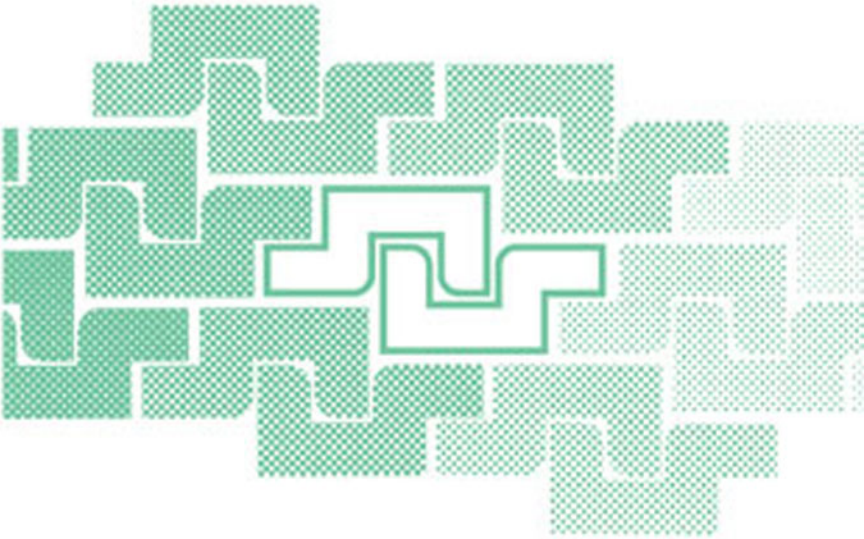

Advances in Earthquake Engineering for Urban Risk Reduction

Edited by

S. Tanvir Wasti
and Guney Ozcebe

NATO Science Series

IV. Earth and Environmental Sciences – Vol. 66

CD-ROM INCLUDED

Advances in Earthquake Engineering for Urban Risk Reduction

NATO Science Series

A Series presenting the results of scientific meetings supported under the NATO Science Programme.

The Series is published by IOS Press, Amsterdam, and Springer in conjunction with the NATO Public Diplomacy Division

Sub-Series

I. Life and Behavioural Sciences	IOS Press
II. Mathematics, Physics and Chemistry	Springer
III. Computer and Systems Science	IOS Press
IV. Earth and Environmental Sciences	Springer

The NATO Science Series continues the series of books published formerly as the NATO ASI Series.

The NATO Science Programme offers support for collaboration in civil science between scientists of countries of the Euro-Atlantic Partnership Council. The types of scientific meeting generally supported are “Advanced Study Institutes” and “Advanced Research Workshops”, and the NATO Science Series collects together the results of these meetings. The meetings are co-organized bij scientists from NATO countries and scientists from NATO’s Partner countries – countries of the CIS and Central and Eastern Europe.

Advanced Study Institutes are high-level tutorial courses offering in-depth study of latest advances in a field.
Advanced Research Workshops are expert meetings aimed at critical assessment of a field, and identification of directions for future action.

As a consequence of the restructuring of the NATO Science Programme in 1999, the NATO Science Series was re-organised to the four sub-series noted above. Please consult the following web sites for information on previous volumes published in the Series.

http://www.nato.int/science
http://www.springer.com
http://www.iospress.nl

Series IV: Earth and Environmental Sciences – Vol. 66

Advances in Earthquake Engineering for Urban Risk Reduction

edited by

S. Tanvir Wasti
Middle East Technical University,
Ankara, Turkey

and

Guney Ozcebe
Middle East Technical University,
Ankara, Turkey

Published in cooperation with NATO Public Diplomacy Division

Proceedings of the NATO Science for Peace Workshop on
Advances in Earthquake Engineering for Urban Risk Reduction
Istanbul, Turkey
30 May – 1 June 2005

A C.I.P. Catalogue record for this book is available from the Library of Congress.

ISBN-10 1-4020-4570-0 (PB)
ISBN-13 978-1-4020-4570-7 (PB)
ISBN-10 1-4020-4569-7 (HB)
ISBN-13 978-1-4020-4569-1 (HB)
ISBN-10 1-4020-4571-9 (e-book)
ISBN-13 978-1-4020-4571-4 (e-book)

Published by Springer,
P.O. Box 17, 3300 AA Dordrecht, The Netherlands.

www.springer.com

Printed on acid-free paper

Printed in the Netherlands.

CONTENTS

CONTRIBUTING AUTHORS

Umut AKGUZEL
Bogazici University.
Dept. of Civil Engineering
80815 Bebek, Istanbul, TURKEY

Sinan AKKAR
Assistant Professor
Middle East Technical Univ.
Dept. of Civil Engineering
06531 Ankara, TURKEY

Ugurhan AKYUZ
Associate Professor
Middle East Technical University
Dept. of Civil Engineering
06531 Ankara, TURKEY

Sergio M. ALCOCER
Director, Institute of Engineering
National Univ. of Mexico
Ciudad Universitaria UNAM
México DF, 04510, MEXICO

Maria ALEXOUDI
Civil Engineer
Aristotle Univ. of Thessaloniki
Dept. of Civil Engineering
54124, Thessaloniki, GREECE

Arzhang ALIMORADI
Dr., Technical Staff
John A. Martin & Associates, Inc.
1212 S. Flower St., Los Angeles
CA 90015, USA

Anastasios ANASTASIADIS
Dr., Civil Engineer
Institute of Engineering Seismology
and Earthquake Engineering
P.O. Box 53-Finikas, Thessaloniki
GREECE

Stelios ANTONIOU
Dr., Chief Programming Specialist
SeismoSoft
Perikleous Stavrou Str.
Chalkis 34100, GREECE

Sotiris ARGYROUDIS
Civil Engineer
Aristotle Univ. of Thessaloniki
Dept. of Civil Engineering
54124, Thessaloniki, GREECE

Mehmet BARAN
Research Assistant
Middle East Technical University
Dept. of Civil Engineering
06531 Ankara, TURKEY

Baris BINICI
Assistant Professor
Middle East Technical University
Dept. of Civil Engineering
06531 Ankara, TURKEY

Dionysis BISKINIS
Univ. of Patras
Dept. of Civil Engineering
Structures Laboratory
P.O.Box 1424
26500 Patras, GREECE

Julian J. BOMMER
PhD, Reader in Earthquake Hazard Assessment
Imperial College
Dept. of Civil and Env. Engineering
London, SW7 2AZ, UK

Stathis N. BOUSIAS
Univ. of Patras
Dept. of Civil Engineering
Structures Laboratory
P.O.Box 1424
26500 Patras, GREECE

Yousef BOZORGNIA
Associate Director
University of California
Pacific Earthquake Engineering Research Center
Richmond, CA 94804-4698, USA

G. Michele CALVI
Professor of Structural Design
Univ. of Pavia
Dept. of Structural Mechanics
Via Ferrata 1
27100 Pavia, ITALY

Juan CARRION
Univ. of Illinois at Urbana-Champaign
Dept. of Civil and Env. Engineering
205 N. Mathews Ave., Urbana, IL
61801, USA

Chiara CASAROTTI
Dr., Post-Doctoral Researcher
ROSE School
EUCENTRE, Via Ferrata 1
27100 Pavia, ITALY

Helen CROWLEY
M.Sc., Doctoral Student
Univ. of Pavia
(ROSE Schoo)
EUCENTRE, Via Ferrata 1
27100 Pavia, ITALY

Serdar CULLU
Graduate Student
Middle East Technical University
Dept. of Civil Engineering
06531 Ankara, TURKEY

Cem DEMIR
Istanbul Technical Univ.
Dept. of Civil Engineering
Structural and Earthquake Engineering Laboratory
34469, Maslak, Istanbul, TURKEY

Uwe E. DORKA
Professor
Univ. of Kassel
D-34125 Kassel, GERMANY

Roberto DURAN
Research Associate
National Univ. of Mexico
Institute of Engineering
Ciudad Universitaria UNAM
México DF, 04510, MEXICO

Amr S. ELNASHAI
Professor
Univ. of Illinois at Urbana-Champaign
Dept. of Civil and Env. Engineering
Urbana, IL 61801, USA

M. Altug ERBERIK
Assistant Professor
Middle East Technical University
Dept. of Civil Engineering
06531 Ankara, TURKEY

Emrah ERDURAN
Middle East Technical University
Dept. of Civil Engineering
06531 Ankara, TURKEY

Ugur ERSOY
Professor
Middle East Technical University
Dept. of Civil Engineering
06531 Ankara, TURKEY

Michael N. FARDIS
Professor
University of Patras
Dept. of Civil Engineering
Structures Laboratory
P.O.Box 1424
26500 Patras, GREECE

Leonardo FLORES
Investigador, CENAPRED
Av. Delfin Madrigal 665
Col. Pedregal de Santo Domingo
COYOACAN CP 04360, MEXICO

Robert J. FROSCH
Associate Professor
Purdue Univ.
School of Civil Engineering
West Lafayette, Indiana, 47907-2051
USA

Quan GAN
Operations Manager
Univ. of Illinois at Urbana-Champaign
Dept. of Civil and Env. Engineering
Urbana, IL 61801, USA

Mihail GAREVSKI
Professor
St. Cyril and Methodius Univ.
Institute of Earthquake Engineering and Engineering Seismology IZIIS
Salvador Aljende 73, 1000 Skopje, MACEDONIA

Wassim GHANNOUM
PhD Student
University of California
Pacific Earthquake Engineering Research Center
Richmond CA 94804-4698, USA

Stephan GLEIM
Dipl.-Ing., Teaching and Research Associate
Univ. of Kassel
D-34125 Kassel, GERMANY

Polat GULKAN
Professor
Middle East Technical University
Dept. of Civil Engineering
06531 Ankara, TURKEY

M. Selim GUNAY
Research Assistant
Middle East Technical University
Dept. of Civil Engineering
06531 Ankara, TURKEY

Scott HAGIE
Technical Staff
John A. Martin & Associates, Inc.
1212 S. Flower St., Los Angeles
CA 90015, USA

Alidad HASHEMI
PhD Student
University of California
Dept. of Civil and Env. Engineering
Berkeley, USA

Viktor HRISTOVSKI
Associate Professor
St. Cyril and Methodius Univ.
Institute of Earthquake Engineering and Engineering Seismology IZIIS
Salvador Aljende 73, 1000 Skopje, MACEDONIA

Alper ILKI
Associate Professor
Istanbul Technical Univ.
Dept. of Civil Engineering
Structural and Earthquake Engineering Laboratory
34469, Maslak, Istanbul, TURKEY

James O. JIRSA
Janet S. Cockrell Centennial Chair
Univ. of Texas at Austin
Dept. of CivilEngineering
Austin, TX 78712-0275, USA

Faruk KARADOGAN
President
Istanbul Technical Univ.
Dept. of Civil Engineering
34469, Maslak, Istanbul, TURKEY

Emre KARAMUK
Istanbul Technical Univ.
Dept. of Civil Engineering
Structural and Earthquake Engineering Laboratory
34469, Maslak, Istanbul, TURKEY

Ilker KAZAZ
Research Assistant
Middle East Technical University
Dept. of Civil Engineering
06531 Ankara, TURKEY

Sung Jig KIM
Univ. of Illinois at Urbana-Champaign
Dept. of Civil and Env. Engineering
Urbana, IL 61801, USA

Dan A. KUCHMA
Univ. of Illinois at Urbana-Champaign
Dept. of Civil and Env. Engineering
Urbana, IL 61801, USA

Nahit KUMBASAR
Professor
Istanbul Technical Univ.
Dept. of Civil Engineering
34469, Maslak, Istanbul, TURKEY

Manuel LÓPEZ
PhD Student
Univ. of Pavia
ROSE Schoo)
EUCENTRE, Via Ferrata 1
27100 Pavia, ITALY

Asli METIN
Middle East Technical University
Dept. of Civil Engineering
06531 Ankara, TURKEY

Christian MEYER
Professor
Columbia University
Dept. of Civil Engineering and
Engineering Mechanics
New York, NY 10027, USA

Eduardo MIRANDA
Assistant Professor
Stanford Univ., Stanford
Dept. of Civil and Env. Eng.
CA 94305-4020, USA

Jack P. MOEHLE
Professor
University of California
Berkeley, CA 94720-1710, USA

Khalid M. MOSALAM
Associate Professor
University of California
Dept. of Civil and Env. Eng.
Berkeley, CA 94720-1710 USA

Farzad NAEIM
Vice President
John A. Martin & Associates, Inc.
1212 S. Flower St., Los Angeles
CA 90015, USA

Dilek OKUYUCU
Research Assistant
Middle East Technical University
Dept. of Civil Engineering
06531 Ankara, TURKEY

Guney OZCEBE
Professor
Middle East Technical University
Dept. of Civil Engineering
06531 Ankara, TURKEY

Gokhan OZDEMIR
Research Assistant
Middle East Technical University
Dept. of Civil Engineering
06531 Ankara, TURKEY

Sevket OZDEN
Assistant Professor
Kocaeli University
Dept. of Civil Engineering
Kocaeli, TURKEY

Onder PEKER
Istanbul Technical University
Dept. of Civil Engineering
34469, Maslak, Istanbul, TURKEY

Rui PINHO
Dr., Associate Professor
EUCENTRE, Via Ferrata 1
27100 Pavia, ITALY

Artur V. PINTO
Construction and Earthquake
Engineering Sector
European Commission
JRC, ELSA Laboratory
2120 Ispra (VA), ITALY

Kyriazis PITILAKIS
Professor
Aristotle Univ. of Thessaloniki
Dept. of Civil Engineering
54124, Thessaloniki, GREECE

Murat SAATCIOGLU
Professor
University of Ottawa
Dept. of Civil Engineering
Ottawa, CANADA

Mete A. SOZEN
Kettelhut Distinguished Professor
Purdue University
School of Civil Engineering
West Lafayette, Indiana, USA

Alex-Loukas SPATHIS
University of Patras
Dept. of Civil Engineering
Structures Laboratory
P.O.Box 1424
26500 Patras, GREECE

Billie F. SPENCER
Univ. of Illinois at Urbana-Champaign
Dept. of Civil and Env. Engineering
Urbana, IL 61801, USA

Marta STOJMANOVSKA
Research Assistant
St. Cyril and Methodius Univ.
Institute of Earthquake Engineering and Engineering Seismology IZIIS
Salvador Aljende 73, 1000 Skopje, MACEDONIA

Haluk SUCUOGLU
Professor
Middle East Technical University
Dept. of Civil Engineering
06531 Ankara, TURKEY

Shunsuke SUGANO
Professor
Hiroshima Univ.
Graduate School of Engineering
1-4-1 Kagamiyama
Higashi-hiroshima 739-8527, JAPAN

Tugrul TANKUT
Professor
Middle East Technical University
Dept. of Civil Engineering
06531 Ankara, TURKEY

Fabio TAUCER
European Commission
Joint Research Centre
ELSA Laboratory
2120 Ispra (VA), ITALY

Ahmet TURER
Assistant Professor
Middle East Technical University
Dept. of Civil Engineering
06531 Ankara, TURKEY

Syed Tanvir WASTI
Professor
Middle East Technical University
Dept. of Civil Engineering
06531 Ankara, TURKEY

Sharon L. WOOD
Professor
Univ. of Texas at Austin
Dept. of Civil Engineering
Austin, TX 78712-0275, USA

Ahmet YAKUT
Associate Professor
Middle East Technical University
Dept. of Civil Engineering
06531 Ankara, TURKEY

Baris YALIM
PhD Student
Florida International Univ.
Dept. of Civil and Env. Engineering
Miami, FL, USA

Guangqiang YANG
Webmaster
Univ. of Illinois at Urbana-Champaign
Dept. of Civil and Env. Engineering
Urbana, IL 61801, USA

M. Semih YUCEMEN
Professor
Middle East Technical University
Dept. of Civil Engineering
06531 Ankara, TURKEY

Ercan YUKSEL
Istanbul Technical Univ.
Dept. of Civil Engineering
Structural and Earthquake
Engineering Laboratory
34469, Maslak, Istanbul, TURKEY

PREFACE

NATO Science for Peace Project 977231 entitled Seismic Analysis and Rehabilitation of Existing Buildings became operational in 2001 and was related to the seismic evaluation and retrofitting of existing buildings in Turkey and the Balkans. It was an ambitious project intended to transfer, adapt and implement and/or develop innovative technologies and methodologies for countries in this region – and, now that it has reached conclusion, appears to have fulfilled its task with great success. In fact, the achievements of this project were also given much prominence at the NATO Istanbul Summit attended by world leaders in June 2004. Many reports, proceedings and papers have been published as a result of the work conducted under this project. The project was launched with a 'kick-off' Workshop in Antalya in May 2001, where it was unanimously decided that as part of Subproject 4 named "Training and Dissemination of Results" the most important item apart from the production of suitable research publications and technical material in the area of the project was the organization of International [as well as national] Workshops to monitor the progress of the whole project and also the associated four subprojects. It was expected that formal submissions at such workshops would later be arranged to form part of the material to be published and disseminated from the project.

In addition to overall support provided by the NATO Public Diplomacy Division, the collaborating institutions in this project were:

- TUBITAK [The Scientific and Technical Research Council of Turkey]
- Middle East Technical University, Ankara, Turkey
- The Greek General Secretariat for Research and Technology
- The University of Texas at Austin, Texas, USA
- The Institute of Earthquake Engineering and Engineering Seismology (IZIIS), University St. Cyril and Methodius, Macedonia[*].

The Scientific and Technical Research Council of Turkey was responsible for the planning and coordination and was the co-sponsor of the project. The project co-coordinators were as follows:

- Prof. Guney Ozcebe, Ankara, Turkey
- Prof. Mihail Garevski, Skopje, Macedonia

[*] Turkey recognizes the Republic of Macedonia with its constitutional name.

- Prof. Michael N. Fardis, Patras, Greece
- Prof. Kyriazis Pitilakis, Thessaloniki, Greece
- Prof. James O. Jirsa, Austin, Texas, USA

NATO Project SfP977231 has brought together leading research personalities in the area of earthquake engineering from several countries for brainstorming sessions, informal discussions, exchanges of ideas via e-mail and, of course, for more formal meetings and workshops. Very many people have given generously of their time and expertise, especially because the very name of the project strikes a responsive chord in all of us. Earthquakes tax engineering ingenuity – and buildings, in the form of houses and homes, are indisputably among the earliest engineering structures.

Highlights of the NATO Project have included a NATO Science for Peace Workshop on Seismic Assessment and Rehabilitation of Existing Buildings organized in Izmir on 13 – 14 May 2003 with support from NATO and TUBITAK [The Scientific and Technical Research Council of Turkey]. The 23 papers of the Workshop were published in the NATO Science Series as Vol. IV/29, and this book of 546 pages has received much attention from the engineering community in all NATO member and partner countries.

The present book contains the Proceedings of the Closing Workshop for Project SfP977231 which spanned the three day period 30 May – 1 June 2005 in Istanbul. The theme was chosen as Advances in Earthquake Engineering for Urban Risk Reduction in order to enable exchange of information, present intermediate analytical/ experimental/other results obtained and to provide a forum for technical discussions related to continuing work in each subproject. The application of state-of-the-art structural analysis and sophisticated experimental techniques for the understanding and mitigation of earthquake damage in order to save lives and property in future earthquakes has formed the core of this multi-national NATO project. Macro-assessment of the seismic safety of buildings in urban areas and cutting-edge rehabilitation methods such as epoxy-bonded Carbon Fiber Reinforced Polymers (CFRP) as well as other ‘occupant friendly’ techniques such as infill strengthening with precast panels comprise important components of the project, and these show great promise for future applications.

The Proceedings comprise the texts of 34 accepted submissions made to the Closing Workshop, which provide an excellent account of ‘where the action is’ in many areas of Earthquake Engineering. It is not surprising – in view of the expertise of the many authors who have made contributions – that the papers cover a remarkable range of topics and though they may not be the last words on earthquake engineering, they are certainly the latest words on the subject. From shaking table tests to infill wall upgrading, from nonlinear analyses to

modern concrete technology, from initial structural assessment to final rehabilitation and from risk to reliability, there are few areas of interest that remain untouched. Research from North America and Europe is well represented, and the NATO members and partner countries in the Balkans that form the components of NATO Project SfP977231 have also made solid contributions to the theme of the Workshop.

Alcocer, Flores and Duran present the latest experimental evidence on the performance of rehabilitation techniques in Mexico, including methods suitable for masonry construction. Sugano provides comprehensive material on the techniques for the strengthening of RC buildings in Japan, mentioning, in particular, the landmark role played by the 1995 Kobe earthquake. The area of FRP [Fiber Reinforced Polymers] applications in strengthening is currently very popular, as indicated by the comprehensive work presented by Binici and Ozcebe, Bousias et al., Ilki et al., Ozden and Akguzel, and Yuksel et al. Ozdemir and Akyuz point out that the anchoring of Carbon Fiber Reinforced Polymers to structural members and infills is often a weak link. They study the effects of concrete compressive strength, anchorage depth, anchorage diameter, and number of fibers on the tensile strength capacity of CFRP anchors. Saatcioglu adds his comprehensive treatment of the retrofitting of non-ductile RC columns to the above. Frosch comes up with an efficient use of precast infill walls for rehabilitation but draws special attention to the connections. Separately, Pinto and Taucer have tested deficient RC frames with and without infill panels The rehabilitation program included retrofitting of a bare frame using selective retrofitting techniques, strengthening of infill panels using shotcrete and retrofitting of frames using K-bracing with shear-link dissipators. Tankut et al. want to transform poorly performing hollow masonry infill walls by using them as filler materials for strong, portable precast concrete panels glued on both sides, which are also dowel connected to the frame members.

Shaking table tests are now an integral part of available experimental tools and the Skopje group, represented by the paper of Garevski et al. give valuable information on three 1/3 scale models of an RC frame building prototype which were designed, constructed and tested on the shaking-table at the IZIIS Laboratory in Skopje in order to verify the validity and applicability of different seismic retrofitting techniques. This is complemented by the paper of Hashemi and Mosalam giving the results of a shake-table experiment at the University of California, Berkeley on a one story reinforced concrete moment resisting frame structure with an unreinforced masonry (URM) infill wall.

In a masterly overview, Jirsa distils the experience from the post-quake rehabilitation of a large number of structures in Mexico City where traditional rehabilitation approaches were used but the number of buildings that were deficient required the development of innovative techniques. Thus, the poor

foundation conditions in the lake bed zone necessitated that foundation rehabilitation be kept to a minimum. Cable bracing systems provided a means of stiffening and strengthening the structure to reduce lateral deformation and provide the lateral capacity required by the code after the 1985 earthquake.

There is a wide range of papers dealing with different types of analysis, from Bommer et al. who use a direct displacement approach for loss assessment in urban areas, to Calvi et al. who employ a similar approach to bridge design. Pinho presents an adaptive pushover algorithm that may be applied to both buildings and bridges. Erberik and Cullu discuss seismic fragility for low and mid-rise RC frame buildings, whereas Gulkan et al. offer an evaluation of approximate nonlinear procedures when applied to shear wall structures. Metin and Akkar investigate the drift demands for stiff moment-resisting frames by subjecting a total of 8 regular frame models with 3- to 9-stories to 40 soil site records. The moment magnitude and source-to-site distance of the ground motion data set is also varied. Pinho et al. discuss the advantages and shortcomings of various currently utilized pushover analyses or nonlinear static procedures which are being preferred over complex nonlinear time history methods. Yakut and Erduran propose a comprehensive performance assessment procedure for RC buildings with masonry infill walls which has been found to give good results when calibrated with observed damage from recent earthquakes in Turkey, and they have extrapolated their results to a pilot study of structural assessment in the Zeytinburnu district in Istanbul. Gunay and Sucuoglu have developed a displacement-based seismic assessment procedure, employing equivalent linear analysis in combination with capacity principles. The procedure, implemented on three case studies, identifies the expected locations of inelastic behavior and reduces the stiffness of members corresponding to these locations. Dorka gives examples of buildings that have been earthquake protected using hysteretic devices. The capabilities of the versatile testing facility for small and large scale structures at the University of Illinois (Urbana-Champaign) are presented by ElNashai et al. Turning to a topic that is often not given its proper place, Wood discusses the similarities and differences between industrial structures in Turkey and the United States, with regard to seismic performance as well as rehabilitation. Rapid screening of RC buildings – particularly deficient ones – needs to be conducted with efficiency both before and after a disaster. Turer and Yalim have proposed preliminary assessment methods that tap into the speed of the Internet to accumulate information data bases dealing with existing buildings. Naeim et al. indicate where the future may lie in terms of automated seismic assessment of buildings. Their paper contains proposed methods that can provide extremely useful information regarding the status of a building immediately after an earthquake by simple and rapid analysis of sensor data and prior to any building

inspections. Ozcebe et al. have combined dedication, analysis and engineering judgment to produce a weighty and impressive paper on the large scale seismic evaluation of RC buildings in the Istanbul district of Zeytinburnu.

In a continuation of their extensive work dealing with the seismic risk in Thessaloniki, Pitilakis et al. expound the steps needed for the development of the urban risk scenario for Greece's second largest city. These include seismic hazard assessment, conducting of a systematic inventory and identification of the typology of the elements at risk, an analysis of their global value and vulnerability, and finally the identification of the weak points of urban systems. Meyer, writing about the latest advances in fiber-reinforced concrete technology informs us that it is now possible to engineer the properties of the material such that it not only becomes very ductile, but also exhibits strain hardening, thereby making it ideally suited for impact-resistant structures as well as for earthquake-resisting structures. Penultimately, Wasti and Ersoy round off the presentations with a critical appraisal of traditional versus emerging rehabilitation techniques in Turkey.

Last, but by no means least, Mete Sozen has spun a fascinating and thought-provoking tale in his Keynote Address, which sets a high and thought-provoking tone for the proceedings. The earthquake that lies hidden in store for Istanbul is dissected over the culinary delights and libations that Istanbul has to offer. Engineering and eloquent expression are a daunting combination and do not always mix, but Mete Sozen has hidden gifts. He can marshal unlikely facts from history and science and folklore to buttress his case. He calls his account 'fiction' – you may prefer to call it a parable if you wish. The story, both somber and uplifting, is an excellent introduction to the city itself, and even Sozen himself – in spirit at least – is not completely concealed in the narration. Perhaps in the nostalgia that grips the whole story there is room for self-questioning, even regret.† The past is another country, indeed.

Syed Tanvir Wasti
Guney Ozcebe

Ankara, September 2005.

---

†In the background of Sozen's narrative, like a refrain or *leit-motiv*, or an insistent whisper, are the words that the Istanbul born poet Cavafy wrote for another city in another ancient land touched by the Mediterranean:

This city will always pursue you.
You'll walk the same streets, grow old
in the same neighborhoods, turn gray in these same houses.
You'll always end up in this city.

FOREWORD

For many years the thrust of experimental and analytical research in earthquake engineering has been directed towards the reduction of seismic risk in urban areas. Because of advances made in research and implementation in design and construction practices it is fair to say that structures designed and built in accordance with today's good practice are expected to fare well even in severe earthquakes. Unfortunately this cannot be said about the vast stock of existing older structures that prevail in many urban areas, particularly in countries in which economic conditions do not support large-scale and expensive seismic upgrading. There the need is largest for simple methods for assessment of seismic vulnerability and for cost-effective means of retrofitting.

This volume on provides insight into many important issues of risk assessment and management and into mature and developing methods for predicting and improving the collapse safety of structures. The papers span a wide spectrum of topics, including state-of-the-art analysis and experimental techniques, but the primary theme is cost-effective reduction of seismic risk. In this respect the volume lays a groundwork that can be used by engineers and decision makers alike to develop plans and guidelines for an effective urban risk reduction program. It can only be hoped that the contributions presented in this volume will be read not only by other researchers and engineers but also by those who are empowered to make decisions that affect implementation of risk mitigation measures. In an urban area like Istanbul the question is not whether or not a strong earthquake will happen, rather when it will happen and what can be done to reduce the resulting human suffering.

We should be thankful to Professors Syed Tanvir Wasti and Guney Ozcebe, Middle East Technical University in Ankara, who have taken the initiative to organize the workshop that has resulted in this excellent compendium of papers on issues of great importance to seismic safety in urban areas.

Helmut Krawinkler
John A. Blume Professor of Engineering
Stanford University
Stanford, CA 94305-4020, USA
November 2005

FROM DUZCE TO THE CITY

METE A. SOZEN
Department of Civil Engineering, Purdue University, West Lafayette, IN 47905.

Alice : "….what is the use of a book without pictures and conversations?"

Figure 1.

Abstract. The manuscript contains a fictional discussion of the earthquake hazard Istanbul sustains and what may be done about it. Of all the fiction surrounding the issue, this may well be the only one that is admittedly so.

Keywords: Istanbul; urban risk; earthquake hazard; drift; lateral forces; PI index

S.T. Wasti and G. Ozcebe (eds.), Advances in Earthquake Engineering for Urban Risk Reduction, 1–18.

Istanbul (the City derives its current name—after having been called Byzantium and then Constantinople-- from a misunderstanding of what its denizens said to the community in the countryside: “Eis tin Poli” or “to the city” whenever they wished to return home) has had her share of catastrophes but none has reached the depth, breadth, and height of what it suffered on 13 April 1204 when the armies wearing the cross of Christ on their shoulders breached her walls. “Since the creation of the world such a vast quantity of booty had never before been taken from one city,” wrote Villehardouin, the historian of the Fourth Crusade. An eyewitness to the human slaughter by the conquerors, Niketas Choniates, noted “Even the Turks are merciful and kind in comparison.” Nicholas Mesarites, another eyewitness, wrote of the conquerors “tearing children from mothers and mothers from children, treating the virgin with wanton shame in holy chapels, viewing with fear neither the wrath of God nor the vengeance of men.” The carnage was hardly a fitting end for the City that had saved Greek literature, philosophy, and learning from extinction and had added durable thrusts of her own in culture from architecture to politics, to law, to music, to literature, to food, and even to table manners.

To contemplate that a catastrophe of similar magnitude, a fault rupture in the Marmara Sea, threatens the City today is not heartening. In recorded history, there have been eight major earthquakes that have caused severe damage in Istanbul. The first set of four occurred during the years 400-740 AD. The second set of four occurred during the years 1500-1900 AD. If the City has survived eight major events, why should one be concerned about the next one? The reason is simple. Until the mid 1900’s there were fluctuations in the City’s population and construction types, but they were not overwhelming. Since 1960, the population of the city has grown immensely. Construction has changed from primarily timber to almost exclusively masonry and concrete, especially for residences. Building structures have been optimized with respect to gravity loads only. The ground covered by the vast residential sectors is mostly new and fraught with potential surprises in ground motion. Unless the City leaders take action to reduce the risk, the next major earthquake event may make 13 April 1204 look like by far the lesser evil.

This manuscript contains a fictional discussion of the earthquake threat to Istanbul and what may be done to reduce the risk. It is not the first fiction on the topic but it may well be the only one that is explicitly so.

What follows is an incomplete extract from a conversation among four structural engineers who had grown up in Istanbul. The conversation took place at Cavit’s Tavern at Cicek Pasaji (Flower Alley or Hristaki’s), a well known watering spot in Beyoglu (Pera), a rather lively district of Istanbul. The four knew Cavit quite well. Cavit had started as an apprentice waiter when the four were in high school. In those days, Cavit was their pass to the world of adults.

He would seat them at an inconspicuous table and serve them. By 1999, Cavit had worked his way up to own the tavern.

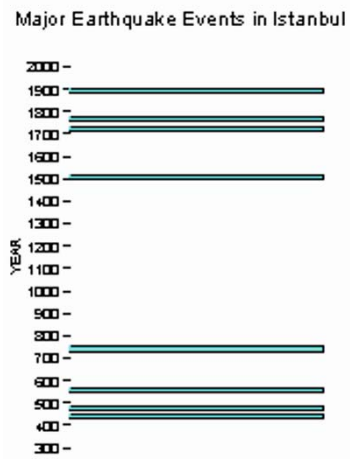

Figure 2.

All four engineers had been very close friends having attended the same middle and high school in Istanbul in mid-twentieth century. After high school, they had gone in different directions. Only one of them, Kerim Dinlemez, had returned to Turkey. The other three lived and worked in different parts of the world. This was their first face-to-face meeting as a group after almost four decades. What brought them together on this occasion was the pair of earthquakes that devastated the region from Yalova to Bolu in 1999 and the threat that a possible third event would pose to Istanbul.

Hajime Shiba, one of the two sons of the Japanese chargé d'affaires in Turkey, had gone to Tokyo after completing high school in Istanbul and won a berth at the University of Tokyo where he eventually obtained his doctorate in architectural engineering. He had remained in the academy and had gone on to an illustrious research and teaching career.

John Tzetzes, the only son of the haute-societé couturier in Istanbul and a descendant of one of the old Phanariot families, had left Istanbul for Argentine in 1956 to continue his schooling as an engineer and had become a builder in that country. Not a single acquaintance had the courage to pronounce his last name. He was known simply as Yani to all his friends. "John" had surfaced after his migration to Argentine.

Arda Dervishian had remained in the United States after he obtained his doctorate specializing in earthquake resistant design. After trying his hand at teaching for a few years, he went into the profession developing an

architectural/engineering firm that earned the reputation of being the best in southern California.

Kerim Dinlemez had also studied in the United States for a graduate degree and had returned to Turkey to launch successful construction and construction materials businesses. During his years in the United States he had remained close to Dervishian. The two men were connected through family ties and their friendship had started when they were toddlers. Their grandfathers had been partners in business. They shared a common distant ancestor, a cantor in Tbilisi, a fact they never acknowledged even to one another possibly because neither could carry a tune.

Figure 3.

Dervishian had gone through a few decades as Dervishoglu on the whim of a registrar before the name was rectified through court action. The Dinlemez transformation during the implementation of the “surname law” of 1934 was more interesting. The patronymic had been Hacidumbatzezade. The registrar was adamant in not accepting it as an appropriate name for a citizen of the secular Turkish Republic. In 1934, Haci was anathema and zade reeked of the Ottoman. When Kerim's grandfather insisted on Dumbatze, the registrar had compromised on Dinlemez (which means does not listen in Turkish) and had, at least for one family, captured the spirit of the Istanbul population.

"This is not the City I left," Tzetzes remarked.

"Certainly you, of all the four of us, did not expect to cross the same river twice," responded Dinlemez, "Indeed, the City has expanded phenomenally. The population had barely exceeded the million mark when you left. You must remember having been told by Mr. Campbell (who had been their favorite teacher at high school) that Byzantium flourished on the bounty of the fish that crossed the Bosphorus twice a year. It is now people, not fish. The 1997 census set it at close to 10 million. Many people who profess inside information--this is the city of rumors-- put it closer to 12 million. There had hardly been any construction in the City as late as the '50s. But the explosion of population and the return (after 1923, Ankara took what revenue there was, and made the urban population recall Claudius fondly for the tax exemption he had granted the City) of a modest amount of capital to Istanbul changed all that (Currently the City is returned less than one fourth of the taxes collected)."

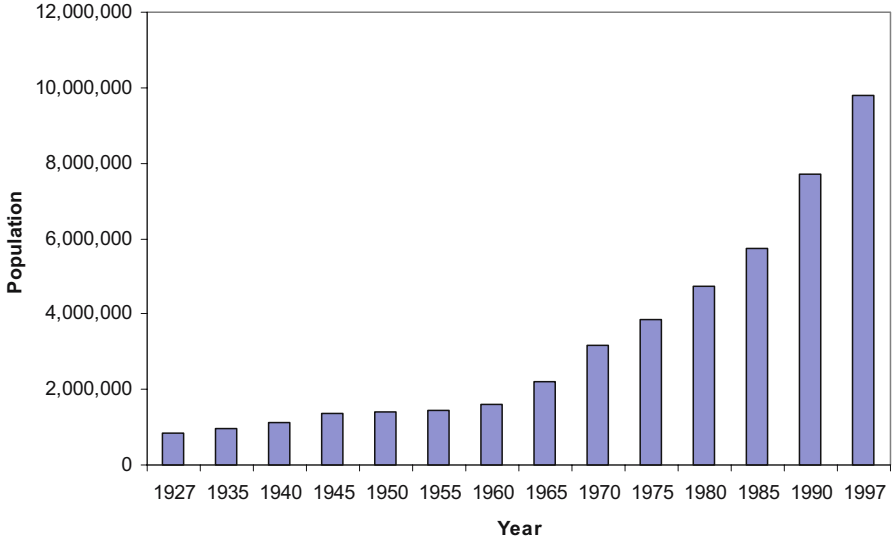

Figure 4.

"In the '70s, the urban population increased by approximately 150,000 souls a year. Since 1980, the annual increase has been close to 250,000. Shelter had to be provided in an environment of acute shortages of material and trained workers in the '70s. Until the Turkish steel mills and the cement factories came in on line, our experience was the construction equivalent of war. We built with hardly half a thought for the future. The citizens of Istanbul demanded shelter and we provided. I and others built for the rich. The poor built for themselves. Inflation that went out of control in the '80s created new conditions to shape our decisions. Never mind the individual owners, even our major corporations built structures intermittently whenever money became available. Continuity of

structure was as dubious as our financial outlook. We built to be able to rent. To rent, the plaster had to be on the walls and the glazing had to be in place. We selected the frames to fit the room plan that we thought would sell. Framing responded to space demands. We cannot blame the random framing and the sterile facades on the architects. Very few of them were involved. We built with whatever materials we could find. In that rush, what was inside the concrete did not appear to matter very much. Back in the 70's, I remember a fellow contractor announcing jubilantly that he had used barbed wire for reinforcement in the girders of an apartment building and it had worked. We were seldom in position to test the steel or the concrete. We had to accept whatever we could find. The forces of gravity tested and sales ruled."

"What did you do about structural details?" Tzetzes was curious.

"We made sure that the column reinforcement stayed in place during casting. We sized sections to handle the gravity shear. But that was about all."

"That means no special transverse reinforcement in columns, no proper development of plain bars?"

"Yes. None."

"What about the codes? Were there any?" asked Dervishian.

Dinlemez scoffed, "Were we not Ottomans? The Republic was replete with codes. An occupancy permit required proof of having satisfied all applicable codes. And there were many that applied. But seldom did owners or renters demand permits. I would not be surprised if I was told that less than half the living and working space in Istanbul has valid permit. We built in the mindset of refugees escaping from the cold."

"Was there no governing authority inspecting your construction?" Tzetzes asked.

“Many," was the answer, "but we thought of our inspection authorities as another layer of tax collectors. Have you not heard of the saying that if Jesus had been mayor of Istanbul he would have been corrupted in six months? The would-be inspectors received their bakshish and left. Yes, we contributed to the corruption. So did they. Any toughening of the inspection criteria seldom improved quality. The only result was a corresponding increase in the sub rosa collection by the inspectors.”

Dervishian persisted, "It is difficult for me to believe that a city with as serious an earthquake risk as Istanbul can build without proper care. You have a well functioning state disaster agency that has correctly placed parts of Istanbul in the highest risk zone. You have well informed faculties in your engineering schools. You have a very demanding modern code for earthquake-resistant design. How could a builder ignore all these?"

Dinlemez was irate, "Currently, our government and our scientists keep telling us that we had been amply warned. I question that. If the authorities had

been sincerely interested in reducing the risk, they would have developed a shared vision of the earthquake threat. If the perception of the risk remains locked within the departments of government or of universities, the risk is not likely to be reduced. Did the municipality enforce the earthquake code? Were their own buildings built in every case with seismic effects in mind? Have the state hospitals all been built to be earthquake-resistant? Did the scientists state in a single voice their concern in language the builders and owners could understand? The answer is a resounding no to all those questions. To boot, our profession did not have the institutional memory. The year 1894 was far too early for it to have made an impact on anyone building in the last thirty years. And, our building technology and media had changed. There were no built-in safety catches, no good habits."

"But you kept having disastrous earthquakes in Anatolia!" Dervishian exclaimed. "Earthquakes between the years 1925 and 1998 resulted in over 50,000 casualties and total loss of 350,000 dwelling units. You did not notice it?"

Dinlemez was untouched. "I can tell that you have been gone a long time from Istanbul. This is Istanbul here and out there, far away, is Anatolia. The earthquakes you talk about might as well have been in Tashkent."

In school Dervishian had prided himself to be the craftsman of the four. But California had made a neo-scientist out of him. He returned to his favorite topic. "As an enlightened person who can put two and two together, you cannot deny the risk sustained by the city. Forget ancient history. Consider only what happened in the 20th. century. We see a diabolical progression of a tear along the North Anatolian Fault. It is disturbingly like a zipper opening. It has left a scar in Thrace in 1912. Since then it appears to have restarted at the eastern end to move sporadically toward the City. And now we witness a sizeable seismic gap close to Istanbul. One does not need a degree in seismology to conclude that there may be a sudden slip along it of as much as five meters or more. Could that build up to a seismic moment magnitude of close to seven? Yes. Would the energy source be close to Istanbul? Yes. You could not have figured that out?"

Dinlemez was defiant, "Dervish, to assign wisdom to the majority of any group is not wise. What makes you think that I had time or wanted to think? Remember that in our ethos, mythos overrides logos. We had and continue to have a preternatural feeling of security based on two myths. The first: Listen to Cavit. He says this building behind us was standing in 1894. And he is certain that it will stand after the next event because, he says, it is built like a rock and built on a rock. Were the City walls not built in the fifth century?"

Tzetzes, who had a proprietary interest in the walls and knew their history quite well, interjected, "But the towers bit the dust in the 447 event and had to

be rebuilt! The damage to the walls reoccurred. Even Anadolu Hisari, the fortress that was built in 1395 on the Anatolian shore of the Bosphorus before the liberation of the City, was once damaged by an earthquake."

Figure 5.

Dinlemez went on," Well, Cavit does not know that. Besides there are many buildings that were here before 1894 and we go about our business in Istanbul believing in those signs. Is this not the land of icons?"

"Your mysticism will not save you." Tzetzes stated. "Severus may have rebuilt the city after totaling it, but the earthquake will not. And your past earthquake damage statistics are irrelevant. You have built yourself a brittle house over terrain yet to be tested. You are the one who reminded me that I cannot cross the same river twice. The City has changed. The ground motion may be surprisingly different."

"Give him quarter," said Shiba. "He did say it was a myth."

Tzetzes was not ready to give up. "Your first article of faith was bankrupted by what happened in Avcilar and what happened to Mihrimah on 17 August 1999."

Undaunted, Dinlemez continued, "Avcilar, as every one knows, was a case of a bunch of bad buildings sitting on even worse ground. In fact, Avcilar strengthens the case for Cavit's rock on rock. About Mihrimah, I say Sinan went overboard in his putative love for the Sultana. He did indeed create a shimmering jewel of a building. But as structure, it lacks the basis of Sinan's successes with his other works: a low ratio of axial load to supporting area

(P/A) begets, in an earthquake, a low ratio of lateral load to resisting area (V/A). In Mihrimah, Sinan threw all caution to the winds. It was also his misfortune to place that shimmering piece of architecture on ground that appears to amplify the seismic waves or so it has in almost all previous events."

Shiba wanted to change the course of the conversation. "What is your other myth?" he asked.

Figure 6.

"The other article of faith is distance." Dinlemez picked up where he had left. "If the earth's crust cracks south of the islands, it will be distant enough not to hurt much of the City. I look at your science Dervish, at your attenuation curves, and I feel good. Yes, I concede the earthquake will happen but distance will save us if our foundation rocks will not."

“I cannot support your faith in our scientists,” responded Shiba.“ You must have noted that attenuation curves are always compared with the data in terms of the logarithm of the peak acceleration. That camouflages considerable scatter. As an engineer, I have always felt we were flimflammed by such presentations. Deviations that may look trivial on a logarithmic plot may be devastating for the buildings. In fact, I have always claimed that they should plot the acceleration ordinates raised to a power, more than one, of the acceleration values in order to provide the right perspective.”

"How can you deny the data?" chimed in Dinlemez. Shiba was unmoved, "I do not deny the data. I ask you to look at them carefully. Do not be lulled to inaction by the averages. You know the old proverb: One can drown in a stream with an average depth of a foot. When it comes to ground motion, one must expect the unexpected."

Dervishian was getting frustrated, "Enough of your rivers, Shiba! What are you leading to?" He was not comfortable with Shiba's deconstructionism.

Shiba continued unperturbed, "I wish to say that whatever the magnitude and wherever the fault, I look at the earthquake history of the City and I conclude that the demand in a finite part of this large city may be pegged by an effective peak ground acceleration of as low as G/3 and as high as twice that value. And that is if I am feeling optimistic. If one means to protect the City, it is a waste of time to deal with dice, to ponder about what will happen where and to which. Suppose I tell you that the probability of occurrence of a peak ground acceleration of G/3 in Istanbul is 70% within the next 50 years. What does that tell you other than the strength of my personal conviction. Can you falsify my position? I am right if it happens and I am right if it does not happen. We do not have a hundred cities to test the statistics. I do not call that engineering. As a matter of fact, I do not believe we even need to divine a demand spectrum. All a good engineer needs to do is to look at the buildings and decide which ones need urgent care."

Dervishian was not about to declare bankruptcy of what he told his clients. "The City is vast. Microzonation, properly done, will reduce the task of prevention by an order of magnitude. As a minimum, it will indicate where to spend the resources and where not to. Granted the 19 August event had a far epicenter but did it not provide any clues as to where the problems may arise?" Tzetzes deflected the question," Shiba-chan (a nickname Shiba had acquired as a ten-year old in his prep year in middle school and had not been able to shake off even after adolescence) is right. Given the fragility of the construction in the City, we need not sweat to determine contours of expected intensity. A flat-rate expectation will do. Besides, I fear that the causative fault may be north of the islands, closer to the city than Dinlemez hopes.

Dervishian conceded. "The City may be a special case. I am willing to throw in the towel with respect to zonation. It may be feasible to concentrate exclusively on identifying the vulnerable. The probability of success in that exercise is much higher than in guessing at intensity variations in the City in detail."

"And?" Dinlemez queried.

"The immediate action must be control of the new construction. If the City is expanding by as much 2.5 % each year, the first frontier is to make certain that the new buildings are reasonably safe," Dervishian suggested.

"That would make a dent," added Tzetzes, "If we have, say, 30 years to the next major event, proper proportioning and detailing of new construction would protect a fraction of the population."

"But how would you control the construction?" Shiba asked. "I have read your code for earthquake resistance insofar as my Turkish allowed me. It is indeed up to date and a very good document. But it is too esoteric to use for low-rise construction. It has too steep a learning curve. The effective action would be to develop a new building code for buildings of seven stories or less based on a simple statement such as having the total cross-sectional area of the walls and the columns satisfying a requirement expressed in terms of a specified story shear and an allowable stress. We have used that approach quite successfully in Japan. You can easily modify it to suit your conditions and experience. There must, of course, be specified minima for reinforcement ratios and a simple definition of a "regular" structure. You could develop such a recipe in less than a month. Any engineer could learn to use it in a day. It has another supreme advantage. It would make inspection very easy.

"That takes us to the middle ages," demurred Dervishian. "In California, we have developed a simpler and intelligent approach."

"How simple?" Dinlemez wanted to know. Subconsciously, he hoped for a solution from the west. No matter how defiant he was about centuries of European brainwash about superiority of western thought, when it came to techne, he looked to the west.

Dervishian went on," The function and value of a building set the requirements for consistent drift and strength. Some buildings, such as hospitals, need to survive the expected earthquake intact. Some others, all they need to do is not to collapse. On the basis of performance demands, we determine the required base shear strength coefficient and limiting story drift ratios. If it is a building on the drawing board, we proportion so it satisfies the strength and drift limits. If it is an existing building, we analyze it to ensure that the drift ratios are not exceeded. If they are, the building is declared unsafe."

"And we are to do this for every building?" asked Dinlemez.

"Yes!"

"I am glad you have not lost your Anatolian humor," chuckled Dinlemez. Shiba could not control himself because he knew Dervishian was serious. He interrupted, "The process is neither simple nor wise. I might consider your scheme for new buildings, but the quality of construction you see around you simply does not merit that sort of attention. How will you obtain the material properties and reinforcement details? If we are bound to be wrong, we might as well be wrong the easy way. The residential and small-business buildings in the City need a solution of the Gordian-Knot type. Knee-jerk analysis in lieu of thinking is a waste of time. Yes, there may be subtle problems that only

analysis may unearth, but much if not all of the vulnerability is abundantly self evident. It is very seldom that a building fails in a complicated way because of mysterious flaws. People get killed in buildings with simple and obvious flaws.

"I still maintain that there is room for drift determination as an indicator of safety," Dervishian insisted.

"Pray tell me how you would do that?" It was Shiba's turn to get testy.

"Elementary," said Dervishian. " But I need your help, Kerim. How would you define the period of the typical building in Istanbul?"

"With or without the nonstructurals?" asked Dinlemez.

"Without."

"I would venture that our representative reinforced concrete residential building would have a calculated period equal to approximately the number of stories divided by seven."

"That is all I need to know," said Dervishian, "It is well known that a "reasonable upper-bound" estimate drift spectrum for the lower bound demand on competent ground of which we speak is 200T, with T in seconds and the result in mm. I assume the amplifier to obtain the roof drift to be 5/4 and the typical story height to be 3 m. The mean drift ratio, in per cent, then becomes $200\times(N/7)\times(5/4)/(N\times30)$ or less than 1.5% which I would consider to be barely tolerable. If the building has walls on all upper stories but none or little at the ground story, then I assume that half the total drift occurs at the ground story. In that case, the drift ratio, again in percent, becomes $200\times(N/7)\times(5/4)\times(1/2)/(30) = 4\%$. That is intolerable and the calculation immediately identifies the vulnerability of buildings with "open first stories."

Shiba asked, "But why do you take this circuitous route to tell me the obvious, that buildings with open first stories are vulnerable?"

Dervishian was discomfited. People did not ask such questions where he worked. They had respect for analysis. 'Because it convinces the building owner that the flaw in the building has been identified through rational analysis."

"Rational!" exclaimed Tzetzes. He had read Aristotle but did not want to get into an argument on etymology. "Clearly, Dervish, yours is no way to skin this cat. I grant you the coefficient of 200 that you seem to pick up from thin air and I shudder to think what you are going to conclude if the event is defined by a PGA of 2G/3 rather than G/3. But I am not willing to give up on the nonstructural walls (at least if they are distributed with reasonable uniformity over the full height of the building).

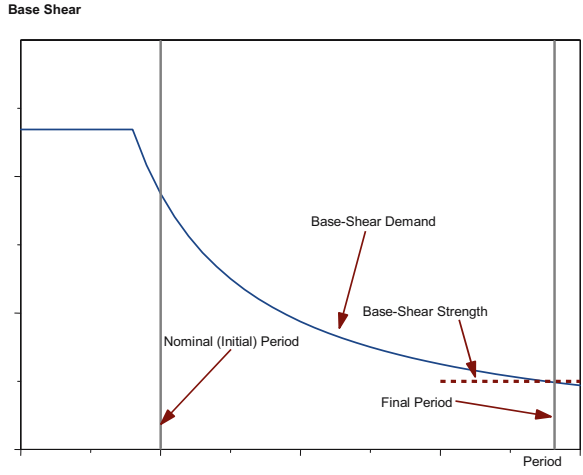

Figure 7.

They do make a substantial difference in strength and stiffness, until, of course, they crumble. And your analysis ignores the add-on story, a story added on after the building had been in service for years, often with no positive connection to the story below. You also forget about the captive column."

Shiba joined the conversation. "The engineer needs to have a feel for the physics of the phenomenon. For that a simple method has been devised. What defines a building structure on the drawing board is its period, however fictitious it may be. We start with that and a relationship for base shear. Most engineers are familiar with the concept and tend to overlook the differences between the responses of systems with one and many degrees of freedom. It is self evident that upon strong shaking, the period moves from its initial value to a higher one. Further, it is plausible to accept that the period will move to the value at which its inherent strength (limiting base shear) will be equal to the base-shear demand. Knowing the limiting base shear and the base-shear demand identifies the period that will be reached. Given that period, one can go the idealized response spectrum (that is coupled with the base shear) and determine the spectral drift. So that in one method the engineer understands why the base shear strength does not have to be as high as the demand at the nominal period."

Shiba explained. "It was brilliant of the Italian engineering community to devise a quick-fix design method, immediately after the 1906 Messina catastrophe, based on a pretense of lateral forces acting on the building. But at best it was a stop-gap method to respond to the exigencies of the day. Basing our thinking on force, it took us a long time and bitter experience to rediscover that toughness was as important as strength, if not more. Any modern design method must be coupled explicitly to drift. Consider the base shear demand. If

one overlooks the differences between responses of structural systems with simple and many degrees of freedom, the variation of base-shear demand with system period provides a comfortable understanding of the forces involved. For a given distribution of lateral forces over the height of the building, it is possible to determine the base-shear strength. It is usually a small fraction of the base-shear demand determined for a linear system. Instead of reducing the demand at that period by mysterious factors, it is better to pretend that the period will increase to a value at which the base-shear strength is equal to the base-shear demand. Then, it is a simple step to conclude that, at that period, the drift response will be higher. This process allows the engineer to relate the behavioral phenomena to the design process and understand what he/she is doing."

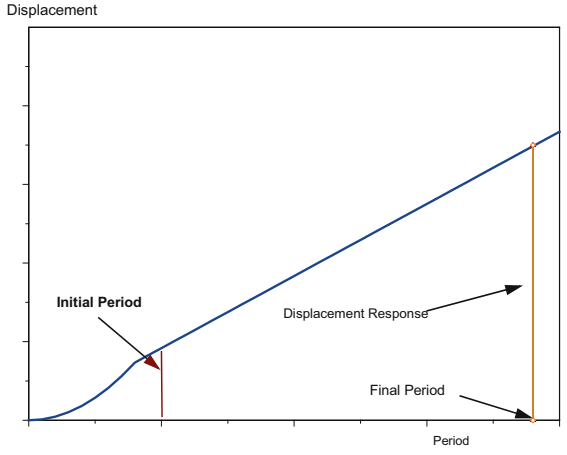

Figure 8.

"We use a much improved version of that in California," announced Dervishian. He was delighted to find common ground with Shiba and hastily sketched curves on a napkin (Figure 9). "It is based on a clever transformation of period, in the shear vs period plot, to displacement. The shear-period and the displacement-period relationships are related to one another. So we simply plot the shear demand against the displacement demand. This plot also provides the axes for plotting the base-shear resistance of the structure as the displacement increases. Where the resistance curve crosses the demand curve is the solution that provides the engineer both the base-shear and drift responses in one fell swoop!"

"Not so fast!" exclaimed Tzetzes (he was renowned for having sat through the movie Casablanca seven times in one week.) "I thought Shiba was dealing with smoke when he explained his simple method, you have gone further into the deep. A question: What is the reasonable error range in the shear demand?"

"In a region of which seismicity has been well established, probably plus or minus 30%."

"I shall accept that. What is the probable error in the resistance curve?"

"I do not think it would be more than 20 %."

Tzetzes was quizzical. "And I presume 20% relates to a given arbitrary arrangement of the lateral forces. Even if I accept your numbers, I find the variation in the crossing point of the two curves to be all over the place. Indeed the procedure is elegant but it provides a false sense of accuracy to the designer."

"How?" asked Dervishian.

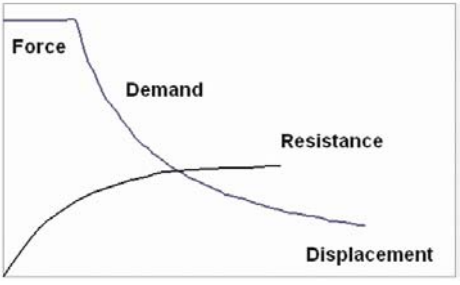

Figure 9.

The two curves look quite crisp and the intersection point appears to be unique, but there is a lot of fuzz hiding behind the curves."

Dinlemez was reaching his limit. "I look to you for a simple solution and you keep wanting to analyze buildings that defy analysis. The structural framing that you fantasize is simply not there. Your science ignores our reality. We need to deal with existing buildings held up by bashibazouk framing systems. You seem to keep thinking about chalkboard examples. Before we came here, Dervish had stated that there were two main rules to earthquake resistance: (1) Maintain elevation –to preserve the people—and (2) maintain shape –to preserve the investment--. You seem to be preoccupied with the second one while our concern is the first. When the big one comes, I am willing to lose the investment in the existing buildings but I am not willing to lose the people. The buildings in Istanbul to which you can apply your fine analytical methods, those with well defined framing systems and known material properties, are not likely to need scrutiny anyway. What you need to tell me with your superior knowledge is which buildings I need to fix and in what order?"

"Then use your Anatolian wisdom," said Tzetzes in a conciliatory tone. "When Nasreddin Hoca fell off the roof and his wife was agonizing over which expert to call to his aid, the Hoca said: Just bring me someone who fell off a roof." You have the experience. You can easily identify the buildings with

open first stories, with captive columns, and with add-on stories. Start with those."

Cavit, who had been listening patiently, chimed in, "I think all four of you believe techne will save the City at no cost. I say it is not techne but money that will save the City. Ali Ihsan Bey, a banker and one of my customers, proposed a much simpler and not so expensive solution. If you start making technical judgments about which building should stay and which buildings should not stay, our lawyers will trip you up in almost all cases. Any action to raze and rebuild may take years. Ali Ihsan Bey has a workable plan. First, the engineers identify the vulnerable buildings. This does not result in a great deal of hassle because the owners are given the option to rebuild or not to rebuild. If they want to rebuild, they get low-interest 30-year loans from a special fund set up for that purpose. Ali Ihsan Bey believes that the initial capital for this purpose, not likely to exceed four billion euros, could be raised by joint efforts of the Turkish Republic and the World Bank. After a few years, the fund would be self-sustaining. What happens to those who do not wish to rebuild? Nothing, but the Municipality maintains a list of the buildings considered to be vulnerable for all prospective buyers and tenants to consult. He says that such a plan would be very efficient and would, in a span of 30 years, reduce the risk to a tolerable level."

"What if the ground motion we fear does not wait for 30 years?" wondered Shiba. Cavit did not consider it a threat, "If it happens this year, all plans would be equally bankrupt. If it happens in five years? Well, I do not think your technical solutions will be any further ahead than Ali Ihsan Bey's financial solution."

Dinlemez seemed to be searching for a compromise. He addresses the three engineers, "May I suggest the grounds for exercising your intellect?"

"What are the grounds," the three asked almost in a single voice. They remembered well his juvenile fixation on pseudophilosophical issues and did not want to get involved in word games.

"I would like for you to think of what happened in Duzce within a time span of three months in 1999. For some sectors of Istanbul, Duzce is a fair metaphor. In Duzce, almost all buildings have light and lightly reinforced concrete frames. More than 80% of the building inventory had four, five, or six stories of approximately 3 m. To describe the relative strengths of these buildings allow me to use the "priority index" or the ratio of the total cross-sectional areas of the columns and walls (the nonstructural filler walls weighted by a factor of 0.1) in the ground floor to the total floor area in the building. On that basis and on that basis alone, can you rationalize what happened in Duzce if I tell you that in the first earthquake (17 Aug. 1999) approximately one-eighth of the structures were severely damaged or destroyed and in the second earthquake

(12 Nov. 1999) approximately one-third (cumulative) of the total was severely damaged or destroyed. To make judgment easier, let us assume that the peak ground accelerations for the first and second events were approximately 0.4G and 0.5G, respectively.

Dervishian was the first to react. “If I judge simply on the basis of the PI distribution you give us, I would say that half the buildings should have sustained severe damage.”

Tzetzes was skeptical about the outcome. “I do not believe any one of us can give you a professionally responsible opinion on the basis of the indices you have given us. Many buildings fail because of singular flaws such as captive columns, discontinuities in construction, bad framing concept, and poor materials or workmanship. How can I infer that from the data you gave me? Besides I’d rather be told the peak ground acceleration than the peak ground velocity. The fault was close to Duzce.”

Dervishian ignored Tzetzes to return to his theme, “One of the most sensible approaches to definition of intensity is the Medvedev system that was used in the former USSR. It is based on considerable experience interpreted wisely. It suggests that even in the worst instance, at the intersection of very strong ground motion and poor construction, one should not expect total devastation. That is the voice of experience not logic. That is why I inferred that only half the building inventory would succumb. Otherwise I would have claimed that most buildings would suffer serious damage.”

“I find your positions contradictory. First you explained that we needed consistent and clever analysis. Now you are telling us that the phenomenological should do,” Shiba observed.

Dinlemez realized that the conversation would move into another cul-de-sac, “Allow me to bring you back to the main issue. The main issue is the anticipated damage in Istanbul. Before we get to that, I want to test your reasoning for predicting post facto the damage that was observed in Duzce.”

“Let me suggest a way,” started Shiba. “I look at the distribution that Kerim gave us and develop a ‘hybrid engine.’” The horizontal axis of the bar chart summarizing the PI indices may be considered to represent increasing demand. If we lost one eighth of the inventory in the first event, putting Medvedev and the PI index together, I say the demand in that event reached and maybe exceeded PI=0.25%. You tell me that the second event was 20 % “stronger.” From our experience in Japan I know that damage increases at an increasing rate with instrumental measurement, be it acceleration or velocity. So I would have guessed that the demand could have “saturated” an “intensity of PI = 0.5 %”. From the bar chart, I infer that 90 % of the construction was within that level of PI. Returning to Medvedev, I find the observation of heavy damage to one third of the inventory plausible.”

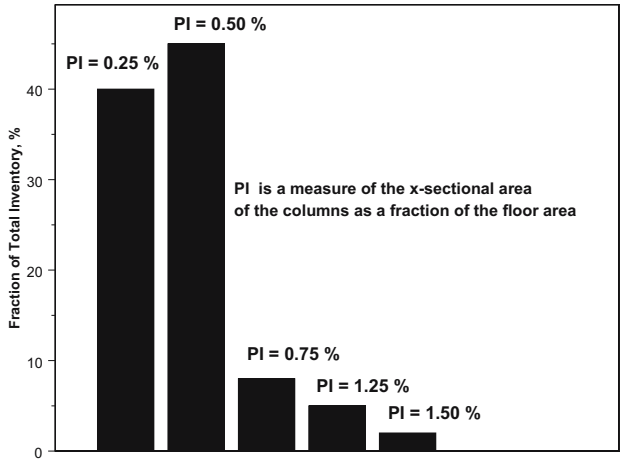

Figure 10.

Dinlemez did not question the logic of the inference. He was interested in results. “If I claim that the PI distribution of the vulnerable buildings in Istanbul, well in parts of Istanbul accessible to our lower-bound motion indexed by G/3, is the same as if not worse than it is in Duzce, what could you tell me about the expected damage?”

Shiba answered after a brief pause, “I cannot tell you how large a portion of the City will suffer the G/3 of which we speak, but I fear that will be compensated by higher demand in parts close to the Marmara. So within the conditions you specified and recognizing that we are assuming a lower demand in the City vs that in Duzce, my optimistic best estimate, in one significant figure, is that the City would lose 10% of its building inventory. That, of course, is based on the assumption that the PI index for almost half the buildings is approximately 0.25 %.”

“And lives?”

“As much as 1 % of the population.”

Dinlemez addressed the other two, “Do you agree?” They nodded their assent.

“Do you realize that your percentages indicate one million people homeless and a hundred thousand lives lost? To boot, the surviving nine million would be in a city without transportation and communication.”

The answer was again in the affirmative.

“And you do not plan to stay here with me and see what we can do, however little, to avert this tragedy in the City where you were born?”

Dervishian, Shiba, and Tzetzes were silent.

Dinlemez concluded, “Then you either do not know how to count or your adopted cultures have dehumanized you.”

RECENT ADVANCES IN THE SEISMIC REHABILITATION OF REINFORCED CONCRETE BUIIDINGS IN JAPAN

SHUNSUKE SUGANO
Hiroshima University, Graduate School of Engineering,
1-4-1 Kagamiyama, Higashi-hiroshima 739-8527, JAPAN
sugano@hiroshima-u.ac.jp

Abstract. The state-of-the-art in seismic rehabilitation of existing reinforced concrete buildings in Japan is described in this paper. Emphasis is placed on advances in research, design and practice after the 1995 Hyogoken-Nambu (Kobe) Earthquake which severely damaged a large number of buildings. Major topics include; 1) Recent research and development of seismic rehabilitation techniques. 2) Performance-based approaches for the design of seismic rehabilitation. 3) Case studies in practice of seismic rehabilitation which utilized new concepts, innovative methods and/or advanced materials.

Keywords: seismic rehabilitation; reinforced concrete; building; jacketing; strength; ductility; advanced material; response control; seismic isolation; seismic control; 1995 Hyogoken-nambu Earthquake; continuous fiber; steel plate

1. Introduction

The Hyogoken-Nambu (Kobe) Earthquake on January 17, 1995 severely damaged a large number of buildings (Architectural Institute of Japan, 1997). The lessons on reinforced concrete buildings learned from this earthquake were;

- Most of the severely damaged buildings were designed and constructed before 1981 when the design code (the building standard law) was revised to the present form (Figure 1).
- New buildings after 1981 generally behaved in a good manner.
- It was supposed that the damage would be significantly mitigated if seismic evaluation and rehabilitation were advanced.

S.T. Wasti and G. Ozcebe (eds.), Advances in Earthquake Engineering for Urban Risk Reduction, 19–31.

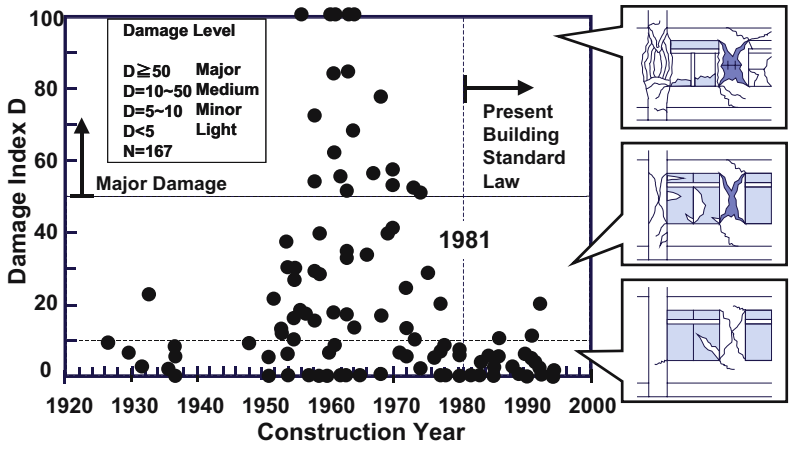

Figure 1. Damage to reinforced concrete school buildings in Kobe City (Architectural Institute of Japan, 1997).

The Kobe Earthquake significantly changed the feature of seismic rehabilitation of existing reinforced concrete buildings. The number of implementations of seismic rehabilitation has been clearly increasing after this earthquake. It is supposed that the change of consciousness and awareness of building owners and users on seismic performance of their buildings pushed up the number of implementations.

Although existing standards and guidelines for seismic rehabilitation do not clearly regulate performance-based approaches, practically the rehabilitation design has been becoming performance-based. Higher level of seismic performance such as “operational” or “immediate occupancy”, which requires maintaining the building function immediately after an earthquake, than the conventional level of performance, such as “life safety” or “collapse prevention”, has often been required. It has been strongly required to minimize influences of rehabilitation on the function, architectural design and/or occupants of the building. Therefore, the construction for rehabilitation must be achieved in a short period without strong influence on serviceability, move of occupants and significant change of architectural design of the building. Recent research and design have been undertaken to overcome these requirements for the seismic rehabilitation. It is also noted that a large variety of rehabilitation techniques have been adopted to overcome the demands described above.

This paper describes the state-of-the-art in seismic rehabilitation of existing reinforced concrete buildings in Japan. Emphasis is placed on advances in research, design and practice of seismic rehabilitation after the Kobe Earthquake. Major topics include;

- Recent research and development of rehabilitation techniques.

- Performance-based approaches for the design of seismic rehabilitation.
- Case studies of seismic rehabilitation, which utilized innovative methods and/or advanced materials.

2. Seismic Rehabilitation Strategy and Techniques

2.1 SEISMIC REHABILITATION STRATEGY

The aim of seismic rehabilitation is to upgrade original seismic performance or to reduce seismic response of an existing building so as to mitigate its earthquake vulnerability. A general approach to upgrade original performance is to strengthen existing structures. Irregularity or discontinuity of stiffness or strength distribution, which may result in a failure or a large distortion of the building, must be eliminated by changing structural configuration. It is effective to add energy dissipating devices so that the seismic response may be reduced (seismic control). Another way to reduce seismic response is to isolate existing building from the ground excitation by extending its fundamental period (seismic isolation). The concept of seismic strengthening, seismic isolation and seismic control is shown in Figures 2 and 3.

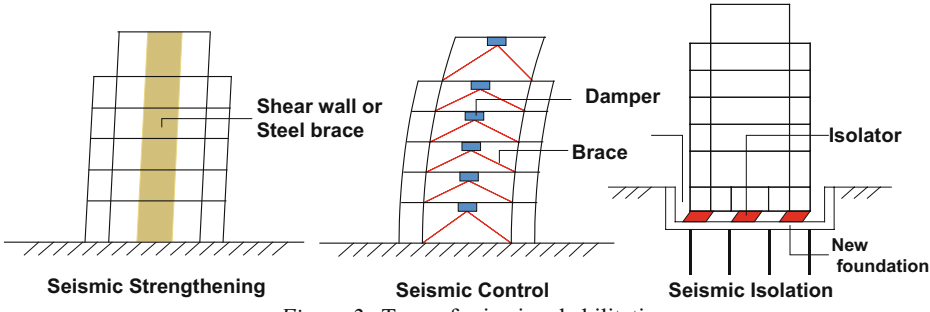

Figure 2. Type of seismic rehabilitation.

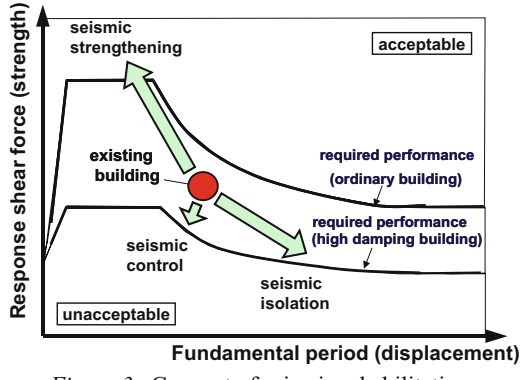

Figure 3. Concept of seismic rehabilitation.

2.2. DEMANDS FOR SEISMIC REHABILITATION

Since the seismic rehabilitation has been applied to many buildings in large variety after the Kobe Earthquake, demands for the seismic rehabilitation have been changing. Recent demands are;

- to avoid loss of building function and evacuation of occupants,
- to avoid change of building design and facade and
- to shorten construction period.

The items to be considered when selecting rehabilitation techniques are;

- influence on building function (lighting, traffic line, usability),
- hindrance associated with construction (noise, vibration, dust, smell),
- effect on foundation system and
- construction cost and period.

Many existing construction techniques have been improved and new techniques and approaches have been developed to meet these demands as well as to provide structural safety.

2.3 RECENT SEISMIC STRENGTHENING TECHNIQUES

2.3.1. Continuous fiber jacketing

The continuous fiber jacketing (Figure 4) to use carbon, aramid or glass fiber sheet is a relatively new technique. This method is characterized by its excellent constructional workability in addition to the characteristics as material which exhibit high levels of anti-corrosion, high strength and lightweight.

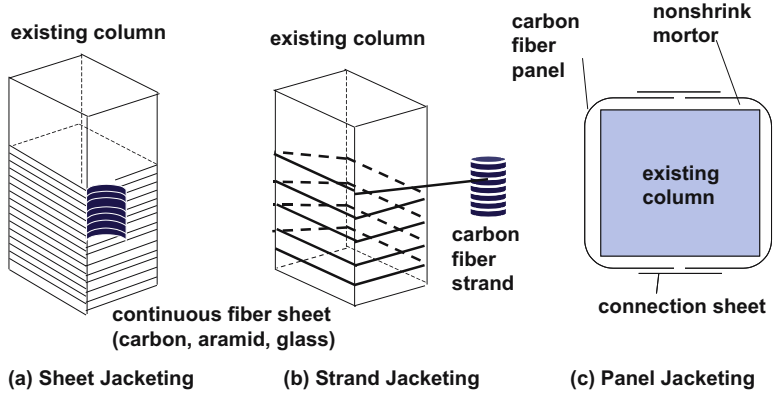

Figure 4. Jacketing columns with new materials.

With these features, it is considered one of the most effective rehabilitation methods today. Until the Kobe Earthquake, this method had been studied by

few institutes and employed by few construction projects. After the Kobe Earthquake, however, various institutes have initiated the research on this method and the guidelines for design and construction have been established. The number of projects adopting this technique has also significantly increased.

Continuous fiber jacketing is applied mainly to brittle columns so that their ductility may be improved. Continuous fibers are used in a form of sheet, strand or panel (Figure 4). They are used generally in a form of continuous fiber sheet to save workmanship in the site. Carbon fiber strands are also used. Carbon fiber panels which are formed in a channel-shape in factory are used to simplify the work in the site and to shorten construction period.

2.3.2. Strengthening by exterior structures

Exterior walls (buttresses), exterior frames or braces and mega-frames in Figure 5 have recently been investigated in many research institutes to apply to buildings where construction can not be achieved inside the building. Because of the previously described strict demands, the case to utilize exterior structures, particularly, exterior braces has been increasing.

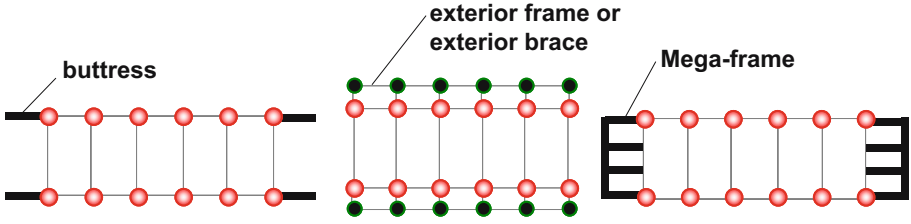

Figure5. Frame strengthening by exterior structures.

3. Advances in Research

3.1 RECENT RESEARCH ON SEISMIC REHABILITATION

One of the advances in research on seismic rehabilitation is that a large number and variety of researches have been undertaken since the Kobe Earthquake by many public and private institutes in order to develop new and innovative techniques or to improve existing techniques. The research and development are aiming at overcoming the previously described strict demands and hard conditions for rehabilitation. Many private organizations, mostly research and development institutes of general contractors, have been developing own rehabilitation techniques to take care of the buildings which they designed and/or constructed.

Recent research subjects are column jacketing with new materials, frame strengthening by means of exterior structures and damper added systems, so on. Accumulated research data has been reviewed in 2000 by the Japan Concrete

Institute (JCI) with respect to the methods to evaluate the behavior of rehabilitated members and buildings (Japan Concrete Institute, 2000). Many of developed techniques have been subjected to reviews of public organizations such as the Building Center of Japan (BCJ) and the Japan Building Disaster Prevention Association (JBDPA) for certificate.

3.2. REVIEW OF RESEARCH RESULTS

Existing test data of column jacketing utilizing new materials such as carbon fiber sheets was reviewed by the JCI in 2000 with respect to restoring force characteristics shown in Figure 6 (Japan Concrete Institute, 2000). The relationship between observed ductility of jacketed columns and the margin of shear strength is shown in Figures 7 and 8. In the case of concrete jacketing, ductility factor was significantly affected by the margin of shear strength (the ratio of shear strength to flexural strength). The correlation factor was 0.97. In the case of steel plate jacketing, the ultimate displacement increased with the increase of the margin of shear strength, however, correlation was not good in comparison with concrete jacketing.

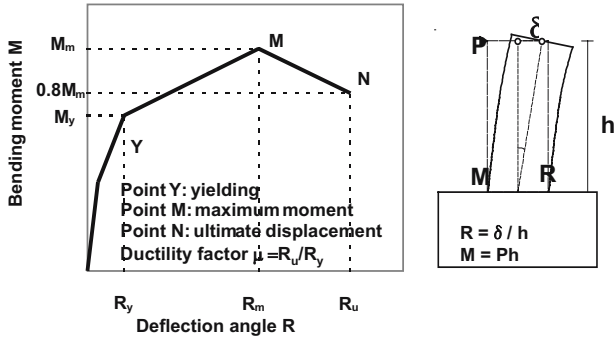

Figure 6. Restoring force characteristics of a jacketed column.

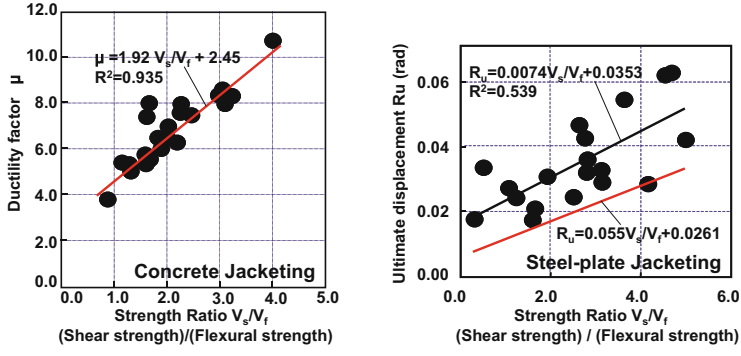

Figure 7. Ductility of columns jacketed with concrete (Japan Concrete Institute, 2000).

As shown in Figure 8, the ultimate displacement of columns jacketed with carbon fiber or aramid fiber sheet was controlled by the ratio of shear strength to flexural strength, though the scatter was large. The relationship between ultimate displacement and the strength ratio and its boundary are expressed with a dashed line and a thin solid line, respectively, in the figure for the columns with shear-span ratio less than 2.5.

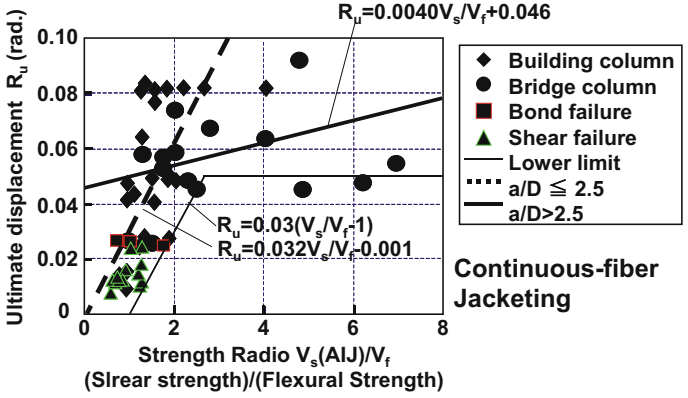

Figure 8. Ductility of columns jacketed with continuous-fiber sheets (Japan Concrete Institute, 2000).

3.3. RESEARCH AND DEVELOPMENT OF NEW TECHNIQUES

In 2000 and 2004 the JCI carried out questionnaire surveys of new techniques for seismic rehabilitation, which were developed by general contractors (Japan Concrete Institute, 2000 and 2004). The total number of general contractors which responded to the surveys was 57.

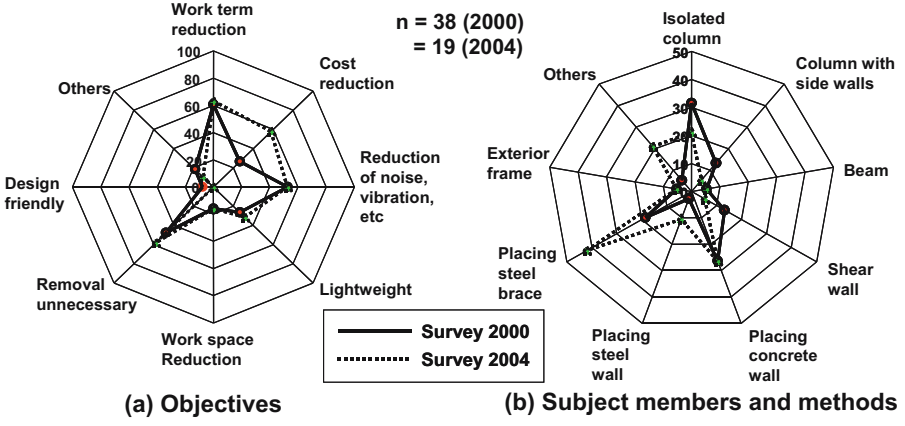

Figure 9. Development of new seismic rehabilitation techniques (Japan Concrete Institute, 2000 and 2004).

The surveys indicated that the keywords of the aims of developing new techniques were 1) short construction period, 2) low cost, 3) reduction of disturbances (noise, dust, etc.) resulting from construction and 4) unnecessity of move of occupants.

Also the surveys indicated that the developed major techniques were 1) placement of steel braces including brace-dampers and exterior-braces, 2) placement of infill-walls with various materials and connections, and 3) column jacketing with various materials. These techniques were developed applying innovative methods or new materials.

4. Advances in Design

4.1. TREND OF THE DESIGN

It is a recent stream to adopt the performance-based design approaches also for existing buildings where the target performance and the level of design earthquakes are clearly specified. In case of the seismic strengthening, the seismic performance is evaluated in terms of the seismic structural index (I_s) shown in Figure 10 (Japan Building Disaster Prevention Association, 1990). Generally the judgment index I_{so} for the seismic evaluation is used as the target performance for seismic rehabilitation. In the case of Kobe Earthquake, the value I_{so}=0.6 is the boundary between major damage or less (Figure 10). Target performance is determined based on importance and function of the building.

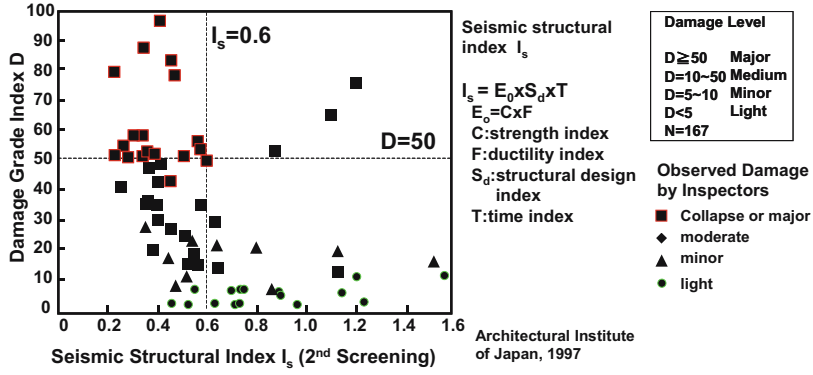

Figure 10. Seismic structural index vs damage level (Architectural Institute of Japan, 1997).

In the case of design for response control rehabilitation utilizing seismic isolation or seismic control, it is required in general to clearly specify design earthquake motions and their level, and the story drift which the building must sustain as shown in Table 1.

Existing experimental data is essential to evaluate the performance of designed members and buildings. When evaluating the performance of building,

Table 1. Design criteria for response control buildings.

		Level of ground motion	
		Max. probable EQ	Safety margin check
Max.velocity of ground motion		Recorded and/or artificial 50 cm/sec or more	Recorded and/or artificial 65 cm/sec or more
Seismic isolation	Superstructure	Interstory drift <1/400 No yielding	Interstory drift <1/200 Sufficient margin to failure
	Isolator	Lateral displacement < 200%	Lateral displacement < 300% or more
Seismic control	Superstructure	Interstory drift <1/200 Sufficient margin of safety to member failure	Interstory drift <1/100 Marginof safety to member failure
	Damping system	Sufficient margin of safety to energy dissipation capacity	Margin of safety to energy dissipation capacity

the index of probable maximum loss (PML), which is defined as the ratio of the maximum loss due to a strong earthquake to the cost for rebuilding, is recently adopted as one of the indices to evaluate the performance of a building. The strong earthquake here is defined generally as the earthquake with 10% probability of exceedance in a 50-year period.

On the other hand, there are many cases where it is impossible to achieve the seismic rehabilitation because the original design and/or function of the building may be completely changed if the rehabilitation is performed.

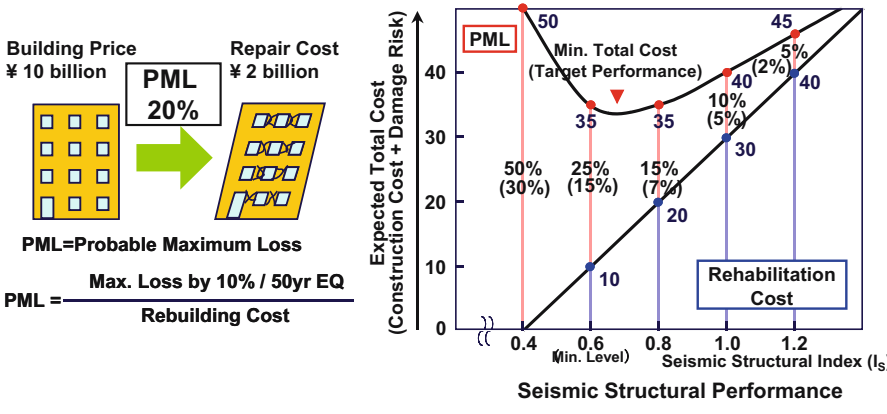

Figure 11. Performance evaluation in terms of PML.

4.2. A CASE STUDY OF THE PERFORMANCE-BASED DESIGN

A Buddhist temple shown in Figure 12 was seismically rehabilitated installing isolation systems at its base (Fujimura, M., et al, 2004). The target performance of the building was “no damage” during the presumed earthquake motions in the site in order to secure its function as a religious facility. It was also aimed

that principle objects of worship would not overturn nor move. The recorded and artificial earthquake motions with the maximum velocity of 50 cm/s were set for design (Table 2). It was expected that acceleration responses would be reduced to 1/3 against input accelerations.

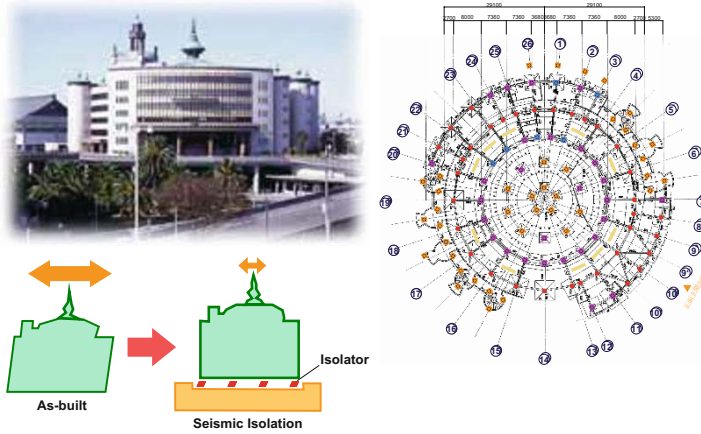

Figure 12. A case study of performance-based design (Fujimura, M., et al., 2004)

Table 2. Target Performance for Max. Probable Earthquakes*

		Target Performance	*Design Criteria*
Upper Structure	Structure	Within the state of allowable stress	Story drift index < 2/1000
	Principal objects Contents	No overturning, no moving	Resp. acceleration < 0.20g
Isolation Story	Isolation devices	Within warranty displacement	Shear deformation < 300%
	Periphery clearance	No pounding	Resp. displacement < 50cm
	Piping system	No damage	Resp. displacement < 50cm

*1) Recorded EQ motions (El Centro 1940 NS, Taft 1952 EW, Hachinohe 1968 NS). Max. Velocity 50cm/s
2) Artificial EQ motions based on the BSL spectrum on the engineering bedrock (max. velocity 35-52 cm/s, acceleration 0.24-0.30g)

5. Advances in Practice

There have been a large number and variety of case studies of seismic rehabilitation of reinforced concrete buildings since the Kobe Earthquake, though the number of implemented buildings is still far from the number of whole existing non-conformed buildings over the country. The questionnaire survey of the Japan Structural Consultants Association (JSCA) in 2003 indicated that the number of implemented private buildings has been clearly increasing since the Kobe Earthquake as

indicated in Figure 13. It is supposed that the change of consciousness and awareness of owners of private buildings after the Kobe earthquake might have pushed up the number of implementations above.

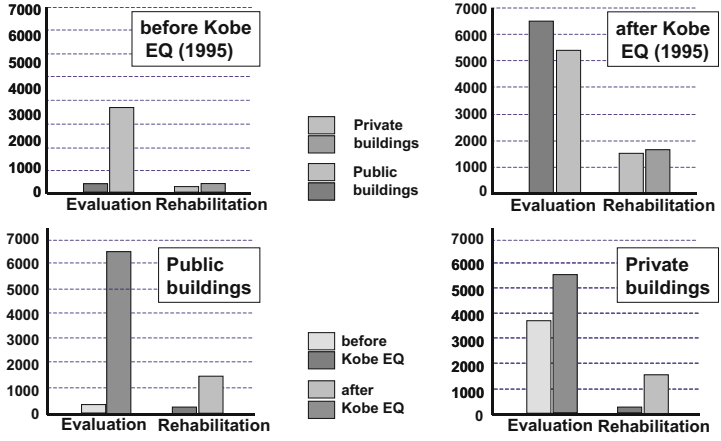

Figure 13. Implementation of seismic evaluation and rehabilitation.(Survey of JSCA, 2003)

It is notable that new rehabilitation techniques such as continuous-fiber jacketing, seismic isolation and seismic control have been adopted in addition to conventional strengthening or reinforcing techniques. The seismic isolation has been applied to the buildings which need higher seismic performance than ordinary buildings, which have valuables inside or which don't accept any change of original design or facade such as historical or monumental buildings. The seismic control is applied to tall and flexible buildings as the method to control the response displacement or as the method which can reduce the number of portions to be rehabilitated in a building.

Photo 1. A strengthening element to match original design (Fujimura, M., et al, 2001)

Photo 1 shows the case of seismic strengthening by “design panels”. In order not to change the facade of the building, the building was strengthened by grid panels of steel which are similar in shape to that of original design. The seismic behavior of the elements was investigated by cyclic loading tests in laboratory.

6. Concluding Remarks

The state of seismic rehabilitation of reinforced concrete buildings in Japan is summarized as follows from the aspect of advances after the Kobe Earthquake.

- A large number and variety of researches have been conducted in many public and private institutes in response to social demands for the seismic rehabilitation, particularly, the demand of “in-service rehabilitation”.
- Performance-based design approaches have often been adopted since the Kobe Earthquake because higher performances than “life safety” have been required in many cases. While the rehabilitation has been impossible in some cases because it would completely change the feature of the building.
- The number of rehabilitated both public and private buildings has been significantly increasing since the Kobe Earthquake and a large variety of rehabilitation techniques have been appropriately applied to these buildings.

References

Japan Building Disaster Prevention Association, 1990, Standards for Evaluation of Seismic Capacity and Guidelines for Seismic Rehabilitation of Existing Reinforced Concrete Buildings (in Japanese)

Japan Building Disaster Prevention Association, 1991, Standard for Inspection of Damage Degree and Guidelines for Restoration Techniques (in Japanese)

Sugano, S., 1996, State-of-the-Art in Techniques for Rehabilitation of Buildings, Proceedings of 11WCEE, Acapulco, Mexico, Paper No. 2175

Architectural Institute of Japan, 1997, Report on the Hanshin-Awaji Earthquake Disaster, Structural Damage to Reinforced Concrete Buildings, Building Series Vol. 1, (in Japanese)

Japan Concrete Institute, 1998, Post-earthquake Restoration and Seismic Rehabilitation of Concrete Structures, 772pp (in Japanese)

Sugano, S., 2000, Seismic Rehabilitation of Concrete Buildings in Japan, Proceeding of 12WCEE, Auckland, New Zealand, Paper No.2324

Fukuyama, H. and Sugano, S., 2000, Japanese Seismic Rehabilitation of Concrete Buildings after the Hyogoken-Nambu Earthquake, Cement and Concrete Composite, Vol. 22, No.1

Fujimura, M., et al., Seismic Isolation Retrofit of Great Sacred Hall, Rissho Kosei-kai, Menshin, Japan Society of Seismic Isolation, No 46, 2004.11 (in Japanese)

Fujimura, M., et al., Seismic Retrofit Utilizing Design Panels, Nikkei Architecture, 2001.6.11 (in Japanese)

Japan Concrete Institute, 2000, A Technical Evaluation of Seismic Rehabilitation of Concrete Structures, 592pp (in Japanese)

Japan Concrete Institute and National Science Foundation, 2000, Proceedings of US-Japan Symposium on Seismic Rehabilitation of Concrete Structures -State of Research and Practice-

Japan Concrete Institute, 2004, Evaluation of Seismic Performance of Concrete Structures Damaged by Recent Earthquakes, 458pp (in Japanese)

CONCRETE OR FRP JACKETING OF CONCRETE COLUMNS FOR SEISMIC RETROFITTING

STATHIS N. BOUSIAS
Structures Laboratory, Department of Civil Engineering, University of Patras, P.O. Box 1424, Patras, Greece

MICHAEL N. FARDIS
Structures Laboratory, Department of Civil Engineering, University of Patras, P.O. Box 1424, Patras, Greece

ALEX-LOUKAS SPATHIS
Structures Laboratory, Department of Civil Engineering, University of Patras, P.O. Box 1424, Patras, Greece

DIONYSIS BISKINIS
Structures Laboratory, Department of Civil Engineering, University of Patras, P.O. Box 1424, Patras, Greece

Abstract. Experimental and analytical work is reported for jacketed concrete columns, including short lap splices at the base. 45 rectangular columns with smooth or ribbed vertical bars are subjected to cyclic flexure with constant axial load. Test parameters are the presence and length of lap splices and the type of retrofitting: concrete jackets over the whole column, or CFRP wrapping of the plastic hinge region at varying number of layers and height of application from the base. A 0.7:1 scale two-storey space frame was also pseudodynamically tested before and after retrofitting. Test results are supplemented with past data, to develop expressions for the yield moment, deflection at yielding and ultimate deflection in cyclic loading, for columns with concrete or FRP jackets, as a function of jacket parameters and the length of lap splice.

Keywords: concrete columns; concrete jackets; deformation capacity; FRP wrapping; lap splices; seismic retrofitting; seismic rehabilitation

S.T. Wasti and G. Ozcebe (eds.), Advances in Earthquake Engineering for Urban Risk Reduction, 33–46.

1. Introduction

Columns are normally the weak links in existing concrete buildings in seismic regions, especially if vertical bars are insufficiently lap-spliced at floor level. To extend the life of these buildings, such column deficiencies should normally be corrected. This paper describes test results on columns with or without lap splices, retrofitted via either wrapping of the plastic hinge region with CFRP sheets, or concrete jacketing of the entire column. Test results supplement those of other experimental campaigns in the literature, in order to develop simple rules and analytical tools for calculation of the effect of concrete or FRP jackets on: (a) yield strength, (b) yield deflection and the associated secant-to-yielding stiffness; and (c) ultimate deflection in cyclic loading, in columns with or without lap splicing at the base.

2. Experimental Campaign

A total of 45 columns were cyclically tested to failure under constant axial load. They include ten unretrofitted columns as control specimens (Table 1), 21 columns retrofitted with CFRP wraps (Table 1) and 14 columns retrofitted with concrete jackets (Table 2). All columns were tested as simple cantilevers fixed in a heavily reinforced rigid footing. Uniaxial cyclic deflections (one cycle with amplitudes increasing by 5mm, up to or beyond column failure) were imposed 1.6m above the top of the footing. The original columns have either 250-by-250mm section with four 14mm smooth (plain) vertical bars with 313MPa yield strength and hooked ends (Q- specimens), or 250-by-500mm section with four 18mm ribbed (deformed) vertical bars with 514MPa yield strength and straight ends. The original columns have a closed perimeter tie at 200mm centres, of smooth 8mm bars with 425MPa yield stress. In 13 columns of each type the vertical bars of the original column are lap-spliced near the base. In Q-type columns the ends of the smooth vertical bars are provided with standard 180^{o}-hooks and are lapped starting at the top of the footing over 15- or 25-bar diameters (specimens L1 or L2, respectively). In R-type specimens the straight ends of the ribbed longitudinal bars are lapped starting at the footing over 15-, 30- or 45-bar diameters (columns L1, L3 or L4, respectively).

The resin-impregnated carbon-fibre-reinforced-polymer (CFRP) wrapping in the retrofitted columns of Table 1 use uniaxial CFRP sheets with Elastic Modulus E_f=230GPa, tensile strength f_{uf}=3450MPa and nominal thickness t_f= 0.13mm. The main objective of the tests in Table 1 is to investigate the effect of lap-splicing in the plastic hinge region of the base, with one parameter of the tests being the lap length and another being the number of CFRP layers and the height of its application from the base. In the columns retrofitted with concrete

jackets, the jacket is 75mm thick on each side and has 20mm ribbed corner bars with yield strength f_{yL}=487MPa in Q-type specimens, or six 18mm bars in R-type ones with yield strength f_{yL}=514MPa, all embedded within the base at the time of casting the original column. The jacket has 10mm closed perimeter ties with yield stress f_{yw}= 599MPa, at 100mm centres. One aim of these tests is to study the effect of measures at the interface for the connection of the new and old concrete, through the first seven tests in Table 2. The other objective is to investigate the effect of lap splicing of vertical bars in the original column, on the basis of the rest of the tests in Table 2.

TABLE 1. Columns retrofitted with FRP jackets: parameters, key results and model predictions

Specimen	lapping (d_{bL}: bar diam.)	FRP jacket: no. of layers –height of application	f_c (MPa)	v= $N/A_c f_c$	M_y (kNm): yield moment with P-Δ		θ_y (%): yield chord rotation		θ_u (%): ultimate chord rotation	
					test	calc.	test	calc.	test	calc.
Q-0	-	unretrofitted	27.0	0.44	66	73.7	0.8	1.15	2.2	2.25
Q-0L1	$15d_{bL}$	controls	30.3	0.41	72.7	80.7	1.05	1.14	2.5	1.95
Q-0L2	$25d_{bL}$		30.3	0.42	72.5	82.1	0.95	1.15	1.6	1.95
Q-0L1a	$15d_{bL}$		28.1	0.63	70.0	86.7	0.8	0.91	1.0	1.45
Q-0L2a	$25d_{bL}$		28.1	0.57	83.0	85.8	0.9	0.98	1.35	1.6
Q-P2H1	-	two – 0.3m	28.2	0.40	77.4	72.3	1.0	1.15	5.0	5.65
Q-P2H2	-	two – 0.6m	28.1	0.45	74.5	78.0	0.95	1.15	4.7	5.4
Q-P4H1	-	four – 0.3m	28.1	0.45	78.3	78.2	1.25	1.2	>6.6	6.45
Q-P4H1a	-	four – 0.3m	28.2	0.48	66.1	80	0.75	1.13	1.9	3.7
Q-P4H2	-	four – 0.6m	28.2	0.44	77.0	77.0	1.15	1.2	6.9	6.55
Q-P2L1H2	$15d_{bL}$	two – 0.6m	30.0	0.40	75.0	76.9	1.2	1.15	6.0	5.55
Q-P4L1H2	$15d_{bL}$	four – 0.6m	30.0	0.40	76.8	78.7	1.1	1.15	6.8	6.55
Q-P4L1H1	$15d_{bL}$	four – 0.3m	27.5	0.44	82.8	77.0	1.1	1.2	6.2	6.4
Q-P2L2H2	$25d_{bL}$	two – 0.6m	30.0	0.43	79.2	82.1	1.2	1.15	6.0	5.4
Q-P4L2H2	$25d_{bL}$	four – 0.6m	30.0	0.42	83.7	78.9	1.4	1.15	6.9	6.5
R-0	-	unretrofitted	31.0	0.26	298.2	285	0.75	1.05	2.5	3.95
R-0a	-	controls	18.3	0.38	290.6	217.5	0.9	0.75	2.5	3.0
R-0L1	$15d_{bL}$		27.4	0.23	225.4	196.3	0.5	0.45	1.9	1.2
R-0L3	$30d_{bL}$		27.4	0.28	279.4	288.0	0.75	1.01	1.9	2.1
R-0L4	$45d_{bL}$		27.4	0.28	283.1	298.5	1.1	1.05	2.5	2.65
R-P2	-	two – 0.6m	32.9	0.23	323.2	276.6	1.0	1.0	4.4	5.4
R-P2a	-	two – 0.6m	18.1	0.37	322.8	278.5	1.0	0.8	5.6	4.75
R-P2L1	$15d_{bL}$	two – 0.6m	26.9	0.30	258.1	288.0	0.65	0.85	3.4	3.1
R-P2L3	$30d_{bL}$	two – 0.6m	26.9	0.28	303.2	293.6	1.0	0.95	4.7	5.3
R-P2L4	$45d_{bL}$	two – 0.6m	26.2	0.28	303.6	293.6	1.15	0.95	5.6	5.3

Specimen	lapping (d_{bL}: bar diam.)	FRP jacket: no. of layers –height of application	f_c (MPa)	$v=N/A_cf_c$	M_y (kNm): yield moment with P-Δ		θ_y (%): yield chord rotation		θ_u (%): ultimate chord rotation	
					test	calc.	test	calc.	test	calc.
R-P2L4a	$45d_{bL}$	two – 0.6m	26.9	0.27	314.0	285.2	0.95	0.97	>2.5	5.65
R-P5	-	five – 0.6m	32.9	0.23	323.2	275.0	1.0	1.0	5.3	6.9
R-P5a	-	five – 0.6m	17.9	0.39	323.3	277.3	1.1	0.8	>6.9	5.7
R-P5L1	$15d_{bL}$	five – 0.6m	27.0	0.28	284.0	281.8	0.95	0.8	5.0	4.65
R-P5L3	$30d_{bL}$	five – 0.6m	27.0	0.29	323.1	300.0	0.95	0.95	>5.6	5.25
R-P5L4	$45d_{bL}$	five – 0.6m	27.0	0.29	322.6	300.0	0.8	0.95	>5.6	5.25

TABLE 2. Columns retrofitted with concrete jackets: parameters, key results, model predictions

Specimen	Connection measures of jacket to the old column	Lap splice	f_c (MPa)		$v=N/A_cf_c$ jcktd. col.[2]	M_y (kNm): yield moment with P-Δ		θ_y (%): yield chord rotation		θ_u (%):ultimate chord rotation	
			old col.	Jacket col.		test	calc.	test	calc.	test	calc.
Q-RCM	monolithic control[1]	-	30.6	-	0.18	251.0	218.5	1.0	1.0	5.3	4.8
Q-RCW	welded U-bars	-	22.9	18.8	0.20	212.3	198	1.15	1.05	5.65	3.9
Q-RCD	dowels	-	27.4	55.8	0.084	225.0	227.8	1.15	0.9	6.25	5.4
Q-RCR	roughening	-	27.7	55.8	0.09	258.2	229	1.2	0.9	5.65	5.35
Q-RCRD	roughening +dowels	-	26.3	55.8	0.09	242.7	229.6	1.0	0.9	5.3	5.35
Q-RC	No treatment	-	26.3	55.8	0.079	233.1	226.5	1.3	0.9	5.3	5.4
Q-RCpd	No treatment pre-damage	-	23.1	24.1	0.168	242.7	205.3	1.25	1.05	5.3	4.2
Q-RCL1	No treatment	$15d_{bL}$	27.5	55.8	0.084	212.9	225.9	1.15	0.9	5.6	5.5
Q-RCL2		$25d_{bL}$	25.6	55.8	0.084	217.5	225.9	1.0	0.9	5.3	5.5
Q-RCL1pd	No	$15d_{bL}$	28.1	20.7	0.25	203.8	230.2	1.0	1.05	4.4	3.75
Q-RCL2pd	treatment, pre-damage	$25d_{bL}$	28.1	20.7	0.27	244.6	232.0	1.1	1.05	5.3	3.65
R-RCL1		$15d_{bL}$	36.7	55.8	0.066	533.2	496.3	1.0	0.75	4.2	3.8
R-RCL3	No treatment	$30d_{bL}$	36.8	55.8	0.066	562.7	466.2	1.0	0.75	3.8	3.85
R-RCL4		$45d_{bL}$	36.3	55.8	0.052	522.5	453.5	1.0	0.75	4.7	3.85

[1]: Monolithic 400-by-400mm control specimen with reinforcement that of the jacket of the jacketed columns

[2]: Calculation of $v=N/A_cf_c$ is based on the f_c value of the jacket.

In all tests behaviour was controlled by flexure. Tables 1 and 2 show key test results (the moment and chord rotation at yielding and the ultimate chord rotation, conventionally defined as the one where resistance drops below 80% of the previous peak resistance during the test), along with the values calculated on the basis of sections 4 (for Table 1) and 3 (for Table 2).

The test results of the unretrofitted Q-type columns in Table 1 show that old-type columns with smooth (plain) bars have low cyclic deformation capacity and energy dissipation, which is however not impaired further by lap splicing of the bars at the base: a lap length as short as 15-bar diameters supplements sufficiently the 180^o hooks for the transfer of forces. The test results of the unretrofitted R-type columns in Table 1 show that old-type columns with ribbed (deformed) bars lap-spliced at the base have reduced cyclic deformation capacity and energy dissipation. If lapping of ribbed bars is at least 45-bar diameters, cyclic deformation capacity is not significantly reduced in comparison to the column with continuous bars and energy dissipation is acceptable. Lapping of straight ends of ribbed bars by as little as 15-bar diameters reduces appreciably flexural resistance and gives rapid post-peak strength and stiffness degradation and low energy dissipation capacity.

The results of the tests of Q-type columns in Table 1 show that there is no systematic effect of the number of layers and the length of application of the FRP, or even of the existence and length of lapping, on the force and cyclic deformation capacity and the rate of strength degradation in FRP-retrofitted columns with smooth bars and hooked ends. Nonetheless, a decrease in lapping seems to reduce energy dissipation in the FRP-retrofitted columns.

The test results in Table 1 for R-type columns show that in FRP-retrofitted columns with straight ribbed bars, five CFRP layers are more effective than two layers; nonetheless, the improvement in effectiveness is not commensurate to the number of FRP layers. Test results also suggest that there is a limit to the improvement due to FRP wrapping: if the lapping of straight ribbed bars is as short as 15 bar-diameters, its adverse effects on force capacity and energy dissipation cannot be fully removed by FRP wrapping.

The test results for concrete-jacketed Q-type columns show that RC jacketing of old-type columns with smooth bars increases their deformation capacity to levels sufficient for earthquake resistance, irrespectively of the presence and length of lap splicing. Previous damage of the old column by cyclic loading beyond its peak resistance does not reduce the effectiveness of the jacket. The results of the present tests, combined with those of previous studies (see section 3), also show that concrete-jacketed old-type columns with smooth bars behave very similarly to a monolithic column with the same geometry and reinforcement as the jacket, almost irrespectively of any special measures to improve the connection of the jacket with the old concrete.

The results of the tests of R-type columns in Table 2 show that concrete jackets are effective in removing the adverse effect of lap-splicing of straight ribbed bars on strength and deformation capacity, even for very short lap lengths. Nonetheless, the adverse effect of very short lapping in the original column on hysteretic energy dissipation is retained in the jacketed column.

3. Strength, Stiffness, Deformation Capacity of Members with RC Jackets

The test results in Table 2, considered together with 39 more tests on jacketed columns without lap splicing in the original column from 11 other sources in the literature, lead to the conclusion that the key strength and deformation parameters of jacketed columns may be computed through appropriate modification of a corresponding monolithic member which has concrete strength f_c over the full section equal to that of the jacket and is considered to resist the axial load with its full section, regardless of the fact that the axial load is originally applied to the old column alone.

The column strength and deformation parameters of interest here are:

- the yield moment, $M_{y,}$,
- the secant-to-yield stiffness determined for the shear span L_s (moment-to-shear ratio) at each end of a concrete member as: $EI_{eff} = M_y L_s / 3\theta_y$, where θ_y is the chord rotation at yielding at the end of interest, and
- the cyclic chord rotation capacity, θ_u, or its plastic part, $\theta_u^{pl} = \theta_u - \theta_y$.

For members with rectangular section and ribbed (deformed) longitudinal bars without lapping in the end region, the value of M_y may be computed from first principles, while those of θ_y and θ_u (or θ_u^{pl}) may be obtained from semi-empirical or purely empirical relations developed by (Biskinis and Fardis, 2004) on the basis of the results of almost 1700 tests and adopted in (CEN, 2005).

Based on the average ratios of (a) the experimental value for the 13 tests in Table 2 and of the 39 additional tests the literature, to (b) the value predicted considering the column as monolithic as above, the following relations were developed in the present study (and adopted in CEN, 2005) for the values of M_y*, θ_y*, θ_u* of the jacketed member, in terms of the values M_y, θ_y, θ_u resulting from the assumptions above, regardless of any lap splicing of vertical bars in the original column:

- For M_y*: M_y *= M_y.
- For θ_y*
  - If the old concrete is connected to the jacket by roughening the interface, with or without any other connection measure: θ_y *= $1.05\theta_y$.

- for any other measure to connect the jacket to the old concrete, or for no such measures: θ_y *= 1.20θ_y.

- For θ_u*: θ_u*= θ_u

4. Strength, Stiffness and Deformation Capacity of Concrete Members with Lap Splices in the Plastic Hinge and/or with FRP-wrapped Ends

4.1 MEMBERS WITH LAP SPLICES IN THE PLASTIC HINGE, BUT WITHOUT FRP-WRAPPING

4.1.1. *Members with smooth longitudinal bars and standard 180^o hooks*

The test results of the five Q-type unretrofitted control columns in Table 1 suggest that the rules developed by (Biskinis and Fardis, 2004) and adopted in (CEN, 2005) for the calculation of M_y and θ_y of members with rectangular section and ribbed longitudinal bars without lapping, can be taken to apply to rectangular columns with smooth longitudinal bars as well, even when these bars are lapped starting at the end section over a lapping $l_o \geq 15d_{bL}$. In such columns, the plastic part of the cyclic chord rotation capacity is reduced via:

- multiplication by $0.0035(60+\min(50, l_o/d_{bL}))(1-l_o/L_s)$, and
- subtraction of the lap length l_o from the shear span L_s, as the ultimate condition is controlled by the region right after the end of the lap.

In the just four available cyclic tests of columns with lap-spliced smooth bars (namely tests Q-0L1, Q-0L2, Q-0L1a, Q-0L2a in Table 1) this gives a median of 0.9 for the ratio experimental-to-predicted cyclic chord rotation capacity and a C.o.V. (Coefficient of Variation) of 30.4%.

4.1.2. *Members with lap-spliced ribbed longitudinal bars*

In order to establish rules for the calculation of the yield moment and the associated deformations, tests R-0L1, R-0L3, R-0L4 in Table 1 are considered together with 78 more tests in the literature on members with rectangular section and ribbed longitudinal bars with lapped straight ends starting at the end section. These results show that in the calculation of:

- the yield moment M_y,
- the yield curvature ϕ_y (which is used in the determination of the parts of the chord rotation at yielding, θ_y, which is due to flexure or to fixed-end rotation due to slippage of the bars from their anchorage zone beyond the member end), and of
- the plastic part of the cyclic chord rotation capacity, θ_u^{pl},

the compression reinforcement ratio should be doubled over the value applying outside the lap splice Moreover, if the straight lap length l_o is less than $l_{oy,min}=0.3d_{bL}f_{yL}/\sqrt{f_c}$, ($f_{yL}$ and f_c in MPa), then M_y, ϕ_y, θ_u and θ_u^{pl} should be calculated with the yield stress of the tensile longitudinal reinforcement, f_{yL}, multiplied by $l_o/l_{oy,min}$. In 81 tested columns with lap splices, this rule gives a median of 1.005 for the ratio experimental-to-predicted yield moment and a C.o.V. of 11.9%. Finally, the part of the chord rotation at yielding which is due to sources of deformation other than flexure or fixed-end rotation due to slippage from the anchorage zone, should be multiplied by the ratio of the yield moment M_y as modified to account for the lap splicing, to the yield moment outside the lap splice. These rules give a median of 0.975 and a C.o.V. of 23.3% for the ratio of experimental-to-predicted stiffness at yielding in 61 columns with lap splices (including the present ones R-0L1, R-0L3, R-0L4).

To establish rules for the cyclic chord rotation capacity, tests R-0L1, R-0L3, R-0L4 are considered together with 37 more tests in the literature on members with rectangular section and ribbed longitudinal bars with straight lapped ends. They show that the plastic part of chord rotation capacity, θ_u^{pl}, decreases with l_o in proportion to $l_o/l_{ou,min}$, if $l_o<l_{ou,min}=d_{bL}f_{yL}/[(1.05+14.5\alpha_l\rho_{sx}f_{yw}/f_c)\sqrt{f_c}]$, where:

- f_{yL}, f_{yw}, f_c (all in MPa) and d_{bL} have been defined previously,
- $\rho_{sx}=A_{sx}/b_w s_h$ is the transverse steel ratio parallel to the direction x of loading (s_h= stirrup spacing), and
- $\alpha_l=(1-0.5s_h/b_o)(1-0.5s_h/h_o)n_{restr}/n_{tot}$, with
- s_h: stirrup spacing,
- b_o, h_o: dimensions of the confined core to the hoop centerline,
- n_{tot}: total number of longitudinal bars along the cross-section perimeter and
- n_{restr}: number of bars laterally restrained by a stirrup corner or a cross-tie.

The value of the chord rotation at yielding, θ_y, to be added to θ_u^{pl} to obtain θ_u, should also account for the effect of lapping if l_o is less than $l_{oy,min}=0.3d_{bL}f_{yL}/\sqrt{f_c}$. In the 40 available cyclic tests of members with lap length less than $l_{ou,min}$ (including R-0L1, R-0L3, R-0L4 in Table 1), this rule gives a median of 1.0 for the ratio of experimental-to-predicted to cyclic chord rotation capacity, θ_u^{pl}, and a C.o.V. of 31.3%.

4.2. MEMBERS WITH FRP-WRAPPING

4.2.1. *Members without lap splicing in the plastic hinge*

According to the available tests on rectangular columns with either ribbed or smooth longitudinal bars and no lapping (including tests Q-P2H1, Q-P2H2, Q-

P4H1, Q-P4H1a, Q-P4H2, R-P2, R-P2a, R-P5, R-P5a of Table 1), the values of M_y and θ_y may be considered as unaffected by FRP wrapping of the member end. In that case, the median of the ratio of experimental-to-predicted value of M_y in 112 tests is equal to 1.04 and its C.o.V. is 18.8%, whilst the median of the experimental-to-predicted-ratio of effective stiffness at yielding in 105 tests is equal to 1.02 and its C.o.V. is 29%. The enhancement of the deformation capacity of the member, θ_u, and the improvement of any lap splices due to FRP sheets wrapped around the member end with the fibres oriented along the perimeter, may be obtained as described in the following paragraphs.

The member deformation capacity will profit from confinement by the FRP wrapping of its end, provided that such wrapping extends up to a distance to the end section which is sufficient to ensure that the yield moment M_y in the unwrapped part is not exceeded before the end section reaches its flexural strength, as this increases due to confinement by the FRP. If this condition is met, the increase of the plastic part of the chord rotation capacity, θ_u^{pl}, may be determined by adding a term due to the FRP to the term describing confinement by the transverse reinforcement, $\alpha\ \rho_{sx} f_{yw}/f_c$, where

- $\rho_{sx}=A_{sx}/b_w s_h$, f_{yw} and f_c were defined previously, and
- $\alpha=(1-0.5s_h/b_o)(1-0.5s_h/h_o)[1-\Sigma_i b_i^2/(6\ b_o h_o)]$ is the familiar confinement effectiveness factor, with:
  - s_h, b_o, h_o: as defined in 4.1.2, and
  - b_i: centerline spacing of the n_{restr} laterally restrained longitudinal bars.

The term describing confinement by the FRP is $\alpha_f f_{f,e}\rho_f/f_c$, where:

- $\rho_f=2t_f/b_w$ is the transverse FRP ratio in the loading direction, x,
- $f_{f,e}=\min(f_{u,f};\ \varepsilon_{u,f}E_f)[1-0.7\min(f_{u,f};\ \varepsilon_{u,f}E_f)\rho_f/f_c]$ is an effective FRP strength, where *$f_{u,}$ and E_f are FRP's strength and the modulus, and $\varepsilon_{u,f}$ is the limit strain, equal to 0.015 for carbon- or aramid-FRP and to 0.02 for glass-FRP.*
- $\alpha_f=1-[(b-2R)^2+(h-2R)^2]/(3bh)$, is the FRP confinement effectiveness factor, where; *b and h are full dimensions of the section, and R is rounding radius at the corner.*

This rule gives a median experimental-to-predicted chord rotation capacity in 90 cyclic tests (including R-P2, R-P5, Q-P2H1, Q-P2H2, Q-P4H1, Q-P4H2) equal to 0.995 and a C.o.V. of 31.2%.

4.2.2. *Members with lap splicing in the plastic hinge region*

The rules given in this section apply to members with:

- rectangular section,

- longitudinal bars lap-spliced over a length l_o at least equal to $15d_{bL}$, starting at the end section, and
- FRP-wrapping of the end region over a length at least equal to $2l_o/3$.
- For smooth longitudinal bars with standard 180° hooks, tests Q-P2L1H2, Q-P4L1H2, Q-P4L1H2, Q-P2L2H2 and Q-P4L2H2 in Table 1 suggest that M_y, θ_y and θ_u may be computed taking into account the FRP according to 4.2.1, neglecting the lap splicing.

For ribbed longitudinal bars with straight ends, M_y, ϕ_y, θ_y can be calculated according to the first paragraph of 4.1.2, except that $l_{oy,min}$ is reduced to $l_{oy,min}=0.2d_{bL}f_{yL}/\sqrt{f_c}$. In 20 tests of columns with such lap splice regions wrapped with FRP, this rule gives a median of 1.065 and a C.o.V. of 9.2% for the ratio of experimental-to-predicted-M_y and a median of 1.01 and a C.o.V. of 22% for the ratio of experimental-to-predicted the effective stiffness at yielding. The rules of 4.1.2 apply for the calculation of the plastic part of the cyclic chord rotation capacity, θ_u^{pl}, as well, except that it is not possible to profit for the same purpose from the benefits of confinement by the transverse bars and the FRP. More specifically, θ_u^{pl} may be estimated as:

- the value obtained from the empirical relations by (Biskinis and Fardis, 2004) and in (CEN, 2005) for members with rectangular section and ribbed bars without lapping, for confinement only by the transverse bars ($\alpha\rho_s f_{yw}/f_c>0$, $\alpha_f f_{f,e}\rho_f=0$), times
- $l_o/l_{ou,min}$, with $l_{ou,min}=d_{bL}f_{yL}/[(1.05+14.5\alpha_{l,f}\rho_f f_{f,e}/f_c)\sqrt{f_c}]$ estimated on the basis of the FRP alone and only the corner bars considered as restrained by the FRP: $\alpha_{l,f}=4/n_{tot}$.
- Then the median of the ratio of experimental-to-predicted θ_u in 16 tests with lap-spliced ribbed longitudinal bars and FRP wrapping (including R-P2L1, R-P2L3, R-P2L4 and R-P5L1 in Table 1) is 0.995 and its C.o.V. is 21.7%.

5. Pseudodynamic Test of a 0.7:1 Scale Two-storey Unsymmetric Structure

A 0.7:1 scale two-storey 3D frame structure has been Pseudodynamically tested, with or without retrofitting of its four columns. The frame is 3.15-by-3.85m in plan (4.5-by-5.5m in full-scale), with a 2m-high ground storey (2.85m in full-scale) and a 2.3m 2nd storey (3.3m in full-scale). Its design, detailing and materials are representative of old RC buildings in Greece, without engineered earthquake resistance. It is an unsymmetric structure, susceptible to torsional response under translational ground motions. The columns of its "flexible side" are 0.7:1 scale models of the Q-type columns tested within the experimental

program of this work, while those of the "stiff side" are 0.7:1 scale models of the R-type columns, except that they also employ smooth bars, lap spliced at floor levels with 180° hooks (Figure 1). Additional concrete masses reproducing the effect of loads other than the self weight (finishings and partitions, quasi-permanent live loads, etc. from a tributary plan area about four times larger than that of the test structure) were mounted on the two floors. The average value of concrete strength at the dates of testing was 32.4 MPa at the ground storey and 30.3 MPa at the 2nd storey. The yield strength of the vertical bars of the columns was 585.5 MPa and 523.3 MPa for their ties.

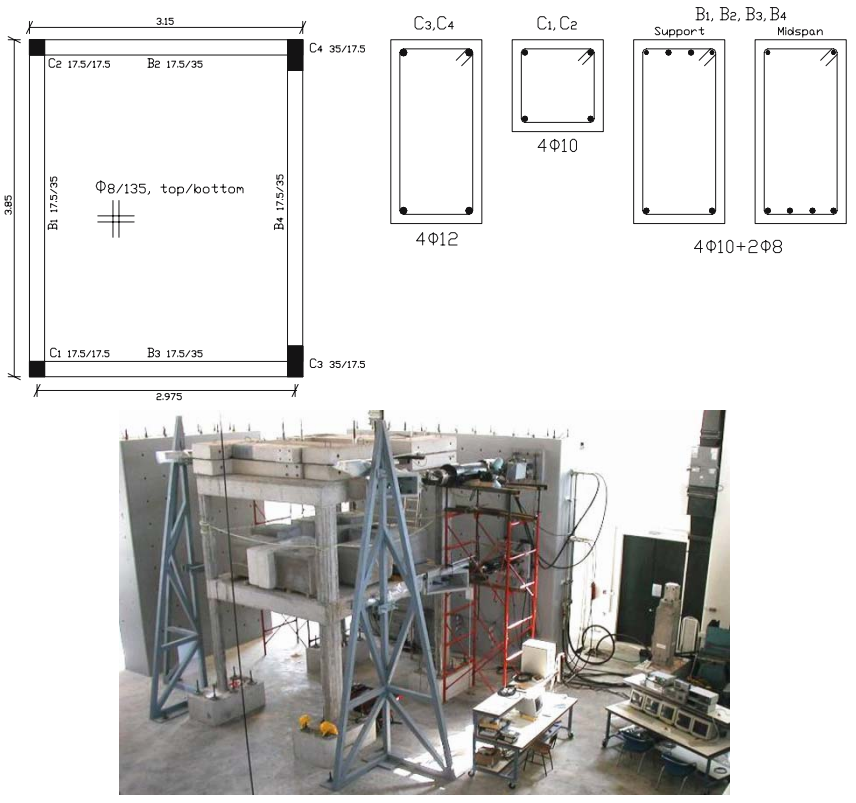

Figure 1. 0.7:1 scale test structure: framing plan, member reinforcement and general view

Pseudodynamic testing was performed with four Degrees-of-Freedom: the displacements of the two floors in the direction of the actuators, plus the two floor rotations with respect to the vertical axis. A 15s long unidirectional input motion was applied (after scaling time by the square root of the scaling factor: $\sqrt{0.7}=0.8366$), fitting well the 5%-elastic spectrum of Eurocode 8 for soil type C (stiff soil), but modulated after one component of the Herzegnovi record from the 1979 Montenegro earthquake.

The unretrofitted version of the test structure was subjected to a series of tests of increasing intensity, up to the input motion scaled to a peak ground acceleration (PGA) of 0.20g (Figure 2). It exhibited strongly torsional response to the unidirectional input motion. Significant damage was inflicted to the frame by this series of tests and had a clear effect on the response. Although wide-spread, structural damage was heaviest at the bottom of the columns – where vertical bars were lap-spliced – and at the beam-column joints.

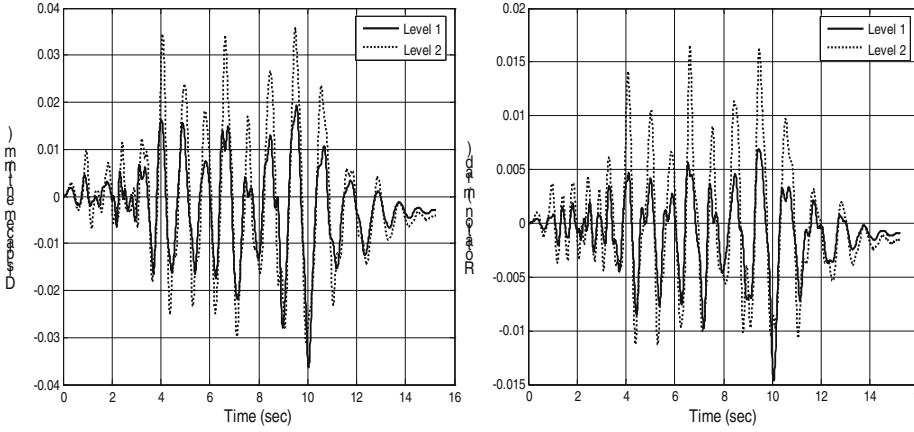

Figure 2. Time-histories of floor displacements and rotations of unretrofitted frame at 0.2g PGA

The test structure was repaired and retrofitted. Repair comprised epoxy grouting of the major cracks, replacement of spalled concrete with non-shrinking mortar and application of a single layer of unidirectional CFRP (with the fibres in the horizontal direction) to the external sides of beam-column joints, extending for a few cm to the side of the beams for anchorage. Retrofitting consisted of wrapping the bottom part of all columns in both storeys with two layers of CFRP (of the same type as that used for the Q- and R-type columns), after rounding their corners to a radius of 30mm. The retrofitted structure was re-tested under the same ground motion, scaled this time to a PGA of 0.30g (Figure 3). Despite the large magnitude of the response displacements (interstorey drifts of the columns of the "flexible side" reaching 4% in the direction of testing and simultaneously 1.75% in the orthogonal direction), further damage was limited to concrete spalling at the (unretrofitted) column tops. It was clear from the response that the structure successfully sustained the increased input motion thanks to controlled slippage of the vertical bars within the beam-column joints of the ground storey and the associated fixed-end rotations of the corresponding column end sections. As a matter of fact, on the "flexible side" the unretrofitted column tops went through drift demands that seem to exceed the ultimate deformation suggested by the test of column Q-0.

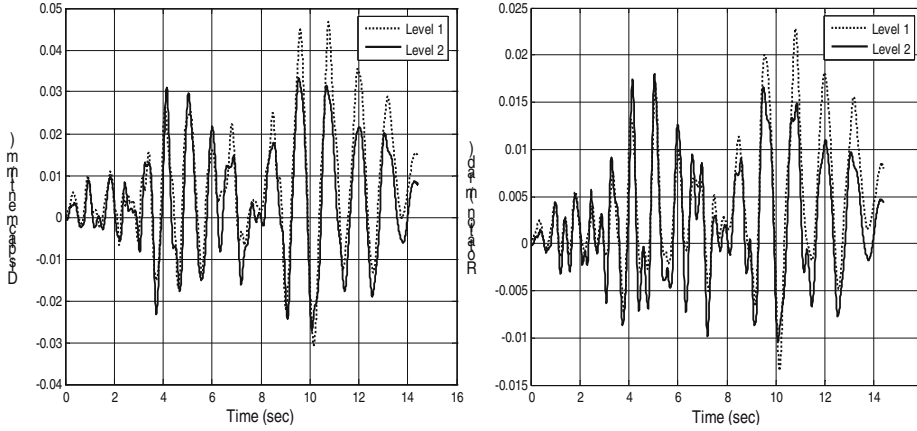

Figure 3. Floor displacement and rotation time-histories at 0.3g for FRP-wrapped column bottoms

6. Conclusions

The effectiveness of concrete jacketing or CFRP wrapping for seismic retrofitting of rectangular concrete columns with poor detailing, and in particular with lap splicing of bars at floor level, was experimentally studied. In addition to the effect of the bond properties of the bars in the original column, parameters studied include the length of the lap splice, the type of connection between the concrete jacket and the old column, the number of layers of CFRP and the length of the member over which FRP wrapping is applied.

The tests of unretrofitted columns show that, for smooth bars with hooked ends, the low deformation capacity and energy dissipation does not depend on lapping length - at least for lapping as short as 15 bar-diameters. Unretrofitted columns with straight ribbed bars exhibit a remarkable loss of deformation capacity and energy dissipation for lap length below 45 bar-diameters.

No systematic effect has been found of the number of layers and the length of application of the FRP, or even of the existence and length of lapping, on the force and cyclic deformation capacity or the rate of strength degradation in FRP-retrofitted columns with smooth bars and hooked ends. A decrease in lap length seems to reduce energy dissipation in FRP-retrofitted columns with smooth bars. In columns with ribbed bars, FRP wrapping cannot fully remove the adverse effects on force capacity and energy dissipation of a very short lapping of straight bar ends (e.g. in the order of 15 bar-diameters) near the base. For such cases, concrete jacketing is far more effective. RC jacketing of columns with smooth bars increases their deformation capacity to levels sufficient for earthquake resistance, irrespectively of the presence and length of lap splicing. Only in columns with ribbed bars and very short lap splices is

some effect of the short lapping retained in the jacketed column, and that adverse effect is limited to the hysteretic energy dissipation of the jacketed column. Previous damage of the old column by cyclic loading beyond its peak resistance does not reduce the effectiveness of the jacket. Concrete-jacketed old-type columns with smooth bars behave similarly to a monolithic column with the same geometry and reinforcement as the jacket, almost regardless to the measures to improve the connection of the jacket with the old concrete.

The test results, supplemented with those of previous investigations, suggest that the yield moment and the flexure-controlled cyclic deformation capacity of jacketed members with jacket longitudinal bars anchored beyond the end section, may be reliably estimated considering the jacketed member as monolithic with f_c value that of the jacket. The drift ratio of the member and the effective stiffness of the jacketed member at incipient yielding may also be similarly estimated, if the interface with the old concrete is roughened. Lack of such roughening increases the drift ratio at incipient yielding and reduces its effective stiffness by about 20%, even when dowels or U-bars welded to the new and the old corner bars are used instead, suggesting that such measures become effective after yielding of the RC-jacketed member.

The present test results, along with experimental results from the literature, were utilized to develop simple rules and analytical tools for the calculation of the flexural strength, the secant-to-yield stiffness and the cyclic deformation capacity of FRP-wrapped columns with or without lap splicing at the base, as a function of jacket parameters. These are modifications or extensions of the corresponding expressions for unretrofitted concrete members without lap splicing. Reference may be made to Eurocode 8 ("Design of structures for earthquake resistance") on "Assessment and Retrofitting of Buildings" (CEN, 2005).

ACKNOWLEDGEMENT

This work was funded partly by NATO (research project SfP977231 of the Science for Peace Program) and partly by the European Commission (research project SPEAR: G6RD-2001-00525, GROWTH Program).

REFERENCES

Biskinis, D.E. and Fardis, M.N., (2004). "Cyclic strength and deformation capacity of RC members, including members retrofitted for earthquake resistance", *Proc. 5th International Ph.D Symposium in Civil Engineering*, Delft, Balkema, pp.1125-1133.

CEN (2005). *European Standard EN1998-3: Eurocode 8: Design of structures for earthquake resistance. Part 3: Assessment and retrofitting of buildings,* Comité Européen de Normalisation, Brussels.

IN SERVICE SEISMIC STRENGTHENING OF RC FRAMED BUILDINGS

TUGRUL TANKUT•
UGUR ERSOY
GUNEY OZCEBE
MEHMET BARAN
DILEK OKUYUCU
Department of Civil Engineering, Middle East Technical University, 06531, Ankara, Turkey

Abstract. An innovative non-evacuation retrofitting technique has been developed for RC buildings, which form the major portion of the existing stock in Turkey. The introduction of cast-in-place RC infill walls, connected to existing frame members, is known to be very effective in improving the overall seismic performance. However, this technique is not suitable since it involves messy construction work and requires evacuation. The idea behind the proposed method is to transform existing hollow masonry infill walls into strong and rigid infill walls by reinforcing them with relatively high strength precast concrete panels epoxy-glued to the wall and dowel connected to the frame members to enhance the lateral stiffness of the frame. The panels to be assembled are small enough to be handled by two workers. All specimens were tested to failure under reversed cyclic quasi-static lateral loading and constant vertical load. All strengthened specimens exhibited superior performance compared to the reference specimens designed to represent the present state of ordinary RC frames with hollow brick infill walls plastered on both sides.

Keywords: seismic strengthening; retrofitting; precast panels; infill walls; connections.

• Tugrul Tankut, Middle East Technical University, Civil Engineering Department, Ankara, Turkey; e-mail: ttankut@metu.edu.tr

S.T. Wasti and G. Ozcebe (eds.), Advances in Earthquake Engineering for Urban Risk Reduction, 47–62.

1. Introduction

A great number of existing building structures require seismic vulnerability assessment followed by seismic retrofitting. The traditional seismic repair techniques that necessitate evacuation cannot be a solution to a problem of this size. Therefore, there is a great need for seismic strengthening techniques that can be applied while the building is still in service. This challenging effort towards the development of innovative retrofitting techniques has been the subject matter of this comprehensive NATO project. The study reported in the present paper concerns the development of one such innovative retrofitting technique, suitable for the most common type of building structures in the region, namely, reinforced concrete frames with hollow brick masonry infill.

The seismic repair technique developed earlier for this kind of building structures has been successfully used in the post-quake repair of damaged buildings. This repair technique aiming at the improvement of the overall system behaviour consists of the introduction of cast-in-place reinforced concrete infill walls properly connected to the existing frame members by epoxy anchored dowels. This repair technique, which proved to be very effective in improving the overall seismic structural performance, is not suitable for pre-quake strengthening of a large number of building structures since it involves messy construction works and requires evacuation of the building.

As already introduced in an earlier paper[1] reporting the very initial stage of the present work, the idea of the newly developed strengthening technique is to convert the existing hollow brick infill wall into a lateral load resisting member by reinforcing it with a comparatively thin layer of relatively high strength precast concrete panels epoxy connected to the wall and the frame members. One single piece of precast concrete member covering the entire wall would definitely be unmanageable, too large to go through doors and too heavy to be carried manually. Hence it has to consist of individual panels of suitable size and weight and to be assembled on the wall by connecting the panels together.

2. Experimental Work

2.1. TEST FRAMES

One-third scale, one-bay two-storey reinforced concrete frames were used as test units. Test units have been designed and constructed to reflect the most common deficiencies observed in local practice, such as strong beam-weak column connections, insufficient confinement, low-grade concrete (C12-C16) and poor workmanship. Realising the problems caused by insufficient lap

length on the column reinforcement that may lead to premature failure in retrofitted structures, it was decided to include this factor among the parameters studied. These frames had their columns fixed to rigid foundation beams. Dimensions and reinforcement of the test frames are illustrated in Figure 1.

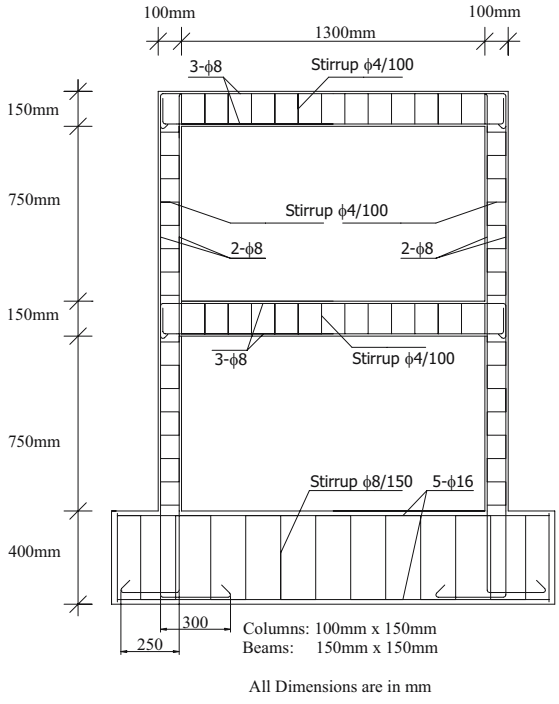

Figure 1. Dimension and reinforcement of test frames

Both the first and second floor frame bays are infilled with scaled brick walls covered with a scaled layer of plaster. Realising the critical consequences workmanship may have on the performance, ordinary workmanship was intentionally employed in wall construction and plaster application to reflect ordinary practice.

2.2. PRECAST CONCRETE PANELS

The major factor considered in the design of precast panels was weight; each piece to be used in actual practice should not exceed 60~70 kg so that it can be handled by two workers. The other important factor was the panel thickness. Considering the relatively high strength of concrete (~40 MPa) to be used in panels, 40~50 mm panel thickness can reasonably be proposed for the actual practice. Since the usual floor height is 2.80~3.00 m and the usual beam depth is around 400~600 mm, a panel arrangement with three layers sounds rather

sensible and leads to a panel size around 700~800 mm in vertical direction, horizontal size being around 600~700 mm. With all these considerations, Types A, C and E (nearly square) were designed. Types B, D and F (strip) reflect a different design approach; they are narrow and full floor height tall.

Since masonry wall thickness is usually less than the frame member width and the wall is eccentrically placed on the external face of the frame, the two possible panel application modes were studied; (i) internal application where the panel layer was nicely surrounded and confined by the frame and (ii) external application where the panel layer had to be extended over the frame members and anchored to the external face of the frame.

Method of connecting precast concrete panels together is a critical issue, since these connections need to be capable of transferring tension and compression as well as shear. Shear keys and welded connections on panel reinforcement were considered essential in the design of the first series of test specimens as illustrated in Figure 2. However, tests on these specimens revealed that integration of the panels with each other and with the hollow brick wall could be achieved satisfactorily by epoxy alone. Welding of bars and shear keys were eliminated in all the following test series, leading to a considerable simplification, and yet a very satisfactory performance could be obtained.

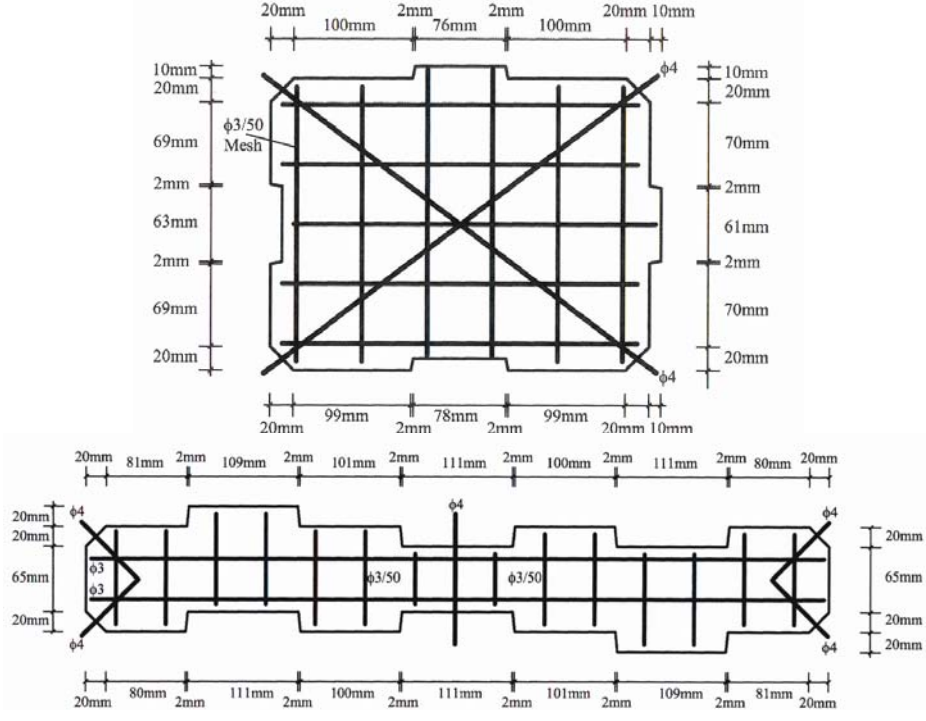

Figure 2. Dimensions and reinforcement of Type A and Type B panels

Although it is obviously best to have epoxy-anchored dowels along the four sides of each panel, the possibility of reducing the number of panel sides having dowels has also been investigated to simplify the technique further and to impove its cost efficiency.

2.3. PARAMETERS STUDIED

More than thirty quasi-static tests (results of twenty-two of them are reported in the present paper) have been performed on one-third scale, one-bay two-storey reinforced concrete frames, besides two shake table tests on three-dimensional test units consisting of two three-bay two-storey frames of similar properties connected with slabs to verify the efficiency of the developed strengthening technique under actual seismic action. In these tests, effects on the performance of the parameters such as (i) panel geometry, (ii) panel-to-panel connections, (iii) panel-to-frame connections, (iv) internal or external applications, (v) lapped splices on column reinforcement, (vi) axial load level in columns and (vii) use of one-storey test frames have been investigated. Additional test series are currently being carried out to study (viii) the effects of infill wall aspect ratio, (ix) the possibility of using lightweight high strength concrete panels and (x) the advantages of using fibre reinforced concrete panels.

Various properties of the test specimens are simply listed in Table 1. Series A consists of one-bay two-floor frame specimens and Series B of one-bay one-floor frames. Panel Types A (square) and B (strip) have shear keys and welded connections; Types C (square) and D (strip) are simple panels with straight edges and no welded connections. Types A to D are used in internal panel applications, whereas Types E (square) and F (strip) are simple panels with straght edges used in external panel applications.

TABLE 1. Characteristic properties of the test specimens

Series (No. of Floors)	Specimen Type	Spec. Id.	Column Steel	Panel Application	Panel Type	Dowel Sides
A (2)	Reference	CR	Continuous	---	---	---
A (2)	specimens	LR	Lapped	---	---	---
A (2)	Complicated	CIA	Continuous	Internal	A	4
A (2)	connection	CIB	Continuous	Internal	B	4
A (2)	Standard	CIC	Continuous	Internal	C	1
A (2)	connection	CID	Continuous	Internal	D	1
A (2)	Reduced	CIC3	Continuous	Internal	C	3
A (2)	dowels	CIC4	Continuous	Internal	C	4
A (2)	Standard	CEE	Continuous	External	E	4
A (2)	dowels	CEF	Continuous	External	F	4

Series (No. of Floors)	Specimen Type	Spec. Id.	Column Steel	Panel Application	Panel Type	Dowel Sides
A (2)	Reduced	CEE1	Continuous	External	E	1
A (2)	dowels	CEER	Continuous	External	E	4 (reduced)
A (2)	Lapped	LIC	Lapped	Internal	C	4
A (2)	steel	LID	Lapped	Internal	D	4
B (1)	Reference	CR	Continuous	---	---	---
B (1)	specimens	LR	Lapped	---	---	---
B (1)	Complicated	CIA4	Continuous	Internal	A	4
B (1)	connection	CIB4	Continuous	Internal	B	4
B (1)	Standard	CIC4	Continuous	Internal	C	4
B (1)	connection	CID4	Continuous	Internal	D	4
B (1)	Lapped	LIC4	Lapped	Internal	C	4
B (1)	steel	LID4	Lapped	Internal	D	4

2.4. MATERIALS

A low strength concrete is intentionally used in the test frames to represent the concrete commonly used in existing building structures. On the other hand, relatively strong concrete should be preferred for the precast panels to provide the required load carrying capacity by using relatively thin layers of concrete, minimising the panel weight. Ordinary cement-lime mortar is used for the plaster, imitating the usual practice. For the same reason, mild steel plain bars are used as reinforcement in both test frames and panels.

SIKADUR-31 epoxy repair mortar was used in panel joints and between the panels and the plaster on the wall. It is a relatively inexpensive two component mortar recommended for reinforced concrete repair works. Its rather viscous structure enables a practical use of this material on vertical surfaces. According to the manufacturer's manual, its setting time is about 45 minutes at room temperature and the tensile strength is nearly 20 MPa which is obviously beyond the strength required in concrete applications.

2.5. LOADING AND SUPPORTING SYSTEM

Figure 3 gives a general view of the test set-up. A reinforced concrete universal base, serving as a rigid foundation for the test unit and enabling various support configurations, has been prestressed to the strong testing floor of the Structural Mechanics Laboratory. Each test frame was cast together with a rigid foundation beam, which was suitably bolted down to the universal base as required. The quasi-static test loading consists of reversed cyclic horizontal load

applied at floor levels, besides constant vertical load around 10 to 20% of the column axial load capacity.

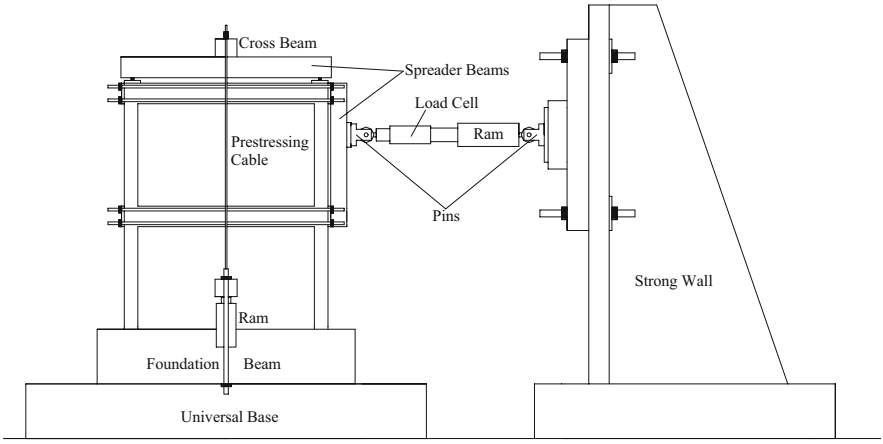

Figure 3. A general view of the test set-up

The vertical load application gear consisted of a hydraulic jack and a load cell placed between a spreader beam and a cross-beam at the top, which was pulled down by two prestressing cables attached to the universal base on either side of the test unit. Having been supported as a simple beam with supports at the column heads as shown in Figure 3, the spreader beam divided the load and transferred two equal components to the two columns. The load was continuously monitored and readjusted during the test.

Reversed cyclic horizontal load was applied by using a double acting hydraulic jack bearing against the reaction wall as illustrated in Figure 3. The loading unit, consisting of the ram and load cell, had pin connections at both ends to eliminate any accidental eccentricity mainly in the vertical direction and tolerating a small rotation in the horizontal direction normal to the testing plane. The load was applied at one third span of the spreader beam to ensure that the load at the second floor level always remained twice as the load at the first floor level. At floor levels, clamps made of four steel bars connected to two loading plates at either end were loosely attached to the test frame to avoid from any unintended interference with the frame behaviour, which might possibly be caused by the external prestressing on the beams. Thus, in both pushing and pulling modes, a horizontal push is applied to the test unit through steel loading pads without inducing any undesirable axial load in the beam.

The infill wall, which had a considerably smaller thickness than the beam width, is placed eccentrically on the exterior side of the beam to reflect the common practice. Thus the contribution of the infill made the frame behaviour somewhat unsymmetrical, and the load applied in the plane of symmetry

created warping, which may lead to significant undesirable out-of-plane deformations, especially towards the end of the test. Rather rigid external steel 'guide frame' attached to the universal base was used to prevent any out-of-plane deformations. Four 'guide bars' two on each side, with roller ends, were attached to the guide frame, and they gently touched the test frame beam, smoothly allowing in-plane sway.

Typical load and displacement histories followed during the tests are illustrated in Figure 4. As can be deduced from the figure, ever-increasing load cycles were applied so far as the specimen was capable of resisting higher loads, and beyond that, deformation controlled loading was performed with ever-increasing displacement cycles, usually in steps of multiples of yield displacement.

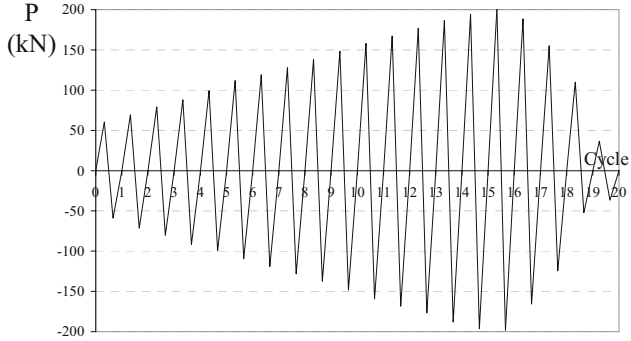

a. Typical loading history

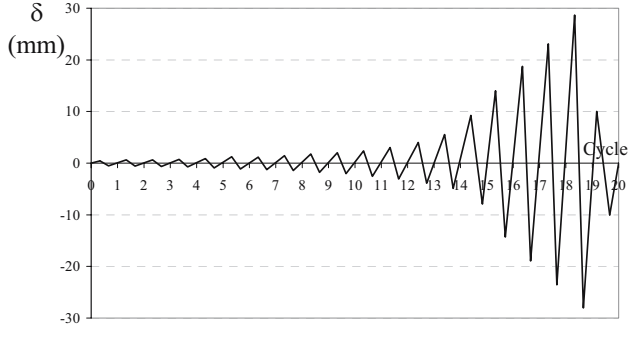

b. Typical displacement history

Figure 4. Typical loading and displacement history patterns

2.6. DEFORMATION MEASUREMENT SYSTEM

All deformations were measured by displacement transducers; using either LVDTs or electronically recordable dial gauges as shown in Figure 5. Sway displacements were measured both at the first and second floor levels. Three

measurements were normally taken at the top level to ensure a reliable collection of these very important data, even in the case of one or two transducers unexpectedly going wrong. Infill wall shear deformations were determined on the basis of displacement measurements along the diagonals.

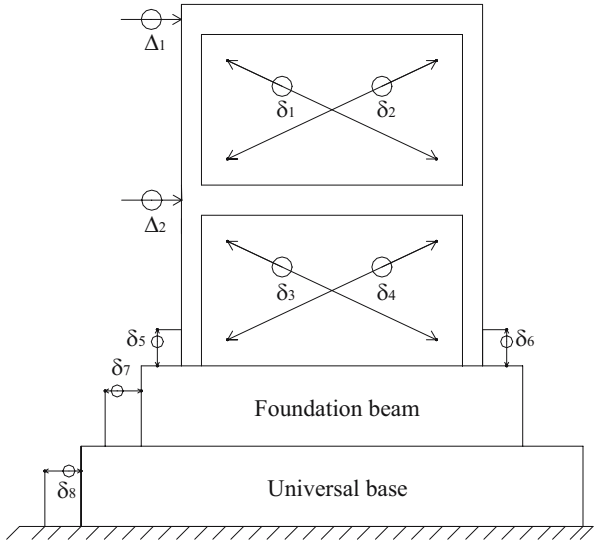

Figure 5. Instrumentation

Displacement measurements taken at the column roots were meant for computation of rotations of the entire test unit. However, they also provided data for monitoring the critical column section deformations; steel yielding in the tension side column, concrete crushing in the compression side column etc. Although it is heavily prestressed to the strong testing floor, the rigid body rotations and displacements of the universal base were also monitored using four dial gauges.

3. Test Results

Table 2 presents the major performance indicators together with short notes explaining the observed behaviour for the twenty-two tests reported in this paper. A little more detailed information is given for each group of tests in the following paragraphs.

Reference Specimens - These specimens were designed and constructed as hollow brick masonry infilled frames with the common deficiencies mentioned earlier in to reflect the common practice. They exhibited typical masonry infilled frame behaviour. The masonry infill considerably contributed to the lateral load capacity at the initial stage, however, this contribution decreased

rapidly as crushing started in the infill leading to behaviour similar to that of the bare frame where significant deformations took place under rather small lateral loads.

TABLE 2. Performance indicators

Series (No of Floors)	Spec. Id	Axial Load N/N_o	Cap. (kN)	Drift Ratio δ/h	Initial Rigidity (kN/mm)	Energy Dis. (kJ)	Remarks on Performance
A (2)	CR	0.19	78.8	0.0042	43.5	6.4	Typical infilled frame behaviour
A (2)	LR	0.30	74.2	0.0033	59.1	4.6	Typical infilled frame behaviour
A (2)	CIA	0.17	192.5	0.0038	123.5	15.3	Wall behaviour, intact panel
A (2)	CIB	0.21	201.3	0.0089	123.4	21.8	Wall behaviour, intact panel
A (2)	CIC	0.19	195.7	0.0084	118.7	20.4	Damage in panel & frame
A (2)	CID	0.19	192.7	0.0066	109.8	17.8	Damage in panel & frame
A (2)	CIC3	0.18	210.6	0.0092	112.7	17.9	Damage in panel & frame
A (2)	CIC4	0.17	218.5	0.0055	125.3	13.4	Wall behaviour, intact panel
A (2)	CEE	0.18	206.6	0.0073	112.8	9.2	Smeared cracking, light damage
A (2)	CEF	0.21	204.3	0.0076	124.6	21.2	Smeared cracking, light damage
A (2)	CEE1	0.15	176.5	0.0057	133.7	9.4	Separation, unsatisfactory perf.
A (2)	CEER	0.20	185.4	0.0059	124.7	16.1	Smeared cracking, light damage
A (2)	LIC	0.17	174.0	0.0062	101.8	17.7	Damage in panel & frame
A (2)	LID	0.22	172.4	0.0029	117.1	8.9	Damage in panel & frame
B (1)	CR	0.25	86.6	0.0036	96.0	5.7	Typical infilled frame behaviour
B (1)	LR	0.13	65.5	0.0053	60.0	8.6	Typical infilled frame behaviour
B (1)	CIA4	0.25	209.9	0.0112	312.0	15.5	Damage in panel & frame
B (1)	CIB4	0.25	197.0	0.0056	308.0	15.1	Damage in panel & frame
B (1)	CIC4	0.25	213.5	0.0105	294.0	9.2	Damage in panel & frame
B (1)	CID4	0.25	254.7	0.0119	276.0	8.4	Damage in panel & frame
B (1)	LIC4	0.13	148.9	0.0125	159.0	14.3	Heavy damage in panel & frame
B (1)	LID4	0.13	199.6	0.0109	280.0	14.4	Heavy damage in panel & frame

Specimens with Complicated Connections - In these specimens, precast concrete panels (square in one, strip in the other) were used to reinforce the hollow brick infill walls. Type A and Type B panels which had shear keys on four sides were epoxy glued to the plastered infill wall and to each other. Furthermore, the bars protruding from the corners were welded to each other and to the epoxy anchored dowels. This intervention led to a significant increase in the capacity and the lateral stiffness, thus to a significantly better seismic performance. The entire test unit behaved nearly as a monolithic cantilever where failure took place at the root in terms of yielding of the steel in the tension side column and concrete crushing and buckling of longitudinal steel in the compression side column.

Specimens with Standard Connection - In the specimens with complicated connections, the epoxy connection between the panels appeared to be sufficiently strong by itself. Based on this observation, shear keys and welded connections were eliminated in the following pair of tests with the aim of simplifying the technique and increasing its cost efficiency. Furthermore, epoxy anchored dowels into the existing frame members were also eliminated with the exception of the dowels into the foundation beam. Some damage was observed in the lower storey infill panel and eventually capacity was exhausted by the failure of the existing frame at the top ends of the lower columns. The capacity and lateral stiffness values achieved were rather close to those obtained in the specimens with complicated connections.

Specimens with Reduced Dowels - Standard panels (Type C and Type D) were used in these specimens with three (to the columns and foundation beam) or four sides having epoxy anchored dowels to observe the effects of the dowel arrangements on the seismic performance. As expected, a better behaviour and a higher capacity were achieved as better connections to the frame were provided.

Specimens with External Panels Having Standard Bolts - It may not always be possible to place the strengthening panels inside the frame such that they are nicely confined by the existing frame members. In such cases, panels need to be placed and glued on the external face of the frame and to be anchored there by means of bolts epoxy anchored into the frame members. Such specimens were tested and this version of the technique has also proved to be equally effective. The specimens where each one of the panels lying on a beam or column was epoxy glued and bolted down to the frame member performed very well and produced an equal capacity and lateral stiffness as the others.

Specimens with External Panels Having Reduced Bolts - The possibility of reducing the number of bolts was investigated in these tests. The specimen where the panels were merely epoxy glued on the frame members without using any anchor bolts could produce a rather high capacity (about 90% of the other strengthened specimens); however, the performance was found unacceptable due to the rapid strength degradation as a result of panel separation at the peak load. For the other specimen, the bolt pattern was based on a finite element analysis to introduce a significant bolt reduction (12 bolts instead of 42), and almost an identical performance as the specimen with 42 bolts could be achieved.

Specimens with Lap Spliced Column Steel - Although they were designed to include the common deficiencies, the specimens mentioned above had continuous column steel. The use of lap splices of inadequate lap length at the column base is another common source of problem. To investigate the effects of this deficiency on the efficiency of the proposed technique specimens (similar

to the ones mentioned in paragraph c) with lap spliced column steel were also tested. Although the capacity achieved was somewhat smaller (about 90% of the others), its behaviour appeared to be perfectly normal and no indication of bond deterioration could be detected at the splice zones. This observation was interpreted as the result of rather high column axial load (about 20% of its uni-axial load capacity) which might have prevented the development of significant axial tension.

Single Storey Reference Specimens - Single storey specimens were introduced to seek the advantages of simpler and less expensive specimens if they could satisfactorily replace the two-storey frames. The single storey reference specimens exhibited typical masonry infilled frame behaviour as briefly explained above in paragraph a.

Single Storey Specimens with Complicated Connection - Precast concrete panels (square in one, strip in the other) had shear keys on four sides and welded connection at their four corners besides the epoxy connection to each other just like the specimens mentioned in paragraph b. As expected, this kind of retrofitting led to a significant increase of the same magnitude in the capacity and the lateral stiffness as observed in the two-storey tests. Some damage occurred in the infill; however, eventual exhaustion came with the failure of frame columns.

Single Storey Specimens with Standard Connection - Straight edge precast concrete panels with no shear keys and no welding (Type C and Type D) were used in these specimens and dowels were provided along the four edges. The observed performance was almost identical to that of the specimens with complicated connection mentioned above.

Single Storey Specimens with Lap Spliced Column Steel - In these specimens, column reinforcement had rather inadequate (20 bar diameter) lap splices; straight edge precast concrete panels (Type C and Type D) were used and dowels were provided along the four edges. Besides, column axial load level was deliberately reduced down to 13% (as opposed to 25% in the others) of the column capacity. Although the overall behaviour was not significantly different than the others, some indication of bond failure were observed at the lap splice zones in the columns, and an appreciable reduction (up to ~25%) took place in the capacity, clearly indicating the importance of the axial load level as a factor controlling the problems caused by inadequately lap spliced column reinforcement.

4. Discussion of Test Results

Envelope load-lateral displacement curves given in Figure 6 indicate a significant increase in the load carrying capacity and significantly delayed

strength degradation, leading to a much better ductility. Specimen performances were also evaluated in terms of load-displacement, ductility, energy dissipation, stiffness degradation etc. Detailed discussions on these issues together with the respective diagrams and tables can be found in the related PhD and MSc theses[2,3,4,5]. They could not be included in the present paper due to space limitations; instead, an overall interpretation of the test results is summarised in Table 3 and interpretation results are summarised in the following paragraphs.

1. The technique developed, that can be described as converting the existing hollow brick infills into lateral load resisting members by reinforcing them with epoxy glued precast concrete panels, proves to be an effective method of seismic rehabilitation of the existing reinforced concrete framed building structures. The performance improvement indicators given in Table 3 clearly exhibit the effectiveness of the proposed technique.

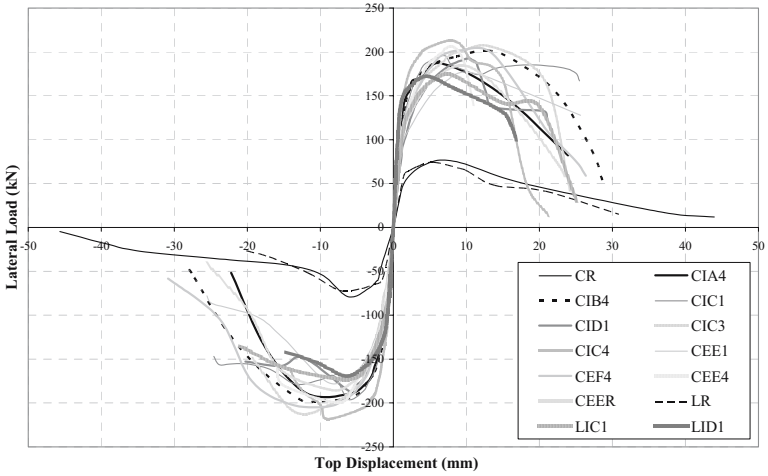

Figure 6. Envelope load-lateral displacement curves

TABLE 3. Performance improvement

	Relative to masonry infilled frame	Relative to bare frame
Lateral load capacity	~ 2.5 times	~ 15 times
Lateral stiffness	~ 3 times	~ 20 times
Ductility	~ 2 times	~ 0.2 times
Energy dissipation	~ 3 times	~ 60 times

2. Specimens, strengthened with straight edge panels connected by epoxy alone, performed very satisfactorily, indicating that the use of shear keys and welded connections could be avoided, thus simplifying the proposed technique and improving its cost efficiency.

3. Proper connections through epoxy anchored dowels (epoxy anchored bolts in the case of external panels) between the existing frame members and the wall strengthening panel are essential especially at the lowermost floor and particularly at the foundation beam level. Although a significant drop in the capacity has not been observed in the specimens where less than four sides were dowel connected to the frame, the performance was observed to be somewhat inferior in such specimens compared to the fully connected ones. It is therefore highly recommended to have dowel connections along all the four sides in the lowermost few floors.
4. In many specimens, final failure has been associated with significant damage in the existing frame columns, indicating that the effectiveness of the developed technique did not depend solely on the properties of the strengthening panel, but also on the properties of the existing frame members. It is therefore obvious that the effectiveness of the intervention can be improved if the existing frame members are strengthened prior to the introduction of the wall strengthening panel. However, this approach would cause the major advantage of the proposed method to disappear, since it would necessitate evacuation besides increasing the cost. Instead, it is recommended to strengthen a few frames more than what is necessary such that each strengthened frame receives a somewhat lower share from the seismic action.
5. Presence of inadequate (20 bar diameter) lap splices in column reinforcement does not seem to adversely affect the effectiveness of the proposed rehabilitation technique significantly, if the column axial load is not less than 20% of its axial load capacity. It is therefore concluded that the lap splice complication can be tolerated to a certain extent, provided the column axial loads are not too low.
6. Similar and compatible results have been obtained from both one-storey and two-storey test frames, indicating that they are equally acceptable as test structures and one-storey frames may be preferred in the cases where the limitations of the testing facility require.
7. The seismic retrofitting technique developed does not require messy construction work and therefore it can be realised while the building is still in service without causing too much disturbance to the occupant. That is why it is called OFR-Occupant Friendly Rehabilitation.
8. The cost of construction is estimated to be of the same order as that of the cast-in-place reinforced concrete infill. However, when the cost of evacuation (i.e., the moving out and moving in expenses together with the rent to be paid during the construction period plus the cost of the

psychological torture the occupant is subjected to) is taken into account, the cost effectiveness of the proposed technique becomes unrivalled. This advantage becomes even more pronounced in the cases of mass retrofitting of thousands of building simultaneously.

9. A major question yet to be answered concerns the method of analysis to be employed in the design of buildings to be retrofitted by this technique. Continuing analytical studies indicate that modelling of a panel strengthened wall as a monolithic shear wall having an equivalent thickness (a function of panel concrete strength, panel thickness, thickness and other properties of the brick wall) may be the basis of a practical and suitable method of analysis. However, another possibility is the modelling of the panel strengthened wall with pin connected diagonal struts of equivalent width (modified Smith approach).

5. Conclusion and Recommendations

5.1. CONCLUSION

The technique developed on the principle of converting the existing hollow brick masonry infill walls, by reinforcing them through epoxy attached precast concrete panels of manageable size, into lateral load resisting structural members, has been verified to be an effective, practical and cost effective seismic retrofitting method that can suitably be used in the seismic rehabilitation of the existing reinforced concrete framed building structures without evacuation and with minimal disturbance to the occupants.

As soon as the ongoing studies on the method of analysis to be employed in the design of buildings to be retrofitted by this technique are completed and a practical and reliable approach is formulated, the method will be made available to the use of the construction industry.

5.2. RECOMMENDATIONS FOR PRACTICE

Seismic rehabilitation using the proposed technique can best be realised by precast concrete companies, since they normally have the skills and equipment required for this kind of rather meticulous concrete element production and handling. The procedure given below can be recommended for a successful application. However, it is natural that these companies will in due course develop their own and probably more efficient procedures.

Following the completion of the rehabilitation design and the decision about the infill walls that will be reinforced as a result of the analytical investigations,

panel dimensions should be determined carefully considering the measurements taken on the actual structure.

Panels designed considering the actual measurements should be manufactured at the factory and brought near the wall they belong to. Standard size panels taken from the stock can be used in most cases together with a limited number of custom made panels specially designed and manufactured for that particular wall.

In the mean time, epoxy anchored dowels should be placed in the existing frame members considering the panel dimensions chosen.

The operation should be completed by epoxy mounting the panels prepared for that particular wall. No surface finishing is normally required since the panels are expected to have sufficiently smooth surfaces.

The most problematic buildings of the existing stock have been identified as the mid-rise (3-8 storey) poor quality residential and office buildings. In the three critical levels of these buildings, namely the basement, ground and first floors, strengthening panels should be properly attached to the frame members along their four sides by epoxy anchored dowels (epoxy anchored bolts in external applications). However, it is possible to reduce the number of dowels in the next three floors and even to eliminate the dowels totally in the floors above that level. On the other hand, it is strongly recommended to double the number of dowels to be anchored in the foundation beams.

References

1. M. Baran, M. Duvarci, T. Tankut, U. Ersoy, G. Ozcebe, Occupant Friendly Seismic Retrofit (OFR) of Framed Buildings, Proceedings, NATO International Workshop on Seismic Vulnerability and Rehabilitation of Existing Structures, Izmir, Turkey, May 2003.
2. M. Duvarci, Seismic Strengthening of Reinforced Concrete Frames with Precast Concrete Panels, MSc thesis, Department of Civil Engineering, Middle East Technical University, Ankara, Turkey, 2003.
3. M. Baran, Precast Concrete Panel Reinforced Infill Walls for Seismic Strengthening of Reinforced Concrete Framed Structures, PhD thesis, Department of Civil Engineering, Middle East Technical University, Ankara, Turkey, 2005.
4. M. Susoy, Seismic Strengthening of Masonry Infilled Reinforced Concrete Frames with Precast Concrete Panels, MSc thesis, Department of Civil Engineering, Middle East Technical University, Ankara, Turkey, 2005.
5. D. Okuyucu, Seismic Strengthening of Reinforced Concrete Framed Structures with Column Lap-Splice Deficiency by Precast Concrete Panels, PhD thesis in progress, Department of Civil Engineering, Middle East Technical University, Ankara, Turkey.

AN EQUIVALENT LINEARIZATION PROCEDURE FOR DISPLACEMENT-BASED SEISMIC ASSESSMENT OF VULNERABLE RC BUILDINGS

M. SELIM GUNAY
Department of Civil Engineering, Middle East Technical University, 06531 Ankara, Turkey

HALUK SUCUOGLU*
Department of Civil Engineering, Middle East Technical University, 06531 Ankara, Turkey

Abstract. Seismic assessment of vulnerable reinforced concrete buildings in Turkey is a challenging task. Considering both the size of the problem and the inadequacy of inelastic analysis methods in the seismic evaluation of large building stocks, it is evident that simple and convenient methods are required. A displacement-based seismic assessment procedure, employing equivalent linear analysis in combination with capacity principles, is developed herein. Briefly, the procedure consists of identifying the expected locations of inelastic behavior and reducing the stiffness of members corresponding to these locations. The procedure is implemented on three case study buildings in order to compare the results with the nonlinear static (pushover) analysis results. Comparisons are based on axial forces and moment capacities of columns, distribution of the locations exhibiting inelastic behavior, chord rotations at the member ends and the base shear capacities of buildings. It is observed that the results obtained by the two procedures are sufficiently close.

Keywords: displacement-based; seismic assessment; equivalent linear analysis; capacity principles; stiffness reduction

* Haluk Sucuoglu, e-mail: sucuoglu@ce.metu.edu.tr

S.T. Wasti and G. Ozcebe (eds.), Advances in Earthquake Engineering for Urban Risk Reduction, 63–78.

1. Introduction

The majority of existing buildings located in the seismically active regions of Turkey do not conform to the minimum safety requirements of modern earthquake engineering. Recent strong earthquakes in the last two decades revealed that a large urban building stock, mainly consisting of low to medium-rise substandard reinforced concrete buildings, is seismically vulnerable. Common weaknesses of these buildings are low concrete quality (usually less than 15 MPa), lack of confinement at critical regions, insufficient anchorage and development lengths, and inadequate structural forms (such as soft or critical stories or strong beam-weak column proportions) for seismic resistance.

Recent developments in performance-based procedures produced powerful tools for the seismic safety assessment of existing buildings (ATC-40, FEMA-356). These methods provide valuable and detailed information on the expected seismic performances of such vulnerable buildings. However, there are two important shortcomings on their effectiveness in handling global seismic safety issues. First, they require inelastic analysis capabilities which are not available to most structural engineering professionals. Moreover, inelastic structural analysis tools are not as standard as the linear elastic analysis methods (Wight et al., 1999). Second, the size of the problem or the number of buildings that has to be assessed before the next earthquake is too large. This time limitation, combined with the necessity for detailed analytical models due to the local weaknesses stated above, introduces the need to consider the global responses rather than the details in seismic assessment. Simpler and more efficient seismic performance assessment procedures may serve to eliminate these shortcomings.

A practical and convenient displacement-based seismic assessment procedure is developed in this study for the seismic assessment of vulnerable reinforced concrete buildings. The procedure combines the advantages of linear procedures with the merits of capacity principles. Three existing buildings in Turkey are used as case study buildings for comparison of the results of this procedure with those obtained from true nonlinear static (pushover) analysis.

2. Equivalent Linearization Procedure

This procedure is a displacement-based assessment method that employs linear elastic static analysis in combination with capacity principles in order to predict the true nonlinear response. It is based on combining the results of a demand analysis (linear elastic) and a capacity analysis in order to obtain an equivalent linear system with reduced stiffness. Outline of the procedure is presented in Figure 1 and the details are explained in the following paragraphs.

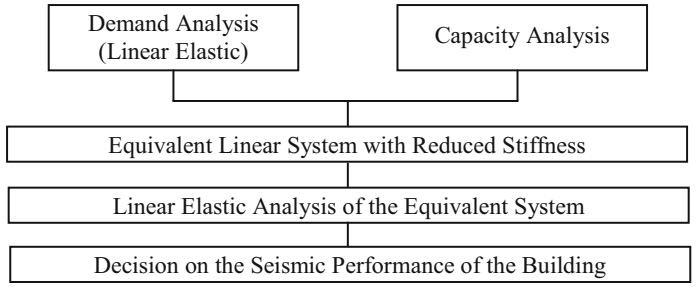

Figure 1. Outline of the equivalent linearization procedure

2.1. DEMAND ANALYSIS

In the demand analysis part, a modal spectrum analysis of the building is performed. However, directions of the internal moments are obtained from the first mode directions. It is assumed that the global system displacements from the linear-elastic modal spectrum analysis and the nonlinear analysis are equal, in accordance with the equal displacement rule. Cracked section stiffness is employed in the linear elastic model according to FEMA-356 (ASCE, 2000) recommendations.

2.2. CAPACITY ANALYSIS

Capacity analysis is conducted in order to decide on the potential yielding member ends. In addition, base shear capacity of the building is calculated as a by-product of the capacity analysis. Steps of the capacity analysis are presented in the form of a flowchart in Figure 2.

2.2.1. *Calculation of the Moment Capacities of Beams (Step 1)*

Flexural capacities of beam end sections are calculated by using the nominal material strengths.

2.2.2. *Calculation of Axial Forces and Moment Capacities of Columns and BCCR Values at the Joints (Steps 2, 3 and 4)*

Axial forces are needed for the calculation of moment capacities of reinforced concrete columns. Under the combination of gravity and earthquake forces, total axial force of a column is equal to the sum of the axial forces due to gravity loading (N_G) and earthquake loading (N_{EQ}).

Axial forces due to gravity loading can be obtained by conducting linear elastic analysis, since it is assumed that there is no inelasticity when only

gravity loads act on the structure. Axial forces due to earthquake loading are bounded by the maximum shear forces that can be transmitted from the beams. Hence, it is suitable to calculate the axial forces due to gravity loading (N_G) by conducting linear elastic analysis and axial forces due to earthquake loading (N_{EQ}) by using limit analysis.

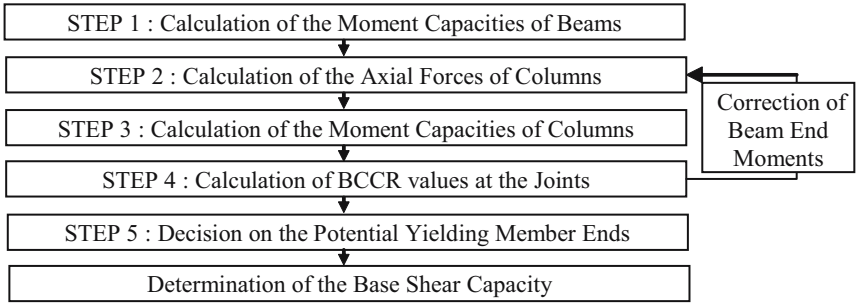

Figure 2. Steps of the capacity analysis

In calculating the axial forces due to earthquake loading (N_{EQ}) by limit analysis, first all the beam-ends are accepted to yield in flexure, in agreement with the direction of the lateral force. Since the axial forces due to gravity loading are available from linear elastic analysis, beam end moments due to gravity loading should be eliminated from limit analysis. Eliminating the end moments due to gravity loading, reserve capacity moment at a beam end is equal to the difference between the moment capacity and the moment due to gravity loading. Beam-end shear forces are then calculated by considering the free body diagrams of the beams. Axial force of a column due to earthquake loading is calculated by using vertical equilibrium, from the free body diagram of the considered column axis (Figure 3). When masonry infill walls are modeled as struts, vertical components of the strut forces should also be considered in the calculation of the axial forces (SF in Figure 3). Axial force capacities of the struts can be used as the strut forces.

The axial force of a column (N) is then calculated as the sum of N_G and N_{EQ}. After calculation of the axial forces, moment capacities can be calculated by using the interaction diagrams of the columns. Up to this stage, all the beam-ends were assumed to yield, however at the joints where the columns are weaker than the beams, column-ends may yield which will prevent the beam-ends to reach their capacities. In order to take this situation into consideration, Beam-to-Column Capacity Ratios (BCCR) are calculated for all joints by dividing the total moment capacity of the beam-ends connecting to the joint by the total moment capacity of the column-ends connecting to the joint. If BCCR for a joint is larger than one, the beam-end moments are corrected by dividing the beam capacity moments by the BCCR value. If BCCR for a joint is smaller

than one, beam-ends are likely to yield and beam-end moments need not be modified.

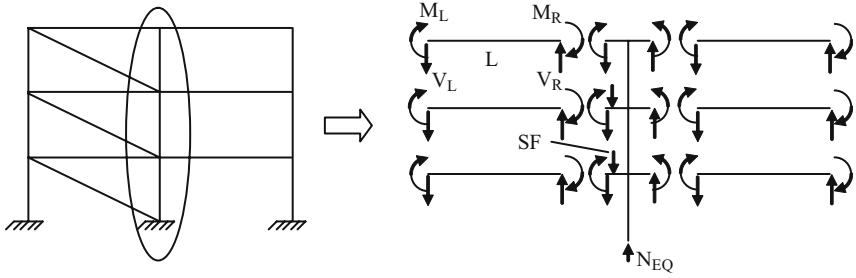

Figure 3. Calculation of axial forces of the columns due to earthquake loading

After modification of the beam-end moments considering BCCR values, the reserve moment at a beam end will be the difference between the modified end moment and the moment due to gravity loading. Using the reserve moments, beam-end shear forces, axial forces due to earthquake loading (N_{EQ}) and total axial forces (N) of the columns are updated. Then column moment capacities and BCCR values are recalculated.

2.2.3. *Decision on the Potential Yielding Member Ends (Step 5)*

If BCCR for a joint is larger than 1.1, column-ends are considered as the potential yielding member-ends. If BCCR is smaller than 0.9, beam-ends are considered as the potential yielding member-ends. Finally, if BCCR is between 0.9 and 1.1, all member ends connecting to the joint are considered to have yielding potential. The reason of using the numbers 0.9 and 1.1 is the possible errors due to the approximate calculation of the axial forces and moment capacities of the columns and BCCR values.

2.2.4. *Determination of the Base Shear Capacity*

Base shear capacity is calculated as a by-product of the capacity analysis. It is calculated by using the global moment equilibrium of the structure (Figure 4).

2.3. EQUIVALENT LINEAR SYSTEM

Combining the results of demand and capacity analysis, an equivalent linear structure with reduced stiffness is obtained. For this purpose, flexural demand-to-capacity ratios (DCR) are first calculated at all potential yielding member ends, by dividing the moments obtained from demand analysis to the moment capacities obtained from capacity analysis. The final distribution of yielding member ends is determined by using DCR values of the potential yielding

member ends. If DCR value at a potential yielding member end is larger than one, that member end is considered as yielding, else it is considered as nonyielding. In addition, bottom story column bases are considered as yielding member ends if they have DCR values exceeding one.

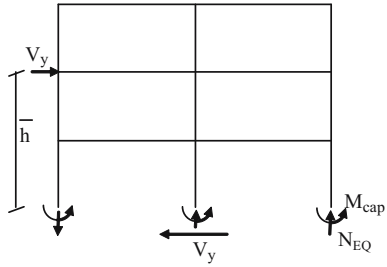

Figure 4. Calculation of base shear capacity using the global equilibrium of the structure

After the determination of final yielding distribution, flexural stiffness of members with yielding ends are reduced by reducing their moments of inertia.

2.3.1. *Reduction of Moment of Inertia (I) of a Member*

With the assumption that the beams and columns are prismatic members, "I" throughout the member is the same. This value is reduced depending on the DCR values and yielding of the member ends.

If there is no yielding at the member ends, "I" is not reduced. If there is yielding at both ends of a member, two assumptions are considered.

1. The inflection point of the member is at the middle (moments at the member ends are equal).
2. Inelastic chord rotation (θ_{in}) is equal to the elastic chord rotation (θ_e) in view of the equal displacement rule (Definition of chord rotation is expressed in Figure 5).

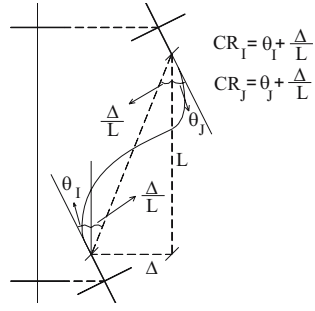

Figure 5. Definition of chord rotation at I and J ends of a frame member

Reduced stiffness can be represented by the slope of the line connecting the origin to the point (θ_{in}, M_y) in Figure 6.

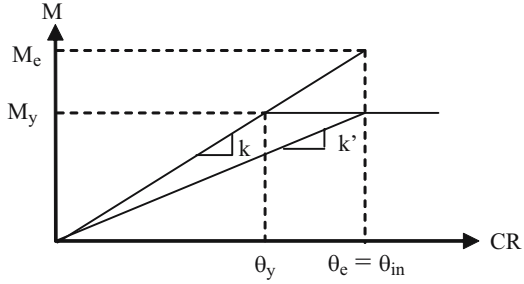

Figure 6. Relation between moment and chord rotation for elastic and elasto-plastic behaviors in case both ends yield

Considering the first assumption, Eq. (1) and Eq. (2) are obtained.

$$M_y = \left(6EI_{cr}/L\right)\theta_y \tag{1}$$

$$M_y = \left(6EI'/L\right)\theta_{in} \tag{2}$$

Considering the second assumption, Eq. (3) is obtained.

$$\theta_e = \theta_{in} \tag{3}$$

Substituting Eq. (3) into Eq. (2), Eq. (4) is obtained.

$$M_y = \left(6EI'/L\right)\theta_e \tag{4}$$

Substituting Eq. (4) into Eq. (1) and rearranging, Eq. (5) is obtained.

$$I_{cr}/I' = \theta_e/\theta_y \tag{5}$$

Considering Figure 6, Eq. (6) is obtained.

$$M_e/M_y = \theta_e/\theta_y \tag{6}$$

Demand-to-capacity ratio (DCR) is defined using Eq. (7).

$$DCR = M_e/M_y \tag{7}$$

Substituting Eq. (7) into Eq. (6), Eq. (8) is obtained.

$$\theta_e/\theta_y = DCR \tag{8}$$

Substituting Eq. (8) into Eq. (5) and rearranging, Eq. (9) is obtained.

$$I' = I_{cr}/DCR \tag{9}$$

Since the DCR values will be different at the two ends of a member, it is suitable to use the maximum DCR of the two ends in order to calculate the

reduced moment of inertia for the member. Hence, in Eq. (9), DCR is the maximum DCR value calculated from both ends, I_{cr} is the cracked section moment of inertia and I' is the reduced moment of inertia.

If there is yielding only at one end of a member, the reduction in the moment of inertia should be less than the case when both ends yield. In this case, same assumptions used in the case when both ends yield are also used. The reduced stiffness can be represented by the slope of the line connecting the origin to the point (θ_{in}, M_{eff}) in Figure 7.

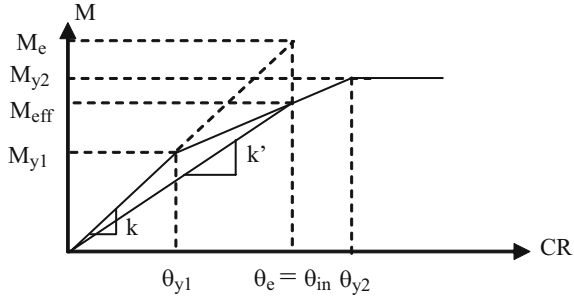

Figure 7. Relation between moment and chord rotation at the nonyielding end for elastic and elasto-plastic behaviors in case one end yields

Following a similar approach to the one indicated above, Eq. (10) is obtained for the reduced moment of inertia in case when one end yields.

$$I' = \frac{I_{cr}}{2} \cdot \left(1 + \frac{1}{DCR}\right) \tag{10}$$

where DCR is the DCR at the yielding end, I_{cr} is the cracked section moment of inertia and I' is the reduced moment of inertia. Reduced moments of inertia for different cases are summarized in Table 1.

TABLE 1. Reductions in the moment of inertia corresponding to different cases.

Case	Reduced Moment of Inertia
No yielding	I_{cr} [1]
Yielding at one end	$(I_{cr} / 2)(1+1 / DCR_Y{}^2)$
Yielding at both ends	$I_{cr} / MAX(DCR_I{}^3, DCR_J{}^4)$

[1] Cracked section moment of inertia, [2] DCR of the yielding end, [3] DCR at end I, [4] DCR at end J

2.4. LINEAR ELASTIC ANALYSIS OF THE EQUIVALENT LINEAR SYSTEM

A second modal spectrum analysis is performed by using the reduced stiffness values, similar to the procedure in section 2.1. The system is pushed to the same global displacement of the unreduced system. The procedure is presented

graphically in Figure 8. This procedure is based on the premise that elastic and inelastic global system displacements are similar, in line with the equal displacement rule. However, reducing the system stiffness from k_o to k_1 leads to a better prediction of inelastic member displacements by the equivalent linearization procedure. Chord rotations are obtained from the second analysis and compared with the chord rotation limits in order to determine the damage states of the members.

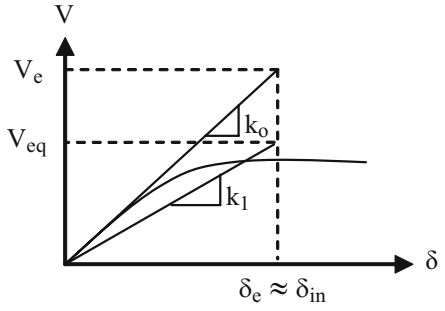

Figure 8. Relation between base shear and displacement for 1st and 2nd analysis

2.5. DECISION ON THE SEISMIC PERFORMANCE OF THE BUILDING

According to the obtained results, decision is made on the seismic performance of the building, depending on the base shear capacity, distribution of yielding member ends and the damage states of the members.

2.6. CONTROLLING SHEAR FAILURE

This procedure can be applied if no member or joint of the structure fails in shear. Therefore, the possibility of shear failure should be controlled. The possibility of shear failure for a member is controlled by comparing the maximum shear forces that can occur at the member-ends with the shear capacity of the member. Maximum shear forces are calculated by considering the free body diagrams of the members in the limit state. BCCR values at the joints should be considered for determination of the moments at the member-ends in the limit state. According to the BCCR value, if there is no yielding at the considered member-end, moment capacity should not be used as the member-end moment, instead the moment obtained by distributing the total moment capacities of the yielding member-ends connecting to the joint should be used. For the calculation of shear capacities, the decrease in the contribution of concrete to shear capacity with increasing curvature ductility should be taken into account (Park, 1998).

3. Case Study Buildings

The results obtained by employing the equivalent linearization procedure are compared with those obtained from nonlinear static analysis by using three case study buildings. Since nonlinear static analysis is based on a single mode, only the first mode is taken into account in the equivalent linearization procedure.

Case study 1 is an eight-story reinforced concrete residential building at Ceyhan, case study 2 is a four-story reinforced concrete building at Dinar and case study 3 is a five story reinforced concrete residential building at Duzce. Structural characteristics of the first two buildings and the observed damage during the 1998 Adana-Ceyhan and 1995 Dinar earthquakes can be found in Sucuoglu et al. (2004). Structural characteristics of the third building and the observed damage during the 1999 Duzce earthquake can be found in Bayili et al. (2002). All the buildings are modeled in 2D and analyzed with the simplified procedure by considering the Ceyhan ground motion of Adana-Ceyhan earthquake, Dinar ground motion of Dinar earthquake and Duzce ground motion of Duzce earthquake respectively.

4. Results

The results of the equivalent linearization procedure are compared with those obtained from pushover analysis using the software Drain-2DX (Prakash et al., 1993). Axial forces and moment capacities of the columns, distributions of yielding member ends, chord rotations at member ends and base shear capacities of buildings are compared. In the following text, results obtained from the equivalent linearization procedure are referred to as “estimated”.

4.1. AXIAL FORCES AND MOMENT CAPACITIES OF THE COLUMNS

Axial forces and moment capacities of the bottom story columns of the five story building at Duzce and four story building at Dinar are presented in Tables 2 and 3 respectively. Estimated axial forces of the columns of the five story building are in very good agreement with the pushover analysis results. Errors are somewhat larger for the columns of the four story building. This result is expected, because the five story building displays a nearly pure beam failure mechanism, whereas the four story building displays a mechanism close to a column failure mechanism. Since axial forces are calculated by using the shear forces that are transferred from the beams, shear forces and the axial forces are calculated more accurately for a structure displaying a beam failure mechanism. Errors in the axial forces are not reflected to the moment capacities except the

columns which are under tension, hence errors in the estimated moment capacities are generally small.

TABLE 2. Comparison of estimated axial forces (AF) and moment capacities (MC) of the bottom story columns of the five-story building at Duzce with those obtained from pushover analysis.

Label	AF Pushover (KN) (1)	AF Estimated (KN) (2)	Ratio (2/1)	MC Pushover (kNm) (3)	MC Estimated (KNm) (4)	Ratio (4/3)
C1	59	62	1.06	47	48	1.00
C2	335	346	1.03	65	65	1.01
C3	1685	1694	1.01	7845	7854	1.00
C4	282	265	0.94	61	60	0.98
C5	1549	1563	1.01	7429	7443	1.00
C6	329	331	1.01	64	65	1.00
C7	449	455	1.01	70	71	1.00
D1	91	91	1.01	49	49	1.00
D2	434	449	1.03	70	70	1.01
D6	91	91	1.01	49	49	1.00
D7	434	449	1.03	70	70	1.01

TABLE 3. Comparison of estimated axial forces (AF) and moment capacities (MC) of the bottom story columns of the four-story building at Dinar with those obtained from pushover analysis.

Label	AF Pushover (KN) (1)	AF Estimated (KN) (2)	Ratio (2/1)	MC Pushover (KNm) (3)	MC Estimated (KNm) (4)	Ratio (4/5)
B1	-230	-146	0.63	47	70	1.50
B2	610	532	0.87	267	255	0.96
B3	604	607	1.00	212	213	1.00
B4	472	440	0.93	178	177	1.00
B5	526	548	1.04	245	250	1.02
B6	502	534	1.06	67	69	1.03
A1	-132	-117	0.88	253	262	1.03
A2	557	577	1.04	68	69	1.01
A3	635	532	0.84	68	67	0.98
A4	488	575	1.18	64	69	1.07
A5	517	445	0.86	66	62	0.95
A6	450	502	1.11	64	67	1.04

4.2. BASE SHEAR CAPACITIES

Base shear capacities of the case study buildings calculated according to capacity analysis part of the equivalent linearization procedure are compared with the results of pushover analysis in Table 4. It is observed that the base shear capacity estimations are quite close to the pushover analysis results.

TABLE 4. Comparison of estimated base shear capacities with the pushover analysis results.

CASE	Pushover (KN)	Estimated (KN)	Estimated / Pushover
Eight Story Building	1 090	1 110	1.02
Four Story Building	736	746	1.01
Five Story Building Y	2 168	2 170	1.00
Five Story Building X	2 014	1 995	0.99

4.3. DISTRIBUTIONS OF YIELDING MEMBER ENDS

Estimated distributions of yielding member ends are generally consistent with the results of pushover analysis (Figures 9-11).

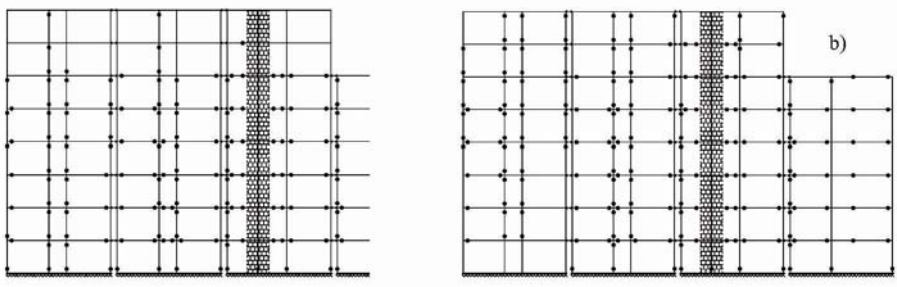

Figure 9. Comparison of distribution of yielding member ends at the eight story building at Ceyhan obtained with a) pushover analysis, b) equivalent linearization procedure

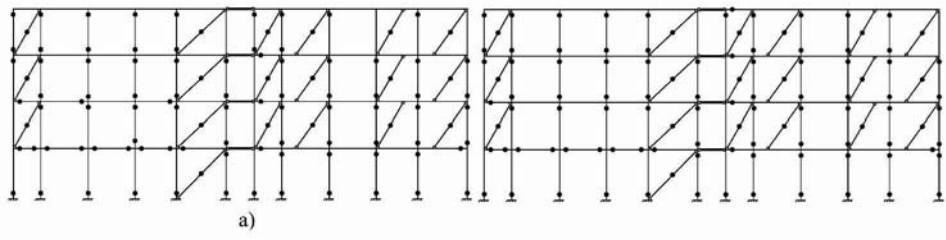

Figure 10. Comparison of distribution of yielding member ends at the four story building at Dinar obtained with a) pushover analysis, b) equivalent linearization procedure

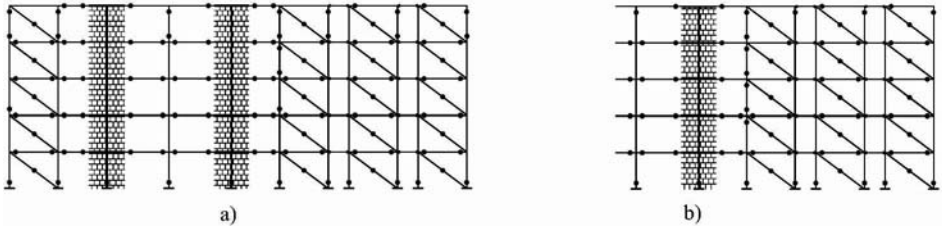

Figure 11. Comparison of distribution of yielding member ends for x direction model of the five story building at Duzce obtained with a) pushover analysis, b) equivalent linearization procedure

4.4. CHORD ROTATION ESTIMATIONS

Chord rotation estimations of the beam and column ends of the x-direction model of the five story building at Duzce are compared with the results of pushover analysis in Figures 12 and 13. In Figure 12, estimated chord rotations are obtained by conducting linear elastic analysis without stiffness reduction whereas in Figure 13, they are obtained by employing the equivalent linearization procedure. It can be observed that there is a significant improvement in the accuracy of the estimations obtained by reducing the stiffness. Chord rotations at the member ends of other case studies are plotted in Figures 14-16. Estimated chord rotations are generally in good agreement with those obtained from pushover analysis. Correlation coefficient is also provided at the inset of each figure, which is not a measure of one to one matching, but a measure of linear dependency.

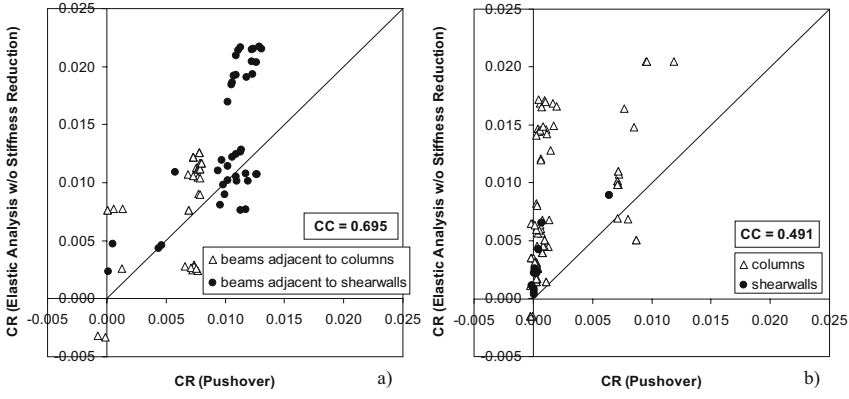

Figure 12. Comparison of chord rotations of a) beams, b) columns of the x direction model of the five-story building at Duzce obtained by employing pushover analysis and elastic analysis (no stiffness reduction)

5. Summary and Conclusions

An equivalent linearization procedure for displacement-based seismic assessment is developed in this study, in which standard linear elastic analysis is used in combination with the capacity principles. Results obtained by the application of this procedure are compared with the results of pushover analysis. It is observed that the base shear capacity is estimated quite close to the pushover analysis results. In addition, estimations of axial forces and moment capacities of the columns, distributions of yielding member ends and the chord rotations are sufficiently accurate. Considering that this procedure uses conventional linear elastic analysis which is simple, standard and familiar

to engineering professionals and that the amount of errors of the demand parameters obtained by the application of the procedure are small compared to pushover analysis results, it can be concluded that this procedure may serve as a simple seismic assessment procedure as an alternative to nonlinear analyses.

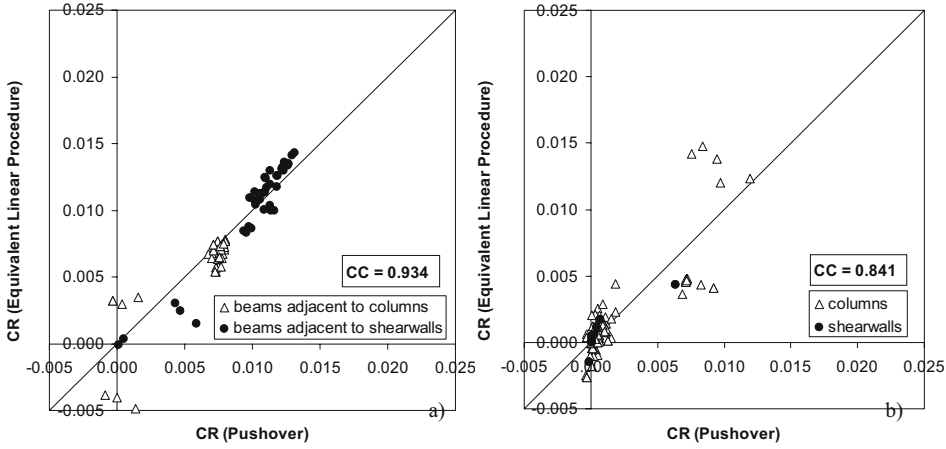

Figure 13. Comparison of chord rotations of a) beams, b) columns of the x direction model of the five story building at Duzce obtained by employing pushover analysis and equivalent linearization procedure

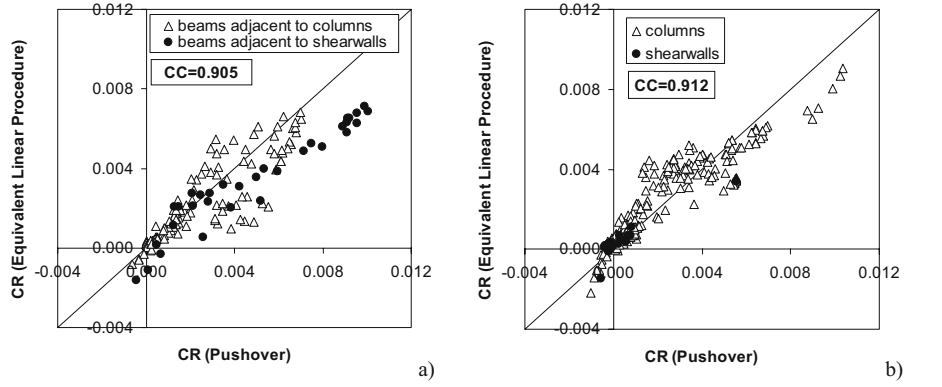

Figure 14. Comparison of chord rotations of a) beams, b) columns of the eight-story building at Ceyhan obtained by employing pushover analysis and equivalent linearization procedure

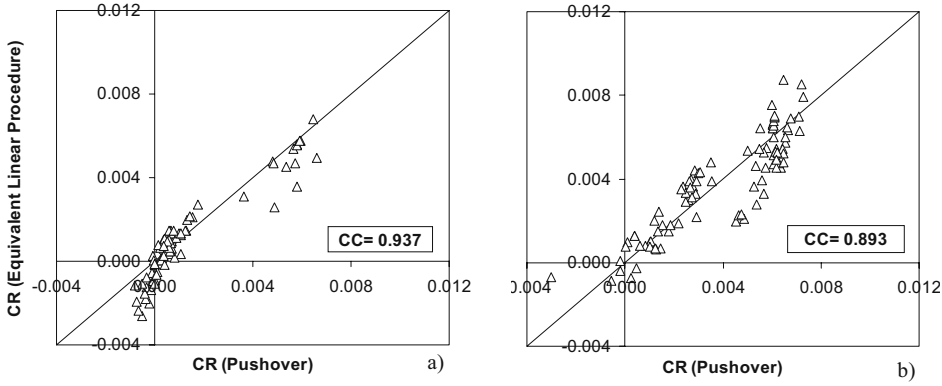

Figure 15. Comparison of chord rotations of a) beams, b) columns of the four-story building at Dinar obtained by employing pushover analysis and equivalent linearization procedure

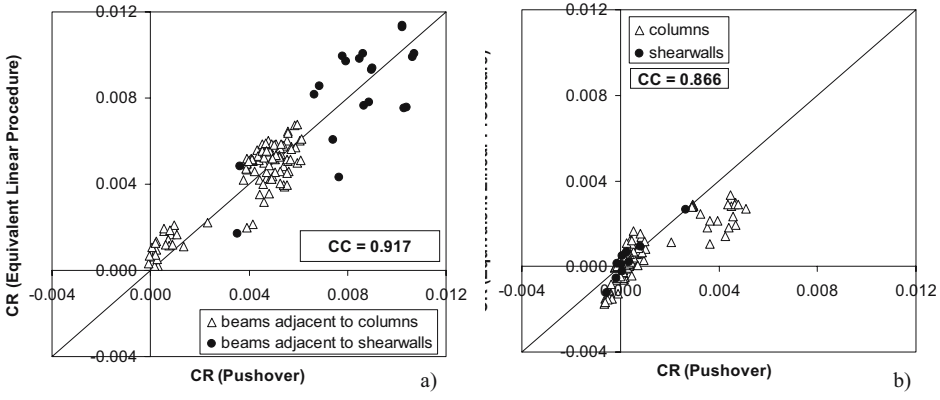

Figure 16. Comparison of chord rotations of a) beams, b) columns of the y direction model of the five-story building at Duzce obtained by employing pushover analysis and equivalent linearization procedure

References

Applied Technology Council, ATC-40, 1996, Seismic Evaluation and Retrofit of Concrete Buildings, Volume 1-2, Redwood City, California.

Bayili, S., 2002, Seismic Performance Assessment of a Residential Building in Duzce During the 12 November 1999 Duzce Earthquake, MS Thesis, Department of Civil Engineering, METU, Ankara.

Federal Emergency Management Agency, FEMA-356, 2000, Prestandard and Commentary for the Seismic Rehabilitation of Buildings, ASCE, Reston, Virginia.

Park, R., 1998, Seismic assessment and retrofitting of reinforced concrete buildings, in: Proceedings of the Fifth International Conference on Tall Buildings, Volume 1, Hong Kong, pp. 56-77.

Prakash V., Powell G.H., Campbell S., 1993, Drain-2DX Version 1.10 User Guide, Department of Civil Engineering, University of California, Berkeley, California.

Sucuoglu H., Gur T., and Gunay M.S., 2004, Performance based seismic rehabilitation of damaged R/C buildings, Journal of Structural Engineering, ASCE. 130(10):1475-1486.

Wight, J.K., Burak B., Canbolat, B.A., and Liang, X., 1999, Modeling and software issues for pushover analysis of RC structures, in: U.S.-Japan Workshop on Performance-Based Earthquake Engineering Methodology for Reinforced Concrete Building Structures, Maui, Hawaii, pp. 133-143.

A DISPLACEMENT-BASED ADAPTIVE PUSHOVER FOR ASSESSMENT OF BUILDINGS AND BRIDGES

RUI PINHO
European School for Advanced Studies in Reduction of Seismic Risk (ROSE School), Pavia, Italy

STELIOS ANTONIOU
SeismoSoft - Software Solutions for Earthquake Engineering

CHIARA CASAROTTI
European School for Advanced Studies in Reduction of Seismic Risk (ROSE School), Pavia, Italy

MANUEL LÓPEZ
European School for Advanced Studies in Reduction of Seismic Risk (ROSE School), Pavia, Italy

Abstract. Estimating seismic demands on structures requires consideration of inelastic behaviour: to this end, the use of nonlinear static pushover analyses, is inevitably going to be favoured over complex, impractical nonlinear time history methods. Currently employed pushover methods subject the structure to monotonically increasing lateral forces with invariant distribution until a target displacement is reached, based on the assumption that the response is controlled by the fundamental mode, unchanged after the structure yields. However, these invariant force distributions neither account for the contributions of higher modes to response, nor for the redistribution of inertia forces due to structural yielding and associated changes in vibration properties. To overcome drawbacks arising from conventional methods, an innovative displacement-based adaptive pushover technique for estimation of the seismic capacity of RC structures is illustrated. Analytical parametric studies on a suite of continuous multi-span bridges and framed buildings show that the novel approach can lead to the attainment of significantly improved predictions, which match very closely results from dynamic nonlinear analysis.

Keywords: displacement-based; adaptive pushover; DAP; buildings; bridges; drift.

S.T. Wasti and G. Ozcebe (eds.), Advances in Earthquake Engineering for Urban Risk Reduction, 79–94.

1. Introduction

A major challenge in performance-based engineering is to develop simple, yet accurate methods for estimating seismic demand on structures considering their inelastic behaviour: the use of nonlinear static procedures, or pushover analyses, is inevitably going to be favoured over complex, impractical for widespread professional use, nonlinear time-history methods.

It is observed that traditional pushover methods, prescribed in a number of seismic design codes for buildings, feature a number of drawbacks, mainly related to the impossibility of a fixed force pattern to accurately model the varying response characteristics of reinforced concrete structures subjected to strong transverse motion. On the contrary, the alternative, and most innovative, displacement-based adaptive pushover algorithm proposed is shown to lead to the attainment of significantly improved predictions, which match very closely results from dynamic nonlinear analysis.

The objectives of the present research are to verify the applicability of different pushover procedures, either adaptive or conventional, to RC structures. Analytical parametric studies have been conducted on a number of regular and irregular bridges and buildings: the effectiveness of each methodology in modelling both global behaviour and local phenomena is assessed by comparing static analysis results with the outcome of nonlinear time-history runs.

2. Pushover Methodologies in Earthquake Engineering

The term ‘pushover analysis’ describes a modern variation of the classical ‘collapse analysis’ method, as fittingly described by Kunnath (2004). The procedure consists of an incremental-iterative solution of the static equilibrium equations corresponding to a nonlinear structural model subjected to a monotonically increasing lateral load pattern. The structural resistance is evaluated and the stiffness matrix is updated at each increment of the forcing function, up to convergence. The solution proceeds until (i) a predefined performance limit state is reached, (ii) structural collapse is incipient or (iii) the program fails to converge. Within the framework of earthquake engineering, pushover analysis is employed with the objective of deriving an envelope of the response parameters that would otherwise be obtained through many possible dynamic analyses, corresponding to different intensity levels.

2.1. NONLINEAR STATIC PUSHOVER IN CURRENT PRACTICE

According to recently introduced code provisions, such as FEMA-356 (BCCS, 2000) and Eurocode 8 (CEN 2002), pushover analysis should consist of subjecting the structure to an increasing vector of horizontal forces with invariant pattern. Both the force distribution and target displacement are based on the assumptions that the response is controlled by the fundamental mode and the mode shape remains unchanged until collapse occurs. Two lateral load patterns, namely the first mode proportional and the uniform, are recommended to approximately bound the likely distribution of the inertia forces in the elastic and inelastic range, respectively.

However, a number of recent studies, summarised in the FEMA-440 (ATC, 2005) report, raise doubts on the effectiveness of these conventional force-based pushover methods in estimating the seismic demand throughout the full deformation range: (i) inaccurate prediction of deformations when higher modes are important and/or the structure is highly pushed into its nonlinear post-yield range, (ii) inaccurate prediction of local damage concentrations, responsible for changing the modal response, (iii) inability of reproducing peculiar dynamic effects, neglecting sources of energy dissipation such as kinetic energy, viscous damping, and duration effects, (iv) difficulty in incorporating three-dimensional and cyclic earthquake loading effects. Krawinkler and Seneviratna (1998) summarised the above with a single statement; fixed load patterns in pushover analysis are limiting, be they first modal or multimodal derived, because no fixed distribution is able of representing the dynamic response throughout the full deformation range.

2.2. THE NEW GENERATION OF PUSHOVER PROCEDURES

In an attempt to include higher modes effects, a number of Multi-Modal Inelastic Procedures (MMP) has been recently developed. These may be referred to as “pushover-based procedures”, as opposed to “pure pushover” analysis methods, since they estimate the seismic demand at one or more specific seismic levels (i.e. “individual point” on the pushover curve) rather than providing a structural capacity curve throughout the whole deformation range. Such methods essentially consist in performing conventional pushover analyses per each mode separately and then estimating the structural response by combining the action effects derived from each of the modal responses (alternatively, the “most critical mode” may be considered in isolation). Paret et al. (1996) first suggested the Multi-Modal Pushover procedure, which was then refined by Moghadam and Tso (2002). Chopra and Goel (2002), on the other hand, have developed and proposed a Modal Pushover Analysis (MPA)

technique, which Hernández-Montes et al. (2004) have then adapted into an Energy-based Pushover formulation.

Although the aforementioned methods constitute a significant improvement over traditional techniques, they still do not account for the damage accumulation, and resulting modification of the modal parameters, that characterise structural response at increasing loading levels. The latter motivated the recent development and introduction of the so-called *Adaptive Pushover* methods whereby the loading vector is updated at each analysis step, reflecting the progressive stiffness degradation of the structure induced by the penetration in the inelastic range. These methods, also termed as incremental response spectrum analysis by some researchers (e.g. Aydinoglu, 2003), can evidently consider the effects of the higher modes and of the input frequency content.

Adaptive procedures have been proposed by Bracci et al. (1997), Sasaki et al. (1998), Satyarno et al. (1998), Matsumori et al. (1999), Gupta and Kunnath (2000), Requena and Ayala (2000), Elnashai (2001), Antoniou et al. (2002), Aydinoglu (2003). The methodologies elaborated by latter four are conceptually identical, with the difference that Elnashai (2001) and Antoniou et al. (2002) implemented the procedure within a fibre analysis framework, allowing for a continuous, rather than discrete, force distribution update to be carried out.

These adaptive procedures have led to an improvement in the agreement between static and dynamic analysis results, thanks to the consideration of: (i) spectrum scaling, (ii) higher modes contributions, (iii) alteration of local resistance and modal characteristics induced by the accumulated damage, (iv) load updating according to the eigen-solutions from instantaneous nonlinear stiffness and mass matrix. However, despite such apparent conceptual superiority, or at least despite its conspicuously more elaborated formulation, the improvement introduced by current force-based adaptive pushover procedures is not-necessarily impressive, with respect to its traditional non-adaptive counterparts, particularly in what concerns the estimation of deformation patterns of buildings, which are poorly predicted by both types of analysis (e.g. Kunnath and John, 2000; Antoniou and Pinho, 2004a; ATC, 2005).

As shown by Kunnath (2004) and López-Menjivar (2004), the main reason for such underperformance seems to be the quadratic modal combination rules (SRSS, CQC) used in computing the adaptive updating of the load vector; these rules will inevitably lead to monotonically increasing load vectors, since the possibility of sign change in applied loads at any location is precluded, whilst it may be needed to represent the uneven redistribution of forces after an inelastic mechanism is triggered at some location. It is thus perhaps equally evident that in order to overcome such limitations, alternative modal combination schemes

should be derived and proposed. In their recent work, Kunnath (2004) and López-Menjivar (2004) make tentative proposals in such direction, which, however, cannot yet be considered as valid for general application.

2.3. DISPLACEMENT-BASED ADAPTIVE PUSHOVER

Antoniou and Pinho (2004b) have proposed, as an alternative solution to the problems highlighted in the previous paragraphs, a paradigm shift in pushover analysis, by introducing the innovative concept of displacement-based pushover. Contrarily to what happens in non-adaptive pushover, where the application of a constant displacement profile would force a predetermined and possibly inappropriate response mode, thus concealing important structural characteristics and concentrated inelastic mechanisms at a given location, within an adaptive framework, a displacement-based pushover is entirely feasible, since the loading vector is updated at each step of the analysis according to the current dynamic characteristics of the structure. And, indeed, this displacement-based pushover algorithm caters for the reproduction of reversal of storey shear distributions (Figure 1) even if a quadratic rule is employed to combine the contribution of the different modes, since the latter are here represented by their displacement vectors, with forces/shear coming as a result of the structural equilibrium to the applied displacement pattern.

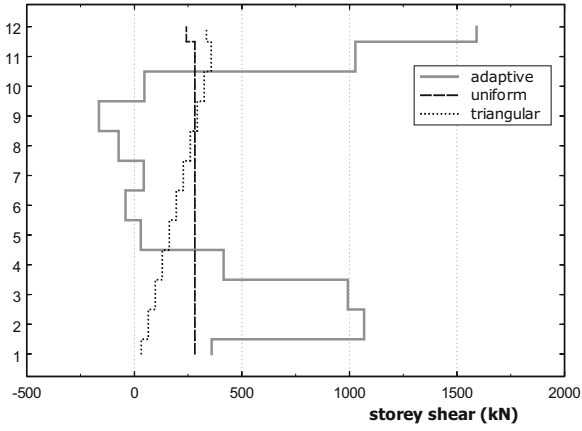

Figure 1. Storey shear distribution for a 12-storey building subjected to pushover analyses using (i) constant uniform force, (ii) constant triangular force and (iii) adaptive displacement loading vectors (Antoniou and Pinho, 2004b)

Hence, by adopting a displacement-based adaptive pushover, not only the attainment of more accurate results (deformation profiles and capacity curves) are warranted, but the entire structural assessment exercise becomes coherent with recent seismic design/assessment trends where the direct use of

displacements, as opposed to forces, is preferred as a recognition of the conspicuous evidence that seismic structural damage is in fact induced by response deformations. In addition, and as far as the effort of the modeler/engineer is concerned, the additional modelling and computational effort requested to run such type of analysis is, with respect to conventional pushover procedures, negligible.

3. Parametric Study

In the current work, the innovative displacement-based adaptive pushover procedure (DAP) proposed by Antoniou and Pinho (2004b) is assessed through an analytical comparative study involving different pushover methods, either single or multi mode, adaptive or conventional, and dynamic nonlinear analysis of reinforced concrete buildings and bridges. The "true" dynamic response is deemed to be represented by the results of the Incremental Dynamic Analysis procedure (IDA) (e.g. Vamvatsikos and Cornell, 2002), which is a parametric analysis method by which a structure is subjected to a series of nonlinear time-history analyses of increasing intensity.

Whilst the application of pushover methods in the assessment of building frames has been extensively verified in the recent past, nonlinear static analysis of bridge structures has been the subject of only limited scrutiny. Due to the marked difference of the two structural typologies, observations and conclusions withdrawn from studies on the latter cannot really be extrapolated to the case of the former, and two different approaches are therefore employed in the subsequent sections. In the case of buildings, the study aimed to explore the potentials of alternative and more effective rules in the proposed adaptive algorithm; for this reason, attention focused on output obtained from single accelerograms, as opposed to the statistical average of all cases, in order to spot structural response peculiarities introduced by individual motions without being smoothed out through results averaging. The dearth of research data, within the framework of bridge applications, implied instead the need of a first comprehensive parametric study, whereby a suite of bridge configurations subjected to a large ensemble of seismic records is analysed in a more statistical perspective.

The Finite Elements Analysis package used in the present work, SeismoStruct (SeismoSoft, 2005), is a fibre-element based program for seismic analysis of framed structures, which can be freely downloaded from the Internet. The program is capable of predicting the large displacement behaviour and the collapse load of framed structural configurations under static or dynamic loading, accounting for geometric nonlinearities and material inelasticity. Its accuracy in predicting the seismic response of building and

bridge structures has been demonstrated through comparisons with experimental results derived from pseudo-dynamic tests carried out on full or large-scale models (e.g. Pinho and Elnashai, 2000; Casarotti, 2004). Further, the package features also the readily availability of the displacement-based adaptive pushover algorithm employed in this study.

3.1. BUILDING PARAMETRIC STUDY

Three different configurations of common RC structures were employed: a 12 storey regular frame, an eight storey irregular frame and a dual wall-frame system. The latter are based on buildings previously designed for different ductility classes and design ground acceleration, on medium soil type 'B' of EC8 (Fardis, 1994), resulting in a total of 12 models, as described in Table 1. The overall plan dimensions of the three configurations are 15m by 20m. The storey height is 3m except the first storey of the irregular set, which is 4.5m high. A detailed description of models and load conditions, as well as of their FE modelling, can be found in López-Menjivar (2004).

TABLE 1. Considered building systems

Structural System	Storeys (Height)	Structure Reference	Ductility Level	Design PGA (g)	Behavior Factor (q)	Tuncracked (s)
Regular Frame	12 (36 m)	RH30	High	0.30	5.00	0.697
		RM30	Medium		3.75	0.719
		RM15	Medium	0.15	3.75	0.745
		RL15	Low		2.50	0.740
Irregular Frame	8 (25.5 m)	IH30	High	0.30	4.00	0.565
		IM30	Medium		3.00	0.536
		IM15	Medium	0.15	3.00	0.613
		IL15	Low		2.00	0.614
Regular Wall-Frame	8 (24 m)	WH30	High	0.30	3.50	0.569
		WM30	Medium		2.625	0.557
		WM15	Medium	0.15	2.625	0.601
		WL15	Low		1.75	0.588

Four input time-histories, consisting of one-artificially generated accelerogram (A975) and three natural records (Loma Prieta earthquake, USA, 1989), were employed: the selection of these four records aimed at guaranteeing a wide-ranging type of earthquake action, in terms of frequency content, peak ground acceleration, duration and number of high amplitude cycles (Antoniou et al., 2002). Upper and lower bounds of the main characteristics of the records are summarised in Table 2, where the significant duration is defined as the

interval between the build up of 5% and 95% of the total Arias Intensity (Bommer and Martinez-Pereira, 1999).

TABLE 2. Bounding characteristics of the employed set of records for buildings

	Peak Ground Acceleration	Peak Response Acceleration	5% Arias Intensity threshold	Significant Duration teff	Total Duration ttot	teff / ttot
Min	0.12 g	0.50 g	1.02 s	7.24 s	10.0 s	22.3%
Max	0.93 g	4.25 g	11.23 s	10.43 s	40.0 s	72.4%

3.1.1. *Analyses and result post-processing*

The two non-adaptive pushover schemes, proposed in the NEHRP Guidelines (ATC, 1997), were applied to each set of buildings: the uniform distribution, whereby lateral forces are proportional to the total mass at each floor level, and the triangular distribution, in which seismic forces are proportional to the product of floor mass and storey height. The adaptive pushover algorithm was used in both its force and displacement-based variants, with spectrum scaling, employing SRSS or CQC modal combination rules.

It is noteworthy that the DAP procedure employed in this building parametric study made use of the interstorey drift-based scaling algorithm, whereby maximum interstorey drift values obtained directly from modal analysis, rather than from the difference between not-necessarily simultaneous maximum floor displacement values, are used to compute the scaling displacement vector. This comes as a reflection of the fact that the maximum displacement of a particular floor level, being essentially the relative displacement between that floor and the ground, provides insufficient insight into the actual level of damage incurred by buildings subject to earthquake loading. On the contrary, interstorey drifts, obtained as the difference between floor displacements at two consecutive levels, feature a much clearer and direct relationship to horizontal deformation demand on buildings. Readers are referred to the work of Antoniou and Pinho (2004b) for further details on this formulation.

The inter-storey drift profiles obtained from each pushover analysis are compared to the drift profiles from the nonlinear dynamic analysis and the standard error of the pushover results, with respect to the dynamic, is calculated as:

$$\text{Error}\,(\%) = 100\sqrt{\frac{1}{n}\sum_{1}^{n}\left(\frac{\Delta_{iD}-\Delta_{iP}}{\Delta_{iD}}\right)} \qquad (1)$$

The interstorey drift profiles are monitored at four different deformation levels: the pre-yield state (0.5% total drift), the point of global yielding (1.0% and 1.5%), where the stiffness changes significantly and the local distributions are rapidly updated, and the deeply inelastic range (2.5%).

The Standard Error of the non-adaptive and adaptive pushover schemes was computed for all the structures and earthquakes that the authors used in their research. In order to spot the presence of possible response peculiarities introduced by individual input motions but smoothed out through results averaging, the standard error is given separately for each time history analysis, as a unique value, averaging the standard error of all the storeys, in the building, and deformation levels.

3.1.2. *Obtained results*

The Mean Standard Error of the DAP, FAP, Triangular and Uniform pushovers, considering all structures and ground motions, are 19.11%, 30.90%, 21.11% and 38.76%, respectively. These overall results seem to indicate only a marginal advantage of DAP with respect to non-adaptive triangular distribution. However, a closer inspection of interstorey drift profiles (Figure 2a) and capacity curves (Figure 2b) for some particularly difficult cases, renders much more conspicuous the gains provided by the employment of displacement-based adaptive pushover in the prediction of the seismic demand/capacity of framed buildings subjected to seismic action.

3.2. BRIDGES PARAMETRIC STUDY

The parametric study has considered two bridge lengths (50 m spans), with regular, irregular and semi-regular layout of the pier heights and with two types of abutments; (i) continuous deck-abutment connections supported on piles, exhibiting a bilinear behaviour, and (ii) deck extremities supported on pot bearings featuring a linear elastic response. The total number of bridges is therefore twelve, as shown in Figure 3, where the label numbers 1, 2, 3 characterise the pier heights of 7 m, 14 m and 21 m, respectively.

A sufficiently large number of records have been employed so as to bound all possible structural responses. The employed set of seismic excitation is defined by an ensemble of 14 large magnitude (6-7.3) small distance (13-30 km) records selected from a suite of historical earthquakes scaled to match the 10% probability of exceedance in 50 years uniform hazard spectrum for Los Angeles (SAC Joint Venture, 1997). The bounding characteristics of the records are summarized in Table 3. Further details on modelling and input can be found in Casarotti (2004).

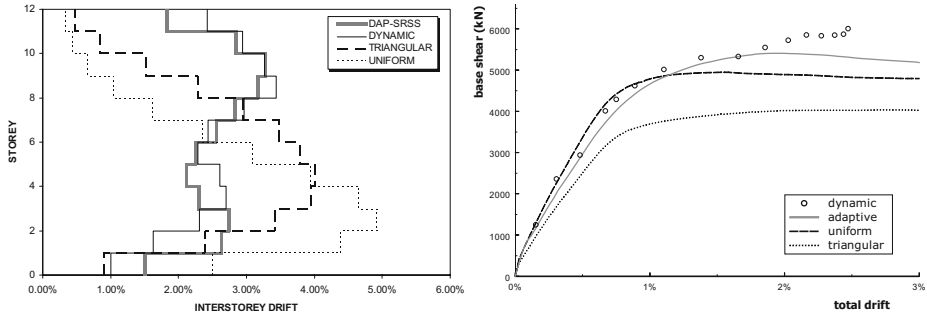

(a) (b)

Figure 2. Representative results obtained with model RM15 subjected to one of the natural accelerograms employed in this study (Hollister)

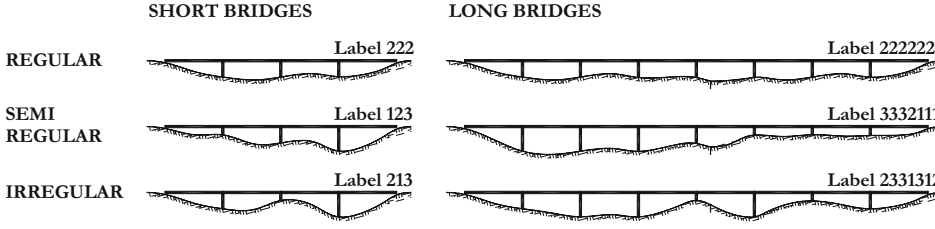

Figure 3. Analysed Bridge Configurations

TABLE 3. Bounding characteristics of the employed set of records for bridges

	Peak Ground Acceleration	Peak Response Acceleration	5% Arias Intensity threshold	Significant Duration teff	Total Duration ttot	teff / ttot
Min	0.30 g	0.84 g	1.25 s	5.3 s	14.95 s	9%
Max	1.02 g	3.73 g	12.5 s	19.66 s	80.00 s	52%

3.2.1. *Analyses and result post-processing*

The response of the bridge models is estimated through the employment of Incremental Dynamic Analysis (IDA), Force-based Conventional Pushover with uniform load distribution (FCPu), Force-based Conventional Pushover with first mode proportional load pattern (FCPm), Force-based Adaptive Pushover with Spectrum Scaling (FAP) and Displacement-based Adaptive Pushover with Spectrum Scaling (DAP). Results are presented in terms of the bridge capacity curve, i.e. a plot of the reference point displacement versus total base shear, and of the deck drift profile.

Each level of inelasticity is represented by the deck centre drift, selected as independent damage parameter, and per each level of inelasticity the total base shear Vbase and the displacements Δi at the other deck locations are monitored. Results of pushover analyses are compared to the IDA median value out of the responses to the 14 records, of each response quantity R, be it total base shear or deck drift:

$$\hat{R}_{i,\,IDA} = \text{median}_{j=1:14}\left[R_{i,j-IDA}\right] \tag{2}$$

Pushover analyses with spectrum scaling (i.e. adaptive pushovers) are statistically treated in an analogous way: medians of each response quantity represent that particular pushover analysis (i.e. FAP or DAP) with spectrum scaling. Finally, the results of each type of pushover are normalized with respect to the corresponding "exact" quantity obtained from the IDA medians, as schematically illustrated in Figure 4, and translated in Eq. (3). Representing results in terms of ratios between the "approximate" and the "exact" procedures, immediately indicates the bias in the approximate procedure, as the ideal target value of the different pushovers is always one.

$$\overline{R}_{i,\,PUSHOVERtype} = \frac{R_{i,PUSHOVERtype}}{\hat{R}_{i,IDA}} \cdots \xrightarrow[\text{ideally}]{} 1 \tag{3}$$

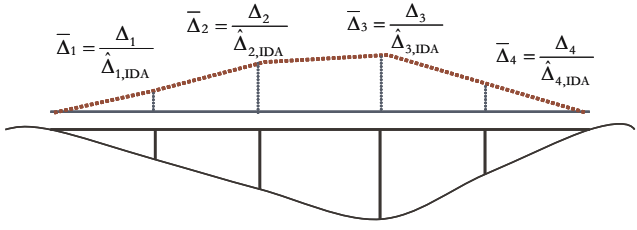

Figure 4. Normalised Transverse Deformed Pattern

Given that fact that a "realistic" capacity curve does not imply reliable estimations of the inelastic displacement pattern at increasing levels of inelasticity, the control of the deformed pattern is of the same relevance of the capacity curve prediction.

Having the same unitary target value, all normalized deck displacements become comparable, and a bridge index BI can measure the precision of the obtained deformed shape. Per each level of inelasticity, such bridge index is defined as the median of results over the m deck locations (Eq. 4a), with the standard deviation measuring the dispersion with respect to the median (Eq. 4b). The latter indicates the stability of the estimate of displacements along the deck: a small scatter means that predicted normalised displacements along the deck are averagely close to their median value BI.

$$BI_{i,\,PUSHOVERtype} = median_{i=1:m}\left(\overline{\hat{\Delta}}_{i,PUSHOVERtype}\right) \tag{4a}$$

$$\delta_{PUSHOVERtype} = \sqrt{\frac{\sum_{i=1}^{m}\left(\overline{\hat{\Delta}}_{i,PUSHOVERtype} - BI_{PUSHOVERtype}\right)^2}{m-1}} \tag{4b}$$

3.2.2. *Obtained results*

Current code recommendations require performing pushover analysis by pushing the entire structure with distributed load. In case of bridges, the additional option of pushing only the deck has been investigated, observing that the superstructure is the physical location where the most of the structural mass, i.e. the source of the inertia forces on the bridge, is usually concentrated and where it is relatively free to be excited. A preliminary investigation indicated a significant improvement in terms of stability and velocity of analysis in case of DAP and a very poor influence on results with the application of the latter option, which is thus recommended and employed in the parametric study.

Two main pertinent observations can be withdrawn from a scrutiny of the capacity curves obtained by the different pushover analyses in Figure 5: first, FCPm tends to significantly underestimate the structural stiffness, mainly due to the fact that, for the same base shear, central deck forces are generally higher compared to the other load patterns, thus results in larger displacement at that location. Then, on occasions, a "hardening effect" in the pushover curve occurs, which is sometimes reproduced only by employing DAP: once piers saturate their capacity, abutments absorb the additional seismic demand, proportionally increasing shear response and hardening the capacity curve.

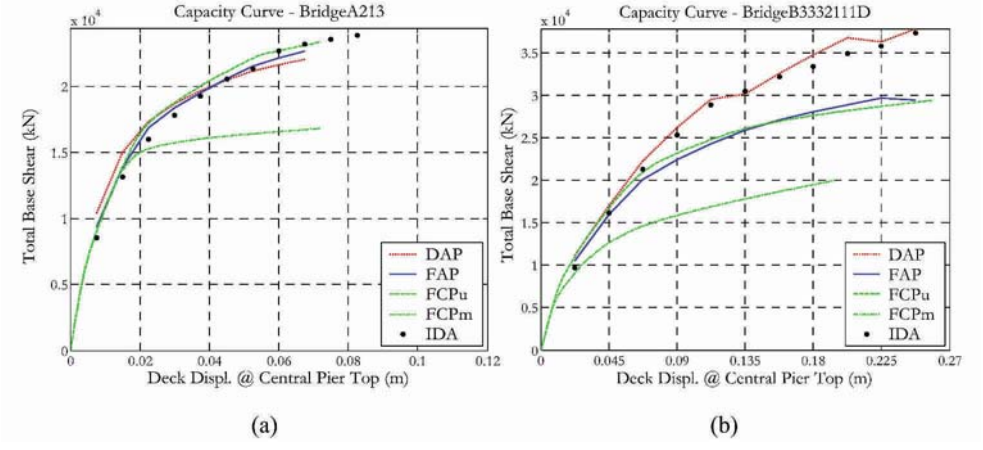

Figure 5. Capacity curve results

In Figure 6, the Bridge Index, as computed at each level of deck centre drift, is plotted as black filled marks so as to cater for an easier comparison with the IDA-normalised deck displacements, represented as empty marks in the background. In this manner, it results immediately apparent the level with which each pushover analysis is able to capture the deformed pattern of the whole bridge, at increasing deformation levels. For the sake of succinctness, only two analysis types are considered, FCPm and DAP, which are those leading to the worst and best predictions, respectively.

Table 4 provides global averages of means, maximum and minimum values of BI and respective dispersion as well as of the normalised total base shear, over the whole bridge ensemble. It is noted that FCPm heavily underestimates predictions, featuring also a very high BI dispersion value, (ii) FCPu performs very well for regular bridges and underestimating otherwise, (iii) DAP features the best overall behaviour, despite the slight underprediction of deformed shape values, with the lowest values of scatter.

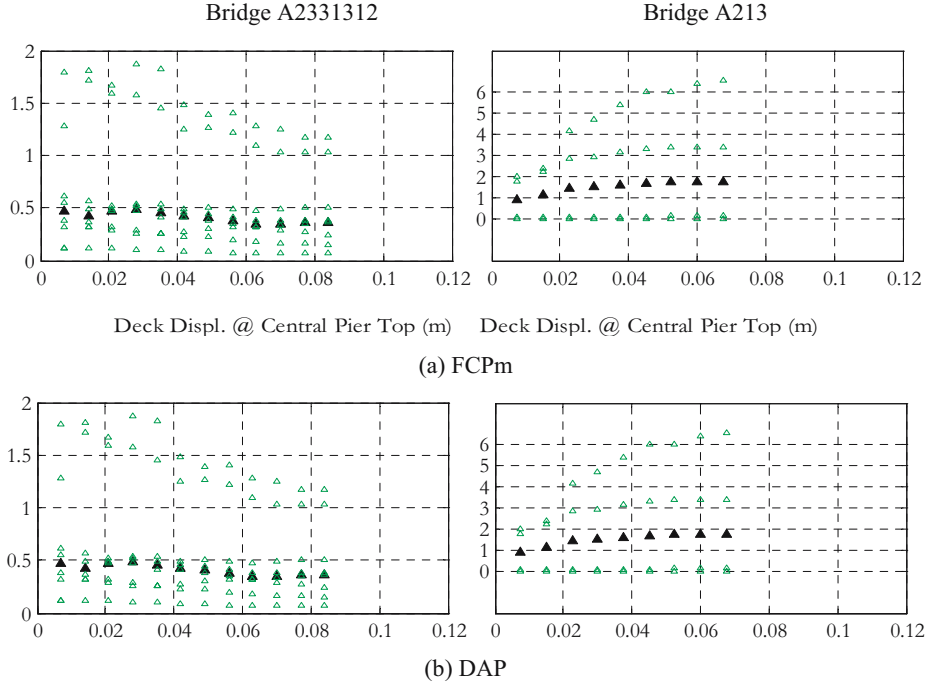

Figure 6. Prediction of the deformed pattern: BI and relative scatter

4. Concluding Remarks

Given that current performance-based design trends require simple, yet accurate methods for estimating seismic demand on structures considering their full inelastic behaviour, in the current work the effectiveness of pushover analysis applied to buildings and bridges has been investigated. In particular, the effectiveness of applying a displacement-based adaptive pushover to estimate the seismic response of buildings and bridges subjected to earthquake action was investigated.

TABLE 4. Global averages of the summaries of results

Means	Bridge Index			Dispersion			Normalised Base Shear		
	Mean	Min.	Max.	Mean	Min.	Max.	Mean	Min.	Max.
FCPm	0.74	0.57	0.92	0.79	0.58	1.00	0.80	0.69	0.95
FCPu	0.87	0.75	1.03	0.24	0.17	0.34	1.03	0.92	1.18
FAP	0.88	0.78	1.01	0.22	0.13	0.34	0.99	0.89	1.10
DAP	0.87	0.78	0.99	0.19	0.14	0.27	1.03	0.95	1.13

It was observed that the employment of such an innovative adaptive pushover technique lead to the attainment improved response predictions, throughout the entire deformation range, in comparison to those obtained by force-based methods, either adaptive or conventional. Indeed, prediction of the global behaviour (capacity curves), as well as of the deformed shapes and shear/moment distributions, proved to be very effective.

In other words, within the scope of buildings and bridge applications, whereas the application of a fixed displacement pattern is a commonly agreed conceptual fallacy, the present work witnesses not only the feasibility of applying an adaptive displacement profile, but also its practical advantages, with respect to other pushover methods.

It is important to observe that a static procedure will never be able to completely replace a dynamic analysis; nevertheless, a methodology has been searched to obtain response information reasonably close to that predicted by the nonlinear dynamic analyses. The innovative displacement-based adaptive pushover method is therefore shown to constitute an extremely appealing displacement-based tool for structural assessment, fully in line with the recently introduced deformation- and performance-oriented trends in the field of earthquake engineering.

Of equally noteworthy status is perhaps the fact that the proposed adaptive pushover schemes are as simple to use as standard pushover methods and have been implemented in an Internet-downloadable Finite Element program, adequate for general usage, and thus rendering the presented analytical methodologies readily available to the practicing and research communities.

ACKNOWLEDGEMENTS

Part of the current work has carried out under the financial auspices of the European Commission through the FP6 Integrated Project LESSLOSS (Risk Mitigation for Earthquakes and Landslides). Such support is gratefully acknowledged by the authors.

References

Antoniou, S., Rovithakis, A., Pinho, R., 2002, Development and verification of a fully adaptive pushover procedure, *Proceedings of the Twelfth European Conference on Earthquake Engineering*, London, UK, Paper No. 822.

Antoniou S. and Pinho, R., 2004a, Advantages and limitations of adaptive and non-adaptive force-based pushover procedures, *Journal of Earthquake Engineering*, **8**(4):497-522.

Antoniou, S., Pinho, R., 2004b, Development and verification of a displacement-based adaptive pushover procedure, *Journal of Earthquake Engineering*, **8**(5):643-661.

Applied Technology Council, 2005, *Improvement of Nonlinear Static Seismic Analysis Procedures*, FEMA-440, ATC, California, USA.

Applied Technology Council, 1997, *NEHRP "Guidelines for the seismic rehabilitation of buildings*, FEMA Report No. 273, Federal Emergency Management Agency, Applied Technology Council, Washington D.C.

Aydinoglu, M.N., 2003, An incremental response spectrum analysis procedure based on inelastic spectral deformation for multi-mode seismic performance evaluation, *Bulletin of Earthquake Engineering*, **1**:3-36.

Bommer, J.J., Martinez-Pereira, A., 1999, The effective duration of earthquake ground motion, *Journal of Earthquake Engineering*, **3**(2):127-17.

Bracci, J.M., Kunnath, S.K., Reinhorn, A.M., 1997, Seismic performance and retrofit evaluation for reinforced concrete structures, *ASCE Journal Structural Engineering*, **123**(1):3-10.

Building Seismic Safety Council, 2000, *Prestandard and Commentary for the Seismic Rehabilitation of Buildings*, FEMA-356, BSSC, Washington D.C., USA

Casarotti, C., 2004, *Adaptive pushover-based methods for seismic assessment and design of bridge structures*, PhD Thesis, European School for Advanced Studies in Reduction of Seismic Risk (ROSE School), University of Pavia, Italy

Chopra, A.K., Goel, R.K., 2002, A modal pushover analysis procedure for estimating seismic demands for buildings, *Earthquake Engineering and Structural Dynamics*, **31**:561-582.

Comité Europeen de Normalization (2002) *Eurocode 8: Design of Structures for Earthquake Resistance - Part 2: Bridges*, PrEN 1998-2: 2003, 2 April 2002, CEN, Brussels, Belgium

Elnashai, A.S., 2001, Advanced inelastic static (pushover) analysis for earthquake applications, *Structural Engineering and Mechanics*, **12**(1):51-69.

Fardis, M.N., 1994, *Analysis and design of reinforced concrete buildings according to Eurocode 2 & 8. Configuration 3, 5 and 6*, Reports on Prenormative Research in Support of Eurocode 8.

Gupta, B., Kunnath, S.K., 2000, Adaptive spectra-based pushover procedure for seismic evaluation of structures, *Earthquake Spectra*, **16**(2):367-392.

Hernández-Montes, E., Kwon, O-S, Aschheim, M., 2004, An energy-based formulation for first and multiple-mode nonlinear static (pushover) analyses, *Journal of Earthquake Engineering*, **8**(1):69-88.

Krawinkler, H., Seneviratna, G.D.P.K., 1998, Pros and cons of a pushover analysis of seismic performance evaluation, *Engineering Structures*, **20**(4-6):452-64.

Kunnath, S.K., 2004, Identification of modal combination for nonlinear static analysis of building structures, *Computer-Aided Civil and Infrastructure Engineering*, **19**:246-259.

Kunnath, S.K., John, A. Jr., 2000, Validity of static procedures in performance-based seismic design, *Proceedings of ASCE Structures Congress*, Philadelphia, USA.

López-Menjivar, M.A., 2004, *Verification of a displacement-based Adaptive Pushover method for assessment of 2-D Reinforced Concrete Buildings*, PhD Thesis, European School for Advances Studies in Reduction of Seismic Risk (ROSE School), University of Pavia, Italy.

Matsumori, T., Otani, S., Shiohara, H., Kabeyasawa, T., 1999, Earthquake member deformation demands in reinforced concrete frame structures, *Proceedings of the US-Japan Workshop on Performance-Based Earthquake Engineering Methodology for R/C Building Structures*, PEER Center Report, UC Berkeley - 79-94, Maui, Hawaii.

Moghadam, A.S., and Tso, W.K., 2002, A pushover procedure for tall buildings, *Proceedings of the Twelfth European Conference in Earthquake Engineering*, London, UK, Paper 395.

Paret, T.F., Sasaki, K.K., Eilbeck, D.H., Freeman, S.A., 1996, Approximate inelastic procedures to identify failure mechanisms from higher mode effects, *Proceedings of the Eleventh World Conference in Earthquake Engineering*, Acapulco, Mexico, Paper 966.

Pinho, R., Elnashai, A.S., 2000, Dynamic collapse testing of a full-scale four storey RC frame, *ISET Journal of Earthquake Engineering*, Special Issue on Experimental Techniques, **37**(4):143-164.

Requena, M., Ayala, G., 2000, Evaluation of a simplified method for the determination of the nonlinear seismic response of RC frames, *Proceedings of the Twelfth World Conference on Earthquake Engineering*, Auckland, New Zealand, Paper No. 2109.

SAC Joint Venture, 1997, *Develop Suites of Time Histories*, Project Task: 5.4.1, Draft Report, March 21, 1997, Sacramento, CA, USA

Sasaki, K.K., Freeman, S.A., Paret, T.F., 1998, Multi-mode pushover procedure (MMP) - a method to identify the effects of higher modes in a pushover analysis, *Proceedings of the Sixth US National Conference on Earthquake Engineering*, Seattle, Washington – Earthquake Engineering Research Institute, Oakland, California.

Satyarno, I., Carr, A.J., Restrep,o J., 1998, Refined pushover analysis for the assessment of older reinforced concrete buildings, *Proceedings of the New Zealand Society for Earthquake Engineering Technology Conference*, Wairakei, New Zealand, pp. 75-82.

Seismosoft, 2004, Seismostruct - A Computer Program for Static and Dynamic nonlinear analysis of framed structures [online], available from URL: http//www.seismosoft.com.

Vamvatsikos, D., Cornell, C.A., 2002, Incremental dynamic analysis, *Earthquake Engineering Structural Dynamics*, **31**(3):491-514.

IN DEFENCE OF ZEYTINBURNU

GUNEY OZCEBE
Middle East Technical University, Department of Civil Engineering, 06531, Ankara

HALUK SUCUOGLU
Middle East Technical University, Department of Civil Engineering, 06531, Ankara

M. SEMIH YUCEMEN
Middle East Technical University, Earthquake Engineering Research Center, Department of Civil Engineering, 06531, Ankara

AHMET YAKUT
Middle East Technical University, Department of Civil Engineering, 06531, Ankara

Abstract. A multiple level assessment of the seismic vulnerability of several thousand buildings in Zeytinburnu, a district in Istanbul with much deficient construction, is presented. Consistent results are obtained from walkdown surveys as well as sophisticated two tier discriminant analyses developed within the framework of NATO SfP project SfP977231.

Keywords: regional assessment; seismic risk; Zeytinburnu

1. Introduction

In the past, severe earthquakes in Turkey and elsewhere have caused extensive losses of life and property. In many countries, even medium size events occurring near densely populated areas may lead to considerable casualties and economic losses. This also applies to the developed regions of the world. For instance in the last 15 years, almost 5,000 people have died in earthquakes occurring in Europe. The 1980 Irpinia Earthquake, with a magnitude of 6.9 in Richter scale, struck Italy, killing 4,580 people and leaving 250,000 without

S.T. Wasti and G. Ozcebe (eds.), Advances in Earthquake Engineering for Urban Risk Reduction, 95–116.

shelter. More recently, on 7 September 1999, an earthquake of magnitude 5.9 on the Richter scale hit Athens. After a week of search and rescue, 143 people were confirmed dead, either in collapsed buildings or by falling elements of buildings or by heart attacks. In this event more than 750 people were injured and thousands of families became homeless. Most recently, in the 1999 Kocaeli earthquake (Richter magnitude of 7.4) the poor performance of vulnerable buildings claimed more than 20,000 lives. These examples emphasize the high vulnerability of the urban environment in earthquake prone regions.

Since the main cause of casualties and other losses during past earthquakes is the poor performance of existing buildings, the determination of the addresses of seismically vulnerable buildings within the existing building stock is a high priority task in the seismic risk reduction of the urban environment. Over the last decade, a lot of effort has been devoted to the problem of how to devise reliable estimates, given the large uncertainties in the pattern of earthquake occurrence, both in time and space and our limited understanding of behavior of the vulnerable elements of the built environment.[1-7] In some of these studies, because of various uncertainties and randomness involved both in seismic demand and capacity, assessment of potential damage is based on statistical and probabilistic techniques.

Current seismic vulnerability evaluation methods can be classified in three main groups depending on their level of complexity. The first level, being the least complex one, is known as "Walkdown Evaluation." First level does not require any analysis and it relies on the past performance of similar buildings. The goal of the walkdown evaluation is to determine the priority levels of buildings that require immediate intervention. This evaluation is applied to all structures in the region for which the assessment is made. The procedures given by FEMA 154[8], FEMA 310[9] Tier 1 and the procedure developed by Sucuoglu and Yazgan[10] are examples of walkdown survey procedures.

Preliminary assessment methodologies are applied when more in-depth evaluation of building stocks is required. These methodologies are generally applied to buildings that are classified in the high-risk group at the end of the first level evaluation, i.e. walkdown evaluation. In this stage, simplified analysis of the building under investigation is performed based on a variety of methods. These analyses require data on the dimensions of the structural and nonstructural elements in the most critical story (generally the ground story). The procedures by FEMA 310[9] Tier 2 and Ozcebe et al.[6] (later complemented by Yakut et al.[7]) can be listed as the examples of preliminary survey procedures. The time needed for a preliminary evaluation of a particular building is about three to four hours. With a trained group of engineers and technicians it is possible to survey large building stocks by employing the preliminary evaluation methodologies within a reasonable time span.

In the third level assessment we have the final (or detailed) vulnerability assessment procedures. The procedures in this group employ linear or nonlinear analyses of the building under consideration. For this reason these procedures require the as-built dimensions and the reinforcement details of all structural elements. Moreover, the layouts of the structural system as well as the mechanical properties of the materials are also needed for the analyses. In general, the buildings that cannot be classified in the first two levels are evaluated in this final stage. The time needed for final evaluation of a particular structure can range from a couple of days to several weeks. The procedures proposed in FEMA 356[11], ATC 40[12], EUROCODE 8[13] and those by Sucuoglu et al.[14] and Park and Ang[15] are examples of third level assessment procedures.

2. The Objective and Scope

The built environment of Istanbul alone consists of about 1,000,000 buildings. It is anticipated that some 50,000 to 70,000 buildings in Istanbul are expected to experience severe damage or collapse if the probable scenario earthquake occurs.[16] Considering that Istanbul is under very high seismic risk, the occurrence of an earthquake with a magnitude of 7 or more on the Richter scale would cause a serious burden on Turkey's development.

Within the scope of NATO Science for Peace project "*NATO SfP977231-Seismic Assessment and Rehabilitation of Existing Buildings*" the tools deemed to be essential for the seismic safety assessment in regional and/or individual scales have been developed and made available to the profession.[6,7]

This paper summarizes the activities of the Middle East Technical University-Earthquake Engineering Research Center (METU-EERC) faculty in this context. METU-EERC is currently leading the pilot implementation of the *"Earthquake Masterplan for the Istanbul Metropolitan Area"* in the Zeytinburnu subprovince. Zeytinburnu, with a population of 240,000 and a building stock with more than 16,000 buildings, is one of the districts of Istanbul that possesses the highest seismic risk. Within the scope of this study, those buildings in the highest risk group were identified through field surveys and screening methods developed by METU-EERC. This pilot project provided a unique opportunity for METU-EERC in testing and verifying the methods developed for large building stocks. During this study METU EERC trained the technical personnel of the Zeytinburnu Municipality, supervised the field work and provided consultancy at every step of this project.

An outline of the applied methodologies and the details of the project activities are provided in the paper.

3. The Walkdown Evaluation Procedure

3.1. GENERAL

This procedure was developed by Sucuoglu and Yazgan in 2003. The details of the procedure are available elsewhere[10] and will not be repeated here. However, for the sake of completeness and the integrity of the work presented here, the proposed methodology will be given in the following paragraphs.

Structural parameters that have to be observed during the field surveys and the value given to each parameter by the observer are explained below.

3.2. SURVEY PARAMETERS

3.2.1. *Number of Stories*

This is the total number of floors above the ground level. If the building is built on a slope and the numbers of stories on either side are different, the larger of the two shall be taken as a representative value.

3.2.2. *Soft Story: No (0); Yes (1)*

A soft story usually exists in a building when one particular story has less stiffness and strength compared to the other stories. This situation mostly arises in buildings located along the side of a main street. The ground stories, which have level access from the street, are employed as a street side store or a commercial space whereas residences occupy the upper stories. Besides, the ground stories may have taller clearances and a different axis system causing irregularity. The combined effect of all these negative features from the earthquake engineering perspective is identified as a soft story.

3.2.3. *Heavy Overhangs: No (0); Yes (1)*

Heavy balconies and overhanging floors in multistory reinforced concrete buildings shift the mass center upwards; leading to increased seismic lateral forces and overturning moments during earthquakes. Reconnaissance studies made after the recent earthquakes in Turkey showed that those buildings possessing such features sustained heavier damage compared to buildings which were regular in elevation. As this building feature can easily be observed during a walkdown survey, it is included in the parameter set.

3.2.4. *Apparent Building Quality: Good (0); Moderate (1); Poor (2)*

The material and workmanship quality, and the care given to its maintenance reflect the apparent quality of a building. A well-trained observer can classify

the apparent quality of a building roughly as good, moderate or poor. A close relationship has been observed between the apparent quality and the experienced damage during the recent earthquakes in Turkey. A building with poor apparent quality can be expected to possess weak material strengths and inadequate detailing.

3.2.5. *Short Columns: No (0); Yes (1)*

Frames with partial infills, band windows in semi-buried basements or mid-story beams around stairway shafts lead to the formation of short columns in concrete buildings. Such columns usually sustain heavy damage during strong earthquakes since they are not originally designed to receive the high shear forces due to shortened heights that they will experience in case of a strong earthquake. Short columns can easily be identified from outside as they are usually located along the exterior frame lines.

3.2.6. *Pounding Effect: No (0); Yes (1)*

When there is no sufficient clearance between adjacent buildings, they pound each other during an earthquake as a result of different vibration periods and consequent non-synchronized vibration amplitudes. Uneven floor levels aggravate the effect of pounding.

3.2.7. *Topographic Effects: No (0); Yes (1)*

Topographic amplification is another factor that may increase the ground motion intensity on top of hills. Besides, buildings located on steep slopes (steeper than 30 degrees) usually have stepped foundations, which are incapable of distributing the ground distortions evenly to structural members above. Therefore these two factors must be taken into account in seismic risk assessment. Both factors can be observed easily during a street survey.

3.3. LOCAL SOIL CONDITIONS

The intensity of ground motion under a building during an earthquake predominantly depends on the distance of the building to the causative fault, and the local soil conditions. Mapping of seismic hazard at micro scale considers both variables. In engineering applications, seismic hazard (or ground motion intensity) is generally mapped in terms of PGA and/or PGV. The PGV usually reflects the effect of soil conditions very well during a large magnitude earthquake.[17] Since there exists a strong correlation between the PGV and the shear wave velocities of local soils,[17] in this study, the PGV is selected the representative parameter of the ground motion intensity.

The PGV map in the JICA report[16] has contour increments of 20 cm/s^2. The intensity zones in Istanbul are expressed accordingly, in terms of the associated PGV ranges.

- Zone I : 60<PGV<80 cm/s^2
- Zone II : 40<PGV<60 cm/s^2
- Zone III : 20<PGV<40 cm/s^2

Based on their number of stories and the seismic hazard level at the site buildings are assigned different base scores as shown in Table 1.

TABLE 1. Base Scores and Vulnerability Scores for Concrete Buildings

	BASE SCORES *(BS)*			VULNERABILITY SCORES *(VS)*					
Number of Stories	Zone I 60 ≤ PGV ≤ 80	Zone II 40 ≤ PGV ≤ 60	Zone III 20 ≤ PGV ≤ 40	Soft Story	Heavy Overhangs	Apparent Quality	Short Column	Pounding	Topographic Effects
1 or 2	100	130	150	0	-5	-5	-5	0	0
3	90	120	140	-15	-10	-10	-5	-2	0
4	75	100	120	-20	-10	-10	-5	-3	-2
5	65	85	100	-25	-15	-15	-5	-3	-2
6 or 7	60	80	90	-30	-15	-15	-5	-3	-2

3.4. BUILDING SEISMIC PERFORMANCE

Once the vulnerability parameters of a building are obtained from walkdown surveys and its location is determined, the seismic performance score *PS* can be calculated by using Eq. (1). The base scores, *BS*, the vulnerability scores, *VS*, and the vulnerability score multiplies, *VSM*, to be used in Eq. (1) are defined in Tables 1 and 2, respectively

$$PS = (BS) - \sum(VSM) \times (VS) \quad (1)$$

The weight of each building vulnerability parameter is evaluated by statistical procedures, based on the Duzce database. Statistical analysis is conducted by the program package SPSS Version 11, using the "Multivariable Stepwise Linear Regression Analysis" procedure. The results are then smoothed, and the weights of the parameters for which there was no available data (soft story, pounding, topography) are assigned by using engineering judgment.

TABLE 2. Vulnerability Parameters, *(VSM)*

Soft story	Does not exist = 0; Exists = 1
Heavy overhangs	Does not exist = 0; Exists = 1
Apparent quality	Good = 0; Moderate = 1; Poor =2
Short columns	Does not exist = 0; Exists = 1
Pounding effect	Does not exist = 0; Exists = 1
Topography effect	Does not exist = 0; Exists = 1

4. Preliminary Assessment

4.1. GENERAL

Up to date procedures on the vulnerability assessment of building structures have primarily focused on the structural system, capacity, layout and response parameters. These parameters would provide realistic estimates of the expected performance when the built structural system reflects the prescribed structural and architectural features. In general, construction practice in Turkey is far beyond reflecting the designed structural system. For this reason, statistical analysis based on the observed damage and significant building attributes would provide reliable and accurate results for regional assessments. In this context, the discriminant analysis technique was used to develop a preliminary evaluation methodology for assessing seismic vulnerability of existing low- to medium-rise reinforced concrete buildings. The main objective of the procedure outlined below is to identify the buildings that are highly vulnerable to damage. The procedure is developed for structures whose structural system is formed by frames or frames and structural walls. The procedure is applicable for cases where the number of stories is less than or equal to 7. The structures described above comprise the majority of the existing RC buildings in Turkey.

Definition of the discriminating parameters and the procedure to be followed are introduced below.

4.2. DEFINITION OF PARAMETERS

Considering the characteristics of the damaged structures and the huge size of the existing building stock in Turkey, the following parameters were chosen as the basic estimation parameters of the proposed method:

1. number of stories (*n*),
2. minimum normalized lateral stiffness index (*mnlstfi*),
3. minimum normalized lateral strength index (*mnlsi*),

4. normalized redundancy score (*nrs*),
5. soft story index (*ssi*),
6. overhang ratio (*or*)

These parameters are briefly defined in the following paragraphs.

4.2.1. *Number of stories (n)*

This is the total number of individual floor systems above the ground level.

4.2.2. *Minimum normalized lateral stiffness index (mnlstfi)*

This index is the indication of the lateral rigidity of the ground story, which is usually the most critical story. If the story height, boundary conditions of the individual columns and the properties of the materials used are kept constant, this index would also represent the stiffness of the ground story. This index is calculated by considering the columns and the structural walls at the ground story. While doing this, all vertical reinforced concrete members with "maximum cross-sectional dimension / minimum cross-sectional dimension ratio" less then 7 are considered as columns. All other reinforced concrete structural members are considered as structural walls. The *mnlstfi* parameter shall be computed based on the following relationship:

$$\text{mnlstfi} = \min(I_x, I_y) \tag{2}$$

I_{nx} and I_{ny} values in Eq. (2) are to be calculated by using Eq. (3).

$$\begin{aligned} I_{nx} &= \frac{\sum (I_{col})_x + \sum (I_{sw})_x}{\sum A_f} \times 1000 \\ I_{ny} &= \frac{\sum (I_{col})_y + \sum (I_{sw})_y}{\sum A_f} \times 1000 \end{aligned} \tag{3}$$

Here:

- $\Sigma(I_{col})_x$ and $\Sigma(I_{col})_y$ are the summation of the moment of inertias of all columns about their centroidal x and y axes, respectively.
- $\Sigma(I_{sw})_x$ and $\Sigma(I_{sw})_y$ are the summation of the moment of inertias of all structural walls about their centroidal x and y axes, respectively.
- I_{nx} and I_{ny} are the total normalized moment of inertia of all members about x and y axes, respectively.
- ΣA_f is the total floor area above ground level.

4.2.3. *Minimum normalized lateral strength index (mnlsi)*

The minimum normalized lateral strength index is the indication of the base shear capacity of the critical story. In the calculation of this index, in addition to the existing columns and structural walls, the presences of unreinforced masonry filler walls are also considered. While doing this, unreinforced masonry filler walls are assumed to carry 10 percent of the shear force that can be carried by a structural wall having the same cross-sectional area. [4-6] As in *mnlstfi* calculation, the vertical reinforced members with a cross-sectional aspect ratio of 7 or more are classified as structural walls. The *mnlsi* parameter shall be calculated by using the following equation:

$$\text{mnlsi} = \min\left(A_{nx}, A_{ny}\right) \tag{4}$$

Here:

$$\begin{aligned} A_{nx} &= \frac{\sum (A_{col})_x + \sum (A_{sw})_x + 0.1\sum (A_{mw})_x}{\sum A_f} \times 1000 \\ A_{ny} &= \frac{\sum (A_{col})_y + \sum (A_{sw})_y + 0.1\sum (A_{mw})_y}{\sum A_f} \times 1000 \end{aligned} \tag{5}$$

For each column with a cross-sectional area denoted by A_{col}:

$$\left(A_{col}\right)_x = k_x \cdot A_{col} \quad , \quad \left(A_{col}\right)_y = k_y \cdot A_{col} \tag{6}$$

Here:

- k_x=1/2 for square and circular columns;
- k_x=2/3 for rectangular columns with $b_x > b_y$;
- k_x=1/3 for rectangular columns with $b_x < b_y$; and
- k_y=1-k_x

For each shear wall with cross-sectional area denoted by A_{sw}:

$$\left(A_{sw}\right)_x = k_x \cdot A_{sw} \quad , \quad \left(A_{sw}\right)_y = k_y \cdot A_{sw} \tag{7}$$

Here;

- k_x=1 for structural walls in the direction of x-axis;
- k_x=0 for structural walls in the direction of y-axis; and
- k_y =1-k_x

For each unreinforced masonry filler wall with no window or door opening and having a cross-sectional area denoted by A_{mw}:

$$\left(A_{mw}\right)_x = k_x \cdot A_{mw} \quad , \quad \left(A_{mw}\right)_y = k_y \cdot A_{mw} \tag{8}$$

Here;

- k_x=1.0 for masonry walls in the direction of x-axis;
- k_x=0 for masonry walls in the direction of y-axis; and
- k_y=1-k_x

8.2.4. *Normalized redundancy score (nrs)*

Redundancy is the indication of the degree of the continuity of multiple frame lines which distribute lateral forces throughout the structural system. The normalized redundancy ratio (nrr) of a frame structure is calculated by using the following expression:

$$\text{nrr} = \frac{A_{tr}(nf_x - 1)(nf_y - 1)}{A_{gf}} \tag{9}$$

Here;

- A_{tr} is the tributary area for a typical column. A_{tr} shall be taken as 25 m^2 if nf_x and nf_y are both greater than and equal to 3. In all other cases, A_{tr} shall be taken as 12.5 m^2.
- nf_x, nf_y are the number of continuous frame lines in the critical story (usually the ground story) in x and y directions, respectively.
- A_{gf} is the area of the ground story, i.e. the footprint area of the building.

Depending on the value of *nrr* computed from Eq. (9), the following discrete values are assigned to the normalized redundancy score (*nrs*):

nrs = 1 for $0 < nrr \leq 0.5$
nrs = 2 for $0.5 < nrr \leq 1.0$
nrs = 3 for $1.0 < nrr$

4.2.5. *Soft story index (ssi)*

On the ground story, there are usually fewer partition walls than in the upper stories. This situation is one of the main reasons for the soft story formations. Since the effects of masonry walls are included in the calculation of *mnlsi*, soft story index is defined as the ratio of the height of first story (i.e. the ground story), H_1, to the height of the second story, H_2.

$$\text{ssi} = \frac{H_1}{H_2} \tag{10}$$

4.2.6. *Overhang ratio (or)*

In a typical floor plan, the area beyond the outermost frame lines on all sides is defined as the overhang area. The summation of the overhang area of each story, $A_{overhang}$, divided by the area of the ground story, A_{gf}, is defined as the overhang ratio.

$$or = A_{overhang} / A_{gf} \tag{11}$$

4.3. PERFORMANCE CLASSIFICATION

The damage index or the damage score corresponding to the life safety performance classification (DI_{LS}) shall be computed from the discriminant function given in Eq. (12).

$$DI_{LS}=0.620-0.246mnlstfi-0.182mnlsi-0.699nrs+3.269ssi+2.728or-4.905 \tag{12}$$

In the case of immediate occupancy performance classification (IOPC), the discriminant function, where DI_{IO} is the damage score corresponding to IOPC, based on these variables is:

$$DI_{IO}=0.808n-0.334mnlstfi-0.107mnlsi-0.687nrs+0.508ssi+3.884or-2.868 \tag{13}$$

In the proposed classification methodology, buildings are evaluated according to both performance levels. The steps to be followed are listed below.

7. Calculate DI_{LS} and DI_{IO} scores by using Eq. (12) and Eq. (13), respectively.
8. Determine the cutoff values for each performance classification by using the relationships given in Eq. (14). The LS_{CVR} and IO_{CVR} values in these relationships shall be obtained from Table 3 based on the number of stories above the ground level. The CMC values are adjustment factors, which introduce the spatial variation of the ground motion in the evaluation process. These values shall be taken from Table 4 based on the location of the building relative to the fault and the soil properties of the site.

$$CV_{LS} = LS_{CVR} + |LS_{CVR}| \times (CMC - 1); CV_{IO} = IO_{CVR} + |IO_{CVR}| \times (CMC - 1) \tag{14}$$

TABLE 3. Variation of LS_{CVR} and IO_{CVR} Values with Number of Stories

n	LS_{CVR}	IO_{CVR}
3	0.383	-0.425
4	0.430	-0.609
5	0.495	-0.001
6	1.265	0.889
7	1.791	1.551

TABLE 4. Variation of CMC Values with Soil Type and Distance to Fault

Soil Classification	Shear Wave Velocity (m/s)	Distance to Fault (km) 0-4	5-8	9-15	16-25	>26
B	>760	0.778	0.824	0.928	1.128	1.538
C	360-760	0.864	1.000	1.240	1.642	2.414
D	180-360	0.970	1.180	1.530	2.099	3.177
E	<180	1.082	1.360	1.810	2.534	3.900

By comparing the CV values with associated DI value calculate performance grouping of the building for life safety performance classification (LSPC) and immediate occupancy performance classification (IOPC) as follows:

If $DI_{LS} > CV_{LS}$ take $PG_{LS}=1$
If $DI_{LS} < CV_{LS}$ take $PG_{LS}=0$
If $DI_{IO} > CV_{LS}$ take $PG_{IO}=1$
If $DI_{IO} < CV_{LS}$ take $PG_{IO}=0$

By examining the performance groupings of the building for LSPC and IOPC, make a decision on the probable expected performance level of the building. In this process, reasoning summarized in Table 5 shall be followed.

TABLE 5. Probable Expected Performance Level Classification

PG_{LS}	PG_{IO}	DECISION
0	0	Low risk group
1	1	High risk group
All other cases		Require further analysis

5. The Earthquake Master Plan for Istanbul

Early in 2002, the Istanbul Metropolitan Municipality extended an invitation to a consortium formed by four leading Turkish universities to prepare an *Earthquake Master Plan for Istanbul,* [18] *(EMPI)*. These universities were the Middle East Technical University (METU), Istanbul Technical University, Bosphorus University and the Yildiz Technical University. The teams from these universities were confronted not only with the issues that will need to be resolved when Istanbul is struck by a large-magnitude earthquake but also with legal, administrative and organizational countermeasures that must be put into effect before the actual event occurs.

The scope of *EMPI* comprised of works to be done in the following areas:

- Assessment of current situation
- Seismic assessment and rehabilitation of existing buildings
- Urban planning issues

- Legal issues
- Financial issues
- Educational issues
- Social issues
- Risk and disaster management issues.

The master plan took into account the high seismic risk faced by Istanbul and findings of the preceding study for Istanbul Metropolitan Municipality under Japanese International Cooperation Agency auspices.

An important aspect of the *EMPI* was the assessment of seismic vulnerability of existing building stock in Istanbul. The main goal in assessing the seismic safety of the existing buildings was to envisage the probable earthquake damage on the existing buildings and to identify those buildings which will probably cause human losses in case of a severe earthquake.

The Master Plan adopted the three tier seismic assessment procedures. For the first and second stage assessments several methodologies (based on deterministic or probabilistic approaches) were recommended. Before generalizing the proposed techniques to the rest of Istanbul, it was also suggested that the validity and suitability of each method should be checked by carrying out pilot area studies.

The methodologies summarized in the previous sections of this paper were among the methodologies cited by the *EMPI*. The pilot implementation of the *EMPI* was adopted by the Zeytinburnu Municipality and it was referred to as the *"Zeytinburnu Pilot Project, ZPP."* Within the framework of Zeytinburnu Pilot Project the methodologies described in Sections 2 and 3 were applied on the Zeytinburnu building stock. Further details of the *ZPP* are given in the following sections.

6. Zeytinburnu Pilot Project

6.1. GENERAL

The findings of the study entitled "A Disaster Prevention / Mitigation Basic Plan in Istanbul Including Seismic Microzonation" carried under the auspices of the Japan International Cooperation Agency[16] pointed out that among the 32 districts of Istanbul; Zeytinburnu possesses a high seismic hazard and that with its existing building stock it is under a very severe seismic threat. Table 6 shows those districts of Istanbul where more than 10 percent of the existing buildings are expected to be under very high risk leading to an estimated death toll of more than one percent. According to this table, about 17 percent of the entire

building stock in Zeytinburnu is expected to experience severe damage or collapse in the case when the scenario earthquake defined in the JICA Report occurs. As this ratio was very high, the Istanbul Metropolitan Municipality decided to carry out the pilot application of the *EMPI* in the Zeytinburnu district. Within the scope of *ZPP* the three-tier seismic safety assessment methodology developed by the *METU* was applied in Zeytinburnu.

6.2. FIRST STAGE EVALUATIONS: WALKDOWN SURVEY

Before starting the walkdown evaluation process, the members of the field team were given a special training program. In this program the forms to be used in the walk-down evaluation survey were introduced to the trainees. The team members were given a basic understanding of some concepts like soft storey formation, short columns, heavy overhangs, etc. The purpose in doing this was to establish a uniformity of approach among the team members in order to minimize possible discrepancies in visual structural evaluations. The entire field team was composed of 50 persons having engineering backgrounds and the whole walkdown survey was completed in approximately two months.

The walkdown survey yielded the complete inventory of the building stock in the Zeytinburnu district. The buildings were identified in terms of their structural systems, their number of stories and their type of use, Tables 7 and 8. Walkdown survey results indicated that there are currently 16,030 buildings in Zeytinburnu. This observation further indicated that within the past 5 years the building stock of Zeytinburnu grew nearly 3.4 percent, which corresponds to an average growth of 0.7 percent per year between 2000 and 2005.

TABLE 6. Top 10 High Seismic Risk Districts of Istanbul (JICA, 2002)

District	Population*	Number of Buildings*	Probable Losses	
			High Risk Buildings (%)	Casualties (%)
Adalar	17,700	6,500	24.8	8.4
Avcilar	231,800	14,000	14.1	1.8
Bahcelievler	470,000	19,700	13.1	1.2
Bakirkoy	206,500	10,000	18.3	1.8
Buyukcekmece	34,700	3,400	10.5	2.2
Bayrampasa	237,800	20,200	12.3	1.5
Eminonu	54,500	14,100	13.9	4.6
Fatih	394,000	32,000	16.0	1.6
Gungoren	272,000	10,600	11.8	1.1
Zeytinburnu	240,000	15,500	16.6	1.9

* The given numbers reflect the 2000 census results.

TABLE 7. Classification of Buildings According to the Type of Structural System

Type of Structural System	Number of Buildings
Reinforced Concrete	13,885
Masonry	1,853
Mixed	135
Steel	143
Wood	14
Total	16,030

TABLE 8. Tabulation of RC Buildings According to the Number of Stories

Number of Stories	≤ 2	3	4	5	6	7	7+	Total
Number of Buildings	1,964	1,455	2,699	4,262	2,304	1,050	151	13,885

For Zeytinburnu, a scenario earthquake of magnitude 7.5 is assumed to take place in the Main Marmara Fault. The seismic hazard used in this study corresponds to an earthquake having 50 percent probability of exceedance within fifty years. Figure 1 schematically shows the expected fault rupture and Figure 2 illustrates the site dependent PGV distribution for the scenario earthquake.

Figure 1. Scenario Earthquake for Istanbul, M_w = 7.5 (after M. Erdik, KOERI)

The walkdown survey yielded a preliminary seismic performance grading of the existing RC buildings in Zeytinburnu relative to each other. This classification, made according to a performance score computed from the visual attributes of the existing buildings, does not necessarily point out the seismic vulnerability of individual buildings. As described in Section 1 this procedure helps the decision makers to establish the priority levels for buildings that require immediate intervention. Since calibration of the walkdown evaluation procedure was based on the observed performance of similar buildings during the past earthquakes, a bigger percentage of the buildings with low performance

scores are expected to perform poorly when compared to those having higher performance scores.

The calculated performance scores of the RC buildings are given in Table 9. It should be noted that Table 9 includes those buildings having seven stories or less since the procedure presented in Section 2 is applicable to such RC buildings. This table shows that the calculated performance scores of the buildings are inversely proportional with the number of stories. In other words, as the number of stories increases the expected seismic performance of the building under investigation gets poorer. Meanwhile, this response is in good agreement with the observations made in the surveillance studies made in the aftermath of the recent earthquakes in Turkey.

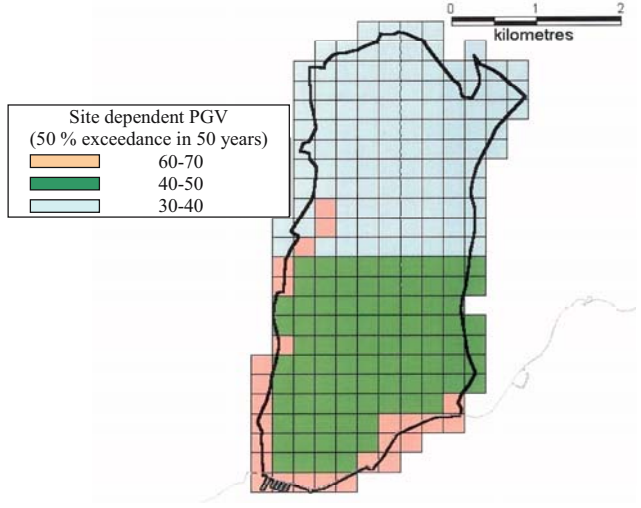

Figure 2. Site Dependent PGV Distribution for the Scenario Earthquake

TABLE 9. Calculated performance scores of RC buildings having 7 stories or less

Number of Stories	Performance Scores				Total
	PS ≤ 30	30 < PS ≤ 60	60 < PS ≤ 100	100 < PS	
1-2	0	0	248 (12.6)	1,716 (87.4)	1,964 (100.0)
3	0	41 (2.8)	1,005 (69.1)	409 (28.1)	1,455 (100.0)
4	28 (1.0)	989 (36.6)	1,563 (57.9)	119 (4.4)	2,699 (100.0)
5	638 (15.0)	2,652 (62.2)	972 (22.8)	0	4,262 (100.0)
6	1,625 (70.5)	593 (25.7)	86 (3.7)	0	2,304 (100.0)
7	848 (80.8)	202 (19.2)	0	0	1,050 (100.0)
Total	3,139 (22.9)	4,477 (32.6)	3,874 (28.2)	2244 (16.3)	13,734 (100.0)

Note: Entries in parenthesis indicate the expected risk distribution in percentages.

Figure 3 shows the spatial distribution of the existing RC buildings in Zeytinburnu with respect to the calculated performance scores. It is interesting to note that majority of the buildings with seismic performance scores less than 20 (red spots in Figure 3), are located along the Cirpici Creek, which provides a natural borderline for Zeytinburnu in the West. As shown in Figure 2 the seismic hazard along this creek is rather high and in this zone the PGV values vary between 50 m/s and 60 m/s. In the same manner, the seismic hazard along the coastal line is also high but the seismic risk in this region is not as high as on the east bank of the Cirpici Creek. This is mainly because those buildings along the coast line are of superior quality and they possess fewer negative attributes when compared to those located along the Cirpici Creek. This observation indicates that the proposed methodology is capable of reflecting the adverse effects of the seismic hazard and the building attributes on the seismic performance classification of buildings.

Figure 3. Spatial Distribution of Buildings with respect to their Calculated Performance Scores

6.3. SECOND STAGE EVALUATIONS: PRELIMINARY ASSESSMENT

In this stage buildings with a seismic performance score of 30 or less were given priority. There were 3,139 buildings in this group of which a representative sample of 2,397 buildings has been studied. In addition, 639 buildings with performance scores greater than 30 were also included in the analyses. The main reason of this inclusion was to assess the correlation between the methods used in the first and the second stage analyses.

In the second stage a total of 3,036 buildings were analyzed. Figure 4 shows classification of these buildings according to their number of stories.

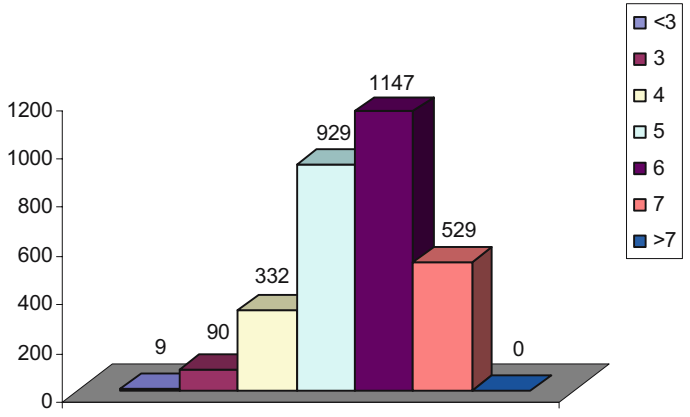

Figure 4. Distribution of Buildings with respect to Their Number of Stories

The field surveys were completed within the first three months of the study. During this phase field teams gathered specific information about the structural system of each building under investigation. This included the following:

- Dimensions of the vertical structural elements, i.e. columns and the structural walls in the critical story (usually the ground floor)
- Dimensions of the nonstructural walls filling the entire frame cell and having no window or door openings (for critical story only)
- Floor area of each story
- Number of continuous frame lines in each direction of the building
- Height of the critical story
- Height of the story immediately above the critical story

The information gathered from the field was later tabulated in a spreadsheet format. After calculating the parameters defined in Section 4 the *PAM* was applied. As shown in Table 10, the buildings were classified in high, moderate and low risk groups according to their estimated seismic performance levels.

Table 10 illustrates that 2,098 buildings out of 3,036 (69.1 percent) were classified in the high seismic risk group. Moreover, as can be revealed from Table 10, while a smaller percentage of the low-rise buildings were in the high seismic risk group, bigger portions of the mid-rise buildings (i.e. 4-7 story buildings) were placed in this category. This trend agrees well with the observations made during the reconnaissance studies performed in the aftermath of the recent earthquakes.

TABLE 10. Results of the Preliminary Assessment Method

Number of Stories	High Risk Group	Moderate Risk Group	Low Risk Group	Number of Buildings
3 or less	10 (10.1)	18 (18.2)	71 (71.7)	99 (100)
4	180 (54.2)	81 (24.4)	71 (21.4)	332 (100)
5	713 (76.7)	170 (18.3)	46 (5.0)	929 (100)
6	808 (70.4)	262 (22.8)	77 (6.7)	1,147 (100)
7	387 (73.2)	119 (22.5)	23 (4.3)	529 (100)
Total	2,098 (69.1)	650 (21.4)	288 (9.5)	3,036 (100)

Note: Entries in parenthesis indicate the expected risk distribution in percentages.

The spatial distribution of those buildings which were classified in the high seismic risk group is given in Figure 5. As in Figure 3, those buildings along the Cirpici Creek were among the most vulnerable ones. As discussed previously this is mainly because of the high seismic hazard of the region and relatively lower building quality in this part of Zeytinburnu.

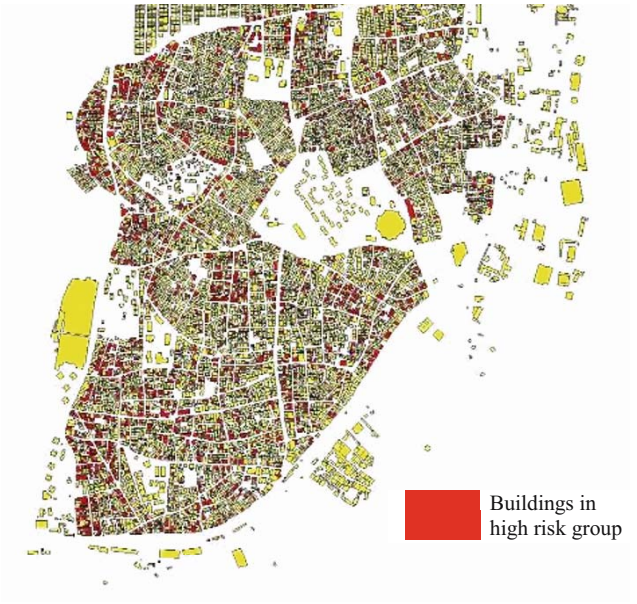

Figure 5. Spatial Distribution of buildings in high risk group

Table 11 compares the results of the walkdown and preliminary assessment methodologies. This table indicates that 1,738 (72.5 percent) of the 2,397 buildings with PS≤30 were classified in the high risk group, showing the consistency of the methodologies. The shifting of 659 buildings (26.5 percent) from high risk group to lower risk groups indicates that the application of *PAM* following the walkdown survey refines the results further.

As mentioned in the previous sections of this paper, the walkdown evaluation methodology provides a priority order for the buildings under investigation. A close inspection of Table 11 indicates that as the performance score of a building gets higher, for that building the probability of being in the high risk group considerably decreases. This is clearly seen when PS≤30 buildings in Table 11 are compared with those with PS>100 buildings. While 72.5 percent of the first group was rated to be in the high risk group, only 16.7 percent of those in the second group were in the high risk group. In a similar manner, the probability of being in the low risk group increases with increasing performance score. While only 6.5 percent of those buildings in PS≤30 group were classified as LRG buildings, more than 55 percent of those buildings in PS>100 group were identified as low risk group buildings by the preliminary assessment methodology. In reality this was the required trend showing that the walkdown survey provides a realistic priority ordering. As some buildings even with very high performance scores can be identified as high risk group buildings by *PAM*, the walkdown evaluation procedure should be complemented by the *PAM*. Those buildings with lower performance scores should be given priority and all existing building stock should be assessed by the use of *PAM*.

TABLE 11. Comparisons between First and Second Stage Assessment Procedures

	PS≤30	30<PS≤60	60< PS ≤ 80	80< PS ≤ 100	100<PS	TOTAL
HRG	1,73 8 (72.5)	258 (66.2)	62 (48.8)	37 (35.6)	3 (16.6)	2,098 (69.1)
MRG	503 (21.0)	81 (20.8)	32 (25.2)	29 (27.9)	5(27.8)	650 (21.4)
LRG	156 (6.5)	51 (13.1)	33 (26.0)	38 (36.5)	10 (55.6)	288 (9.5)
TOTAL	2,397 (100.0)	390 (100.0)	127 (100.0)	104 (100.0)	18 (100.0)	3,036 (100.0)

Note: Entries in parenthesis indicate the predicted risk distributions in percentages.

7. Summary and Conclusions

This paper presents a seismic vulnerability assessment application on a regional scale. In the introductory parts of the manuscript a multi tier assessment methodology was summarized and in the second part the details of the field applications were introduced and the findings were presented.

The pilot implementation of the *"Earthquake Master Plan for Istanbul"* was made in the Zeytinburnu district of Istanbul. Of the 16,030 buildings surveyed in the first tier, 3,036 buildings were selected for further investigation in the second tier. At the end of the second tier study 2,098 buildings (mostly having 4 stories or more) were rated in the high seismic risk group.

Comparisons made between the results of the first tier and the second tier investigations indicated that, in general, both methodologies were yielding consistent results, which further indicated that walkdown survey provides a realistic priority ordering for the second tier investigations. Therefore it is concluded that when applied together these methodologies lead to more refined and more reliable seismic risk estimations on a regional scale.

It was also shown that some buildings, which were assigned very high performance scores at the end of first tier, may be ranked in the high seismic risk group buildings by the second tier survey, which is also referred as *PAM* in this paper. For that reason, it was concluded that the walkdown evaluation procedure should be complemented by the *PAM*. In doing this, those buildings with lower performance scores should be given priority and, in the long run, the entire building stock in the region should be screened by the use of *PAM*.

ACKNOWLEDGMENT

The authors express their appreciation to the authorities of the Zeytinburnu Municipality, the Istanbul Metropolitan Municipality Disaster Coordination Center and the IBB Bimtas Inc for their productive collaboration through the course of the Zeytinburnu Pilot Project.

References

1. Y. K. Wen, H. Hwang, and M. Shinozuka, Development of Reliability-Based Design Criteria for Buildings Under Seismic Load, Technical Report No. 94-0023, National Center for Earthquake Engineering Research, University at Buffalo, 1994, p. 172.
2. C. Kircher, R. K. Reitherman, R. V. Whitman, and C. Arnold, Estimation of Earthquake Losses to Buildings, *Earthquake Spectra-EERI,* **13**(4), 703-720, (1997).
3. D. S. Brookshire, S. E. Chang, H. Cochrane, R. A. Olson, A. Rose, and J. Steenson, Direct and Indirect Economic Losses from Earthquake Damage, *Earthquake Spectra-EERI,* **13**(4), 683-701(1997).
4. M. A. Sozen, and A. F. Hassan, Seismic Vulnerability Assessment of Low-Rise Buildings in Regions with Infrequent Earthquakes, *ACI Structural Journal*, **94**(1), 31-39, (1997).
5. P. Gulkan, and M. A. Sozen, Procedure for Determining Seismic Vulnerability of Building Structures, *ACI Structural Journal,* **96**(3), 336-342, (1999)
6. G. Ozcebe, M. S. Yucemen, V. Aydogan and A.Yakut, Preliminary Seismic Vulnerability Assessment of Existing Reinforced Concrete Buildings in Turkey- Part I: Statistical Model Based on Structural Characteristics, in: *Seismic Assessment and Rehabilitation of Existing Buildings*, edited by S.T. Wasti and G. Ozcebe, (Kluwer Academic Publishers-KAP, Doortrecht, 2003), pp. 29-42
7. A. Yakut, V. Aydogan, G. Ozcebe and M. S. Yucemen, Preliminary Seismic Vulnerability Assessment of Existing Reinforced Concrete Buildings in Turkey -Part II: Inclusion of Site

Characteristics, in: *Seismic Assessment and Rehabilitation of Existing Buildings*, edited by S.T. Wasti and G. Ozcebe, (KAP, Dordrecht, 2003), pp. 43-58

8. Federal Emergency Management Agency, Washington, D.C. (1988), FEMA 154: Rapid Visual Screening of Buildings for Potential Seismic Hazards - A Handbook, p. 162.
9. Federal Emergency Management Agency, Washington, D.C. (1998), FEMA 310: Handbook for the Seismic Evaluation of Buildings -A Prestandard, p. 400.
10. H. Sucuoglu and U. Yazgan, Simple Survey Procedures for Seismic Risk Assessment in: Urban Building Stocks, in: *Seismic Assessment and Rehabilitation of Existing Buildings*, edited by S.T. Wasti and G. Ozcebe, (KAP, Dordrecht, 2003), pp. 97-118.
11. Federal Emergency Management Agency, Washington, D.C. (2000), FEMA 356: Prestandard and Commentary for the Seismic Rehabilitation of Buildings, p. 481.
12. Applied Technology Council, California (1996) ATC-40: Seismic Evaluation and Retrofit of Concrete Buildings, p. 612.
13. European Committee for Standardization, Brussels, (2004), Eurocode 8: Design of structures for earthquake resistance Part 3: Strengthening and repair of buildings - Draft No:7, p.89
14. H. Sucuoglu, T. Gur, and M. S. Gunay, Performance-based seismic rehabilitation of damaged reinforced concrete buildings, *Journal of Structural Engineering-ASCE*, **130**(10), 2004, pp. 1475-1486.
15. Y. J. Park and A. H. S. Ang, Mechanistic Seismic Damage Model For Reinforced-Concrete, *Journal of Structural Engineering-ASCE*, **111**(4), 1985, pp 722-739.
16. Japan International Co-operation Agency and Istanbul Metropolitan Municipality, Tokyo-Istanbul, (2002), The Study on A Disaster Prevention / Mitigation Basic Plan in Istanbul including Seismic Microzonation in the Republic of Turkey, Final Report.
17. D. J. Wald, V. Quitariano, T. H. Heaton, H. Kanamori, C. W. Scrivner, and C. B. Worden, Trinet Shake Maps: Rapid Generation of Peak Ground Motion and Intensity Maps for Earthquakes in Southern California, *Earthquake Spectra*, **15**(3), 1999, p. 537-555.
18. Istanbul Metropolitan Municipality Construction Directorate Geotechnical and Earthquake Investigation Department, Istanbul (2003), Earthquake Master Plan for Istanbul, p. 1344.

AUTOMATED POST-EARTHQUAKE DAMAGE ASSESSMENT OF INSTRUMENTED BUILDINGS

FARZAD NAEIM
John A. Martin & Associates, Inc.
1212 S. Flower St., Los Angeles, CA 90015, USA.

SCOTT HAGIE
John A. Martin & Associates, Inc.
1212 S. Flower St., Los Angeles, CA 90015, USA.

ARZHANG ALIMORADI
John A. Martin & Associates, Inc.
1212 S. Flower St., Los Angeles, CA 90015, USA.

EDUARDO MIRANDA
Stanford University, Stanford, CA 94305, USA.

Abstract. A set of methodologies for automated post earthquake damage assessment of instrumented buildings are presented. These methods can be used immediately after an earthquake to assess the probability of various damage states in the N-S and E-W directions and throughout the height of each building. The methods have been applied to more than 40 CSMIP instrumented buildings which have recordings from more than one earthquake. The results indicate that the proposed methods, when used in combination, can provide very useful information regarding the status of a building immediately after an earthquake by simple and rapid analysis of sensor data and prior to any building inspections.

Keywords: earthquakes; damage assessment; fragility functions; wavelet analysis; instrumentation; automated; remote

1. Introduction

This paper provides an overview of an exhaustive investigation to determine the feasibility of an automated approach to post-earthquake damage assessment of

S.T. Wasti and G. Ozcebe (eds.), Advances in Earthquake Engineering for Urban Risk Reduction, 117–134.

instrumented buildings and establishment of a coherent set of techniques and methodologies to achieve the objective of automated post-earthquake damage assessment.

The objective of this project was to use and study strong-motion data from instrumented buildings with several earthquake records to determine the threshold of measures of motion that would provide guidance to the building officials, in a manner consistent with ATC-20, for determining whether to inspect the building or evacuate it based on the records taken from the building. The proposed measures are such that they can be computed directly from recorded data of instrumented buildings.

Due to publication space constraints this paper provides only a preview of the methodologies developed and a small number of representative examples. A full report which is currently in preparation (Naeim et al., 2005) will contain detailed information regarding various methodologies implemented and the results of application to numerous instrumented buildings. In addition, papers are being prepared for submission to scientific journals that document certain major developments achieved during this project (Alimoradi et al 2005a; Alimoradi et al., 2005b).

Automated damage assessment (ADA) provides an incentive for building owners to instrument their buildings and has the potential of significantly adding to the inventory of instrumented buildings so critically needed for development and evaluation of existing and future design provisions. Elimination or reduction of possible false alarms produced by ADA procedures is a major concern. Therefore, we assess damage using several independent techniques and provide the degree of confidence in terms of probability of occurrence with each of our damage assessments.

Robust ADA methodologies should be able to provide increasingly more accurate estimates of post-earthquake damage when more information is available regarding the building and its contents. With our approach, preliminary damage estimates are provided based on the sensor data and a general understanding of the building and its contents. More accurate damage estimates may be obtained if more detailed information regarding the structural system and contents are available such as detailed fragility curves for various components.

The more specific the information that ADA provides, the more useful it is. We provide damage estimates per floor in each direction of the building. Damage estimates may be based on the maximum response values per floor or response values at the geometric center of each floor's diaphragm.

In more ways than one this project is a natural continuation of last year's effort which resulted in development and dissemination of the CSMIP-3DV software system (Naeim et al., 1994). We utilized and expanded on the

information that we generated regarding 80 CSMIP instrumented buildings contained in the CSMIP-3DV database in order to evaluate, rank, and combine various potential methods to achieve reliable automated post-earthquake damage detection. These enhancements include:

- Calculation of instantaneous and envelope values of story forces and story shears, as well as hysteretic diagrams for these parameters.
- Calculation of instantaneous and envelope values of floor accelerations, velocities and floor spectral attributes.
- Application of numerous fragility curves (Aslani and Miranda 2003; FEMA 2004; Porter and Kiremidjian 2001) for probabilistic assessment of damage to structural and nonstructural systems and components.
- Investigation of possible use of FEMA-356 (ASCE 2000) tables and/or linear/nonlinear response analyses for damage assessment.
- Investigation of the use of Wavelet Analysis techniques for damage assessment
- Development of a new rapid system identification technique based on the use of Genetic Algorithms (Alimoradi, et al 2005a) and approximate mode shapes (Miranda and Taghavi 2005; Alimoradi, et al 2005b) for identifying building periods, mode shapes, and changes in dynamic characteristics of buildings during their response to earthquake ground motions.
- Investigation of the use of the Fuzzy Logic Theory (Revadigar and Mau 1999) for combining information obtained from various methods and techniques.

2. Classes of Potential Damage Indicator Parameters

Several categories of techniques for automated damage assessment based on building records were evaluated.

2.1. "SIMPLE" OR "DESIGN ORIENTED" MEASURES

These include demand/capacity ratios based on the following measures.

1. Comparison of base shear inferred from the records with the capacity level values suggested by the applicable code or used in design.
2. Comparison of maximum inter-story drifts inferred from records with the capacity level values suggested by the applicable code or used in design.

3. Comparison of observed peak ground acceleration obtained from the records with the capacity level values suggested by the applicable code or used in design.
4. Comparison of relevant response spectral entities for a number of modes, combined using an appropriate spectral combination technique, with the capacity level values suggested by the applicable code or used in design.

2.2. PROBABILITY-BASED MEASURES

These include the fragility functions developed by PEER/NSF, utilized by HAZUS-MH and proposed by Porter and Kiremidjian as well as an attempt to cast FEMA-356 limit-state tables in a pseudo fragility function form for possible damage assessment. These are probabilistic damage measures for various floors and contents which are developed utilizing one or more of the following indicators:

- Peak inter-story drift ratios
- Peak floor accelerations
- Peak floor velocities
- Floor response spectra
- Story shears inferred from recorded motions

2.3. WAVELET CHARACTERISTIC MEASURES

These are signal processing measures based on wavelet analyses in which the high-frequency content of the signal is separated from its low frequency content in order to provide information on the timing and extent of changes in the frequency and amplitude characteristics of the sensor data.

2.4. DAMAGE MEASURES BASED ON STRUCTURAL IDENTIFICATION

These are damage measures inferred from changes in the dynamic characteristics of the building such as elongation of natural periods or a change in the dominant mode of behavior of the building during an earthquake(i.e., a change from shear dominated deformation shape to a flexural dominated shape or vice versa).

2.5. CLASSIFICATION OF DAMAGE STATES

Consistent with ATC-20 (Applied Technology Council, 1989), the damage state suggested by each damage indicator are classified in one of the following four categories:

- No Damage
- Slight Damage
- Moderate Damage
- Severe Damage

3. Use of Fragility Curves for Damage Assessment

As will be shown later in this paper, the various fragility curves proved to be the most useful tools for post-earthquake damage assessment. Once engineering demand parameters have been computed based on interpreted data from the sensors, damage in specific stories can be estimated through the use of fragility functions. A fragility function relates structural response with various levels of damage. Unlike deterministic values recommended in FEMA-356 (ASCE, 2000), fragility functions take into account the uncertainty on the structural motions that trigger different levels of damage. In particular, a fragility function supplies the probability that the structure will reach or exceed a particular damage level.

Available experimental data on various types of structural components permit the development of fragility functions. Recent research at PEER (Aslani and Miranda, 2003) indicates that fragility functions for many structural components can be assumed to follow a lognormal distribution. Fragility curves implemented in HAZUS also utilize a lognormal shape. Examples of probabilities of experiencing light (dm1) and severe (dm2) cracking in reinforced concrete slab-column connections as a function of interstory drift ratio are shown in Figure 1.

As shown in this figure severe cracking in slab-columns connections has been observed in specimens subjected to interstory drift ratios as low as 0.5% while in others as large as 1.6%. Rather than categorically stating that severe cracking occurs at a particular level of interstory drift, fragility functions describe how the probability of reaching or exceeding this level of damage increases as the interstory drift ratio imposed in the building increases. As shown in the figures the lognormal distribution captures quite well the observations from experimental results.

Fragility functions assumed to follow a lognormal probability distribution are defined by only two parameters for each damage state. One parameter

describes the engineering demand parameter at which a 50% probability of reaching or exceeding a damage state occurs and the other parameter describes the dispersion in the data. An example of fragility functions for three damage states is presented in Figure 2.

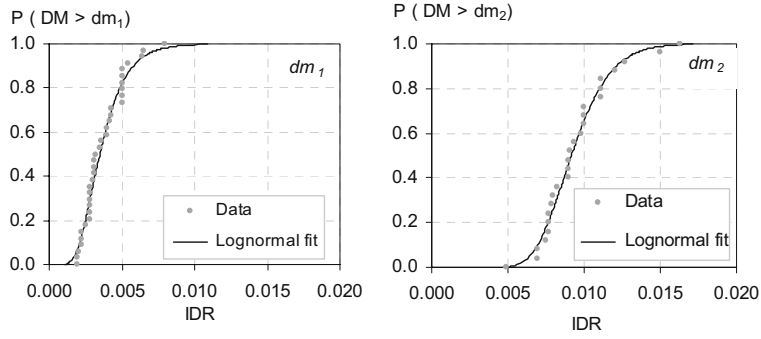

Figure 1. Example of fragility functions to estimate damage in reinforced concrete buildings with slab-column connections as a function of interstory drift (After Aslani and Miranda, 2003)

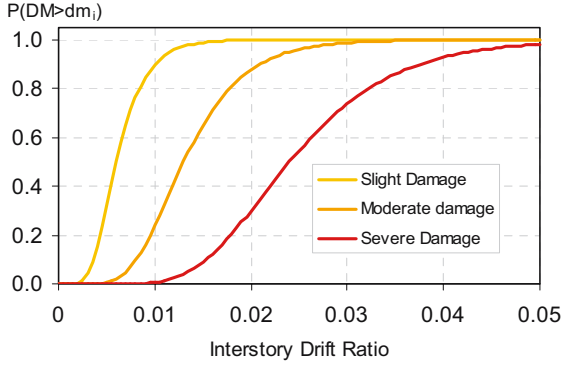

Figure 2. Example of drift-based fragility functions for three damage states

Once the fragility functions have been defined, the probability of being in one of the damage states is easily computed as the difference between two consecutive damage states. An example of damage being within one of the various damage states is shown in Figure 3.

In can be seen that, for this example, stories with interstory drift demands of 1% would have a very small probability (about 10%) of not having damage, a high probability of having slight damage (about 65%), a small probability of experiencing moderate damage (about 20%) and essentially no chance of experiencing severe damage. However, stories experiencing an interstory drift demand of 2.5% would certainly experience some degree of damage: about 5% probability that the damage is slight, about 40% that is moderate and about 55% of experiencing severe damage.

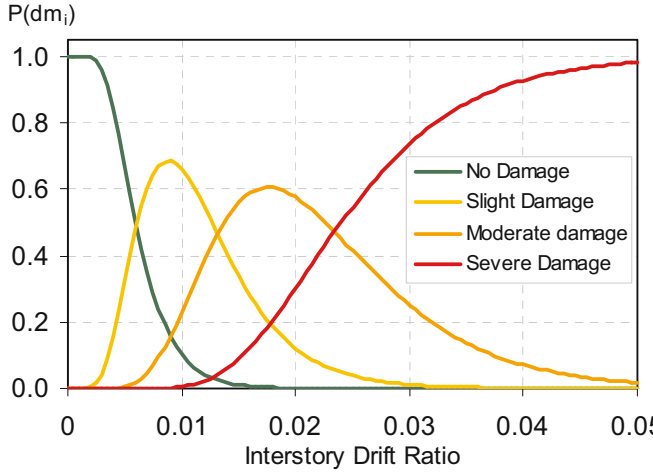

Figure 3. Probabilities of being in various damage states as a function of the level of interstory drift demand

The fragility-based damage assessment algorithms provide the decision makers with a number of options for estimating structural and nonstructural damage in a CSMIP-instrumented building:

1. Apply the HAZUS-MH fragility functions for various FEMA categories of buildings and regions
2. Apply the PEER/NSF fragility functions or fragility functions provided by other researchers
3. Use the deterministic values provided by FEMA-356; or
4. Use their own fragility functions obtained from detailed structural analyses of the building performed prior to the earthquake(s).

4. Examples

An overview of the utility and limitations of various ADA techniques evaluated and implemented during this study are provided by examination of two instrumented buildings. Details of application to other buildings will be included in our final report to CSMIP (Naeim, et al., 2005). The two selected building examples are:

1. The Imperial Valley County Services Building response to the 1979 Imperial Valley earthquake, and
2. The Van Nuys 7 Story Hotel response to the 1992 Landers and Big Bear, and the 1994 Northridge earthquakes.

4.1. EXAMPLE -- IMPERIAL VALLEY COUNTY SERVICES BUILDING

This six story building has been the subject of numerous studies (Figure 4a). A reinforced concrete building with discontinuous shear walls, it suffered severe damage in the form of collapse of the first floor concrete columns at the ground floor during the 1979 Imperial Valley earthquake (Figure 4b). The building was subsequently demolished. The irregular structural system, interruption of exterior walls at the second floor, and sudden transfer of loads at that plane were major contributors to the failure of this building. A sketch of the building depicting sensor locations is shown in Figure 5.

(a) A view of the building (b) Failure of columns at the base

Figure 4. Imperial County Services Building (Photo Credits: BAREPP and USGS)

System identification using GA optimization in the East-West direction indicates that the initial fundamental period of this building was about 0.7 sec. This period was elongated to 1.5 sec. towards the end of the record (Figure 6). Comparison of input elastic spectra at the base with a typical unreduced code spectrum for seismic zone 3, where this building was located, provides little to work with as far as damage assessments are concerned (see Figure 7). First, the elastic demand/capacity ratios in the E-W and N-S directions look about the same. Second, comparison of modal base shear demand and assumed capacities are not far apart from each other. Third, no information pertaining to the significant attributes of the building particular to this structure, such as irregularity, discontinuity of shear walls can be inferred from spectral comparisons. Fourth, the E-W and N-S picture do not vary by much although the building is significantly weaker in the E-W direction. Finally, no information regarding the possible distribution of damage throughout the height of the structure can be obtained from Figure 7. This illustrates the disadvantages of using design-based approaches as tools for automated post-earthquake damage assessment.

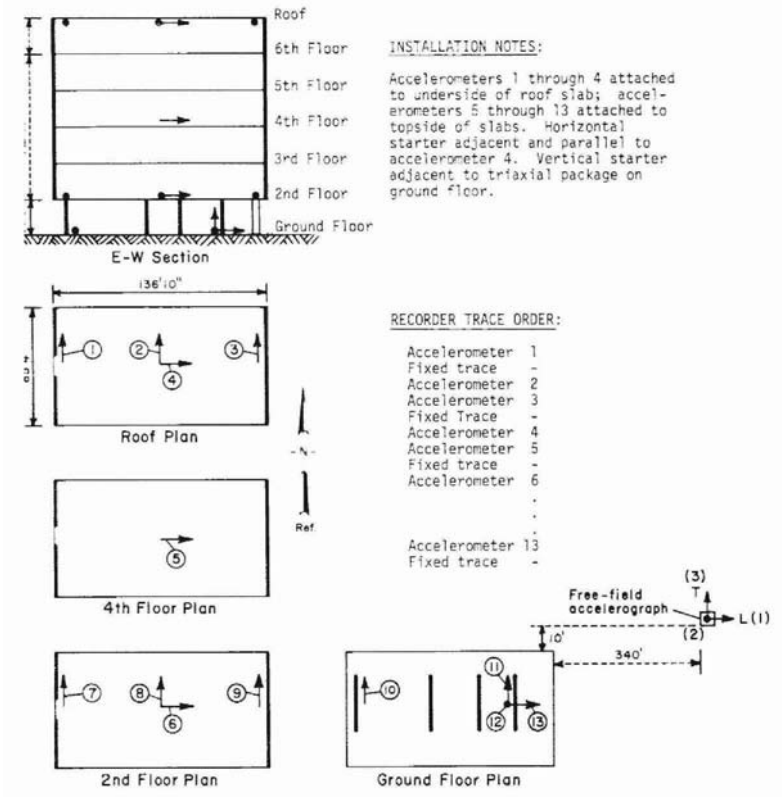

Figure 5. Sketch and sensor layout for Imperial County Services Building (from McJunkin and Ragsdale 1980)

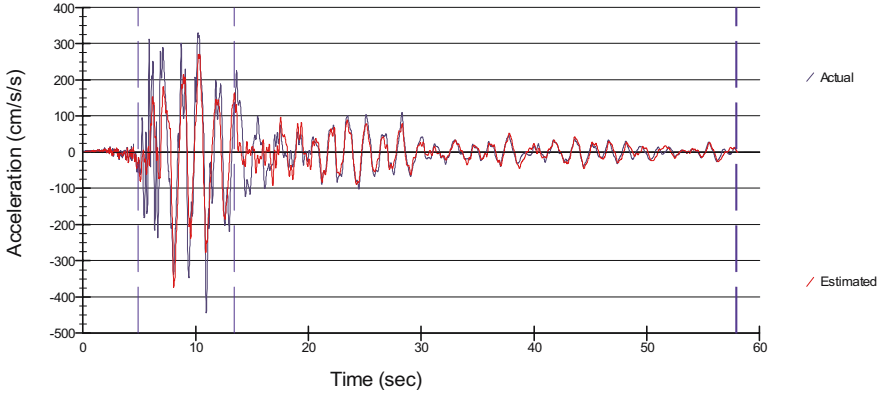

Figure 6. Recorded and GA identified response in the E-W direction at the roof

Instantaneous and maximum values of interstory drifts of CSMIP instrumented buildings after an earthquake can be easily and immediately estimated using tools such as CSMIP-3DV (Naeim et al., 2004). These drift

values were proven to be of immense value in automated damage assessment. A glimpse at the E-W and N-S lateral displacements and story drifts (Figures 8 and 9) reveals that the drift demands in the E-W direction were significantly larger than those in the N-S direction. Furthermore, a drift of 3.5 inches at the first floor is inferred from sensor data in the E-W direction while the maximum drifts in the upper floors are limited to about 1.0 inch. Evaluation of the shear-displacement hysteretic plots (Figure 10) indicates significantly larger excursions and softening of the first floor in the E-W direction.

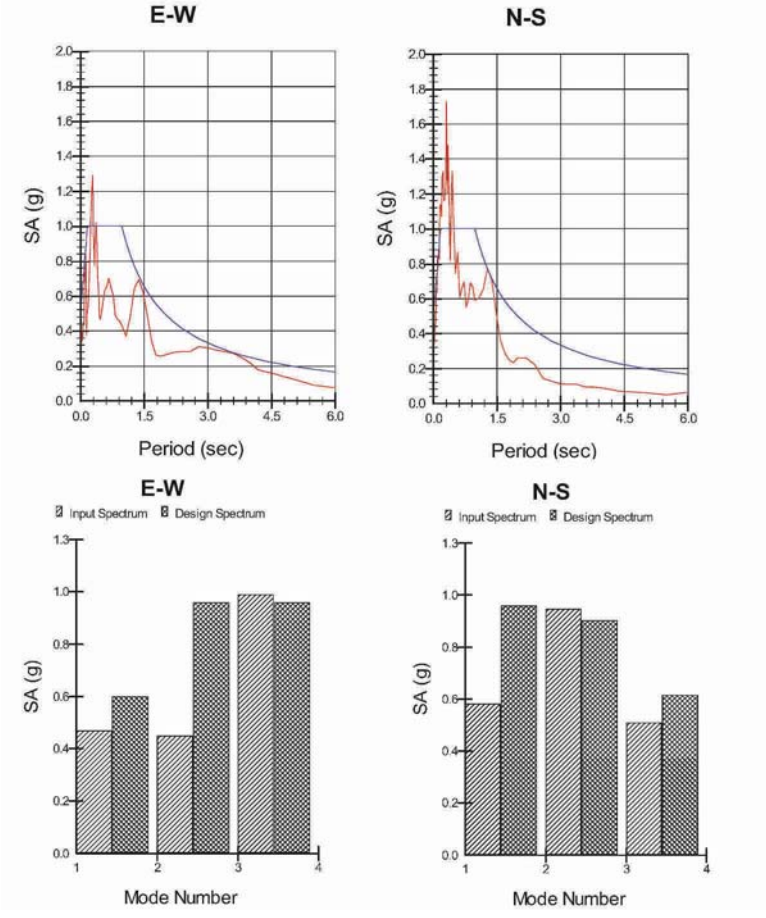

Figure 7. Comparison of the recorded response spectra (5% damped) at the base of the building with a typical "design" spectrum for seismic zone 3 and corresponding elastic modal demands

Surprisingly, completely independent approaches using interstory drift indices provide similar and very useful results. For example, if we use HAZUS-MH fragility curves based on interstory drifts for this type of building (C1M or C2M, older building), we obtain 85% probability of severe damage and 15%

probability of moderate damage at the first floor in the E-W direction (see Figure 11). This is exactly where the column failures occurred. In the N-S direction at the same floor the probability of severe damage is estimated at less than 11% and probability of moderate damage at 78%. The damage at the upper floors of this building was limited as the failure of the first floor columns produced a relatively rigid pin-based block. This is also reflected in these damage estimates. In the E-W direction the probabilities of severe, moderate, slight and no damage are constant from the second floor to roof at 6%, 76%, 16% and 1%, respectively. In the N-S direction these values are 0%, 11%, 47%, and 42% respectively.

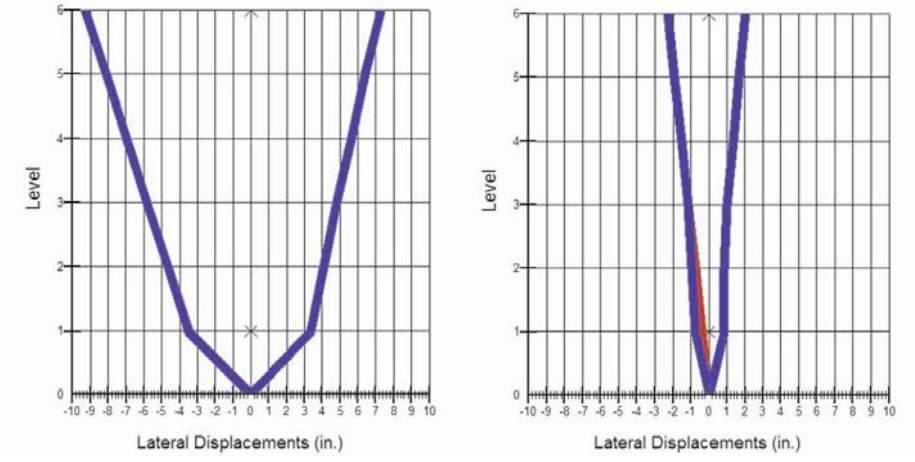

(a) E-W (b) N-S

Figure 8. Maximum lateral displacements in the E-W and N-S directions

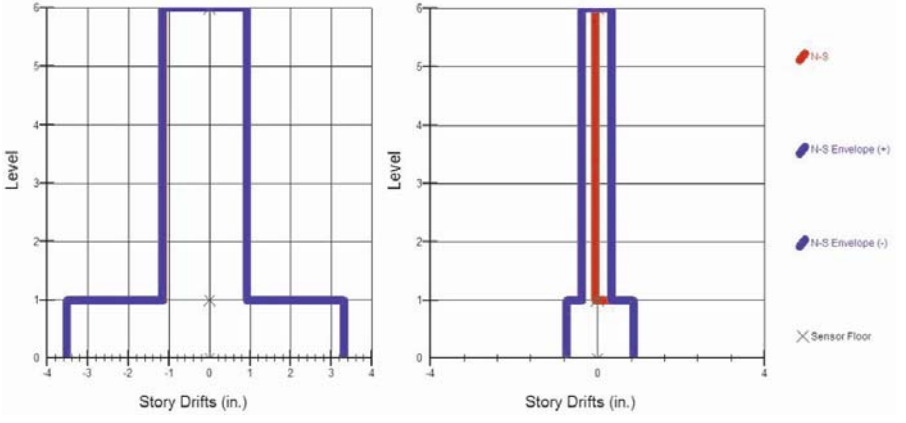

(a) E-W (b) N-S

Figure 9. Maximum interstory drifts in the E-W and N-S directions

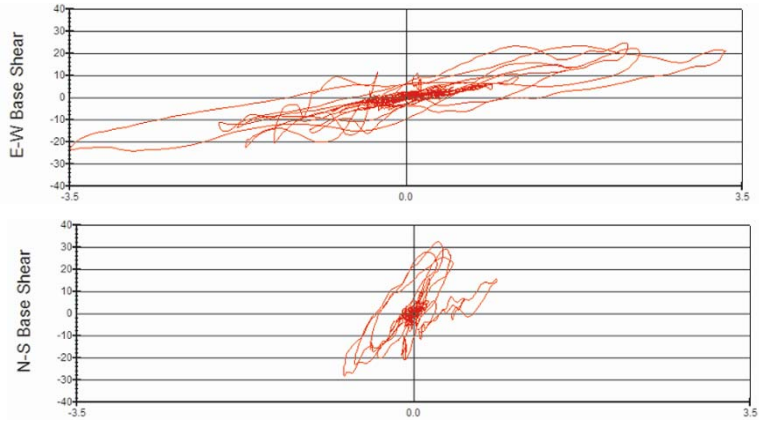

Figure 10. First floor shear-displacement hysteretic loops (E-W on top, N-S at the bottom)

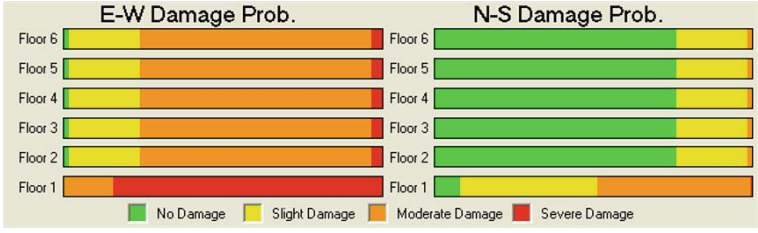

Figure 11. Damage probability established based on HAZUS-MH drift-based fragility curves for older concrete buildings clearly identifies the first floor in the E-W direction as the zone of severe damage

Use of the PEER/NSF fragility curves for flexural behavior of nonductile R/C columns provides similar useful information (Figure 12). Based on this approach, the probability of severe damage to the first floor columns in the E-W direction is 74% and in the N-S direction is 19%. The probability of the severe column damage in upper floors is only 14% in the E-W direction and 0% in the N-S direction. The elegance of the PEER/NSF fragility curves is that the probability of damage based on various damage mechanisms and various components can be estimated. For example, using the fragility curves developed for old RC beam-column joints, one obtains the severe damage probability for the beam-column joint as 0% while the probability of slight damage to these joints is 81% at the first floor in the E-W direction.

Even FEMA-356 tables intended for nonlinear performance analyses such as Table 6-8 can be cast into a fragility curve for the purposes of automated post-earthquake damage assessment. For example, one can assume a certain level of elastic drift and apply some adjustment factors to take into consideration the inherent conservatism of FEMA-356 tabulated limit states. For instance, if we assume the building can take 0.005 of interstory drift angle

within its elastic limit, do not apply any adjustment factors, and use the mean secondary values provided in FEMA-356 Table 6-8 for nonconforming columns in flexure (see Figure 13), then our damage assessment would indicate a 100% probability of exceeding the secondary Collapse Prevention (CP-S) for the first floor columns in the E-W direction (Figure 14). Based on this analysis, all columns in upper floors are within the Immediate Occupancy (IO) limit state.

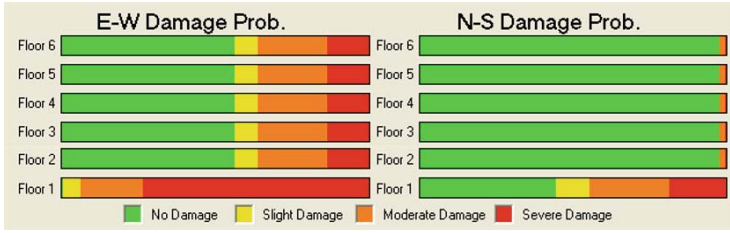

Figure 12. Damage probability established based on PEER/NSF fragility curves for nonductile R/C columns under large gravity loads clearly identifies the first floor columns in the E-W direction as the zone of severe damage

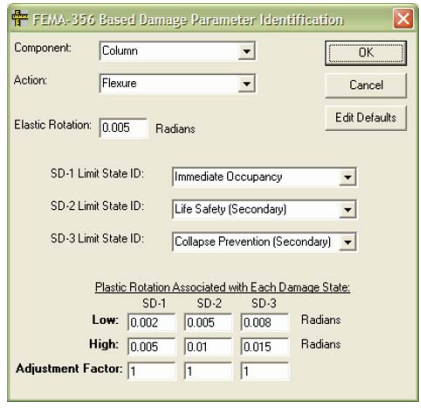

Figure 13. Assumptions used in converting FEMA-356 tabulated values to a fragility curve for nonductile R/C columns

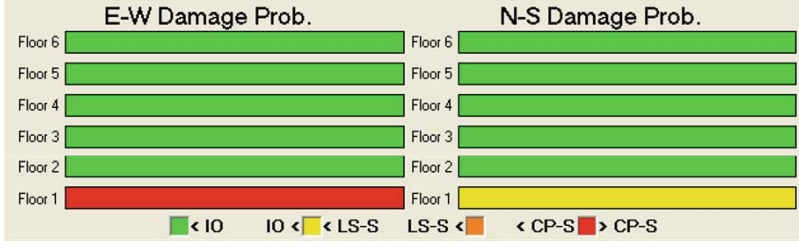

Figure 14. Damage probability established using Tables contained in FEMA-356 for limit-states of nonductile concrete columns clearly identifies the first floor in the E-W direction as the zone of severe damage

In summary, use of sensor data to estimate interstory drifts and application of various fragility curves, if available at the time, could have provided excellent post-earthquake damage assessment of this building.

4.2. EXAMPLE -- THE VAN NUYS 7-STORY HOTEL

This 7-story nonductile concrete frame building (Figures 15 and 16) is probably the most studied instrumented building in the world. We applied ADA to records obtained from three earthquakes: 1992 Landers, 1992 Big Bear, and 1994 Northridge earthquake. The building did not suffer damage during the 1992 events but did suffer significant structural damage during the 1994 Northridge earthquake in the form of shear failure of columns at the 4th floor on the exterior E-W frame on the south face of the building.

Figure 15. The Van Nuys 7-Story Hotel and damage to its fourth floor columns during the 1994 Northridge earthquake

Fragility analysis for 1992 Landers and Big Bear earthquakes using HAZUS-MH, PEER/NFS and FEMA-356 parameters all indicate that this building did not suffer structural damage during these two earthquakes (See Figure 17 for an example). The picture, however, is entirely different for the 1994 Northridge earthquake where all three methods indicate a high probability of extensive damage to the middle floors of the building (Figures 18 and 19). Please note that contrary to the Imperial Valley Services Building, no sensors

were installed in this building on the floor that was damaged. Therefore, the estimates are provided by interpolation between sensors at other floors. As a result the ADA procedures assign possibility of damage to several floors in the building and cannot pinpoint the exact floor at which the damage occurs.

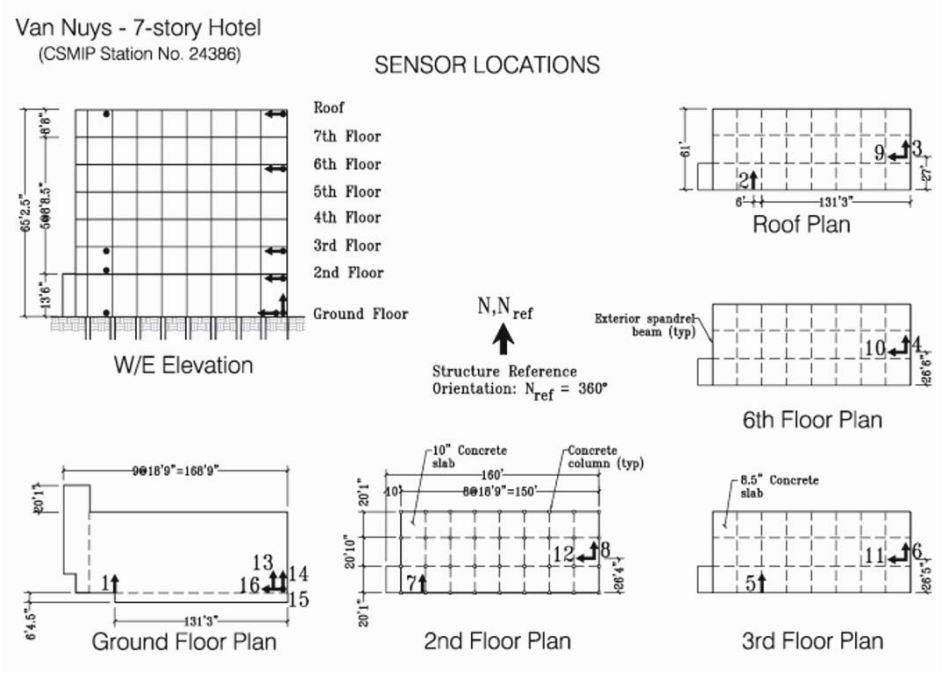

Figure 16. Sketch and sensor layout for the Van Nuys 7 Story Hotel

Our experience indicates that wavelet analysis shows promise if the results of wavelet analysis details are compared to those obtained from an earthquake in which the building was known to be not damaged (baseline earthquake). Otherwise, the possibility of false alarms based on wavelet analysis is high. Here, we use 1992 Big Bear as the baseline earthquake to estimate damage probability during the 1994 Northridge earthquake.

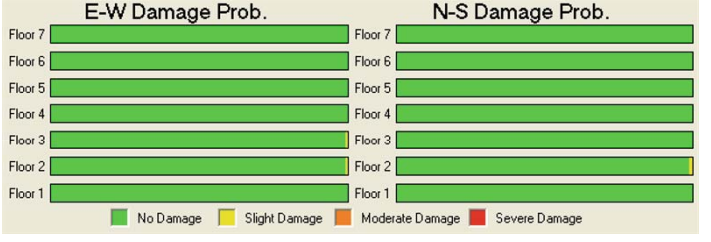

Figure 17. Damage probability established based on HAZUS-MH drift-based fragility curves for older concrete buildings indicates no damage during the Big Bear and Landers earthquakes

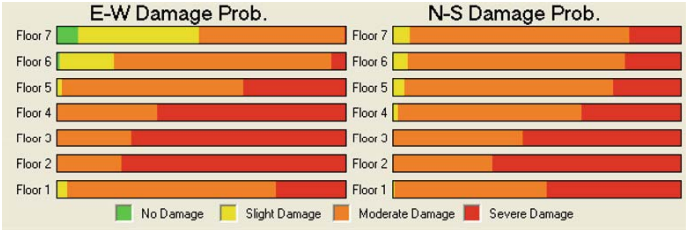

Figure 18. Damage probabilities established based on HAZUS-MH drift-based fragility curves for the 1994 Northridge earthquake show 100% probability of moderate to severe damage at the second to fourth floors

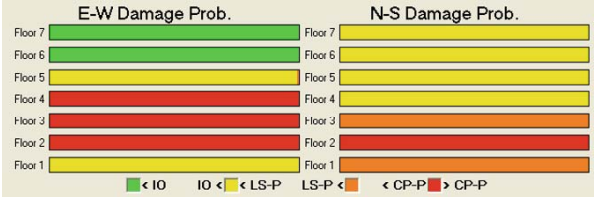

Figure 19. Damage probabilities established using FEMA-356 Tables indicate 100% probability of exceeding Collapse Prevention limit state at second to fourth floors in the E-W direction

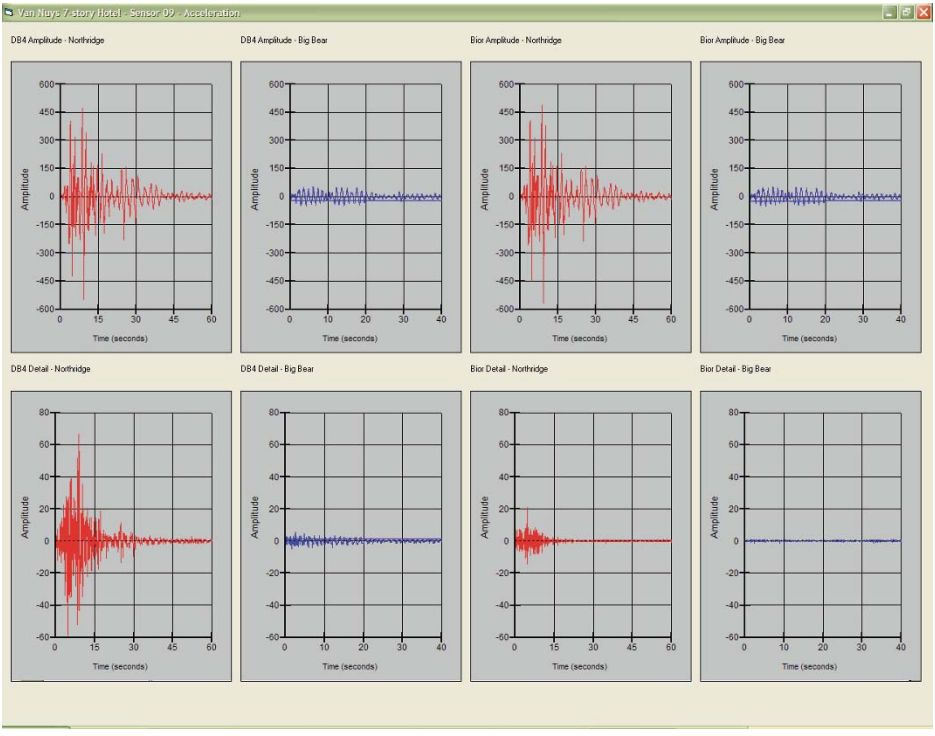

Figure 20. Amplitudes (top) and details (bottom) for a DB4 wavelet analysis of sensor data for the 1994 Northridge and the 1992 Big Bear earthquakes

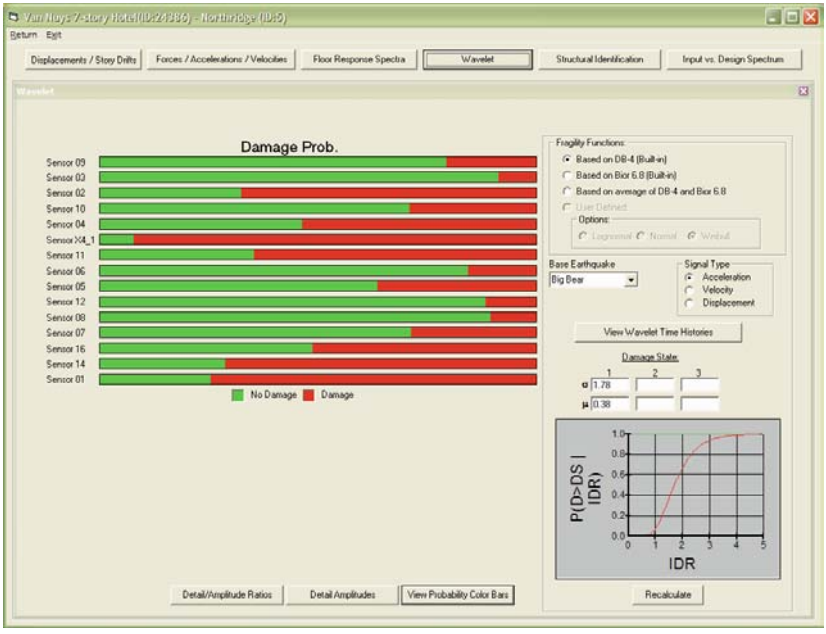

Figure 21. Damage probabilities obtained by wavelet analysis for the 1994 Northridge earthquake

5. Conclusions

A set of methodologies for automated post earthquake damage assessment of instrumented buildings were presented. It was shown that these methods can be used immediately after an earthquake to assess the probability of various damage states in the N-S and E-W directions and throughout the height of each building. The methods have been applied to more than 40 CSMIP instrumented buildings which have recordings from more than one earthquake. The results indicate that the proposed methods can provide extremely useful information regarding the status of a building immediately after an earthquake by simple and rapid analysis of sensor data and prior to any building inspections.

ACKNOWLEDGMENTS

Funding for this project was provided by State of California, California Geologic Survey, Strong Motion Instrumentation Program (SMIP) under Contract Number 1003-781.

The authors wish to express their gratitude to the members of the consulting panel of experts consisting of Professors Wilfred Iwan, S.T. Mau, and Eduardo Miranda.

The opinions expressed in this paper are those of the author and do not necessarily reflect the views of the California Strong Motion Instrumentation Program or John A. Martin and Associates, Inc.

References

Alimoardi, A., and Naeim, F., 2005a, Identification of Linear and Nonlinear Seismic Response using Genetic Algorithms, in preparation.

Alimoardi, A., Miranda, E., Taghavi, S, and Naeim, F., 2005b, Automated Identification of Linear and Nonlinear Structural Systems using Genetic Algorithms and Approximate Mode Shapes, in preparation.

American Society of Civil Engineers (ASCE), 2000, *Prestandard and Commentary for the Seismic Rehabilitation of Buildings*, Washington, D.C.

Applied Technology Council (ATC), 1989, *Procedures for Postearthquake Safety Evaluation of Buildings, Redwood City*, CA.

Aslani, H., and Miranda, E., 2003, Probabilistic Assessment of Building Response During Earthquakes, in: *Applications of Statistics and Probability in Civil Engineering*, Der Kiureghian, Madanat and Pestana (eds), Millpress, Rotterdam.

California Strong Motion Instrumentation Program (CSMIP), 1995, Processed Data for Los Angeles 2-story Fire Command Control Building from the Northridge Earthquake of 17 January 1994, Report No. OSMS 95-01A.

Federal Emergency Management Agency (FEMA), 2004, *HAZUS-MH Technical Manual*, Washington, D.C.

McJunkin, R.D., and Ragsdale, J.T., 1980, Compilation of Strong Motion Records and Preliminary Data from the Imperial Valley Earthquake of 15 October 1979, Preliminary Report 26, Office of Strong Motion Studies, California Division of Mines and Geology, Sacramento, CA.

Miranda E., and Taghavi S., 2005, Approximate Floor Acceleration Demands in Multistory Buildings: I Formulation, *Journal of Structural Engineering*, **131**(2):203-211.

Naeim, Farzad, 1997, Performance of 20 Extensively Instrumented Buildings during the 1994 Northridge Earthquake – An Interactive Information System, A report to CSMIP, John A. Martin & Associates, Inc.

Naeim, F., Lee, H., Bhatia, H., Hagie, H., and Skliros, K., 2004, CSMIP Instrumented Building Response Analysis And 3-D Visualization System (CSMIP-3DV), *Proceedings of the SMIP-2004 Seminar*.

Naeim, F., H., Hagie, H., Alimoradi, A., and Skliros, K., 2005, Automated Post-Earthquake Damage Assessment and Safety Evaluation of Instrumented Buildings, A report to CSMIP, John A. Martin & Associates, Inc., in preparation.

Porter and Kiremidjian, 2001, Assembly-Based Vulnerability of Buildings and its Uses in Seismic Performance Evaluation and Risk-Management Decision-Making, Report No. 139, John A. Blume Earthquake Engineering Research Center, Stanford, CA

Revadigar, S. and Mau, S.T., 1999, Automated Multi-criterion Building Damage Assessment from Seismic Data, *Journal of Structural Engineering*, ASCE, **125**(2):211-217.

A DETAILED SEISMIC PERFORMANCE ASSESSMENT PROCEDURE FOR RC FRAME BUILDINGS

AHMET YAKUT*
Depatment of Civil Engineering, Middle East Technical University, 06531, Ankara, Turkey

EMRAH ERDURAN
Depatment of Civil Engineering, Middle East Technical University, 06531, Ankara, Turkey

Abstract. A detailed seismic performance assessment procedure has been developed for RC frames with masonry in-fill walls. The procedure is based on member damage functions developed for the primary components: columns, beams and in-fill walls. Investigations carried out to determine the influence of a number of parameters on the damageability of components were combined with experimental data to develop component damage functions expressed in terms of member deformations. The component damage states are combined taking into account their importance to determine the story and building level damage states used to assess its performance. The procedure has been calibrated and compared with other procedures by predicting the observed performance of buildings exposed to recent earthquakes in Turkey. It was observed that the damage experienced by most of the components of these buildings was predicted satisfactorily, and that the observed building damage states were captured. It has been applied to several existing representative buildings located in Zeytinburnu to evaluate their performance under an expected future earthquake. The procedure can be used for a reliable performance assessment as well as performance-based design of RC frame structures.

Keywords: Reinforced Concrete Frame; Seismic Assessment; Damage Functions; component importance; performance evaluation

* Ahmet Yakut, Depatment of Civil Engineering, Middle East Technical University, 06531, Ankara, Turkey; e-mail:ayakut@metu.edu.tr

S.T. Wasti and G. Ozcebe (eds.), Advances in Earthquake Engineering for Urban Risk Reduction, 135–150.

1. Introduction

Reinforced concrete buildings constitute the majority of the building stock throughout the world, especially in developing countries. Due to their poor performance under major earthquakes occurring in the last decade, significant research has been initiated to assess the vulnerability of the existing building stock and to provide means of improving the expected seismic performance of the vulnerable buildings. The available seismic performance assessment procedures are classified based on the degree of sophistication involved, in addition to the quality of data in hand and the purpose of the assessment. Quick performance assessment procedures using only superficial data that reflect the general properties of the building, mostly architectural features, provide a crude index that is used to rank a group of buildings to determine their priority for further evaluation. An improved but preliminary step is to use additional information including certain structural features of the building to assess its vulnerability by identifying unsafe buildings using simple and practical procedures. The buildings identified as vulnerable in the preliminary or quick assessment phases require more thorough evaluations before a mitigation measure is proposed.

Detailed assessment procedures generally require a full blown seismic analysis of the building to determine the forces and deformations experienced by its components under a presumed level of earthquake intensity.

The general tendency in most assessment procedures is to determine an index that reflects the vulnerability or damageability of the structure. In their State-of-the-Art Review, Williams and Sexsmith (1995) grouped the damage indices as local and global. The local damage indices are defined for individual elements, whereas global damage indices are given for the entire structure. The local damage indices are generally defined in terms of ductility, interstory drift, stiffness degradation, dissipated energy or various combinations of these terms. One of the best-known and widely used local damage indices is the one developed by Park and Ang (1985). This damage index is expressed as a linear combination of the normalized displacement and dissipated energy (Eq. 1).

$$D = \frac{\delta_m}{\delta_u} + \beta_e \frac{\int dE}{F_y \delta_u} \tag{1}$$

The first term in Eq. (1) is the ratio of the maximum attained deformation to the ultimate deformation capacity of the member under static loading (δ_u). The second term accounts for the effect of the dissipated hysteretic energy on the accumulated damage. The term $\int dE$ is the total hysteretic energy absorbed by

the element of interest; F_y is the calculated yield strength and β_e is a coefficient for cyclic loading effect. This model can also be used to assess the damage of the entire building. The global damage index was defined as the weighted average of the damage indices of all the elements, where the weighing coefficient of an element is equal to the ratio of the energy absorbed by that element to the sum of the energy absorbed by all of the elements.

The global damage indices were grouped into two by Williams and Sexsmith (1995). The first group is called the weighted average damage indices and is based on the weighted average of the damage scores of all the elements. An example to this group of global damage indices was summarized above. The other group is based on the variation of modal parameters due to the sustained damage. These methods are based on the natural frequencies or they may use the mode shapes to locate the damage (Roufaiel and Meyer, 1987; DiPasquale and Cakmak, 1987).

A number of widely used assessment procedures (FEMA 356, 2000; ATC-40, 1996; Eurocode 8, 2003) compare the demands with the recommended values of member capacities varying with the level of the performance objectives employed. Each member is classified as either force-controlled or displacement controlled, depending on its mode of behavior. The outcome of the evaluation is a decision on the capacity of the member as such it meets the criteria of the target performance level or not. No guidelines are provided on how to make a decision on the building as a whole. In other words, only member level information and evaluation is carried out. The main difference between the Eurocode 8 (2003) and the other two documents is that, Eurocode 8 uses a force based criterion for shear critical members rather than a displacement based one.

A major drawback of the procedures proposed by FEMA (2000), ATC (1996) and Eurocode (2003) is that no guidelines are provided on how to assess the performance of the whole building based on the member level evaluations carried out and the final decision remains to the judgment of the engineer performing the assessment.

This article presents a detailed assessment procedure that is applied to individual buildings. The procedure is based on the behavior of the individual components comprising the structural system. The component vulnerabilities are expressed in the form of a damage curve that relates a response parameter to the physical damage. Columns, beams and masonry infill walls are considered as structural components that contribute to the lateral load capacity of the RC frame buildings, so damage curves have been developed for these components only.

2. Outline of the Procedure

The procedure presented in this article is a detailed vulnerability assessment procedure carried out for an individual building under a given ground motion or design spectrum. The outline of the procedure is explained in this part. The response parameters that have been used as pertaining to seismic damage are the interstory drift ratio for columns and infill walls and the chord rotation for beams.

The steps involved in the procedure developed are summarized below

Step 1 – Data Collection: The developed methodology requires a nonlinear analysis, either static or dynamic, of the given building. For this, first of all, some data must be collected about the building at hand. This data includes the design drawings, as-built dimensions of the building, the condition of the building and the material properties, preferably obtained from in-situ tests.

Step 2 – Nonlinear Analysis & Determination of the Member End Deformations: The computer model developed may be a two dimensional or a three dimensional model, based on the choice of the user. Similarly, the user chooses the type of nonlinear analysis (nonlinear static analysis or nonlinear time history analysis) that will be used. If a nonlinear static analysis is carried out, the capacity curve obtained as a result of this analysis must be used to determine the performance point of the building under the prescribed ground motion or response spectrum, using the procedures available in literature such as the Capacity Spectrum Method summarized in ATC-40 (1996), the Displacement Coefficient Method of FEMA-356 (2000) or the Constant Ductility Spectrum Method. The member end deformations at this performance point will be recorded and used in the subsequent steps. If a nonlinear time history analysis is carried out, then the maximum member end deformations will be recorded.

Step 3 – Determination of the Member Damage Scores: The maximum member end deformations obtained as a result of the nonlinear analysis will be input in the damage functions developed to compute the damage score of each member.

Step 4 – Determination of the Story and Building Damage Scores: Once the damage score for each member is determined, then the weighted average of these damage scores is computed to determine the damage score of each story and finally of the entire building. The weighing coefficients used here depend on the contribution of each member in resisting the seismic forces and named as component importance factors. Approximate values for the component importance factors were developed and are given in a tabular format.

The final step of the procedure is the determination of the performance of the building based on the computed building damage score.

The first two steps of this procedure are familiar to the engineers; hence these parts will not be elaborated in this article. The details of the third step are given elsewhere (Erduran and Yakut, 2004a, 2004b) so the last step will be summarized in the forthcoming sections.

3. Component Damage Functions

For each type of component, numerical analyses and experimental test results have been used to develop damage curves. Extensive numerical analyses have been carried out to determine parameters affecting damageability of RC members. For the columns and beams, damage curves for shear behavior and three ductility levels of flexural behavior have been developed. The damage curves developed for the components of a RC frame with masonry infill walls are discussed briefly next.

3.1. COLUMN DAMAGE CURVES

As a result of the numerical analyses carried out, it was observed that the main parameters affecting the ultimate ductility of the columns were the amount of transverse reinforcement (ρ_s) and the axial load level (N/N_o; N_o being the nominal axial load capacity of the column). The column ductility levels are determined based on their $\rho_s/(N/N_o)$ values. If the $\rho_s/(N/N_o)$ value for a column is less than 5%, then the ductility level of this column is deemed to be low. If that value is between 5% and 10%, then the column is considered to be moderately ductile. Finally if $\rho_s/(N/N_o)$ value exceeds 10%, then the ductility level is stated to be high.

The main damage criterion used in the development of the damage curves for reinforced concrete columns is the ductility index which is defined as the given drift divided by the yield drift. In this study, four main damage levels are defined: negligible, light, moderate and heavy. For the first three damage levels crack widths were used to establish the ductility indices. To compute the crack widths, the expression proposed by Frosch (1999) was used. The ductility index corresponding to the heavy damage state was obtained from the cyclic load-deformation curves of the tested columns rather than the capacity curves of the analyzed columns. The capacity curves may overestimate the ultimate ductility of the columns, since the pushover analysis can not take the strength degradation due to cyclic loading into account. To determine the ultimate ductility of the columns, cyclic test data of 33 columns, which were obtained from the NISTIR report (Taylor et al., 1997), were used.

The other parameters affecting the damageability of RC columns are the yield strength of longitudinal reinforcement (f_{yk}) and the slenderness of the

column (L/i). These two parameters affect the yield drift ratio of the columns. Since the damage criterion set in this study depends on the ductility levels (ratio of a certain drift ratio to the yield drift ratio), these two terms affect the damageability of the columns at every stage. The effect of yield strength of longitudinal reinforcement and slenderness of the column was reflected in the damage curves as correction factors. To obtain the most appropriate form for the damage curves, the drift ratios corresponding to the four damage levels were plotted, and the most suitable functional form was observed to be the one given in Eq.(2).

$$\text{Damage}(\delta) = \left[1 - e^{-\left(\frac{\delta}{a}\right)^b}\right] g(\delta) \tag{2}$$

where

$$g(\delta) = 0.5\left[1 - \cos\left(\frac{\pi\ \delta}{c}\right)\right] \text{ if } \delta \leq c \tag{3.a}$$

$$g(\delta)=1 \text{ if } \delta > c \tag{3.b}$$

In Eqs. (2) and (3), δ represents the interstory drift ratio and a, b, and c are the equation parameters. The values of these parameters were obtained using the least squares curve fitting technique for each ductility level and are given in Table 1 with the corresponding damage curves presented in Figure 1 which displays a damage curve for the columns that are expected to fail in shear.

TABLE 1. Values of equation parameters for damage curves of RC columns

Parameter	Low Ductility	Moderate Ductility	High Ductility
a	0.0119	0.0170	0.0205
b	1.4206	1.1021	0.9859
c	0.0093	0.0123	0.0144

The correction factors for the slenderness (C_s) of the column and the yield strength of longitudinal reinforcement (C_{fy}) are given in Eqs. (4) and (5), respectively.

$$C_s = 0.045\left(\frac{L}{i}\right) \tag{4}$$

$$C_{fy} = 0.4\left(\frac{f_y}{439}\right) + 0.6 \tag{5}$$

The drift ratios obtained as a result of the structural analysis should be corrected by $1/C_s$ and $1/C_{fy}$ before they are used in the damage curves.

These damage curves are for columns whose predominant failure mode is flexure. A separate curve for shear critical columns was also formed and presented in Figure 1.

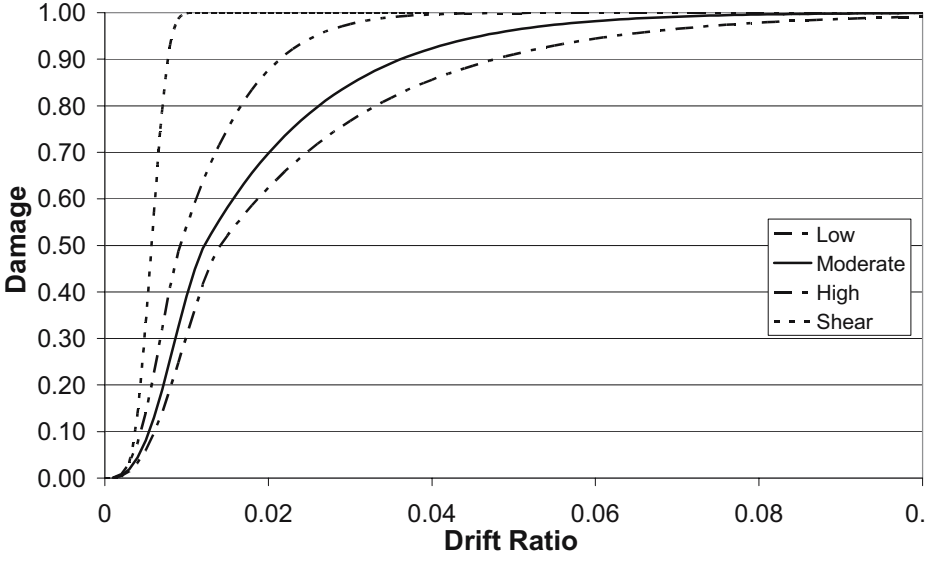

Figure 1. Damage curves for RC columns

3.2. BEAM DAMAGE CURVES

The beams are grouped into three according to their $(\rho_s f_{ck}(\rho'/\rho))/(f_{yk}\rho)$ values; f_{ck} is the compressive strength of concrete, f_{yk} is the yield strength of longitudinal reinforcement, ρ' and ρ are the ratios of compression and tension reinforcements, respectively. If the $(\rho_s f_{ck}(\rho'/\rho))/(f_{yk}\rho)$ value for a beam is less than 0.25%, then the ductility level of this beam is low. The limiting value of $(\rho_s f_{ck}(\rho'/\rho))/(f_{yk}\rho)$ for moderate and high ductility levels determined from the parametric analyses is 1%. If the $(\rho_s f_{ck}(\rho'/\rho))/(f_{yk}\rho)$ of a beam exceeds 1%, the ductility level of this beam is high, otherwise it is assumed to be moderate.

After a database of sufficient size was formed, the damage curves for RC beams were developed. The functional form for the damage curves was the same with that of the columns. However, this time the independent parameter was the rotation (θ) rather than the interstory drift ratio (δ). The values of the equation parameters were determined for the three ductility levels using the least squares curve fitting technique and are given in Table 2. Figure 2 presents the damage curves for the beams of three ductility levels. In these damage

curves, the depth of the beams was constant and equal to 500mm. If the depth of the beam (d) analyzed is different from 500 mm, the rotation value obtained from the structural analysis must be divided by the C_d computed from Equation 6 before it is used in the computation of the damage score of that beam.

$$C_d = \left(\frac{d}{500}\right)^{-1} \tag{6}$$

TABLE 2. Values of equation parameters for damage curves of RC beams

Parameter	Low Ductility	Moderate Ductility	High Ductility
a	0.0118	0.0172	0.0340
b	2.8000	1.5000	1.05000
c	0.0100	0.0140	0.0140

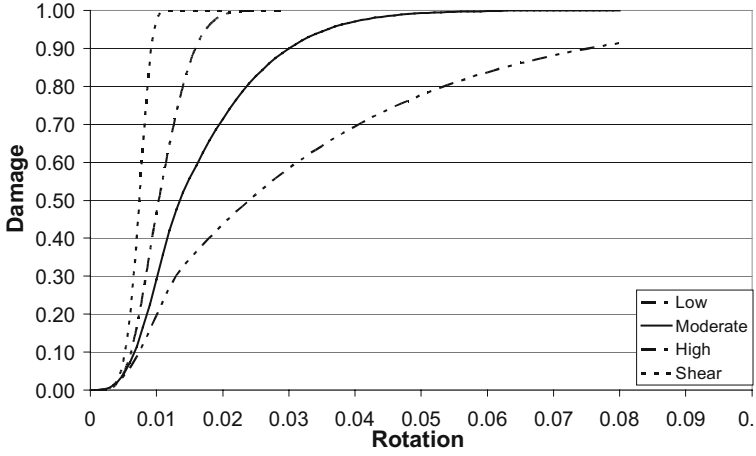

Figure 2. Damage curves developed for RC beams

As in the case of columns, these damage curves are for flexure critical members and a separate curve for shear critical members was also developed and presented in Figure 2 together with the other curves.

3.3. INFILL WALL DAMAGE CURVES

Brick infills are generally treated as non-structural elements and their contribution is neglected in the practical design applications. However, past earthquakes revealed that the presence or non-existence of brick infills significantly influences the seismic behavior of a building. Hence, for a reliable seismic assessment, the infills of brick infilled reinforced concrete frames were taken into account and drift based damage curves were developed.

The major parameter that affects δ_y (yield drift ratio) of infill walls is the non-dimensional term, $(f_m L^2)/(E_I dh)$, where f_m and E_I are the compressive strength and Young's modulus of the infill material, L is the bay length, h is the height and d is the diagonal length of the infill panel. Hence, the analyzed infills were grouped into four according to their $(f_m L^2)/(E_I dh)$ as summarized in Table 3.

For the drift based damage curves of the brick infills, the functional form given for columns and beams was once again employed. The equation parameters a, b and c were modified to reflect the brittle behavior of the infills. The values of these parameters are summarized in Table 4 and the developed damage curves are presented in Figure 3.

TABLE 3. Grouping of infills

Group	$(f_m L^2)/(E_I dh)$ value
1	<0.0015
2	between 0.0015 and 0.0020
3	between 0.0020 and 0.0025
4	<0.0025

TABLE 4. Equation parameters developed for the damage curves developed for brick infills

Parameter	Group 1	Group 2	Group 3	Group 4
a	0.0030	0.0042	0.0055	0.0070
b	7.0000	10.0000	12.0000	15.0000
c	0.0020	0.0020	0.0020	0.0020

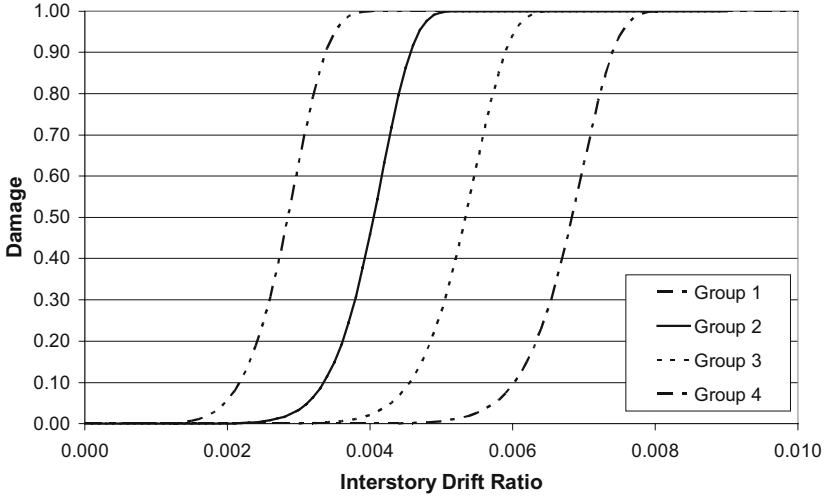

Figure 3. Damage curves developed for brick infills

4. Component Importance Factors

Once the damage scores for each member of the building is determined, these damage scores must be combined to determine the damage score of the building in order to assess its vulnerability. The most appropriate way to combine the component damage scores seems to be taking their weighted average. The main problem in the weighted average procedure is the determination of the weighing coefficients for each member which are called "*Component Importance Factors*". These importance factors must reflect the importance or contribution of each component in resisting the seismic forces. To determine these importance factors, a procedure is developed and applied on several buildings to propose approximate values for the importance factor of each component. The contribution of each component to the energy dissipation capacity of the entire structure was chosen as the criterion to evaluate the importance of that component.

The energy dissipation capacity of the building is computed as the area under its pushover curve, a plot of base shear force versus roof displacement (E_0). To determine importance of a component in a given story to this capacity that component is virtually removed from the system in that story by assigning hinges to its ends that diminishes its load carrying capacity. Then the building is re-analyzed to obtain a new pushover curve and the corresponding energy dissipation from its area (E_i). Obviously the area E_i is smaller than E_0 and their ratio provides an indication of the contribution of the selected component to the energy dissipation capacity. Applying this procedure to all components in each story a number of energy dissipation capacities are computed for each case. For example, to represent the damage occurring in the first story beams of the structure, moment releases were applied at both ends of these beams. For the infills, the infills of a story were removed from the frame to represent the damage occurring during an earthquake.

So for a five story, the energy dissipation capacities of the original frame, E_o, and the 15 damage cases are obtained. The importance of a component in resisting the seismic forces is inversely proportional to the ratio of the energy dissipated by the corresponding damage case to that dissipated by the original frame, E_o. In addition to this, the sum of the importance factors for all the components of a building must add up to 1. For this, the ratio E_o/E_j for each damage case was summed and the importance factor obtained for each component was normalized by this sum. In other words, the importance factor for a component is given as:

$$IF_j = \frac{E_0}{E_j} \Bigg/ \sum_{i}^{3n} \frac{E_0}{E_j} \tag{7}$$

where, j represents the damage case corresponding to the member of interest and n is the number of stories.

The procedure developed above was applied on several buildings with different material and geometrical properties to develop approximate values for the importance factors of the components of brick infilled reinforced concrete frames. It was observed that, the material and geometrical properties of the frames do not have significant effect on the component importance factors and the approximate values given in Tables 5 to 7 were obtained as the mean component importance factors.

The importance factors computed using the above procedure is not for a single member. Instead, they reflect the importance of all the members of the same type located in the same story. To compute the importance of each column, the weighted average of the importance factor for all of the columns of a story must be taken where the weighing coefficient is the moment of inertia of the column. Simply taking the average of the importance factor computed using the above formulation for the beams and columns would be sufficient for determining the importance factor of a single beam or a single infill. A more detailed summary regarding the development of importance factors was reported elsewhere (Erduran and Yakut, 2004c). The importance of first story columns becomes more dominant as the number of stories increase whereas for beams and infill walls it appears to be same for each floor.

TABLE 5. Importance factors for columns

		Number of Stories of the Building						
		2	3	4	5	6	7	8
Story Number	1	0.375	0.250	0.233	0.174	0.193	0.165	0.144
	2	0.375	0.250	0.233	0.174	0.193	0.165	0.144
	3		0.250	0.233	0.174	0.193	0.165	0.144
	4			0.053	0.174	0.058	0.165	0.144
	5				0.053	0.058	0.030	0.043
	6					0.058	0.030	0.043
	7						0.030	0.043
	8							0.043

5. Performance Evaluation of the Building

According to the damage criterion set in this study, there are mainly four damage levels: negligible, light, moderate and heavy. In addition to this, the performance of the buildings under a given earthquake is mainly grouped into

three as immediate occupancy (IO), life safety (LS) and collapse prevention (CP). The first two of the damage levels used in this study correspond to the immediate occupancy performance criterion. The moderate damage state corresponds to the life safety performance criterion whereas the heavy damage level corresponds to the collapse prevention. Recalling the damage scores assigned to the four damage levels, the damage scores corresponding to the performance levels are summarized in Table 8.

Once the damage score of each story and the entire building is computed, their performance levels are evaluated using Table 8. However, to be able to take the local failures that may exist in a single story of a building such as soft story, an additional criterion was also set. According to this criterion, if the damage score of a story exceeds 70%, then the performance level of the building is accepted to be collapse prevention regardless of the damage score of the entire building.

TABLE 6. Importance factors for beams

		Number of Stories of the Building						
		2	3	4	5	6	7	8
Story Number	1	0.075	0.053	0.042	0.034	0.029	0.025	0.022
	2	0.075	0.042	0.037	0.032	0.027	0.024	0.021
	3		0.031	0.032	0.029	0.026	0.023	0.020
	4			0.028	0.027	0.024	0.022	0.020
	5				0.024	0.023	0.021	0.019
	6					0.021	0.020	0.018
	7						0.019	0.018
	8							0.017

TABLE 7. Importance factors for infills

		Number of Stories of the Building						
		2	3	4	5	6	7	8
Story Number	1	0.055	0.037	0.028	0.022	0.018	0.016	0.014
	2	0.055	0.037	0.028	0.022	0.018	0.016	0.014
	3		0.037	0.028	0.022	0.018	0.016	0.014
	4			0.028	0.022	0.018	0.016	0.014
	5				0.022	0.018	0.016	0.014
	6					0.018	0.016	0.014
	7						0.016	0.014
	8							0.014

TABLE 8. Damage scores and corresponding performance levels

Damage Score	Performance
0% - 10%	Immediate Occupancy (IO)
10% - 50%	Life Safety (LS)
50% - 100%	Collapse Prevention (CP)

6. Application to Zeytinburnu

The proposed procedure has been applied to several buildings damaged from past earthquakes for verification and calibration purposes. It has been shown that the observed seismic performances of the case study buildings have been predicted satisfactorily. The procedure has also been used for assessment of several RC frame buildings located in Zeytinburnu district of Istanbul and surveyed under the pilot project initiated to determine expected performance of the buildings in Zeytinburnu.

In the assessment of the buildings located in the Zeytinburnu district, the elastic response spectrum proposed in the National Earthquake Hazards Reduction Program (NEHRP) document (2001) was used to represent a ground motion with a probability of exceedance of 50% in 50 years. The major parameters in this response spectrum are the spectral acceleration at short periods (S_{DS}) and the spectral acceleration at the period of 1 sec (S_{D1}). The response spectrum used in this study can be fully defined for each ground motion and site once these two values are known. The S_{DS} and S_{D1} values that define the ground motion each building will be exposed to under a certain scenario earthquake.

Within the scope of this study, the detailed assessment of 10 mid-rise buildings (3-6 stories) with variable material properties was carried out. Table 9 presents the properties of the buildings assessed together with the S_{DS} and S_{D1} values for each building.

All of the buildings were modeled in 3D in SAP2000 and the nonlinear static analysis was carried out to determine the capacity curve of the buildings together with the modal analysis. Then, these capacity curves were bilinearized to determine the yield base shear force (V_y), yield roof drift ratio (δ_y), ultimate base shear force (V_u) and the ultimate drift ratio of (δ_u) of the buildings. The target displacement of each building under the specified ground motion was computed using the displacement coefficient method summarized in FEMA 356 (2000). Once the displacement demand is determined, the assessment procedure summarized above was applied on each building to determine expected performance of each member, each story and the entire building under the given ground motion. Table 10 summarizes the bilinear capacity curve parameters,

target roof drift ratio under the given elastic spectrum (δ_t), maximum story damage score, building damage score and the expected performance of each building.

As shown in Table 10 one of the ten buildings assessed was found to be immediately occupiable under the given ground motion. Five buildings were found to suffer moderate damage and the remaining 4 were found to experience either heavy damage or collapse. The results of the assessment shows that the buildings with favorable material properties will probably not suffer heavy damage or collapse, while the ones with poor material properties are highly vulnerable to devastating earthquakes.

TABLE 9. Properties of the assessed buildings in Zeytinburnu district

Building ID	Plan Area (m^2)	# of Stories	f_{ck} (MPa)	f_{yk} (MPa)	S_{DS} (g)	S_{D1} (g)
BLD1	165	6	27	420	0.767	0.454
BLD2	100	4	9	220	0.692	0.412
BLD3	70	5	16	220	0.698	0.417
BLD4	98	5	8	220	0.729	0.432
BLD5	80	5	10	220	0.873	0.692
BLD6	91	4	15	220	0.873	0.692
BLD7	147	5	11	220	0.699	0.416
BLD8	269	3	16	420	0.698	0.417
BLD9	83	6	13	220	0.735	0.435
BLD10	145	4	15	220	0.714	0.424

TABLE 10. Results of the assessment of the buildings in Zeytinburnu district

BLD ID	T (sec)	V_y/W	δ_y (%)	V_u/W	δ_u (%)	δ_t (%)	Max Story Damage (%)	Bluilding Damage Score (%)	Perf.
BLD1	0.627	0.32	0.14	0.49	1.32	0.58	10.85	5.60	IO
BLD2	0.644	0.11	0.17	0.13	1.24	0.94	28.22	26.06	LS
BLD3	0.921	0.06	0.19	0.07	1.29	1.01	54.20	25.16	LS
BLD4	1.430	0.04	0.25	0.06	1.51	1.51	90.05	42.67	CP
BLD5	0.996	0.03	0.13	0.04	1.24	1.24	77.12	40.88	CP
BLD6	0.672	0.10	0.23	0.11	1.85	1.75	88.41	52.16	CP
BLD7	0.798	0.09	0.14	0.13	1.28	0.95	63.09	28.77	LS
BLD8	0.519	0.25	0.34	0.29	1.68	0.85	33.71	19.27	LS
BLD9	1.340	0.05	0.29	0.08	2.02	1.36	68.49	31.99	LS
BLD10	0.792	0.11	0.15	0.13	1.04	1.03	71.86	46.01	CP

7. Conclusions

The procedure developed for reinforced concrete frames with masonry in-fill walls provides an objective way to assess the performance of an individual building. It relies on the behavior of its components determined from experimental as well as numerical studies. The effects of the significant parameters on the performance of the components were incorporated on their damage curves.

The decision regarding the expected future performance of an existing building is quite challenging and it is believed that this procedure provides a tool not for only reliable performance assessment but also for performance based design of reinforced concrete buildings with infill walls.

The procedure has been calibrated and verified on a number of case study buildings that have suffered various degrees of damage dring some recent earthquakes, showing quite satisfactory predictions.

References

Applied Technology Council (ATC), 1996, Seismic evaluation and retrofit of concrete buildings, *ATC-40*, California

Building Seismic Safety Council for the Federal Emergency Management Agency, 2001, NEHRP recommendations for seismic regulations for new buildings and other structures, Washington DC

Chopra A. K. and Goel R. K., 1999, Capacity-demand-diagram methods for estimating seismic deformation of inelastic structures: SDF systems, *Technical Report PEER-1999/02*, Pacific Earthquake Engineering Research Center, University of California at Berkeley, Berkeley, California

DiPasquale E. and Cakmak A. S., 1987, Detection and assessment of seismic structural damage, *Technical Report NCEER-87-0015*, National Center for Earthquake Engineering Research, State University of New York, Buffalo NY

Erduran E. and Yakut A., 2004a, Drift based damage functions for reinforced concrete columns" *Computers and Structures*, **82**: 121-130

Erduran E. and Yakut A., 2004b, Drift Based Damage Functions for Components of RC Structures, *13th World Conference on Earthquake Engineering,* Vancouver, Canada

Erduran E. and Yakut A., 2004c, Development of Component Importance Factors for RC Buildings, *6th International Congress on Advances in Civil Engineering*, Bogazici University, Istanbul, October.

European Committee for Standardization, 2003, Eurocode 8: Design of structures for earthquake resistance Part 3: Strengthening and repair of buildings – Draft No:4, *Eurocode 8*, Brussels

Federal Emergency Management Agency (FEMA), 2000, Prestandard and commentary for the seismic rehabilitation of buildings, *FEMA-356*, Washington, DC

Frosch R. J., 1999, Another look at cracking and crack control in reinforced concrete, *ACI Struct. J.*, **96**(3): 437-442

Park Y. and Ang A. H, 1985, Mechanistic seismic damage model for reinforced concrete, *J. Struct. Eng.*, **111**(4): 722-739

Roufaiel M. S. L. and Meyer C, 1987, Reliability of concrete frames damaged by earthquakes, *J. Struct. Eng.*, **113**(3): 445-457

Williams M. S. and Sexsmith R. G, 1995, Seismic Damage Indices for Concrete Structures: A State-of-the-Art Review, *Earthquake Spectra*, **11**(2): 319-349.

ASSESSMENT OF SEISMIC FRAGILITY CURVES FOR LOW- AND MID-RISE REINFORCED CONCRETE FRAME BUILDINGS USING DUZCE FIELD DATABASE

M. ALTUG ERBERIK*
Department of Civil Engineering, Middle East Technical University, Ankara 06531, Turkey

SERDAR CULLU
Department of Civil Engineering, Middle East Technical University, Ankara 06531, Turkey

Abstract. This paper focuses on the generation of fragility curves for low-rise and mid-rise reinforced concrete frame buildings, which constitute approximately 75% of the total building stock in Turkey and which are generally occupied for residential purposes. These buildings, which suffered extensive damage after recent earthquakes, are not designed according to the current code regulations and the supervision in the construction phase is not adequate. Hence the buildings possess many deficiencies like irregularities in plan and elevation, weak column-strong beam connections, poor concrete quality, inadequate detailing of reinforcement in hinging zones, etc. In this study, the test bed, which represents the characteristics of the aforementioned frame buildings, is selected as the Duzce field database. The influence of ground motion characteristics, structural input parameters, sampling techniques, sample size, type of hysteresis model and limit state definitions on the response statistics is investigated and fragility curves for low- and mid-rise reinforced concrete structures in Turkey are proposed as an end product.

Keywords: fragility; reinforced concrete buildings; sampling techniques; capacity curve; limit states

*M. Altug Erberik; e-mail: altug@metu.edu.tr

S.T. Wasti and G. Ozcebe (eds.), Advances in Earthquake Engineering for Urban Risk Reduction, 151–166.

1. Introduction

This paper focuses on low-rise and mid-rise reinforced concrete frame buildings, which constitute approximately 75% of the total building stock in Turkey and which are generally occupied for residential purposes. Observations related to the reinforced concrete frame buildings which suffered heavy damage or even collapsed after recent earthquakes are as follows:

- Most of the buildings are not designed according to the current code regulations;
- Seismic behavior is not taken into consideration in the architectural design and during selection of the structural system;
- Supervision in the construction phase is not adequate which in turn induces deficiencies like poor concrete quality, inadequate detailing of reinforcement, etc.

The tool that is employed to assess the seismic performance of low-rise and mid-rise reinforced concrete frame buildings is the fragility curve in this study. By definition, fragility curves provide estimates of the probabilities of reaching or exceeding various limit states at given levels of ground shaking intensity for an individual structure or population of structures[1].

During the construction of fragility curves for building structures, it is necessary to consider the country-specific characteristics of the building stock. The reason is that the construction practice may differ substantially in different countries and since the differences in the country-specific characteristics of building structures are directly reflected in the fragility curves, this may lead to erroneous estimates in terms of earthquake damage and loss. However, this fact has usually been ignored and the results obtained from fragility analysis of building structures in other countries have been employed in the earthquake loss estimation and master-plan studies in Turkey. Hence the main goal of the study is to determine the fragility of low-rise and mid-rise reinforced concrete frame buildings by considering the country-specific structural characteristics.

2. Duzce Field Database

The inventory used in this study is composed of 28 reinforced concrete buildings extracted from a building database of approximately 500 buildings in Duzce, which has been affected by two major earthquakes in 1999. Post-earthquake damage assessments of the buildings are also available. The database under concern has been used before by other researchers[2-4]. In this particular study, it is employed as the field data to conduct a very detailed sensitivity analysis based on fragility curves. By using this field data, the effects

of various input and response parameters and methods on the fragility functions are investigated.

General properties of the buildings in the database are listed in Table 1. Number of stories of the selected buildings ranges from 2 to 6. The building database is divided into two sub-groups: buildings with two and three stories are regarded as low-rise (LR) and buildings with four to six stories are considered as mid-rise (MR).

TABLE 1. General properties of the buildings in Duzce field database

Code	Construction Year	No. of Stories	Building Class	Building Height (m)	Concrete Strength (MPa)	Observed Damage
B01	1985	6	MR	16.3	15	Moderate
B02	1985	6	MR	16.1	14	Moderate
B03	1978	5	MR	14.4	17	Severe
B04	1991	5	MR	14.4	20	None
B05	1985	5	MR	13.8	20	Light
B06	1997	5	MR	14.3	20	None
B07	1985	3	LR	8.3	20	Moderate
B08	1989	4	MR	13.5	20	Moderate
B09	1977	4	MR	11.4	17	Moderate
B10	1975	5	MR	14.6	22	None/Light
B11	1962	2	LR	6.3	14	None
B12	1975	3	LR	8.3	9	Light
B13	1975	3	LR	8.9	14	Moderate
B14	1993	4	MR	11.6	17	Light
B15	1999	3	LR	8.9	13	Light
B16	1982	4	MR	11.6	22	Moderate
B17	1980	3	LR	8.4	9	Light
B18	1970	2	LR	6.3	17	Light
B19	1972	2	LR	5.6	9	Light
B20	1995	3	LR	8.3	14	Light
B21	1990	2	LR	6.1	17	Light
B22	1982	3	LR	8.1	10	Moderate
B23	1985	2	LR	5.8	14	None
B24	1973	3	LR	9.7	17	None
B25	1994	4	MR	12.3	14	Light
B26	1992	5	MR	14.7	13	Moderate
B27	1984	4	MR	12.5	10	Moderate
B28	1981	3	LR	9.6	10	Moderate

3. Individual Building vs. Stock of Buildings

To estimate the seismic vulnerability of a specific building type, two different approaches can be considered. In the first approach, each building in the stock is investigated individually and the vulnerability of the building stock is obtained by combining the fragility information associated with each building. Very detailed models and analysis procedures are employed; hence the results will be highly accurate. On the other hand, this approach is physically impractical and economically unfeasible. The second approach is to conduct the fragility studies by using the statistical properties of the building population. Simple models and methods are employed in this approach. The advantage of this approach is that it is simple and economically feasible. In addition, the non-technical decision makers prefer such simple and rapid estimates of anticipated losses to develop the proper judgment to execute their mitigation plans. However obtained results will be crude and the limitations of the models or the methods should be clearly understood.

In this study, fragility functions of low-rise and mid-rise reinforced concrete structures are constructed by considering the population statistics as explained above. The buildings are further classified as "bare frame" or "infilled frame" according to the absence or presence of masonry infill walls in the analytical models to examine their effect on seismic response. Hence there are four different sub-classes of frame buildings: low-rise bare frame, low-rise infilled frame, mid-rise bare frame and mid-rise infilled frame. The abbreviations used for these sub-classes throughout the text are LR_BR, LR_INF, MR_BR and MR_INF, respectively. Each building is represented by an equivalent Single-Degree-of-Freedom (SDOF) system with three structural parameters: Period (T), strength ratio (η) and the post-elastic stiffness as a fraction of the elastic stiffness (α). These parameters are obtained from the push-over analysis of the model frames in two orthogonal directions by using the bilinearization approach proposed by FEMA356 [5]. Capacity curves and the corresponding capacity spectra of the structural models were obtained by the analysis software SAP2000 [6] and the results can be found elsewhere[2]. Examples of capacity spectrum are shown in Figure 1.a for mid-rise infilled frames. Similarly, bilinear representation of one of the curves in Figure 1.a (the one in solid black) is illustrated in Figure 1.b. As a result, the building population is characterized by the structural parameters T, η and α .

The main statistical descriptors (mean, μ and standard deviation, σ) of each variable for each sub-class obtained after the bilinearization process are listed in Table 2. The following observations are based on the statistical outcomes:

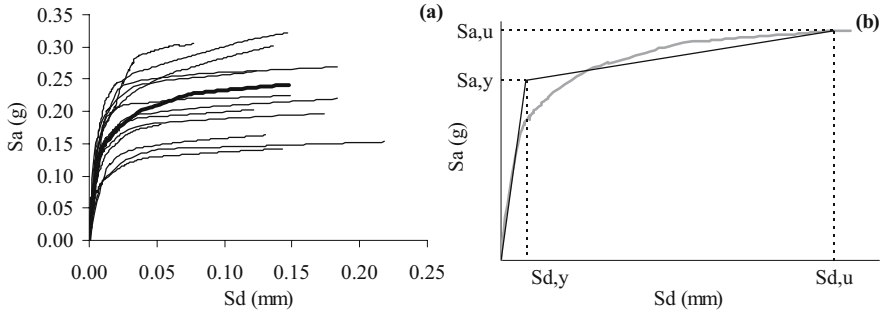

Figure 1. a) A sample taken from the capacity spectra obtained for MR_INF frames, b) bilinear representation of the capacity spectrum represented by the solid line in part (a)

- The increase in stiffness and strength is significant in both low-rise and mid-rise structural models by the addition of infill walls when compared with the corresponding values of the bare frame models.
- In terms of the parameters T and η, the dispersion (variability) in low-rise building statistics is more significant than the one in mid-rise building statistics.
- Low-rise building models possess higher strength ratios.
- The variation in parameter α is very high.

4. Procedure for Generating Fragility Curves

There are several ways to generate seismic fragility curves. The method used in this study can be explained as follows:

TABLE 2. Main statistical descriptors of each sub-class of buildings after bilinearization

Parameter	Building Class	Bare Frame		Infilled Frame		All Frames	
		μ	σ	μ	σ	μ	σ
T	Low-rise	0.372	0.113	0.288	0.095	0.330	0.112
	Mid-rise	0.521	0.092	0.437	0.107	0.479	0.107
η	Low-rise	0.225	0.093	0.289	0.109	0.257	0.105
	Mid-rise	0.133	0.036	0.163	0.049	0.148	0.045
α^*	Low-rise	2.20	2.15	1.40	1.21	1.80	1.78
	Mid-rise	2.50	2.32	2.00	1.99	2.25	2.15

*Post-elastic stiffness values are in percent of the initial stiffness.

- It is based on SDOF analysis. Hence, the equivalent SDOF structural parameters are obtained from the bilinearized capacity curve corresponding to each building model. For each sub-class, statistical descriptors of the SDOF parameters (mean and standard deviation) are obtained.

- Nonlinear time history analysis is employed. Structural variability is taken into account by considering the structural input parameters as random variables, and ground motion uncertainty is taken into account by selecting a set of records with different characteristics. Ground motion records should be selected carefully so that the set should cover the whole range of hazard intensity in terms of the selected hazard parameter.
- After the analyses are conducted, response statistics are obtained in terms of maximum displacement. At this stage, damage-motion relationship can be easily constructed, where the horizontal axis is the hazard parameter to be used in the fragility analysis and the vertical axis is the demand parameter (i.e. maximum displacement response).
- The limit states in terms of maximum displacement are established. The best way to quantify the limit states is to employ the capacity curve of the structure where one can monitor the structural performance step by step.
- By using demand statistics and limit state values, the probability of exceedance of each limit state at a specific hazard level can be obtained. Finally computed conditional probability is plotted with respect to hazard parameter. This plot is defined as the fragility curve for that limit state.

5. Reference Fragility Curves

The main goal of this study is to investigate the sensitivity of different parameters or procedures on the final fragility curves. To achieve this, a reference set of fragility curves are required for the sake of comparison. Generation of the reference fragility curves for low-rise and mid-rise reinforced concrete structures of Duzce database is explained below in detail.

5.1. INPUT DATA FOR STRUCTURAL SIMULATIONS

After bilinearization process, three structural input parameters (T, η, α) were obtained from the capacity curve of each structural model. Among these input parameters, T and η are considered as random variables. A normal distribution is assumed for these parameters. The sample size is 28 considering both orthogonal directions. The validity of the normal distribution for each parameter in each sub-class is verified by the *chi-square goodness of fit* test. The variation of η with T for each sub-class is presented in Figure 2 with the corresponding correlation coefficient. The third parameter, α is considered as a deterministic parameter. Mean value is considered for each sub-class.

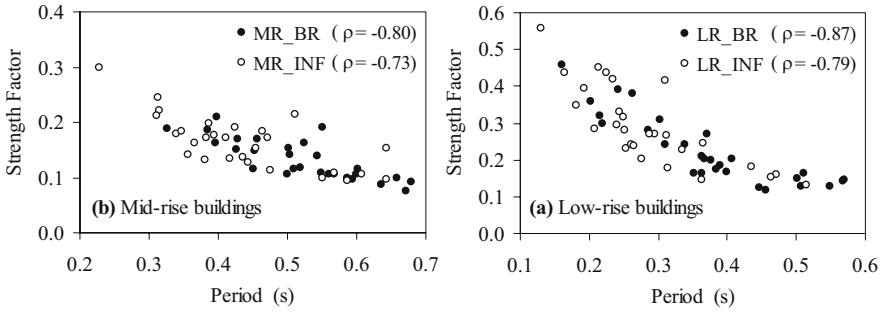

Figure 2. The variation of η with T for a) low-rise building sub-classes, b) mid-rise building sub-classes

5.2. GROUND MOTION SET

The reference hazard parameter is considered as Peak Ground Velocity (PGV) and selection of the ground motion set is carried out accordingly. There are 100 ground motion records in the dataset from different parts of the world (North America, Europe, Asia) covering a wide range of characteristics. Peculiar ground motions records due to extreme near-field and soil site effects are not included. The dataset is divided into 20 bins with intervals of 5 cm/s, each bin having five records within. The purpose of such a classification is to distribute the response statistics evenly in the whole hazard intensity range. The statistics in Figure 3 provide general information (peak ground acceleration, magnitude, closest distance to fault and site conditions) about the characteristics of the ground motion dataset.

5.3. RESPONSE STATISTICS

The response statistics in terms of maximum displacement are obtained by conducting inelastic SDOF time history analyses. The structural input parameters are η, T (random variables) and α (deterministic parameter) as explained in the above sections. The Clough stiffness degrading model [7] is employed in order to take into account the inelastic behavior. The viscous damping ratio, ξ is taken as 5%. Maximum response is monitored for all structural simulation triplets (T, η, α) at each ground motion hazard intensity. This is illustrated in Figure 4 for MR_INF sub-class. Hence there are 28 (no. of simulations in a sub-class)*5 (no. of records in a ground motion bin)=140 response data points in a vertical bin, where a normal distribution is fitted to calculate the probabilities of exceedance. For the whole range of hazard intensity, 140*20 (no. of ground motion bins)=2800 response data points are calculated.

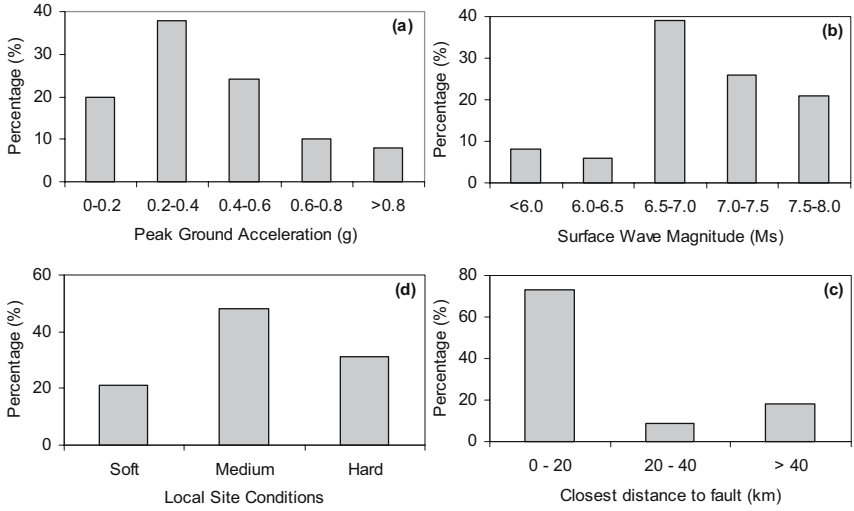

Figure 3. General characteristics of the ground motion data set in terms of a) peak ground acceleration, b) surface wave magnitude, c) closest distance to fault, d) local site conditions

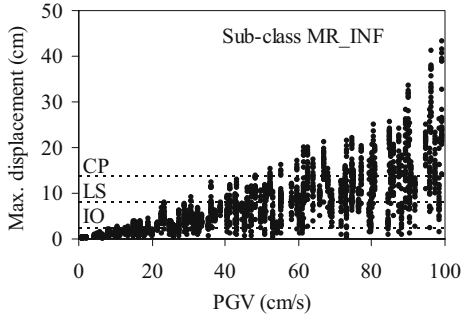

Figure 4. Response statistics (maximum displacement vs. PGV) for sub-class MR_INF

5.4. ATTAINMENT OF LIMIT STATES

Limit states, or in other words the performance levels, play a significant role in the construction of the fragility curves. Well-defined and realistic limit states are of paramount importance since these values have a direct effect on the fragility curve parameters.

Limit States considered in this study are Immediate Occupancy (IO), Life Safety (LS) and Collapse Prevention (CP). The definitions of these limit states in terms of global drift ratio are provided in FEMA356 [5] document. In this study, the limit states are established in terms of both global drift ratio and spectral displacement.

The approach used in this study to attain the limit states is a simple one and based on the utilization of the bilinear representation of each capacity curve. Accordingly, IO limit state is considered as the drift ratio (or spectral displacement) at the intersection point of the lines representing the elastic stiffness (initial period) and post-elastic stiffness, respectively. Analytically, this point represents the state when the yield base shear capacity of the building is exceeded. CP limit state is considered as the ultimate drift ratio (or spectral displacement) where a collapse mechanism occurs. LS limit state is considered as the drift ratio (or spectral displacement) in half way between the other two limit states for the sake of simplicity. Hence three limit states are established for the buildings in each sub-class. The statistics of the limit states for each sub-class is listed in Table 3 in terms of global drift ratio for the sake of comparison with the previously published specifications.

TABLE 3. Statistics for limit states of the building sub-classes in terms of global drift ratio

Limit States	LR_BR		MR_BR		LR_INF		MR_INF	
	μ (%)	σ (%)	μ (%)	σ (%)	μ (%)	σ (%)	μ (%)	σ (%)
IO	0.28	0.09	0.26	0.10	0.23	0.07	0.22	0.09
LS	0.88	0.21	0.77	0.26	0.85	0.20	0.75	0.26
CP	1.48	0.35	1.27	0.44	1.47	0.36	1.28	0.44

The numbers in Table 3 indicate that the presence of infill walls have an influence especially on the IO limit state. This is an expected outcome since serviceability limit state is closely related to the stiffness of the structure. The mean global drift ratio values range between 0.2% - 0.3%, 0.75% - 0.90% and 1.25% - 1.5% for IO, LS and CP limit states, respectively. When these values are compared with the ones proposed in different specifications [5,8] and studies [9,10], it is observed that the values are in the same range, but differences exist. Especially, the differences are more significant when CP limit state values are compared. However, these differences are justifiable on grounds of specific structural characteristics of Turkish buildings, or in other words, the Duzce database used in this study. Due to construction practice in Turkey, the buildings are more brittle than the ones considered in the relevant specifications. Hence they are generally heavily damaged or they collapse without experiencing large inelastic deformations.

5.5. GENERATION OF FRAGILITY CURVES

The mean values of limit states for each sub-class are placed on the corresponding response statistics plot in terms of maximum displacement response (see horizontal lines in Figure 4 as an example for MR_INF sub-

class). In the response statistics plot, each vertical bin of scattered demand data corresponds to an intensity level in terms of PGV. A normal distribution is fitted to the demand data and the statistical parameters (mean and standard deviation) are calculated for each PGV intensity level. The next step is to calculate the probability of exceedance of each limit state for a given intensity level. Then the calculated probability of exceedance values can be plotted as a function of the hazard parameter PGV. As the final step, a lognormal distribution can be fitted to these data points, to obtain the final smooth fragility curves. The reference fragility curves for low-rise and mid-rise reinforced concrete buildings with infill walls are illustrated in Figure 5.

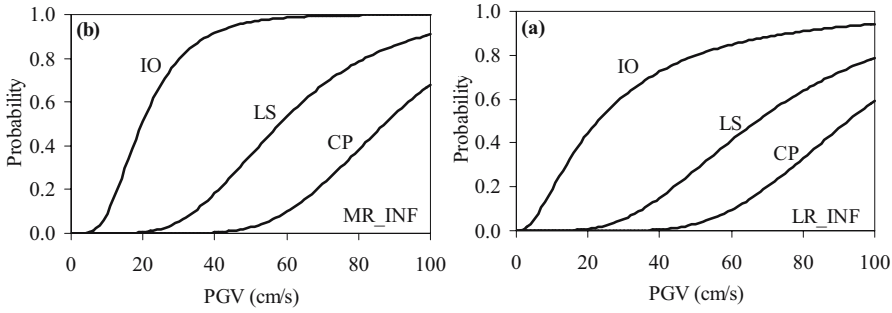

Figure 5. Reference fragility curves for (a) low-rise and (b) mid-rise reinforced concrete buildings with infill walls.

6. Sensitivity Analysis based on Fragility Curves

The sensitivity analysis is carried out to investigate the influence of different parameters on the final fragility curves by isolating the effect of each parameter to be examined. In this study, the influence of the post-elastic stiffness ratio, sampling method, sample size, hysteresis model type and limit state definition are considered in the sensitivity analysis.

6.1. INFLUENCE OF POST-ELASTIC STIFFNESS RATIO

As explained above, three parameters are involved in the structural simulation phase. Among these parameters, post-elastic stiffness ratio (α) was taken as a deterministic (constant) parameter while generating the reference fragility curves. However, it is worth investigating the difference in the final fragility functions when this parameter is also taken as a random variable. Therefore, instead of using mean values of α for each sub-class, the value obtained from the bilinearization process for each building is employed in the structural simulation. Keeping all the other parameters the same, the fragility curves are

generated again with the same ground motion set and limit state values and then compared with the reference fragility. The comparison is presented in Figure 6 for sub-classes LR_INF and MR_INF. The solid black curves represent the reference fragility functions where α is constant (deterministic) and the gray curves represent the new fragility functions where α is variable (probabilistic). It is observed that the use of α as a deterministic or a probabilistic parameter does not have a significant effect on the final fragility curves.

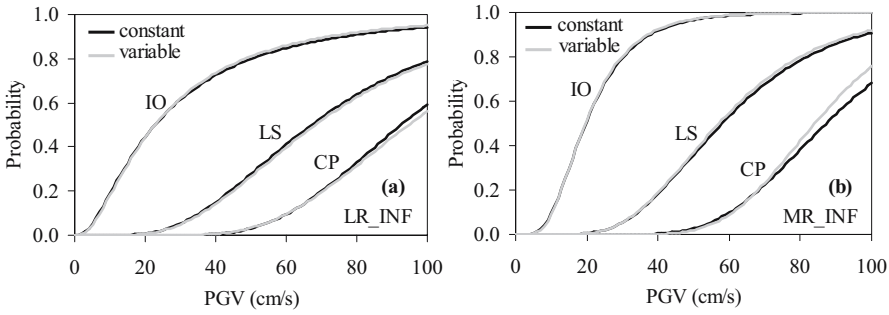

Figure 6. The influence of α on fragility curves for sub-classes (a) LR_INF and (b) MR_INF

6.2. INFLUENCE OF SIMULATION AND SAMPLING TECHNIQUES

Different simulation techniques have been employed in the study. In the first technique, which was used before by other researchers in the generation of fragility curves[4], a range is selected for each random variable (T and η) in each sub-class and the range is divided into a specific number of equal intervals. Hence a rectangular grid of input data is obtained for each sub-class. Figure 7.a is an example of such a mesh type generation for sub-class MR_INF. In this study, the selected ranges for each sub-class are divided into five equal intervals, forming a 6x6 (sample size is 36) input data grid.

The second and the more enhanced alternative is to employ sampling techniques for the generation of the structural simulation data. Among these techniques, Latin Hypercube Sampling (LHS) is the most suitable one for structural simulations with small sample size. Developed by McKay et al.[11], it is a technique that provides a constrained sampling scheme instead of random sampling according to the direct Monte Carlo Method, which requires a very large sample size in order to achieve the required accuracy. In the original LHS technique, the correlation between the random variables is not taken into account. However, Figure 2 clearly indicates that there is a strong correlation between the random input parameters T and η employed in this study. Hence a MATLAB code is established that can generate random (T, η) pairs for each sub-class by using LHS technique with rank correlation technique proposed by

Iman and Conover [12]. The random pairs generated by this code are illustrated in Figure 7.b for sub-class MR_INF.

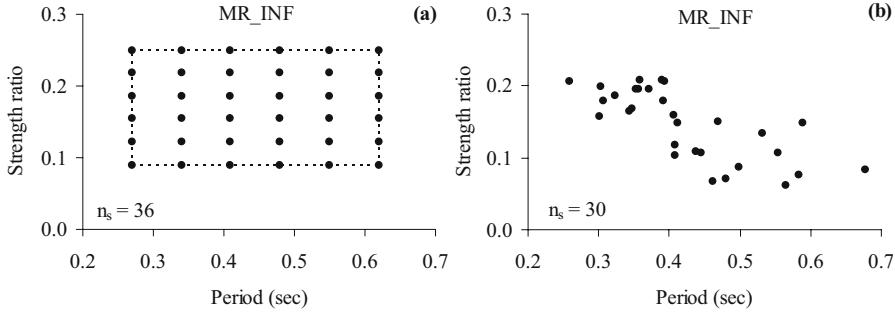

Figure 7. Mesh type (uniform) sampling, b) LHS technique with rank correlation

The influence of different sampling techniques on the final fragility curves is illustrated in Figure 8 for sub-classes LR_INF and MR_INF. The curves are very close to each other, for IO limit state and slightly different for LS and CP limit states. Hence it can be concluded that employing different sampling techniques does not affect the fragility functions drastically.

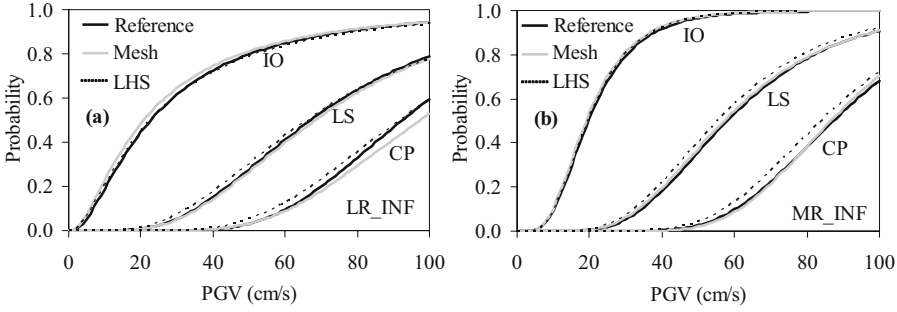

Figure 8. Comparison of different sampling techniques on final fragility curves for sub-classes (a) LR_INF and (b) MR_INF

6.3. INFLUENCE OF SAMPLE SIZE

In order to investigate the effect of sample size on the fragility functions, structural simulations with 30, 75 and 150 (T, η) pairs are generated using LHS technique with rank correlation. Hence, the fragility curves are obtained using sample sizes of 30, 75 and 150, keeping all the other parameters constant. In Figure 9, the fragility functions with n_s=30, 75 and 150 for sub-classes LR_INF and MR_INF are compared. It is clearly observed that the sample size does not have a significant effect on the final curves. This is an expected result since LHS is an effective technique for simulations for small sample size.

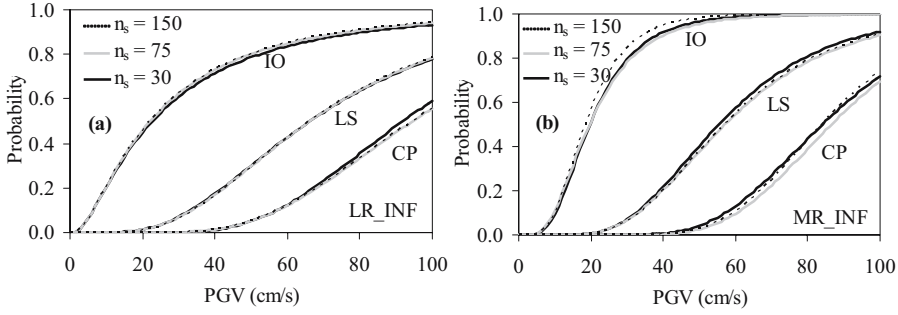

Figure 9. Comparison of fragility curves with different sample sizes (n_s=30, 75, 150) for sub-classes (a) LR_INF and (b) MR_INF

6.4. INFLUENCE OF LIMIT STATE DEFINITION

In the reference fragility curve generation, the variabilities in ground motion and structural characteristics are taken into account and the demand statistics are obtained accordingly. The limit states, which represent the capacity of the structure at some predetermined thresholds, are assumed to be constant (deterministic) parameters. However, a great deal of uncertainty is also involved in the attainment of limit states. Therefore, it is necessary to investigate the influence of considering deterministic or probabilistic limit states on the fragility curves.

As opposed to assigning the mean values for each limit state (IO, LS, CP) and sub-class in the deterministic approach, the statistical descriptors for each limit state (Table 3) are utilized in the probabilistic approach. While calculating the probabilities of exceedance, the limit state is not a single constant value. Based on the assumed probability distribution, a new value is generated for each limit state at each hazard intensity level.

The fragility curves obtained by using deterministic and probabilistic limit states are compared in Figure 10. It is observed that there is a significant difference, between two sets of curves. Fragility functions become more sensitive to limit state definition especially at large PGV levels. The results reveal the fact that the variability in deformation capacity deserves special attention. The limit states should be established with special care since they have an impact on the final fragility curves.

6.5. INFLUENCE OF DEGRADING HYSTERESIS BEHAVIOR

In the generation of reference fragility curves, the employed hysteresis model was the Clough model. This is a stiffness degrading model with stable hysteresis loops and high energy dissipation capacity. It generally simulates

well-detailed, slightly degrading, newly constructed structural systems. However, the structural systems modeled in this study are existing structures with many deficiencies. It is very probable that they will exhibit significant stiffness and strength degradation with low energy dissipation capacity. Hence, the sensitivity of the fragility curves to degrading structural systems should also be investigated.

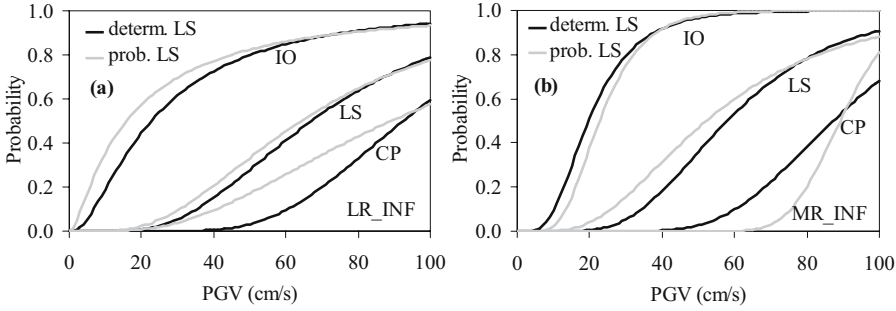

Figure 10. Comparison of the effect of using deterministic or probabilistic limit states in the generation of fragility curves for sub-classes (a) LR_INF and (b) MR_INF

An energy-based hysteresis model is employed with two parameters α and β in order to account for the degradation characteristics of structural systems. The details of the hysteresis model can be found elsewhere [13]. The degrading parameters were calibrated before by using the experimental results obtained from cyclic column tests[14]. Accordingly, the values assigned to the model parameters for simulating severely degrading structural systems are $\alpha = 0.3$ and $\beta = 0.7$. The generated curves are compared with the reference fragility curves in Figure 11. The reference fragility curves are shown as black lines whereas the ones ontained with the energy-based degradation model are shown in gray colour. Furthermore, the curves are grouped according to the limit states they represent: dotted curves for IO limit state, solid curves for LS limit state and dashed curves for CP limit state. It is obvious that there is a great difference between the two sets of curves. Hence, the degradation characteristics of the structural model have a major influence on the final fragility curves. However it should be noted that the curves are generated by using simple SDOF analyses; the results cannot be generalized before obtaining these two sets of curves by using inelastic MDOF analyses of the considered structural systems.

7. Summary and Conclusions

In this study, reference fragility curves are generated for different classes of reinforced concrete structures by using Duzce field database. Furthermore, the sensitivity of the parameters and techniques involved in the generation process

are investigated. Hence each time, the fragility curves are regenerated and compared with the reference fragility curves. Considering the fact that the results are based on the specific characteristics of the limited structural database used in this study, the following conclusions can be stated:

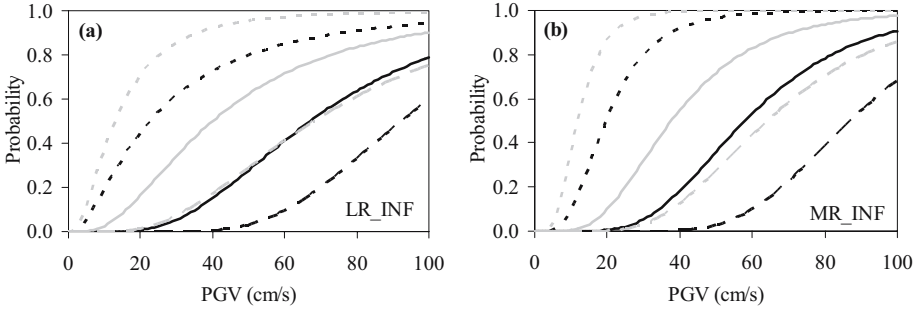

Figure 11. Comparison of the effect of strength degradation characteristics in the generation of fragility curves for sub-classes (a) LR_INF and (b) MR_INF

- Among the three main SDOF structural parameters (period, strength factor and post-elastic stiffness ratio), the variability in the post-elastic stiffness ratio does not have a significant effect on the fragility functions.
- Simulation techniques, from the simplest one (mesh-type generation) to the most enhanced one (LHS technique with rank correlation) does not influence the final fragility curves to a great extent.
- Sample size seems not to affect the final fragility functions.
- Uncertainty in the capacity should be taken into account by quantification of the variability in the limit states considered since the sensitivity of the fragility curves to limit state definitons seems to be high.
- Degradation characteristics seem to have a drastic influence on the final fragility curves, especially in the case of severe strength degradation.

References

1. M.A. Erberik and A.S. Elnashai, Seismic Vulnerability of Flat-Slab Structures, Mid-America Earthquake (MAE) Center, Report No. 03-06, University of Illinois at Urbana-Champaign, IL, 2003, p.182.
2. A. Yakut, N. Yilmaz, and S. Bayili, Analytical Assessment of Seismic Capacity of RC Frame Buildings, International Conference on Skopje Earthquake - 40 Years of European Earthquake Engineering SE40EEE, Skopje-Ohrid, 2003.

3. V. Aydogan, Seismic Vulnerability Assessment of Existing Reinforced Concrete Buildings in Turkey, Master Thesis, Department of Civil Engineering, Middle East Technical University Ankara, 2003.
4. S. Akkar, H. Sucuoglu, and A. Yakut, Displacement-Based Fragility Functions for Low and Mid-rise Ordinary Concrete Buildings, Earthquake Spectra (in press), 2005.
5. Federal Emergency Management Agency, FEMA 356 Prestandard and Commentary for the Seismic Rehabilitation of Buildings. American Society of Civil Engineers, Washington DC, 2000.
6. Computers and Structures, Inc., SAP2000 Nonlinear, Version 7.21, Structural Analysis Program, Berkeley CA, 2000.
7. R.W. Clough and S.B. Johnston, Effect of Stiffness Degradation on Earthquake Ductility Requirements, Proceedings, Second Japan National Conference on Earthquake Engineering, 1966, pp.227-232.
8. SEAOC, Performance Based Seismic Engineering of Buildings, Vision 2000 Committee, Structural Engineers Association of California, Sacramento, California, 1995.
9. A. Ghobarah, On Drift Limits Associated with Different Damage Levels, Proceedings of the International Workshop Bled, Slovenia, PEER Report No.2004/05.
10. K.M. Mosalam, G. Ayala, R.N. White and C. Roth, Seismic Fragility of LRC Frames with and without Masonry Infill Walls, Journal of Earthquake Engineering, Vol. 1, No. 4, 1997, pp. 693-720.
11. M.D. McKay, W.J. Conover and R.J. Beckman, A Comparison of Three Methods for Selecting Values of Input Variables in the Analysis of Output from a Computer Code, Technometrics, Vol.221, 1979, pp. 239-245.
12. R.L. Iman and W.J. Conover, A Distribution Free Approach to Inducing Rank Correlation Among Input Variables, Communications in Statistics, Vol. 11 (3), 1982, pp. 311-334.
13. H. Sucuoglu and, M.A. Erberik, Energy Based Hysteresis and Damage Models for Deteriorating Systems, Earthquake Eng. and Str. Dyn., Vol. 33, 2004, pp. 69-88.
14. H. Sucuoglu and M.A.Erberik, Evaluation of Inelastic Displacements in Deteriorating Systems using an Energy-based Approach, Proceedings of the International Workshop Bled, Slovenia, PEER Report No.2004/05, pp. 421-433.

SEISMIC REHABILITATION OF LOW-RISE PRECAST INDUSTRIAL BUILDINGS IN TURKEY

SHARON L. WOOD
Department of Civil, Architectural, and Environmental Engineering, University of Texas at Austin

Abstract. The seismic performance of low-rise industrial buildings in Turkey and the US are compared. Although the structural systems are very different, both are vulnerable to earthquake damage. Rehabilitation schemes used in southern California to improve the performance of tilt-up structures are proposed as an option for Turkish construction.

Keywords: industrial buildings; precast members; tilt-up construction; diaphragms

1. Introduction

Precast concrete members form the primary lateral-force resisting system in the vast majority of the warehouse and light industrial facilities in northwest and central Turkey (Karaesmen, 2001). The most common structural system for these facilities is shown in Figure 1. The precast columns are fixed at the foundation level and the cantilevered columns provide all the lateral resistance for the structure.

Structural damage and collapse of precast buildings was widely reported throughout the epicentral regions of the 1999 Kocaeli and Duzce earthquakes (Atakoy, 1999; EERI, 2000). Two types of structural damage were frequently observed: flexural hinges at the base of the columns and pounding of the precast elements at the roof level (Figure 2).

In contrast to the precast frames used in Turkey, concrete tilt-up wall panels are commonly used to construct one-story industrial structures in the US (Figure 3). The wall panels are cast horizontally at the site and then tilted into the vertical position. The panels are positioned around the perimeter of the building and connected to a flexible roof diaphragm.

S.T. Wasti and G. Ozcebe (eds.), Advances in Earthquake Engineering for Urban Risk Reduction, 167–177.

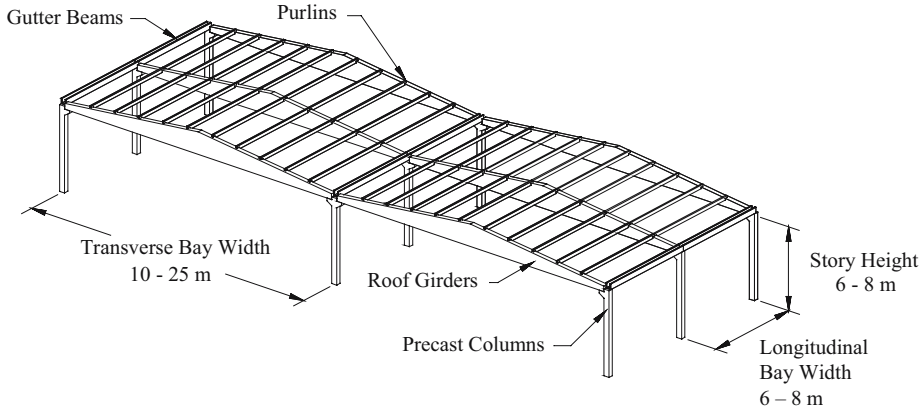

Figure 1. Typical configuration of one-story industrial building

Figure 2. Common structural damage in one-story industrial buildings

Tilt-up systems have exhibited poor seismic response in a number of earthquakes, including the 1964 Alaska, 1971 San Fernando, and 1994 Northridge events. Most frequently, the connections between the wall panels and flexible diaphragms failed. Localized collapse of sections of the roof is common and often accompanied by collapse of the wall panels in the out-of-plane direction (Figure 4).

In response to the risk associated with these structures, the City of Los Angeles developed an ordinance (Division 91) for seismic rehabilitation of the most vulnerable tilt-up structures (those constructed before 1976). The

guidelines require that the connections between the wall panels and roof be strengthened, sub-diaphragms and cross building ties be added in the roof, and continuous chords be provided between adjacent wall panels.

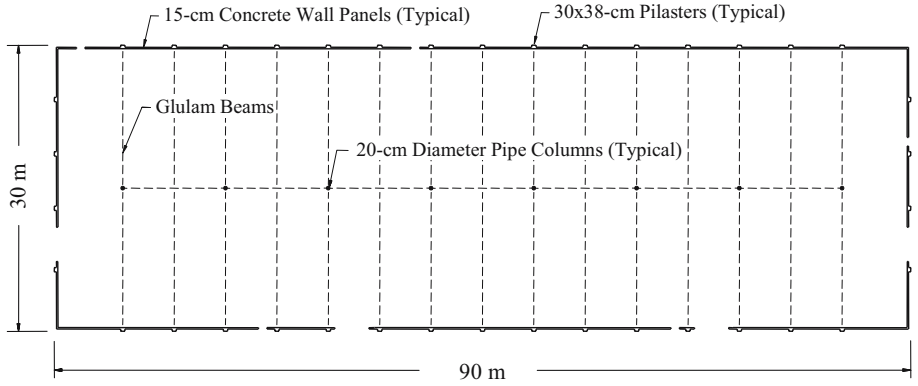

Figure 3. Floor plan of typical tilt-up warehouse in the western US

Figure 4. Damage to tilt-up warehouse during 1994 Northridge earthquake (EERI, 1996)

While the ordinance was not formally adopted until after the 1994 Northridge earthquake, approximately 60 tilt-up structures were rehabilitated in 1993 using preliminary versions of the guidelines. These rehabilitated structures exhibited significantly better response during the Northridge earthquake than older structures than had not been rehabilitated and newer structures that were designed using building codes that had been modified in response to the 1971 San Fernando earthquake (EERI, 1996; Lyons and Gebhart, 1996).

Although the structural systems used in the US and Turkey for low-rise industrial buildings are very different, both systems were developed to provide large interior spaces at low cost. Experience in the US has demonstrated that the performance of tilt-up buildings can be improved by increasing the strength of the diaphragms. A similar approach may also be appropriate for precast industrial buildings in Turkey.

2. Precast Structural Systems used in Turkey

The single-story industrial buildings common in Turkey are characterized by long-span roof girders which provided large open areas needed for manufacturing (Figure 1). The buildings tend to be rectangular in plan with one to four bays in the transverse direction and ten to thirty bays in the longitudinal direction. Transverse bay widths range from 10 to 25 m, longitudinal bay widths range from 6 to 8 m, and story heights range from 6 and 8 m.

The base of each precast column is typically grouted in a socket footing (typically precast) to form a fixed connection. Long-span roof girders are oriented along the transverse axis of the building and are supported on column corbels. The depth of these girders often varies along the length, forming a triangular shape. Beams with U-shaped cross sections are oriented along the longitudinal axis of the building. These beams function as gutters to collect water from the roof. Purlins span between the roof girders at regular intervals.

The precast roof girders, gutter beams, and purlins are pinned at both ends. Vertical dowels extend up from the supporting member and the horizontal elements were cast with vertical holes near their ends to accommodate these dowels. The holes were filled with grout in most buildings. In some cases the dowels were threaded, and nuts were installed before grouting.

Typically, lightweight materials, such as metal decking or asbestos panels, are used to form the roof. The roof is designed to provide environmental protection for the building, but does not serve as a structural diaphragm. Clay tile infill is typically used for the exterior walls, but precast concrete wall panels are also used. The connection details for the wall panels are such that the panels do not contribute to the lateral stiffness of the building, however.

During the summers of 2000 and 2001, researchers from the University of Texas, Kocaeli University, Bogazici University, Middle East Technical University, Purdue University, and the University of Minnesota visited more than 60 precast industrial buildings in northwest Turkey. A few had been rehabilitated following the 1999 earthquakes. Two rehabilitation schemes are shown in Figure 5. In one case, a steel lattice had been welded around the columns to increase their flexural capacity and in the other case the corbels that support the roof beams had been enhanced. Both of these strategies have

benefits, but they may not be sufficient to reduce the risk of collapse in the most vulnerable precast industrial buildings.

Figure 5. Observed seismic rehabilitation schemes in one-story industrial buildings

Posada (2001, 2002) investigated the relationship between column size and expected damage during the 1999 earthquakes. A one-story precast industrial building in Adapazari that sustained light damage during the Kocaeli earthquake was selected as the prototype structure for this study. The building is 80 by 200 m in plan. The transverse bay widths are 20 m, the longitudinal bay widths are 7.5 m, and the story height is 7 m.

As indicated in Table 1, column dimensions were varied from 40 by 40 cm to 80 by 80 cm in the study. It should be noted that the overwhelming majority of the columns in one-story industrial buildings were 50 by 40 cm or smaller. The largest precast columns observed were 80 by 75 cm at a one-story, automotive manufacturing plant near Golcuk. The cross-sectional dimensions and mass of the roof girders, gutter beams, purlins, roofing materials, and cladding in the prototype building were used in all analyses.

The columns were assumed to have longitudinal reinforcement ratios of 2%. The compressive strength of the concrete was taken as 30 MPa and the yield stress of the steel was assumed to be 420 MPa. The calculated periods of the idealized structures assuming fixed column bases and cracked cross-sectional properties are also reported in Table 1.

The inelastic response of the columns was compared with the demand from the 1999 earthquakes. Eleven ground motion records were used in the study. All of the recording stations were within 20 km of the surface trace of the faults of the 1999 earthquakes (EERI, 2000). Records from Bolu, Duzce, and Yarimca were used to determine the spectral characteristics for soft soil sites, while records from Arcelik, Gebze, Izmit, and Sakarya were used to determine the

spectral characteristics for stiff soil/rock sites. The earthquake displacement demand was estimated using an elastic response spectrum with 2% damping (Shimazaki and Sozen, 1984).

TABLE 1. Column sizes considered in parametric study

Column Dimensions		Calculated
Depth (cm)	Height (cm)	Period* (sec)
40	40	1.56
45	45	1.24
50	50	1.03
55	55	0.86
60	60	0.74
65	65	0.64
70	70	0.57
80	80	0.44

* Calculated periods correspond to cracked cross-sectional properties.

The analyses indicated that columns larger than 50 by 50 cm were sufficient to resist the maximum demand at the stiff soil/rock sites without yielding (Figure 6). At sites with these soil conditions, the mean displacement demands during the 1999 earthquakes were typically less than 1% of the story height for columns of this size and the rehabilitation strategies shown in Figure 5 are expected to be sufficient.

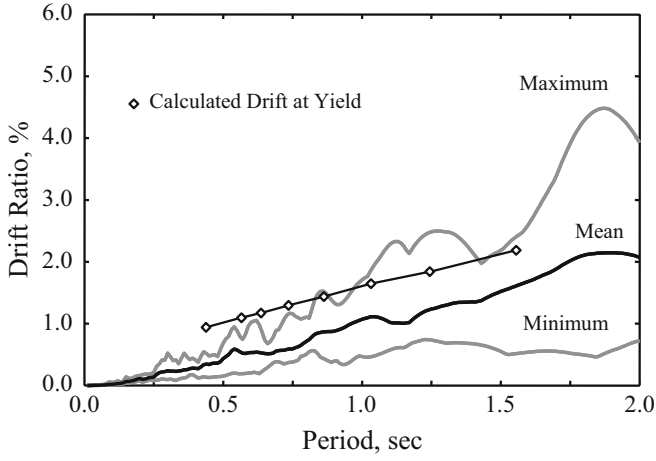

Figure 6. Comparison of drift demand at stiff soil/rock sites with calculated drift at yield

In contrast, the displacement demands are considerably larger at soft soil sites (Figure 7). Only columns larger than 70 by 70 cm had sufficient capacity

to resist the maximum displacement demand at the soft soil sites and columns sizes most representative of practice would be expected to fail under the mean displacement demand.

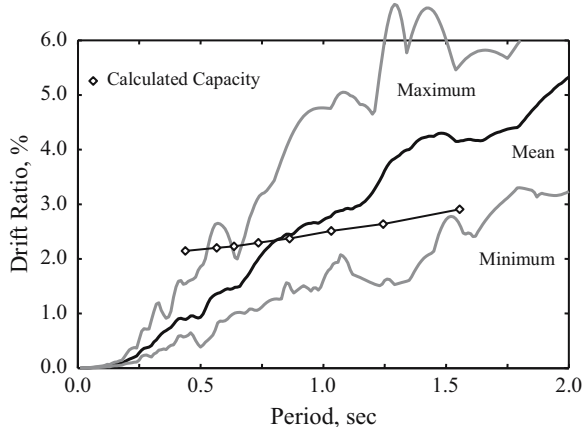

Figure 7. Comparison of drift demand at soft soil sites and calculated drift capacity

Because the columns provide all the lateral stiffness for the precast industrial structures and because moments can not be redistributed within the structural system, the development of a single flexural hinge at the foundation level constitutes the onset of collapse. Simply increasing the flexural capacity of the columns is not likely to be sufficient to prevent collapse of structures subjected to expected level of ground motion at the soft soil sites. Additional rehabilitation measures are required to prevent the collapse in these cases.

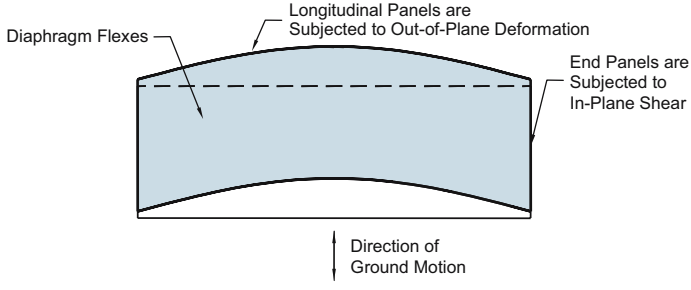

Figure 8. Expected response of tilt-up system with flexible diaphragm

3. Tilt-Up Structural Systems used in the US

Single-story, tilt-up industrial buildings are common in the western US. The structures tend to be rectangular in plan and the structural system is characterized by perimeter walls and a flexible roof diaphragm (Figure 8). The

wall panels are typically 15 to 20-cm thick, 6 to 9-m wide, and 9 to 10.5-m tall. Timber roof systems with plywood sheathing are most common in tilt-up construction; however, steel joists and metal decks are also used.

Within the roof, glulam beams are analogous to the roof girders in the Turkish structures and span in the transverse direction of the building. The glulam beams are often supported on pilasters, which are small, cast-in-place columns that connect adjacent wall panels. Sawn timber members are used as the purlins and subpurlins. The purlins span between adjacent glulam beams, typically at a spacing of 2.4 m on center, and the subpurlins span between adjacent purlins at a spacing of 0.6 m on center. Metal hangars are used to connect the ends of the purlins and subpurlins to the supporting members.

In structures designed before the 1971 San Fernando earthquake, the connections (Figure 9) between the roof and wall panels did not have sufficient strength or deformation capacity to resist the out-of-plane inertial forces induced in the panels (Hamberger et al., 1988). As a result, the wall panels often pulled away from the roof during earthquakes (Figures 4, 10).

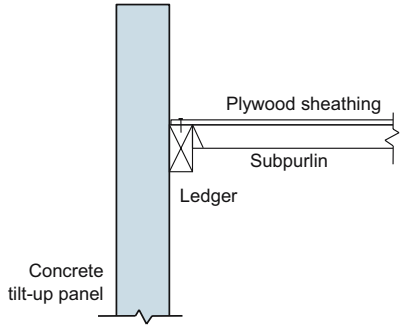

Figure 9. Typical wall anchorage details in tilt-up buildings constructed before 1971

Figure 10. Separation of wall panels from roof diaphragm during 1971 San Fernando earthquake (NISEE, 2005)

More than 400 of the 1,200 tilt-up buildings in the San Fernando Valley suffered significant structural damage during the 1994 Northridge earthquake (EERI, 1996). The extent of the damage was not surprising. The excellent performance of structures that had been voluntarily rehabilitated is notable, however. Lyons and Gebhart (1996) provide a detailed evaluation of three tilt-up buildings in Chatsworth that were adjacent to each other. The plan dimensions of all three were approximately 60 by 55 m. Buildings A and B were designed and constructed before the 1971 San Fernando earthquake, while Building C was designed and constructed in the late 1970s after numerous changes had been made to the building codes in response to the San Fernando earthquake. Critical elements of Building A were strengthened in 1993 using the proposed Division 91 guidelines. Portions of the roof collapsed in both Buildings B and C, but no structural damage was observed in Building A.

The rehabilitation measures taken by the owner of Building A are documented in Lyons and Gebhart (1996) and summarized below:

- Anchors were added to attach each purlin and subpurlin to the tilt-up wall panels (Figure 11). These anchors provide a direct load path from the roof member to the wall panel and do not rely on the eccentric load path through the ledger in the original construction (Figure 9).

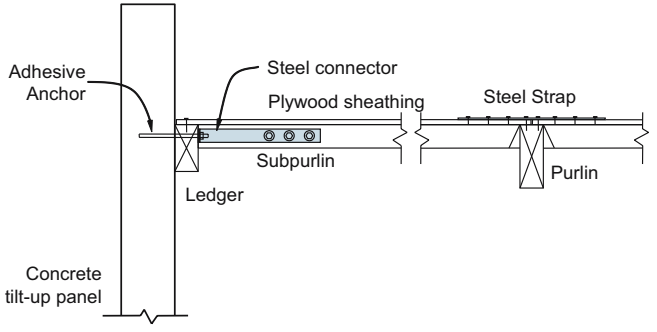

Figure 11. Wall anchorage details after rehabilitation

- Anchors were added to connect the glulam beams to the pilasters and the wall panels.
- Subdiaphragms were created by tying the purlins together through the glulam beams along three lines (Figure 12).
- Splices in the glulam beams were strengthened using bolted plates.
- Continuous angles were attached to the wall panels below the existing ledgers to serve as chord elements in the diaphragms.
- The number of nails used to attach the plywood sheathing to the purlins and subpurlins was increased.

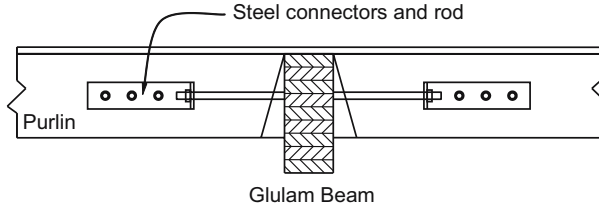

Figure 12. Connections between glulam beams and purlins after rehabilitation

Most of these measures are readily accomplished with timber members and they highlight the importance of the diaphragm in the seismic performance of tilt-up construction. When the diaphragm lacks sufficient strength, key connections fail during an earthquake, the structural members move relative to each other, and collapse ensues. Satisfactory performance is only achieved when the roof diaphragm has the strength to deform and transfer inertial loads as intended (Figure 8).

4. Conclusions

Although the structural systems are very different, the precast industrial buildings in Turkey and tilt-up structures in the US have many similarities. Both types of structural systems are inexpensive to construct, provide large interior spaces needed for manufacturing and warehouse facilities, and are susceptible to collapse during earthquakes. Experience in southern California has shown that the seismic response of tilt-up buildings is improved dramatically when the strength of the roof diaphragm is sufficient to prevent structural members from moving relative to each other.

Translating this experience to Turkey will require detailed evaluation because developing the appropriate connection details for precast members is more difficult and the inertial forces induced at the roof are larger due to the mass of the roof system. However, due to the large demands expected at soft-soil sites, the seismic performance of the Turkish structures is not likely to improve unless the roof is incorporated as part of the lateral-force-resisting system in these structures.

ACKNOWLEDGEMENTS

The field observations of damaged industrial buildings in Turkey and parametric study described in this paper were sponsored by the US National Science Foundation under grant CMS-0085337. The opinions expressed in this paper are not necessarily those of the sponsor.

The assistance of Ugur Ersoy, Erhan Karaesmen, Guney Ozcebe, and Tugrul Tankut (Middle East Technical University), Sevket Ozden (Kocaeli

University), Sami And Kilic (Bogazici University), Michael E. Kreger, Julio A. Ramirez and Mete A. Sozen (Purdue University), Catherine W. French and Arturo E. Schultz (University of Minnesota), Mauricio Posada and Eric B. Williamson (University of Texas), the Turkish Precast Concrete Association, and numerous engineers at GOK, Pekintas, Set Betoya, and Yapi Merkezi, is gratefully acknowledged.

References

Atakoy, H. ,1999, *17 August Marmara Earthquake and the Precast Concrete Structures Built by TPCA Members*, Turkish Precast Concrete Association, Ankara, Turkey.

EERI, 1996, Tilt-Up-Wall Buildings, Northridge Earthquake Reconnaissance Report, Vol. 2, *Earthquake Spectra*, Supplement C to Vol. 11, Earthquake Engineering Research Institute.

EERI, 2000, 1999 Kocaeli, Turkey, Earthquake Reconnaissance Report, *Earthquake Spectra,* Supplement A to Vol. 16, Earthquake Engineering Research Institute.

Ersoy, U., Tankut, T., and Ozcebe, G., 1999, *Damage Observed in the Precast Framed Structures in the 1998 Ceyhan Earthquake and their Rehabilitation*, Department of Civil Engineering, Middle East Technical University, Ankara, Turkey.

Hamburger, R., McCormick, D.L., and Hom, S., 1988, Performance of Tilt-Up Buildings, 1987 Whittier Narrows Earthquake Reconnaissance Report, *Earthquake Spectra*, Vol. 4, No. 2, Earthquake Engineering Research Institute.

Karaesmen, E., 2001, *Prefabrication in Turkey: Facts and Figures*, Department of Civil Engineering, Middle East Technical University, Ankara, Turkey.

Lyons, R.T. and Gebhart, K., 1996, Three Tilt-Up Buildings, *1994 Northridge Earthquake, Buildings Case Studies Project*, Seismic Safety Commission, State of California.

NISEE, 2005, *EQIIS and Karl Steinbrugge Image Database*, National Information Service for Earthquake Engineering, University of California at Berkeley, http://nisee.berkeley.edu/.

Posada, M., 2001, *Performance of Precast Industrial Buildings during the 1999 Earthquakes in Turkey*, M.S. Thesis, Department of Civil Engineering, University of Texas, Austin.

Posada, M. and Wood, S.L., 2002, Seismic Performance of Precast Industrial Buildings in Turkey, *Proceedings*, 7th U.S. National Conference on Earthquake Engineering, Earthquake Engineering Research Institute, Boston, MA, Paper 543.

Shimazaki, K. and M.A. Sozen, 1984, Seismic Drift of Reinforced Concrete Structures, *Research Reports*, Hazama-Gumi Ltd., Tokyo. (in Japanese).

SEISMIC RISK MITIGATION THROUGH RETROFITTING NON-DUCTILE CONCRETE FRAME SYSTEMS

MURAT SAATCIOGLU
Department of Civil Engineering, the University of Ottawa, Ottawa, CANADA

Abstract. A large proportion of existing buildings across the world consists of non-ductile structural systems. Performance of structures during recent earthquakes has demonstrated seismic vulnerability of these systems. The majority were designed prior to the enactment of modern seismic codes, while some were designed more recently in areas where code enforcement can not be ensured. These structures constitute significant seismic risk, especially in large metropolitan centers. Because it is economically not feasible to replace a large segment of the existing infrastructure with seismically superior systems, retrofitting non-ductile systems remains to be a viable seismic risk mitigation strategy. The objective of this paper is to highlight recent research at the University of Ottawa in Canada on seismic retrofit strategies for such systems. Specifically, projects on i) concrete frames with unreinforced masonry (URM) infill walls retrofitted with surface bonded FRP sheets, ii) non-ductile reinforced concrete frames braced by diagonal prestressing, and iii) the use of active control and smart structure technology for seismic retrofitting non-ductile reinforced concrete frames are presented. Research findings indicate that the application of these retrofit techniques produces good to excellent improvements in strength and inelastic deformability of otherwise seismically deficient non-ductile systems.

Keywords: active control; fibre-reinforced-polymers (FRP); masonry walls; prestressed concrete; reinforced concrete; seismic retrofit; smart structures.

1. Introduction

Previous earthquakes have demonstrated that the majority of structural failures can be blamed on seismically deficient structures, resulting in loss of lives,

S.T. Wasti and G. Ozcebe (eds.), Advances in Earthquake Engineering for Urban Risk Reduction, 179–194.

economic losses and tremendous grief for the society. These structures constitute a large portion of the existing infrastructure worldwide. Buildings designed prior to the enactment of modern seismic design guidelines, as well as those built more recently without appropriate seismic design and detailing practices pose particularly high seismic risk. In spite of improved knowledge on earthquake resistant design of structures during the last three decades, seismic risk worldwide remains high because of lack of code enforcement in many countries. It is economically not feasible to replace seismically deficient structures with those that conform to current codes and standards. Therefore, seismic retrofitting remains an effective seismic hazard mitigation strategy. Recent developments in new and innovative seismic retrofit methodologies offer great potentials for seismic risk reduction.

A comprehensive research program is currently underway at the University of Ottawa to develop improved seismic retrofit strategies. The research program consists of both experimental and analytical investigations. The specific areas of research include; retrofitting non-ductile concrete frames with diagonal prestressing, strengthening infill masonry walls with FRP sheets, active control of frame buildings to minimize seismic deformations and forces, and column retrofitting by either external transverse prestressing or FRP wrapping. Salient features of research projects on retrofitting non-ductile concrete frames with and without masonry infill walls are presented in this paper.

2. Non-ductile Concrete Frames with or without Masonry Infill Walls

A large number of existing buildings have non-ductile reinforced concrete frames with or without unreinforced masonry (URM) infill walls as their lateral load resisting systems. These buildings were primarily designed and detailed to resist gravity loads. A common approach to providing lateral bracing to these non-ductile frames is to build properly designed and detailed reinforced concrete walls between the columns[1]. This approach has been applied successfully over the years when it was possible to either fill in existing bays with reinforced concrete walls or replace some of the existing masonry walls in both directions with reinforced concrete walls.

It has been a common practice to consider the infill walls as non-structural elements though they often interact with the enclosing frame, sometimes creating undesirable effects. These elements may contribute to the increase in strength and stiffness of the frames, though they are not capable of developing inelastic deformations. Any seismic improvement to be expected from URM infills is limited to the elastic range of the material. However, the elastic behaviour can not be guaranteed during strong seismic excitations, and subsequent brittle failure may lead to disastrous consequences. Buildings that

were designed for higher seismic forces than those corresponding to the elastic threshold of URM need to be protected during seismic response. Two retrofit techniques have been developed to achieve this goal, one consisting of epoxy-bonded carbon fiber reinforced polymer (CFRP) sheets and the other diagonal prestressing.

2.1. CFRP SHEETS FOR RETROFITTING R/C FRAMES WITH MASONRY INFILL WALLS

Experimental research was conducted to investigate the performance of nonductile reinforced concrete frames with masonry infill walls, retrofitted with surface bonded carbon fiber reinforced polymer (CFRP) sheets. Three half-scale reinforced concrete frames were designed on the basis of the 1963 edition of the ACI 318 Building Code[2], representing the frames of old buildings. Unreinforced concrete block masonry walls were used as infill panels. The frame wall assemblies were constructed and tested under uniformly distributed gravity loads and incrementally applied lateral deformation reversals. The first specimen (BL-1) was built to reflect the majority of existing buildings constructed prior to 1970's, with a gravity-load designed frame. Figure 1 illustrates the details of the specimen.

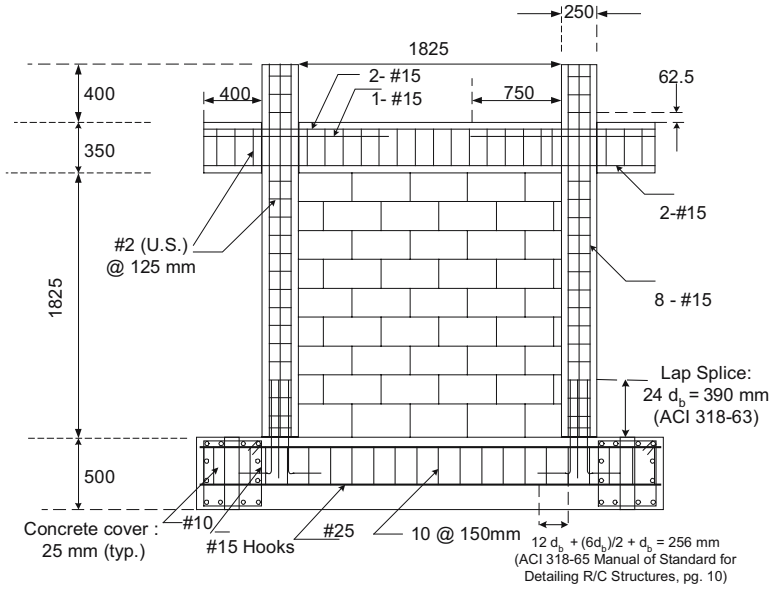

Figure 1. Details of frames with masonry infill walls

The specimens were constructed in stages; first the foundation, followed by the frame. A professional contractor was hired to build the masonry infills to

implement the actual practice in industry. Two of the specimens were built for retrofitting with CFRP sheets. Important aspects of the retrofit strategy were; i) the amount and arrangement of CFRP sheets and ii) the possibility of delamination of sheets and measures against it. It was decided to retrofit one of the walls (BL-2) with two layers of CFRP sheets per face, covering the entire wall surface, where each layer of fibers was oriented diagonally to be parallel to one of the wall diagonals, as shown in Figure 2(a), and the other layer was oriented to have the fibers parallel to the opposite diagonal. This resulted in four layers of sheets, two per wall face. The diagonal orientation of fibers was selected to increase their efficiency since their primary function was to resist diagonal tension. The other specimen was retrofitted with diagonal strips of CFRP sheets where the strip width was equal to the width of the CFRP sheet (625 mm), creating an X pattern, as illustrated in Figure 2(b). Two strips of sheets were used on each side, one strip along each diagonal. This resulted in a symmetric retrofitting with a total of four strips.

Specially designed CFRP anchors were developed and used to minimize/eliminate the separation of CFRP sheets from the enclosing frame. This was done by drilling holes in frame members adjacent to the wall with approximately 45-degree inclination towards the centre of the frame elements and inserting the anchors to be epoxy glued into the concrete. The anchors were produced in the laboratory by twisting strips of CFRP sheets and folding into two, as illustrated in Figure 3(a). A hammer drill was used to make approximately 50 mm deep, 12 mm diameter holes in columns and beams for the FRP anchors, as shown in Figure 3(b). Wooden pieces were inserted into the anchor holes during the placement of CFRP sheets, as guides, and also to avoid filling of the holes with epoxy. This is illustrated in Figure 3(c). The anchors were placed and epoxy glued after the application of surface bonded CFRP sheets, as depicted in Figure 3(d).

(a) Specimen BL-2 b) Specimen BL-3

Figure 2. FRP retrofitted walls

(a) FRP anchor (b) Anchor holes (c) Wooden Guides (d) Anchors in place

Figure 3. Application of FRP anchors

The specimens showed a significant participation of the walls in the frame response. The walls were able to stiffen the frames during the initial stages of loading. Specimen BL-1, without the retrofit, experienced gradual stiffness degradation under reversed cyclic loading. Progressive cracking of masonry units and mortar joints led to the dissipation of energy, without affecting the strength of the frame. The lateral drift was controlled by the stiffening effect of the wall. Of particular interest was the simultaneous degradation of strength and stiffness of the wall and the frame. The initial resistance was provided mostly by the wall. The load resistance was gradually transferred to the frame through progressive cracking and softening of the wall. The eventual failure of the unretrofitted specimen was caused by the hinging of columns within the reinforcement splice regions near the ends, while a significant portion of the cracked infill wall remained intact. Figure 4 shows the hysteretic force-lateral drift relationship for the unretrofitted frame-wall assembly. The relationship indicates that the peak load of 273 kN was attained in the direction of first load excursion at approximately 0.25% lateral drift ratio and remained constant up to about 1% drift, though there was substantial stiffness degradation during each cycle of loading. Gradual strength decay was observed after 1% drift, and the assembly failed due to the failure of concrete columns in their reinforcement splice regions at about 2% drift ratio.

The retrofitted specimens showed a substantial increase in elastic rigidity and strength. The initial slope of the force-deformation relationship was high, corresponding to that of uncracked wall stiffness and remained at the uncracked stiffness level until the specimens approached their peak resistances. This was especially true for specimen BL-2 where the entire wall surface was covered with FRP sheets. It was clear that the FRP control of cracking helped improve the wall rigidity. Specimen BL-2 resisted a peak load of 784 kN in the direction of first load excursion, indicating an improvement of approximately a factor of 3. The peak load was attained at approximately 0.3% lateral drift ratio. The FRP sheets maintained their integrity until after the peak resistance was reached.

There was no delamination observed throughout the test. However, the FRP sheets started rupturing gradually near the opposite corners in diagonal tension. This resulted in strength decay. By about 0.5% lateral drift, approximately 25% of the peak load resistance was lost. The load resistance continued to drop during subsequent deformation reversals and the resistance dropped to the level experienced by the unretrofitted specimen at approximately 1% drift ratio. The behaviour beyond this level was similar to that of the unretrofitted specimen, and the failure occurred at 2% drift ratio. The hysteretic relationship recorded during testing is illustrated in Figure 4(b).

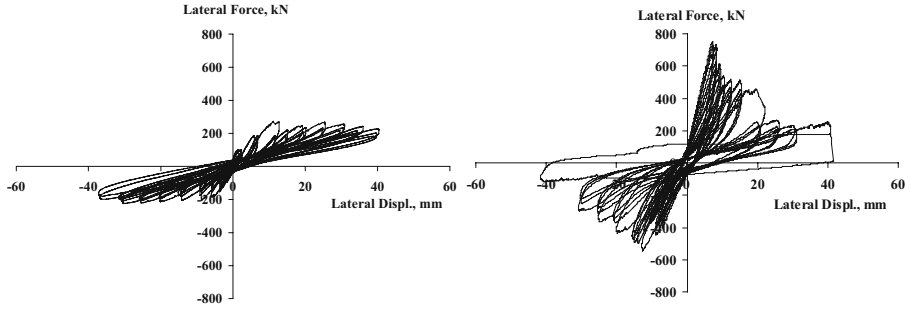

(a) Specimen BL-1 (b) Specimen BL-2

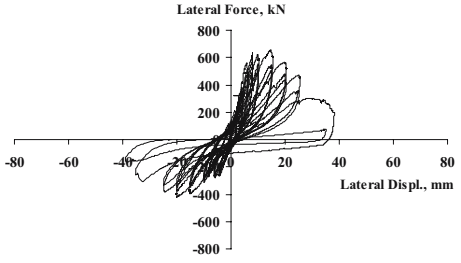

(c) Specimen BL-3

Figure 4. Hysteretic relationships for frame-block wall systems

Specimen BL-3 initially behaved similar to BL-2. Test observations indicated no visible cracking during the initial cycles at 0.1% and 0.3% drift ratios. Some noise was heard during these initial load applications, indicating signs of local stretching and possible debonding from the blocks locally. However there was no sign of damage. The lateral drift ratio of 0.3% was attained at 558 kN and 278 kN of loading in the push and pull modes, respectively. The specimen remained essentially intact, without any serious damage, and continued resisting additional loads. Some local debonding and buckling of FRP strips was observed in compression, which subsequently had

to stretch before it could develop full resistance. The maximum lateral load resistance of 659 kN occurred at 0.75 % lateral drift ratio during pushing. The improvement in load resistance due to the retrofit resulted in 2.4 times the lateral load resistance recorded in unretrofitted specimen (659/273). The maximum tensile strain on FRP occurred when the maximum load resistance of specimen was attained and was measured to be 5302 micro strain at the centre of the bottom corner of tension FRP strip. The specimen sustained somewhat lower resistance when pulled, developing 424 kN of resistance at 1.0 % drift ratio. This was attributed to local debonding and buckling of strips in compression during the initial load excursion, which resulted in reduced load resistance upon load reversal. However the FRP remained well anchored to the surrounding frame elements because of the FRP anchors used.

The hysteretic relationships indicated that there was no significant improvement in deformability beyond 0.5% lateral drift, which corresponded to the onset of FRP rupturing followed by column failure at about 1% lateral drift, because of column splice failures as typically observed in older frames. This observation indicates that the seismic retrofit strategy for non-ductile frame wall assemblies should be based on elastic design, unless individual frame members are retrofitted for improved deformability. Single layers of CFRP strips of 625 mm width and 0.9 mm thickness (after impregnation in epoxy to form a composite material) on both sides of the masonry wall (with 700 MPa coupon strength) was sufficient to increase the elastic load resistance by about 2.5 times in the direction of original load excursion and by about 2.0 upon load reversal. Analysis of the frame-wall assembly with a simple analytical model, consisting of flexural frame elements, a diagonal strut for the masonry wall and a diagonal tie for the FRP strip produced fairly accurate capacity calculations in the original direction of loading. It may be prudent to reduce the contribution of FRP ties based on coupon strength by a factor of 2.0 to account for the possibility of local fiber buckling in compression before they are subjected to tension under reversed cyclic loading. Further research is needed to establish the characteristics of FRP sheets bonded on masonry walls under reversed cyclic loading.

Analytical research was conducted to investigate the dynamic response of a non-ductile reinforced concrete frame building with and without FRP retrofitting of the infill walls. A 5-storey reinforced concrete frame building was designed on the basis of the National Building Code of Canada[3] (NBCC-2005), for seismically active city of Vancouver. The design strength was then reduced to 1/3 of the code required level to simulate a seismically deficient older building of 1970's, as the comparison of the seismic base shear levels between 1970's design practice and that required by the current building code indicated approximately a factor of 3 increase in the design base shear level.

The plan and elevation views of the structure are shown in Figure 5. The structure was retrofitted by surface bonded carbon FRP sheets with 700 MPa coupon strength, placed along the diagonals of interior bays of external frames. This is illustrated in Figure 5(b). Two different retrofits were considered. First, a single layer of FRP strip was placed along each diagonal on only one side of the wall. Then, the amount of FRP was increased to provide single layer of FRP strips on both sides. The structure was modelled and analysed using computer software DRAIN-RC[4] with hysteretic models for flexure, shear and anchorage slip of the frame elements. The infill walls were modelled by elastic truss elements, as diagonal compression struts, and the FRP strips were modelled as diagonal tension ties. The average stress of 85% of coupon strength (0.85*700 MPa = 595 MPa) was specified as the FRP tie strength. The structure was subjected to a NBCC-2005[3] code compatible artificial design earthquake record to investigate the performance of buildings retrofitted with FRP strips relative to that of the unretrofitted building.

The analysis results are shown in Figure 6 in the form of maximum inter-storey drift demands. The unretrofitted structure showed a maximum drift demand of about 2.4% at the second storey level. The drift demand was reduced to approximately 1.5% by retrofitting the exterior frames with a single FRP strip on **one side** of the middle bays. At the maximum drift level, the maximum tensile stress computed in FRP strips was equal to the average rupturing strength of strip (595 MPa). The drift demand was further reduced to about 1% when a single layer of FRP strip was placed on **both** sides of infill walls in the middle bays of exterior frames. In this case the maximum tensile stress in FRP was reduced to 541 MPa. The analysis results indicate that the FRP retrofit technique tested in the laboratory has the potential of successful use in practice, reducing drift demands in non-ductile buildings significantly, promoting elastic response.

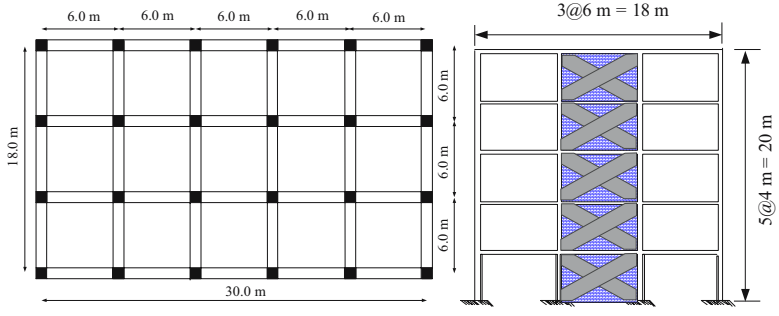

(a) Plan view (b) Elevation view of exterior frames

Figure 5. 5-storey frame building retrofitted with diagonal FRP strips

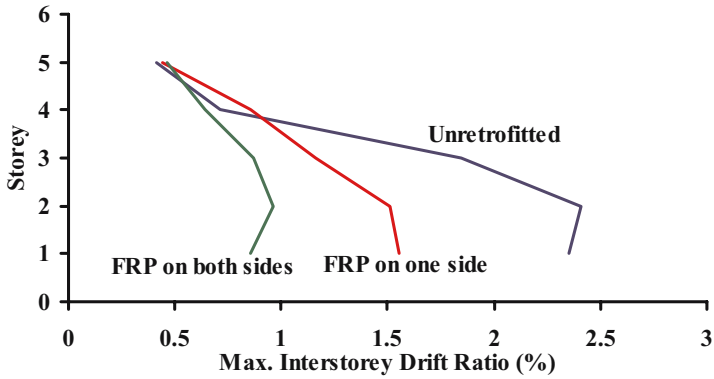

Figure 6. Drift demands established through dynamic analysis

2.2. DIAGONAL PRESTRESSING NON-DUCTILE CONCRETE FRAMES FOR SEISMIC RETROFITTING

Diagonal prestressing non-ductile concrete frames for improved lateral bracing and seismic performance is currently being investigated at the University of Ottawa as a seismic retrofit technology. Combined experimental and analytical research is being carried out to establish force-deformation hysteretic characteristic of diagonally prestressed frames.

Figure 7 illustrates two frame-masonry infill assemblies with brick infill wall. The walls were constructed using double layers of hollow clay bricks. Both specimens were loaded vertically by means of prestressing strands to simulate gravity design loads before they were subjected to incrementally increasing lateral deformation reversals. Specimen BR-1 was tested as the reference specimen, representing the characteristics of unretrofitted frame-infill wall structures. Specimen BR-2 was prestressed diagonally using #15 seven-wire strands (with 15.24 mm nominal diameter and 140 mm^2 area) along each diagonal, one on each side. Each strand was prestressed to 75 kN resulting in a total prestressing force of 150 kN along each diagonal. Diagonal tension forces generated during loading resulted in further stretching of the strands, increasing the initial prestressing force. This resulted in sufficiently high lateral bracing forces to control displacements while also controlling diagonal cracking in the walls.

The results indicate that the retrofit scheme introduced provided additional strength and deformability, improving the overall system behavior. Figure 8 illustrates hysteretic relationships for the two specimens.

(a) Control specimen BR-1 (b) Retrofitted specimen BR-2

Figure 7. Frame-brick infill wall assemblies

Figure 8 indicates an increase of approximately 100% in lateral load resistance due to diagonal prestressing. The maximum load resistance was attained at about 1% drift ratio. As deformations increased, some strength decay was observed due to the gradual failure of the infill wall. However, the reduction in load resistance was compensated significantly by the increase in diagonal prestressing due increased diagonal tension. Therefore, approximately 50% of the increase in load resistance was maintained until 3% lateral drift, improving inelastic deformability significantly.

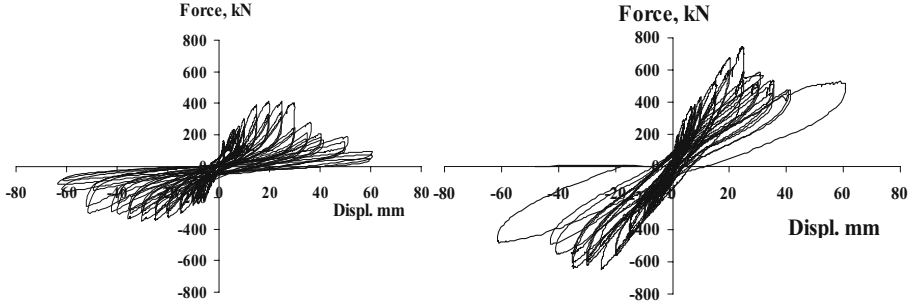

(a) Specimen BR-1 (b) Specimen BR-2

Figure 8. Hysteretic relationships for frame-brick wall systems

Analytical research was also carried out to investigate the feasibility of the retrofit technique for practice. A 5-storey reinforced concrete frame building was designed to represent a seismically deficient old structure with member capacities as low as 1/3 the design strength required by the current National Building Code of Canada[3] (NBCC-2005). Figure 9 shows the plan and elevation views. The external frames were diagonally prestressed in the middle bay, along the height of the structure. The structure was analyzed in the short direction under incrementally increasing lateral seismic forces (pushover

analysis). The load was increased until either the current level of design base shear of 2000kN was attained or the structure collapsed. The frame elements were modeled to represent inelastic behavior with bi-linear force-deformation relationships. The prestressing stands were modeled as diagonal ties. Two #15 7-wire strands (with 15.24 mm nominal diameter and 140 mm^2 area. each) were placed in the middle bay of external frames, one on each side. This resulted in the use of 4 strands per floor, in each diagonal direction, for the entire building. The results are shown in Figure 10 in terms of the first-storey drift ratios. The unretrofitted structure was able to resist 65% of the NBCC-2005[3] seismic base shear when it developed a stability failure due to excessive deformations. The 5% interstory drift sustained by the unretrofitted structure at its peak force resistance is unrealistically high as non-ductile frames would have experienced significant strength decay beyond approximately 1% to 2% drift ratios, depending on whether the columns have splice deficiencies. This was not captured by the analysis since the force-deformation model assigned to individual members did not incorporate the effect of strength decay.

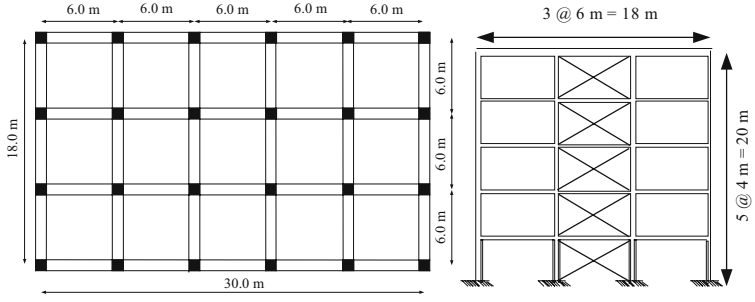

(a) Plan view (b) Elevation view of exterior frames

Figure 9. 5-story frame structure retrofitted with diagonal prestressing

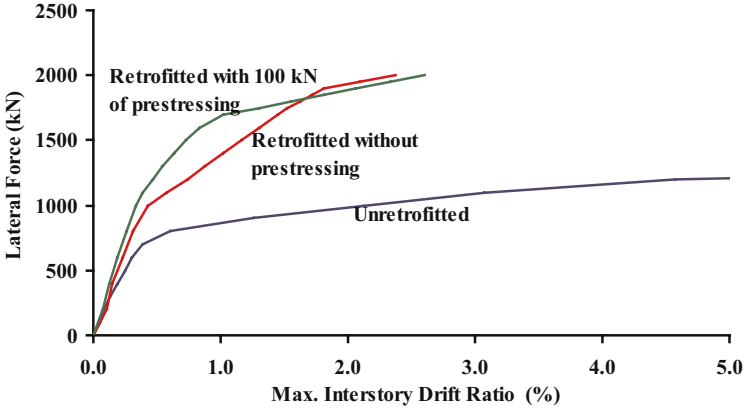

Figure 10. First story drift ratio under incrementally increasing lateral load

Retrofitting with a single non-prestressed 7-wire strand of 140 mm^2 area per side of the interior bay of each exterior frame (two strands per floor per exterior frame in each diagonal direction) was able to reduce the drift demand to approximately 2.6% at full lateral load (1.5 times the load that was sustained by the unretrofitted structure). When the strands were prestressed to approximately 40% of the specified ultimate strand strength (100 kN per strand), the structure became initially stiffer, developing lower drift ratios until the strands started yielding due to further tensioning during response. At about 85% of the maximum load, the prestressed building developed 1% storey drift, as compared with 1.5% storey drift in the building retrofitted with unprestressed strands. When the NBCC-2005[3] design force level was reached at about 2.6% drift ratio, the prestressed strands had already exceeded the initial yield stress of 1600 MPa, developing post-yield stresses of up to 1772 MPa. Unprestressed strands in the companion building developed a maximum of 1717 MPa tensile stress at the same load level, corresponding to a slightly lower drift ratio of 2.4%. The same structure was subsequently retrofitted with twice as many #15 strands, with a total of 8 strands per floor in each diagonal direction (4 per external frame). The strands were prestressed to 100 kN/cable initially. The results indicated that the first storey drift reduced to 0.65% at maximum NBCC-2005 lateral load of 2000 kN. The maximum tensile stress at this stage was 1384 MPa, significantly below the yield level. As expected, there is a clear relationship between the number of prestressing strands used and the level of initial prestressing to attain a specific level of drift ratio. This needs to be established through analysis during retrofit design.

The effectiveness of diagonal prestressing under seismic conditions was also investigated by conducting dynamic inelastic analyses of the same 5-storey building, with and without retrofitting. The structure was subjected to a NBCC-2005[3] code compatible artificial earthquake record. The results are summarized in Figure 11, in terms of maximum inter-storey drift demands.

The figure demonstrates that the drift demand of 2.4% for the unretrofitted building can be reduced substantially through diagonal prestressing.

2.3. ACTIVE SEISMIC CONTROL OF NONDUCTILE FRAME BUILDINGS

Among the options considered for seismic rehabilitation, a new approach has been emerging in the form of a smart structure technology for seismic risk mitigation. This technique involves active control of structural response during seismic excitations.

Seismic structural control includes the computation of control forces during an actual seismic event and the application of these forces to reduce or minimize the effects of earthquakes. Two seismic response quantities gain

importance in structural control; i) lateral drift and ii) earthquake induced inertia forces. Both of these response quantities are affected significantly by inelasticity, which is unavoidable in reinforced concrete structures under strong earthquakes.

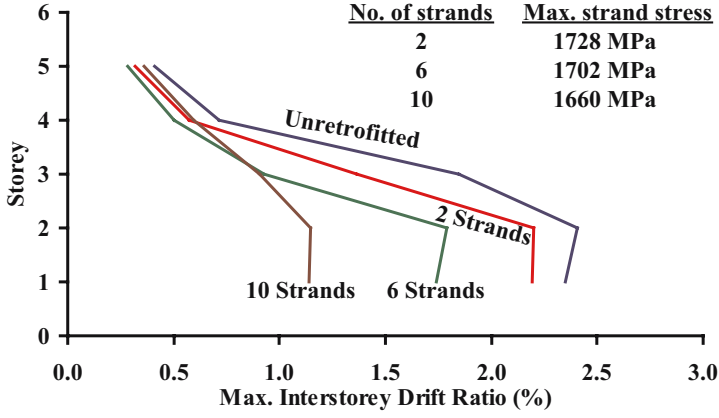

Figure 11. Maximum storey drift under design earthquake (Initial prestressing :100 kN/strand)

A method of active structural control was developed by Shooshtari and Saatcioglu[5], applicable to R/C frame structures responding in the inelastic mode of deformations. The technique involves the solution of the dynamic equation of motion while employing the instantaneous optimum control algorithm. The equation of motion of an n degree-of-freedom system, subjected to ground excitations and control forces, can be written as shown below:

$$Ma + Cv + Ku = Ea_g + Df_c \qquad (1)$$

where, M, C and K are mass, damping and stiffness matrices, respectively; a_g and f_c are vectors which determine ground acceleration and control force; and a, v and u are response acceleration, velocity and displacement, respectively. Matrix E represents the degree of freedom in which the ground acceleration is applied, and matrix D shows the location of control forces.

Computer software was developed for the application of the control algorithm employed. The technique was demonstrated analytically to produce significant control of deformations in concrete frame structures, reducing seismic vulnerability of non-ductile structures. The application of the approach was illustrated using a 3-storey concrete frame structure, shown in Figure 12. The structure was designed to be seismically deficient in terms of strength and deformability. It was analyzed in the short direction under the N-S component of 1940 El Centro earthquake record, with and without active control. The

frames were equipped with control hardware, as illustrated in Figure 12(b). The control forces were applied through actuators placed on floor slabs and the prestressing strands attached to beam column joints, diagonally. During an earthquake, the sensors trigger the control system, which records the ground motion as well as the response of structure. This information is fed into a local computer which establishes the stiffness of structure (based on recorded deformations) and solves Eq. (1) for required corrective control forces. These forces are then applied to the structure. The effect of control forces on dynamic response of the building is incorporated during the next time step. Figure 13 illustrates roof displacement time histories with and without active control in the short direction, showing a significant drift control through active structural control.

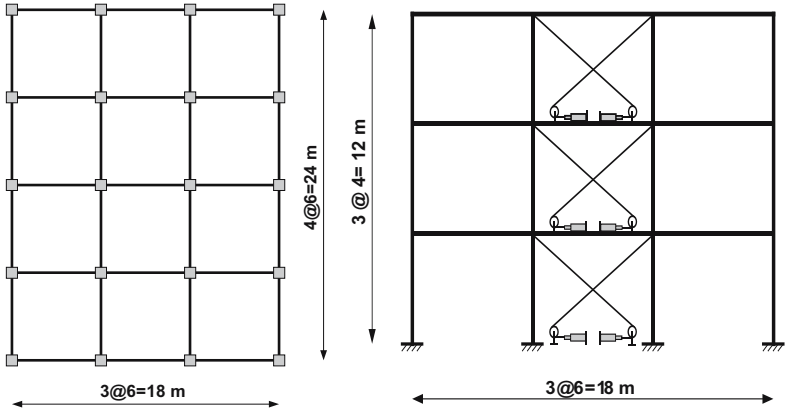

(a) Plan view (b) Elevation of external frames

Figure 12. 5-story frame building retrofitted by an active control system

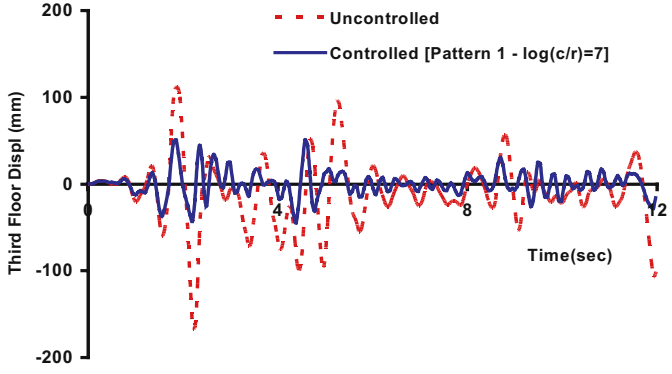

Figure 13. Roof displacement time histories of the 3-storey frame building as affected by active control

The above technique is one of the early attempts to control seismic induced deformations (and hence damage) through active force control. The technology requires further development for application in practice, though similar technologies utilizing active mass dampers have already been used in Japan in a number of buildings. Currently, the technology is being verified at the Structures Laboratory of the University of Ottawa through pseudo-dynamic testing of large scale components and small scale shake table testing of models.

3. Conclusions

The following conclusions can be drawn from the seismic retrofit research presented for non-ductile frame buildings, presented in the paper:

- FRP sheets can be used to retrofit masonry infill walls in non-ductile reinforced concrete frames, increasing seismic force resistance very substantially. However, no ductility enhancement can be achieved. Therefore, seismic retrofit design for surface bonded FRP applications should be based on elastic seismic response. It is sufficient to use diagonal strips of FRP as diagonal ties, instead of covering the entire wall surface, although the latter results in better crack and damage control for unreinforced masonry walls.
- Diagonal prestressing of non-ductile concrete frames results in substantial lateral bracing, increasing lateral load resistance of frames significantly. The technology is easy to apply, using readily available prestressing hardware.
- Active control and smart structure technology offer a great potential for seismic retrofitting non-ductile frames. However, the hardware for the technology needs further progress to address some of the practical problems.

References

1. Canbay, E., Ersoy, U., and Ozcebe, G. (2003), Contribution of RC infills to the seismic behavior of structural systems, ACI STRUCTURAL JOURNAL 100 (5): 637-643 SEP-OCT 2003
2. ACI Committee 318. (1963)., Building code requirements for reinforced concrete and commentary (ACI 318-63), American Concrete Institute, Detroit, U.S.A.
3. NBCC-2005. (2005)., National building code of Canada, National Research Council of Canada, Ottawa, Ontario, Canada.

4. Saatcioglu, M., Shooshtari, A., and Alsiwat, J. (1997)., Computer program for dynamic inelastic response history analysis of reinforced concrete structures, Ottawa-Carleton Earthquake Engineering Research Centre, Research Report: OCEERC 97-18, Dept. of Civil Engineering, the University of Ottawa, Ottawa, Canada.
5. Shooshtari, M. and Saatcioglu, M. (2004)., Active structural control of concrete structures for earthquake effects, Proceedings of the 13th World Conference on Earthquake Engineering, Vancouver, Canada.

HYDE-SYSTEMS FOR EARTHQUAKE PROTECTION OF RESIDENTIAL BUILDINGS

UWE E. DORKA
University of Kassel, Kurt-Wolters-Str. 3, D-34125 Kassel, Germany

STEPHAN GLEIM
University of Kassel, Kurt-Wolters-Str. 3, D-34125 Kassel, Germany

Abstract. The development of the Hyde system, a structural control concept for earthquake protection, is summarized. Recent results of large scale tests at ELSA (JRC-Ispra) confirming the concept are presented. It is shown that designing residential or mixed commercial-residential buildings as Hyde systems provides a more economic and sustainable structure. This concept is particularly suited to retrofit soft storey buildings with little effort and negligible interference with tenant activities.

Keywords: Earthquake design; earthquake retrofit; sustainable structures; structural control; Hyde system; soft storey building; residential building; mixed residential-commercial building

1. Introduction

All over this world, recent earthquakes have demonstrated the vulnerability of large numbers of residential or mixed residential-commercial buildings. The standard type building is the reinforced concrete frame designed as a frame but with masonry in-fill, poor seismic detailing and often a soft ground floor. These structures collapse in a brittle fashion in great numbers. They are cheap to build but unfit to resist earthquakes because a typical designer cannot anticipate their collapse mechanism, a typical contractor cannot execute all the details in the required fashion and typical quality control cannot detect all the "minor" mistakes (like insufficient lap splices, reinforcement placing or hooks in stirrups) that are so important for their behavior during an earthquake. Code

S.T. Wasti and G. Ozcebe (eds.), Advances in Earthquake Engineering for Urban Risk Reduction, 195–208.

design procedures and detailing requirements do not take these practical limitations into account: Codes should document current good practice, not require a structure that will not be built under typical circumstances.

Since it is not possible to assess the earthquake response of a typical structure in a typical design situation, it is better to conceive a structural system first that is suitable for the application, then design it and make sure that it is built that way. This requires the designer to consciously implement a suitable mechanism and control its motion under earthquakes in a few defined locations. In short: to construct a structural control system. It can be shown that rigid body mechanisms controlled by stiff-plastic devices in their links are most suitable for earthquake protection since they prevent vibrations in the structure that would lead to stress amplifications. The devices put a physical limit to the forces in the structure through their plastic limit and dissipate most of the input energy in the links between the rigid bodies. All in all, the result is small forces completely under the control of the designer who can now perform a conventional and safe design on the rigid bodies that can safely be constructed with typical methods and under reasonable quality control. Special attention only need to be paid to a few select locations in the links between the rigid bodies where the required motion capacity must be provided and a few select devices must be placed correctly and with care – a clear focus that can be addressed everywhere.

2. Structural Control Concepts Suitable for Earthquake Protection

Fortunately, the designer does not have to "invent" a new structural control system for each new building. A few standard types have emerged that are applicable in many situations. They are: Base Isolation (BI), Hyde Systems (HS), Tendon Systems (TS), and Pagoda Systems (PS) with their principal mechanisms given in Figure 1.

The one known most is BI but the one with the longest success record is PS. It is an "accidental" mechanism inherent in the Japanese pagoda allowing it to perform its famous "snake dance" during an earthquake[1]. After a history of about 1200 years littered with earthquakes, not a single pagoda has been destroyed by one: An impressive proof of the versatility of this control concept which obviously is most suitable for slender structures. Unfortunately, no modern structure has been built this way.

On the other hand, the TS system has been used, namely in the retrofit of the ancient bell tower in Trignano, It.[2]. Vertical cables were placed in the four corners of this tower and anchored in the foundations. Their tension is controlled by shape memory alloy devices placed on top. The rigid blocks of this tower have formed by cracking during the Reggio Emilia earthquake and

can now still move against each other dissipating energy by friction but they cannot topple.

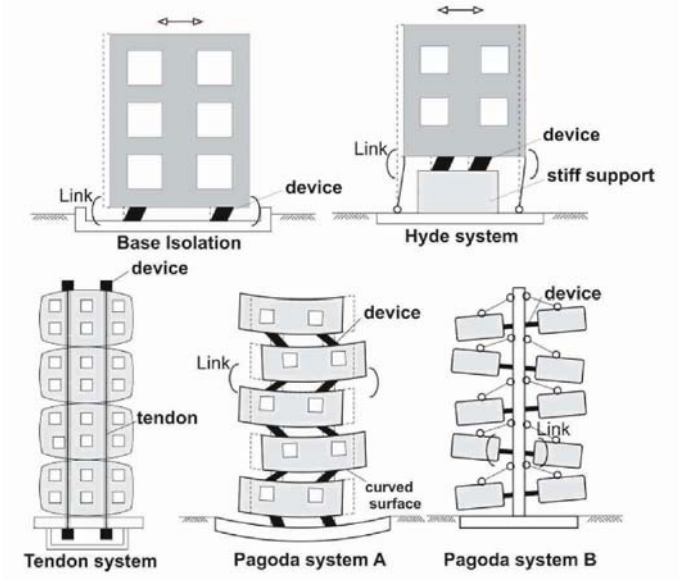

Figure 1. Structural control concepts with rigid body motions suitable for earthquake protection

With BI sufficiently covered in the literature and some codes, this paper now concentrates on the Hyde system.

3. Hysteretic Device System Concept

As described in[3] and shown in Figure 1, a HYDE system consists of two main parts: A Primary Horizontal load bearing System (PHS) and a Secondary Horizontal load bearing System (SHS).

The PHS must be very stiff in order to concentrate horizontal displacements in its Seismic Links (SLs). There, stiff-ductile "Hysteretic Devices (Hydes) are placed. They must show almost ideal stiff-plastic behaviour by use of dry friction or yielding. Then, already small movements in the links cause plastic energy dissipation transmitting only the maximum friction or yield forces to the adjacent rigid structural blocks. These conventional structures are thus protected from overloading. A well designed Hyde system dissipates around 85% percent of the earthquake's input energy and thus leads to small link displacements and forces. The conventional part of the structure is designed using the link forces as static loads against quasi-linear limit states.

A variety of inexpensive devices that may be used as Hydes is available. A small overview is given in[3] – but one of the best and least expensive is the shear

panel made of mild steel that has recently been optimised for this purpose (see next section).

The SHS must stabilise this mechanism with respect to the P-Δ effect during non-linear action of the PHS. It must therefore act in parallel to the PHS and its stiffness should only be selected for this purpose. Any additional stiffness will draw energy away from the PHS and thus diminish the efficiency of the Hyde system. The required stiffness of the SHS may be computed by linear static stability analysis with vertical loads present during the earthquake but without considering the stiffness of the PHS.

In the literature on new earthquake protection concepts for buildings, one usually finds two distinctions: the base isolation concept and "the rest", often referred to as "added damping systems", "added damping and stiffness systems" or "systems with supplemental energy dissipation devices"[4]. Such latter systems are also often referred to as "structural control". The unsuspecting reader might therefore place a Hyde system into this category and try to apply design concepts developed on the principle of "adding some form of damping" to an otherwise conventional structure. This is a dead end because these design concepts fail to address the most important part of any structural control system: the underlying basic mechanism.

Conventional structures with added dissipators do not have such unique mechanisms. The literature is full of "structural control" studies where conventional moment frames that develop plastic hinges are equipped with additional dissipators. From a structural control point of view, the basic mechanism here is first of all a hinged frame and the devices are the plastic hinges. This is not a very efficient mechanism against earthquake loading since it invites vibrations with large stress amplifications before it even becomes a controllable mechanism. This is further obscured and complicated by adding a parallel system of some kind through the additional dissipators and their support structure. This approach might have some limited advantages but nothing is "controlled" here and therefore, such systems fail to qualify as true structural control concepts and cannot match their performance and advantages.

This has been demonstrated by extending a comparative study between conventional frame systems and their retrofit by "added damping" systems to a rehab with a Hyde system considering large, near-field California earthquake situations with accelerations of more than 1g. It was shown in the original study[5] that added damping (using viscous, yielding or friction devices) may prevent collapse of the original frame under most circumstances but cannot prevent severe damage and a complete economic loss of the building whereas the Hyde system lived up to its expectation[6] that even under such severe conditions, only the shear panel devices selected here would have to be

replaced. It is worth mentioning that the number (and therefore costs) of devices in the "added damping" systems was about 5 times of those in the Hyde system.

When applying a true control concept like the Hyde system, substantial economic advantages can be achieved. A first advantage is the reduction in costs for the conventionally designed rigid blocks that don't require anymore hundreds of complicated and costly "seismic" details like welded or heavily reinforced frame corners and column end details. The extra costs for a few simple devices, like shear panels, and their connections are more than offset by this.

The next advantage is after an earthquake. Instead of a complete economic loss which is typical for conventional structures even if they remain standing, only a few devices need to be replaced, an important aspect in the context of sustainable construction.

And then there is the huge demand in rehab where such systems have unique advantages. The Hyde system, for example, is ideal in retrofitting soft storey structures since the soft storey is already an ideal place for the required seismic link. Interference is limited to a few locations in the ground floor and tenant activity is hardly affected, an important financial aspect for any rehab where even tenant relocation is often required when using conventional techniques.

The rehab of the Allstate Building in Seattle, USA[7] demonstrated this with a Hyde system that was 60% cheaper than any other concept and this does not even account for tenant relocation which was not an issue in this project.

4. Validation of Hyde System Concept

Efficient numerical models, optimised shear panel and friction devices and a concept for a design procedure have been proposed and used in many studies like in a retrofitting concept for large panel buildings[8] or the infamous RC-frame with masonry infill[9] but have been validated only recently in large scale pseudo-dynamic tests on two specimens at the ELSA laboratory of the JRC in Ispra, It.[10]. One specimen was a ½ -scale 3-storey steel frame with composite floors. The other was a full-scale 3-storey RC-frame with masonry infill in the upper floors.

Both were subjected to a synthetic acceleration time history with a response spectrum compatible with Eurocode 8 at 2% damping for stiff soils and a peak ground acceleration of 0.30g. In addition, the strong motion phase of the Kocaeli earthquake, scaled to the same peak acceleration, was chosen to include a natural Mediterranean near field event because of its higher spectral accelerations in the low frequency range.

The steel frame was converted into a Hyde system by stiffening the upper floors with simple steel braces and implementing shear panels in the ground floor between the floor beams and inverted V-braces (Figure 2). The tests confirmed the rigid body motion of the upper floors and the required concentration of deformation in the shear panels. These showed stable hysteresis loops (Figure 3) even after cyclic plastic buckling of the web set in and initial cracks developed at the centre of the web and along the flange welds after 10 repeats of the maximum event. No cracks developed in the web corners being specifically designed to transfer the high stresses produced by the tension diagonals that alternately form when cyclic plastic web buckling occurs.

Figure 2. Steel frame mock-up at ELSA converted to a Hyde system using shear panel devices

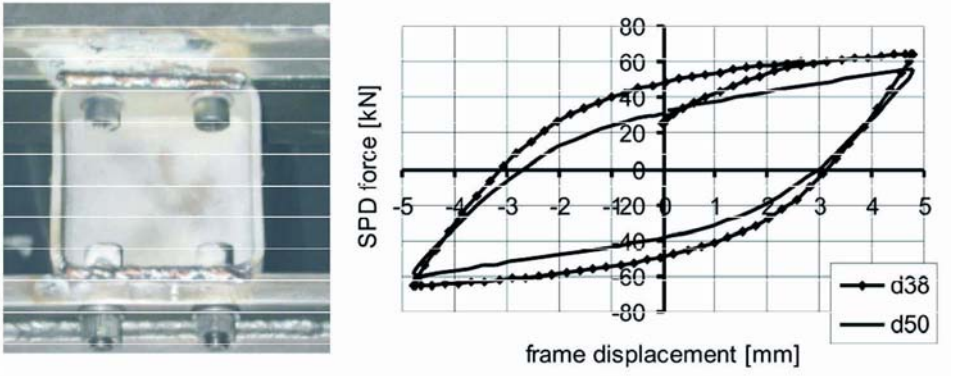

Figure 3. Shear panel device with plastic web buckles and stable hysteresis loop before (d38) and after (d50) cyclic plastic web buckling occurred

The tests also confirmed the modelling approach developed for Hyde systems which is based on static condensation of a refined FE-model using only a few dynamic DOFs in the floors and an elasto-plastic hysteresis model in the seismic link (see example in chapter 5). Furthermore, the tests demonstrated the importance of local detailing in the seismic link, especially the connections. The first design (pre-stressed bolts) failed due to rapid loss of pre-stressing requiring subsequent welding to activate the full capacity of the shear panels.

The RC-frame was converted into a Hyde system by adding simple masonry walls to the upper floors and prefabricated RC-panels with friction connections in the ground floor (Figure 4). In these connections, friction between RC-panels and steel plates was controlled by packages of non-linear disc springs[11] that allow the adjustment and checking of the clamping force with an accuracy of 2% by simply measuring the thickness of the package. Together with prescribed surface treatment and local detailing (size and placing of holes, local reinforcement, local thickness of panels etc.), a stable and highly accurate hysteresis loop is produced (Figure 5). After an event, these devices need not be replaced. Simply releasing and retightening the bolts will do since in the released state, the SHS will automatically re-centre the seismic link.

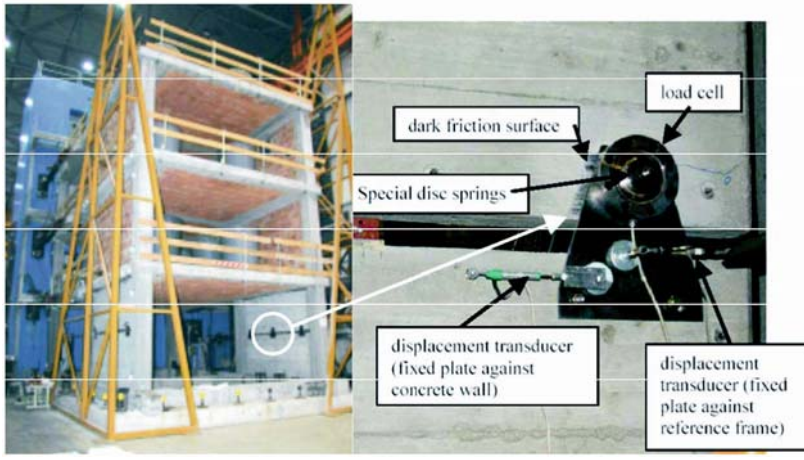

Figure 4. RC-frame mock-up at ELSA converted into a Hyde system using prefabricated wall elements and simple friction devices

Due to test limitations (large stiffness can destabilize a pseudo-dynamic test), the required masonry walls in the upper floors could not be placed and the rigid body was not correctly achieved. The comparison between the energy curves of the retrofitted steel frame and the RC-frame (Figure 6) show that still too much kinetic energy enters the RC-structure and is converted into potential energy causing stresses and some local cracking in the masonry especially in corners of windows and doors. Thus, although an improvement was achieved

and again, the numerical model was validated, only an improved design with more masonry walls in the upper storeys revealed the full potential of the Hyde system in a subsequent numerical analysis.

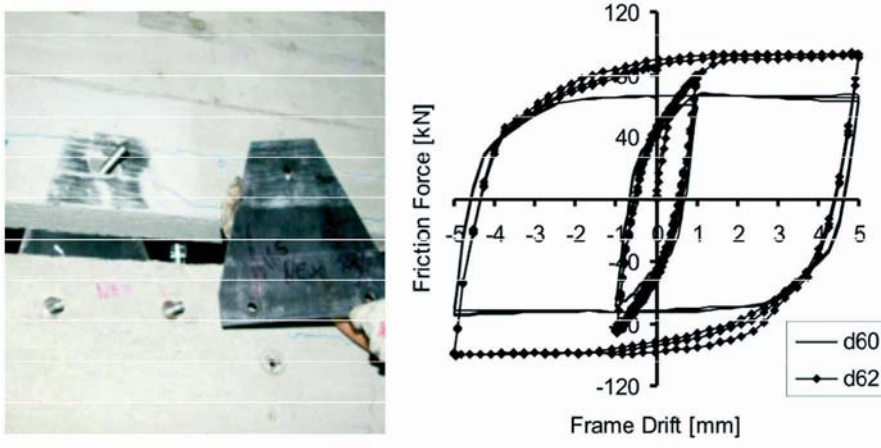

Figure 5. Friction device showing the desired wear on the concrete surface and stable hysteresis loop for 4 (d60) and 6 (d62) disc springs in one package

With the basic knowledge of how to design a Hyde system now firmly established and its virtues demonstrated, an application study for a real building follows.

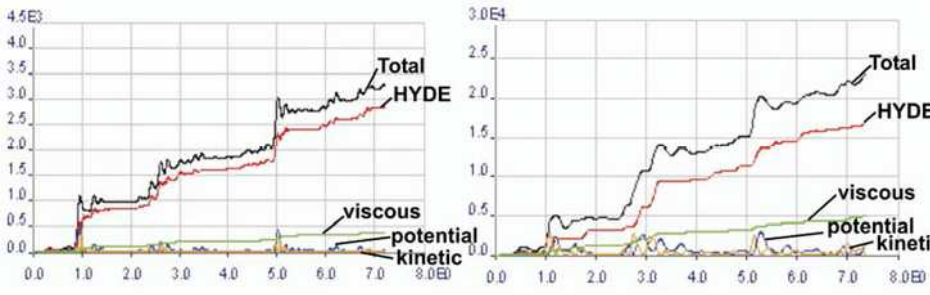

Figure 6. Comparison of energies: Steel frame mock-up (left) and RC-frame (right) both after modification to Hyde systems which was not completely achieved with the RC-frame showing a still too large percentage of kinetic and potential energy

5. A Hyde System for a Residential Building in Skopje

The building given in Figure 7 is a typical modern residential structure in the Republic of Macedonia. As a conventional structure, it is built as an RC-frame stiffened with RC shear walls and masonry walls serving as the main divisions between apartments. Well designed and built with state of the art

technology and quality control, they can be expected to protect their inhabitants during a major earthquake. Then why start a public-private-partnership (PPP-project between the University of Kassel, IZIIS and a local contractor) to look into a Hyde system? Because a Hyde system should improve the economy of such buildings before and after an earthquake.

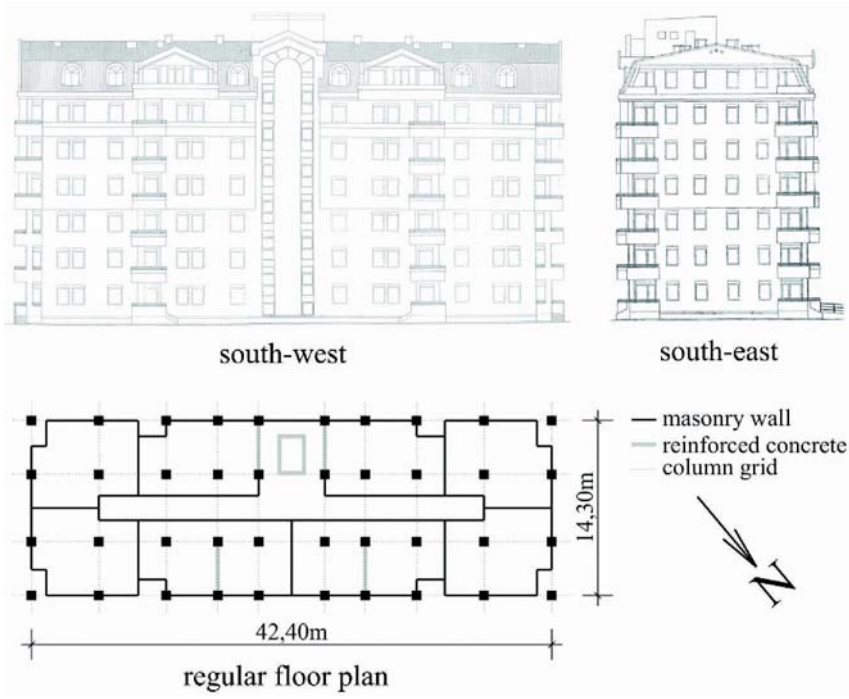

Figure 7. A typical residential building in Skopje

To show this, a re-design was performed that provides the necessary link, the rigid body on top and an SHS that is not too stiff (Figure 8). The link consists of RC-walls (separated from the adjacent columns to allow for the link movement) with shear panels. The SHS is a light horizontal RC-frame acting in parallel to the link and the rigid body on top is achieved by simple masonry walls between columns with greatly reduced x-sections that do not require seismic details. Specific details are only required for the connections of the shear panels. Even the RC-walls in the link do not require typical "seismic" details in their connections to the structure because of the force limit provided by the shear panels.

The design of this limit force is done by establishing a design curve using time history analysis. In this case, 3 natural records scaled to 0.35g maximum

(Figure 9) were used. The refined and condensed numerical models are given in Figure 10. Initially, a large stiffness is used in the link.

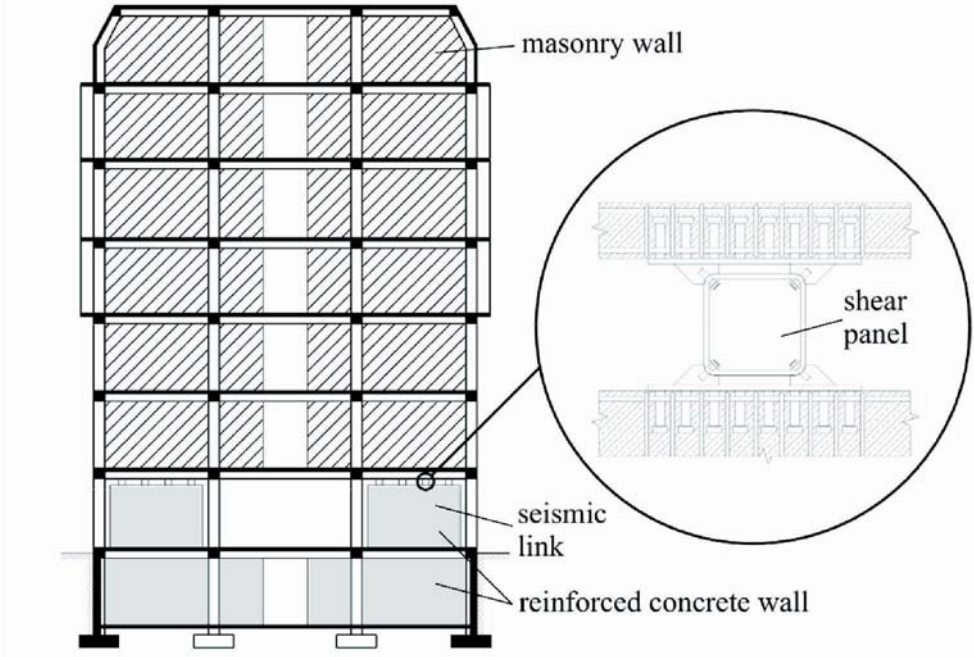

Figure 8. The building in Figure 7 re-designed as a Hyde system using only inexpensive masonry walls for stiffening the upper floors

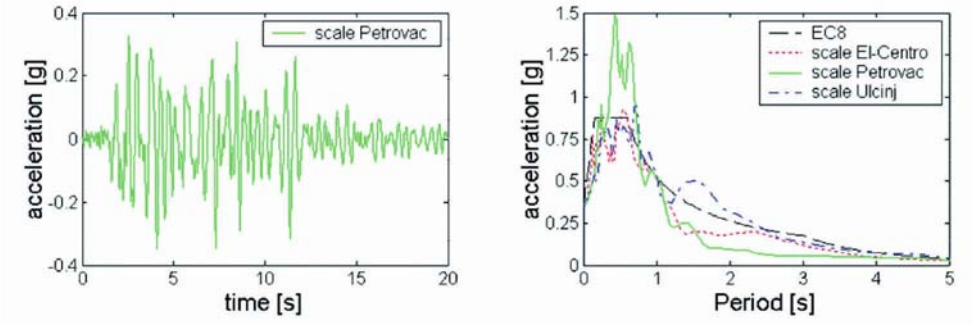

Figure 9. Time history of the Petrovac earthquake and linear response spectra of excitations used in the design

The design curve is bounded by two linear states: The fully stiffened link (no Hyde action) and the structure without Hydes (soft storey). The design limit is given as a deformation limit in the link derived from the quasi-linear limit state of the frame corners in the SHS (Figure 11). Introducing this limit into the

design curve (Figure 12) yields the design Hyde force. A subsequent stiffness reduction in the link (the RC-walls) until this has an effect yields an economic link design.

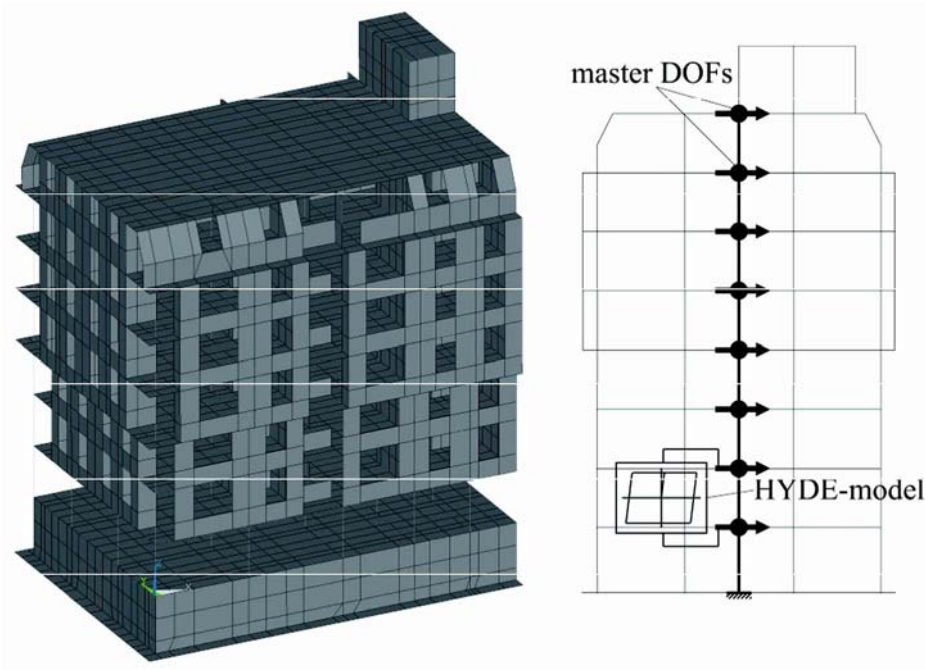

Figure 10. Refined and condensed FE-models for numerical studies on Hyde systems

Comparing the stresses in the conventional structure and in the Hyde system for an extreme event (Figure 13) shows that the Hyde system is more tolerant to increased earthquake demand and thus comprises a more sustainable structure with little or no demand for repair after an earthquake although it has far fewer seismic details and thus can be built with less cost. The newly designed shear panel connections allow easy replacement of deformed devices.

The same structural concept can be realized for mixed residential and commercial buildings since the ground floor is now open. In this case, more "transparent" shear panel supports like the inverted V-braces of the steel frame mock-up in the ELSA tests will be more appropriate.

For an existing building with a soft storey, such a concept can be implemented with ease since a natural place for the seismic link is already provided. Interference with the building's use is minimal even during the retrofit. Considering that such buildings are very common in many cities and are the most vulnerable type today, the Hyde system offers an inexpensive and speedy solution to this very pressing problem.

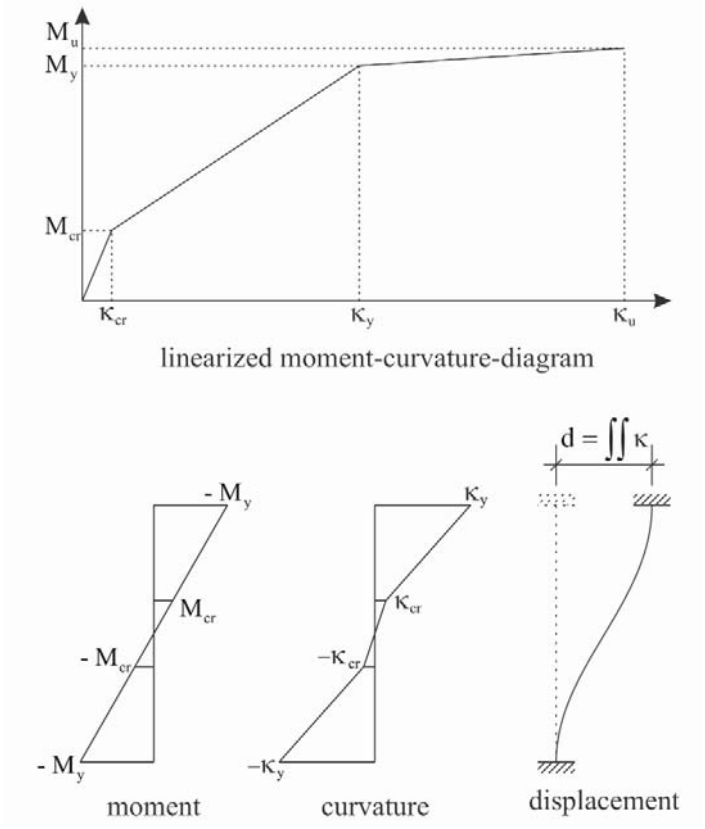

Figure 11. Design limit defined by quasi-linear behavior of the SHS frame columns

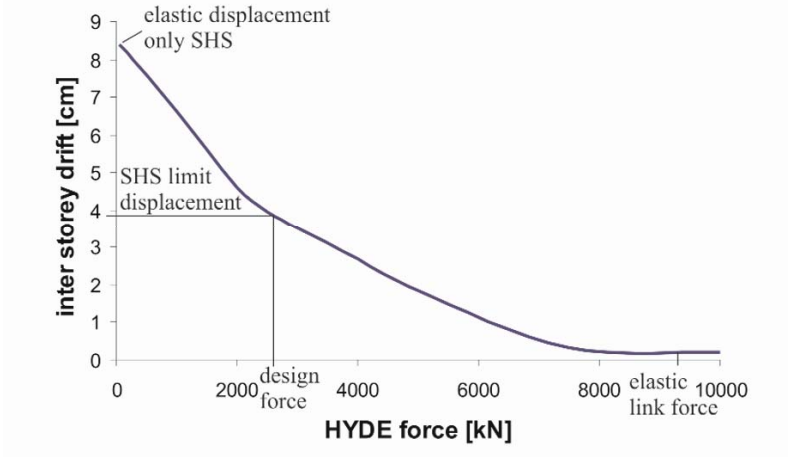

Figure 12. Design curve with boundaries and design point

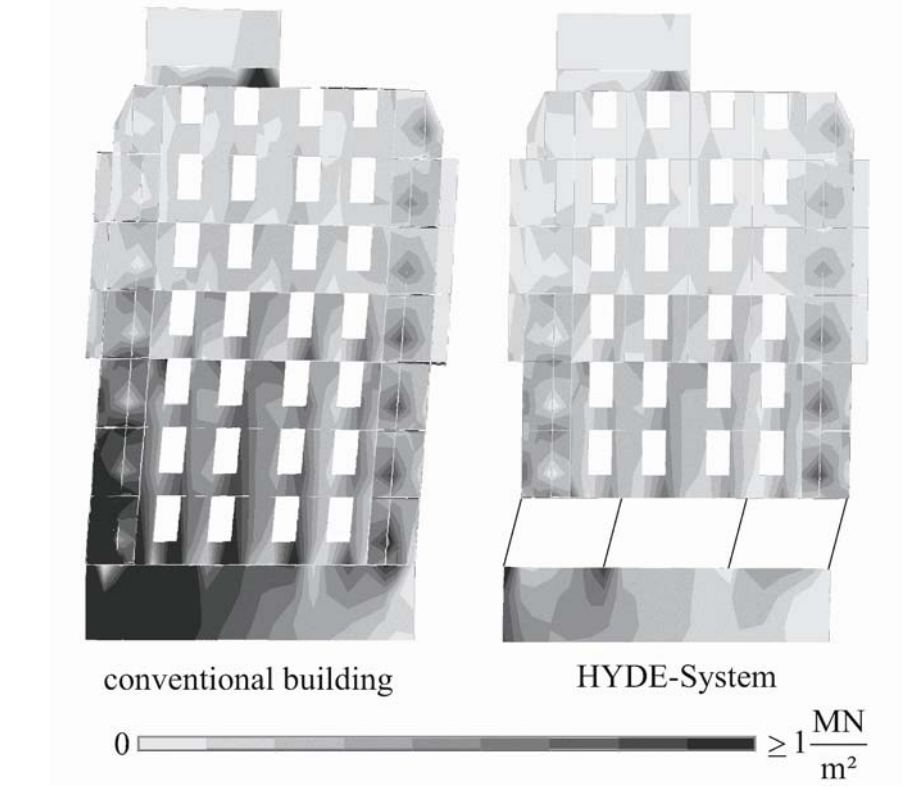

Figure 13. Comparison of maximum linear principal stress distributions for the conventional design (left) and the Hyde system (right). Maximum deformation under 0.35g Petrovac

6. Summary and Conclusions

This paper summarizes the developments of the Hyde system, a particular kind of structural control concept suitable for earthquake protection. It presents results of large scale tests at ELSA (JRC-Ispra) confirming the modeling and design approach that has been developed over a period of years and a study for a residential building in Skopje that is part of a public-private partnership project to demonstrate the advantages of new approaches to earthquake safe structures.

Designing residential or mixed commercial-residential buildings as Hyde systems provides a more economic and sustainable structure in an earthquake environment. This structural control concept needs only inexpensive devices like shear panels to control a rigid body mechanism and can be used to retrofit soft storey buildings with little effort and negligible interference with tenant activities.

References

1. K. Nakahara, T. Hisatoku, T. Nagase, Y. Takahashi, Earthquake response of ancient five-story pagoda structure of Horyu-ji Temple in Japan. *12th[th]World Conf. Earthq. Eng.* paper no. 1229/11/A (2000),
2. M.G. Castellano, M. Indirli, A. Martelli, J.J. Azevedo, G.E. Sincraian, D. Tirelli, V. Renda, G. Croci, M. Biritognolo, A. Bonci, A. Viskovic, Seismic protection of cultural heritage using shape memory alloy devices - an EC funded project (ISTECH). *International Post-SmiRT Conference Seminar on Seismic Isolation, Passive Energy Dissipation and Active Control of Vibration of Structures,* 213-235 (1999)
3. U.E. Dorka, Hysteretic device system for earthquake protection of buildings. *5th US Nat. Conf. Earthq. Eng.*, 775-785 (1994)
4. R.D. Hanson, T.T. Soong, Seismic design with supplemental energy dissipation devices. Publ. No. MNO-8, *Earthq. Eng. Res. Inst*. (EERI), Oakland, CA. (2001).
5. A. Filiatrault, R. Tremblay, Wanitkorkul, Performance evaluation of passive damping systems for the seismic retrofit of steel moment-resisting frames subjected to near-field ground motions. *Earthquake Spectra* 17(3), 427-456 (2001).
6. K. Schmidt, U.E. Dorka Comparative studies of steel frame retrofitted with HYDE system and added damping system subjected to near-field earthquakes*. 40SEEE, Skopje, Macedonia* (2003).
7. UE. Dorka, G.A. Conversano, Seismic retrofit of Allstate Building. *IABSE Symp., San Francisco, CA,* 145-150 (1995).
8. U.E. Dorka, A. Ji, E. Flygare, A hysteretic device system for earthquake retrofit of large panel buildings. *11th European Conf. Earthq. Eng.*, (1998).
9. U.E. Dorka, K. Schmidt, Retrofitting of buildings with masonry infill using HYDE concept. *12[th] European Conf. Earthq. Eng*., paper 206 (2002).
10. K. Schmidt, U.E. Dorka, G.E. Magonette, F. Taucer, Retrofitting of a steel frame and a RC frame with HYDE systems. *Report EUR21180EN, European Commission, Ispra* (2004).
11. K. Roik, U.E. Dorka, Fast online earthquake simulation of friction-damped systems. *SFB 151-Report Nr.15, Sonderforschungsbereich Tragwerksdynamik Ruhr-Universität Bochum*, Germany, (1989).

LEARNING FROM EARTHQUAKES TO IMPROVE REHABILITATION GUIDELINES FOR REINFORCED CONCRETE BUILDINGS

JAMES O. JIRSA
Department of Civil Engineering, University of Texas, Austin

Abstract. Development of design guidelines and updating of such documents is usually accomplished through a combination of laboratory studies and field experience. In the case of rehabilitation design, the problems are complex and the variety of different situations is immense. Furthermore, the issues are not easily studied in parts or in small scale because of the complexity of the interactions between different elements of the existing structure and between the existing structure and new elements added during rehabilitation. As a result, one of the best sources of information for understanding the behavior of existing structures before or after rehabilitation is reconnaissance studies after an earthquake occurs. The 1985 Mexico City earthquake provided an opportunity to carry out such studies. The lessons of Mexico City are relevant to other mega-cities, such as Istanbul, located in regions of high seismicity. The objective of this presentation is to describe some of those studies so that the mitigation efforts to reduce the risk posed by existing buildings can benefit from the Mexico City experience.

Keywords: Rehabilitation; field studies; guidelines; construction techniques

1. Mexico City 1985 Earthquake

Greater Mexico City with a population of about twenty million people is one of the world's largest metropolitan areas. The rapid increase in population prior to 1985 led to the construction of large housing projects and a highly concentrated urban environment. The urban area has about 800,000 buildings with a mix of both modern structural systems and old traditional structures. It is situated in the

S.T. Wasti and G. Ozcebe (eds.), Advances in Earthquake Engineering for Urban Risk Reduction, 209–227.

Valley of Mexico which is underlain by a complex soil formation that has been a continuing challenge for structural engineers.

On September 19, 1985, a major earthquake occurred along the Pacific coast of Mexico and produced extensive destruction. In Mexico City, over 10,000 deaths were recorded. The local site conditions led to high amplification of the ground motion and about 400 buildings were severely damaged or collapsed (Fundacion ICA, 1988). The estimated total direct damage was 4 billion dollars. Mexico City became an enormous natural laboratory in which many modern structural systems were subjected to large lateral forces and cyclic displacements.

After the 1985 earthquake, rehabilitation of damaged structures and strengthening of undamaged structures had to meet updated and increased requirements imposed by the Mexico City Building Code (Rosenblueth, 1985 and Norena, et al., 1989). Structures had to be repaired or rehabilitated as soon as possible after the earthquake to meet the concerns of inhabitants regarding the safety of their buildings. To meet this challenge engineers came up with inventive solutions even though there was not enough experimental data available and little design guidance that could be utilized.

2. Documentation of Damage and Rehabilitation

The main objective of this report is to describe retrofitting techniques used in Mexico City that may be most applicable to common Turkish structures. Like Mexico City, the most prevalent structural systems are reinforced concrete frames with masonry infills. The infills provide considerable stiffness but are quite weak and fail in a brittle manner. In Figures 1 and 2, typical reinforced concrete construction in the two countries is shown.

Figure 1. Typical Turkish residential reinforced concrete construction

Figure 2. Typical Mexican residential reinforced concrete construction

2.1. REHABILITATION STUDIES PRIOR TO 1985

There were a number of buildings that were damaged in 1985 that had been repaired following earthquakes in 1957 and 1979. However, it was not possible to learn much from the performance of the repaired structures because records of the construction were not available. Exceptions include two buildings that were rehabilitated prior to the 1985 earthquake and which performed very well that event. Reports by Del Valle, 1980 and by Foutch, et al., 1989 provide information on the seismic performance of the building shown in Figure 3 during the 1985 earthquake. The structure had solid masonry infills in the long direction and was braced with an external steel tension bracing system that was bolted to the spandrel beams. The columns were strengthened with steel jackets to carry the vertical forces from the braces. Figure 4 shows the plate attached to the spandrel beam and the column jacket. The reports on this structure serve as an excellent model for documenting rehabilitation work. Unless information is available on the condition of the structure before rehabilitation and on details of the rehabilitation scheme, little will be learned from a study of the structure following a future event.

There were a few other structures that had been repaired in previous earthquakes but there was little information available regarding the damage or the rehabilitation.

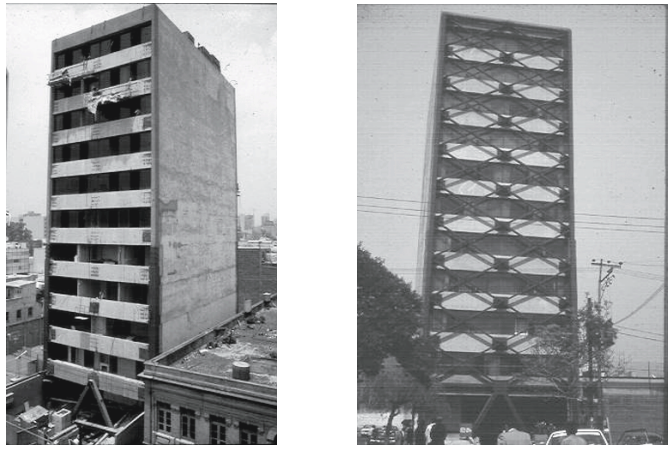

Figure 3. Eleven-story structure braced before 1985

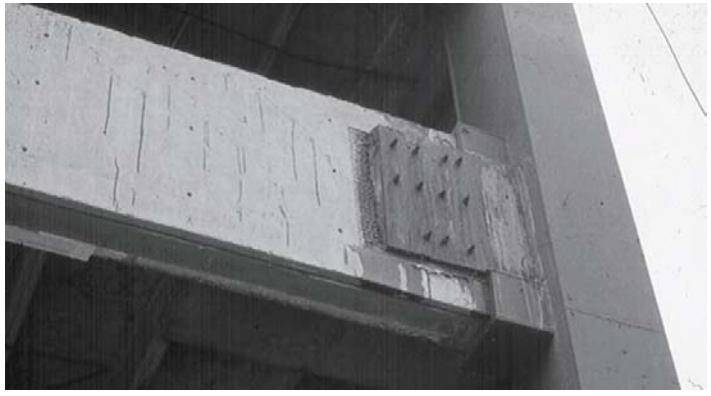

Figure 4. Detail of brace connection and column jacket

2.2. DAMAGE DATA

The soil in Mexico City had a significant effect on the distribution of the damage. The lake bed zone of the Valley of Mexico contains deep deposits of clay with high compressibility. The first hard layer is found from 20 to 35m. deep and has been used to support buildings on point bearing foundations. Below the first hard layer there is another layer of highly compressible clays with a thickness between 9 and 15m. At depths greater than 55m., heavily consolidated sands form what is known as the deep hard layer.

Most of the buildings damaged during the 1985 earthquake were located in the lake bed zone. A comparison between accelerograms recorded on the hill zone and on the lake bed zone shows the importance of the site effects on the ground motion for this earthquake. The peak ground acceleration registered at

the hill zone was 34 gals and at the lake zone was 168 gals. The dynamic properties of the soil at the lake bed zone had great influence on the amplification of seismic waves.

Another important characteristic of the 1985 earthquake was the almost harmonic motion registered in the lake zone and the high energy content at periods greater than one second. The predominant lake bed response occurred at a period of about 2.0 sec. As a result, buildings having long fundamental periods in the 1 to 2.5 sec. range were the most affected by the earthquake. Buildings located in the lake zone that had an initial natural period slightly below the predominant period of the earthquake suffered the greatest damage. As yielding and damage occurred during the strong motion, the building period became longer and closer to the predominant period of the lake bed. Even small period changes resulted in significantly higher structural response. The duration of strong motion between about 40 and 70 seconds and the harmonic characteristics of the ground motion created significant ductility demands on buildings and increased both the extent and level of damage.

Many of the engineered buildings that were seriously damaged during the 1985 earthquake were medium height, reinforced concrete buildings (6 to 15 floors) that had natural periods close to period of the dominant ground motion. The dynamic response of these moment-resisting frame structures was greatly amplified. Buildings with masonry bearing walls performed quite well during the earthquake. Bearing wall buildings were generally less than 5 stories high and were much stiffer than framed buildings of comparable height.

In Table 1, information on 379 buildings that partially or completely collapsed or were severely damaged during the 1985 earthquake is summarized (Iglesias and Aguilar 1988). The buildings are listed according to structural type and number of stories. Concrete buildings represent 86% of the total, 47% were built between 1957 and 1976, and 21% were built after 1976. Damage was concentrated in buildings with 6 to 15 stories and most of these mid-rise buildings were concrete structures.

Table 2 lists the main modes of failure that were observed in the 1985 earthquake. The results were obtained from a survey of 331 buildings in the most affected zone in Mexico City that represented the majority of severely damaged or collapsed buildings (Meli 1987).

Structural configuration problems were a major cause of failure. Most configuration problems were associated with the contribution of non-structural elements to the building response, especially in corner buildings where two perpendicular facades were infilled with masonry walls, and the facades facing the street were left open. Of the buildings that suffered collapse or severe damage, 42 percent were corner buildings (Rosenblueth and Meli, 1986).

TABLE 1. Summary of Damage

TYPE OF STRUCTURE	EXTENT OF DAMAGE	NUMBER OF STORIES <5	6-10	11-15	>15	TOTAL
R/C Frames	Collapse	37	47	9	0	93
	Severe	23	62	14	0	99
R/C Frames &	Collapse	0	1	0	0	1
Shear Walls	Severe	2	1	2	1	6
Waffle Slab	Collapse	20	31	6	0	57
	Severe	6	33	19	1	59
Waffle Slab &	Collapse	0	0	0	0	0
Shear Walls	Severe	0	2	3	0	5
R/C Frames &	Collapse	3	0	0	0	3
Beam-Block Slab	Severe	0	1	2	2	5
Steel Frames	Collapse	6	1	3	1	10
	Severe	0	2	1	3	6
Masonry Bearing Walls	Collapse	8	0	1	0	9
	Severe	19	1	1	0	21
Masonry B. Walls with R/C	Collapse	1	0	0	0	1
Frames in Lower Stories	Severe	3	1	0	0	4
TOTAL	Collapse+Severe	128	183	61	7	379

TABLE 2. Type of Damage (Meli, 1987)

MODE OF FAILURE OBSERVED	% OF CASES
Shear in columns	16
Eccentric compression in columns	11
Unidentified type of failure in columns	16
Shear in beams	9
Shear in waffle slab	9
Bending in beams	2
Beam-column joint	8
Shear and bending in shear walls	1.5
Other sources	7
Not possible to identify	25

Changes in stiffness or mass over the height of the building also were a contributing factor to the damage observed in the 1985 earthquake. Changes in stiffness were due to drastic changes in the structural configuration (wall discontinuities, column location), to a reduction in the size or the longitudinal and transverse reinforcement in columns, or to the location and number of infill walls. Abrupt mass changes resulted from floor dead loadings which were considerably greater than that for which the building had been designed

originally. Concentration of files in government buildings and stacking of materials in buildings used as warehouses were common causes of failure.

Building pounding was quite common during the 1985 earthquake because of the proximity of adjacent buildings. Mexico City codes explicitly limited the distance between buildings, however this limitation proved to be insufficient mainly because of the intensity of the ground motion and large inelastic deformations. Base rotations may also have contributed up to 50% of the lateral motion. Minimum spacing limitations between buildings stipulated in the code were not always met. In some cases, accumulation of materials during building construction filled the gap between buildings. Much of the column damage can be attributed to pounding especially when the slab levels of two adjacent buildings did not coincide.

The lack of sources of good quality aggregates for the production of concrete in Mexico City also contributed to a decrease in the modulus of elasticity of concrete. Such structures may have been more flexible than assumed in the Code. Severe pounding problems were common because the elastic modulus was less than expected and the stiffness was reduced when elements were damaged during cyclic deformations (Rosenblueth and Meli, 1986).

While the ground motions in Turkey and Mexico may be somewhat different, there are many similarities—buildings located on soils that liquefy, structural systems that have quite rigid masonry infill walls that provide stiffness at low deformation levels but tend to fail and leave a flexible, weak frame, sometimes poor quality control of materials and construction, and a large inventory of very similar structures.

2.3. REHABILITATION REQUIREMENTS AND FEATURES

Concern for life safety led to the upgrading of undamaged structures to new lateral force levels specified by codes. Many undamaged school buildings have been rehabilitated. However, in Mexico City, most of the structures that were rehabilitated were damaged either during the 1985 earthquake or in a previous event. A brief overview of some of the materials and techniques used follows.

2.3.1. *Materials*

Resins were generally used to repair cracks or to replace small quantities of damaged concrete. They were also used to anchor or to attach new steel and concrete elements because of the high bond characteristics of the material. In Mexico City, there was not much experience using this material for construction and many projects were done without qualified supervision.

Concrete was widely used as a repair material to replace damaged sections, increase the capacity of an element, and/or add new lateral force resisting

elements to an existing structure. For monolithic action between the new and old materials, shrinkage was sometimes controlled with the use of volume stabilizing additives. (Teran 1988). Old concrete surfaces were generally roughened. The old surface was saturated prior to casting the new section to avoid water loss from the fresh mix to the existing section. Resin or a water-cement mix on the old concrete surface was sometimes applied to improve bond between the two materials (Iglesias, et al. 1988). Shotcrete was used to repair and strengthen concrete and masonry walls and to jacket concrete elements. The concrete surface was prepared prior to shotcreting in the same manner as for cast in place concrete to enhance bond between the two materials.

Mortars and grouts of sand, cement, and water were used to repair cracks in damaged concrete or masonry elements. In some cases epoxy grouts were used when high shear force transfer, low shrinkage, and positive bond were required (Teran 1988). Large gaps were filled with dry pack; a sand-cement mix with minimum water content. The material was packed into position and the quality of the installation was dependent on workmanship and on the space available to place and consolidate the material.

2.3.2. *Rehabilitation Techniques*

A report on the rehabilitation work in Mexico City and details of 12 case studies in which different techniques were used was prepared by a team of US and Mexican engineers (Aguilar, et al., 1996, Brena 1990).

MODIFICATION OF EXISTING ELEMENTS

In Mexico City, concrete jacketing was the most common technique used to increase the axial, flexural, and shear strength of existing elements. Increases in ductility and stiffness were also achieved. Jacketing was performed by adding longitudinal and transverse reinforcement or a welded wire mesh surrounding the original section and covering it with new cast in place concrete or with shotcrete. To be able to develop yield in the longitudinal bars, continuity had to be provided at the ends of the element. For columns this was done by extending bars through the slabs as shown in Figure 5. For beams, the reinforcement was extended through the column core or was bent around the original column. Steel jackets were used primarily for strengthening columns, especially in cases where column forces were increased because new bracing systems were added to the structures. In most cases, the jackets consisted of angles at the corners with straps welded to provide a continuous hoop around the column as shown in the Figure 5. Contact between the steel elements and the concrete surface was required for the steel jacket to be effective. Contact was achieved by using concrete or resin grouts between the two materials.

Figure 5. Examples of column jacketing

In many structures, material was added to increase the thickness of wall and slab elements that were damaged or that had inadequate strength for design lateral loads. To obtain monolithic behavior, the existing material surface was prepared prior to the addition of the new concrete section. Adequate shear transfer was achieved by roughening the old concrete surface and using epoxy grouted dowels embedded in the concrete interface. The wall reinforcement was made continuous over the height of the building to insure proper wall behavior. Holes were bored into the slab to allow continuity of longitudinal reinforcement, improve the force transfer between the wall and the slab, and allow better concrete compaction near the wall-slab interface. Because the lake zone has such difficult soil conditions, many structures were rehabilitated with beam and column jackets to strengthen the existing moment-resisting frame (Figure 6) and avoiding costly modifications to the foundation.

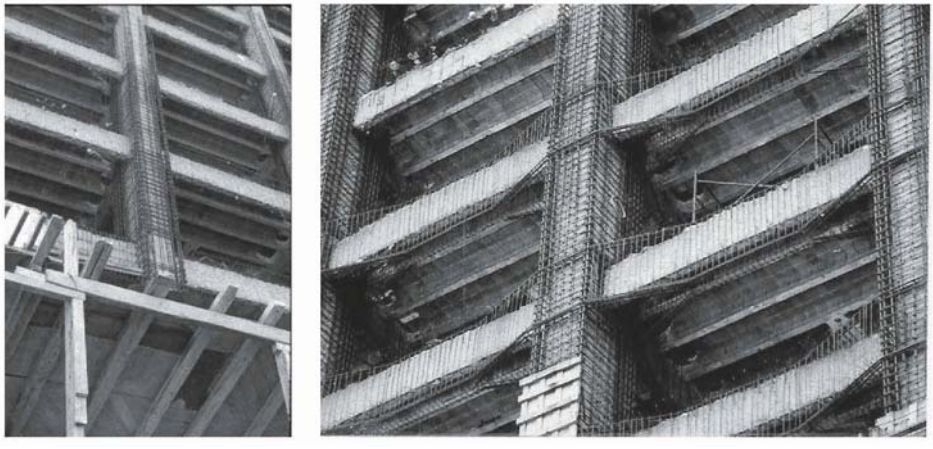

Figure 6. Jacketing of moment-resisting frame

ADDITION OF NEW WALLS

Concrete shear walls were often used to eliminate stiffness eccentricities in a building or to increase lateral load carrying capacity. The new walls were located in the perimeter of the structure thereby reducing interior interference. If there were beams in the perimeter frames, the walls had to be offset to pass the longitudinal reinforcement. Structural wall were attached to existing columns whenever possible so that gravity forces would reduce the uplift generated at the ends of the wall due to overturning moments as lateral loads were applied. Figures 7 and 8 show several different arrangements of new wall elements.

Figure 8 shows the addition of new "wing wall" elements to a moment resisting frame. The distributed wall elements provide increased lateral capacity but do not impose large forces to the foundation as would the new walls shown in Figure 7.

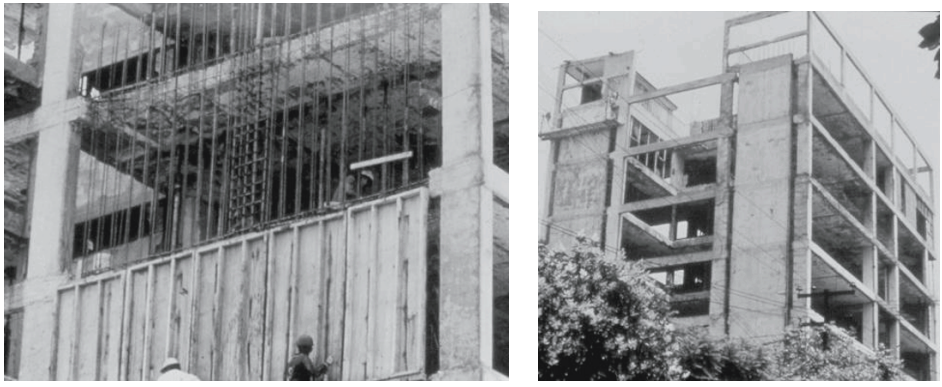

Figure 7. Addition of wall

Figure 8. Addition of distributed wall elements

ADDITION OF STEEL BRACES

The main problem to be addressed when using this technique was anchorage of steel elements to the existing concrete structure. Welded connections were also used to attach steel braces to the existing concrete elements. In this case, collars or steel jackets surrounded the columns. Welding against steel column jackets provided a very good alternative because the axial forces generated by the steel braces can be carried by the strengthened columns. In other cases, steel elements located in the perimeter frames were fixed at the floor levels to the exterior face of the columns.

Infill braces were used when the existing beams and columns had adequate shear capacity to resist the lateral forces induced by the braces. To achieve adequate performance of the bracing system, the deformational characteristics of the concrete structure and the braces have to be matched such that the ultimate capacities of the two systems are reached almost simultaneously. Some steel bracing systems in Mexico City used elements (angles, channels, plates, rods) with high slenderness ratios to avoid buckling and connection problems. Such braces provide lateral resistance primarily through tension. In Figure 9, several steel bracing systems are shown.

Figure 9. Steel bracing systems

ADDITION OF CABLE BRACING

Tension braces or cables were used to eliminate the problems associated with inelastic buckling of bracing systems and to take advantage of the original structure with minimal modifications. The application of a prestressing tensile force improved the behavior of the system under service conditions. With this technique, an increase in stiffness of the original structure was obtained. Also,

the repaired structure was expected to behave elastically for a wider range of ground motions. However, care had to be taken to avoid creating a structure that would go into resonance with the ground motion since there was no energy dissipation through elastic behavior.

Cable braces were used effectively to upgrade undamaged low to medium rise buildings in Mexico City that had to be redesigned for the higher level of forces specified by the codes. The cable system and the existing structure had to interact to achieve acceptable structural response. In many cases the axial loads generated by the cables required that columns be strengthened by one of the techniques described previously. Use of cable bracing seems particularly appropriate for rehabilitation of many reinforced concrete systems in Turkey. These systems have flexible beam-column or slab-column frames with masonry infills providing stiffness and lateral strength but with very limited deformation capacity. Therefore, the reduction of lateral deflection and increasing the lateral strength of the system become the major issues for rehabilitation. Examples of the use of cable braces in Mexico City are presented in the following section.

3. Use of Cable Bracing in Mexico City

3.1. EXAMPLE 1—FOUR STORY CLASSROOM/LABORATORY BUILDING

The four story, reinforced concrete building housed classrooms and laboratories and was located in the lake bed zone of Mexico City. In one direction, the building had 15 bays, with a total length of 101 m. In the short direction, there was one 8.00 m. bay and a 3.75 m. cantilever on one side. The building plan and elevation are shown in Figure 10.

The floor system was a reinforced concrete waffle slab supported on concrete columns that have a rectangular cross section (25 or 35x100 mm.). The columns in the first two stories had more longitudinal and transverse reinforcement than in the upper two stories. The building was supported on a box foundation that is approximately 4 m. deep and partially compensates for the weight of the structure. Partition walls in the restroom and stairway areas were solid clay bricks and the rest of the interior partition walls were hollow clay brick reinforced with #3 bars at every intersection or edge or at a maximum spacing of 1.2 m. The partition walls were to be isolated from the lateral force-resisting system by a 10 mm. gap but the gap was generally not provided in the original construction and the partition walls became part of the lateral force resistance.

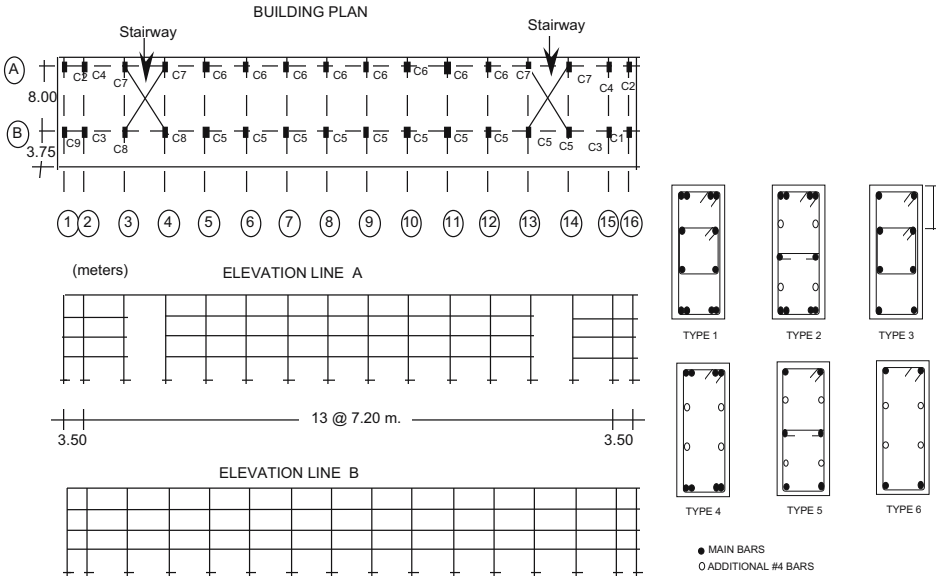

Figure 10. Plan and elevation of building, column details

3.1.1. *Description of Damage after the 1985 Earthquake*

The 1985 earthquake produced cracks (>1mm) in columns around stairway areas, particularly those in line A. The arrangement of perimeter walls resulted in reduction of the clear height of the columns in line A. The building was retrofitted not only because of the damage that occurred but because changes in seismic regulations in the Mexico City Code required Group A structures (school buildings are included in Group A) to be upgraded to resist higher design forces as specified in the code.

3.1.2. *Strengthening Procedure*

The structure was retrofitted using a cable bracing system in the longitudinal direction along column lines A and B. Several bracing configurations were analyzed in order to obtain a bracing system in which the braces and the original structure would reach their capacities at approximately the same displacement level. The configuration selected is shown in Figures 11.

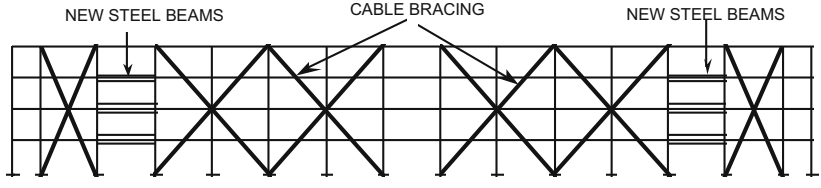

Figure 11. Arrangement of cable braces

The bracing consisted of ½ in. diameter cables, post-tensioned only at 10% of their capacity to prevent sagging. The details of the cables passing through a slab-column joint can be seen in Figure 12. The solution was viable because of the way in which the main longitudinal reinforcement was arranged in the columns. Since the original structure consisted of a waffle slab there were no beams at the joints. Drilling the cable ducts through the joints was a difficult task in the construction procedure.

Because the waffle slab was interrupted in the bays that correspond to the stairway areas (between lines 3 and 4; and between lines 13 and 14, see Figure 10), steel beams were provided for continuity between the bays bordering the stairway area Figure 13. Columns in the stairway areas showed the most cracking after the earthquake.

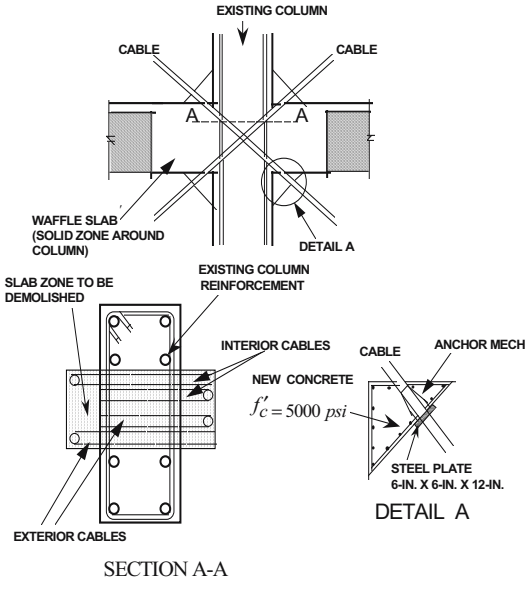

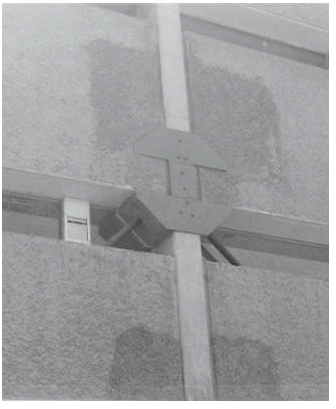

Figure 12. Details of cable connection at column-floor intersection

Figure 13. Added beams in stairway areas for continuity between braced bays

Since the vertical component of the cables resulted in large compressive loads on some of the columns, the columns were strengthened with steel angles or plates located at the corners of the columns. To increase the lateral strength in the short direction of the building, the infill masonry walls in the stairway areas (lines 3,4, 14 and 15) were strengthened with wire mesh and shotcrete was added on both faces of the walls.

The appearance of the structure is almost unchanged following the addition of the cables as can be seen in Figure 14.

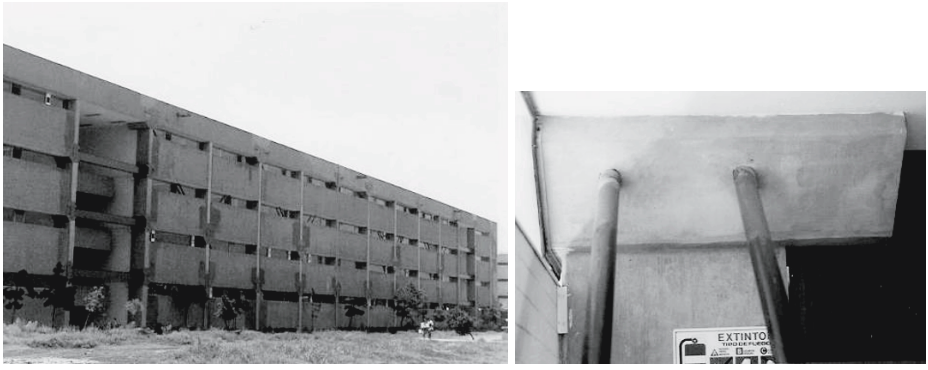

Figure 14. Exterior and interior appearance of building after rehabilitation.

3.2. EXAMPLE 2—PUBLIC SCHOOL BUILDINGS

Many school buildings in Mexico City are two to four story reinforced concrete slab column frames with a number of bays in the long direction but only one bay in the short direction with an overhang that serves as a canopy of hallway on the front of the building such as that shown in Figure 15 after rehabilitation with cable bracing.

In Figure 16, the reinforcement cages for the cable anchorages at the column footing and on the roof are shown. Figure 17 shows other school buildings with the cable bracing in place.

3.3. EXAMPLE 3--10 STORY STRUCTURE

Cable bracing was used to rehabilitate a 10-story structure that was located in lake bed zone. The structure had steel beam-column frames in both directions with and lightweight concrete floors. Lateral resistance in the short direction was provided by a structural wall. The structure is shown in Figure 18 and the connection of the cable anchorages to the frames are shown in Figure 19.

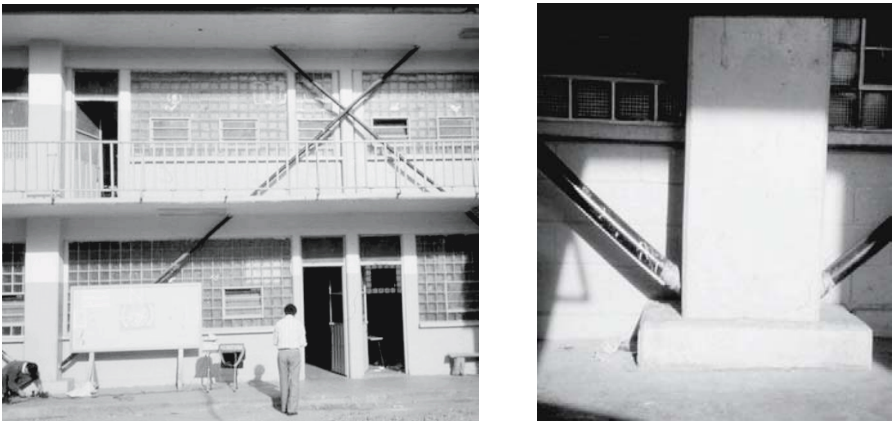

Figure 15. Typical school building

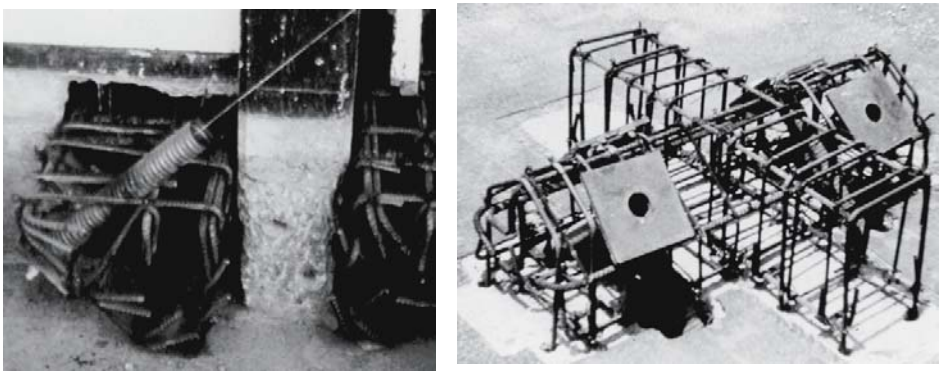

Figure 16. Reinforcement for cable anchorage elements

Figure 17. Cable-braced school buildings

Figure 18. Views of cable bracing on 10-story structure

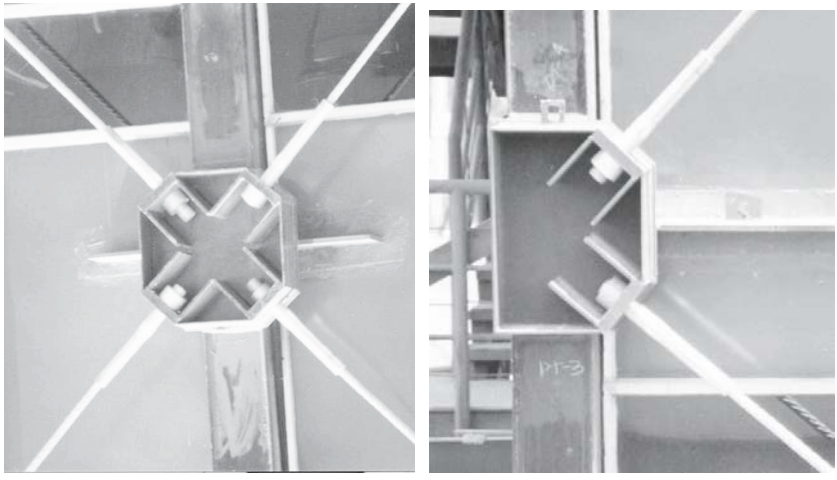

Figure 19. Cable anchorages welded to steel frame

3.4. SUGGESTIONS FOR FUTURE ACTION

While a number of different rehabilitation techniques used in Mexico City were studied and reports prepared, the archiving of such data is often overlooked and forgotten. The lessons learned in future events will hinge on knowledge of the details of the rehabilitation undertaken and of the response of the structure. While damage assessment can provide much insight, instrumentation of buildings would add immeasurably to the knowledge gained.

4. Summary and Conclusions

The problem of rehabilitating a large inventory of deficient structures is one that most large urban areas in active seismic regions will have to address. To mitigate the risks posed by these structures, rehabilitation schemes are needed that are affordable and easily constructed. The Mexico City experience provides many lessons in that regard. Various traditional rehabilitation approaches were used but the number of buildings that were deficient required the development of some innovative techniques. The poor foundation conditions in the lake bed zone required that foundation rehabilitation be kept to a minimum. Cable bracing systems provided a means of stiffening and strengthening the structure to reduce lateral deformation and provide the lateral capacity required by the code after the 1985 earthquake.

That experience provides important information for other urban regions. Mexican engineers involved in the rehabilitation effort shared information with colleagues around the world. There was support for documenting the work done so that the performance of the rehabilitated buildings could be assessed using information about the original construction, previous damage, and details of the techniques used to modify the performance. The archiving of such information should be supported following future major urban earthquakes.

Although some structures were instrumented in Mexico City, cost generally precludes extensive instrumentation of more than a few existing structures. However, government agencies and private owners should be encouraged to provide as much instrumentation as possible to maximize the knowledge that can be gained following future earthquakes. Such lessons will have a major impact on codes and on construction practices.

ACKNOWLEDGMENTS

The enthusiastic participation of Mexican engineers and researchers was critical to gathering the information that has been discussed in this paper. Without their willingness to discuss their work, lessons learned and the benefits of their experience would have been greatly diminished. The efforts of Jorge Aguilar, Sergio Brena, Enrique del Valle, Jesus Iglesias, Marianela Picado, and Manuel Jara are greatly appreciated. Special mention must be made as to the contribution of Structural Engineer Jose Maria Rioboo who provided much of the information regarding cable braced buildings and was one of the early proponents of the technique. The National Science Foundation provided funding for workshops and for preparation of a report on the Mexico City case studies.

References

Aguilar, J., Brena, S. F., del Valle, E., Iglesias, J., Picado, M., Jara, M., Jirsa, J. O., 1996, Rehabilitation of existing reinforced concrete buildings in Mexico City: Case studies, PMFSEL Report 96-3, University of Texas at Austin.

Breña, S. F., An overview of rehabilitation techniques used in reinforced concrete buildings in Mexico City, Thesis, Master of Science in Engineering, The University of Texas at Austin, December 1990.

Del Valle, E., 1980, Some lessons learned from the March 14 Earthquake in Mexico City, *Seventh World Conference on Earthquake Engineering*, Vol. 4, Istanbul, Turkey, pp. 545-552.

Departamento del Distrito Federal, 1993, *Reglamento de Construcciones para el Distrito Federal*, Gaceta Oficial, Vol. II, No. 218, Mexico City.

Fundacion ICA, A.C., 1988, Experiencias derivadas de los sismos de septiembre de 1985, Limusa, Mexico, D.F.

Iglesias, J. and Aguilar, J., 1988, Identificación de daños ocasionados por los sismos de 1985, 1979 y 1957 en la Zona Metropolitana, Estudios de Sismicidad en el Valle de Mexico, *3a Parte, Capitulo III, Anexos I and II, Departamento del Distrito Federal and Centro de las Naciones Unidas para los Asentamientos Humanos* (HABITAT), Mexico, D.F.

Iglesias, J., Robles, F., De La Cera, J. and Gonzalez, O., 1988, Reparación de estructuras de concreto y mamposteria, Universidad Autónoma Metropolitana, Mexico, D.F.

Foutch, D.A., Hjelmsted, K., and Del Valle, E., 1989, Investigation of two buildings shaken during the 19 September 1985 Mexico Earthquake, *Report on Lessons Learned from the 1985 Mexico Earthquake*, EERI, Report 89-02, pp. 161-165.

Meli, R., 1987, Evaluation of performance of concrete buildings damaged by the September 19, 1985 Mexico Earthquake; *The Mexico Earthquakes-1985: Factors Involved and Lessons Learned*, ASCE, pp. 308-327.

Norena, F., Castaneda, C. and Iglesias, J., 1989, The Mexico Earthquake of September 19, 1985 evaluation of the seismic capacity of buildings in Mexico City, *Earthquake Spectra*, Earthquake Engineering Research Institute, **5**(1):19-24.

Rosenblueth, E. and Meli, R., 1986, The 1985 Earthquake: Causes and effects in Mexico City, *Concrete International*, May 1986, pp. 23-34.

Rosenblueth, E., Emergency regulations and the new building code, *The Mexico Earthquakes-1985: Factors Involved and Lessons Learned*, *ASCE*.

Teran, A., 1988, Review of repair techniques for earthquake damaged reinforced concrete buildings, Thesis, Master of Science in Engineering, The University of Texas at Austin, December.

SEISMIC RISK SCENARIOS FOR AN EFFICIENT SEISMIC RISK MANAGEMENT: THE CASE OF THESSALONIKI (GREECE)

KYRIAZIS PITILAKIS*
Aristotle University of Thessaloniki, Department of Civil Engineering, P.O.B. 450, 54124, Thessaloniki, Greece

MARIA ALEXOUDI
Aristotle University of Thessaloniki, Department of Civil Engineering, P.O.B. 450, 54124, Thessaloniki, Greece

SOTIRIS ARGYROUDIS
Aristotle University of Thessaloniki, Department of Civil Engineering, P.O.B. 450, 54124, Thessaloniki, Greece

ANASTASIOS ANASTASIADIS
Institute of Engineering Seismology & Earthquake Engineering, P.O. Box 53-Finikas, Thessaloniki, Greece

Abstract. This paper presents the methodology developed in the framework of the RISK-UE project for the creation of earthquake-risk scenarios in urban systems. The main steps of the methodology are illustrated through an application in Thessaloniki. It is shown that RISK-UE methodology is a general and modular methodology, based on seismic hazard assessment, systematic inventory and typology of the elements at risk, analysis of their global value and vulnerability, and identification of the weak points of urban systems. The vulnerability assessment of building stock, monuments, and lifelines together with the appropriate estimations of the socio-economic consequences (debris, causalities, serviceability dysfunctions, direct/ indirect losses etc) for different earthquake risk scenarios, can operate as a valuable tool for the seismic risk management in urban areas and the development of efficient mitigation plans.

Keywords: seismic scenarios; risk; vulnerability; urban systems; hazard; RISK-UE.

* Prof. Kyriazis Pitilakis, Aristotle University of Thessaloniki, Department of Civil Engineering,, P.O.B. 450, 54124, Thessaloniki, Greece; e-mail: pitilakis@geo.civil.auth.gr.

S.T. Wasti and G. Ozcebe (eds.), Advances in Earthquake Engineering for Urban Risk Reduction, 229–244.

1. Introduction

The seismic protection of metropolitan areas with substantial demographic and building growth, high population density, important administrative, commercial, industrial and residential buildings, extended networks of interconnected infrastructures and variety of daily activities (all referring as elements at risk), dictates a reliable mitigation strategy. Especially when large parts of population are affected and human health and quality of life are threatening, advanced approaches for the seismic risk management are of first priority targets. As a result of the many uncertainties associated with typology of elements at risk, seismic hazard estimation, vulnerability analysis and definition of damage states or losses, the seismic risk assessment is undoubtedly a very complicated task. In Europe until recently there was no general and commonly accepted methodology for constructing earthquake-risk scenarios and assessing the seismic risk of building stock, lifelines, essential facilities and monuments.

This paper presents briefly the general and modular procedure for performing earthquake-risk scenarios in urban areas as it was developed during the RISK-UE project (Mouroux et al., 2004), through an application to the city of Thessaloniki. The methodology takes into consideration the distinctive features of European towns and structures, the European characteristics of seismic hazard and seismicity and the global value of elements at risk. A spatio-temporal evaluation method for the calculation of direct and indirect losses in GIS environment is conducted as well. The flowchart of the proposed seismic risk assessment and risk management methodology, with emphasis to lifelines, is illustrated in Figure 1 (Pitilakis et al., 2004).

2. The City of Thessaloniki

Thessaloniki is located in the eastern part of Mediterranean in the Northern Greece (Macedonia, Thrace). It is the second largest city in Greece (1,048,151 people) after Athens and an important administrative, economic, industrial, academic and cultural centre at national scale. The urban area of Thessaloniki (area of the city = 13130Ha, 1991) consists of 17 districts with the more important the municipality of Thessaloniki (density: 216 people/Ha).

Thessaloniki has been struck by several earthquakes and considerable losses have been reported (Papazachos and Papazachou, 1997). The urban area is located on the Axios-Vardar seismogenic zone, which is adjacent to Servomacedonian massif, one of the most seismotectonically active regions in Europe. The latest major earthquake occurred in June 1978 with an epicenter located at a distance of about 25km NE of the city, a focal depth of about 8 km

and a magnitude of M=6.5 (IMM=VII-VIII). 45 people were killed and the city suffered from major problems for several months and years in some cases.

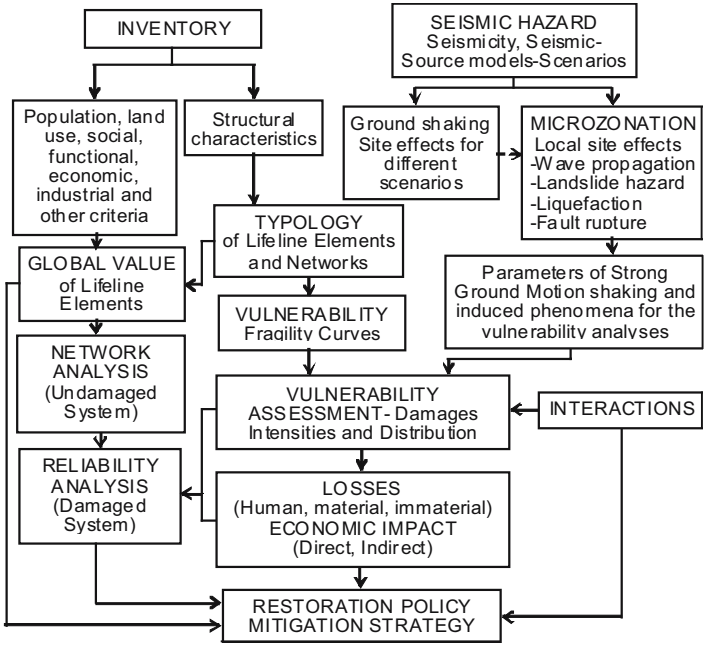

Figure 1. Flow-chart of the RISK UE methodology

3. Earthquake Hazard Assessment

3.1. GEOLOGY, TECTONICS, SEISMICITY

The urban area of the city is situated on three main large-scale geology structures. The first formation includes the metamorphic substratum, the second is composed by alluvial deposits and the third formation composed by recent deposits. A detailed geological map is presented in Figure 2.

3.2. GEOTECHNICAL ZONATION OF THE THESSALONIKI URBAN AREA

A detailed geotechnical map was produced (Anastasiadis et al., 2001), based on data provided by an extended program of geotechnical investigations (boreholes, CPT's, water wells), geophysical surveys (cross holes, down holes, surface seismics), microtremors measurements, classical geotechnical and special soil dynamic tests (resonant column, cyclic triaxial), (Pitilakis et al. 1992, Pitilakis and Anastasiadis, 1998, Raptakis et al. 1994a, Raptakis et al.

1994b, Raptakis 1995). The geotechnical map illustrated in Figure 3, together with various thematic GIS maps, such as the one presented in Figure 4, describe the spatial distribution and the thickness of each soil formation. Nine different soil formations are needed to fully describe the subsoil conditions in the city as is shown in Table 1.

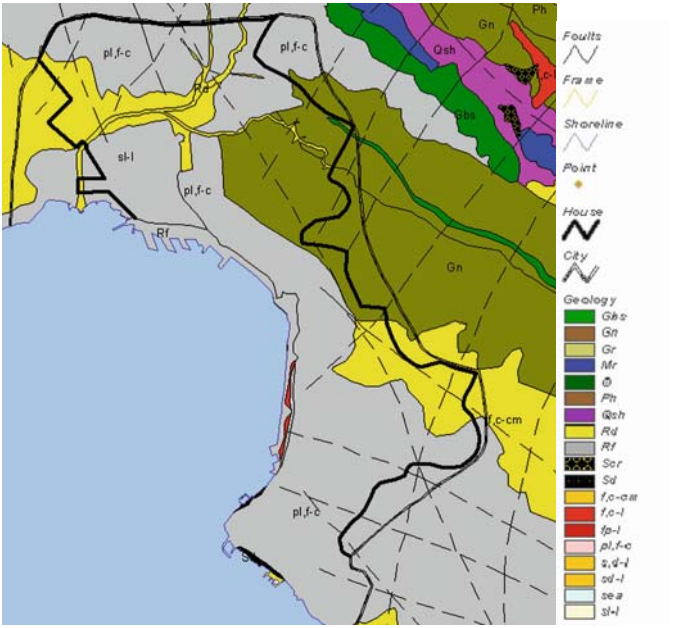

Figure 2. Geological map of Thessaloniki

TABLE 1. Description of soil formations and mean physical and mechanical properties

Formation		Description	V_S (m/s)	V_P (m/s)	Q_S
A	Surficial	Artificial fills, demolition materials and debris parts	200-350 (250)	400-1700	8-20 (15)
B1		Very stiff sandy-silty clays to clayey sands, low plasticity	300-400 (350)	1900	15-20 (20)
B2		Soft sandy-silty clays to clayey sands, low to medium plasticity	200-300 (250)	1800	20-25 (20)
B3		Stiff to hard high plasticity clays	300-400 (350)	1800	20-40 (30)
C		Very soft bay mud and silty sands	120-220 (180)	1800	20-25 (25)
D		Alluvial deposits, sandy-silty clays to clayey sands-silts, low strength, high compressibility	150-250 (200)	1800	15-25 (20)

Formation		Description	V_S (m/s)	V_P (m/s)	Q_S
E		Stiff to hard sandy-silty clays to clayey sands	350-700 (600)	2000	6-30 (30)
F	Subbase	Very stiff to hard low to medium plasticity clays to sandy clays, overconsolidated with rubble and thin layers of gravels	700-850 (750)	3200	50-60 (60)
G		Green Schists & Gneiss	1750-2200 (2000)	4500	180-200 (200)

3.3. SEISMIC HAZARD

Seismic hazard in case of vulnerability analysis and risk assessment of urban areas must be specified according to the needs of particular elements at risk, as well as the models used to describe the vulnerability. In addition, due to the large extent of lifeline systems, it should describe the spatial variability of ground motion considering the local soil conditions, and thus it is absolutely necessary to perform site-specific seismic hazard analyses, considering the seismicity, geology and tectonics of the area and the geotechnical zonation, which is a key issue for a reliable modelling and evaluation of site-effects.

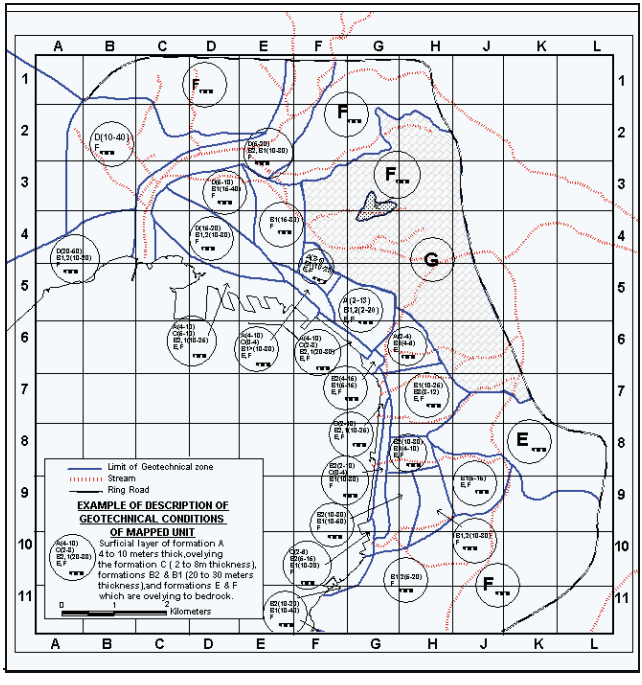

Figure 3. Detailed geotechnical zonation of Thessaloniki with different geotechnical zones

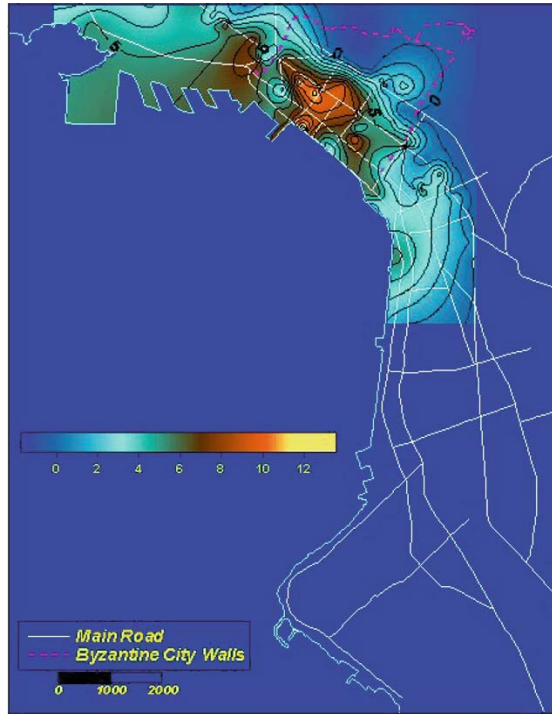

Figure 4. Example of thematic map giving the thickness of formation A (artificial fills)

In case of Thessaloniki, five seismic hazard scenarios were developed: two deterministic and three probabilistic with 475 years recurrence period. The deterministic scenarios were developed according to the maximum credible (1978 earthquake) and the maximum historical earthquake (Assiros), while the probabilistic according to uniform distribution of the seismicity in seismic source zones and to concentrated seismicity in two seismic fault zones (Alexoudi et al., 2002). The results of these studies in terms of PGA at outcrop conditions will be used at the next step of the site specific ground response analyses.

3.4. SITE RESPONSE ANALYSIS

For the ground response analyses, 1D soil profiles were constructed in 301 sites and five different real accelerograms were selected to describe, after appropriate scaling, the seismic input according to seismic hazard study (Anastasiadis et al., 2002).

For an earthquake scenario with 10% probability of exceedance in 50 years, the characteristics of the calculated seismic motions at the free surface, in terms of maximum amplification ratio, peak ground parameters (PGA, PGV, PGD),

spectral values, and ground strains along the city of Thessaloniki, organized through GIS environment are shown in Figures 5 and 6. The evaluation of permanent ground displacements due to liquefaction phenomena was performed in a narrow area of the coastal zone of the central Thessaloniki, where loose and saturated cohesionless soil deposits appear.

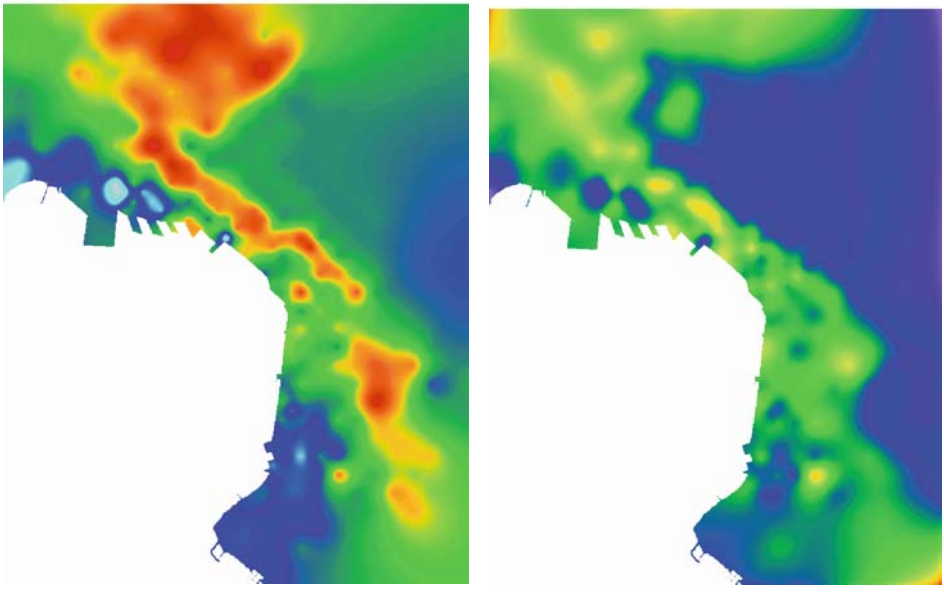

Figure 5. Distribution of mean spectral acceleration (g's) on the surface at 0.0s (left) and 0.6s (right)

The elaboration of all results stemming from site classification and theoretical computations led to the definition of seismic zones and the corresponding mean response spectra.

4. Urban System Exposure

International practice led crisis-management-and-assistance specialists to identify the strategic/important issues for three main periods of urban functioning: normal, crisis (during and few hours after the earthquake) and recovery (that extends days or months after the event). For every element at risk a relative value was given through suitable indicators that comprised the individual characteristics of the component and its importance to urban environment and essential facilities. In order to evaluate and classify the urban components such as residential, commercial and building stock areas, it was necessary to divide the urban fabric of the study area (central part of Thessaloniki) in 20 homogeneous units, mainly based on the primary land use.

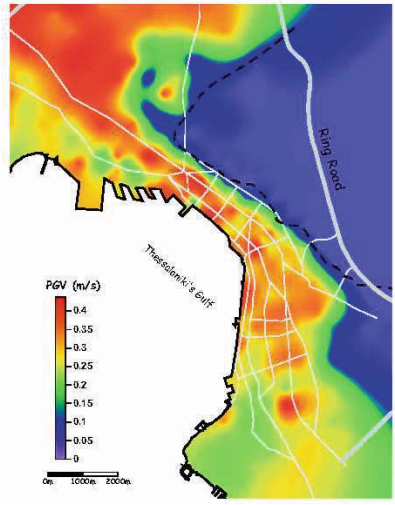

Figure 6. Distribution of mean PGV (m/s) values

The analysis of each element (area, point or line) is based on the following urban components: population, activity, urban space, functions and identity of the city. An urban indicator characterizes each component, while appropriate quantitative or qualitative criteria were used in order to identify the measuring units of each indicator. According to the considered period, the relevant indicators are selected for each element at risk and a score for each indicator from 0 to 1 was assigned according to its relative importance based on expert judgment. A decision making process was followed according to Saaty (1980) based on suitable questionnaires to quantify the weighting factor of the element at risk. Finally, the global value was calculated and the main, important and secondary issues were identified. Various thematic maps in GIS format were produced such as those in Figures 7 and 8, presenting the spatial distribution of the importance of the study elements at risk (Alexoudi et al., 2005).

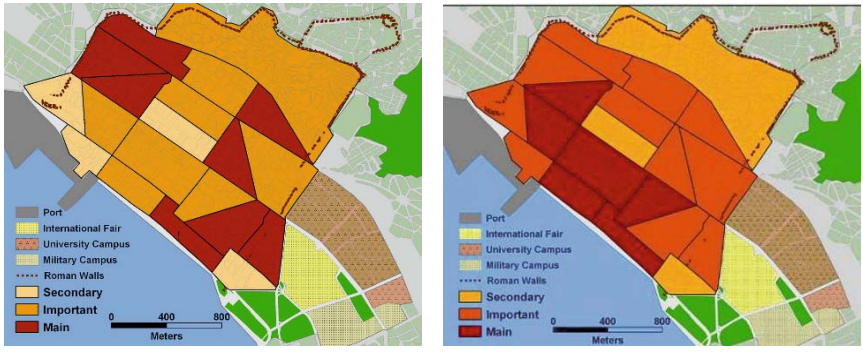

Figure 7. Main, important and secondary issues of residential (left) and trade (right) land use in terms of urban units for the central area of Thessaloniki in the crisis period

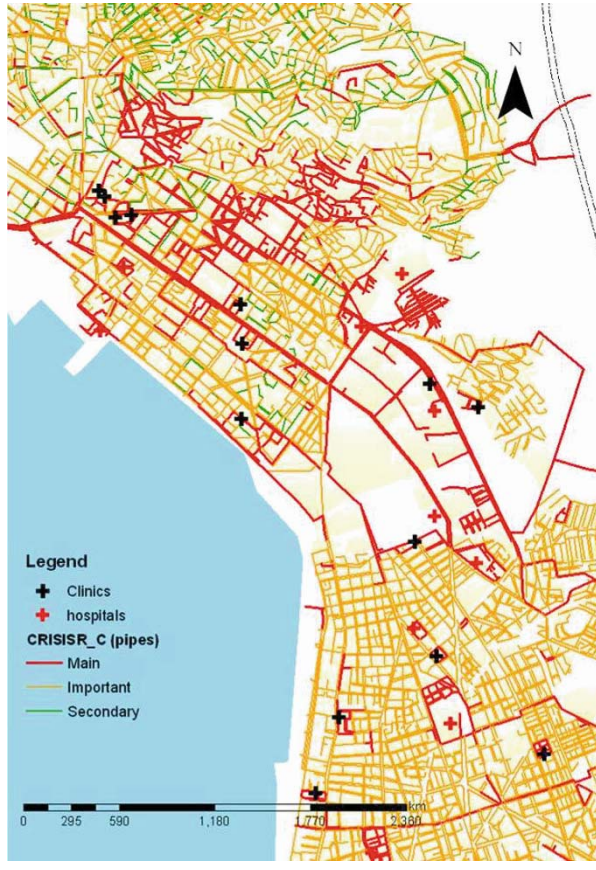

Figure 8. Urban importance of water system. Scenario: Residential use. Period: Crisis

5. Vulnerability Assessment of Current Buildings

For the vulnerability assessment of the building stock, capacity curves, as well as fragility curves (in terms of PGA) were developed for all typologies of R/C and URM buildings present in Greece using a "hybrid" approach (Kappos 2001). Two levels were used for the vulnerability of building stock, level I: fragility curves in terms of PGA and level II: fragility curves in terms of spectral displacement, Sd (Milutinovic and Trendafiloski, 2003). The results for the input seismic hazard scenario (Microzonation study scenario with 475 years return period) were obtained in terms of damage distribution (DS or tag colour), weighted damage factors for each building block, and finally economic loss (repair cost), for the study area that covers the 40% of the Thessaloniki municipality. Table 2 and Figure 9 give the damage state distribution of each damage state.

TABLE 2. Total number of buildings in each damage state

	Damage State	DS0 none	DS1 slight	DS2 moderate	DS3 substantial-heavy	DS4 very heavy	DS5 collapse
Level I	Number of buildings	654	6813	6430	3002	1201	1079
	Percentage (%)	3.41	35.53	33.52	15.65	6.26	5.63
Level II	Number of buildings	3595	7748	3827	2101		1908
	Percentage (%)	18.74	40.40	19.95	10.96		9.95

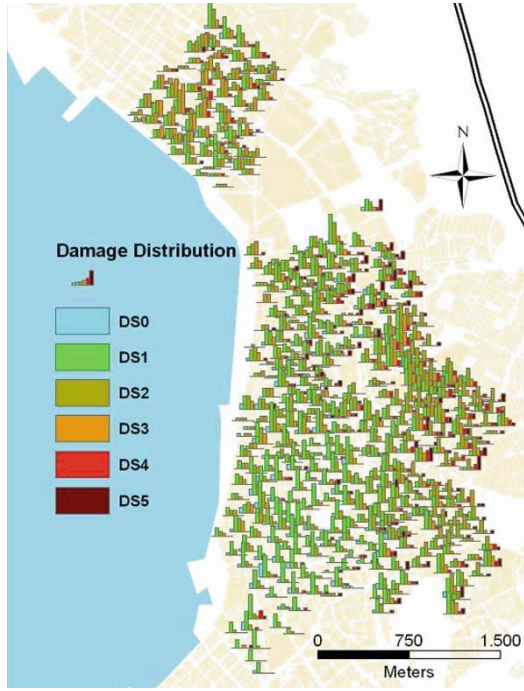

Figure 9. Number of buildings suffering damage states DS0 to DS5 in each building block

6. Vulnerability Assessment of Lifelines

The vulnerability assessment of lifelines was performed for the following systems: roadway, port, gas, telecommunication, potable water and waste-water. The collection of inventory data is essential in order to define the typology of each lifeline element and to assign the appropriate fragility curve or function (Pitilakis et al., 2004). Normally, a detailed inventory using questionnaires is mandatory for each element at risk (i.e. see Table 3 for water-pipelines). However, in most cases this is extremely difficult if not impossible. Table 4 presents the typology of most usual structural types of RC bridges in

Thessaloniki, classified according to the number of spans, column bent type, span continuity and seismic design level.

Fragility curves or functions, relate the probability of the component damage to the level of seismic hazard. The fragility curves that were used for the risk assessment of lifelines in Thessaloniki were mainly empirical, obtained from the international bibliography such as HAZUS'99 (NIBS, 1999). The damage states are described either with an expert opinion on damage's level (i.e. qualitative approach), or using appropriate indexes for the functionality or serviceability of the system (Pitilakis et al., 2004). The expected damage level of each lifeline network depends on the seismic hazard scenario, the individual characteristics of the components and the selected fragility model. An example of fragility functions that were used for the vulnerability assessment of pipelines is given in Table 5 together with an evaluation of damage states in Table 6.

TABLE 3. Inventory for water system pipelines

Detailed inventory for water pipelines
General information: Geographic location (coordinates), Location of pressure reduction valves (coordinates), Exact location of connections (coordinates), Location of manhole (central, smaller), Location of isolation valves, of SCADA, In case of failure: Isolation of pipe segments (area coverage, number of customers). Geometrical and construction detail: Length (m), Type (fragile, ductile), Diameter (mm), Thickness (mm), Elevated or buried, Material, Strain: σy, σf (MPa), Connection type (compression coupling, bell & spigot, heat fusion, arc or oxyacetylene gas weld), Rotation tolerance, Depth (m), Type of coating, Type of lining, Type of protection material (if any), Operational characteristics (free-flow, with pressure), Operation pressure (atm), Directivity of flow, Year of construction, Corrosion (yes, no, possible, unknown), Description of construction technique, History of failures/ repairs (not only from earthquakes but also from operation use), Method of repair. Urban & economic characteristics: Type of customers served (important, common), Connection with essential/ critical facilities (e.g hospitals, clinics etc), Alternative routing, Time of emptying pipe segment, Economic cost of construction, Cost of reconstruction if damaged by an earthquake.
Basic features of water pipelines
Geographic location, Diameter, Thickness, Material, Connection type, Operational characteristics, Distances between connections, Type of customers served, Connection with essential/ critical facilities, Description of construction technique, Alternative routing, Location of manhole, Location of valves, isolation valves etc, Location of SCADA, Economic cost of construction.

TABLE 4. Typology of R/C bridges in Thessaloniki

Spans	Column bent type	Span continuity	Design
Single span		-	Conventional (<1986)
			Seismic (>=1986)
Multiple spans	Single column	Simple support	Conventional
			Seismic
		Continuous	Seismic
	Multiple column	Simple support	Conventional
			Seismic
		Continuous	Seismic

TABLE 5. Fragility relations for water pipes subjected to wave propagation and permanent ground deformation

Induced hazard	Vulnerability model (R.R.)	Lognormal standard deviation β
Wave propagation (ALA, 2001a,b)	K_1* 0.241*PGV	1.15
Ground failure (ALA, 2001a,b)	K_2*11.223*$PGD^{0.319}$	0.74

R.R. =repair rate= repairs / km

K_1, K_2: coefficients according to various pipe material, joint type, soil conditions and diameter size

PGV: Peak Ground Velocity (m/s)

PGD: Permanent Ground Displacement (m).

TABLE 6. Pipeline Vulnerability Risk

Vulnerability Class	Repair Rate (R.R)	Vulnerability Risk
High	1.4< R.R	Break
Moderate- High	0.7< R.R ≤ 1.4	
Moderate	0.1< R.R ≤ 0.7	Leak
Low- Moderate	0.01< R.R ≤ 0.1	
Low	0.001<R.R ≤ 0.01	None
No-damage	0 ≤R.R≤ 0.001	

The input seismic hazard scenario for the seismic risk assessment of lifelines was based on the detailed microzonation study of the city in terms of peak ground velocity, peak ground acceleration or spectral acceleration for ground shaking and permanent ground displacement for ground failure, depending on the element at risk. The restoration process was defined in some cases, mainly based on the extent of damage, manpower, equipment, expertise, company organization and interaction between other lifelines. Finally, various maps were produced, illustrating the distribution of expected damage or the restoration process for each element at risk such as those presented in Figures 10 and 11.

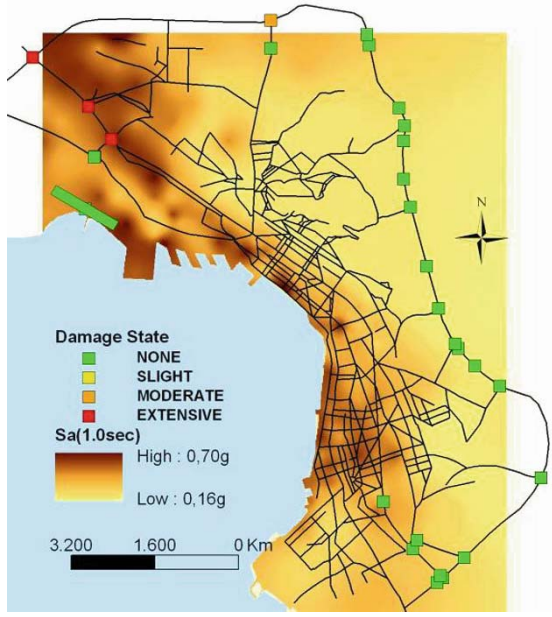

Figure 10. Estimated damage for bridges

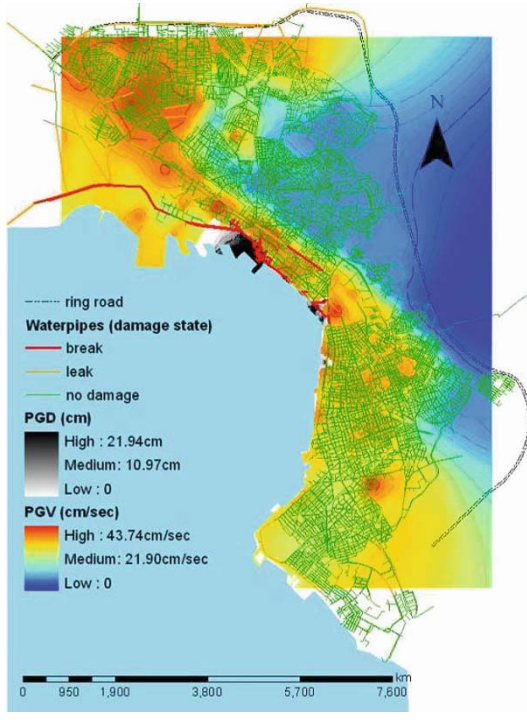

Figure 11. Estimated damage for water system

7. Earthquake Risk Scenarios

The debris and casualties due to collapse of buildings were estimated for the selected earthquake scenario in the study area. Two types of debris are calculated: Type 1, reinforced concrete and steel and Type 2, brick, wood and other. The number of casualties is a function of various parameters such as the complete damage state probability, the occupancy rate, the time of occurrence of the earthquake, the type of building or the response of the community. Table 7 shows the breakdown of computed casualties according to Coburn and Spence, 2002 model, for both level I and II approaches. However, the estimated casualties are probably overestimated as the experience from past earthquakes in Greece reveals that the number of death rate is quite low compared to other countries for the same seismic magnitude.

TABLE 7. Breakdown of casualties

	Level I		Level II	
Time of earthquake	12:00	24:00	12:00	24:00
Dead or unsavable	246	360	216	291
Life threatening cases needing immediate medical attention	216	310	210	287
Injury requiring hospital treatment	261	371	241	323
Light injury not necessitating hospitalization	234	319	237	323

Such combination could be implemented by a double-entrance table as the one given for pipes in Table 8. An application example is presented for the water system of Thessaloniki in Figure 12.

TABLE 8. Risk analysis matrix showing seismic retrofit priorities

Urban Risk/ Seismic Risk	Issues		
	Main	Important	Secondary
Breaks	1st priority	1st priority	2nd priority
Leaks	2nd priority	3rd priority	3rd priority

8. Restoration Policy- Mitigation Strategy

Mitigation strategy includes pre-earthquake actions and an efficient restoration policy immediately after the seismic event. The identification of the “main”, “important” and “secondary” elements at risk in “normal period” provides a prioritization of the importance according to functional, social and economic criteria and satisfies the daily demand for serviceability. The evaluation of the “global value” in crisis period, the vulnerability assessment of the element at risk and the essential human and material resources are essential steps for the development of an efficient recovery plan.

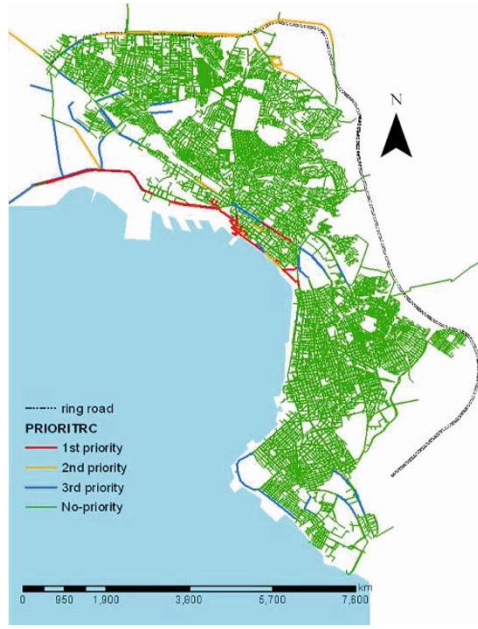

Figure 12. Replacements priorities for the water system of Thessaloniki (mitigation strategy)

9. Conclusions

RISK-UE methodology provides a valuable framework to the scientific community, local actors, emergency planners and decision makers, to understand the seismic risk, to estimate the induced direct and indirect damage and to apply pre-, co- and post-seismic measures in order to reduce losses. However, further research is needed on issues such as the casualty and debris estimation models or the fragility functions of lifeline elements, in order to take into account the characteristics of European typology and construction practice.

Considering the application of the methodology to Thessaloniki, an efficient mitigation policy can be developed based on the expected damage of building stock, lifeline systems and urban environment, taking into account the urban importance and functional relations between the different elements at risk.

In conclusion the organization of mitigation policies is a political and economic decision, not based on emotion or public feeling which, however, should be seriously considered. The selection of the acceptable risk and the appropriate seismic scenarios should combine the level of detail of the seismic hazard, the will of central and local actors, the financial capability of the community and the country without neglecting the epistemic and physical uncertainties involved in every path of any earthquake risk reduction policy.

References

ALA, 2001a, Seismic Fragility Formulations for Water Systems. *Part 1 – Guideline*. American Lifelines Alliance (ALA), ASCE-FEMA, 104 p.

ALA, 2001b, Seismic Fragility Formulations for Water Systems. *Part 2 – Appendices*. American Lifelines Alliance (ALA), ASCE-FEMA, 239 p.

Alexoudi M, Hatzigogos Th., Pitilakis K, 2002, Earthquake- hazard assessment in Thessaloniki, Greece, Level I: Probabilistic & Deterministic Approach, *Proceedings of the International Conference of Earthquake Loss Estimation and Risk Reduction*, 25 & 26 Oct. Bucharest.

Alexoudi M, Hatzigogos Th., Pitilakis K., 2005, Advanced methodology for mitigation strategy of water system. The case of Thessaloniki (Greece), *Proceedings of 1st International Conference on Urban Disaster Reduction (1ICDR),* January 18-20, Kobe, Japan.

Anastasiadis A, Apessou M, Pitilakis K, 2002, Earthquake- hazard assessment in Thessaloniki, Greece, Level II: Site Response Analyses, *Proceedings of the International Conference of Earthquake Loss Estimation and Risk Reduction*, 25 & 26 Oct. Bucharest.

Anastasiadis, A., Raptakis, D., and Pitilakis, K., 2001, Thessaloniki's Detailed Microzoning: Subsurface Structure as basis for Site Response Analysis, *Pure and Applied Geophysics – PAGEOPH*, **158** (12): 2597-2633.

Coburn, A., Spence, R., 2002. Earthquake Protection. John Wiley Ltd., Chichester, England.

Kappos, A.J., 2001, Seismic Vulnerability Assessment of Existing Buildings in Southern Europe, *Keynote lecture, Proceedings "L'Ingegneria Sismica in Italia",* Potenza/Matera, Italy, Sept.

Milutinovic, Z. V. and Trendafiloski, G. S., 2003, WP4 Report Vulnerability of current buildings. RISK-UE project, "An advanced approach to earthquake risk scenarios with applications to different European towns", Contract: EVK4-CT-2000-00014. (http://www.risk-ue.net/)

Mouroux, P., Bertrand, E., Bour, M., Le Brun, B., Depinois, S. and Masure, P., 2004, The European RISK-UE project: an Advanced Approach to Earthquake Risk Scenarios. *Proc. of the 13th World Conf. on Earthquake Eng.*, Vancouver, Canada, paper 3329 (CD-ROM).

NIBS, National Institute of Building Science, 1999, Direct physical damage to lifelines-transportation systems-utility systems. In: Earthquake loss estimation methodology. *HAZUS. Technical manuals.* Federal Emergency Management Agency (FEMA), Washington, Vol. 2.

Pitilakis, K., Anastasiadis, A., and Raptakis, D., 1992, Field and Laboratory Determination of Dynamic Properties of Natural Soil Deposits. *Proc.of the 10th World Conf. on Earthquake Engineering,* Madrid, **5**: 1275-1280

Pitilakis, K., and Anastasiadis, A., 1998, Soil and Site Characterization for Seismic Response Analysis, *Proceedings of the XI ECEE*, Paris 6-11 Sept. 1, Inv.Lectures, pp.65-90.

Pitilakis K., Alexoudi A., Argyroudis S., Monge O., and Martin C., 2004, Chapter 9: Vulnerability and Risk Assessment of Lifelines, in: *Assessing and Managing Earthquake Risk*, C.S. Oliveira, A. Roca and X. Goula, ed., Springer Publ., (in press).

Raptakis, D., 1995, Contribution to the Determination of the Geometry and the Dynamic Characteristics of Soil Formations and their Seismic Response, *Ph.D. Thesis* (in Greek), Dep. of Civil Engineering, Aristotle University of Thessaloniki.

Raptakis, D., Anastasiadis, A., Pitilakis, K. and Lontzetidis, K., 1994a, Shear Wave Velocities and Damping of Greek Natural Soils, *Proceedings of the 10th European Conference on Earthquake Engineering,* Vienna, Austria, **1**: 477-482.

Raptakis, D., Karaolani, E., Pitilakis, K., and Theodulidis, N., 1994b, Horizontal to Vertical Spectral Ratio and Site Effects: The Case of a Downhole Array in Thessaloniki (Greece), *Proceedings of XXIV General Assembly*, *ESC*, Athens, Vol.III, pp.1570-1578.

Saaty TL., 1980, The Analytic Hierarchy Process. New York: McGraw-Hill, 1980.

THE MULTI-AXIAL FULL-SCALE SUB-STRUCTURED TESTING AND SIMULATION (MUST-SIM) FACILITY AT THE UNIVERSITY OF ILLINOIS AT URBANA-CHAMPAIGN

AMR S. ELNASHAI*
BILLIE F. SPENCER
DAN A. KUCHMA
GUANGQIANG YANG
JUAN CARRION
QUAN GAN
SUNG JIG KIM
Department of Civil and Environmental Engineering, University of Illinois at Urbana-Champaign, Urbana, IL 61801, USA

Abstract. The Multi-Axial Full-Scale Sub-Structured Testing and Simulation facility (MUST-SIM) is a state-of-the-art physical and analytical simulation environment capable of representing the inelastic seismic response of full-scale structure-foundation-soil systems. Three Load and Boundary Condition Boxes (LBCBs) provide full hybrid action-deformation control at each of their three contact points. An L-shaped prestressed concrete wall provides the reaction structure for testing of full scale sub-structures while a suite of advanced analysis software is available for analytical simulation. The paper describes four sets of simulations under investigation. These are an RC bridge and a steel building, at scales between 1:1 and 1:16. Early results using a new concept of integrated simulation combining analytical and experimental components are reported on complex structure-foundation-soil bridge systems.

Keywords: pseudo dynamic; hybrid simulation; testing facility; substructure; bridge.

* Professor Amr Elnashai, Department of Civil and Environmental Engineering, University of Illinois at Urbana-Champaign, 205 N. Mathews Ave., Urbana, IL 61801, USA; e-mail: aelnash@uiuc.edu

S.T. Wasti and G. Ozcebe (eds.), Advances in Earthquake Engineering for Urban Risk Reduction, 245–260.

1. Introduction

The investigation tools of earthquake performance assessment are i) laboratory testing, ii) computer analysis, and iii) collecting data from regions hit by destructive earthquakes. Each of the three tools has advantages and drawbacks. Experimental testing is an essential and powerful tool. However, requirements for testing of large structures often exceed the capabilities of a single experimental facility. Analytical modeling also suffers from serious shortcomings, where many important response and failure mechanisms remain beyond the realms of accurate constitutive representation. Field observations, as realistic as they are, suffer from lack of control of the exposed sample, incomplete knowledge of the input motion and uncertainty about the underlying soil properties. As a result, only an integrated approach would provide the means to reliably investigate the seismic performance of complex structure-foundation-soil systems (Elnashai et al., 2004).

As a node of the George E. Brown Network for Earthquake Engineering Simulations (NEES), MUST-SIM facility at UIUC allows advanced experimental and computational simulations of full-scale structure-foundation-soil systems to be conducted. The facility is currently used on four sets of simulations at two different scales, ranging between 1:1 and 1:16. The first project investigates the response of a reinforced concrete bridge under simultaneous horizontal and vertical seismic excitation. The second one analyzes and compares the response and performance of a steel building with various types of bolted semi-rigid connections. These simulations fully utilize the NEES approach to aid in providing the basis to mitigate the effect of earthquakes on existing infrastructure and furnishing data upon which enhanced design procedures may be derived.

2. UIUC MUST-SIM Facility

The MUST-SIM facility is one of the fifteen NEES experiment sites that provides distributed experimental-computational simulation capabilities to the earthquake engineering community. The MUST-SIM facility has many advanced features, and is well-suited to run the Pseudo Dynamic (PSD) tests. The principle components of the MUST-SIM facility are shown in Figure 1.

An important feature of the MUST-SIM facility is the large reaction wall (shown in Figure 2), used for anchoring test specimens and loading devices. This L-shaped post-tensioned concrete strong wall of 15.2 × 9.1 × 8.5 × 1.5 m (length × width × height × thickness, respectively) enables testing of full scale sub-structures.

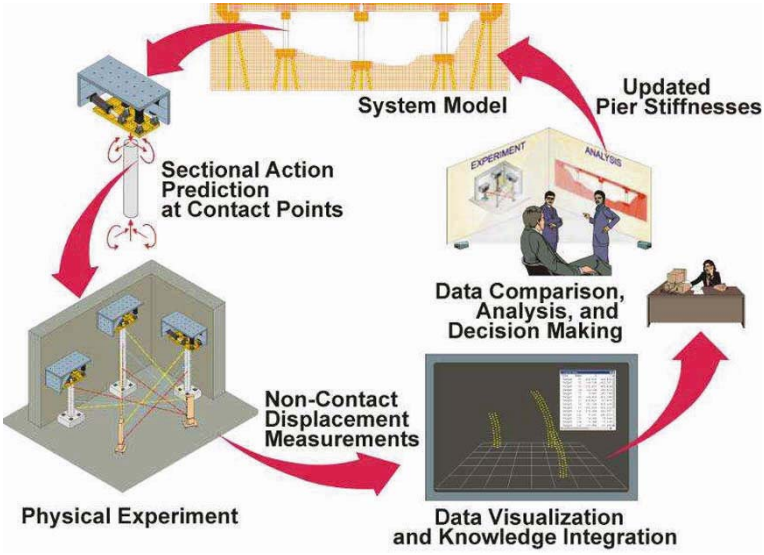

Figure 1. Principle components of MUST-SIM facility

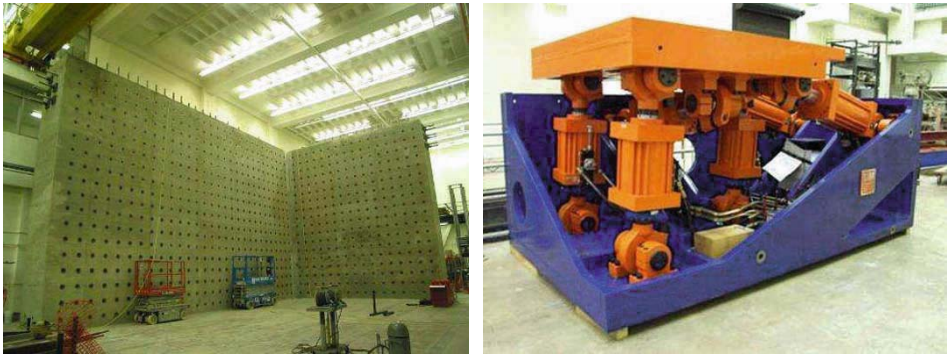

Figure 2. Reaction wall and LBCB in the MUST-SIM facility

The UIUC MUST-SIM facility also features three large scale high capacity and precision Load and Boundary Condition Boxes (LBCBs). Through the use of the LBCBs, researchers can displace a test specimen in 6 DOF, easily applying combinations of shear, axial force, and moment (Figure 2). Each LBCB is a self-reacting assembly of actuators and swivel joints with control software capable of imposing any combination of six actions (forces and moments) and six deformations (displacements and rotations) to test specimens connected to its loading platform. In addition, the LBCBs are capable of imposing motions on the test structures from the results of concurrently-running numerical models of the surrounding structure-foundation-soil system employing pseudo-dynamic and sub-structuring testing methods.

Three types of non-contact instruments, which include Krypton K-600 Dynamic Measurement Machine (DMM), Stress Photonics Gray Field Polariscope (GFP-1200), and Close-Range Digital Photogrammetry, are available at the facility. These state-of-the-art non-contact instruments have been used to display and analyze the deformations and response of large structures in 3D with unprecedented high spatial resolution and allow near real-time model updating for the model-based simulation.

An integral part of the MUST-SIM facility is a fully functional model consisting of a $1/5^{th}$ scale reaction structure, $1/5^{th}$ scale LBCBs (Figure 3) and dedicated servo- controllers. The $1/5^{th}$ scale laboratory allows users with diverse research backgrounds to have full access to the MUST-SIM facility and to understand the capability and limitations of the facility. Also, the laboratory will provide the pre-test verifications before using the large scale facility.

Figure 3. 1/5th scaled reaction wall and LBCB in the MUST-SIM facilities

Recognizing the need for a central control system for multi-site testing, the University of Illinois simulation coordinator, UI-SIMCOR, was developed for multi-site substructure PSD test and simulation (Kwon et al. 2005). During the development of this coordination system, the following key components were sought:

- Integration scheme for PSD tests.
- Communication amongst sub-structured components.
- Sub-structuring (sub-division) of the complex system.

One of the notable advantages in UI-SIMCOR is that it allows all sub-structured components to be analyzed or physically loaded statically. The dynamic components of structural tests are contributed by UI-SIMCOR through a PSD algorithm. The α-Operator Splitting method (Nakashima et al., 1990; Shing et al., 1996) is used as the integration scheme. Another significant advantage of the simulation coordinator is the ease with which it allows

integrated response to be determined from numerous separate subdivisions of the overall system. Distant geographically distributed sub-structured components can be integrated and tested as a fully interacting system, allowing multiple laboratories to be used for large and complex tests.

3. Bridge Experiment

The first application concerns the assessment of the effect of vertical earthquake ground motion on the shear capacity and imposed demand on RC bridge piers. This project is motivated by the pier shear failure of the Collector-Distributor 36 of Santa Monica (I-10) Freeway during the 1994 Northridge earthquake. The Collector-Distributor 36 forms part of a pair of off-ramps from the eastbound carriageway on the I-10 Freeway at La Cienega-Venice Under-crossing and was designed and constructed between 1962 and 1965. The structural configuration is shown in Figure 4.

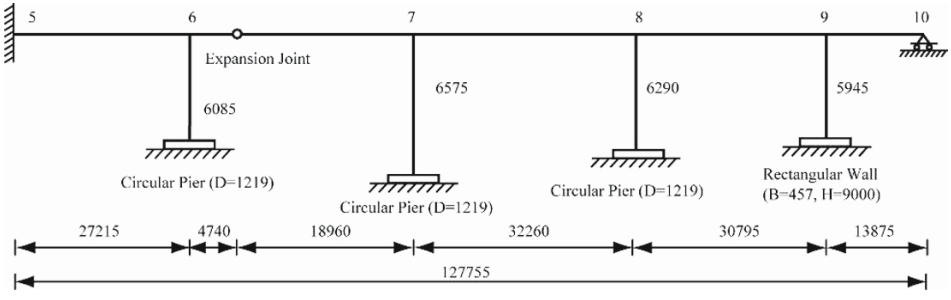

Figure 4. Layout of Collector-Distributor 36 of Santa Monica Freeway

After the Northridge earthquake, there was no visible damage on either the ramp deck or the abutment. However, the piers experienced varying levels of damage. In particular, pier 6 experienced spectacular failure. As shown in Figure 5, shear failure occurred in the lower half of the pier. The concrete cover completely spilled over the height and the concrete core disintegrated. Moreover, all the reinforcement bars buckled symmetrically and the transverse hoops opened, leaving the pier with large permanent axial deformation. There is evidence that the collapse of this pier is partly attributed to the instantaneous reduction of shear strength caused by vertical ground motion and the resulting fluctuation of the pier axial load (Broderick and Elnashai, 1995; Papazoglou and Elnashai, 1996).

Characteristics of the vertical component of ground motion has much higher frequency content than the horizontal component, which often coincide with the vertical period of RC members, thus causing large response values, especially with regard to forces. Elnashai et al. (2005) indicated that the horizontal and

vertical periods of vibration increased significantly when the vertical ground motion was considered, and the variation of axial force and contribution of vertical ground motion to the axial force increase as the vertical-to-horizontal (V/H) peak ground acceleration ratio increases. Simulation results also showed that arrival time interval between horizontal and vertical ground motion have no noticeable effect on the axial force (Elnashai et al. 2005).

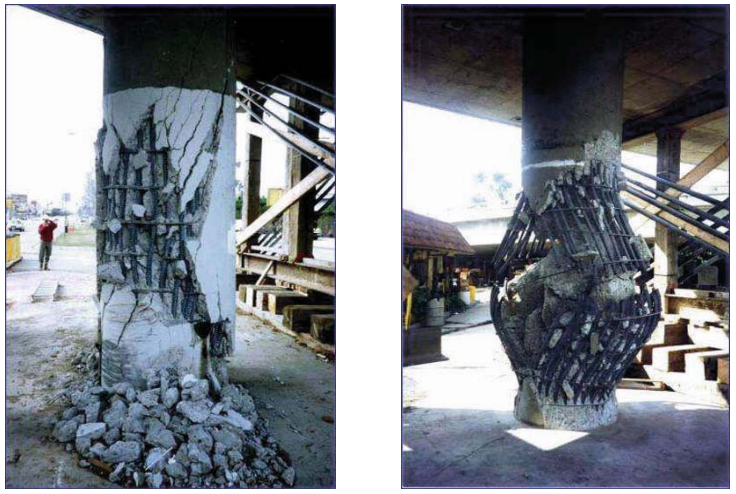

Figure 5. Shear failure caused by fluctuation of axial load

As changes in the balance between supply and demand in axial, moment and shear are difficult to predict by simple models, the best way to investigate the vertical ground motion effect is by experimental testing. However, laboratories are restricted by scale and capacity, especially when dealing with problems of even medium span bridges. To overcome the above difficulties in experiment, advanced distributed testing and hybrid testing-analysis methods employing pseudo-dynamic techniques and sub-structuring can be employed. This method allows important effects such as the influence of axial force variation on the shear deformation and failure of RC members, especially bridge piers, to be investigated.

3.1. SETUP FOR LARGE SCALE SIMULATION AND COMPONENTS RESULTS

To investigate the effect of vertical ground motion and soil-structure-interaction on earthquake response of bridges, Multi-Site Soil-Structure Foundation Interaction Test (MISST) will be conducted by using the NEES equipment sites at UIUC, Lehigh University and Rensselaer Polytechnic Institute (RPI). The MISST simulation is intended to provide a framework for testing complex bridge systems including their underlying soil and varying axial force.

In order to utilize these NEES experimental facilities and for simplification, the bridge is assumed to have three piers, as shown in Figure 6. Masses are placed on the deck since the hybrid test will be conducted for the piers under static conditions while the dynamic response will be obtained from an analytical model of the deck. The initial load corresponding to the deck self-weight is applied to the top of the piers as a static load.

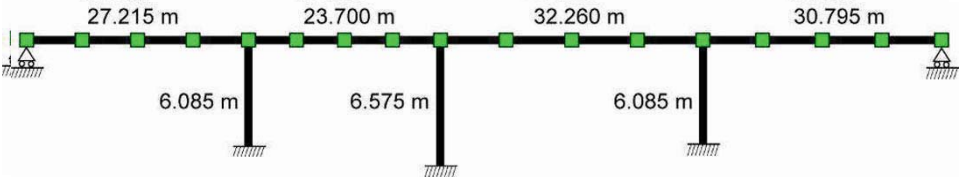

Figure 6. Layout of model structure

To accommodate the load limitations at the experimental facilities, half scaled piers were designed for use at both UIUC and Lehigh equipment sites. As shown in Figure 7, the overall structure is subdivided into 5 static modules. The dynamic characteristics of these components are accounted for in UI-SIMCOR. Two components are analytical models while the remaining three are experimental. The test components are:

- Module 1: Four decks and second pier including soil 2 – NCSA
- Module 2: First pier – UIUC
- Module 3: Third pier – Lehigh
- Module 4: Soil 1 – RPI
- Module 5: Soil 3 – NCSA

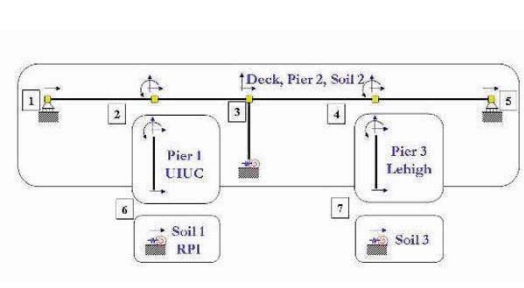

a. Substructure

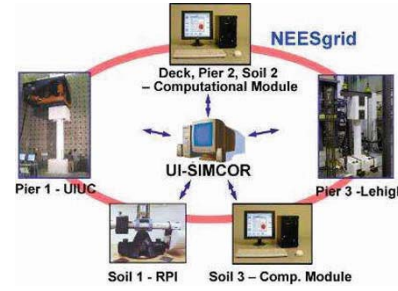

b. Distributed hybrid simulation test

Figure 7. Substructure configuration of MISST experiment

Due to the complexity of the system and the size and capacity requirements for testing, only component tests have been undertaken to date. Figure 8 shows

the results of the component test that was conducted at the MUST-SIM facility. The pier behaved as predicted and failure observed is similar to that seen in the Santa Monica Bridge shown in Figure 5. From Figure 8, one can see that significant failure due to shear capacity reduction was observed at 507 kN with a corresponding displacement of 51.3 mm. This result was very close to the calculated shear capacity of 533.78 kN by using the shear equation suggested by Priestly et al. (1994). An analytical model has also been created in Zeus-NL (Elnashai et al., 2002) using shear springs based on the Modified Compression Field Theory. Its comparison with experimental results is presented in Figure 8.

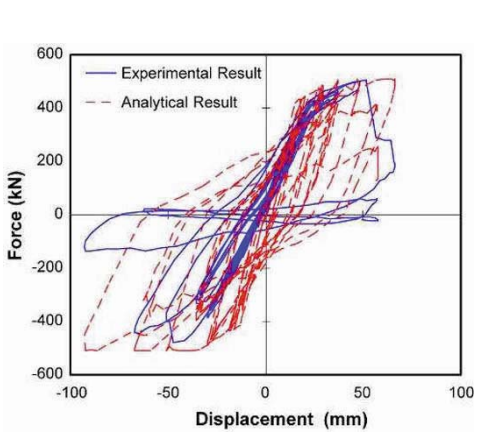

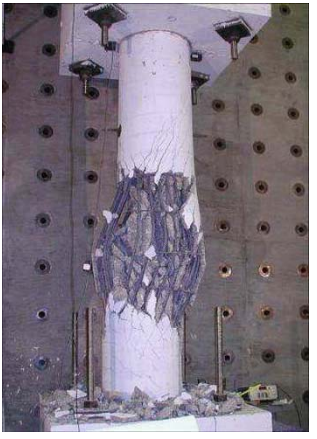

a. Comparison with analytical result b. Failure in the laboratory

Figure 8. Preliminary pier test result

3.2. SETUP FOR SMALL SCALE TESTS

Additional sub-structured tests will be performed utilizing the $1/5^{th}$ scale MUST-SIM laboratory. The small scale testing will serve to determine the specific test parameters for the large scale and to verify the capabilities of the small scale facility. The structure will be subdivided as above and piers 1 and 3 will be experimentally tested at UIUC. The model piers will be $1/16^{th}$ and $1/20^{th}$ scaled representations of the prototype. As exact similitude cannot be fulfilled with the prototype structure due to difficulties in obtaining suitable reinforcing steel, the small scale piers were designed to have similar axial-moment capacity when compared to the prototype. The relaxation of similitude requirements was deemed acceptable for the scope of the current project, where the investigation focuses on the difference in behavior between testing with and without vertical motion effects. Shear strength of the model piers will be controlled by stirrup

spacing. Although several configurations will be tested, a representative 1/10th scaled section is shown in Figure 9 along with the small scale testing setup.

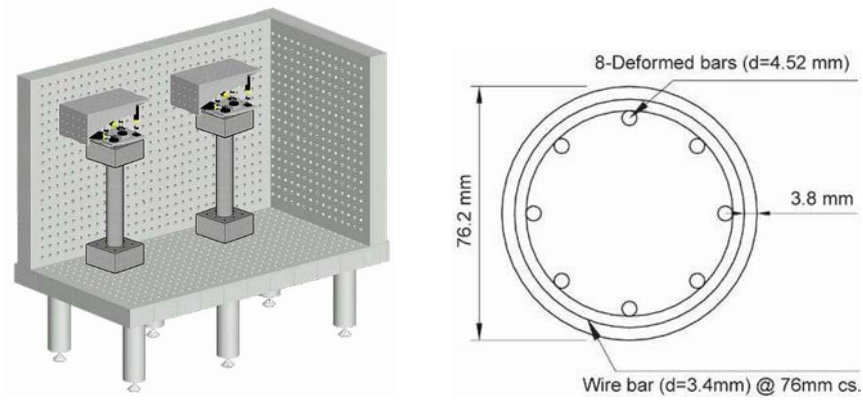

Figure 9. Experimental setup and section properties

Wire commonly used in welded mesh reinforcement will be utilized for reinforcement in the model piers. Sizes D2.5 and W1.4 will be used for longitudinal and transverse reinforcement respectively. A micro-concrete mix will used to model the prototype concrete. Work is in progress to create a micro-concrete mix that can represent the compressive stress-strain relationship and tensile strength of the prototype concrete.

4. Semi-Rigid Steel Frame

The second application investigates the response of steel moment resisting frames with semi-rigid connections. Objectives of this study are: (a) to compare the behavior of semi-rigid frames to that of rigid frames under realistic earthquake loads, (b) to experimentally evaluate the influence of connection behavior on the overall frame performance, and (c) to develop and validate numerical models for semi-rigid connections that would allow accurate predictions of frame response.

Traditionally steel moment resisting frames with fully welded connections have been considered as one of the most ductile and effective systems to resist seismic loads providing the necessary rigidity for lateral stability and significant energy dissipation. During the Northridge earthquake of 1994, several steel building suffered severe damage at the welded beam-to-column connections. These connections designed to behave in a ductile manner showed brittle fractures even in areas that experienced moderate seismic forces. This deficiency of welded connections was ratified one year later by the 1995 Kobe earthquake. Bolted connections provide an attractive alternative to the use of

welded connections, thus avoiding the use of welds which are prone to crack initiation. Additional advantages of semi-rigid connections compared to welded connections are its simplicity of fabrication and field installation.

4.1. BOLTED SEMI-RIGID CONNECTIONS

Bolted beam-to-column connections use bolts and other elements such as angles, plates, or T-stubs to transfer the forces from beam to column. Semi-rigid connections allow some relative rotation between beam and column, therefore its rotational stiffness is an important parameter. Common types of semi-rigid connections include top and seat angle connection, end plate connection, and T-stub connection. Connections can also be classified based on strength. Full strength connections are capable of transferring the full plastic moment from beam to column, while partial strength connections transfer only a fraction of beam plastic moment to column. Semi-rigid connections designed with partial strength can be conceived as the weak link and energy dissipating element under the capacity design philosophy, implying that the column strength does no need to exceed the beam capacity, resulting in more economical structures.

Although studies have shown the feasibility of using semi-rigid frames to resist seismic forces (Nader and Asteneh, 1992; Elnashai and Elghazouli, 1994; Elnashai et al., 1998), this type of systems has not been used extensively on earthquake resistant design mainly due to its relative large flexibility, which would yield larger deformations when compared with fully-rigid frames. However, because of their longer period, semi-rigid frames attract lower inertial loads than their rigid counterparts, which may offset the effect of the increased flexibility, hence resulting in a better solution with maybe even lower displacements (Elnashai and Elghazouli, 1994; Elnashai et al., 1998). Therefore, in order to investigate the behavior of structures with semi-rigid connections, it is essential to analyze the response of the whole moment resisting frame subjected to the earthquake, as opposed to applying quasi-statically a predefined displacement time history to the connection. The technique selected for testing the connections in this study is the pseudo dynamic method, which allows experimentally testing the connections while simultaneously considering the effect of the system behavior under realistic seismic loads.

4.2. EXPERIMENTAL PROGRAM AND TEST SET-UP

The structure considered in this investigation is a two-bay three-story steel moment resisting frame with bay width 30 ft and story height 13 ft, as shown in Figure 10(a). The frame structure will be tested at the MUST-SIM facility using

the pseudo dynamic method with the sub-structuring technique (Nakashima et al., 1990; Shing et al., 1996). The components to be tested experimentally were selected as having the largest demands from a nonlinear static pushover analysis of the frame. These are the first-story-exterior connection, and the lower part of the interior column, as shown in Figure 10(b). The rest of the structure, illustrated in Figure 10(c), is modeled computationally using ZEUS-NL (Elnashai et al., 2002). UI-SIMCOR is used for the pseudo dynamic sub-structured simulation.

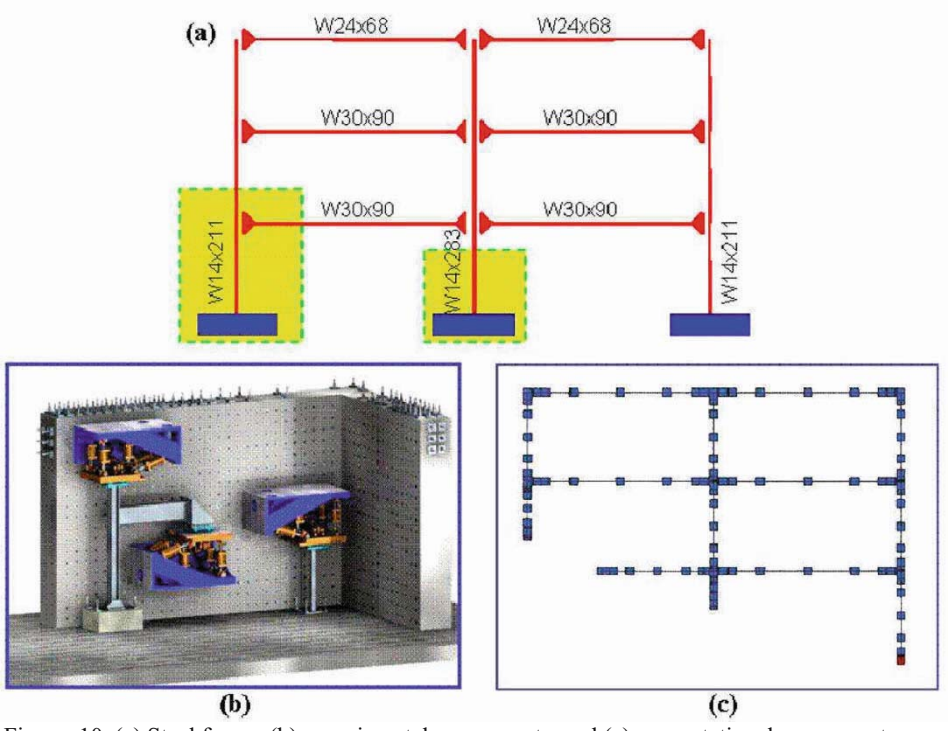

Figure 10. (a) Steel frame, (b) experimental components, and (c) computational component

The experimental program includes the pseudo dynamic testing of the steel frame for three different beam-to-column connection types. The frame will be tested with (i) fully rigid welded connections (for comparison purposes), (ii) end-plate semi-rigid connection with 50% partial strength, and (iii) end-plate semi-rigid connection with 70% partial strength.

4.3. SMALL SCALE MODELS

Because the sub-structuring technique is used for the evaluation of the frame, any of the different components (joint subassembly, interior column, or

remaining frame) can be substituted by computational models or by experimental specimens, either full or reduced scale, while still performing the simulation on the entire prototype structure. Two types of scaled models of the experimental components will be tested using the $1/5^{th}$ scale facility. The first model, intended to remain elastic, was constructed using aluminum standard I-shapes. This model was developed only for the welded rigid connection. The length scale factor is 5.25 and the modulus of elasticity scale factor is 2.9. Since this model is designed to remain elastic, the length scale factor was selected based on the section modulus of inertia, and dimensions of the specimen were adjusted accordingly. The scaled model is shown on Figure 11.

The second type of model, capable of yielding, is designed for the rigid connection and also for the two semi-rigid end-plate connections. The design of these models has the complexity of matching elastic (stiffness) parameters as well as strength, while keeping the forces generated below the limits of the $1/5^{th}$ scale LBCBs. A length scale factor of 6.0 was selected for these models. Because the cost and time required testing the scaled models is relative small compared to their full scale counterparts, scaled models will prove to be valuable in testing control algorithms, pseudo dynamic methods, semi-rigid connection modeling, and allowing analysis of a broader range of semi-rigid connections.

Figure 11. Scaled model

4.4. CONNECTION MODELING

An accurate computational model of the semi-rigid connections is extremely important. It is required in order to conduct analytical studies before testing. During the sub-structured pseudo dynamic test, the computational model is used to obtain the response of the portion of the frame that it is not tested experimentally, and after the test the numerical model is updated and used to

conduct parametric studies. Modeling of semi-rigid connections is complex because of its nonlinear behavior. Component-based models (Madas and Elnashai, 1992; Swanson and Leon, 2000; Faella et al., 2000) allow modeling the connection using several linear or nonlinear spring elements to represent the different components. This can easily be implemented on nonlinear finite element frame analysis software. This model can also be used to derive multilinear moment-rotation curves which can be implemented using a single rotational-spring element at the connection. For an extended end-plate connection, the stiffness and strength of the connecting elements can be determined using equivalent T-stubs as proposed by Yee and Melchers (1986) and more recently applied by Faella (2000). Each equivalent T-stub has four components that contribute significantly; these include bending in the column flange, tension in the column web, bending in the end plate, and tension in the bolts. These models are implemented in ZEUS-NL finite element analysis program. Detailed three dimensional finite element models are also developed to verify the accuracy of the simpler models. The initial stiffness of the semi-rigid connections will be updated prior testing by conducting a pre-test in the linear range. This pre-test is also required to get the initial stiffness for the α-Operator Splitting method (Nakashima et al., 1990) used for numerical integration during the pseudo dynamic simulation.

Distributed pseudo dynamic computational only simulations were conducted using UI-SIMCOR replacing the experimental components with the following numerical finite element models implemented in ZEUS-NL: (a) beam-column-joint subassembly, (b) interior column, and (c) remaining portion of the frame, as shown on Figure 12.

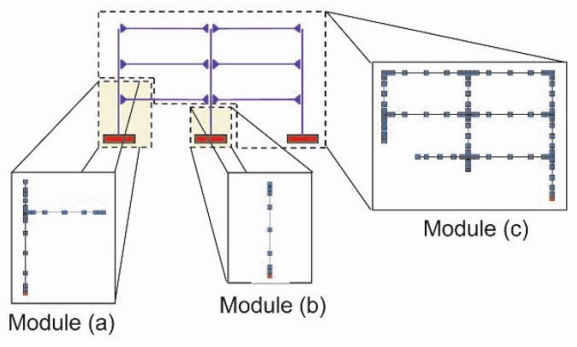

Figure 12. Distributed computational simulation

These simulations allow checking the computational models, the communication, and more importantly that the limits of the actuators on the LBCBs are not exceeded. Figure 13 shows the response of the frame with rigid connections to the Yarimca record from the Kocaeli (Turkey) 1999 earthquake.

Figure 13 (left) corresponds to the elastic scaled model and the full scale structure subjected to 10% of the record and Figure 13 (right) shows the response to 100% of the record of the inelastic scaled model compared to the full scale model.

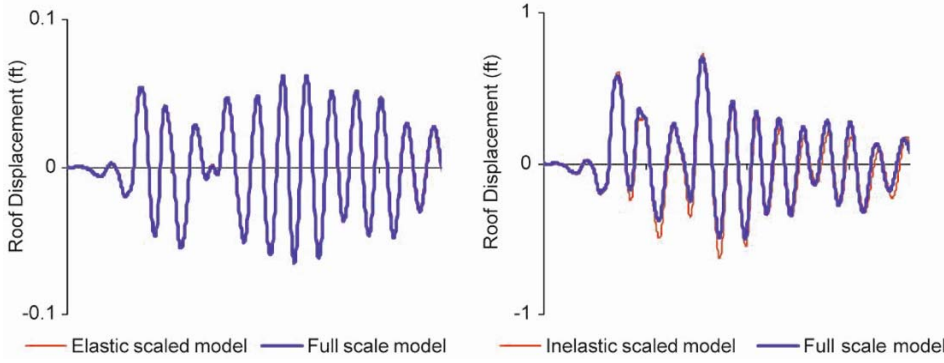

Figure 13. Results from distributed computational simulation

The response from the elastic scaled model is identical to the full scale version. The response of the inelastic scaled model is not as good as the scaled elastic counterpart, but it is considered acceptable.

5. Conclusions and Future Plans

The NESS MUST-SIM facility provides a state-of-the-art environment for conducting distributed pseudo-dynamic testing of full-scale structural and interacting soil-structure systems. Two investigations that are being carried out at this facility are presented.

Analytical results and field observations indicate that the effect of the vertical ground motion is particularly important in concrete structures. A complex bridge system has been selected for tests taking into account the effect of vertical input motion and soil-structure interaction.

The important role of beam-to-column connections in the seismic stability of steel frames was confirmed by several post-earthquake investigations. The use of semi-rigid connections provides a very attractive solution in terms of performance as well as fabrication and installation costs. A three-story two-bay frame is selected for this study. Because connection characteristics greatly influence the frame response, testing of this system requires including the entire frame in order to obtain realistic assessments of its performance.

The physical size of the above two systems makes full scale testing of the complete structures very difficult if not impossible. Hybrid distributed simulation and the advanced features of the MUST-SIM facility provide the

best way to test the critical components while considering all features of interaction within the complex system.

ACKNOWLEDGEMENT

The MISST experiment is funded by National Science Foundation under grant reference 0406812. Many individuals at UIUC and elsewhere have contributed significantly to the experimental setup and analytical framework including Oh-Sung Kwon, Tom Nagle, Narutoshi Nakata, John Barry, Ryan Hopeman, Curtis Holub, Johanna Gonzales, Joseph Shield, Nicholas Berdette and Nathan Rende. The Mid-America Earthquake Center provided support for the first and second authors and provided the analysis platform for the simulations. The MAE Center is a National Science Foundation Engineering Research Center (ERC), funded through contract reference EEC-9701785. Finally, the research teams at Lehigh and RPI are gratefully acknowledged.

References

Broderick, B.M., and Elnashai, A.S., 1995, Analysis of the failure of Interstate 10 freeway ramp during the Northridge earthquake of 17 January 1994, *Earthquake Engineering and Structural Dynamics*, 24:189–208.

Elnashai, A.S., and Elghazouli, A.Y., 1994, Seismic Behavior of Semi-rigid Steel Frames, *J. Construct. Steel Research*, 29:149–174.

Elnashai, A.S., Elghazouli, A.Y., and Denesh-Ashtiani, F.A., 1998, Response of semi-rigid steel frames to cyclic and earthquake loads, *Journal of Structural Engineering*, **124**(8):857–867.

Elnashai, A.S., Papanikolaou, V., and Lee, D., 2002, Zeus NL – A system for inelastic analysis of structures, Mid-America Earthquake Center, University of Illinois at Urbana-Champaign, Program Release Sept. 2002.

Elnashai A.S., Spencer Jr., B.F., Kuchma, D, Ghaboussi, J., Hashash, Y., and Gan, Q., 2004, Multi-axial full-scale sub-structured testing and simulation (MUST-SIM) facility at the University of Illinois at Urbana-Champaign, *Proceedings of 13th World Conference on Earthquake Engineering*, Vancouver, Canada, Paper No. 1756.

Elnashai, A.S. et al., 2005, Analysis and distributed hybrid simulation of shear-sensitive RC bridges subjected to horizontal and vertical earthquake ground motion, *Proceedings of 36th US-Japan Workshop on Wind and Earthquake*.

Faella, C., Piluso, V., and Rizzano, G., 2000, *Structural steel semi-rigid connections: Theory, design, and software*, CRC Press.

Madas, P.J., and Elnashai, A.S., 1992, A component-based model for the response of beam-column connections. *Proceedings of 10th World Conference of Earthquake Engineering*, Madrid, Spain.

Nader, M.N., and Astaneh-Asl, A., 1992, Seismic behavior and design of semi-rigid frames, *Rep. No. UCB/EERC-92/06*, Environmental Engineering Research Council, University of California, Berkeley, California.

Nakashima, M., Kaminosono, T., Ishida, M., and Ando, K., 1990, Integration techniques for substructure online test, *Proc. 4th U.S. National Conf. on Earthquake Engineering*, Palm Springs, CA, II, 515–524.

Kwon, O.S., Naktata, N., Elnashai, A.S., and Spencer, Jr., B.F., 2005, A framework for multi-site distributed simulation and application to complex structural systems, *Journal of Earthquake Engineering*, in press.

Papazoglou, A.J., and Elnashai, A.S., 1996, Analytical and field evidence of the damaging effect of vertical earthquake ground motion, *Earthquake Engineering and Structural Dynamics*, 25:1109–1137.

Priestley, M.J.N., Verma, R., and Xiao, Y., 1994, Seismic shear strength of reinforced concrete columns, *Journal of Structural Engineering*, **120**(8):2310–2329.

Shing, P.B., Nakashima, M., and Bursi, O.S., 1996, Application of pseudo dynamic test method to structural research, *Earthquake Spectra*, **12**(1):29–56.

Swanson, J.A., and Leon, R.T., 2000, Bolted steel connections: Test on T-stub components. *Journal of Structural Engineering*, **126**(1):50–56.

Yee, Y.L., and Melchers, R.E., 1986, Moment-rotation curves for bolted connections, *Journal of Structural Engineering*, Vol. 112, January.

RECENT EXPERIMENTAL EVIDENCE ON THE SEISMIC PERFORMANCE OF REHABILITATION TECHNIQUES IN MEXICO

SERGIO M. ALCOCER*
Institute of Engineering, National University of Mexico, UNAM
LEONARDO FLORES
National Center for Disaster Prevention, CENAPRED, Mexico
ROBERTO DURAN
Institute of Engineering, National University of Mexico, UNAM

Abstract. Observed performance in the laboratory of masonry and structural concrete walls and columns rehabilitated by jacketing is reported. Improved behavior is discussed in terms of strength, stiffness, and energy dissipation and deformation capacity. In general, wall and column jacketing, when properly detailed, provide a reliable rehabilitation technique suitable for the rehabilitation of highly vulnerably structures.

Keywords: walls; columns; jacketing; shear strength; mortar; concrete; masonry; fasteners; steel jacketing; steel angles; steel straps; strengthening; repair; rehabilitation

1. Introduction

Mexico, as well as other countries, has a large inventory of buildings designed and constructed according to old building codes. The performance of these structures under earthquakes has been typically characterized by moderate to severe damage, and even by total or partial collapse. Masonry and structural concrete are the most common materials used in these buildings; masonry accounts for more than 50% of the total construction industry in Mexico. In order to reduce their seismic vulnerability, it is necessary to rehabilitate

* Sergio M. Alcocer, Director, Institute of Engineering, UNAM, Edificio Fernando Hiriart, Ciudad Universitaria, México DF, 04510, México; e-mail: salcocerm@iingen.unam.mx.

S.T. Wasti and G. Ozcebe (eds.), Advances in Earthquake Engineering for Urban Risk Reduction, 261–274.

structural elements so that a better response, in terms of strength, stiffness, deformation capacity and energy dissipation capacity, is attained.

To better understand resistance mechanisms, as well as to assess and develop guidelines for seismic rehabilitation, series of experimental programs on masonry and concrete structures have been carried out. The effectiveness of different rehabilitation schemes and, when needed, of distinct devices for connecting masonry walls and concrete frames to reinforced concrete or reinforced mortar walls has been assessed. Full-scale specimens, tested under cyclic loads, have been studied in detail.

In this paper, observed performance of wall and columns specimens rehabilitated by jacketing is discussed in general terms. A complete discussion of the experimental data can be found elsewhere (Alcocer, 1993; Alcocer and Jirsa, 1993; Alcocer et al., 1996; Alcocer and Durán-Hernandez, 2002; Alarcón and Alcocer, 1999; Flores et al., 1999).

2. Wall Jacketing

Wall jacketing in Mexico is typically made of a cement mortar or concrete cover reinforced with a steel welded wire mesh (SWWM) or a "chicken wire" mesh that is attached to the existing walls. For this new addition to work with the existing structural walls, it is essential that earthquake-induced shear forces be transferred to the jacket, and from there to the foundation, by means of fasteners, shear keys or a combination thereof.

Wall jacketing is particularly suitable when low tensile strength materials are used, and when walls are poorly interconnected. This is generally the case of informally built housing, where technical participation of engineers or architects is lacking, and which use local, typically weak, materials.

2.1. WALL JACKETING IN ADOBE CONSTRUCTION

Adobe construction is typically found in small villages, mainly in the countryside. The structural system consists of one-story perimeter load-bearing walls, 3-m high and 300-to-600-mm thick. Typical roofs consist of timber trusses that support shingles and clay tiles. Earthquake damage is frequently exacerbated by aging and lack of maintenance.

Previous studies on rehabilitation schemes of Mexican adobe houses (Hernandez 1979) have indicated that construction of a perimeter tensile chord on top of the walls, or wall jacketing with a mortar cover reinforced with a 1.9 mm diameter wire mesh were viable options for reducing the likelihood of collapse. To further evaluate the efficiency of connectors and mesh size on wall jacketing, three full-scale adobe load-bearing walls were built and tested.

Control specimen, A1, was an unreinforced adobe wall. After it was tested, A1 was repaired with a "chicken wire" mesh covered with mortar, and was retested (specimen A1R). Specimens A2 and A3, of similar geometry to A1, were strengthened without prior damage by means of a mortar jacket. In A2, jacket reinforcement consisted of SWWM made of gage-10 wire (3.43-mm diameter) with nominal yield stress of $f_y = 490$ MPa and equally spaced at 150 mm in orthogonal directions. In wall A3, a "chicken wire" mesh was used. "Chicken wire" mesh is made of gage-20 wire spaced at 50 mm, $f_y = 640$ MPa. The cover mortar had a 1½:4½ volume ratio of Portland cement and sand. Mortar jackets were, on the average, 30-mm thick and were hand-placed on both wall faces.

Strengthening guidelines have recommended fastening the SWWM on both wall faces by means of steel cross ties placed through the wall thickness in holes perforated with hand drills (UNDP 1983). Such holes are thereafter filled with some epoxy or cement-based mortars. This recommendation is suitable for urban adobe construction, where drill hammers and trained labor are readily available. Due to the limited applicability of this fastening technology in Mexican rural houses, a simple and inexpensive solution, yet technically sound, was searched for. In all cases, commercially available galvanized steel staples were used for fastening the steel meshes. Staples were made of gage-9 wire (3.76-mm diameter), with $f_y = 390$ MPa, 38-mm long and were installed at 300-mm spacing (10 staples/m²). Steel staples were then found to be easy to install (just by hammering into the adobe wall) and very inexpensive (0.16 USD a piece).

The measured axial compressive strength of adobe blocks was $f_p^* = 2.65$ MPa; the compressive strength of adobe prisms was $f_m^* = 0.62$ MPa; and the diagonal compressive strength of adobe walls obtained was $v_m^* = 0.03$ MPa. The dimensions of the specimens were 2.5×2.5×0.35 m. Walls were constructed according to the local practice in rural Mexico. The horizontal reinforcement ratios, p_h, of specimens A1R, A2 and A3, based on adobe wall area, were 0.007%, 0.035% and 0.007%, respectively.

On one face of all rehabilitated walls, the SWWM was fastened directly in contact with the adobe wall and then covered with mortar. On the other face, the SWWM was fastened after a first 10-mm mortar cover was placed on the wall; the mesh was then finally covered with mortar until it reached the final 30-mm thickness. Specimens were tested under a constant vertical stress of 0.07 MPa.

Final crack patterns and hysteresis loops are shown in Figure 1. In A1, one inclined shear crack following the mortar joints controlled the behavior. Hysteresis loops were quite stable and with good energy dissipation capacity. Strength was reached at over 0.4% drift ratio, for a corresponding shear stress of 0.034 MPa. After repair, A1R was retested. Failure mode was changed to

sliding of the wall as a rigid body. This occurred at a shear stress of 0.05 MPa (based on adobe area) that in turn corresponded to a static friction modulus of 0.76. To fail the specimen, horizontal and vertical loads were then monotonically applied to simulate a large diagonal compression test. Strength was reached at a diagonal stress of 0.2 MPa (six times the original strength).

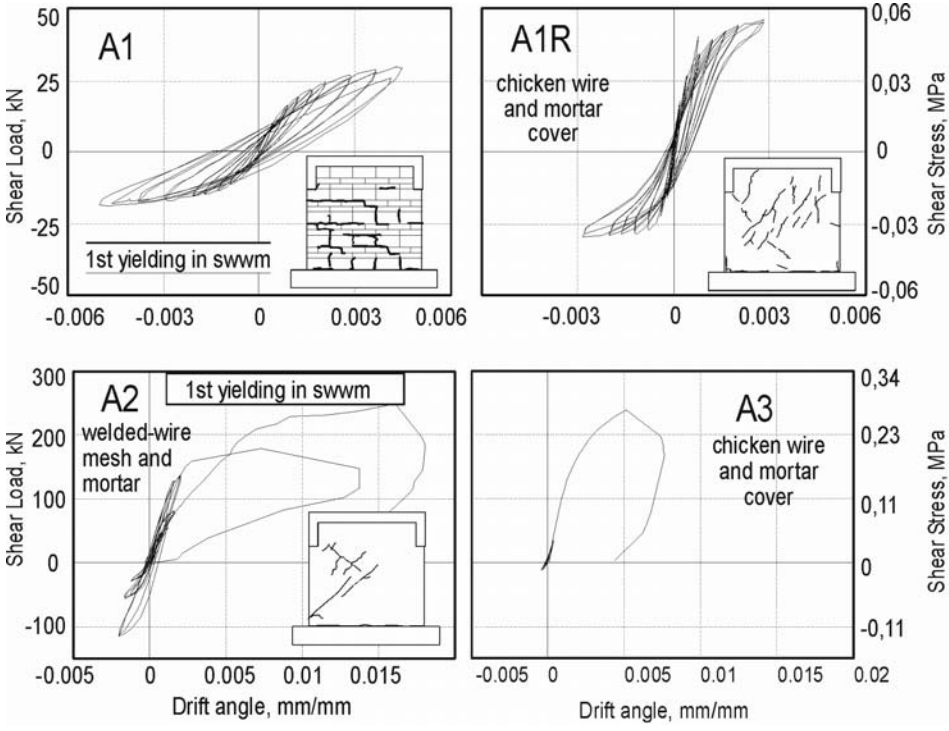

Figure 1. Crack patterns and hysteretic behavior of adobe walls

Similarly to A1R, specimens A2 and A3 were initially tested under cyclic loads. Prior to sliding of the walls, specimens were then tested monotonically through a diagonal compression load. Measured strengths were equivalent to diagonal stresses of 0.28 and 0.27 MPa, respectively (based on the adobe area only). Strengths attained corresponded to large cracks on the mortar and the yielding of the SWWM. A more uniform distribution of cracks was observed in wall faces where a first mortar cover was placed prior to fastening the SWWM. In both faces, staples remained anchored to the wall, even in locations close to the large diagonal cracks.

2.2. WALL JACKETING IN CONFINED MASONRY CONSTRUCTION

Confined masonry is the most popular construction system in urban and areas. In this system, load-bearing walls are intended to resist both vertical and in-plane lateral loads, and are confined through vertical and horizontal RC tie-columns and bond-beams, which, in turn, are for improving strength, deformation capacity and structural integrity. Although this system has performed excellently under very intense earthquakes, moderate-to-severe damage has been observed when confinement location and detailing are substandard. For such cases, wall jacketing is one rehabilitation technique suitable for improving its lateral strength, stiffness and toughness.

Wall jacketing has been studied on a one two-story, three-dimensional confined masonry structure and on four full-scale isolated confined masonry walls. Specimens were built with hand-made burnt clay bricks joined with a Portland cement mortar. Specimen dimensions, reinforcement details and mechanical properties of materials are presented in Figure 2. All specimens were designed to fail in shear.

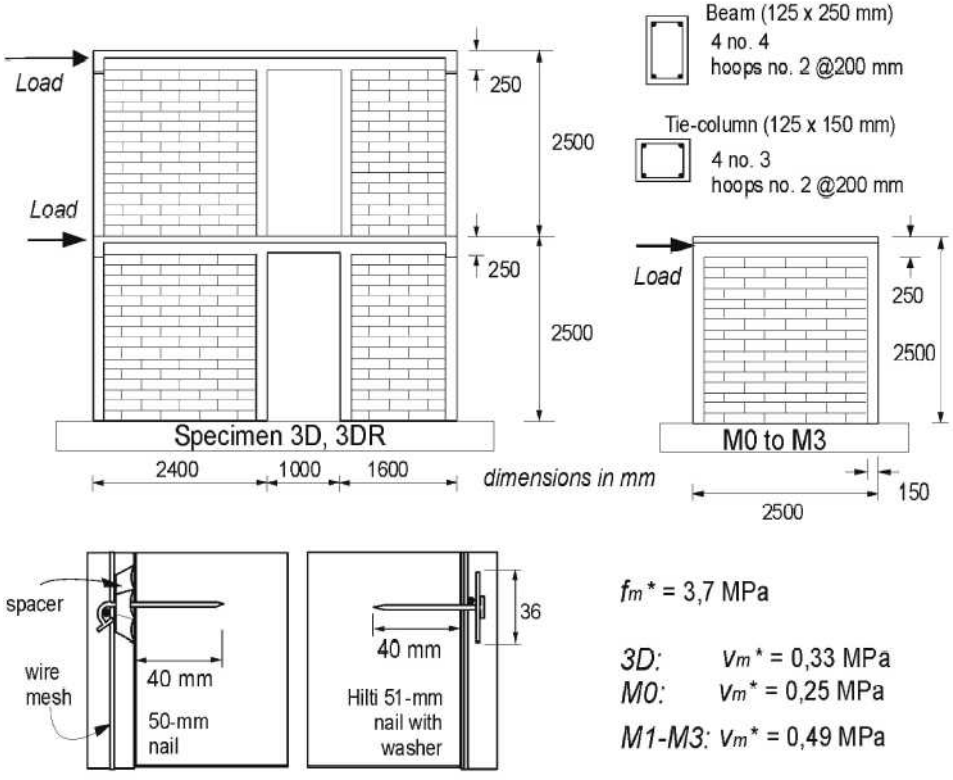

Figure 2. Characteristics of clay brick walls

Specimen 3D was firstly tested by applying lateral displacements controlled by drift angle. Consistent with actual damage patterns observed after earthquakes, distress was concentrated in the ground story walls. Therefore, only such walls were repaired. Crushed and spalled tie-column concrete was removed and replaced by concrete with similar mechanical characteristics. Largest masonry cracks were filled with mortar and brick debris. Finally, the exterior face of the walls was jacketed with a mortar and a SWWM. The specimen was retested using the same displacement history (Alcocer et al. 1996). Common steel nails for timber construction, 50-mm long and made of gage-10 wire were used to fasten the SWWM. Fasteners were placed by carefully hammering them into the wall at the grid intersections. The nail head was then bent around the wire intersection to secure the mesh in position. Fastener density was 9/m². The meshes were placed in the mid-thickness of the mortar cover, so that a 7-mm spacer was used between the wall and the mesh. This has been a typical fastening technology used in Mexican practice.

In the isolated wall series, M0 was the control specimen. M1 to M3 were undamaged confined masonry walls strengthened with wall jackets on both faces, in which the horizontal reinforcement ratios were 0,072, 0,147 and 0,211%, respectively. In M1 and M2, with meshes made of gages-10 (3.43 mm) and -6 (4.88 mm) wire respectively, same fasteners in 3DR were used. However, no spacers were provided, so that the mesh was placed against the masonry wall. The amount of fasteners was different in the two faces, namely 5 and 11/m². For M3, where a steel mesh with a 6.35 mm wire diameter was used, Hilti ZF-51 fasteners were installed. This 51-mm long nail made of gage-10 wire was used in combination with a 36-mm diameter metal washer also supplied by Hilti. Fasteners were powder driven at the intersection of vertical and horizontal mesh wires with the DXE72 tool. The washer was intended to clamp the vertical and horizontal wires at the intersection. Again, no spacers were used. During construction it became evident that this fastening technology was installed faster and is more reliable than the typical hand-driven nails. The speed of installation offset the higher cost of the Hilti-type fasteners as compared to the inexpensive nails.

Final crack patterns and hysteresis loops are shown in Figure 3. Jacketed specimens exhibited a very uniform distribution of cracks and increased strength as compared to those in the control specimens (3D and M0). At same drift levels, crack widths in jacketed specimens were smaller than those recorded in control structures. In 3DR, at drifts to 0.46%, it became apparent that nails had been pulled out. This was attributed to the increased shear flexibility of the nail-spacer system and the reduced anchorage length of the nail into the masonry, when compared to the same nail without spacer used in M1 and M2. M1 failed after fracture of SWWM horizontal wires that led to

shearing off the lower ends of the tie-columns. In M3, Hilti-type fasteners were found to be firmly anchored into the masonry after the test had been finished.

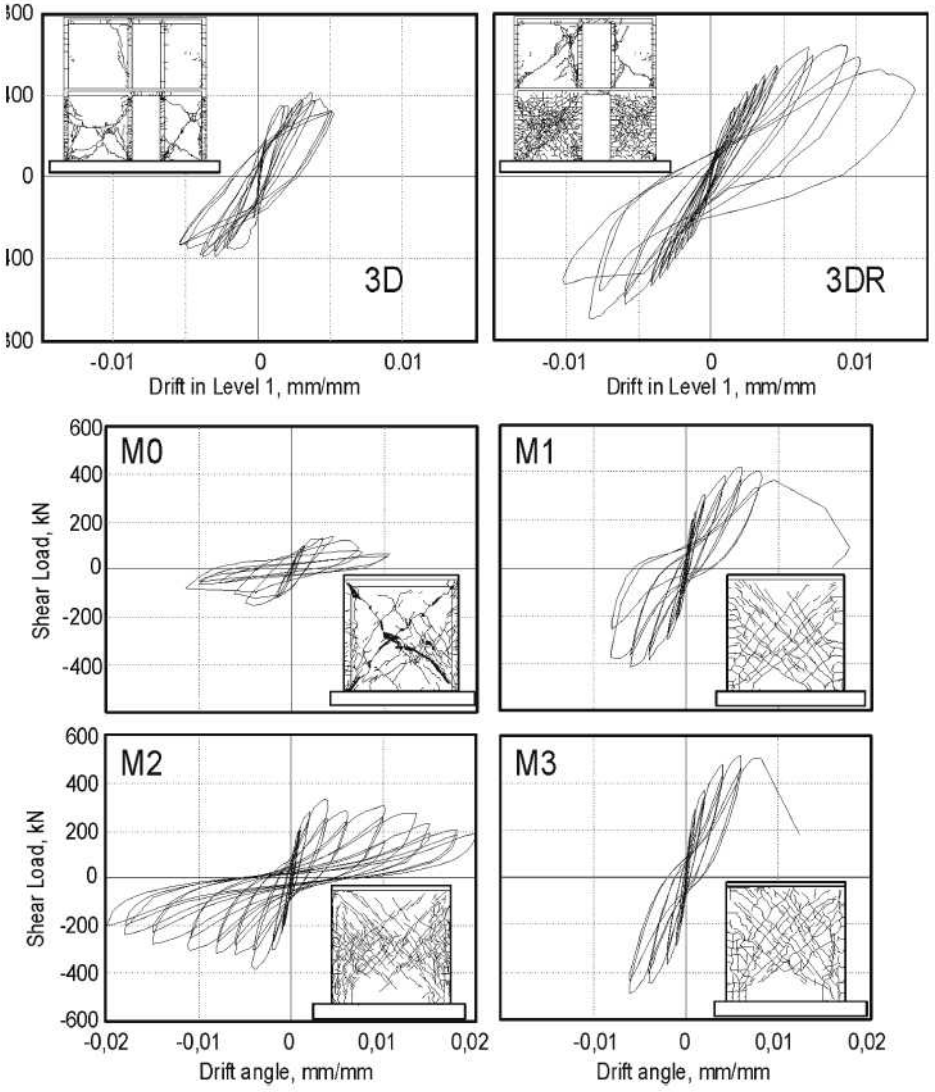

Figure 3. Final crack patterns and hysteresis curves of jacketed clay brick walls

2.3. WALL JACKETING OF CONCRETE MASONRY INFILLS

One of the techniques used to improve performance of reinforced concrete, RC, frames infilled with concrete masonry units, CMU, has been the addition of new RC walls attached to both the existing frame and the CMU infills. Such

walls had been typically added from the exterior side, on the perimeter of the building. That has been possible because infills and perimeter frames are flush. To achieve a positive shear transfer and monolithic behavior between the new and existing elements, dowel bars have been used; however, the detailing, number and distribution varied, depending upon the design office and the contractor. Some required epoxied dowels in both the masonry infill and the RC frame; others only in the frame. In some cases, dowels in the walls were just epoxied at the mortar joints, whereas in other instances the dowels passed through the walls and were welded to small 6.4-mm thick steel plates inside the building. This variety of solutions had, evidently, very different costs.

To assess the effectiveness of this upgrading scheme, as well as the performance of different fastening solutions, four specimens were built and tested (Figure 4). Structures represented 1:1.3 scaled models of a one bay of a prototype building. T0 was the control specimen. In the strengthened (undamaged) specimen TP, epoxied dowel bars were placed in the perimeter RC frame, whereas in TD, dowel bars were distributed both in the frame and in the infilled masonry wall. Preliminary studies on isolated small specimens indicated that dowels with welded steel plates on the back of the wall performed as well as epoxied dowel bars placed in the mortar joint and embedded 80 mm into the wall thickness (Flores et al., 1999). Moreover, the latter solution was evidently more cost-effective. A two-component commercial epoxy resin was used to install the dowel bars. In TH, Hilti ZF-72 powder driven fasteners with a 25-mm spacer were installed. The spacers, made of a steel square tube, were provided to locate the SWWM in the mid-thickness of the concrete jacket. In the design of fasteners of all structures tested, it was assumed that transfer of forces between the existing and new elements would be developed through shear friction.

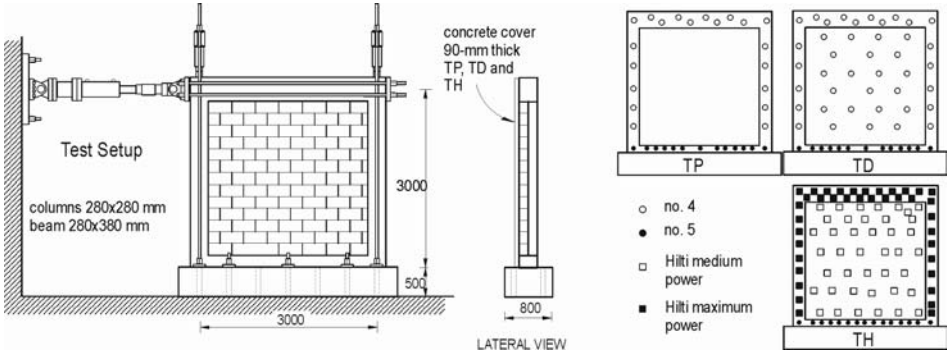

Figure 4. Characteristics of RC frames infilled with CMU

Final crack patterns and hysteresis loops are shown in Figure 5. Damage in T0 was controlled by shear-compression of the masonry infill. Specimens TP

and TD showed a very similar behavior in terms of their uniform crack distribution and hysteretic curves. Failure was triggered by shear—compression cracking and crushing of the infill. Analysis of strain gage data indicated that strains in the dowel bars on the masonry infill were negligible, thus suggesting that their participation in transferring forces was minimal. Indeed, shear transfer was accomplished through shear friction between the wall and the RC frame (where dowels were actually strained), and by means of bond between the CMU and the RC jacket (Flores et al., 1999). Fasteners in TH did not perform as intended, since at drifts to 0.4%, it was apparent that the anchorage was lost and that further shear transfer was impaired. Substandard performance was a combination of the excessive shear flexibility of the fastener due to the spacer, as well as of its reduced anchorage depth. During installation, part of the energy released by the powder charge was rebound due to the elastic deformation of the spacer, thus leaving the remainder energy to actually drive the fastener into the infill.

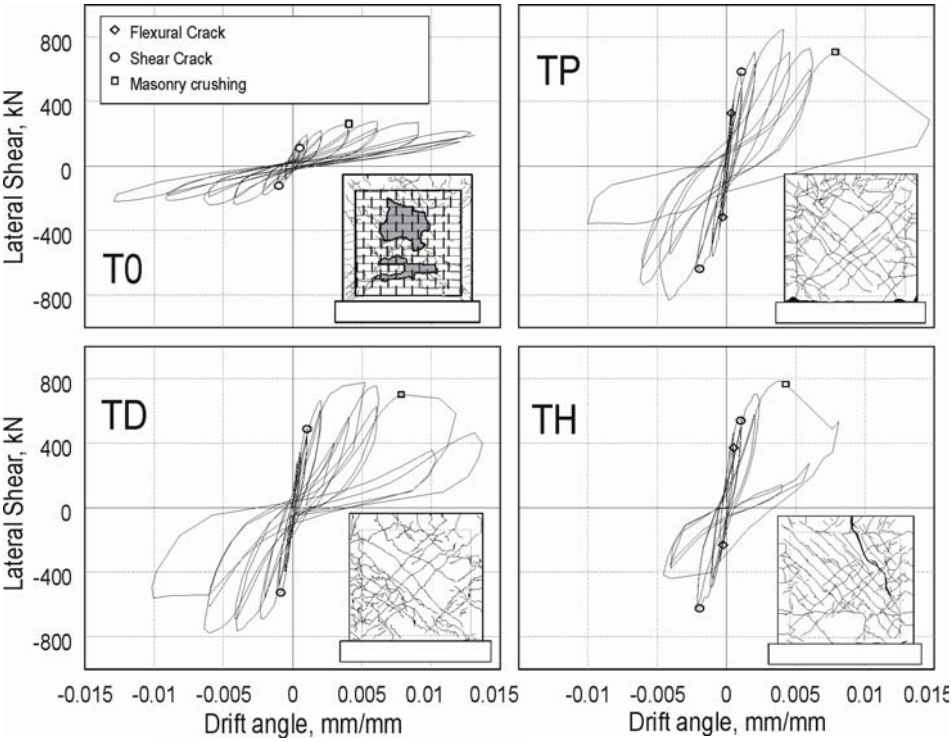

Figure 5. Final crack patterns and hysteresis curves of jacketed concrete masonry infills

3. Column Jacketing

3.1. CONCRETE JACKETING

Concrete jacketing of frame members has been one of the most prevalent rehabilitation schemes used in Mexico. Its advantage of maintaining the frame as the lateral-force resisting system is overcast by the need in some cases to increase lateral stiffness (typically through new walls or braces), and by the need to deploy a large work force. Suitability of concrete jacketing was assessed under a US-Mexico research program developed after 1985. Research results have been published extensively (Alcocer and Jirsa 1993; Alcocer, 1993).

3.2. STEEL JACKETING

Aimed at assessing the performance of concrete columns rehabilitated with steel jackets made of angles and straps, a series of four large-scale reinforced concrete columns was constructed (Alcocer and Duran-Hernandez, 2002). Specimens corresponded to a 0.8-scale model of columns of existing building BL that was rehabilitated after the 1985 Mexico City earthquakes, and which is under study. Two experimental variables were studied, i.e. detailing of the reinforcement, and the level of damage in the specimen before the test. The first column was tested to failure (test C-99); this column satisfied the detailing requirements of modern RC standards for seismic design, such as those in Chapter 21 of the ACI 318-99. This specimen will not be discussed in detail here. Second specimen (C-66) was intended to emulate a column at the ground story of BL; this column was also tested to failure. The longitudinal and transverse reinforcement of C-66 satisfied the requirements of the 1966 Mexico City Building Code (Departamento, 1966). The third specimen (C-66-R) was similar to C-66 and was first tested to a drift angle to 1% (test C-66*). Then the column was rehabilitated with steel jackets and was retested to failure (test C-66-R). It was considered that damage in this type of columns at 1% drift was similar to that observed in BL during the 1985 event, and was still repairable. Specimen C-66-S was similar to C-66 and was undamaged prior to jacketing to assess the effect of a damaged core on the response. All columns were tested under a constant axial compression load equivalent to $0.15\ f'_c\ A_g$, which was found to be the axial load level at the ground story in building BL.

Column dimensions and reinforcement details are shown in Figure 6. Jackets of C-66-R and C-66-S were the same as those provided in building BL. Horizontal steel straps were welded to corner angles through fillet welds. Similarly to the jacketed columns in BL, jacketed specimens had wider steel

plates welded onto the angles at the column ends. Concrete compressive strength at time of test was 27.9 MPa on the average. Specified yield stress of column reinforcement was 412 MPa; steel jackets were made with A36 steel. The gap left between the concrete column and the steel flat bars (straps) and end plates was filled with a high-strength grout.

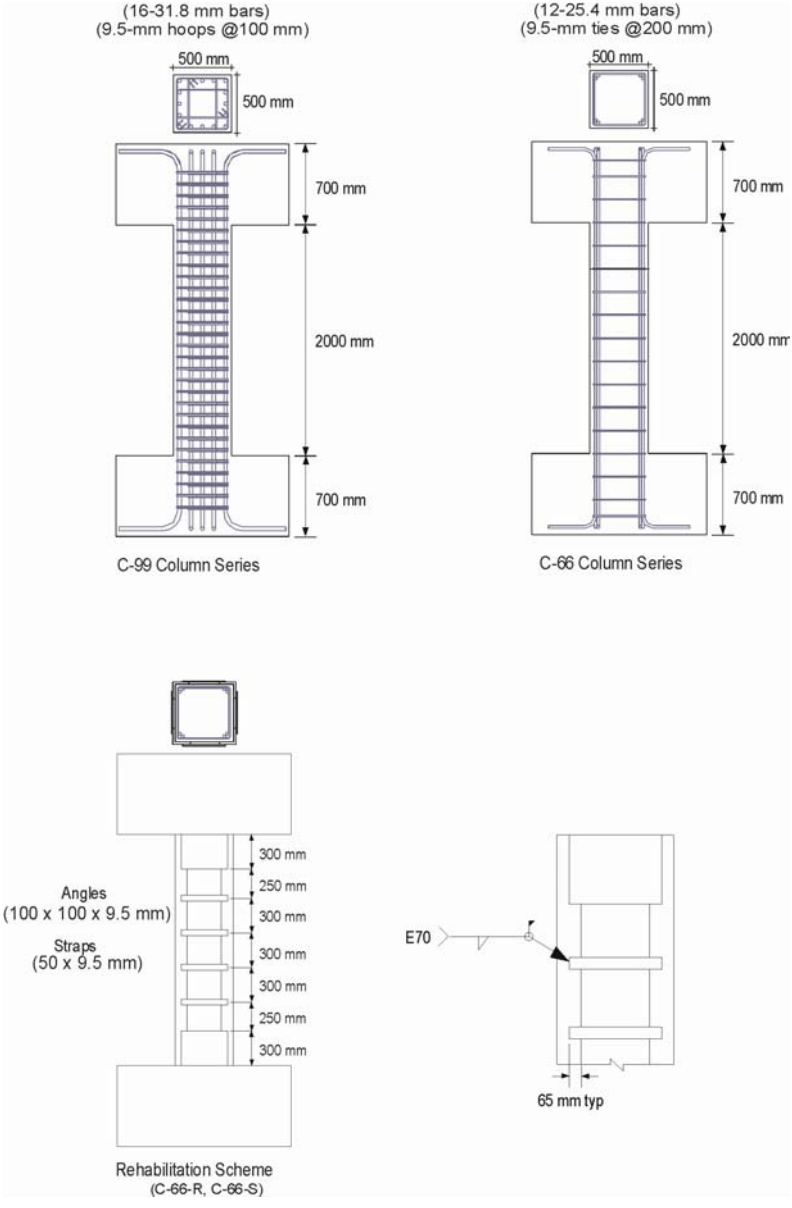

Figure 6. Column dimensions and reinforcement details

The EW lateral load versus interstory drift curves are presented in Figure 7. The ultimate story shears corresponding to column shear failure and column hinging (at the bottom and at both ends) are also shown in the figure. For specimens C-66-R and C-66-S, the contribution of the steel jacket to shear strength was added to the shear resistance provided by reinforced concrete. The shear contribution of the jacket was calculated assuming a plastic mechanism under lateral loads that consider flexural hinging at both ends of all flat bars along the height of the column, and from measured material properties and dimensions. The contribution of the jacket was simply added to the concrete and stirrup contributions.

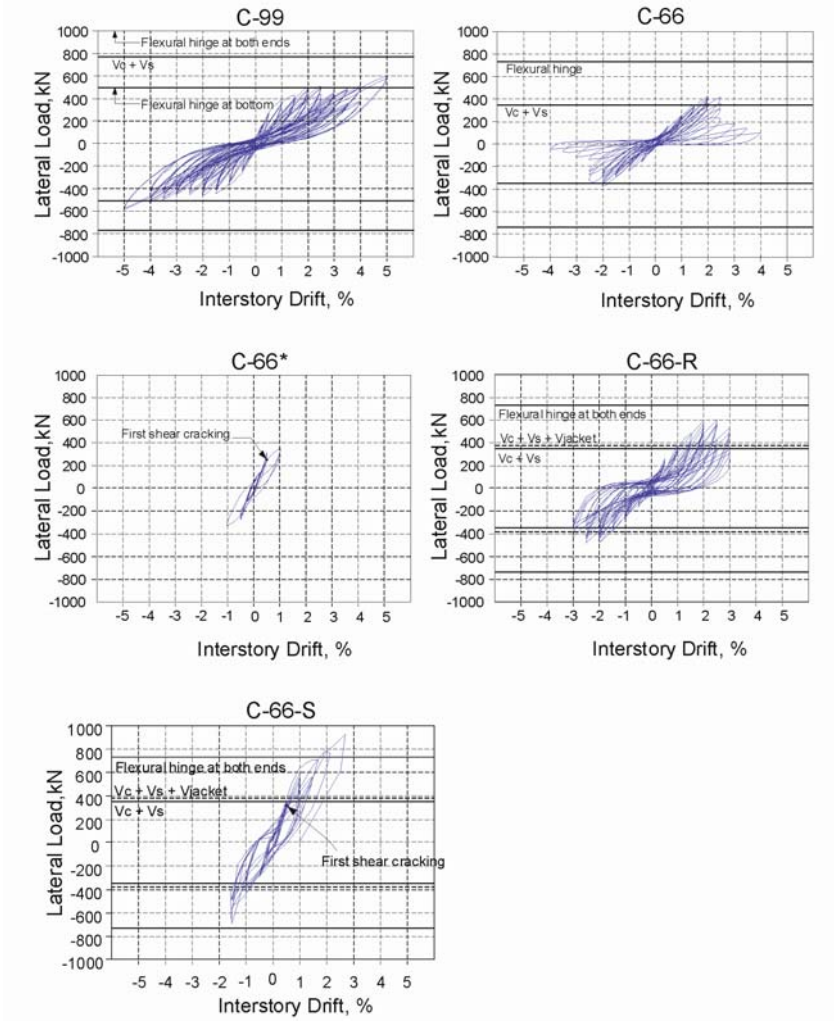

Figure 7. EW story shear - interstory drift hysteresis curves

For rehabilitated columns, loops at similar drifts, exhibited better energy dissipation capacity (wider hysteresis loops) than that of C-66. This is credited to the participation of the steel jacket. In terms of strength, both C-66-R and C-66-S exhibited a superior behavior as compared to C-66. The participation of the steel jacket to the load carrying capacity of the column is therefore evident. Test C-66-S had to be interrupted when the maximum actuator load capacity was reached (1000 kN, approximately).

The lateral stiffnesses at the first loading peak of all columns were comparable, thus suggesting that the contribution to lateral stiffness of the steel jacketing, both in a damaged and in an undamaged column, was minor and could be disregarded for design purposes.

Regarding specimens' crack patterns, C-66 and C-66* experienced a large number of fine inclined cracks with few horizontal cracks; failure of C-66 was characterized by a wide inclined crack. For C-66-R, new inclined cracks were formed suggesting the formation of inclined strut action of the concrete against the steel skeleton. Similarly to C-66-R, specimen C-66-S exhibited inclined cracking and spalling that indicates strut action. The average inclination of the struts, with respect to the vertical axis, is 35 degrees. It can be argued that the strut action is an indication of the development of a truss mechanism where the steel angles and straps are involved as truss chords and ties, respectively.

4. Conclusions and Recommendations

Based on the observations made during the tests and on the analysis of the instrumentation, in general, it can be concluded that wall and column jacketing, when properly detailed, are reliable rehabilitation techniques, suitable for improving structure strength, stiffness and toughness. For this improvement to be achieved, careful detailing and installation of fasteners should be exercised. Recommendations given below are applicable to systems with similar material and structural characteristics as those tested.

For adobe rehabilitation, wall jacketing reinforced with either SWWM or chicken-wire meshes is recommended. To achieve shear transfer, steel staples, 38-mm long, made of gage-9 wire and hammered into the adobe wall, proved to be a strong and stiff fastening system. Prior to the installation of the staples, it is recommended to place a 10-mm thick mortar cover on the adobe wall. Final mortar thickness should be of the order of 25-to-30 mm.

In clay brick masonry, for light gage meshes (up to 4.11-mm wire diameter), 50-mm long steel nails driven into the wall can be used as fasteners. However, powder-driven connectors are most cost-effective and reliable. Nine connectors per m^2 are recommended. In clay brick construction, SWWM should be installed directly against the masonry wall without using spacers.

The addition of a new RC wall connected to existing infilled RC frames through epoxied dowel bars performed satisfactorily. Because bond between new concrete and existing infill could be very large (by removing paint and finishes, and/or by building shear keys onto the infill), only perimeter bars are needed. To connect a new RC wall, it is recommended to design the fasteners so that its shear strength, based on a shear friction model, is at least 1.5 times the maximum shear force expected to be resisted by the jacketed wall.

Steel jacketing made of angles and straps improved the behavior of columns by a combination of truss mechanism and concrete confinement. Plastic deformations suggest the formation of a mechanism in which flat bars ends hinged in bending through the jacket height. Such assumption should be adopted when designing the welds between straps and angles. Angle size should be proportioned to exert confinement onto the column corner.

References

ACI Committee 318, *Building Code Requirements for Structural Concrete (318-99) and Commentary (318R-99)*, American Concrete Institute, Farmington Hills, MI, 1999.

Alcocer S.M. and Jirsa J.O., 1993, Strength of reinforced concrete frame connections rehabilitated by jacketing, *Structural Journal, American Concrete Institute*, **90**(3): 249-261.

Alcocer S.M., 1993, R/C frame connections rehabilitated by jacketing, *Journal of Structural Engineering, American Society of Civil Engineers*, **119**(5): 1413-1431.

Alcocer, S.M., Ruiz, J., Pineda, J.A. and Zepeda, J.A., 1996, Retrofitting of confined masonry walls with welded wire mesh, *Proceedings of the Eleventh World Conference on Earthquake Engineering*, Acapulco, Mexico, paper no. 1471.

Alcocer S.M, and Durán-Hernández R., 2002, Seismic performance of a RC building with columns rehabilitated with steel angles and straps, *Proceedings Fifth American Concrete Institute International Conference*, Cancún, México, 531-552.

Alarcón, P. and Alcocer S.M., 1999, Ensayes experimentales sobre rehabilitación de estructuras de adobe (In Spanish), *Proceedings of XII Mexican Congress on Earthquake Engineering*, Morelia, Mexico, I: 209-217.

Departamento del Distrito Federal, 1966, *Mexico City Building Code*, Mexico, D.F., 104 pp.

Flores, L.E., Marcelino, J., Lazalde, G. and Alcocer, S.M., 1999, *Evaluación experimental del desempeño de marcos con bloque hueco de concreto reforzado con malla electrosoldada y recubrimiento de concreto*, National Center for Disaster Prevention, Mexico, IEG/03/99.

Hernández, O., Meli, R. and Padilla M., 1979, *'Refuerzo de vivienda rural en zonas sísmicas'*; Institute of Engineering, UNAM, Mexico.

UNDP/UNIDO, 1983, Repair and strengthening of reinforcing concrete, stone and brick masonry buildings, RER/79/015, *Building Construction under Seismic Conditions in the Balkan Regions Vol. 5*, UN Industrial Development Programme, Vienna, Austria.

CFRP OVERLAYS IN STRENGTHENING OF FRAMES WITH COLUMN REBAR LAP SPLICE PROBLEM

SEVKET OZDEN•
Kocaeli University, Department of Civil Engineering, Kocaeli, TURKEY

UMUT AKGUZEL
Bogazici University, Department of Civil Engineering, Istanbul, TURKEY

Abstract. This study is part of a research program within the framework of NATO Project 977231 "Seismic Assessment and Rehabilitation of Existing Buildings" led by METU. A new seismic retrofitting method by using CFRP cross overlays is experimentally investigated. Five specimens were tested to highlight the effect of brick infill and epoxy bonded CFRP overlays on the strength and behavior of poorly detailed reinforced concrete frames. The main deficiencies of the one-third scale one-bay, two-story frames tested were low concrete strength, insufficient column lap splice length, poor confinement, and inadequate anchorage length of beam bottom reinforcement. In all specimens beams were stronger than columns and no joint shear reinforcement was used.

Keywords: reinforced concrete; rehabilitation; fiber-reinforced polymer; loading; strength

1. Introduction

Observations made after the recent earthquakes revealed that many existing structures located in seismic regions have inadequate lateral strength, ductility and stiffness. Among the other factors, non-ductile frame structures with unreinforced masonry infill have a significant role in contributing to the

• Sevket Ozden, Kocaeli University, Department of Civil Engineering, Veziroglu Campus, Izmit, Kocaeli

S.T. Wasti and G. Ozcebe (eds.), Advances in Earthquake Engineering for Urban Risk Reduction, 275–284.

disastrous consequences of the earthquakes. Countries of seismically active regions such as Turkey, Greece, Japan, Italy and Mexico, have suffered extensive damage due to catastrophic effects of recent earthquakes.

Lately, a significant amount of research has been devoted to the study of various strengthening techniques to enhance the seismic performance of the predominant structural system of the region, which is reinforced concrete frames with unreinforced masonry infills. The use of CFRP materials offers important advantages such as ease of application, minimum disturbance to the occupants and savings in construction cost and time in addition to their advanced mechanical properties. The main objective of the study was to understand the performance and failure mechanism of the reinforced concrete frames strengthened with CFRP overlays applied to the masonry infill panels. It is anticipated that the use of FRP on masonry will involve walls resisting in-plane and out-of-plane loads and, possibly, in-fill panels. Indeed, the majority of the work conducted to date has been on the out-of-plane capacity of walls with externally applied FRP. Therefore, it is obvious that the number of experimental and theoretical studies on the relevant subject is very limited.

2. Experimental Study

Due to the limitations in testing facilities, five test specimens, namely U1 (bare frame), U2, U3, U4 and U5 (infilled frames), were designed to one-third scale one-bay, two-story frames [1]. Reinforcement detail of the specimens is shown in Figure 1. The properties of the test specimens and materials are summarized in Table 1.

TABLE 1. The properties of the test specimens and materials

Specimen	Type	Long. Reinforcement		Lap Splice Length (mm)	f_c' (MPa)	f_m' (MPa)
		Columns	Beams			
U1	Bare	4-8 mm	6-8 mm	160	15.4	-
U2	Infilled	4-8 mm	6-8 mm	160	14.8	5.5
U3	Infilled	4-8 mm	6-8 mm	160	16.1	5.1
U4	Infilled	4-8 mm	6-8 mm	160	15.3	3.8
U5	Infilled	4-8 mm	6-8 mm	160	14.4	4.7
Material	Type	f_y (MPa)	f_u (MPa)	E (MPa)		
Steel	Stirrup	241	423	198,600		
	Long.	380	518	194,400		
CFRP		N/A	3,500	230,000		
Epoxy		N/A	30	3,800		

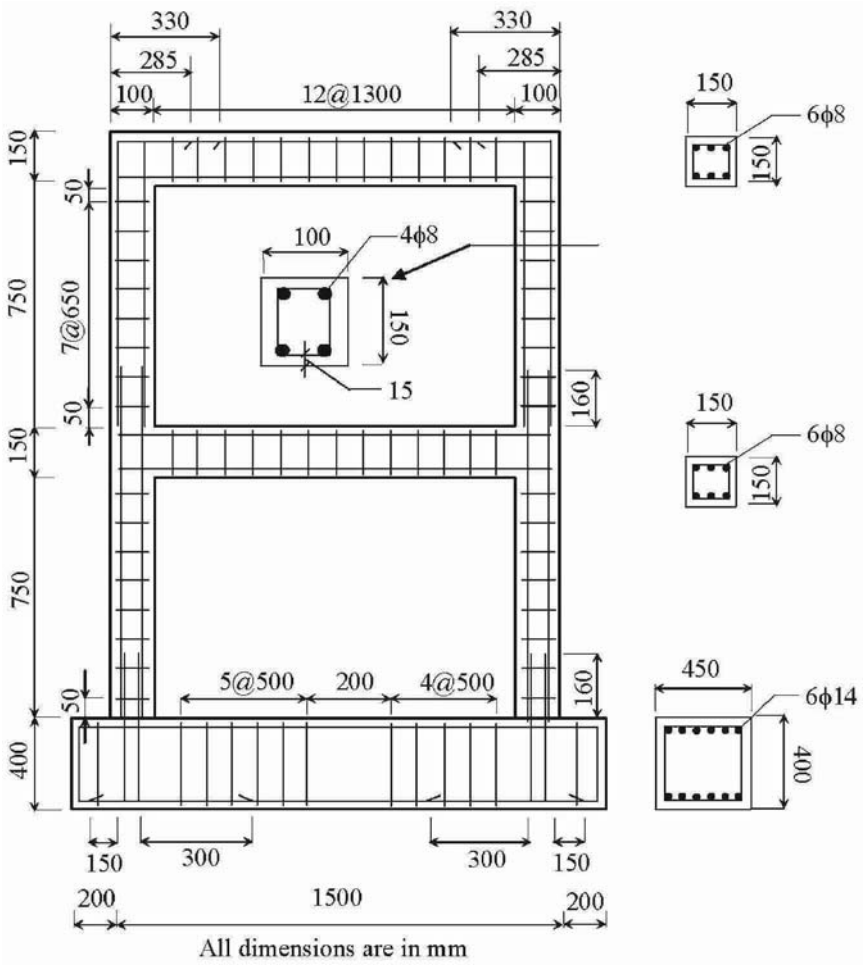

Figure 1. Reinforcement detail

Lateral loading was applied with a displacement controlled 250 kN capacity hydraulic actuator. For the bare-frame test specimen, the horizontal cyclic loading was applied to the second story beam level only, while the load was divided into two by a steel spreader beam and applied both at the first and second story levels for brick infilled specimens such that two thirds of the applied load goes to the upper story level. Axial load (N/No=0.10) was applied by means of a vertical load distributing beam to the columns evenly. Test set-up can be seen in Figure 2. Loading pattern consisted of two-phase: load control was used till the specimen reached yielding point; and displacement control was used such that the top deflection reached integer multiples of the yield displacement in both directions. Each test continued until the specimen experienced a significant loss of capacity.

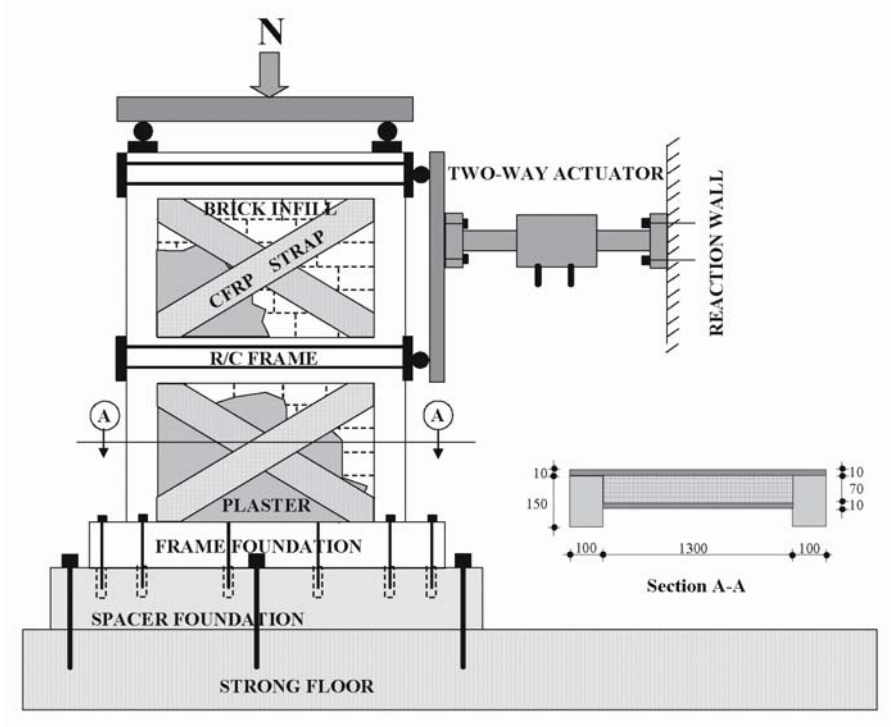

Figure 2. Test set-up

Electronic data acquisition system with control feedback was used to measure the level of applied load, displacements and rotations. In all the specimens, reversed cyclic load level and the frame top displacement were monitored to apply the predetermined loading regime. Curvature measurements on bare frame columns were made to highlight the effect of inadequate lap splice length. Out of plane displacements were recorded both for the bare frame and infilled frame specimens, although the infilled frame ones were restrained against such deformations by means of a steel frame constructed in the test rig. For infilled specimens shear deformations on the brick infill, horizontal base slip, and frame base rocking also measured. The measurements were relative to the frame foundation in all the specimens.

3. Observed Behavior of Test Specimens

Specimen U1: First cracks observed at a load level of 7kN on the base of lower left column. In the 7th cycle (10kN) specimen reached its yielding capacity. After the drift level of 1.65% the lateral load capacity of the specimen stabilized under the increasing lateral displacements. The failure of the system was a

typical frame failure. It turned into a mechanism by the formation of plastic hinges in the beam-column joints and in the columns especially at the lap splice regions.

Specimen U2: First cracks observed at a load level of 40kN through the second story brick wall. In the 8th cycle (55kN, 0.14% drift) specimen reached its yielding point. At a drift level of 0.34% sliding was observed between the first story wall panel and beam. After the drift level of 0.55% crack propagation stabilized and separation of the infill panel into four parts completed. The failure mechanism can be identified as a combination of flexure, sliding and crushing of the infill panel at compression regions due to compression strut formation. Damage accumulation and final conditions of the front faces of the infilled specimens can be seen in Figure 3.

Specimen U3: was the first specimen strengthened by means of CFRP overlays applied as cross diagonal strut and placement of anchor dowels into the predetermined locations. The main idea was to investigate the behavior of CFRP sheets and anchor dowels efficiency during the test. Moreover, separation and crushing of the infill from the frame along the compression struts as seen in Specimen-U2 necessitated the using of CFRP sheets as cross-overlays. Close-ups from the CFRP application process and anchor details are shown in Figure 4. First cracks observed at a load level of 35kN in the first and the second story infill panels. In the 12th cycle (75 kN, 0.18% drift) specimen reached its yielding point. At a drift level of 0.31% delamination of CFRP overlay began to form at the frame foundation near both columns and sliding was observed between the beam and first story infill panel. At a drift level of 0.65% separation of the first story panel from the foundation, fracture of CFRP cross overlays and debonding of anchor dowels observed. In the following cycles, at drift level of 0.9%, the cross CFRP overlay sheets buckled and started to debond from the plaster as a result of compression and tension struts. Anchor dowels failed by forming a pull-out cone at the foundation level on both faces.

Specimen U4: Number and depth of the anchor dowels increased. In addition; rectangular CFRP flag sheets applied to each panel corner to prevent the crushing of brick due to the compression strut, additional anchor dowels were aligned in the same direction with cross-overlays. First cracks observed at a load level of 55kN on the first story left columns just above the rectangular CFRP flag. In the 13th cycle (95kN, 0.2% drift) specimen reached its yielding point. At a drift level of 0.34% pre-formed cracks especially located on the bottom of the columns widened suddenly. Columns and the frame foundation separated completely. At further drift levels separation of frame base from foundation and rocking was more pronounced due to complete bond loss of anchor dowels and excessive slip deformation on the columns. Till the end of the test, the specimen remained intact without any crushing of brick infill corner

joints and delamination of CFRP from the concrete cover did not appear. Moreover no significant buckling or rupture of CFRP overlay was observed. However, it was revealed that depth of the anchor dowels was not sufficient. The problem of lap-splice in columns governs the capacity and post-failure behavior.

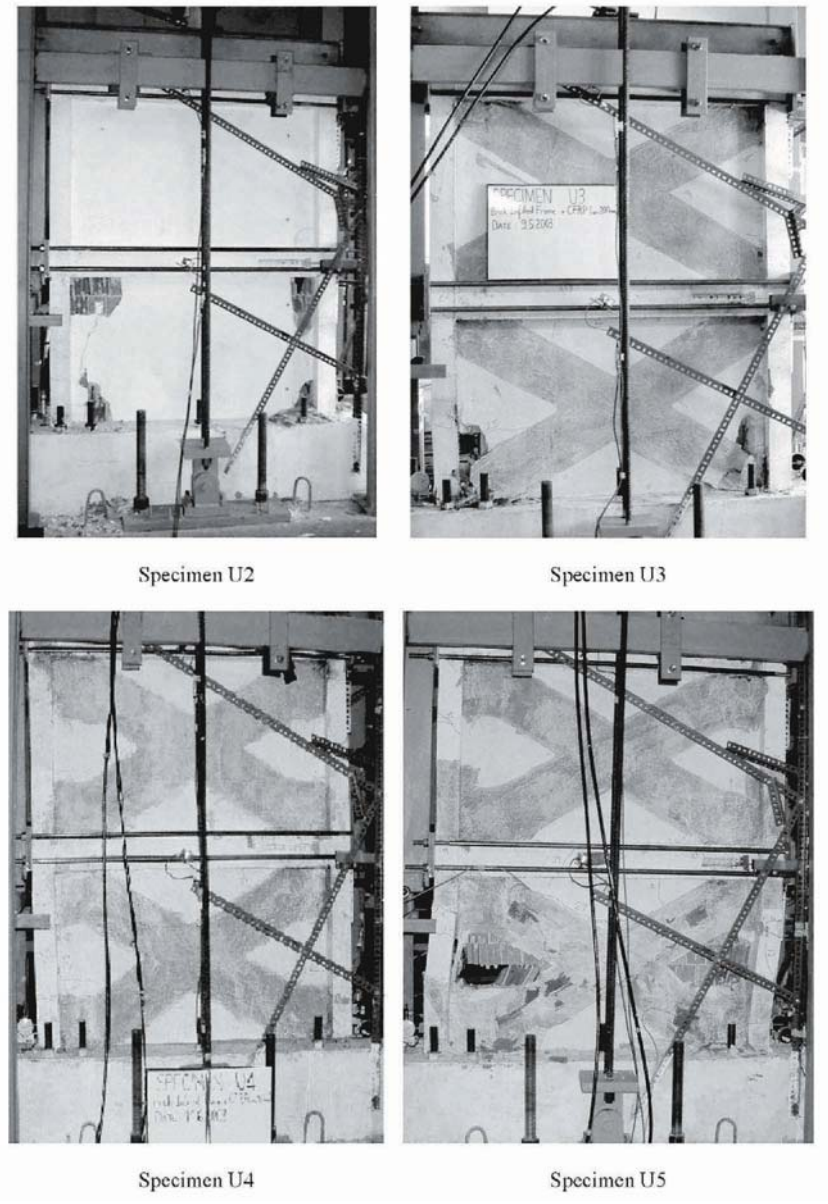

Figure 3. Damage accumulation

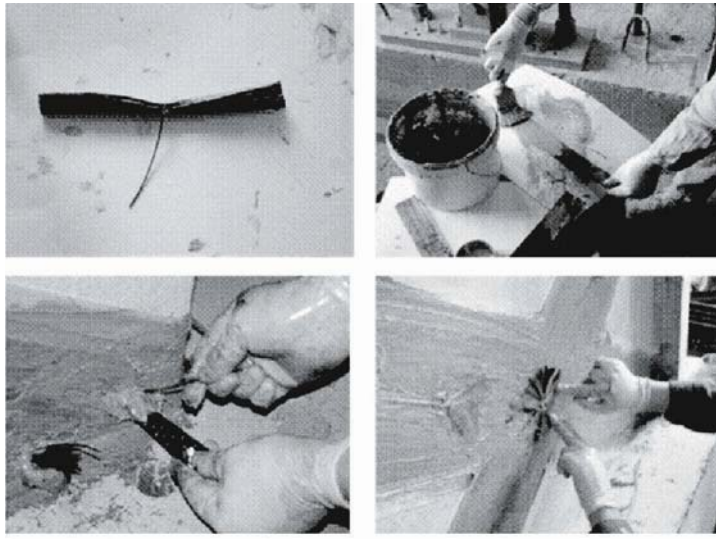

Figure 4. CFRP anchor application

Specimen U4: The number and depth of the anchor dowels were increased. In addition; rectangular CFRP flag sheets were applied to each panel corner to prevent the crushing of brick due to the compression strut, additional anchor dowels were aligned in the same direction with cross-overlays. First cracks observed at a load level of 55kN on the first story left columns just above the rectangular CFRP flag. In the 13th cycle (95kN, 0.2% drift) specimen reached its yielding point. At a drift level of 0.34% pre-formed cracks especially located on the bottom of the columns widened suddenly. Columns and the frame foundation separated completely. At further drift levels separation of frame base from foundation and rocking was more pronounced due to complete bond loss of anchor dowels and excessive slip deformation on the columns. Till the end of the test, specimen remained intact without any crushing of brick infill corner joints and delamination of CFRP from the concrete cover did not appear. Moreover no significant buckling or rupture of CFRP overlay was observed. However, it was revealed that depth of the anchor dowels was not sufficient. The problem of lap-splice in columns governs the capacity and post-failure behavior.

Specimen U5: The strengthening process for Specimen U5 consisted of two phases. First phase was similar to that of U4 except the increment in the depth of foundation level anchorage length up to 12cm. Extra anchor dowels at foundation level with increased anchoring depth together with continuity CFRP sheets along the column splice regions were used. To satisfy the required longitudinal reinforcement at foundation and 1st story level additional CRFP sheets were bonded on the exterior faces of the columns. Afterwards, by

wrapping around each column with one layer of CFRP sheet strengthening was finished. First cracks observed at a load level of 55 kN on the left column at the intersection region of the CFRP column wrap. In the 16th cycle at a load level of 95 kN debonding and peeling off was suddenly occurred on the cross overlay CFRP sheets and boundary separation between the columns and the brick infill wall transpired. In the 17th cycle (115 kN) specimen reached its yielding point. After the drift level of 1.39% sudden drop in load capacity observed due to the complete failure of CFRP overlay sheets by means of rupture through the sliding shear plane along the bed joints which is 300 mm above the foundation.

4. Discussion of Test Results

Response envelope curves are developed by connecting the peak values of each cycle for all specimens (Figure 5). Load bearing capacities of all strengthened frames tested are significantly higher than that of the bare frame (Sp-U1) and the unstrengthened infilled specimen (Sp-U2). Although there was a significant strength enhancement in Sp-U5 (1.94 times that of Sp-U2), the enhancement in displacement capacity was more pronounced (5.3 times that of Sp-U2).

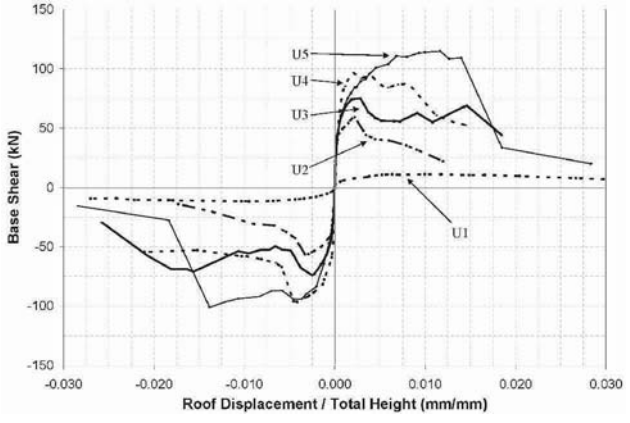

Figure 5. Response envelope of specimens

Moreover, the tangent slopes of the load-displacement curves which are called “tangent stiffness” were calculated for each specimen. These representative slopes referred to each forward and backward cycle are all calculated from the experimental load-displacement curves. The degradation of normalized tangent slopes for the forward and backward cycles with corresponding specific roof story drift ratio are given in Figure 6. The drift ratio exceeds 2 percent for bare frames and 0.5 percent for infilled frames, and the amount of stiffness degradation was more than 90 percent for almost all specimens beyond a drift level of 1 percent.

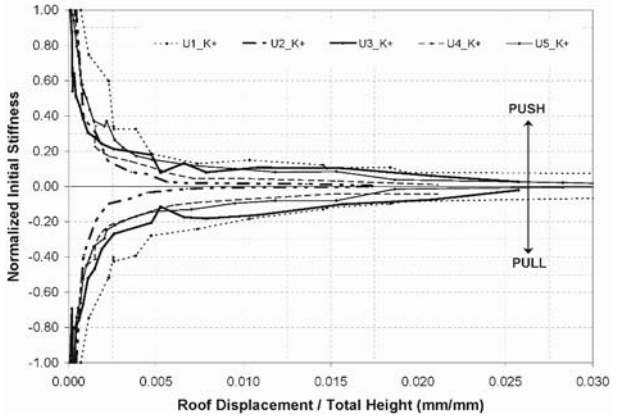

Figure 6. Variation of initial stiffness for each forward and backward cycle

The degree of closing of the existing cracks when the load is reversed is reflected in the load displacement curves with an increased residual deflection. Variation of residual displacement ratio with increasing drift levels is shown in Figure 7.

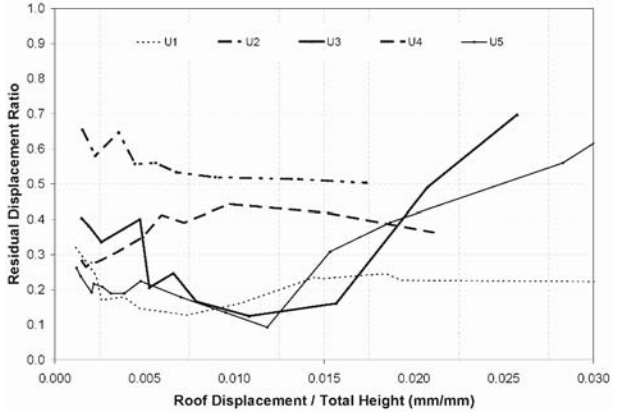

Figure 7. Variation of residual displacement ratio

It is obvious that the capability of a structure to dissipate energy which is defined as the area enclosed by the experimental load-displacement hysteresis loops has a strong influence on its response to an earthquake loading. All specimens except bare frame (Sp-U1) dissipated almost the same amount of energy up to the 0.5% roof drift ratio. Sp-U5 exhibited an increase of 30% in maximum energy and a 20% increase in strength when compared to precedent strengthened specimen, Sp-U4. At 2% drift level, Sp-U5 dissipated 1.5 times more energy than the specimens U3 and U4, while it was 4.5 times greater than the Specimen-U1.

5. Conclusions

The proposed X-overlay CFRP reinforcement scheme with flag sheets and special anchorage details resulted in a significant enhancement in the response of the brick infilled RC frame specimens under reversed cyclic loading. The strengthened specimens yielded a gradual and prolonged failure, a higher base shear, more energy dissipation and apparent post peak strength. However, stiffness enhancement of the specimens was critically low. The interstory drift limit values which are the constraints for rehabilitation of the existing structures should be revised. What is critical here is the reliance on a retrofit analysis and design which limits the story drift to an amount which would prevent any major degradation of the masonry. Test results revealed that an interstory drift level of 0.35% to 0.50% may be a limiting value preventing the CFRP modified masonry from degradation.

ACKNOWLEDGMENTS

The authors gratefully acknowledge the technical support of Bogazici University Structures Laboratory where all the experiments were conducted and financial support from METU-Civil Engineering Department Projects (NATO, Scientific Affairs Division Grant No: SfP977231 and TUBITAK, Grant No. YMAU-ICTAG-I 575). The support of Sika Yapi Kimyasallari A.S., who supplied the materials used in this study, is also gratefully acknowledged.

References

Akguzel, U., Seismic *Retrofit of Brick Infilled R/C Frames with Lap Splice Problem in Columns*, MS thesis, Department of Civil Engineering, Bogazici University, Istanbul, Turkey, 2003.

SEISMIC RETROFIT OF INFILLED REINFORCED CONCRETE FRAMES WITH CFRP COMPOSITES

ERCAN YUKSEL
ALPER ILKI*
GULSEREN EROL
CEM DEMIR
H. FARUK KARADOGAN
Istanbul Technical University, Faculty of Civil Engineering
Maslak, 34469, Istanbul, Turkey

Abstract. Although the infill walls are not considered as structural members during design, the observations made after earthquakes have shown that they are important resources of strength, stiffness and damping under lateral loads. Preventing premature damage of infill walls during earthquakes by keeping them in their locations can help the structure maintain its lateral strength, stiffness and damping characteristics, as well as vertical strength. In this study, six reinforced concrete frames, two bare, two infilled and two with CFRP retrofitted infill walls, were tested under constant vertical load and reversed cyclic lateral loads. Test data were evaluated in terms of strength, stiffness and failure mechanisms and it is concluded that retrofitting of infill walls by applying CFRP composites in diagonal directions, provides significant enhancement in lateral strength and stiffness.

Keywords: CFRP, infill wall, masonry, reinforced concrete frames, retrofitting.

* Asst. Prof. Dr. Alper Ilki, I.T.U., Civil Engineering Faculty, 34469, Maslak, Istanbul, Turkey. Tel:+90 212 285 38 38, Fax : +90 212 285 38 38, e-mail : ailki@ins.itu.edu.tr

S.T. Wasti and G. Ozcebe (eds.), Advances in Earthquake Engineering for Urban Risk Reduction, 285–300.

1. Introduction

It is well known that many existing structures in seismic areas of the world are poorly designed and constructed. During the design and construction of these types of structures, the recent codes and the up-to-date construction methodologies were not followed. As a result, structural members of this type of structures may experience extensive damage during earthquakes. In order to overcome these deficiencies, research on the utilization of new retrofitting techniques, in the aim of developing appropriate and economical repair and retrofit techniques, is essential.

It is a common assumption to neglect the effects of infill walls on the lateral strength and stiffness of RC structures during design. This kind of approach may lead to misprediction of the real behavior of structures, as the observations made after the recent major earthquakes in Turkey and research performed throughout the world have shown that infill walls are important resources of strength, stiffness and damping under lateral loads. These contributions of infill walls may be lost by premature damage during earthquakes. It may be an effective strengthening technique to keep infill walls in place by retrofitting the infill and RC frame elements together and forcing them to work as a whole until the end of the earthquake. Using Fiber Reinforced Polymers (FRP) for this kind of retrofit is recently an appealing area for the researchers.

Most common types of FRP materials are glass (GFRP), carbon (CFRP), and aramid (AFRP) fibers. CFRP sheets are preferred for retrofitting of structures due to their high tensile strength, low weight, immunity to corrosion, easy application and availability in various dimensions. There are also some disadvantages as, FRP composite systems lose strength under high temperatures, are affected by environmental conditions and behave linear elastic until failure[1, 2, 3] as well as being relatively expensive.

In this study, six reinforced concrete frames, two bare, two with infill walls and two with CFRP retrofitted infill walls were tested under constant axial load and reversed cyclic lateral loads. The idea was to understand the behavior of CFRP retrofitted infilled RC frames experimentally and collect data to be used in theoretical work. At the end of the tests, it was seen that retrofitting of infill walls with CFRP composites in diagonal direction provided significant enhancement in lateral strength and stiffness. Prior to this study, a set of similar specimens were tested under vertical and lateral load, where lateral load was applied only to the second stories of the specimens[4].

1.1. EXPERIMENTAL WORK

The geometry, reinforcing details, expected ultimate strength of the specimens and the loading protocol were decided mainly considering, the applications in practice, the room and loading capacities of laboratory and the structural features of earlier tests carried out at different institutions5, 6. Six two story-one bay reinforced concrete frames were tested under constant column axial load and reversed cyclic lateral loads. Some of the structural features of the specimens are tabulated in Table 1. In Table 1, f'_c is the standard cylinder characteristic strength obtained at the end of 28 days.

TABLE 1 . General characteristics of the specimens

Specimen	f'_c (MPa)	Bare/Infill walls	Longitudinal Reinforcement	Retrofit
BC-0-1-14	14	Bare	Continuous	No
BL-0-1-8.6	8.6	Bare	Lap spliced	No
IC-0-1-11	11	Plastered Infill Walls	Continuous	No
IL-0-1-17	17	Plastered Infill Walls	Lap spliced	No
IC-C1-1-10	10	Plastered Infill Walls	Continuous	CFRP diagonals
IL-C1-1-8.6	8.6	Plastered Infill Walls	Lap spliced	CFRP diagonals and confinement of lap spliced zones

During the specimen production process, six two story-one bay frames with 160 mm × 240 mm column and 240 mm × 240 mm beam cross-sections were cast. Three of the frames had continuous longitudinal reinforcement, while the other three had deficient lap splices. As presented in Figure 1, 12 mm diameter plain longitudinal bars in the columns had $20d_b$ (i.e. 240 mm) lap splice length at critical sections to represent the lap splice deficiencies encountered frequently in practice. Although mild steel was used, no hooks were formed for longitudinal bars at the end of the splices.

In the next step, four of these RC frame specimens were eccentrically infilled with 135 mm × 200 mm × 200 mm brittle bricks that were cut in half in transverse direction to the holes. Low strength brittle bricks, which are widely used in nonstructural partitioning walls in Turkey, were selected as the infill material. The compressive strength in the direction of the holes of this type of brittle bricks was between 2.5-10 MPa. The void ratio of bricks was around 60%. The water:cement:lime:sand volumetric mixture proportions of the mortar was 1:1:0.5:4.5 and the thickness of the mortar layer was around 10 mm. As existing structures are generally plastered, these four infilled frames were also plastered similar to the practical applications. Different stages of infilled frame specimen production process are presented in Figure 2.

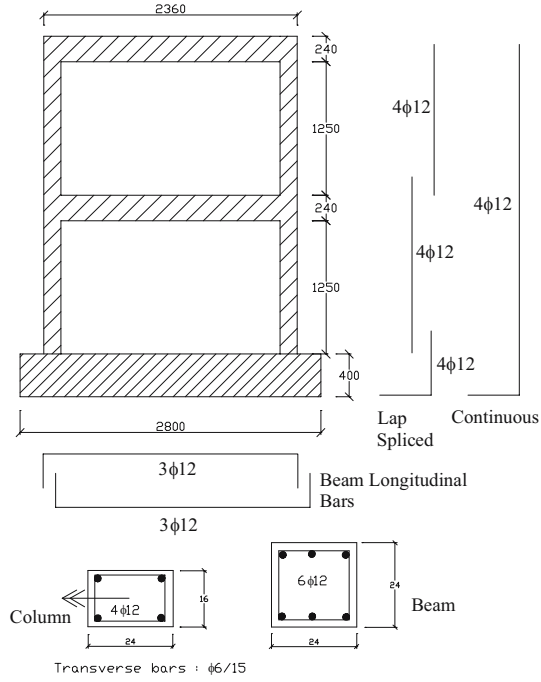

Figure 1. Dimensions and reinforcing details of the specimens (dimensions in mm)

Figure 2. Different stages of fabrication

After application of the plaster, two of the specimens were retrofitted with CFRP sheets. CFRP configuration and detailing, which are the key issues for a satisfactory improvement in the behavior, were previously studied by partner institutions. The final configurations and detailing determined by those institutions [5, 6] have shown that;

- CFRP sheets applied over the infill walls in diagonal directions were quite effective,
- CFRP layers should be extended over the frame members and sufficiently anchored to them,

- Deficient lap splice regions should be strengthened by bonding additional CFRP sheets in vertical direction and then wrapping the columns with at least one layer of CFRP sheet in transverse direction,
- Anchors made up with CFRP should be used to connect CFRP sheets to the infill and to the frame members in order to prevent debonding.

The general appearance of the retrofitted specimens with continuous and lap spliced longitudinal reinforcements are presented in Figure 3. The first stage of retrofitting is same for both cases. A single layer of CFRP sheet was bonded in diagonal directions on both sides of the infill walls of upper and lower stories using epoxy resin. Diagonal CFRP on two sides of infill were connected to each other by means of anchors made of CFRP sheets. The load to be carried by diagonal CFRP sheets were spreaded over a relatively larger area with additional CFRP sheets at the corners of the wall. The fibers of these two layers of CFRP were oriented in two perpendicular directions, namely horizontal and vertical directions and they were connected to the beam/column by two CFRP anchors. Connection of diagonal CFRP sheets to the foundation was maintained by CFRP anchors as well. In order to make these connections, holes were drilled in frame elements and foundation, with 120 mm and 200 mm depths respectively, cleaned thoroughly and filled with epoxy. CFRP sheets were then folded and placed into the holes, see Figure 4. The fibers that were left outside were spread and bonded on the wall using epoxy resin. Different stages of CFRP application are presented in Figure 5.

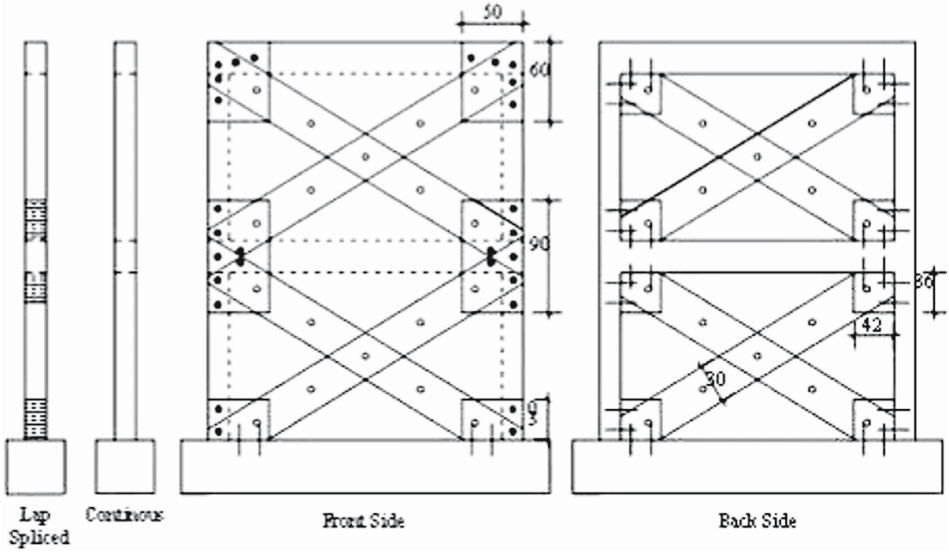

Figure 3. General view of the retrofitted specimens (dimensions in cm)

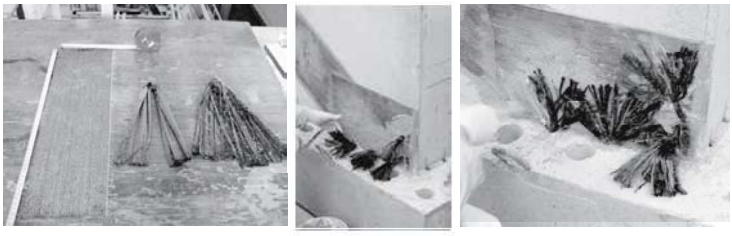

Figure 4. Preparation of CFRP anchors

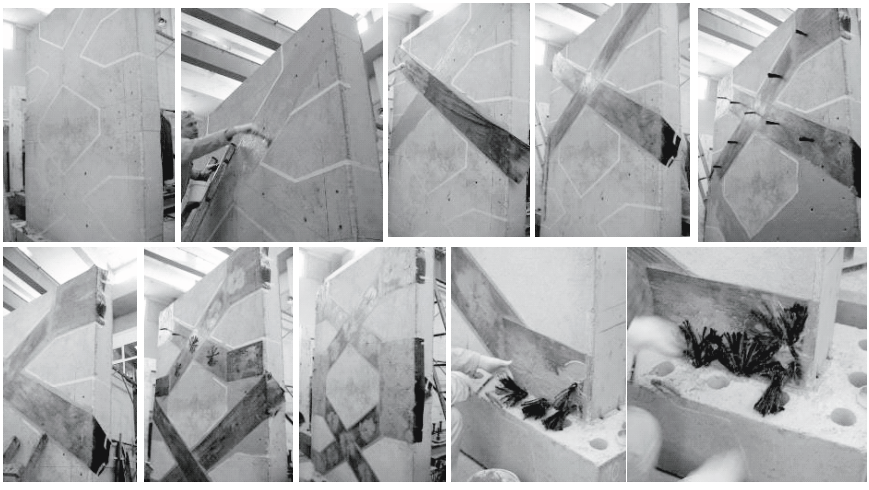

Figure 5. CFRP application stages of front side of the specimens

In addition to the retrofitting procedure explained above, for the specimen with lap splice deficiency, some extra measures were taken as presented in Figure 6. Corners of the columns at lap splicing regions were rounded to prevent stress concentrations. In order to suppress the lap splice deficiency, CFRP sheets with fibers in vertical direction, were bonded on the sides of the column, parallel to the column longitudinal reinforcement, see Sheet A in Figure 6. The amount of CFRP was selected to have the same tensile capacity as the lapped longitudinal reinforcement at tension side of the columns. Then two CFRP anchors were placed at the foundation level (Sheet B in Figure 6) and spreaded over Sheet A. Finally one layer of transverse CFRP sheet (Sheet C in Figure 6) was bonded on Sheet A, confining the column and extending over the infill wall. CFRP application stages of lap splice area are shown in Figure 7.

It should also be noted here that at the first test of IL-C1-1-8.6 the depths of CFRP anchors into the foundation were not sufficient enough to transfer the tensile forces from diagonal CFRP sheets to the foundation, so anchors were pulled out and an early failure was observed. Before it was retested, damage at the lower corners of the first story infill wall was repaired, CFRP anchors were rebuilt and epoxy was injected into the bending cracks of first story columns.

During the stages of concrete casting, standard cylinder specimens were cast, cured in the same way as frames, and tested for determining compressive strength of concrete. Results of 28 days standard cylinder compression tests are given in Table 1. 12 mm diameter plain steel reinforcement was used for longitudinal beam and column bars. The stress-strain relationships of mild reinforcing steel obtained experimentally are shown in Figure 8.

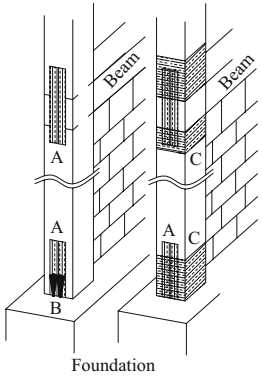

Figure 6. Retrofitting stages for lap splice deficiency (schematic)

Figure 7. Retrofitting stages for lap splice deficiency

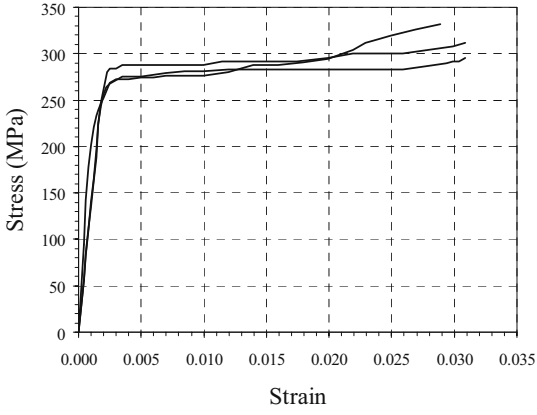

Figure 8. Stress-strain relationships of longitudinal reinforcement

TABLE 2. Mechanical properties of CFRP

Fiber Type	Fiber Orientation	Weight (g/m^2)	Fabric Design Thickness (mm)	Tensile Strength of Fibers (Nominal) (N/mm^2)	Tensile Elastic Modulus of Fibers (Nominal) (N/mm^2)	Strain at Rupture of Fibers (Nominal) (%)
High Str. CF	0° Uni-directional	220± 10%	0.12	4,100	231,000	1.7

2. Testing Setup

The general view of a specimen at the testing stage is shown in Figure 9, together with the necessary adapter pieces and devices used for applying lateral and vertical loads on to the specimen. An adapter foundation specially cast for these specimens was used to supply the required fixation to the strong floor of the laboratory.

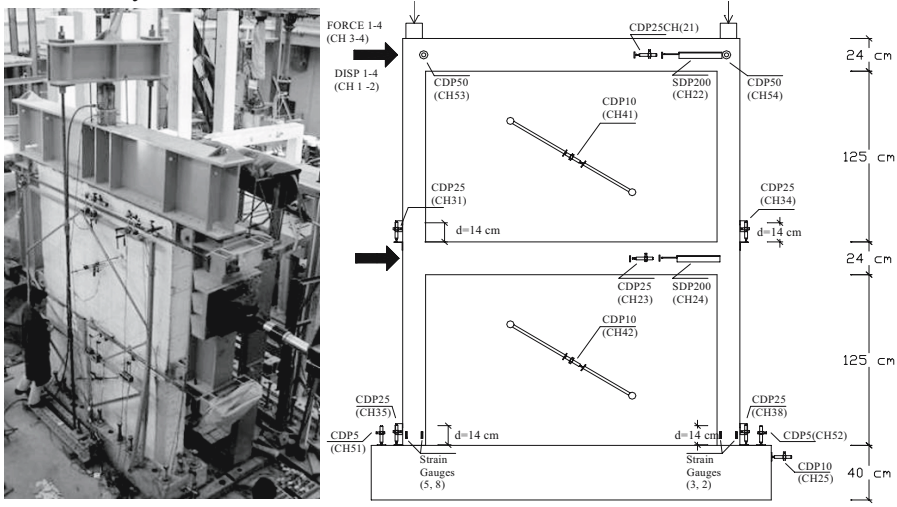

Figure 9. The general view of a specimen at the testing stage and locations of measuring devices

Displacement controlled testing facilities were utilized for loading of the specimen. MTS actuators, having ± 250 kN loading and ± 300 mm displacement capacities, were used for this purpose. As the capacity of a single actuator was not adequate for testing of retrofitted specimens, twin actuators mounted on the reaction wall were used simultaneously for these specimens. The point loads were acted at first and second story levels through a rigid steel adapter with hinged steel connections at beam levels. In order to prevent possible secondary torsional effects, the application point of loads was

approximately the center of rigidity of specimens. In the case of eccentrically placed infill walls this had more importance and extra provisions were taken for safety and reliability of the tests and all out of plane displacements were recorded to observe the magnitude of inevitable torsion.

Axial force, that was approximately 23% of the axial load capacity of reinforced concrete columns, was applied to each column by a hydraulic jack through a steel beam and measured by a load cell, Figure 9. Axial load capacity of columns was obtained by taking the contributions of concrete (28 days standard cylinder strength was used) and longitudinal reinforcement into account. Essentially the total target displacement reached after each increment was imposed to the specimen only once at each cycle. The whole displacement protocol referred for that purpose is shown in Figure 10 and corresponding drift ratios (δ/H) are given in Table 3.

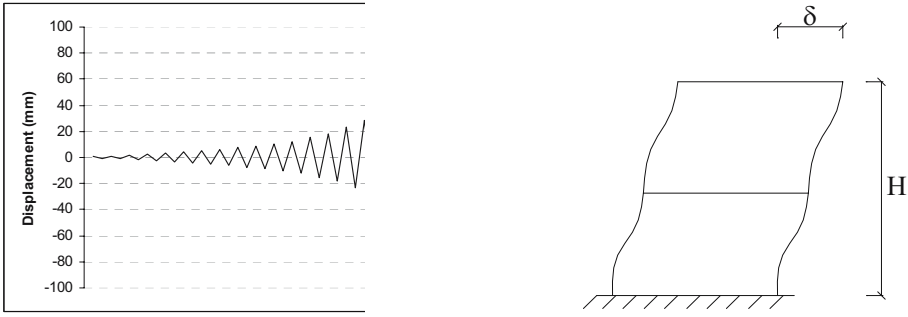

Figure 10. The displacement protocol

TABLE 3 . Displacements and drift ratios corresponding to the displacement protocol

Target Top Disp. (mm)	Top Story Drift Ratio (δ/H)	Target Top Disp. (mm)	Top Story Drift Ratio (δ/H)	Target Top Disp. (mm)	Top Story Drift Ratio (δ/H)
± 0.47	% 0.016	± 7.55	% 0.264	± 32.90	% 1.150
± 0.94	% 0.032	± 9.00	% 0.315	± 37.60	% 1.315
± 1.65	% 0.057	± 10.50	% 0.367	± 47.00	% 1.643
± 2.35	% 0.035	± 12.00	% 0.419	± 56.40	% 1.972
± 3.20	% 0.111	± 15.40	% 0.539	± 65.80	% 2.300
± 4.00	% 0.139	± 18.50	% 0.647	± 75.20	% 2.629
± 5.05	% 0.177	± 23.50	% 0.822	± 84.60	% 2.958
± 6.10	% 0.213	± 28.20	% 0.986	± 94.00	% 3.287

Lateral displacements at story levels, foundation and specimen in-plane and out of plane movements, critical column section rotations and infill walls diagonal deformation values were measured and recorded by means of linear variable displacement transducers (LVDTs). In addition to these measurements, achieved strains of column longitudinal bars at critical column sections were measured with strain gauges. The measuring system is shown in Figure 9.

3. Test Results

Experimentally found base shear versus top displacement curves of bare and infilled frame specimens with continuous longitudinal reinforcement, namely BC-0-1-14 and IC-0-1-11 are drawn together in Figure 11. It can be seen from these curves that lateral stiffness of infilled frame, IC-0-1-11, is significantly high and ultimate load of IC-0-1-11 is approximately 4 times higher than that of bare frame, BC-0-1-14. However, it should be pointed out that this increase could not be sustained until high displacement levels. Damage was accumulated at beam-column joints and foundation levels of first story columns of BC-0-1-14. Unlikely, at the infilled frame IC-0-1-11 less damage had been observed at beam-column joints and bending cracks at the columns of IC-0-1-11 were more spreaded along the height of first story columns, mostly at the levels where transverse reinforcements existed, Figure 12. Although a few diagonal cracks formed, corner crushing was the main damage observed at the infill wall of the first story. There was no apparent damage at the frame elements and the wall of the second story. As new cracks formed at the upper part of the first story columns, propagating into beam-column joints at displacement level 15.4 mm, which is the top story drift ratio (δ/H) %0.539, a decrease at peak loads were observed, see A and B at Figure 11. These cracks were widened at displacement level 23.5 mm (δ/H: %0.822) and at the next displacement level failure of first story column had been occurred due to these shear cracks, Figure 12. It should also be pointed out that the separation of infill wall from the frame elements and a wide diagonal crack on the wall comprised important damage at this displacement.

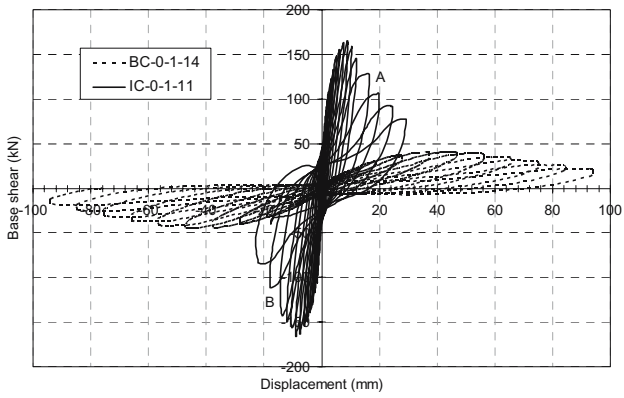

Figure 11. Base shear versus top displacement curves of BC-0-1-14 and IC-0-1-11

Experimentally found base shear versus top displacement curves of bare and infilled frame specimens with lap splice deficiency, namely BL-0-1-8.6 and IL-

0-1-17 are drawn together in Figure 13. The stiffness and lateral load capacity of infilled frame IL-0-1-17 is significantly higher than bare frame BL-0-1-8.6. Damage at BL-0-1-8.6 and IL-0-1-17 was very similar to BC-0-1-14 and IC-0-1-11, respectively. Bending cracks at the first story columns, a wide diagonal crack and corner crushing of first story infill wall, and shear cracks at the upper parts of the first story columns were the major damage observed at IL-0-1-17, Figure 14. There was no significant damage at the frame elements and the wall of second story. The shear crack, formed at the upper part of the first story column at displacement level 18.5 mm (δ/H: %0.647), was widened at further displacement levels. As the concrete at this area were crushed and longitudinal reinforcements were buckled, failure was taken place at displacement level 23.5 mm (δ/H: %0.822). The effects of this shear crack can be seen in the base shear versus top displacement diagram, see A and B in Figure 13.

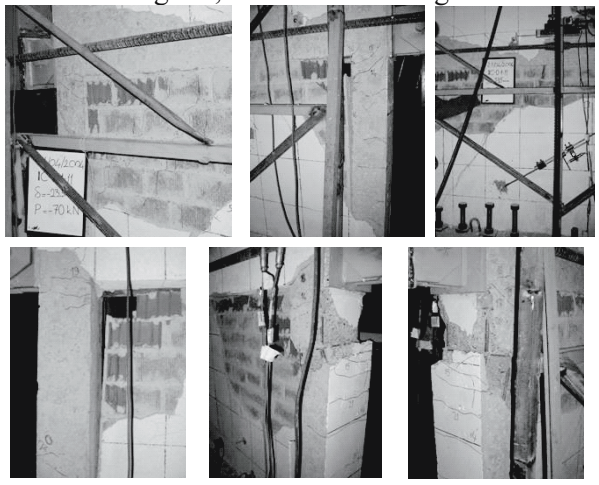

Figure 12. Damage of IC-0-1-11 at different displacement levels

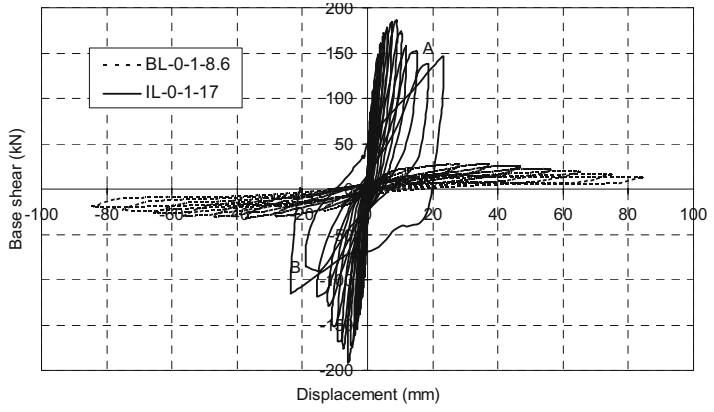

Figure 13. Base shear versus top displacement curves of BL-0-1-8.6 and IL-0-1-17

Experimentally found base shear versus top displacement curves of CFRP retrofitted infilled frame specimens with and without lap splice deficiency, namely IC-C1-1-10 and IL-C1-1-10 are shown in Figures 15 and 16, respectively. Both retrofitted specimens experienced bending cracks formed at first story columns, as infilled specimens. Debonding of diagonal CFRP, mostly in vicinity of the corners had started at displacement level 9 mm (δ/H: %0.315) for IC-C1-1-10, Figure 17. Contrary to the other specimens, diagonal cracks were observed at the second story infill wall. The plaster was crushed and debonding of CFRP increased at 12 mm displacement (δ/H: %0.419) and this noticeable increase of the damage resulted as the decrease at peak load, see A at Figure 15. Shear cracks were formed at the upper part of the first story columns and two diagonal CFRP were broken one by one under tension at displacement level -18.5 mm (δ/H: %0.647). The sudden decrease at the load caused by CFRP rupture can be seen at B, Figure 15. The other two diagonal CFRP in other direction were also broken at the next cycle, see C at Figure 15. After all diagonal CFRP had been broken, base shear versus top displacement curve moved closer to the bare frame curve, see D and E at Figure 15. The shear cracks at the columns were widened, crushing of the concrete had been

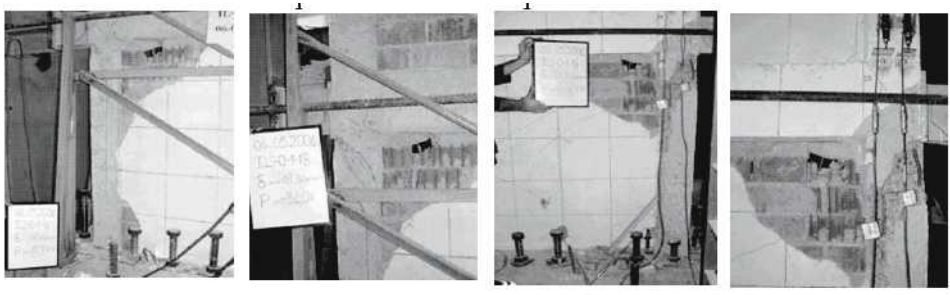

Figure 14. Damage of IL-0-1-17 at different displacement levels

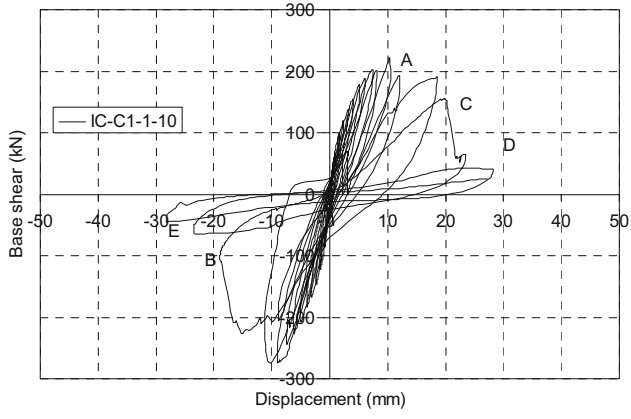

Figure 15. Base shear versus top displacement curve of IC-C1-1-10

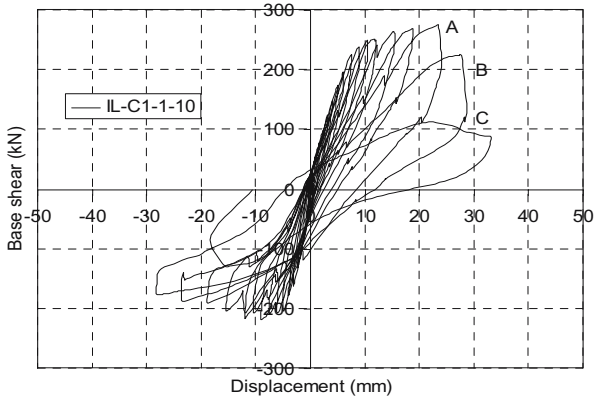

Figure 16. Base shear versus top displacement curve of IL-C1-1-10

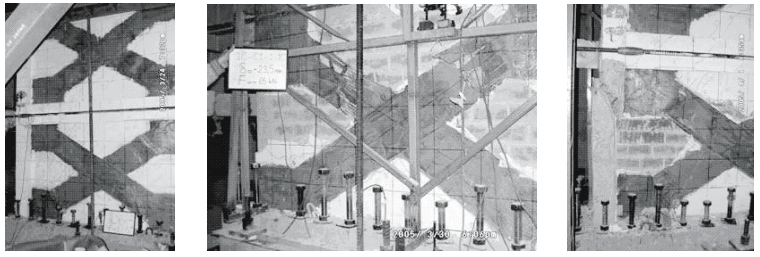

Figure 17. Damage of IC-C1-1-10 at different displacement levels

Similar kind of damage was observed for IL-C1-1-10. Diagonal CFRP were debonded from the wall and broken at displacement level 23.5 mm, i.e. δ/H: %0.822, see A and B in Figure 16. Bricks were crushed, (C in Figure 16) and after the last diagonal CFRP was broken, test was ended because of the safety precautions of actuators, Figure 18.

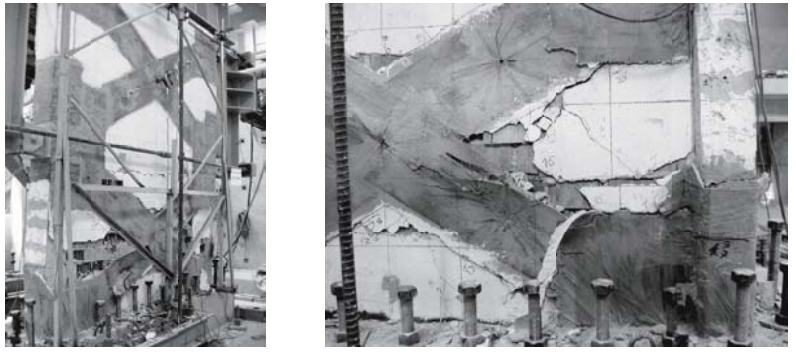

Figure 18. Damage of IL-C1-1-10 at different displacement levels

Envelopes of base shear-top displacement curves of all specimens with and without lap splice deficiency in are shown together for having better comparisons in Figure 19.

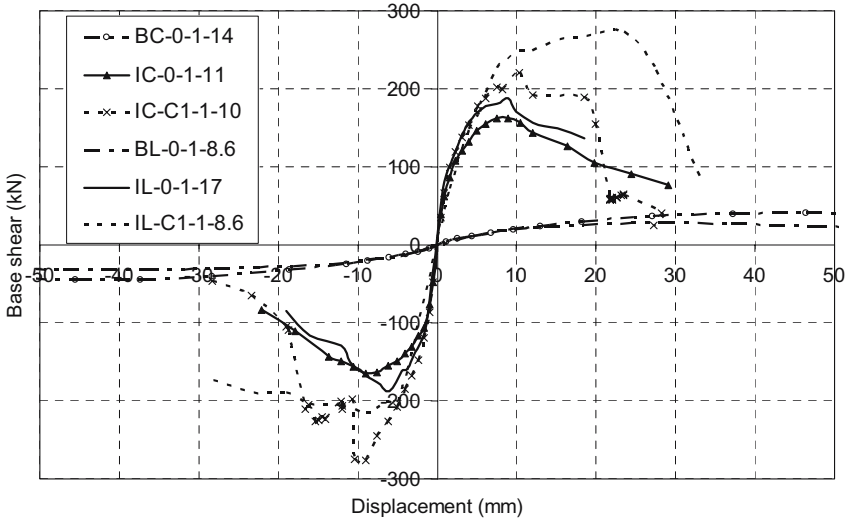

Figure 19. Envelopes of base shear versus top displacement curves of all specimens

4. General Observations and Conclusions

The results that have been reached by the evaluation of base shear-top displacement curves, failure modes and observations made during tests, are presented below.

1. Application of two point lateral loads at story levels by a rigid beam controlled the failure mechanisms of specimens and as a result, no significant damage had been occurred at frame elements and infill walls of second story. The critical sections were the upper parts of the columns and infill walls of first story.
2. The lateral strength and stiffnesses of the infilled specimens are significantly higher than bare frame specimens. The damage accumulated at the beam-column joints and lower parts of the first story columns at bare frame specimens, while bending cracks were spreaded along the columns at infilled specimens. This damage formation indicates that bare frame specimens' frame type behavior changed into shear wall type behavior by the introduction of infill walls.
3. Although one or two diagonal cracks were formed on the infill walls, crucial damage of the infills, prior to retrofitting of the specimens, was corner crushing. The contribution of infill walls to the lateral load capacity of specimen seemed to end after corner crushing.

4. Retrofitting the specimens by CFRP prevented corner crushing and diagonal cracks spreaded over the whole infill. Although the infill walls were severely damaged at the end of the tests, total collapse of infill walls was not observed.
5. CFRP anchors placed into the foundation and frame elements worked properly until the end of the tests. CFRP anchors that connected diagonal CFRP sheets on both sides of the infill walls, prevented CFRP from debonding
6. Retrofitting infilled frame specimens by CFRP increased lateral load capacities and lateral stiffnesses. The sudden load drops, observed at base shear versus top displacement curves due to diagonal CFRP rupture, showed that the contribution of diagonal CFRP on overall behavior is substantial. It should also be noted that even all the diagonal CFRP sheets were broken, the specimens continued carrying lateral load and the base shear versus top displacement curves moved closer to curves of bare frame specimens.
7. After having compared the results, it can be said that the number of displacement reversals before failure was increased by the help of CFRP. In the other words the energy dissipation capacity of the system was increased by the means of CFRP application.
8. The initial stiffnesses of unstrengthened infilled specimens IL-0-1-17 and IC-0-1-11 were very close to each other but the ultimate lateral load of IL-0-1-17 was approximately %15 higher than IC-0-1-11. Although this proportion was expected to be vice versa, as IL-0-1-17 had lap splice deficiency, it should be noted that the compression strength of the concrete used at IL-0-1-17 was higher then IC-0-1-11.
9. The test results of IL-C1-1-8.6 indicate that the behavior of the specimen at pulling and pushing was not symmetrical. Simply because of that, the results of IL-C1-1-8.6 can not be generalized for lap splice improvement.
10. Two more CFRP retrofitted infilled frame specimens, one with lap splice deficiency and the other without, will be tested as the final part of this study. CFRP sheets will be applied only on one side of the specimens.

ACKNOWLEDGEMENTS

This study is financially supported by NATO (Project: 977231) and TUBITAK (Project: TUBITAK-ICTAG-I 575). The assistance of Burcin Malekkiani and staff of I.T.U. Structural and Earthquake Engineering Laboratory are acknowledged.

References

1. ACI Committee 440, *Guide for the Design and Construction of Externally Bonded FRP Systems for Strengthening Concrete Structures*, ACI, Farmington Hills, MI, 2001.
2. Externally Bonded FRP Reinforcement for RC Structures, Technical Report, FIB Bulletin 14, July, 2001.
3. T. C. Triantafillou, Strengthening of Masonry Structures Using Epoxy-Bonded FRP Laminates, *Journal of Composites for Construction,* **2**(2), May, 1998.
4. F. Karadogan, E. Yuksel, A. Ilki, Exterior Carbon or Glass Fibers Used To Strengthen Ordinary RC Frames with Brittle Partitioning, *Seismic Assessment and Rehabilitation of Existing Buildings, NATO SfP977231, International Advanced Research Workshop*, 335-356Izmir, Turkey, 2003.
5. U. Akgüzel, Seismic Retrofit of Brick Infilled R/C Frames with Lap Splice Problem in Columns, Msc. Thesis, Bogazici University, Istanbul, 2003.
6. U. Ersoy, G. Ozcebe, T. Tankut, U. Akyuz, E. Emrah, I. Erdem, Strengthening of Infilled Walls with CFRP Sheets, *Seismic Assessment and Rehabilitation of Existing Buildings, NATO SfP977231, International Advanced Research Workshop*, 305-334,Izmir, Turkey, 2003.

AXIAL BEHAVIOR OF RC COLUMNS RETROFITTED WITH FRP COMPOSITES

ALPER ILKI•
ONDER PEKER
EMRE KARAMUK
CEM DEMIR
NAHIT KUMBASAR
Istanbul Technical University, Civil Engineering Faculty, 34469, Maslak, Istanbul, Turkey

Abstract. Fifteen RC columns and one plain concrete column with inadequate transverse reinforcement were tested under uniaxial compression after being jacketed externally with carbon fiber reinforced polymer (CFRP) sheets. CFRP layer thickness, cross-section shapes and concrete strength were the test parameters. External confinement of columns with CFRP sheets resulted in an increase in the strength and ductility. The behavior of the CFRP jacketed columns was also predicted by the proposed stress-strain model. There was reasonable agreement between analytical behavior and experimental data.

Keywords: carbon; columns; concrete; confinement; ductility; fibers; strength

1. Introduction

It is well known that a high percentage of existing structures in earthquake prone regions of the world need to be strengthened for reducing the risk of heavy loss of life and economic losses. These structures were constructed according to older codes and/or inadequate construction practice. Particularly in developing countries, the seismic performance of the structures may be

• Asst. Prof. Dr., Alper Ilki, Istanbul Technical University, Faculty of Civil Engineering, 34469, Maslak, Istanbul, Turkey. Telephone: +90 212 285 3838, fax: +90 212 285 3838, e-mail: ailki@ins.itu.edu.tr

S.T. Wasti and G. Ozcebe (eds.), Advances in Earthquake Engineering for Urban Risk Reduction, 301–316.

significantly poor due to insufficient ductility and low concrete strength. The structural members of this type of structure may experience severe damage due to low deformability and axial capacity of the structural members. Jacketing vertical structural members with high strength CFRP composite sheets can enhance both deformability and axial capacity of the members significantly, as well as preventing the buckling of the longitudinal reinforcement.

The introduction of advanced polymer composites in the civil infrastructure has been a very rapid process and the extraordinary properties of these materials have enabled the design engineers to have greater confidence in the materials' potential and consequently to use them in various constructions including the strengthening of buildings (Hollaway, 2003). Consequently, many research projects were carried out on strengthening of existing structural members with these materials. Karbhari and Gao (1997), Toutanji (1999), Saafi et al. (1999), Fam and Rizkalla (2001) and Becque et al. (2003) developed extensive experimental data for cylinder specimens, for a variety of fiber types, orientations and jacket thickness, either for FRP jacketed concrete or concrete filled FRP tubes. Demers and Neale (1999), Lin and Liao (2004) and Ilki et al. (2004a) tested reinforced concrete columns of circular cross-section with FRP jackets. Rochette and Labossiere (2000), Wang and Restrepo (2001), Shehata et al. (2002) and Ilki et al. (2004b), tested square and rectangular concrete columns confined by FRP composites. The concrete strength of the specimens tested by Ilki et al. (2004b) was around 10 MPa. Xiao and Wu (2000) investigated the effect of concrete compressive strength and thickness of CFRP jacket and proposed a simple bilinear stress-strain model for CFRP jacketed concrete. Tan (2002) tested half scale reinforced concrete rectangular columns with a section aspect ratio of 3.65 under axial loads and investigated the effects of fiber type and configuration and fiber anchors on the strength enhancement of the columns. Ilki and Kumbasar (2002) tested both damaged and undamaged cylinder specimens, which were externally confined with different thickness of CFRP jackets, under monotonic increasing and cyclic compressive stresses. Based on experimental results they proposed simple expressions for ultimate strength and corresponding axial strain of CFRP jacketed concrete. Lam and Teng (2002) carried out an extensive survey of existing studies on FRP confined concrete and proposed a simple model based on a linear relationship between confined concrete strength and lateral confining pressure provided by FRP composites, which was quite similar to the model proposed by Ilki and Kumbasar (2002) before. Ilki and Kumbasar (2003), after testing CFRP jacketed concrete specimens with square and rectangular cross-sections, modified the expressions that they proposed earlier, to cover non-circular cross-sections. Lam and Teng (2003a, 2003b) proposed design oriented stress-strain models for both uniformly and non-uniformly confined concrete members. Ilki

et al. (2004c) tested FRP jacketed low strength concrete members with circular and rectangular cross-sections, and stated that when the unconfined concrete quality was lower, the efficiency of the FRP jackets was higher. De Lorenzis and Tepfers (2003), stated that none of the available models could predict the strain at peak stress with reasonable accuracy. Bisby et al. (2005) evaluated and modified available analytical confined concrete models to provide the best fit to the experimental data base. Tastani and Pantazopoulou (2004) studied the structural behavior of FRP confined corrosion damaged square columns with reinforcement details representative of pre-1980s.

In this study, experimental results on the uniaxial compressive behavior 15 reinforced concrete columns and 1 concrete column jacketed with CFRP sheets are presented. The average unconfined concrete strength was 31.0 MPa for 10 specimens, while the remaining 6 specimens had an average unconfined concrete strength of 15.9 MPa. The parameters of the experimental work were the thickness of CFRP jacket, cross-section shape, and unconfined concrete strength. After the tests of unconfined and CFRP jacketed specimens, it was observed that the contribution of the CFRP jackets to deformability and/or strength enhancement was remarkable for specimens with circular and non-circular cross-sections. The strength enhancement was more effective for circular cross-sections, while ultimate axial strains were higher for square and rectangular cross-sections. Although original specimens without adequate internal transverse reinforcement experienced premature buckling of the longitudinal bars, this phenomenon was delayed significantly after CFRP sheet jacketing. According to the test results, CFRP jackets were more effective in the case of low concrete strength. The compressive strengths and the corresponding axial deformations of the columns were also predicted by the empirical equations proposed by the authors before, (Ilki et al. 2004c). It was seen that these predictions were in reasonable agreement with experimental results.

Although extensive experimental data is available on FRP confined concrete, most of these studies are on small size cylinders without longitudinal and transverse reinforcement, and the unconfined concrete strengths of almost all of the tested specimens are in the range of medium to high. In this study, relatively larger size specimens with longitudinal and transverse reinforcement and different cross-section shapes were tested under uniaxial compression. Six of the specimens with different cross-sectional shapes were constructed using low strength concrete to investigate the effects of concrete quality. For simulating the columns of the existing structures, particularly in developing countries, plain reinforcement was used for all specimens.

2. Experimental Work

In this study, 15 reinforced concrete columns and 1 concrete column with circular, square and rectangular cross-section were tested under uniaxial compression. 3 specimens with circular, 4 specimens with square and 3 specimens with rectangular cross-sections with the height of 500 mm were constructed using medium strength concrete (f'_c: 31.0 MPa) and 3 specimens with circular, 3 specimens with square cross-sections were constructed using low strength concrete (f'_c: 15.9 MPa). Longitudinal reinforcement ratios, ρ_l, were around 0.01 and the concrete cover was 25 mm (outside of the hoops) for all specimens. To prevent stress concentrations around the corners of the non-circular specimens, corners were rounded with a radius of 40 mm. For all different cross-sections, the spacing of the transverse reinforcement, s, was chosen as approximately 14.5 times of the diameter of the longitudinal bars to allow buckling of longitudinal reinforcing bars under axial stresses, and for representing frequently met transverse bar spacing in relatively older structures. The specimens were tested after being jacketed with 3 or 5 plies of CFRP sheets. Specimen names were given in the form of; NS (normal strength) – R (cross-section type, either Rectangular or Circular) – 2 (cross-sectional aspect ratio for square and rectangular specimens) – 175 (spacing of the transverse bars in the test zone, in mm) – 3 (number of CFRP plies) – 40 (corner radius for square and rectangular specimens, in mm). General characteristics of the specimens are given in Table 1. In this table f'_c, b, h, D, l and n are unconfined standard cylinder strength at the age of 180 days, width, depth, diameter, length of the specimen and number of CFRP plies, respectively.

TABLE 1. Specimen characteristics

Specimen	f'_c (MPa)	Section Properties				Reinforcement		n
		Section Type	b or D (mm)	h (mm)	l (mm)	Longitudinal	Transverse	
LS-C-145-0	15.9	Circular	250		500	6-10 mm	8 mm@145 mm	0
LS-C-145-3	15.9	Circular	250		500	6-10 mm	8 mm@145 mm	3
LS-C-145-5	15.9	Circular	250		500	6-10 mm	8 mm@145 mm	5
LS-R-1-200-0-40	15.9	Square	250	250	500	4-14 mm	8 mm@200 mm	0
LS-R-1-200-3-40	15.9	Square	250	250	500	4-14 mm	8 mm@200 mm	3
LS-R-1-200-5-40	15.9	Square	250	250	500	4-14 mm	8 mm@200 mm	5
NS-C-145-0	31.0	Circular	250		500	6-10 mm	8 mm@145 mm	0
NS-C-145-3	31.0	Circular	250		500	6-10 mm	8 mm@145 mm	3
NS-C-145-5	31.0	Circular	250		500	6-10 mm	8 mm@145 mm	5
NS-R-1-200-0-40	31.0	Square	250	250	500	4-14 mm	8 mm@200 mm	0
NS-R-1-200-3-40	31.0	Square	250	250	500	4-14 mm	8 mm@200 mm	3

Specimen	f'_c (MPa)	Section Properties				Reinforcement		n
		Section Type	b or D (mm)	h (mm)	l (mm)	Longitudinal	Transverse	
NS-R-1-200-5-40	31.0	Square	250	250	500	4-14 mm	8 mm@200 mm	5
NS-R-1-000-3-40	31.0	Square	250	250	500	-	-	3
NS-R-2-175-0-40	31.0	Rect.	150	300	500	4-12 mm	8 mm@175 mm	0
NS-R-2-175-3-40	31.0	Rect.	150	300	500	4-12 mm	8 mm@145 mm	3
NS-R-2-175-5-40	31.0	Rect.	150	300	500	4-12 mm	8 mm@145 mm	5

Ready mixed concrete was used for both medium and low strength concrete specimens. The concrete mix-proportions and fresh concrete characteristics for medium (NS) and low strength (LS) concrete are given in Table 2, respectively. For both mixtures, ordinary Portland cement with 28 days compressive strength of 42.5 MPa and a mid-range superplasticizer were used, where the maximum aggregate size was around 10 mm. For the medium and low strength concrete, Water/Cement ratios were 0.74 and 1.4 and Water/Binder ratios were 0.74 and 1.1, respectively. The 180 days standard cylinder strength, f'_c, was 31.0 MPa and 15.9 MPa, respectively for medium and low strength concrete.

TABLE 2. Mix-proportion (kg/m^3), fresh concrete properties (cm)

Concrete	Cement	Water	Sand	CS	Gravel	Admix.	Fly Ash	Slump	fdast
NS	285	210	413	496	925	1.43	-	20-23	30
LS	150	210	638	286	982	1.14	40	20-24	31

CS: crushed sand, fdast: flow diameter after slump test

For longitudinal reinforcement 10 mm, 14 mm and 12 mm diameter bars were used for specimens with circular, square and rectangular cross-sections, respectively. For transverse reinforcement 8 mm diameter bars were used for all specimens. A clear cover of 20 mm was formed for longitudinal reinforcement at the bottom and top faces of the specimens for preventing direct loading of reinforcing bars. Only mild plain bars were used both for longitudinal and transverse reinforcement for reflecting the columns of existing relatively older structures in developing countries. The mechanical properties and details of reinforcing bars are given in Table 3 and Figure 1, respectively.

TABLE 3. Mechanical properties of reinforcing bars

Bar Type	Nominal d_b (mm)	f_y (MPa)	ε_y	$f_{s,max}$ (MPa)	$\varepsilon_{s,max}$	f_{su} (MPa)	ε_{su}
ϕ8	8.0	476	0.0024	-	-	-	-
ϕ10	10.1	367	0.0018	523	0.19	377	0.27
ϕ12	12.2	339	0.0017	471	0.23	335	0.30
ϕ14	13.8	345	0.0017	477	0.23	294	0.31

d_b: bar diameter, f_y: yield strength, ε_y: yield strain, $f_{s,max}$: tensile strength, $\varepsilon_{s,max}$: strain corresponding to $f_{s,max}$, f_{su}: ultimate stress, ε_{su}: ultimate elongation

CFRP sheets behave linear elastically till rupture. The effective thickness of the CFRP sheets was 0.165 mm per ply. The geometrical and mechanical properties of the CFRP sheets are given in Table 4. In this table f^*_{fu} , E_f, ε^*_{fu} and t_f are the tensile strength, elasticity modulus, ultimate rupture strain and effective thickness, respectively. These properties are taken from the specifications of the manufacturer.

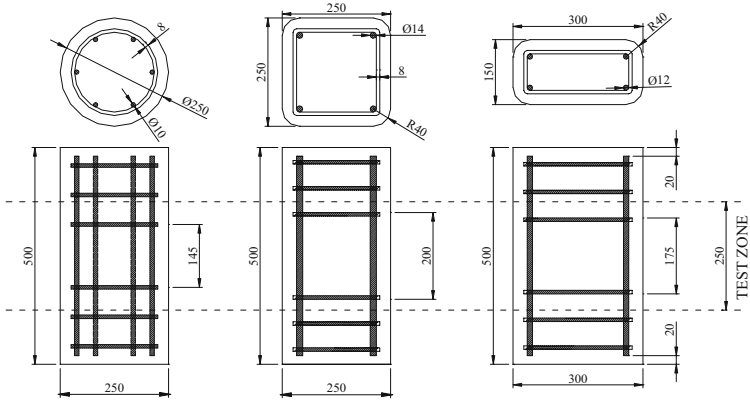

Figure 1. Details of reinforcing bars

TABLE 4. Geometrical and mechanical properties of CFRP

f^*_{fu} (MPa)	E_f (GPa)	ε^*_{fu}	t_f (mm)	Unit weight (kg/m^3)
3,430	230	1.5%	0.165	1,820

Specimens were produced in the Structural and Earthquake Engineering Laboratory of Istanbul Technical University and cured for 7 days. The specimens were tested after being jacketed with 3 or 5 plies of CFRP sheets. All of the retrofitted specimens were jacketed externally by unidirectional CFRP sheets in transverse direction with 0-degree orientation. Before jacketing the specimens with CFRP sheets, surface preparation procedure was carried out. This procedure included sanding, cleaning, forming one layer of epoxy-polyamine primer and one layer of epoxy putty. Then epoxy adhesive was used for bonding CFRP sheets on the specimens. Additional layers of epoxy adhesive were applied between the CFRP jacket plies and on the outer ply of CFRP jacket. The compressive and tensile strengths of the epoxy system were around 80 and 50 MPa, respectively. Tensile elasticity modulus and ultimate elongation of the epoxy system were around 3000 MPa and 0.025, respectively. The steps during jacketing were carried out with great care to prevent stress concentrations due to surface irregularities and to obtain the tight fitting of the CFRP jackets on the specimens. For obtaining satisfactory bonding, 150 mm overlap was formed at the end of the wrap. The specimen production steps can be seen in Figure 2.

Figure 2. Specimen preparation

3. Test Setup

The specimens were tested under monotonic uniaxial compressive loads by using an Amsler universal testing machine with the capacity of 5000 kN. Two different gage lengths were used for measurement of average axial strains by displacement transducers. For this purpose, four transducers in the gage length of 270 mm and six transducers in the gage length of 500 mm were used, Figure 3. Axial and transverse strains at mid-height were also measured by surface strain gages with the gage length of 60 mm for all of the specimens. For specimens with circular cross-section, two vertically and two horizontally bonded strain gages were used with 180 degree intervals around perimeter, for non-circular specimens vertical strain gages were bonded on two opposite sides. For specimens with square cross-sections two horizontal strain gages were bonded on two opposite sides. For rectangular specimens two horizontal strain gages were bonded on short and long sides. To obtain the deformations of the longitudinal and transverse reinforcement, strain gages were used with the gage lengths of 5 and 3 mm, respectively. For data acquisition a 50 channel TML-ASW-50C switch box and a TML-TDS-303 data logger were used. The general appearance of the test setup is shown in Figure 3.

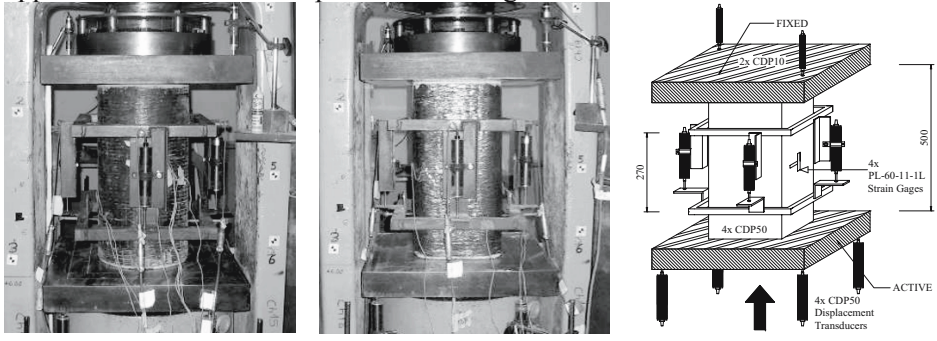

Figure 3. Test setup

4. Test Results

The test results are presented in Table 5. As observed for the NS specimens with circular, square and rectangular cross-sections, the ratios of confined concrete compressive strength to unconfined concrete member strength (f'_{cc}/f'_{co}) were 2.7, 1.6 and 1.5 for 3 plies and 3.6, 2.2 and 1.8 for 5 plies of CFRP jackets, respectively. For the LS specimens with circular and square cross-sections, f'_{cc}, increased 4.2 and 2.8 times for 3 plies and 6.3 and 3.2 for CFRP jackets of 5 plies, respectively. Note that unconfined concrete member strength, f'_{co} was assumed to be 85% of the standard cylinder strength (f'_c). Test results showed that CFRP jackets were more effective in the case of low concrete strength and strength enhancement was more significant for circular specimens, while only slight difference was observed between the strength enhancements of square and rectangular specimens. The axial strains corresponding to CFRP jacketed concrete strengths (ε_{cc}), for the NS specimens with circular, square and rectangular cross-sections were 16.5, 16.5 and 17.0 times that of unconfined concrete (ε_{co}) for 3 plies and 22.0, 26.0 and 20.5 for 5 plies of CFRP jackets, respectively. For the LS specimens with circular and square cross-sections, ε_{cc}, increased 21.5 and 27.5 times for 3 plies, 32.5 and 34.5 times for CFRP jackets of 5 plies, respectively. The axial strain corresponding to unconfined concrete strength, ε_{co}, was assumed equal to 0.002. For the NS specimens, the transverse strains on CFRP jackets at failure, ε_{ch}, were between 0.012 and 0.015 independent of the jacket thickness, with an average of 0.013, which is about 87% of the manufacturer's value. For the LS specimens with square cross-sections, ε_{ch} was 0.015. Only strain gages that could work until failure were taken into consideration. Rupture of CFRP sheets was generally around mid-height of the testing zone. Rupture of CFRP sheets was 3-4 vertical cuts with heights of 40-70 mm for jackets of 3 plies. More vertical cuts with lower heights for jackets of 5 plies were observed. For square and rectangular specimens, the rupture of sheets was around the corners just after the rounded portion. The number and height of vertical cuts were similar with circular specimens (Figure 4). Damage pattern was similar for NS and LS specimens.

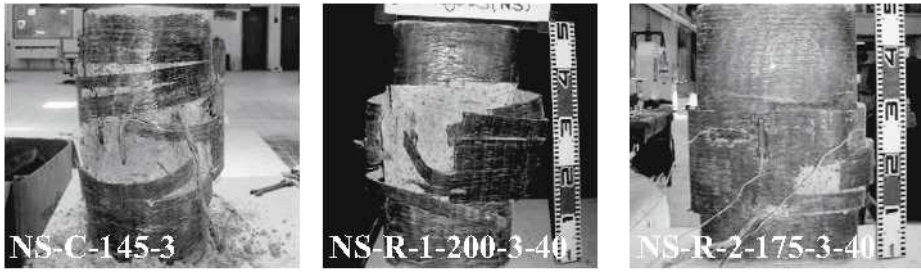

Figure 4. Specimens after test

TABLE 5. Test results

Specimen	f'_{co} (MPa)	f'_{cc} (MPa)	ε_{cc}	ε_{ch}	κ_a	ρ_f	$\frac{f'_{cc}}{f'_{co}}$	$\frac{\varepsilon_{cc}}{\varepsilon_{co}}$
LS-C-145-3	13.5	56.1	0.043	0.007*	1.00	0.0079	4.2	21.5
LS-C-145-5	13.5	84.8	0.065	0.013*	1.00	0.0132	6.3	32.5
LS-R-1-200-3-40	13.5	37.4	0.055	0.015	0.66	0.0079	2.8	27.5
LS-R-1-200-5-40	13.5	51.6	0.069	0.015	0.66	0.0132	3.2	34.5
NS-C-145-3	26.4	71.8	0.033	0.012	1.00	0.0079	2.7	16.5
NS-C-145-5	26.4	94.3	0.044	0.013	1.00	0.0132	3.6	22.0
NS-R-1-200-3-40	26.4	42.0	0.033	0.014	0.66	0.0079	1.6	16.5
NS-R-1-200-5-40	26.4	58.3	0.052	0.015	0.66	0.0132	2.2	26.0
NS-R-1-000-3-40	26.4	41.1	0.024	0.013	0.66	0.0079	1.6	12.0
NS-R-2-175-3-40	26.4	40.6	0.034	0.012	0.56	0.0099	1.5	17.0
NS-R-2-175-5-40	26.4	47.8	0.041	0.014	0.56	0.0165	1.8	20.5

f'_{co} : unconfined concrete member strength, f'_{cc}: confined concrete strength, ε_{cc} : ultimate axial strain in 500mm gage length, ε_{ch} : maximum measured transverse strain in 60 mm gage length, κ_a : efficiency factor, ρ_f : ratio of wrapping material to the concrete cross-section, *out of order before reaching peak stress

The axial stress – axial strain relationships in the gage length of 500 mm, for the NS specimens with circular, square and rectangular cross-sections are given in Figure 5. As seen in this figure, significant enhancement in strength and deformability was provided by CFRP jacketing. As the thickness of the jacket increased, the enhancement in the axial stress-axial strain behavior became more remarkable.

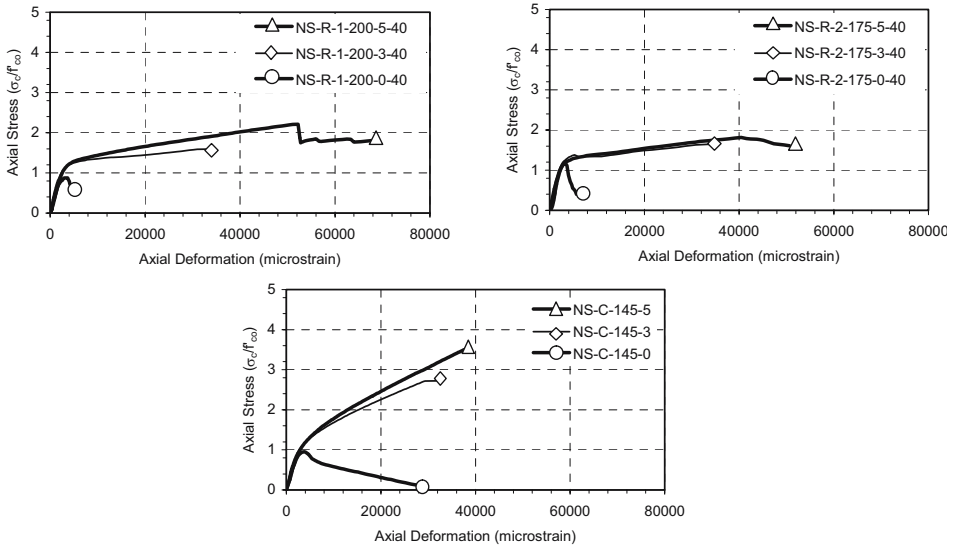

Figure 5. Axial stress – axial strain relationships for NS specimens

The axial stiffness of the specimens did not show a tendency to increase with increasing jacket thickness. All stress-strain relationships are given with the non-dimensional vertical axis and while determining the stress-strain relationship of confined concrete, the stress contribution of longitudinal reinforcing bars was subtracted. The axial stress of the longitudinal bars, $\sigma_{s(\varepsilon)}$ was calculated from Eqs. (1) and (2) before strain-hardening. In the strain-hardening region, for 10 diameter bars Eq. (3), for 12 mm and 14 mm bars Eq. (4) was used for calculating stress in the longitudinal bars, respectively. These equations were obtained from tensile coupon tests. In these equations, E, ε_s, ε_y and ε_{sh} represent elastic modulus, axial deformation of the longitudinal bars, steel yielding strain and strain corresponding to strain-hardening, respectively.

- For $\varepsilon_s < \varepsilon_y$: $\sigma_{s(\varepsilon)} = E \times \varepsilon_s$ (1)
- For $\varepsilon_y < \varepsilon_s < \varepsilon_{sh}$: $\sigma_{s(\varepsilon)} = f_y$ (2)
- For $\varepsilon_s > \varepsilon_{sh}$: 10 mm bars; $\sigma_{s(\varepsilon)} = -5148.5 \times \varepsilon_s^2 + 1997.6 \times \varepsilon_s + 329.1$ (3)
- For $\varepsilon_s > \varepsilon_{sh}$: 12-14 mm bars; $\sigma_{s(\varepsilon)} = -2993.2 \times \varepsilon_s^2 + 1376.9 \times \varepsilon_s + 318.7$ (4)

For obtaining the net stress of the specimen σ_{net}, Eq. (5) was used. In this equation P, A_s and A_c are axial load, area of longitudinal reinforcement and concrete cross-sectional area, respectively.

$$\sigma_{net} = \frac{P - \left(\sigma_{s(\varepsilon)} \times A_s\right)}{A_c - A_s} \tag{5}$$

It should also be noted that although the major contribution of the enhancement in strength and deformability was provided by the external CFRP jacket, the internal transverse reinforcement had also some influence. The contribution of internal transverse reinforcement was minimal for the specimens with circular, square and rectangular cross-section. In Figure 6, the comparison of axial and transverse deformations obtained from internal reinforcement and surface strain gages of circular specimen NS-C-145-3 are presented. As seen in this figure, since the spacing of transverse reinforcement was relatively high, the tensile strains of transverse reinforcement were below yield strain. The axial strains of longitudinal reinforcement and surface strain gages were similar. It should also be noted that the longitudinal reinforcement yielded as a result of increasing axial stress.

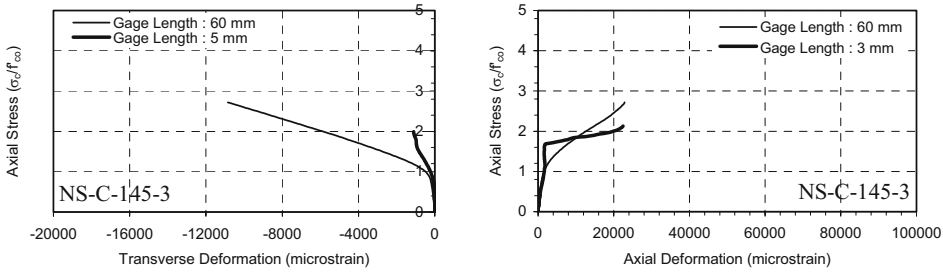

Figure 6. Comparison of internal reinforcement strain gages and surface strain gages

As seen in Figure 7, ultimate transverse strains of CFRP jackets were around 0.012~0.015, independent of the jacket thickness. Transverse strains were around the same level for the specimens with rectangular cross-sections. For the LS specimens, transverse strains were around 0.013~0.015, independent of the jacket thickness.

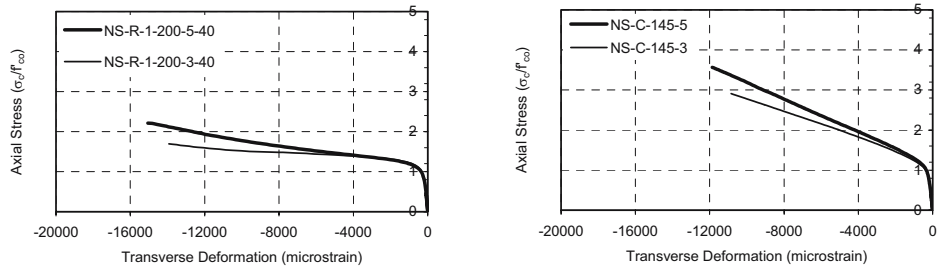

Figure 7. Axial stress – transverse deformation relationships for NS specimens in 60 mm gage length

For the same thickness of CFRP jacket, all the specimens with circular, square and rectangular cross-section experienced enhancement in strength and deformability. While the strength enhancement was more remarkable for the specimens with circular cross-section, specimens with square and rectangular cross-section exhibited higher axial deformations, particularly for jackets of 5 plies.

The effect of unconfined concrete strength on the axial stress-axial strain relationships is demonstrated in Figure 8. As seen in this figure, CFRP jackets were more effective in the case of low concrete strength in terms of strength and deformability enhancement.

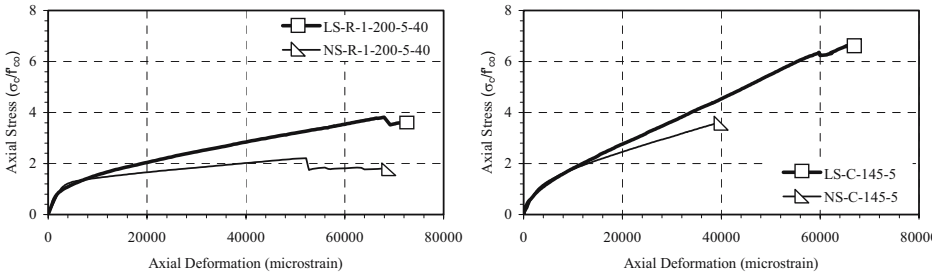

Figure 8. Comparison of LS – NS specimens with circular and square cross-sections in 500 mm gage length

5. Prediction of Confined Concrete Strength and Corresponding Axial Strain

For prediction of ultimate strengths and axial strains of CFRP jacketed specimens, the empirical equations proposed by Ilki et al. (2004c) were used, (Eqs. 6 and 7). These equations were proposed based on experimental results obtained from the specimens with circular and rectangular cross-sections. In previous equations, f'_{cc} and ε_{cc} are the confined concrete strength and corresponding axial strain, b and h are the width and depth of the rectangular member, f'_l is the effective lateral confinement stress and ε_{co} is the strain corresponding to unconfined concrete strength and it is assumed as 0.002 in this study. For specimens with circular cross-section, the h/b ratio was given as 1.

$$\left[\frac{f'_{cc}}{f'_{co}}\right]_{CFRP} = \left[1 + 2.4\left(\frac{f'_l}{f'_{co}}\right)^{1.2}\right] \tag{6}$$

$$\left[\frac{\varepsilon_{cc}}{\varepsilon_{co}}\right]_{CFRP} = \left[1 + 20\left(\frac{h}{b}\right)\left(\frac{f'_l}{f'_{co}}\right)^{0.5}\right] \tag{7}$$

Effective lateral confinement stress, f'_l can be obtained by Eq. (8). In this equation, κ_a is the efficiency factor that is to be determined based on the section geometry as the ratio of effectively confined cross-sectional area to the gross cross-sectional area, E_{frp} and ρ_f are the tensile elasticity modulus and ratio of wrapping material to the concrete cross-section, respectively. The ultimate tensile strength of FRP sheets wrapped around concrete members ($\varepsilon_{h,rup}$) is assumed to be 70% of the ultimate strain corresponding to tensile strength of FRP (ε_{frp}). A similar result was also predicted by Lam and Teng (2003a) before, where they used a range between 58.6% and 85.1% depending on the FRP material instead of 70%.

$$f_l' = \frac{\kappa_a \rho_f \varepsilon_{h,rup} E_{frp}}{2} \tag{8}$$

While predicting the confined concrete strength and corresponding axial strain, the contribution of internal transverse reinforcement (ITR) was also taken into account. For this purpose, the empirical equations proposed by Mander et al. (1988) were used for strength and ultimate axial strain, respectively, (Eqs. 9 and 10). After determining the strength and deformability enhancements provided by the external CFRP jacket and the internal transverse reinforcement separately, the total enhancement in strength and corresponding strain was calculated by using Eqs. (11) and (12). The predictions for the enhancements provided by CFRP jacket and ITR are presented in Table 6.

TABLE 6. Comparison of experimental and analytical results

Specimen	Experimental		Analytical		f'_l (FRP)	f'_l (ITR)	$\frac{f'_{cc(FRP)}}{f'_{co}}$	$\frac{f'_{cc(ITR)}}{f'_{co}}$	$\frac{f'_{cc_{exp}}}{f'_{cc_{analy}}}$	$\frac{\varepsilon_{cc_{exp}}}{\varepsilon_{cc_{analy}}}$
	f'_{cc} (MPa)	ε_{cc}	f'_{cc} (MPa)	ε_{cc}	(MPa)	(MPa)				
LS-C-145-3	56.1	0.043	39.0	0.039	9.56	0.72	3.24	1.34	1.44	1.10
LS-C-145-5	84.8	0.060	57.5	0.049	15.93	0.72	4.73	1.34	1.48	1.33
LS-R-1-200-3-40	37.4	0.055	27.7	0.030	6.31	0.18	1.98	1.09	1.35	1.81
LS-R-1-200-5-40	51.6	0.069	38.7	0.038	10.51	0.18	2.77	1.09	1.33	1.82
NS-C-145-3	71.8	0.033	49.9	0.028	9.56	0.72	1.71	1.18	1.44	1.18
NS-C-145-5	94.3	0.044	65.9	0.034	15.94	0.72	2.31	1.18	1.43	1.29
NS-R-1-200-3-40	42.0	0.033	38.9	0.022	6.31	0.18	1.43	1.05	1.08	1.50
NS-R-1-200-5-40	58.3	0.052	48.6	0.028	10.52	0.18	1.80	1.05	1.20	1.88
NS-R-1-000-3-40	41.1	0.024	37.7	0.022	6.31	-	1.43	-	1.09	1.11
NS-R-2-175-3-40	40.6	0.034	39.0	0.043	6.75	0.03	1.47	1.01	1.04	0.80
NS-R-2-175-5-40	47.8	0.041	49.3	0.056	11.25	0.03	1.86	1.01	0.97	0.74
								Average	1.26	1.32
								S. Deviation	0.19	0.32

$$\left[\frac{f'_{cc}}{f'_{co}}\right]_{ITR} = \left[-1.254 + 2.254\sqrt{1+\frac{7.94 f'_l}{f'_{co}}} - 2\frac{f'_l}{f'_{co}}\right] \tag{9}$$

$$\left[\frac{\varepsilon_{cc}}{\varepsilon_{co}}\right]_{ITR} = \left[1 + 5\left(\frac{f'_{cc}}{f'_{co}} - 1\right)\right] \tag{10}$$

$$\left[\frac{f'_{cc} - f'_{co}}{f'_{co}}\right]_{TOTAL} = \left[\frac{f'_{cc}}{f'_{co}} - 1\right]_{CFRP} + \left[\frac{f'_{cc}}{f'_{co}} - 1\right]_{ITR} \tag{11}$$

$$\left[\frac{\varepsilon_{cc} - \varepsilon_{co}}{\varepsilon_{co}}\right]_{TOTAL} = \left[\frac{\varepsilon_{cc}}{\varepsilon_{co}} - 1\right]_{CFRP} + \left[\frac{\varepsilon_{cc}}{\varepsilon_{co}} - 1\right]_{ITR} \tag{12}$$

For combined contribution of FRP jacket and internal transverse reinforcement, Wang and Restrepo (2001) have determined the effective lateral confinement stresses provided by FRP jacket and internal transverse reinforcement separately and then used the model proposed by Mander et al. (1988) for concrete confined by internal steel reinforcement by replacing the transverse confinement stress provided by internal reinforcement with the total transverse confinement stress provided by internal reinforcement and external FRP jacket.

6. Conclusions

After the uniaxial compression tests on medium and low strength circular, square and rectangular reinforced concrete columns without sufficient transverse reinforcement, the following conclusions were derived.

The CFRP jackets increased the compressive strength and corresponding axial strain of the columns with circular, square and rectangular cross-sections. For the NS specimens, confined concrete compressive strength (f'_{cc}) and corresponding axial strain (ε_{cc}) increased between 1.5~3.6 times and 16.5~26.0 times, respectively. For the LS specimens, f'_{cc} and ε_{cc} increased between 2.8~6.3 times and 21.5~34.5 times, respectively While the strength enhancement was more pronounced for circular cross-sections, deformability enhancement was greater for rectangular cross-sections. The increase in deformability was significant even in the case of rectangular cross-sections with h/b ratio of 2.

Although the spacing of transverse bars in the test zone and the diameter of longitudinal bars were chosen for allowing buckling of the longitudinal bars, in the case of CFRP jacketed specimens, the premature buckling of the longitudinal reinforcement was prevented and the contribution of longitudinal reinforcing bars to the axial resistance and ductility was maintained until very large axial strains. It is apparent that the possible tendency of longitudinal bar buckling did not have a negative influence on the behavior of CFRP sheets.

Independent of the jacket thickness, the measured maximum transverse deformations of CFRP jackets for NS and LS specimens were between 0.012~0.015 and 0.013~0.015, respectively.

The test results showed that CFRP jackets were more effective in the case of low concrete strength in terms of strength and deformability enhancement.

The empirical equations, proposed by the authors earlier, predicted the compressive strength and corresponding axial strains of the specimens with a reasonable accuracy.

ACKNOWLEDGMENTS

This study is a part of FP6 Project: LESSLOSS. The authors wish to thank Yapkim-Degussa Construction Chemicals Company, Set Italcementi Group, Mr. Tayfun Pala, Mr. Bulent Turgut and Mr. Metin Tiryaki for their contributions during the preparations of the specimens. The assistance of Mr. Volkan Koc and Mr. Esen Yilmaz during experiments is also acknowledged.

References

Becque, J., Patnaik, A.K., and Rizkalla, S.H. 2003, Analytical models for concrete confined with FRP tubes, *J. Compos. Const.,* **7**(1): 31–38.

Bisby, L.A., Dent, A.J.S., Green, M.F. 2005, Comparison of confinement models for fiber–reinforced polymer–wrapped concrete, *ACI Structural Journal*, **102**(1):62–72.

De Lorenzis, L., and Tepfers, R. 2003, Comparative study of models on confinement of concrete cylinders with fiber-reinforced polymer composites, J. *Compos. Const.,* **7**(3):219–237.

Demers, M., and Neale, K.W. 1999, Confinement of reinforced concrete columns with fibre-reinforced composite sheets-an experimental study, *Can. J. Civ. Eng.,* **26**(2):226–241.

Fam, A.Z., and Rizkalla, S.H. 2001, Confinement model for axially loaded concrete confined by circular fiber-reinforced polymer tubes, *ACI Struct. Jour.,* **98**(4):451–461.

Hollaway, L.C. 2003, The evolution of and the way forward for advanced polymer composites in the civil infrastructure, *Cons. and Build. Mats.,* **17**:365–378.

Ilki, A., and Kumbasar, N. 2002, Behavior of damaged and undamaged concrete strengthened by carbon fiber composite sheets, *Struct. Eng. and Mech.,* **13**(1):75–90.

Ilki, A., and Kumbasar, N. 2003, Compressive behaviour of carbon fibre composite jacketed concrete with circular and non–circular cross–sections, *Journal of Earthquake Engineering*, **7**(3):381–406.

Ilki A., Peker O., Karamuk E., Kumbasar N., 2004a External confinement of low strength brittle reinforced concrete short columns, *International Symposium on Confined Concrete, Changsha, China*, on CD–ROM.

Ilki A., Koc V., Peker O., Karamuk E., Kumbasar N., 2004b, Strengthening of RC Columns with Inadequate Transverse Reinforcement *The Second Int. Conf. on FRP Comps. in Civil Engineering, 8–10 Dec. 2004, Adelaide, Australia*, 211–218.

Ilki, A., Kumbasar, N., and Koc, V. 2004c, Low strength concrete members externally confined with FRP sheets, *Struct. Eng. and Mech.,* **18**(2):167–194.

Karbhari, V.M., and Gao, Y. 1997, Composite jacketed concrete under uniaxial compression–verification of simple design equations, *ASCE Journal of Materials in Civil Engineering,* **9**(4):185–193.

Lam, L., and Teng, J.G. 2002, Strength models for fiber–reinforced plastic–confined concrete, *J. Struct. Eng.*, **128**(5):612–623.

Lam, L., and Teng, J.G. 2003a, Design–oriented stress–strain model for FRP–confined concrete, *Construction and Building Materials*, **17**:471–489.

Lam, L., and Teng, J.G. 2003b, Design–oriented stress–strain model for FRP–confined concrete in rectangular columns, *Jour. of Reinf. Plast. and Comps*., **22**(13):1149–1186.

Lin, H., Liao, C., 2004, Compressive strength of reinforced concrete column confined by composite material, *Composites Structures*, **65**:239–250

Mander, J.B., Priestley, M.J.N., and Park, R. 1988, Theoretical stress–strain model for confined concrete, ASCE *Journal of the Strucural Division*, **114**(8):1804–1826.

Rochette, P., and Labossiere, P. 2000, Axial testing of rectangular column models confined with composites, *ASCE Jour. of Comp. for Cons*., **4**(3):129–136.

Saafi, M., Toutanji, H., and Li, Z. 1999, Behavior of concrete columns confined with fiber reinforced polymer tubes, *ACI Mat. Journal*, **96**(4):500–509.

Shehata I.A.E.M., Carneiro L.A.V., Shehata L.C.D., 2002, Strength of short concrete columns confined with CFRP sheets, *Mat. and Struct*., **35**(245):50–58.

Tan, K.H. 2002, Strength enhancement of rectangular reinforced concrete columns using fiber–reinforced polymer, *J. Compos. Const*., **6**(3):175–183.

Tastani, S.P., and Pantazopoulou S.J., 2004, Experimental evaluation of FRP Jackets upgrading RC corroded columns with substandard detailing, *Engineering Structure,* **26**:817–829

Toutanji, H.A. 1999, Stress–strain characteristics of concrete columns externally confined with advanced fiber composite sheets, *ACI Mat. Jour*., **96**(3):397–404.

Wang, Y.C., and Restrepo, J.I., 2001, Investigation of concentrically loaded reinforced concrete columns confined with glass fiber–reinforced polymer jackets, *ACI Structural Journal*, **98**(3):377–385.

Xiao, Y., and Wu, H., 2000, Compressive behaviour of concrete confined by carbon fiber composite jackets, *ASCE Journal of Materials in Civil Engineering*, **12**(2):139–146.

COLLAPSE OF LIGHTLY CONFINED REINFORCED CONCRETE FRAMES DURING EARTHQUAKES

JACK P. MOEHLE•
Pacific Earthquake Engineering Research Center, University of California, Berkeley, USA

WASSIM GHANNOUM
Pacific Earthquake Engineering Research Center, University of California, Berkeley, USA

YOUSEF BOZORGNIA
Pacific Earthquake Engineering Research Center, University of California, Berkeley, USA

Abstract. Post earthquake studies show that the primary cause of reinforced concrete building collapse during earthquakes is the loss of vertical-load-carrying capacity in critical building components leading to cascading vertical collapse, rather than loss of lateral-load capacity. In cast-in-place beam-column frames, the most common cause of collapse is failure of columns, beam-column joints, or both. This study emphasizes failure of columns using data from laboratory studies. Failure models are incorporated in nonlinear dynamic analysis software, enabling complete dynamic simulations of building response including component failure and progression of collapse. This approach enables more realistic simulation of building collapse than is possible using simplified assessment procedures, and provides insight into the conditions that cause collapse and the variability of collapse as a function of input ground motions.

Keywords: collapse; column failure; beam-column joint failure; nonlinear dynamic analysis; drift history

• Jack P.Moehle, e-mail: moehle@peer.berkeley.edu

S.T. Wasti and G. Ozcebe (eds.), Advances in Earthquake Engineering for Urban Risk Reduction, 317–332.

1. Introduction

Post earthquake studies show that the primary cause of reinforced concrete building collapse during earthquakes is the loss of vertical-load-carrying capacity in critical building components leading to cascading vertical collapse, rather than loss of lateral-load capacity. In cast-in-place beam-column frames, the most common cause of collapse is failure of columns, beam-column joints, or both. Once axial failure occurs in one or more components, vertical loads arising from both gravity and inertial effects are transferred to adjacent framing components. The ability of the frame to continue to support vertical loads depends on both the capacity of the framing system to transfer these loads to adjacent components and the capacity of the adjacent components to support the additional load. When one of these conditions is deficient, progressive failure of the building can ensue.

Post-earthquake reconnaissance of reinforced concrete buildings provides some insight into the prevalence of collapse among populations of heavily shaken buildings. Otani (1999) reports damage statistics of reinforced concrete buildings, with damage defined in three categories:

1. Operational damage (light to minor damage): columns or structural walls were slightly damaged in bending, and some shear cracks might be observed in non-structural walls;
2. Heavy damage (medium to major damage): spalling and crushing of concrete, buckling of reinforcement, or shear failure in columns were observed, and lateral resistance of shear walls might be reduced by heavy shear cracking; and
3. Collapse (partial and total collapse), which also included those buildings demolished at the time of investigation.

Figure 1 presents the distribution of damage for four earthquakes reported by Otani (1999). For the 1985 Mexico earthquake, data are restricted to the lakebed zone of Mexico City; for the 1990 Luzon, Philippines earthquake, data are from Baguio City; for the 1992 Erzincan, Turkey earthquake, data are from two heavily damaged residential areas of Erzincan; and for the 1995 Kobe earthquake, data are from areas of highest seismic intensity in Kobe and restricted to buildings constructed before enforcement of the 1981 Building Standard Law. Figure 1 shows that even in areas of highest damage in famously damaging earthquakes, the collapse rates of lightly detailed reinforced concrete buildings are relatively low.

Given the relatively low collapse rate shown in Figure 1, it is reasonable to conclude that refined engineering tools might be useful to identify those buildings that are most collapse prone, so that resources could be focused on

seismic mitigation of those buildings. By reducing the number of buildings urgently requiring retrofit from a large number to a small fraction of that number, mitigation programs that are stymied by huge retrofit costs may become more tractable. Ultimately, this is one of the main objectives of this work reported here.

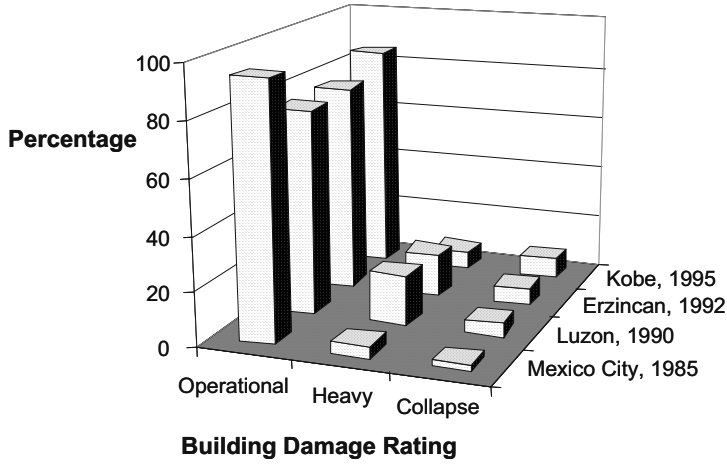

Figure 1. Damage statistics from four earthquakes

Small steps have been made toward the development and implementation of refined engineering tools for building response simulation near and beyond the collapse initiation stage. Laboratory studies of reinforced concrete columns with light transverse reinforcement have identified primary variables that contribute to loss of column axial-load capacity. These models have been implemented in nonlinear dynamic analysis software that can be used to simulate building collapse during earthquake shaking. In one example, the software is used in a limited study to simulate building response to a series of strong ground motions recorded within a relatively small region during the 1994 Northridge earthquake. The results provide some insight into the collapse of building frames as well as the influence of local ground motion on collapse. The following text details some of these developments.

2. Shear and Axial Load Failure of Reinforced Concrete Columns

Of primary interest in this study is the behavior of reinforced concrete columns with relatively light transverse reinforcement and with proportions that enable the column to yield in flexure prior to developing shear or axial failure. Columns with these details and proportions may be able to sustain moderately

large lateral deformations prior to failure; a challenge is to estimate the lateral drift at which failure occurs.

For a column that yields in flexure, the lateral strength is limited to the flexural strength, and therefore can be calculated with relatively high accuracy. The column may subsequently sustain apparent shear failure. Although the details of the mechanism leading to shear failure are not fully understood, it is postulated that crack opening and tensile straining reduce the shear-carrying capacity of the concrete through loss of aggregate interlocking but primarily excessive strain demand on the compression zone, while spalling and bond distress lead to degradation of the transverse reinforcement contribution. To identify whether shear failure is likely, it is necessary to estimate whether the shear strength will degrade to a value approaching the flexure strength.

Sezen and Moehle (2004) report a model for shear strength of columns that initially yield in flexure. The empirical model is based on theoretical concepts of shear resistance but is calibrated to test data. The shear strength is defined as

$$V_n = V_s + V_c = k\frac{A_{st} f_{yt} d}{s} + k\left(\frac{0.5\sqrt{f_c'}}{a/d}\sqrt{1+\frac{P}{0.5\sqrt{f_c'}A_g}}\right)0.8A_g \quad \text{(MPa)} \tag{1}$$

where V_s and V_c are shear contributions assigned to steel and concrete; k is a parameter equal to 1 for $\mu_\delta \leq 2$, equal to 0.7 for $\mu_\delta \geq 6$, and varies linearly for intermediate μ_δ values; μ_δ = displacement ductility; A_{st} = area of shear reinforcement parallel horizontal shear force within spacing s; f_{yt} = yield strength of transverse reinforcement; d = effective depth (=0.8h, where h = section depth parallel shear force); P = axial compression force; f_c' = concrete compressive strength (MPa); A_g = gross section area, and a/d = shear span/effective depth (value limited between 2 and 4). Figure 2 compares measured and calculated shear strengths. The mean ratio of measured to calculated strength and its coefficient of variation are 1.06 and 0.15.

If shear strength degrades to below flexure strength, shear failure is anticipated. Elwood and Moehle (2004) developed an empirical model to estimate deformation at shear failure using the same data as shown in Figure 2. For this model, shear failure was defined as the loss of twenty percent of the maximum shear strength. The data show that deformation at shear failure decreases with increasing shear stress, increasing axial stress, and decreasing transverse reinforcement index. According to the model, deformation at shear failure is defined as

$$\frac{\delta_s}{L} = \frac{3}{100} + 4\rho'' - \frac{1}{40}\frac{v}{\sqrt{f_c'}} - \frac{1}{40}\frac{P}{A_g f_c'} \geq \frac{1}{100} \quad \text{(MPa)} \tag{2}$$

where ρ'' = transverse steel ratio and v = nominal shear stress. Figure 3 compares results from tests and from Equation (2). The mean ratio of measured to calculated strength and its coefficient of variation are 0.97 and 0.34.

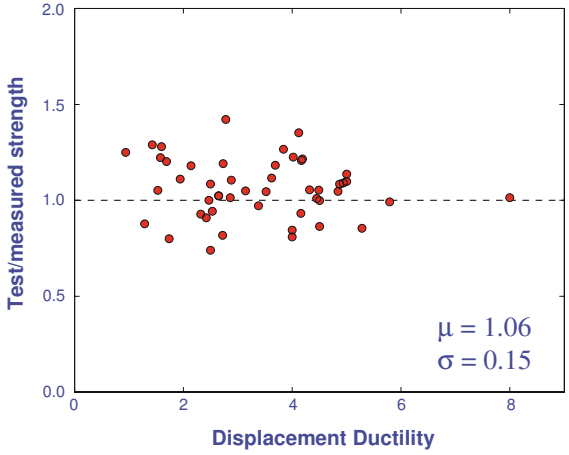

Figure 2. Ratios of strengths measured during tests to strengths calculated by the strength model

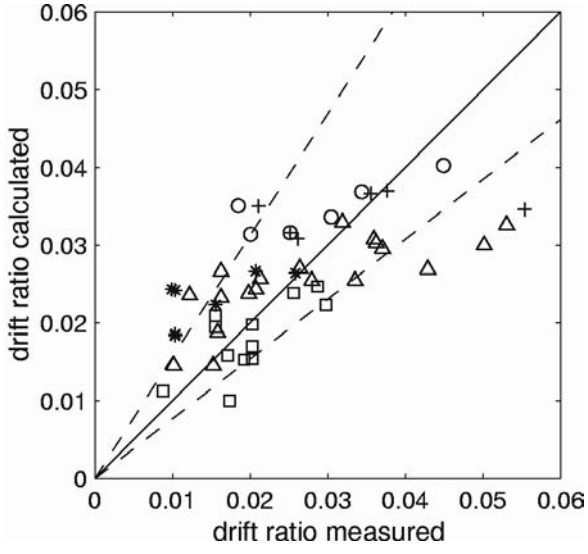

Figure 3. Displacement capacity measured and calculated by Equation (2)

Axial load failure may coincide with onset of shear failure or may occur at larger drift. Elwood and Moehle (2004) use concepts of shear-friction and experimental data to derive an expression for the drift at axial load failure of columns initially yielding in flexure, then developing shear failure, and finally developing axial failure. The drift at shear failure is estimated as

$$\delta_a = \frac{4}{100} \frac{1+\tan^2\theta}{\tan\theta + P\left(\frac{s}{A_{st} f_{yt} d_c \tan\theta}\right)} \tag{3}$$

in which θ = critical crack angle (assumed = 65 deg) and d_c = depth of the column core measured parallel to the applied shear. Figure 4 compares results of tests and Equation (3).

It is important to note that the models presented were for columns with rectangular cross section, relatively light and widely spaced transverse reinforcement, subjected to unidirectional lateral load. Additional data are needed to validate models for other conditions

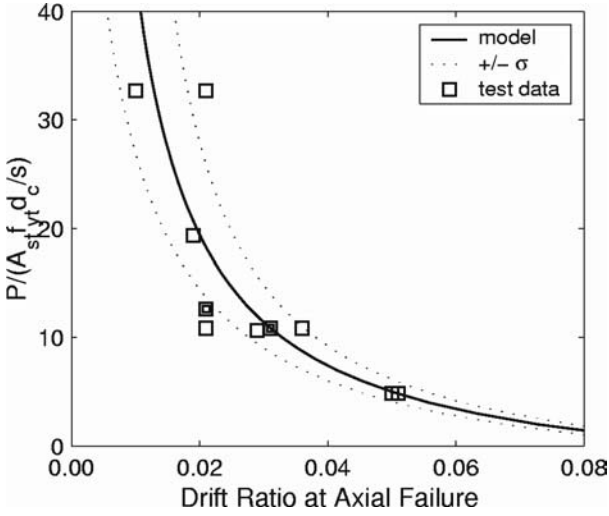

Figure 4. Drift capacity curve based on shear-friction model

3. Implementation of Axial Failure Model in OpenSees

Shear and axial failures were modeled in OpenSees by adding at the end of the columns zero-length Limit State spring elements developed by Elwood (2002) (Figure 5). These elements have differing backbone curves before and after failures are detected. Prior to shear failure, the shear springs are elastic with stiffness corresponding to the shear stiffness of the column. Once the element reaches the limit curve defined by an empirical shear-drift relation (Elwood 2002) the shear spring backbone curve is modified to a degrading hysteretic

curve (Figure 6). The shear degrading slope K_{deg} is calibrated based on observations from previous tests (Nakamura and Yoshimura, 2002), which have shown that axial failure is initiated when shear strength degrades to about zero.

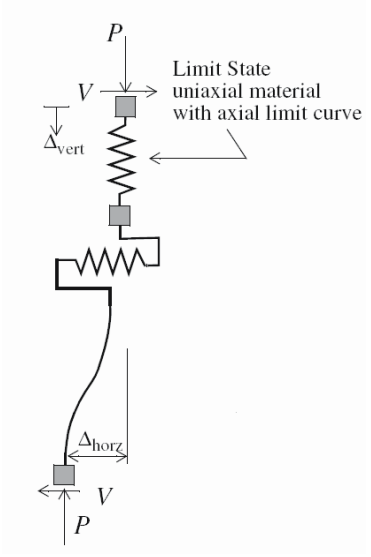

Figure 5. Zero-length springs

Similarly, the zero-length axial springs have a "rigid" backbone prior to reaching the axial load-drift limit curve (Elwood 2002) (Figure 6). This limit curve is defined by the shear-friction model and, hence, assumes that shear failure has already occurred in the element. Once the column element reaches that drift limit curve its axial load-vertical deformation backbone is modified to a degrading hysteretic material model. Because the shear-friction model only describes compression failures, the backbone is only redefined for compressive axial loads. Beyond the initiation of axial failure, a coupling effect exists between the horizontal and vertical deformations where an increase in horizontal drift causes an increase in vertical deformation. This effect is modeled in the vertical spring element with an iterative procedure that keeps the column response on the horizontal drift-axial load curve defined by the shear-friction model. When the earthquake motion reverses direction, the vertical spring backbone is redefined to an elastic response with a reduced elastic stiffness to account for the damage in the column. This modification also halts the axial degradation in the column as it is assumed that the critical shear crack closes which prevents any further sliding along that crack.

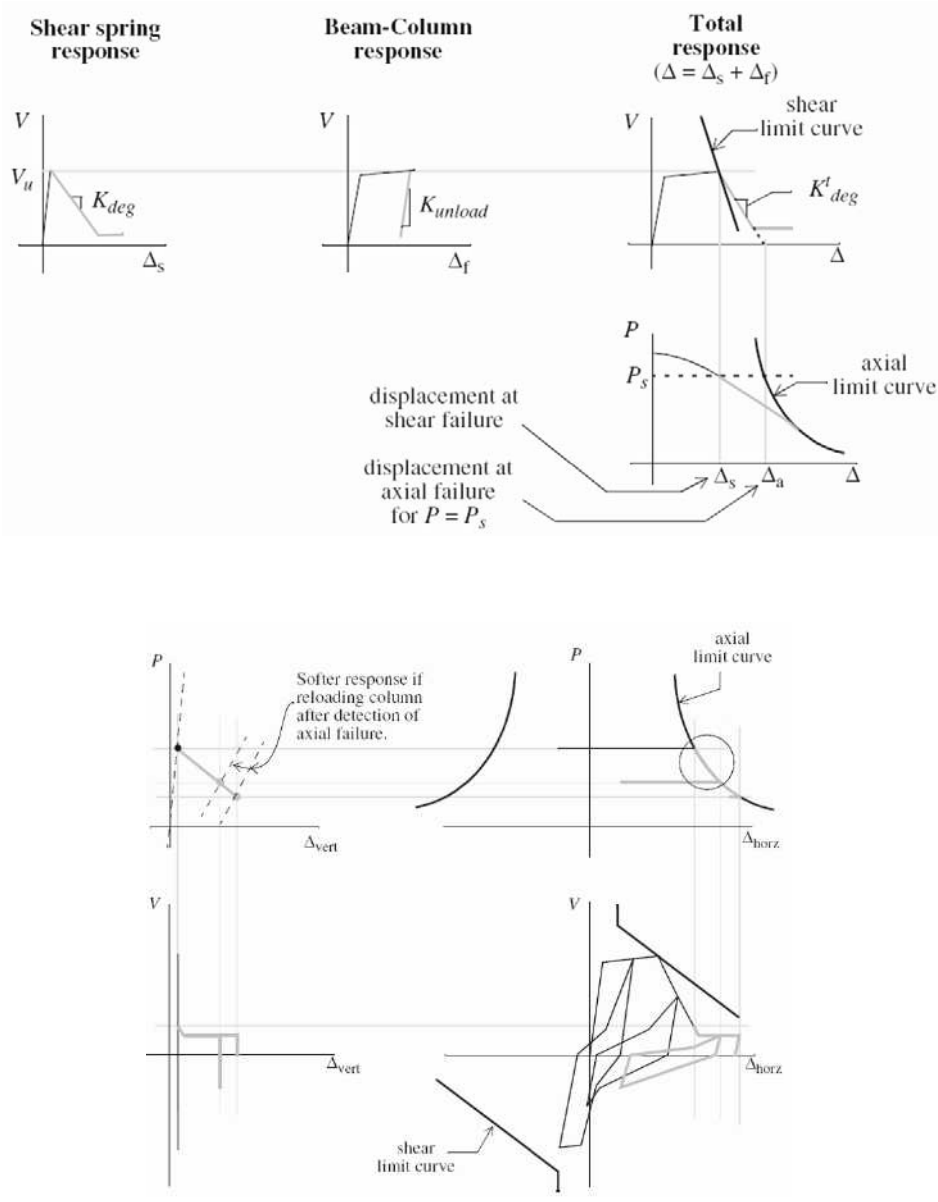

Figure 6. Shear and axial zero-length element responses and limit curves (Elwood 2002)

4. Study of the Dynamic Response of a Building Frame

4.1. BUILDING FRAME DESCRIPTION

As an illustration of the use of the models and implementation described previously, a 3-bay, 3-story RC frame was analyzed for a series of different ground motions. The building frame was dimensioned to represent typical 1960s and 1970s office building construction in California. The building frame (Figure 7) was designed for third-scale shake table testing at the University of California, Berkeley under an ongoing research effort aimed at understanding non-ductile RC frame collapse mechanisms. Two of the columns in this frame have non-ductile detailing with widely spaced ties, 90º hooks, and no ties in the joints, while the other two columns have ductile detailing as per ACI 318-2002 recommendations. The ductile columns are to better control the collapse of the structure during shake table testing.

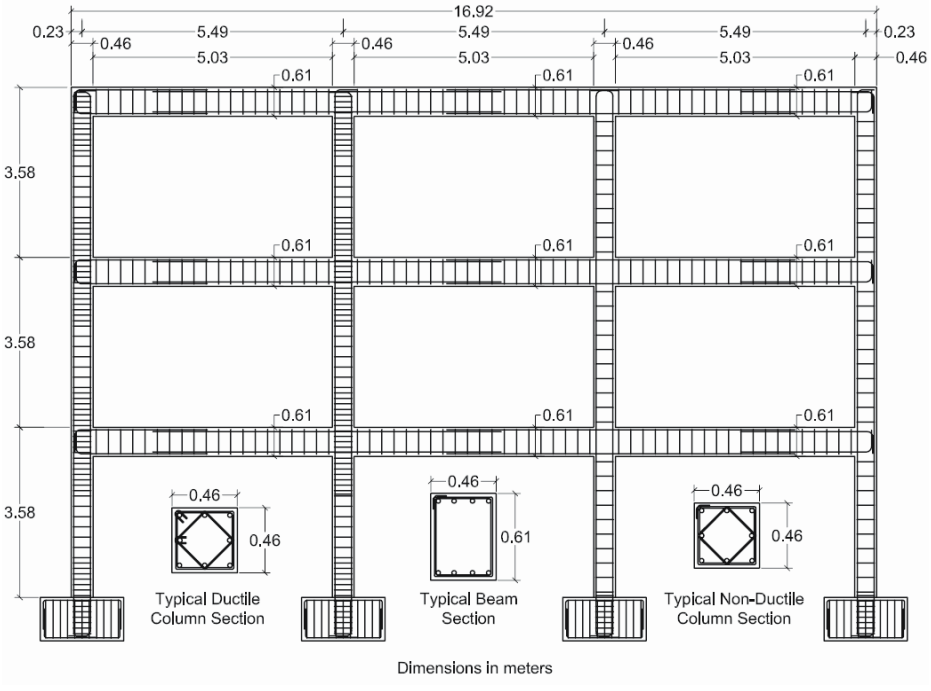

Figure 7. Frame details

Beam depth and reinforcement were chosen to create a weak-column strong-beam mechanism as well as to reduce joint shear stresses. The resulting concentration of damage in the non-ductile columns is intended to force axial collapse in these columns at high drifts. The beam reinforcement details are

typical of those in moment-resisting frames built in the 1960s and 1970s in California.

Masses added to the frame for the dynamic analysis are equivalent to those expected considering dead loads for a two-way slab system typical of office building construction. The masses result in approximately $0.1A_g f'_c$ axial load on the first-floor center columns. The resulting structure has initial elastic first-mode period of 0.60 sec.

Target concrete cylinder strength f'_c is 24.6 MPa and target steel yield strength f_y is 486 MPa. Concrete is modeled in OpenSees using the concrete01 uniaxial material model (Kent-Scott-Park model with a degraded unloading/reloading stiffness according to Karsan and Jirsa). Concrete is modeled with no tension strength. Steel is modeled using the steel01 model (bilinear with kinematic hardening). Flexure, shear and axial effects of components were modeled, and slip of longitudinal reinforcement from joints was considered using rotational springs at column and beam ends. Effects of splices were not modeled.

4.2. SELECTED EARTHQUAKE GROUND MOTIONS

The structural model is subjected to seven ground accelerations recorded during the 1994 Northridge, California, earthquake. By choosing the records from a single earthquake, the earthquake-to-earthquake variability of ground motions is excluded from the analysis. Additionally, by selecting a set of recording sites located in the same general area, spatial variability of the recorded ground motion is relatively reduced. The selected strong motion recording stations are listed in Table 1.

TABLE 1. Strong ground motion records used in this study

Station	R_{seis} (km)	R_{rup} (km)	NEHRP site class	V_{s30} (m/s)	PGA (g)	PGV (cm/s)
Sylmar - Converter Sta East	6.20	5.19	C	370.52	0.64	93.60
Sylmar - Olive View Med FF	6.20	5.30	C	440.54	0.71	100.70
Sylmar - Converter Sta	6.30	5.35	D	251.24	0.74	109.90
Jensen Filter Plant	6.40	5.43	C	373.07	0.50	102.70
Newhall - W Pico Canyon Rd.	6.70	5.48	D	285.93	0.38	79.10
Newhall - Fire Sta	7.00	5.92	D	269.14	0.59	85.70
Rinaldi Receiving Sta	7.40	6.50	D	282.25	0.63	110.10

Notes: R_{seis} = Campbell & Bozorgnia distance to seismogenic portion of the fault plane; R_{rup} = Distance to fault rupture plane; *NEHRP = U.S. National Earthquake Hazard Reduction Program; V_{s30} = Average shear-wave velocity in the top 30-meter of soil; PGA = Peak ground acceleration, geometric mean of the two horizontal components; PGV = Peak ground velocity, geometric mean of the two horizontal components*

The locations of the recording stations, along with the epicenter and the surface projection of the fault rupture plane are mapped in Figure 8. As provided in Table 1, the selected recording stations constitute a closely spaced cluster of sites located between 5.19 and 6.5 km from the fault plane. The sites have either NEHRP site class 'C' or 'D'. The shear-wave velocity in the top 30-meter of soil is in the range of 251 to 441 m/s (see Table 1).

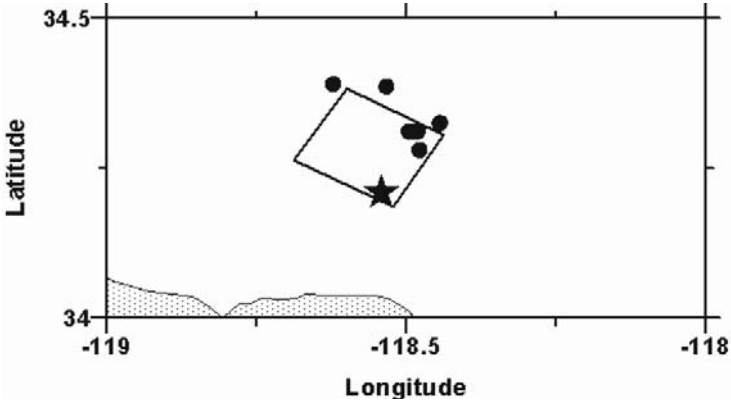

Figure 8. The 1994 Northridge, California, earthquake: epicenter (star symbol), surface projection of the fault plane, and locations of the selected recording stations (solid circles) are marked

Figure 9 shows 5% damped elastic response spectra of the horizontal ground motions at the selected sites. This figure shows the variability of the ground motion as elastic structural response is concerned. The effects of such variability on nonlinear dynamic response of the structural models will be discussed in the next section.

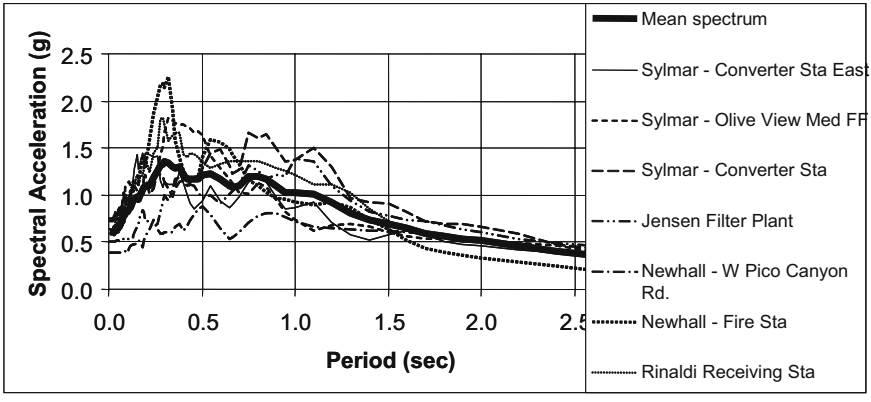

Figure 9. Response spectra for 5% damping of the selected 1994 Northridge records. The spectra are for the geometric mean of the two horizontal components

The site classifications at the recording stations, average shear-wave velocity at top 30-m of soil, various distance measures, and the processed ground motion records have been obtained from the recently enhanced and expanded PEER strong motion database. The expanded PEER ground motion database includes strong motion records at more than 3,000 stations recorded in more than 170 worldwide earthquakes from 1935 to 2003.

4.3. ANALYSIS RESULTS

Dimensioning and detailing of the frame were chosen to concentrate damage in the non-ductile columns at the first floor level, with little or no damage in the upper floor columns prior to collapse. A non-linear static analysis with a first-mode horizontal loading pattern was performed to identify the critical response and damage stages for the structure (Figure 10).

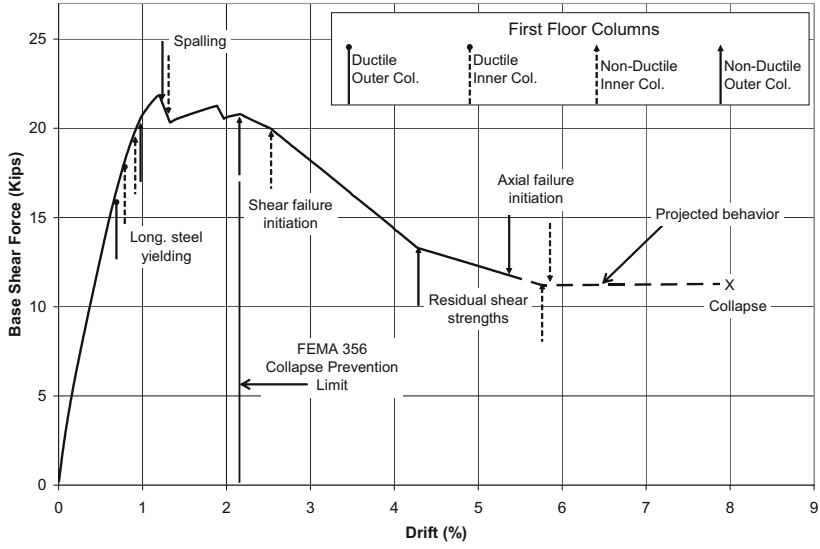

Figure 10. First-floor drift versus base-shear response

The calculated response and damage sequence for the frame is as follows:

1. Yielding of all first floor column longitudinal steel occurs at a first floor horizontal drift of approximately 0.8%.
2. At approximately 2% horizontal drift, shear failures are initiated in the non-ductile columns.
3. Between approximately 2% and 7% horizontal drift, there is a gradual loss of shear capacity in the non-ductile columns until a residual shear/friction capacity is reached

4. At that drift level loss of axial load capacity in the non-ductile columns is initiated. It is important to note that these particular drift levels are mainly a function of the axial load on the columns.
5. As the structure is pushed to even higher drifts, it collapses on the non-ductile side of the frame dragging the ductile side with it. A drift of 8% on the first floor was deemed the collapse drift for this frame. This final stage can be altered by choosing "stronger" framing on the ductile side in which case only a partial collapse would have been observed.

This displacement-controlled behavior prompted the use of the first floor drifts as the damage parameter for comparison among the different ground motion simulations. Figure 11 shows the first floor drift responses for the seven ground motions. Table 2 summarizes the maximum drift values as well as the behavior of the frame.

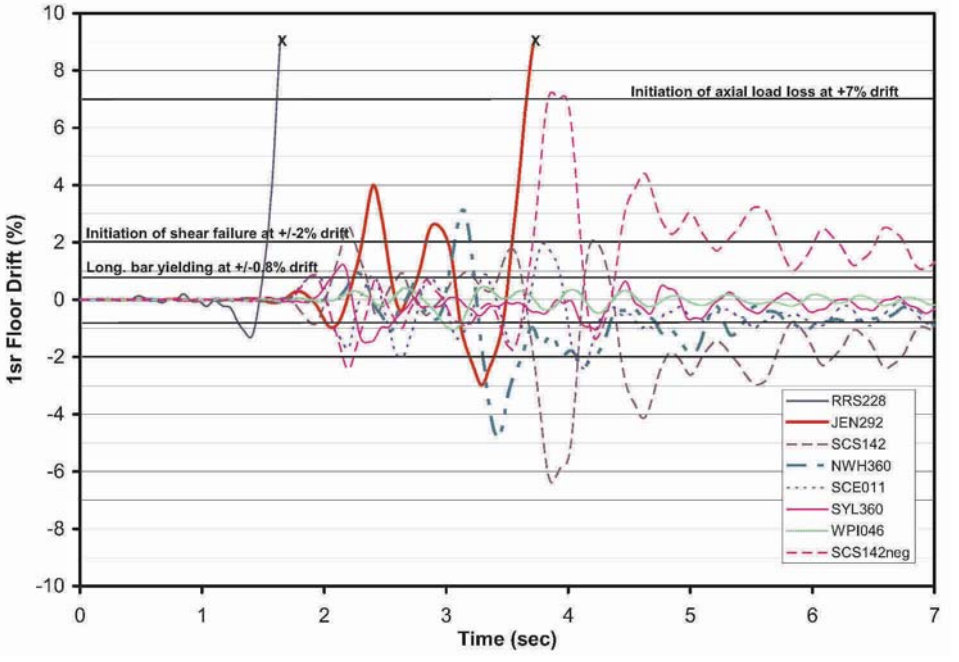

Figure 11. First-floor drift response history

The results summarized in Table 2 show tremendous variation in the frame responses when subjected to ground motions obtained from the same earthquake at sites of close proximity. These responses ranged from almost no yielding of the longitudinal steel to complete collapse of the frame.

It is evident here that local geological and soil conditions have significant effects on the earthquake response of a structure. As well, observing that the

analysis results were obtained using the strongest directional component of the ground motions suggests that the orientation of the structure can have a significant effect on its response. This point was demonstrated with the SCS142 ground motion to which the frame was subjected in the East-West direction as well the West-East direction. For the EW direction which increased the axial load in the non-ductile columns at peak drift due to frame action, axial load carrying capacity degradation was calculated in these columns. As for the other direction, which imparted significant uplift on the non-ductile columns at peak drift, no axial degradation was calculated.

TABLE 2. Summary table of first floor drifts and frame damage

Ground Motion	Max. / Min. 1st Floor Drift	Damage
RRS228	> 9% / -1.3%	complete collapse of frame
JEN292	> 9% / -3.0%	complete collapse of frame
SCS142	2.5% / -6.4%	longitudinal steel yielding in all 1st floor columns - shear failure up to residual in non-ductile 1st floor columns - no axial load carrying capacity degradation
SCS142neg*	7.2% / -2.4%	longitudinal steel yielding in all 1st floor columns - shear failure up to residual in non-ductile 1st floor columns - axial load loss initiation in non-ductile 1st floor columns – no collapse
NWH360	3.1% / -4.8%	longitudinal steel yielding in all 1st floor columns - shear failure initiation with only partial degradation in non-ductile 1st floor columns
SCE011	2.0% / -2.4%	longitudinal steel yielding in all 1st floor columns - shear failure initiation with only slight degradation in non-ductile 1st floor columns
SYL360	1.2% / -1.5%	longitudinal steel yielding in all 1st floor columns
WPI046	0.5% / -1.0%	longitudinal steel just yielding in all 1st floor columns

** SCS142neg is the negative of the SCS142 ground motion (180° rotation)*

The dynamic analysis results (Figure 11) suggest that the response of any given building structure is rather sensitive to the details or the ground motion. Among populations of collapse-prone buildings, only a small fraction may sustain collapse in any given earthquake. Different earthquakes of similar scale but different detail may produce very different collapse scenarios. Thus, the

small collapse rates of Figure 1 may not necessarily equate to equivalently small rates of seismic upgrading requirements. Upgrading of many buildings may be necessary if collapse mitigation is to be realistically achieved.

It should be noted that the frame analysis software used here has relatively limited validation – therefore, the outcome of this analysis should be considered preliminary and only suggest the path forward. Additional shake table tests are needed for validation of the software.

5. Conclusions

A model for shear and axial failure of lightly-confined reinforced concrete columns is developed for columns that sustain shear and axial failure following initial flexural yielding. Lateral strength can be estimated relatively accurately as the lateral force corresponding to flexural yield. Propensity for shear failure can be identified using a shear strength model in which shear strength following flexural yield degrades with increasing deformation demand. The drift at shear failure varies with transverse reinforcement amount and inversely with nominal axial and shear stresses. Drift at axial failure varies with transverse reinforcement and inversely with axial load.

The model is implemented in nonlinear dynamic analysis software to demonstrate the feasibility of conducting nonlinear dynamic analysis including shear and axial failure of columns. A three-story building model is subjected numerically to a series of ground motions recorded at stations located between 5.19 and 6.5 km from the fault plane of the 1994 Northridge earthquake. Response of the frame is found to be sensitive to the ground motions, with responses to individual ground motions varying from almost no yielding of longitudinal steel to total collapse. The results suggest that observed low collapse rates during strong earthquake shaking may not be reflective of small numbers of collapse-prone buildings but instead may be a manifestation of the vagaries of the ground motion. Experimental studies to validate the numerical results, and additional numerical studies to identify the characteristics of strong ground motion best correlated with collapse, are needed.

ACKNOWLEDGMENT

This work was supported by the Pacific Earthquake Engineering Research Center through the Earthquake Engineering Research Centers Program of the National Science Foundation under award number EEC-9701568. Any opinions, findings, and conclusions or recommendations expressed are those of the authors and do not necessarily reflect those of the National Science Foundation. Ground motion data were obtained from the PEER ground motion database (http://peer.berkeley.edu)

References

Elwood, K., and Moehle, J., 2005, Drift Capacity of Reinforced Concrete Columns with Light Transverse Reinforcement, *Earthquake Spectra*, Earthquake Engineering Research Institute, **21**(1):71-89.

Elwood, K., 2002, Shake Table Tests and Analytical Studies on the Gravity Load Collapse of Reinforced Concrete Frames, Doctoral Dissertation, University of California, Berkeley.

Elwood, K., and Moehle, J., 2004, Evaluation of existing reinforced concrete columns, *Proceedings*, 13th World Conference on Earthquake Engineering, Vancouver.

Nakamura, T., and Yoshimura, M., 2002, Gravity Load Collapse of Reinforced Concrete Columns with Brittle Failure Modes, *Journal of Asian Architecture and Building Engineering*, **1**(1):21-27.

OpenSees, 2004, *Open System for Earthquake Engineering Simulation*, PEER Center, University of California, Berkeley, http://opensees.berkeley.edu

Otani, S., 1999, RC Building Damage Statistics and SDF Response with Design Seismic Forces, *Earthquake Spectra*, Earthquake Engineering Research Institute, **15**(3):485 - 501.

Sezen, H., and Moehle, J., 2004, Shear Strength Model for Lightly Reinforced Concrete Columns, *Journal of Structural Engineering*, ASCE, Vol. 130, No. 1692.

EVALUATION OF APPROXIMATE NONLINEAR PROCEDURES FOR OBSERVED RESPONSE OF A SHEAR WALL STRUCTURE

POLAT GULKAN*
Earthquake Engineering Research Center, Department of Civil Engineering, Middle East Technical University, 06531 Ankara, Turkey

AHMET YAKUT
Earthquake Engineering Research Center, Department of Civil Engineering, Middle East Technical University, 06531 Ankara, Turkey

ILKER KAZAZ
Earthquake Engineering Research Center, Department of Civil Engineering, Middle East Technical University, 06531 Ankara, Turkey

Abstract. This article presents an analytical study carried out to investigate seismic response of a lightly reinforced stiff shear wall structure subjected to ground motions classified as near- or far-field. A five-story lightly reinforced shear wall model structure that has been studied both experimentally and analytically in the context of a coordinated research project has been employed. Several response parameters were obtained by linear and nonlinear analyses under a suite of 55 ground motion records on firm soils. Additional analyses are performed to investigate the validity and range of applicability of the most widely used approximate displacement based analysis procedures. The approximate procedures considered are found to be deficient in representing the actual response of the structure employed here regardless of the type of excitation.

Keywords: near-field; far-field; approximate procedure; shear wall; pushover analysis

* Polat Gulkaŋ, Department of Civil Engineering, Middle East Technical University, 06531 Ankara, Turkey; Tel: +90-312-210 2446, Fax: +90-312-210 1193 E-mail: a03516@metu.edu.tr

S.T. Wasti and G. Ozcebe (eds.), Advances in Earthquake Engineering for Urban Risk Reduction, 333–351.

1. Introduction

The increasing use of simplified procedures in performance-based earthquake engineering has led to comprehensive research resulting in improved techniques applicable for buildings with regular features. The nuclear engineering community has initiated research to investigate the validity of simplified displacement based procedures for near field response of stiff structures built for nuclear facilities. In view of this, a series of benchmark shaking table experiments were carried out in the Saclay Nuclear Center, France. One particular specimen, CAMUS1, has been further studied numerically under a coordinated research program sponsored by the International Atomic Energy Agency (IAEA) and JRC. This specimen is a 1/3-scale model of a 5- story reinforced concrete building, a typically representative example for stiff nuclear structures (Combescure, 2002). In the first phase of the investigations, a reliable and representative analytical model of the tested specimen was developed based on the successful duplication of physical conditions and loadings imposed during the tests. The experimentally measured results were predicted numerically with a reasonable level of accuracy (Kazaz et al., 2005). This article is complementary to the first phase, and deals with the analytical assessment of the seismic response of the CAMUS1 under a suite of fifty-five ground motion records. The ground motion set selected for the study contains representative far and near field earthquake excitations recorded on firm soils. The near-fault records used in this study do not necessarily exhibit the forward directivity characteristic, i.e. a long-duration pulse of high velocity dominating the event. Only a few records we use contain such dominant velocity pulses.

The response of the structure calculated using nonlinear response history analyses is considered as “exact,” because the analytical model constructed has successfully predicted the response (including local strains, curvatures, shear forces and moments) of the specimen on the shaking table in the preceding stage. The structure is then re-analyzed using approximate static procedures. The results are examined to evaluate accuracy and validity of the approximate nonlinear static analysis procedures for similar types of structures. Most nonlinear response procedures are based on the dynamics of SDOF systems, so this exercise also provides an understanding of the degree of extrapolation that is acceptable in arriving at estimates of the response of MDOF systems.

1.1. ANALYTICAL AND EXPERIMENTAL MODEL

The experimental program consisted of testing a 1/3-scale representative component of a 5-story reinforced concrete shear wall building on shaking table at Commissariat a l’Energie Atomique (CEA) in the Saclay Nuclear Center.

The specimen, named CAMUS1, had a total mass of 36 tons with additional masses attached to it. The walls had no openings, and were linked by square slabs (1.7m × 1.7m). A heavily reinforced concrete footing allowed anchorage to the shaking table. The total height of the model was 5.10 m. They had a width of 1.7 m and thickness of 6 cm. The specimen had a measured fundamental natural frequency of 7.24 Hz. The dimensions and the mass distribution of the specimen are shown in Figure 1. The experimental study provided the measured response quantities of the model shear walls subjected to different input seismic motions.

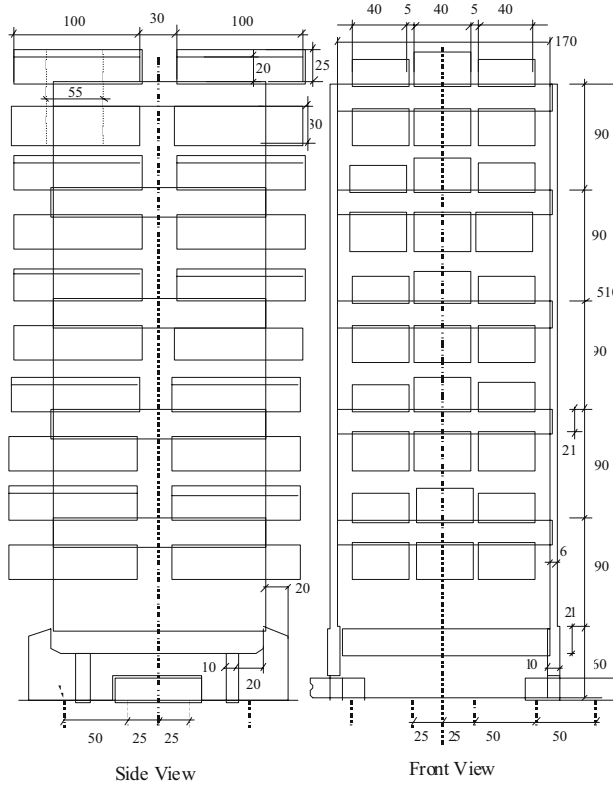

Figure 1. View of the CAMUS specimen and sketch of the walls and masses

A finite element model of the tested shear walls as shown in Figure 2 was created in ANSYS V7.0 (2002). The actual material properties and boundary conditions in the experiment were implemented in the model to reflect the required aspects of the test specimen. The finite element model of the test specimen has a computed fundamental frequency of 7.28 Hz.

The experimentally measured and numerically computed response quantities including top story displacement, base shear, bending moment at the base, top story horizontal accelerations and the local results such as strains were found to be in good agreement. The results, given in detail elsewhere (Kazaz et al., 2005) clearly indicate that the analytical model developed here is able to display the inelastic response of the tested specimen quite satisfactorily. The same model has been employed in this study to perform further analyses for a suite of 55 ground motions.

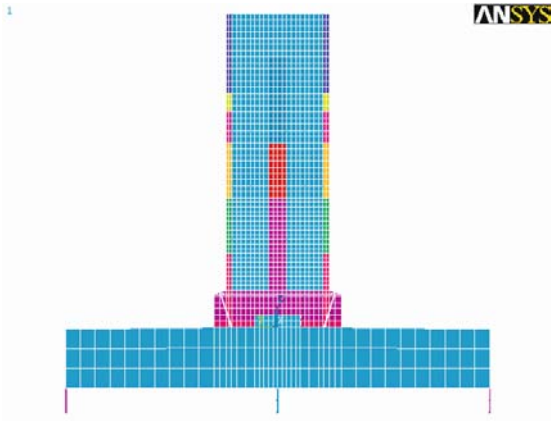

Figure 2. The model created in ANSYS

1.2. GROUND MOTION DATABASE

The selected ground motion set consists of 55 records obtained from 20 earthquakes of which 31 are near-field seismograms. The database was intended to cover both NFE and FFE records. These ground motion records were classified according to their site-to-source distance based on the recommendations given by Martinez-Pereira and Bommer (1998). The records used in the analyses were intended to reflect the characteristics of firm site ground motions, i.e., wave forms rich in high frequency content and effective in the short period range on a narrow period interval (0.1-0.4 sec). The ground motions used in the experimental and analytical studies are listed in Table 1. Some records were generated by scaling the original ground motions. Since the model is a 1/3 scale of a real structure, the ground motions used in the analyses were also scaled in the time axis by a factor of $1/\sqrt{3}$. Ground motions named as Run1 through Run4 are signals that were used in the shaking table experiments. Run1 is a synthetic ground motion and Run2 is the 1957 San Francisco Earthquake recorded in Golden Gate Park. Run3 and Run4 were obtained by scaling Run1 and Run2, respectively. The rest are natural records.

2. Pushover Analyses

A complete time history analysis is quite demanding and computationally expensive as compared to static analysis. As an alternative, nonlinear static pushover analyses are carried out by applying lateral forces at the mass locations of the structural system, assuming that they will account for the distribution of inertia forces acting at the story levels during the dynamic excitation of the structure. This procedure can provide considerable insight for the nonlinear behavior of the structure although it conceals unresolved uncertainties and approximations. The load patterns that are typically used in the pushover analyses are calculated by utilizing modal analyses of the structure. The first mode shape or a combination of modes is used as the representation of the dynamic loading. In the elastic range of the dynamic excitation, results obtained with these prescribed load patterns agree with the exact solution in many cases.

The CAMUS structure was analyzed using the pushover analysis procedure to compare with the "exact" results. A triangular lateral load pattern representing the contribution of each story mass to the inertia force relative to the sum of inertia forces was utilized since the dynamic behavior of the model was observed to be dominated by the first mode. The pushover curve is plotted in Figure 3 which also displays the results of nonlinear dynamic analyses from the ground motions contained in the dataset.

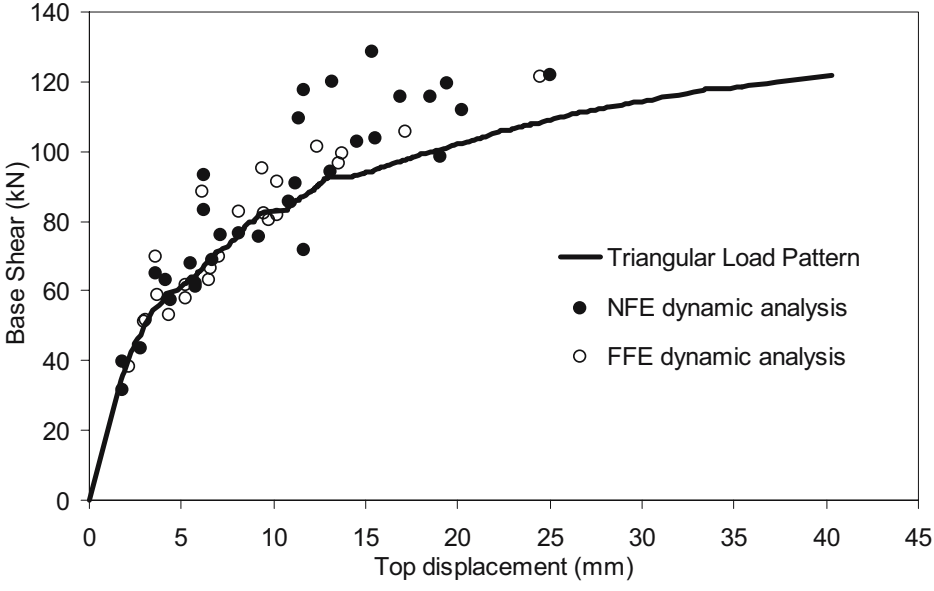

Figure 3. Pushover curve compared with dynamic analysis results

3. Displacement Based Procedures

The motivation for research dealing with the development of simplified procedures that are used to estimate the inelastic displacement demand of structures has essentially been to find an alternative approach as substitute to nonlinear response history analyses that involve analytical complexity and computational expense. These simplified procedures generally rely on the reduction of MDOF systems to equivalent SDOF representations. The two most commonly used procedures of this nature are the Capacity Spectrum Method of ATC-40 (1996), and the Displacement Coefficient Method contained in FEMA 356 (2000). These procedures have been evaluated by many researchers, highlighting their weaknesses as well as their adequacy. Sometimes conflicting findings have led to uncertain and incompatible conclusions on their range of validity. Unlike many previous investigations that either deal with SDOF systems (Miranda, 2001; Miranda et al., 2002; and Chopra et al., 2003) or generic MDOF systems (Chintanapakdee and Chopra, 2003), this study evaluates the accuracy of these procedures for the CAMUS1 model that has been studied experimentally and analytically. It is based on nonlinear response history analyses under a comprehensive suite of ground motions. In addition, the nonlinear analyses of the equivalent SDOF systems and a proposed modification to the CSM have been carried out to test their success in matching the exact results.

3.1. SDOF ANALYSES

The inelastic response (generally the roof displacement with which damage may be associated) of a MDOF system can be estimated from the corresponding equivalent SDOF system in varying degrees of accuracy depending on the particular ground motion used in the analysis and the structural properties of the MDOF system. There is a divergence between the ductility demands imposed on multistory buildings and SDOF systems. Two particular parameters give rise to the differences between the “input” and “output” ductility demands (deformations) of SDOF and MDOF systems. These are higher mode contributions and inter-story drift demands (local response behavior of MDOF system). These two characteristics cannot be incorporated directly into the structural characteristic of a SDOF system, where they are subsumed in a single bilinear force-deformation relation. So in cases where the contribution of these two parameters to the structural response is limited or negligible a good estimation of global deformation demand of a MDOF system can be obtained, otherwise the contribution of these effects must be taken into account with certain correction coefficients.

TABLE 1. Ground motions used in the analyses

No.	Earthquake	Date	Station	Soil Type	M_W	CD (km)	ED (km)	HD (km)	Record Type	PGA (cm/s^2)	PGV (cm/s)
1	Run1	-	synthetic	-	-	-	-	-	FFE	236.4	15.45
2	Run1	-	synthetic, scaled to 0.1g	-	-	-	-	-	FFE	98.1	6.42
3	Run1	-	synthetic, scaled to 0.2g	-	-	-	-	-	FFE	196.2	12.84
4	Run1	-	synthetic, scaled to 0.3g	-	-	-	-	-	FFE	294.3	19.26
5	Run1	-	synthetic, scaled to 0.4g	-	-	-	-	-	FFE	392.4	25.68
6	Run1	-	synthetic, scaled to 0.5g	-	-	-	-	-	FFE	490.5	32.1
7	Run2 (San Francisco), U.S.A	22.05.57	Golden Gate Park, comp 100°	Rock (Chert)	5.3	8	11.5	15.2	NFE	126	5.97
8	Run2 (San Francisco)	22.05.57	Golden Gate Park, c100° , scaled to 0.2g	Rock (Chert)	-	8	11.5	15.2	NFE	196.2	9.3
9	Run2 (San Francisco)	22.05.57	Golden Gate Park, c100° , scaled to 0.3g	Rock (Chert)	-	8	11.5	15.2	NFE	294.3	13.95
10	Run2 (San Francisco)	22.05.57	Golden Gate Park, c100° , scaled to 0.4g	Rock (Chert)	-	8	11.5	15.2	NFE	392.4	18.6
11	Run2 (San Francisco)	22.05.57	Golden Gate Park, c100° , scaled to 0.5g	Rock (Chert)	-	8	11.5	15.2	NFE	490.5	23.25
12	Run2 (San Francisco)	22.05.57	Golden Gate Park, c100° , scaled to 0.6g	Rock (Chert)	-	8	11.5	15.2	NFE	588.6	27.91
13	Run3 (San Francisco.), U.S.A	22.05.57	Golden Gate Park, c100°, scaled to 1.11g	Rock (Chert)	-	8	11.5	15.2	NFE	1080.8	31.66
14	Run4		- Synthetic	Rock	-	-	-	-	FFE	401.9	41.07

No.	Earthquake	Date	Station	Soil Type	M_W	CD (km)	ED (km)	HD (km)	Record Type	PGA (cm/s^2)	PGV (cm/s)
15	Bingöl, Turkey	01.05.03	Mins.of Settl.and Pub.Works Bldg. NS comp.	NEHRP B	6.4	9	12	-	NFE	534.6	26.68
16	ChiChi, Taiwan	20.09.99	CHY074 NS comp.	Rock	7.8	-	-	-	FFE	155	23.58
17	Compano Lucano, Italy	23.11.80	Sturno EW comp.	Rock	6.87	14	32	-	FFE	316.8	54.66
18	Compano Lucano, Italy	23.11.80	Sturno NS comp.	Rock	6.87	14	32	-	FFE	212.2	33.53
19	Coyote Lake, U.S.A	06.08.79	Gilroy # 6, c320□	USGS (B)	5.7	3.1	9.7	13.6	NFE	314.6	21.91
20	CR2_10R	-	USEE synthetic database	Hard Rock	7	-	169	-	FFE	259.2	20.25
21	Friuli, Italy	06.05.76	Tolmezzo, Diga Ambiesta EW comp.	Rock	6.3	-	27	-	NFE	310	32.63
22	Friuli, Italy	06.05.76	Tolmezzo, Diga Ambiesta NS comp.	Rock	6.3	-	27	-	NFE	350.3	20.62
23	Ito-Oki, Japan	09.07.89	Shiofuzaki EW comp	Rock	5.3	-	3	-	NFE	189.2	25.37
24	Ito-Oki, Japan	09.07.89	Shiofuzaki EW comp, scaled by factor 2	Rock	5.3	-	3	-	NFE	378.4	50.73
25	Ito-Oki, Japan	09.07.89	Shiofuzaki EW comp, scaled by factor 2.5	Rock	5.3	-	3	-	NFE	473	63.42
26	Ito-Oki, Japan	09.07.89	Shiofuzaki EW comp, scaled by factor 3	Rock	5.3	-	3	-	NFE	567.6	70.1
27	Kocaeli, Turkey	17.08.99	Izmit EW comp.	Rock	7.4	-	11		NFE	222.7	54.28
28	Lazio Abruzzo, Italy	07.05.84	Scafa NS comp.	Rock	5.7	-	60	-	FFE	129.2	9.73

No.	Earthquake	Date	Station	Soil Type	M_W	CD (km)	ED (km)	HD (km)	Record Type	PGA (cm/s^2)	PGV (cm/s)
29	Lazio Abruzzo, Italy	07.05.84	Scafa EW comp.	Rock	5.7	-	60	-	FFE	123.3	7.27
30	Lazio Abruzzo, Italy	07.05.84	Scafa NS comp., scaled to 2PGA	Rock	5.7	-	60	-	FFE	258.4	19.47
31	Lazio Abruzzo, Italy	07.05.84	Scafa EW comp., scaled to 2PGA	Rock	5.7	-	60	-	FFE	246.6	14.55
32	Loma Prieta, U.S.A	18.10.89	Gilroy – Gav. College Geol. Bldg., c0□	Sandstone Dep. over	7	3	28.7	33.7	NFE	349.1	29.21
33	Loma Prieta, U.S.A	18.10.89	Gilroy – Gav. College Geol. Bldg., c90□	Sandstone	7	3	28.7	33.7	NFE	310.1	22.99
34	Loma Prieta, U.S.A	18.10.89	Gil. Arr. # 1, Gavil. Coll., c0□	Rock	7	2.8	28.4	-	NFE	426.6	31.91
35	Loma Prieta, U.S.A	18.10.89	Gil. Arr. # 1, Gavil. Coll., c90□	Rock	7	2.8	28.4	-	NFE	433.6	33.84
36	Montenegro	15.04.79	Herceg Novi EW comp.	Rock	7.04	29	65	-	FFE	251	12.88
37	Montenegro	15.04.79	Herceg Novi NS comp.	Rock	7.04	29	65	-	FFE	220	13.85
38	Morgan Hill, U.S.A	24.04.84	Gilroy # 6, c90□	USGS (B)	6.1	6.1	35.9	-	NFE	280.4	36.59
39	Morgan Hill, U.S.A	24.04.84	Gilroy # 6, c0□	USGS (B)	6.1	6.1	35.9	-	NFE	214.8	11.26
40	MYG011, Japan	26.07.03	MYG011 NS comp.	Rock	6.2	-	32	-	FFE	324.1	8.37
43	Northridge, U.S.A	17.01.94	Mt. Wilson Caltech Seismic St., c360°	Granitic Rock	6.7	36.7	44.6	-	FFE	228.5	7.58
44	Northridge, U.S.A	17.01.94	Mt. Wil. Cal.S.St., c360° scaled by factor 2	Granitic Rock	6.7	36.7	44.6	-	FFE	457	15.16

No.	Earthquake	Date	Station	Soil Type	MW	CD (km)	ED (km)	HD (km)	Record Type	PGA (cm/s2)	PGV (cm/s)
45	Northridge, U.S.A	17.01.94	L.A. City Terrace, c180°	Sedimentary Rock	6.7	35.8	38.3	-	FFE	311.1	14.02
46	Parkfield, U.S.A	28.06.66	Cholame Shan., California Ar.# 5, c355°	USGS (C)	6.1	7.1	36.8	-	NFE	347.8	23.23
47	Sierra Madre, U.S.A	28.06.66	Mt. Wilson Caltech Seismic Station	Granitic Rock	5.8	9.9	6.4	-	NFE	196.2	7.53
48	Tabas, Iran	06.09.78	Tabas, scaled by factor 0.5	Stiff Soil	6.5	3	52	-	NFE	459.4	57.1
49	Tottoriken , Japan	06.10.00	Gashyo Dam EW comp	Rock	6.6	-	3	-	NFE	531.6	50.57
50	Tottoriken, Japan	06.10.00	Gashyo Dam EW comp, scaled by factor 0.5	Rock	6.6	-	3	-	NFE	265.8	25.28
51	Tottoriken, Japan	06.10.00	Gashyo Dam EW comp, scaled by factor 0.75	Rock	6.6	-	3	-	NFE	398.7	37.93
52	Umbro Marchigianio, Italy	26.09.97	Nocera Umbra EW comp.	Rock	5.9	4	11	-	NFE	754.42	29.86
53	Whittier Narrows, U.S.A	01.10.87	LA, Griffith Park Obser., scaled by factor 2	Rock	6.1	21.9	21.5	26	FFE	267.6	15.17
54	Whittier Narrows, U.S.A	01.10.87	Tarzana, Cedar Hill Nurs., c0° scaled by 0.5	USGS (B)	6.1	41.1	43.4	-	FFE	198.7	9.61
55	Whittier Narrows, U.S.A	01.10.87	Tarzana, Cedar Hill Nursery, c0°	USGS (B)	6.1	41.1	43.4	-	FFE	397.5	19.22

A nonlinear SDOF system with bilinear force-deformation relation with some post elastic-stiffness can be described completely with the following parameters; T (elastic period), ξ (damping), either of m (mass) or k (stiffness of the system in the elastic range), $\eta=f_y/W$ (yield base shear coefficient), and α (post elastic stiffness coefficient). Yield base shear coefficient (η), or base yield strength (f_y), given in Eq. (1) is determined in the design stage for a desired ductility level under a postulated ground motion effect that defines the constant ductility response spectrum.

$$f_y = \frac{A_y}{g} W \tag{1}$$

In the above equation, A_y is the pseudo acceleration corresponding to yielding of the SDOF system with pre-defined ductility level and W is the weight of the structure.

To determine the response of the CAMUS structure by employing equivalent SDOF systems, a representative SDOF model of the MDOF structure was obtained. The accuracy of this approximate procedure depends strongly on how well various structural aspects of the MDOF are represented by the corresponding SDOF system. It is also important to note that the change in the initial slope of pushover curve due to bilinearization requires a change in the natural period of the system that is modified with $T_{eff}=T_n.(K_i/K_{eff})^{0.5}$.

The roof displacements calculated using the equivalent SDOF models having bilinear hysteretic behavior is plotted against the exact roof displacements obtained from nonlinear time history analysis of MDOF structure as shown in Figure 4. For motions that impose large inelastic displacements the equivalent SDOF model underestimates the displacements regardless of the type of ground motion. The response of elastic SDOF system gave better results than the inelastic one in many of the cases.

Although the multistory structure was assumed to respond predominantly in the first mode, in the later stages of nonlinearity the results of SDOF model deviated from the exact displacements, causing significant underestimates of global displacement demand. This can be attributed to the influence of local response as opposed to the global response. Upon yielding at any level, significant ductility demands were imposed on particular sections due to inelastic excursions. It should be noted that this observation contravenes the behavior of frame structures that have reduced roof displacement due to local concentration of inelasticity, such as at a soft story. The inelastic displacement demands computed using the equivalent SDOF systems tend to underestimate the global roof displacement of the structure (Figure 4.b).

3.2. CAPACITY SPECTRUM METHOD (CSM)

The capacity spectrum method initially characterizes seismic demand using a reduced elastic response spectrum. This spectrum is plotted in ADRS format which allows the demand spectrum to be "overlaid" on the capacity spectrum for the building. The intersection of the demand and capacity, if located in the linear range of the capacity, would define the actual displacement for the structure; however this is not normally the case as most of analyses include some inelastic nonlinear behavior (ATC 40, 1996).

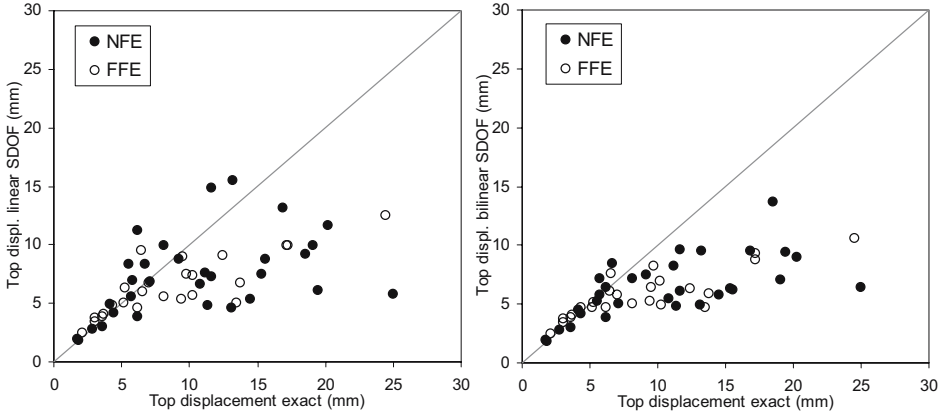

(a) Linear model (b) Inelastic bilinear model

Figure 4. Comparison of "exact" non-linear analyses and SDOF model results

The Nonlinear Static Procedures in ATC-40 is based on the Capacity Spectrum Method originally developed by Freeman et al. (1975) that uses equivalent linearization. In equivalent linear methods, the inelastic deformation demand of a nonlinear system is approximated by the elastic response of an equivalent elastic SDOF system that has a smaller stiffness and larger damping than the inelastic system. The relationship between effective damping (β_{eff}) and the displacement ductility ratio (μ) adopted by ATC-40 procedure is given in Eq. (2) based on the post elastic stiffness ratio (α) and the hysteretic behavior type factor (κ).

$$\beta_{eff} = 0.05 + \kappa \frac{2(\mu - 1)(1 - \alpha)}{\pi\mu(1 + \mu\alpha - \alpha)} \tag{2}$$

The procedure defined in ATC 40 was applied to the model structure in order to compute its inelastic displacement demands for the set of ground motions considered in this study. The results were distinctively investigated for NFE and FFE records and are compared with the exact values in Figure 5.a.

Although no clear evidence of superiority of one set of results on the other was observed, a relatively better correlation for NFE earthquakes is notable.

A clear outcome is that the Capacity Spectrum Method significantly underestimates the inelastic displacements for both NFE and FFE records when the ductility demand is high. The principal reason for this outcome is the unrealistic reduction in the demand, i.e. reduced elastic response spectrum, owing to exaggerated damping values. The estimated damping value to take into account the inelastic behavior in the system is well above twenty percent in many of the cases.

A possible remedy to overcome this problem would be to use other methods that are based on more realistic assumptions for computing the equivalent viscous damping. The substitute damping (β_S) given in Eq. (3) was proposed by Gulkan and Sozen (1974) to determine the equivalent viscous damping that considers approximately the influence of inelastic excursions. Here, μ is the ductility factor that describes the ratio of maximum displacement excursion to the displacement at the yield.

$$\beta_S = (1+10(1-1/\sqrt{\mu}))/50 \tag{3}$$

The underlying principle in Eq. (3) is based on the idea that the response of reinforced concrete structures to strong earthquake motions is controlled by two basic phenomena: reduction in stiffness and increase in energy dissipation capacity. Furthermore, the maximum dynamic response of reinforced concrete structures, represented by SDOF systems, can be approximated by linear response analysis using a reduced stiffness and a substitute damping.

Equation 3 was incorporated into the algorithm of CSM procedure as described in ATC-40 instead of the equivalent viscous damping to compute the inelastic displacements demands. The results obtained by substitute damping were superior to those obtained by equivalent damping as shown in Figure 5.b. This finding emphasizes the significance of the accuracy in calculating the damping used in the CSM.

A recent document, FEMA 440 (2004), devoted to evaluating existing approximate displacement-based procedures to address their drawbacks proposes a procedure that uses the effective period (T_{eff}) and equivalent viscous damping (β_{eff}) expressions given in Eqs. (4) and (5), respectively, to obtain improved results when applying the CSM procedure. In these equations, the constants A, B, C, D, G, H, I and J depend on the hysteretic model and the post elastic slope of the capacity curve. For the shear wall structure employed here the coefficients are: A=4.61, B=-0.95, C=10.9, D=1.6, G=0.12, H=-0.02, I=0.17 and J=0.12, respectively.

For $\mu < 4.0$: $$\beta_{eff} = A(\mu - 1)^2 + B(\mu - 1)^3 + \beta_0 \tag{4a}$$

$$T_{eff} = \left[G(\mu - 1)^2 + H(\mu - 1)^3 + 1\right]T_0 \tag{4b}$$

For $4.0 \le \mu \le 6.5$: $$\beta_{eff} = C + D(\mu - 1) + \beta_0 \tag{5a}$$

$$T_{eff} = \left[I + J(\mu - 1) + 1\right]T_0 \tag{5b}$$

The results of the improved procedure are compared with the exact inelastic displacement demands in Figure 5.c. An immediate observation is that the tendency to underestimate the displacements as the inelasticity increases in the system observed for the conventional CSM procedure is also true for the new procedure.

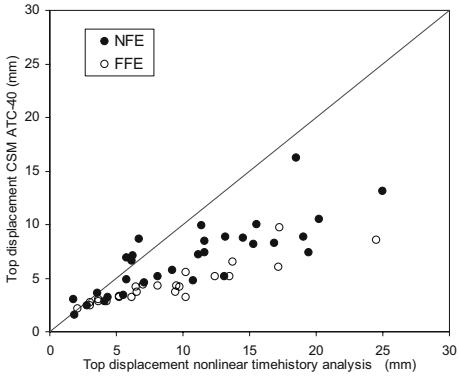

(a) ATC-40 CSM

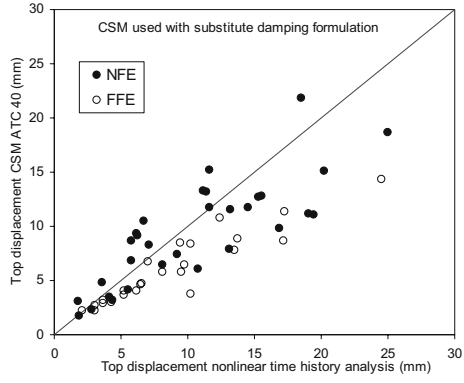

(b) ATC-40 CSM with substitute damping

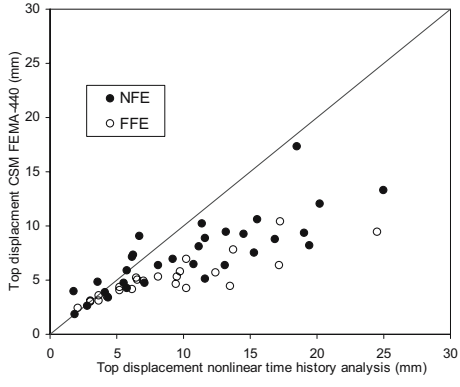

(c) FEMA-440 CSM

Figure 5. Comparison of CSM results with different effective period and damping formulation

The findings of our analyses presented here are in conflict with the observations made by other researchers as presented in FEMA 440. Our results are valid for the structure employed here, a stiff multi-story structure with a

fundamental period of 0.145 sec, and seems to suggest that CSM in ATC-40, a widely used approximate nonlinear analysis procedure, underestimates the displacement demands. The evaluation of results presented in FEMA 440 and elsewhere (Akkar and Miranda, 2005) however, indicates the opposite trend that for structures with fundamental periods smaller than 0.5 sec, the CSM of ATC-40 overestimates the results by a large margin.

There might be two main reasons for this inconsistency. The first is that we use an actual stiff structure whereas the FEMA-440 evaluations are based on the SDOF analyses. This, however, seems not to be the case because our SDOF analyses show quite good agreement with the CSM estimates as shown in Figure 6.a. Thus the main reason appears to stem from the solutions of SDOF systems that represent unrealistically stiff structures. The SDOF systems employed in other research programs display unrealistic ductility ratios, as can be observed in Figure 6.b that presents commonly used relationships for strength reduction factor (R), ductility demand (μ) for a given period (T). At small periods representing stiff structures, the ductility demand of the system increases drastically reaching values in the order of tens which could not be attained by real structures. This indicates that for stiff structures SDOF-based evaluations of approximate procedures can be misleading because of the very small displacements involved.

$$\delta_t = C_0\, C_1\, C_2\, C_3\, Sa \frac{T_e^2}{4\pi^2} g \tag{6}$$

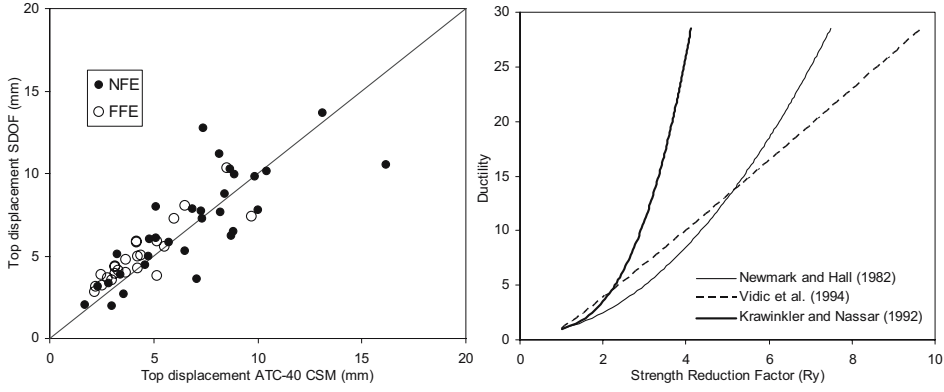

(a) (b)

Figure 6. (a) Comparison of SDOF model analyses and ATC-40 Capacity Spectrum Method, *(b)* Relationship for strength reduction factor (R) and ductility ratio (μ) for T=0.14 sec

3.3. DISPLACEMENT COEFFICIENT METHOD (DCM) IN FEMA 356

A simpler procedure, the Displacement Coefficient Method, is proposed in FEMA 273/356 (2000) to predict the inelastic displacement demand using the building's capacity curve and the elastic site-specific response spectrum. The displacement demand is calculated using Eq. (6) that takes into account various structural parameters and the ground motion through adjustment coefficients.

The coefficient C_0 relates the top floor displacement of the structure to the displacement of an equivalent single degree of freedom system (SDOF). C_1 modifies the elastic displacement to obtain the corresponding inelastic displacement. The coefficient C_2 depends on the structural system and varies with the hysteretic behavior. The increase in the displacement demand due to P-Δ effect is taken into account through the coefficient C_3. This approximate procedure is applied to a system that has bilinear capacity curve so the original curves are needed to be idealized which would have an effective fundamental period (T_e).

The DCM was applied to the model structure here to determine its approximate inelastic displacement demand under the ground motion set considered. The "exact" roof displacements compared with results from the DCM are given in Figure 7.

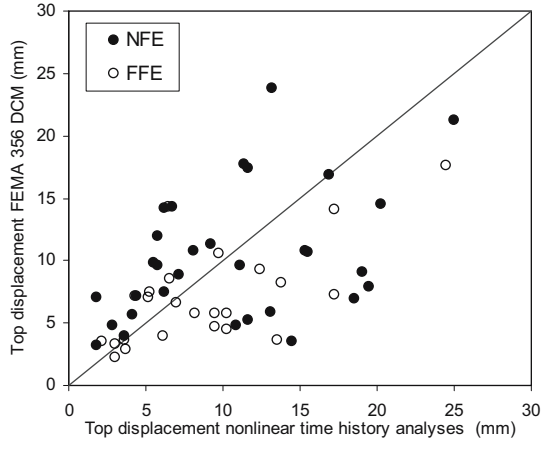

Figure 7. Top displacements obtained from DCM for NF and FF earthquakes

It is observed from the figure that the estimates of roof displacement are improved in comparison to the results of the CSM. The better prediction capacity can be attributed to the coefficients (C_1, C_2 and C_3), that all amplify the response and take into account effects arising from nonlinearity utilized in DCM. However, the dispersion is quite significant, especially for NFE records. The equivalent SDOF solutions presented in Figure 4.b reveal that the exact

inelastic displacement demands are underestimated which is inconsistent with the findings of other research, such as Miranda and Ruiz-Garcia (2002), and FEMA 440. The main reason for the discrepancy arises from the differences in results between the elastic perfectly plastic hysteretic models and bilinear models. The structure we have used has significant post elastic yield stiffness that reduces the inelastic displacement significantly, especially at large displacement ductility demand as compared to elastic perfectly plastic models that are mostly employed by earlier research.

The characteristics of the ground motion set employed as well as the structure considered here exercise significant influence on the observed discrepancies. The wall type structures are too stiff to display large inelastic deformations leading to small ductility ratios and insignificant strength reduction values. Therefore, the inelastic displacement ratios (C_1) based on SDOF solutions appear not to be applicable to the structures with high yield strength capacity similar to that employed here.

The accuracy of DCM depends strongly on the system and the ground motion because the coefficients in Eq. (6) are derived from the analyses of SDOF systems that themselves are not uniformly capable of representing adequately the behavior of the MDOF system considered in this investigation as discussed in the preceding sections.

4. Discussion and Conclusions

The results derived for this particular short-period structural assembly must be carefully interpreted to judge their general applicability. There exists a complex interaction between the types of ground motions used and the response these would generate in the analytical model of a particular test specimen. Our analytical model did not respond exclusively in the inelastic range for all input records, although for most trials it did, so the ductility demand varied from less than 1 to 6. The base motions fell into two groups defined as near- and far-field. We have been preoccupied with the global displacement because this is the quantity that best correlates with damage potential and performance evaluation.

The results obtained from nonlinear time history analyses indicated that stiff structures that are typically used for nuclear facilities respond to both near and far field records on firm soils in similar manner.

The equivalent SDOF systems are not adequate in representing the actual performance especially in the region of significant nonlinearity even for systems where elastic response is dominated by the first mode. The procedures such as DCM in FEMA 273 that use coefficients derived from the SDOF analyses must be re-examined before extrapolating their applicability in general.

Among the approximate procedures implemented here DCM of FEMA-273 yielded the most satisfactory results. The worst predictions were obtained from the CSM in ATC-40, the major reason being the over estimation of the viscous damping leading to severely underestimated displacements. A significant improvement leading to more accurate predictions of the response was achieved when the substitute damping was incorporated into the CSM, although it appears that even smaller damping should be invoked for better prediction.

The results based on SDOF analyses might be misleading for stiff structures that are incapable of exhibiting large inelastic deformations. As other research has also confirmed the SDOF results imply unrealistically large ductility ratios for these structures, but large ductility demand does not translate into large damping ratios.

ACKNOWLEDGEMENTS

The investigation presented here has been in part jointly sponsored by the International Atomic Energy Agency and the Joint Research Center of European Commission under grant No. 20788-2003-05 F1ED ISP TR. We owe a debt of gratitude to Vito Renda, Deputy Head of Unit, ELSA-JRC for his continued support. The constructive comments of Dr. Sinan Akkar are gratefully acknowledged. The findings, opinions and conclusions presented in this article are those of the authors, and do not necessarily reflect views of either of the sponsors.

References

Akkar , S. D. and Miranda, E. Statistical Evaluation of Approximate Methods for Estimating Maximum Deformation Demands on Existing Structures. *Journal of Structural Engineering* 2005, ASCE **131**(1):160-172.

ANSYS Engineering Analysis System, ANSYS, Inc. South Pointe, Canonsburg, Pennsylvania, 2002, Release 7.0 UP20021010.

ATC 40 Seismic Evaluation and Retrofit of Concrete Buildings, Volume 1; *Applied Technology Council*, California Seismic Safety Commission, 1996.

Chintanapakdee, C. and Chopra, A. K. Evaluation of Modal Pushover Analysis Using Generic Frames. *Earthquake Engineering & Structural Dynamics* 2003*,* 32:417–442.

Chopra, A. K., Goel, R. K. and Chintanapakdee, C. Statistics of Single-Degree-of-Freedom Estimate of Displacement for Pushover Analysis of Buildings. *Journal of Structural Engineering* 2003, ASCE **129**(4):459-469.

Combescure, D., 2002, IAEA CRP-NFE Camus Benchmark: Experimental Results and Specifications to the Participants. *Rapport DM2S, SEMT/EMSI/RT/02-047/A*.

FEMA 356 Pre-standard and Commentary for the Seismic Rehabilitation of Buildings; *Federal Emergency Management Agency*, Washington, D.C, 2000.

FEMA 440 Improvement of nonlinear static seismic analysis procedures, Draft Camera-Ready. *Applied Technology Council*, California Seismic Safety Commission, 2004.

Freeman, S. A., Nicoletti, J. P., and Tyrell, J.V. Evaluations of Existing Buildings for Seismic Risk: A case study of Puget Sound Naval Shipyard, Bremerton. Proceedings of First U.S. NCEE, EERI, Berkeley, Washington, 1975, 113-122.

Gulkan, P. and Sozen, M., A. Inelastic Response of Reinforced Concrete Structures to Earthquake Motions. *ACI Journal* 1974, December, 604-610.

Kazaz, I., Yakut, A. and Gulkan, P., 2005, Numerical Simulation of Dynamic Shear Wall Tests: A Benchmark Study. Submitted to *Computers and Structures*.

Martinez-Pereira, A. and Bommer, J. J., 1998, What is the Near-field?. *In Seismic Design Practice into the Next Century*, 245-252, eds. Booth, E., Balkema.

Miranda, E. Estimation of Inelastic Deformation Demands of SDOF Systems. *Journal of Structural Engineering* 2001, ASCE **127**(9):1005-1012.

Miranda, E., Akkar, D. S. and Ruiz-Garcia, J. ATC-55: Summary of Evaluation of Current Nonlinear Static Procedures-SDOF Studies; *Applied Technology Council*, California Seismic Safety Commission, 2002.

Miranda, E. and Ruiz-Garcia, J. Evaluation of Approximate Methods to Estimate Maximum Inelastic Displacement Demands. *Earthquake Engineering and Structural Dynamics* 2002, **31**(3):539-560

Nassar A.A. and Krawinkler H. Seismic Demands for SDOF and MDOF Systems. *Report No.95*, John A. Blume Earthquake Engineering Center, Stanford University, 1991.

Newmark, N. M. and Hall, W. J. Earthquake Spectra and Design. EERI, Berkeley, CA, 1982.

Vidic, T., Fajfar, P. and Fischinger, M. Consistent Inelastic Design Spectra: Strength and Displacement. *Earthquake Engineering and Structural Dynamics* 1994, **23**(5):507-521.

ASSESSMENT AND RETROFIT OF FULL-SCALE MODELS OF EXISTING RC FRAMES

ARTUR V. PINTO*
ELSA Laboratory, Joint Research Centre, European Commission
2120 Ispra (VA), Italy

FABIO TAUCER
ELSA Laboratory, Joint Research Centre, European Commission
2120 Ispra (VA), Italy

Abstract. Pseudo-dynamic (PSD) tests on two full-scale models representative of existing non-seismic resisting RC frame structures are described. The testing program covered several aspects, namely the assessment of seismic performance of existing frames without and with infill panels, retrofitting of a bare frame using Selective Retrofitting techniques, strengthening of infill panels using shotcrete and retrofitting of frames using K-bracing with shear-link dissipators. The main results from the PSD tests are summarized and discussed and conclusions are drawn. The tests on the bare and infilled frames showed the high vulnerability of existing structures constructed in the 60's and confirmed the beneficial effects of infill panels. Important improvements, in terms of seismic performance, were achieved by retrofitting of the frames. However, strengthening of the existing infill panels in poorly detailed frames may lead to dangerous 'local' failures, such as shearing out of the external columns.

Keywords: Pseudo-dynamic tests; existing RC structures; earthquake assessment; seismic retrofit; bare and infilled frames

* Artur V. Pinto, ELSA Laboratory, TP 480, Joint Research Centre, 21020 Ispra (VA), Italy; email: artur.pinto@jrc.it

S.T. Wasti and G. Ozcebe (eds.), Advances in Earthquake Engineering for Urban Risk Reduction, 353–367.

1. Introduction

In the framework of the ICONS Research Network research programme on assessment and retrofit of existing structures (Pinto 1998), full-scale reinforced concrete frames were tested pseudodynamically at the ELSA laboratory. Two frames representative of design and construction practice of the 60's in most European Mediterranean countries were tested in order to assess the vulnerability of bare and infilled structures and to investigate various retrofitting solutions/techniques.

The design of the test frames was performed at LNEC by Carvalho et al. (1999). The retrofitted solution for the bare frame was designed by Elnashai and Pinho (1999) and was based on a rational intervention, balancing strength, stiffness and ductility. The retrofitting solution with K-bracing in series with a shear-link dissipator was designed by Bouwkamp et al. (2001). Additionally, an infilled frame with strengthened infill panels was also tested (Pinto et al., 2002b). Strengthening of the masonry panels was made through a concrete layer with an embedded steel mesh using shotcrete (Pinto et al. 2002b).

The full-scale models were subjected to input motions with increasing intensities until reaching failure.

This paper describes the test structures, testing set-up and loading and presents the main results and conclusions from the pseudo-dynamic (PSD) tests carried out at the ELSA laboratory.

2. Design and Construction of the RC Frames

Figure 1 shows the general layout of the structure; a 4-storey reinforced concrete frame with three bays; two of 5 *m* span and one of 2.5 *m* span. The inter-storey height is 2.7 *m* and a 0.15 *m* thick slab of 2 *m* on each side was cast together with the beams. Equal beams (geometry and reinforcement) were considered at all floors and all the columns, with the exception of the wider interior one, have equal geometric characteristics along the height of the structure (0.40 or 0.3 *m* × 0.20 *m*). The stocky column has a rectangular cross-section with dimensions 0.60 *m* × 0.25 *m* on the first and second storeys and 0.50 *m* × 0.25 *m* on the third and fourth storeys. All beams in the direction of loading are 0.25 *m* wide and 0.50 *m* deep, while transverse beams are 0.20 *m* wide and 0.50 *m* deep. The concrete slab thickness is 0.15 *m*. The column reinforcement splice and stirrup details should be noted, as these are representative of the lack of confinement common in non-ductile reinforced concrete structures. The longitudinal reinforcement of all (four) columns has lap splices of (700 *mm*) at the base of the 1st and the 3rd storey.

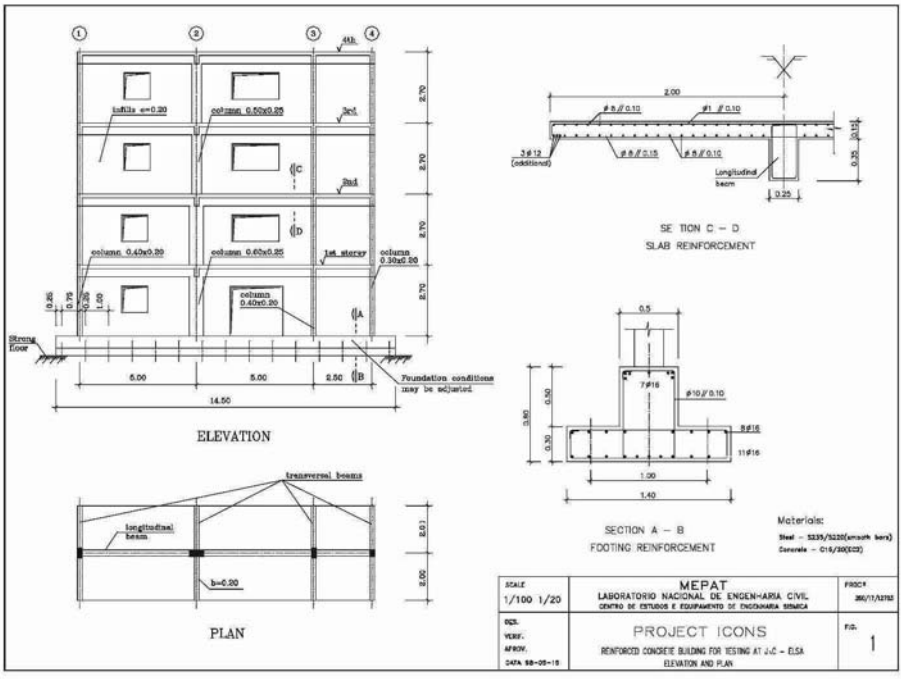

Figure 1. Plan and elevation views of the concrete frame and the masonry infilled building

The materials considered during the design phase (Carvalho et al., 1999) were a low strength concrete, class C16/20 (Eurocode 2) and smooth reinforcing steel (round smooth bars) of class FeB22k (Italian standards). Tests on samples of the materials used in the construction of the structure were carried out and the following results were obtained: a) for the concrete - mean strength values for all casting phases, f_{cm}=15 *MPa*, b) for the steel (mean values) - yielding stress, f_{sy}=350 *MPa*, ultimate strength, f_{su}=453 *MPa*, ultimate deformation, ε_{su}=24% ('nominal' values: f_{sy}=250 *MPa*, f_{su}=365 *MPa*).

The vertical loads were defined in order to simulate the dead loads other than the self-weight of the frame, considering that parallel frames have a distance of 5.0 *m* (the frame model includes a 4.0 *m* wide slab, which requires additional vertical load accounting for the missing slab portion). These additional vertical loads are: weight of slab: 25 × 0.15 =3.75 kN/m^2; weight of finishings: 0.75 kN/m^2; weight of transverse beams: 2.5 *kN/m; w*eight of masonry infills: 1.1 kN/m^2 of wall area (it is considered that these walls exist both over longitudinal and transverse beams). The live loads were also included as part of the additional vertical loads and amount to 1.0 kN/m^2 (quasi-permanent value).

The input seismic motions were defined as being representative of a moderate-high European seismic hazard scenario (Pinto, 1998). Hazard

consistent acceleration time series (15 seconds duration) were artificially generated, yielding a set of twelve uniform hazard response spectra for increasing return periods. The acceleration time histories used in the pseudo-dynamics tests correspond to 475, 975 and 2000 years return periods earthquakes with 0.22, 0.29 and 0.38*g* PGA respectively.

3. Bare Frame (BF) Tests

The bare frame was subjected to one PSD earthquake test corresponding to 475 years return period (475-yrp) and subsequently to a second PSD test with a 975-yrp input motion. Results from these tests are given in Figure 2, in terms of storey displacement. The 975-yrp test was stopped at 7 seconds of the 15 seconds accelerogram due to imminent collapse at the 3rd storey (see details of the stocky column at the 3rd storey in Figure 3). Storey shear versus storey drift (for all storey levels) are shown in Figure 4.

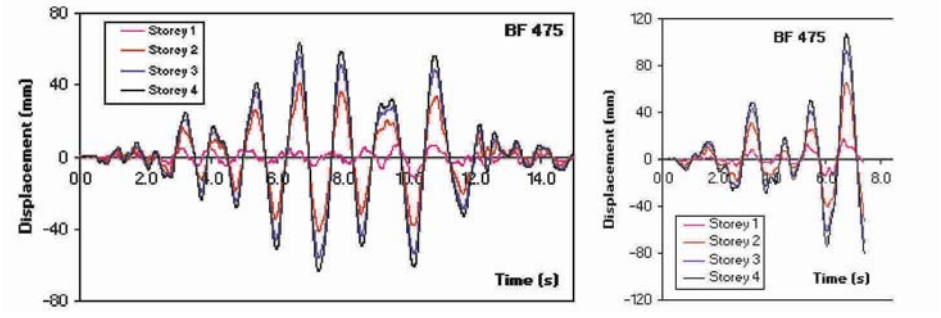

Figure 2. Storey displacement time histories - BF tests: 475-yrp and 975-yrp

Figure 3. Four-storey R/C models: a) General view of the mounting phase (left), b) Stocky column reinforcement at the 3rd storey (lap-splicing) (centre), c) Column failure at the 3rd storey at the bars termination zone during the BF975 test

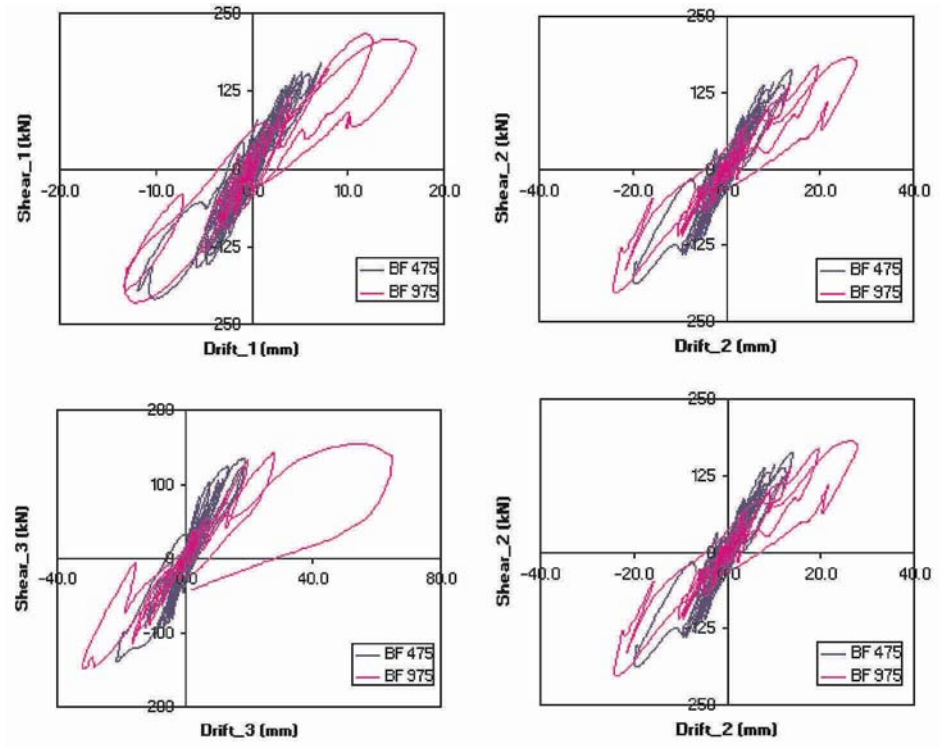

Figure 4. Storey shear - drift diagrams for the BF tests: BF475 and BF975

4. Selective Retrofitted Specimen (SR)

Following the two earthquake tests on the bare frame, the damaged parts of the structure were repaired. The 'spalled' concrete was removed and the cracks were injected with epoxy, the surfaces were cleaned and the selective retrofitting scheme, proposed by the research group at the Imperial College of London (Elnashai and Pinho, 1999; Pinho, 2000) was applied.

The selective retrofitting solution involved two types of interventions in the wide internal column (stocky column). A *strength-only* intervention was implemented in the wide column at the 3rd and 4th storeys to reduce the large differential in flexural capacity verified at level 3. This intervention scheme consisted in using external re-bars embedded in a non-structural concrete (for protection purposes). Moreover, a *ductility-only* intervention was accomplished at the first three storeys in the wide column, where large inelastic deformation demand was expected. This intervention was achieved by the addition of external confining steel plates at the critical zones (at the base and at the top of

the member). Furthermore, to minimize the risk of shear failure, additional plates were also added at mid-height of the columns.

The initial testing programme for the selective retrofitting (SR) frame was similar to the bare frame (BF) programme. However, in view of the results obtained for the SR975 test, which led to rather small demands and damage, it was decided to perform an additional test with higher intensity. This test was expected to inflict more significant damage on the structure without compromising the integrity of the structure for the next strengthening solution foreseen for this specimen (K-bracing with shear-link). A 2000-yrp earthquake was adopted for this high-level test. Time histories of the storey displacements for the 475-yrp and 2000-yrp tests are given in Figure 5 and maximum values of drift and shear are collected in Table 1.

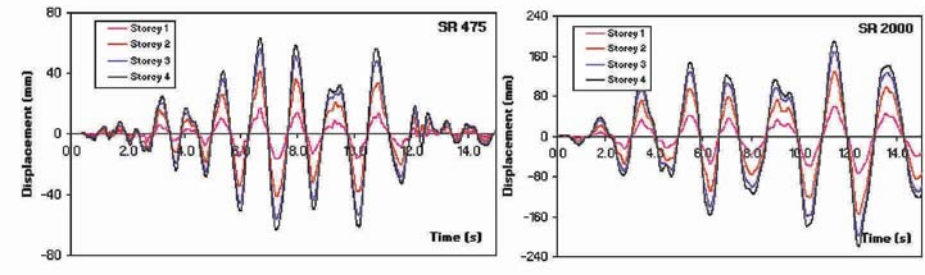

Figure 5. Storey displacement time histories (mm) - SR tests: 475-yrp, and 2000-yrp

5. Bare Frames – Original (BF) *vs* Selective Retrofitted (SR)

While it is important to quantify both the BF and SR test demands and ultimate capacities, it is also useful to highlight the effectiveness of the retrofit solutions provided to the frame.

The tests performed on the bare frame showed concentration of inter-storey drift demands and consequent damage of the stocky column in the 3rd storey (Figure 3). A three-hinge mechanism developed in the structure and was primarily due to its vertical irregularity in terms of stiffness and strength resulting from the change in cross-section size and reinforcement of the strong central column. The selective retrofitting addressed and solved the irregularity problem of the structure (see Figure 6). In spite of the fact that no substantial differences exist between the BF and SR drift demands for the 475-yrp tests, the 3rd storey large drift demand of the bare frame for the 975-yrp test vanishes for the retrofitted frame and the comparable top displacement demands result from much more uniform storey drift in the retrofitted frame. Furthermore, the retrofitted frame was able to withstand an input motion intensity 1.8 times the nominal one, in terms of PGA, without collapse and with reparable damage,

while the bare frame collapsed during the 975-yrp test corresponding to an input motion 1.3 times the nominal intensity (PGA = 2.18 m/s^2).

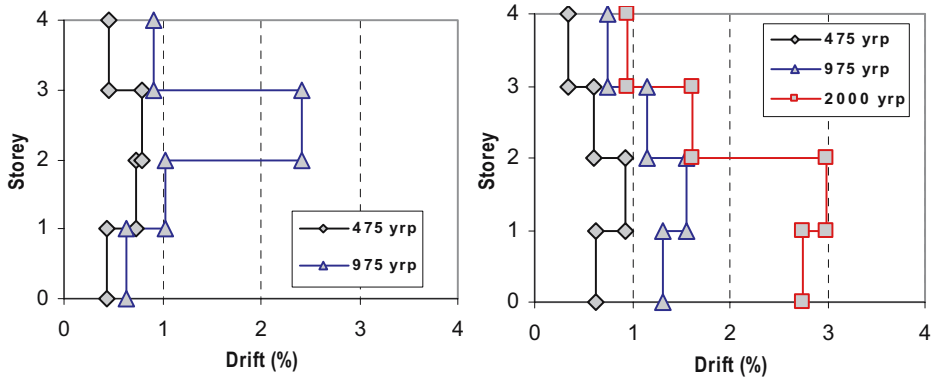

Figure 6. Maximum inter-storey drift profiles for (a) the bare frame (BF) (left) and (b) the retrofitted frame (SR)

From the shear-drift diagrams, it is apparent that the peak shear force at the 3rd storey was reached for a drift of 1.8% with subsequent important decrease in strength (imminent collapse). Furthermore, there was evidence of premature shear failure in the stocky column at the 1st and 3rd storeys (lap-splicing zones) for storey drifts of approximately 0.4%. Tests on the other frame with infill panels have also shown similar column shear crack initiation for 0.4% drift in the 1st storey and severe (dangerous) shear cracking for storey drifts of 1.3%.

The results from the SR tests have shown rather improved seismic performance. The retrofitting operation addressed and solved the irregularity problem and the confining steel plates definitively increased the limited deformation capacity of the central stocky column. In fact, drift demands were rather uniformly distributed in the first three storeys for the three earthquake tests and reached values much higher than the values of the bare frame tests. Inter-storey drifts of 2.8 and 3.0% were reached at the first and second storeys respectively without loss of load carrying capacity. It is noted that the 2.8% drift in the first storey is twice the ultimate drift identified from the original (non-retrofitted) frame. Therefore, it is concluded that the deformation capacity of the first storey, at least, doubles the original deformation capacity of the structure (see values in Table 1).

There are other aspects that should be highlighted from the test campaigns on the original (BF) and retrofitted (SR) frames, namely: 1) As expected, the strong-beam weak-column deformation/dissipation mechanism (storey mechanism) is the only one activated for all tests. However, slight higher demands in the beams were apparent for the retrofitted frame; 2) There is a strong concentration of inelastic demands at the member ends, leading to

equivalent plastic hinge lengths much lower than the empirical values proposed in literature (calculated plastic hinge lengths are 40% of the empirical values). This is a direct consequence of the poor bond characteristics of the smooth round rebars, which leads to extremely high slippage with concentration of deformations at the member (beam and column) extremities; 3) The values calculated for the slab participation are also much lower than the values proposed in the design codes and also lower than the values estimated from tests on building structures with corrugated steel rebars (approximately 45% lower). This is also a direct consequence of the poor bond characteristics of the smooth round steel reinforcement also used in the slabs; 4) The test results confirmed that lap-splicing at the base of columns, particularly in existing structures with smooth round rebars with extremity hooks, poor detailing and low shear/confinement reinforcement ratios, develop premature shear cracks at the bar termination zones for inter-storey drifts of approximately 0.4%. This shear cracks dictate dangerous shear failure of the columns for inter-storey drifts in the range of 1.3~1.8%.

TABLE 1. Maximum values of drift and base-shear for all earthquake tests

Test	Inter-Storey Drift – (%)				Global Drift (%)	Base Shear (kN)
	Storey 1	Storey 2	Storey 3	Storey 4		
BF 475	0.44	0.74	0.80	0.46	0.56	209.0
BF 975	0.63	1.03	2.41	0.91	1.08	216.7
SR 475	0.63	0.92	0.60	0.34	0.59	212.2
SR 975	1.31	1.56	1.16	0.74	1.08	261.1
SR 2000	2.75	2.98	1.62	0.94	2.03	285.9
IN 475	0.12	0.12	0.08	0.06	0.09	754.0
IN 975	0.43	0.27	0.15	0.11	0.21	846.5
IN 2000	1.29	0.22	0.12	0.09	0.38	543.2
SC 475	0.14	0.22	0.11	0.09	0.14	703.9
SC 975	0.22	0.31	0.15	0.11	0.19	820.1
SC 2000	1.30	0.89	0.23	0.14	0.61	838.6

6. Masonry (Brick) Infilled Frame (IN)

An identical RC frame with masonry infill panels was also constructed and subjected to a series of earthquake tests. Figure 1 shows the general layout of the structure including infill panels and the type and location of the openings. The 150 mm thick infill-walls (non-load bearing) were constructed after casting and transferring the reinforced concrete frame inside the ELSA laboratory. Representative materials and construction techniques were used, namely: Italian

hollow clay (ceramic) blocks horizontally perforated, with the following dimensions: 0.12 *m* thick, 0.245 *m* base-length and 0.245 *m* height. According to the classification of masonry units in Eurocode 6, the hollow blocks belong to Group 3. The infill walls were constructed with the block units bedded on the 0.120 *m* × 0.245 *m* face with the holes running in the horizontal direction (0.12 *m* thick). The mortar joints were approximately 1.5 *cm* thick, for both vertical and horizontal joints. A 1.5 *cm* thick plaster was applied on both sides of the walls. The same mortar was used for bed joints and plaster, and was manually prepared with a proportioning of 1:4.5 (Hydraulic binder : Sand).

The infilled frame specimen was subjected to three consecutive PSD earthquake tests corresponding to 475, 975 and 2000 years return periods. During the 2000-yrp PSD test the masonry infills at the 1st storey collapsed and the test was stopped at ~5 seconds. Results from these tests are given in Figure 7 in terms of storey displacements and maximum inter-storey drift profiles.

For the 475-yrp test, overall, the infilled frame structure showed a very good behaviour. A lateral global drift of only 0.08% (roof displacement divided by frame height) was reached. The maximum inter-storey drift occurred at the 1st (ground) storey and was equal to 0.12%, and decreased with increasing storey level to a value of about 0.07% at the 4th storey. As might be expected, the level of damage corresponding to these levels of drift was minor. The 1st storey hysteresis loops (shear force versus drift) suggest that significant damage had just started to occur and that the maximum storey shear strength was nearly attained in this test.

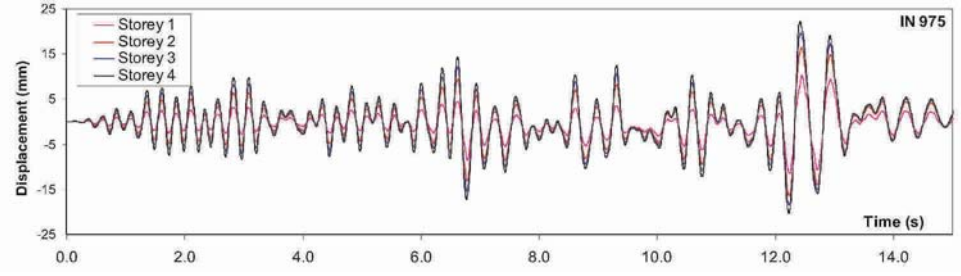

Figure 7. Storey displacements time-histories for the SR 975-yrp test

The 975-yrp earthquake caused a significant amount of damage to the masonry infills in the ground storey of the concrete frame, with some minor damage to the beam-column joints and to several columns at this level. Smaller amounts of damage in similar locations were noted in the 2nd storey. No significant damage was observed in the upper two stories. The main difference, however, was observed in the infill panels. During the 975-yrp test, shear cracking became significant in all 3 of the 1st storey infill panels. This is also evident in the storey shear force versus drift hysteresis loops. The 1st storey

shear strength of approximately 800 *kN* was reached at a storey drift of 0.15% and had reduced to approximately 650 *kN* at a drift of 0.4%. The 2nd storey hysteresis loops also indicate that the ultimate storey shear strength was reached (approximately 800 *kN*), but little softening was observed since the storey drifts at this level never exceeded 0.2% in the negative direction and 0.3% in the positive direction. Storey drifts in the upper two stories essentially never exceeded 0.1% drift, hence there was no significant inelastic behaviour exhibited in the storey hysteresis loops, which is consistent with the lack of observed damage in those two storeys at the conclusion of testing. In summary, at the end of this test, it was found that all members of the concrete frame and the infill in the upper three stories were in good condition. The ground storey infill was severely damaged - too much to be retrofit without replacement.

After the 975-yrp test, the infill frame had become a soft-storey infill frame structure. Nevertheless, it was subjected to the 2000-yrp earthquake signal in order to study how the lateral strength dropped off with increasing drift. To protect the frame and ensure that subsequent tests on retrofit techniques could be performed on the structure, the 2000-yrp test was terminated roughly after 6 seconds once the ground storey drift reached approximately 1.5%. The storey shear versus drift hysteresis loops illustrate clearly that the load deflection characteristics approach those of the bare frame as the drifts increase to values in excess of 1% (see Figure 8).

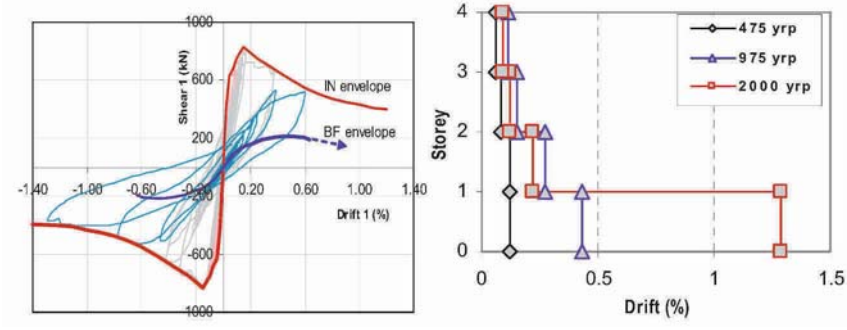

Figure 8. Infill (IN) tests: a) 1st storey shear-drift diagrams and BF and IN envelope curves, b) Maximum drift profiles

The damage patterns at the end of this test were essentially more severe versions of what had been observed in the 975-yrp test. For example, significant shear cracks (approximately 4 *mm* wide) developed in the bottom metre of the 1st storey of column 2. Spalling of cover concrete also occurred in column 2 at this location. The previous cracking patterns in the other frame elements, however, showed no significant change. On the other hand, what remained of the 1st storey infill after the 975 yrp test was severely damaged during this test. When this test was terminated the 1st storey shear strength had dropped by more

than 50%, to less than 400 *kN*. The overall structural behaviour was definitely that of a soft-storey structure. The maximum drift at the top of the structure was 40 *mm* and almost all the drift (35 *mm*) occurred in the 1st storey. Most of the remaining 5 *mm* of drift occurred in the 2nd storey. Consequently, very little new damage occurred in the upper three storeys of the structure.

7. Shotcrete Infilled Frame (SC)

After replacement of the damaged infill panels, shotcrete was applied to part of the walls and new earthquake tests were carried out. On the basis of the analyses of the test results from the previous tests and from visual inspection it was decided to replace only the 1st storey infill walls and to shotcrete the external short-bay at all 4 storeys. The new infill panels were rebuilt with the same geometry and materials as the original walls.

The retrofitting solution applied to the infill walls consisted of a concrete layer with an embedded reinforced steel mesh, which was deemed to improve the post-peak behaviour of the walls. The shotcrete applied to the shorter external panels (one side/face only) at all storey levels consisted of a 26 *mm* thick concrete layer, with an embedded welded steel mesh (5 mm // 0.10, S500, ribbed, grade 500 *MPa*). A 'light connection' (clamps) between the shotcrete layer and the masonry walls was provided at nine points. It is noted that these clamps were not specifically designed to work as dowels, and were used to keep in place the steel reinforcing mesh for the shotcrete works. It is believed that these "connectors" had a beneficial effect on the behaviour of the final wall-shotcrete system, avoiding premature buckling of the shotcrete layer. The final arrangement of the infilled shotcrete frame comprises: 1) at the 1st storey: a) a short panel with a new infill wall (with plaster on both sides) and a shotcrete layer (with 26 *mm* thickness and embedded steel mesh); b) a central long-panel with a new infill wall (with a door opening and plaster on both sides); and, c) an external long-panel with a new infill wall (with a window opening and plaster on both sides); 2) at the 2nd, 3rd and 4th storeys: a) a short panel with an existing infill wall (with plaster on both sides) and a new shotcrete layer (with 26 *mm* thickness and embedded steel mesh); b) a central long-panel with an existing infill wall (with a central window opening and plaster on both sides); and, c) an external long-panel with an existing infill wall (with a window opening and plaster on both sides). It is noted that the existing infills at the 2nd, 3rd and 4th storeys had suffered minor damage after having been subjected to the previous earthquake tests.

The infilled shotcrete frame was subjected to the same earthquakes as the infilled frame; the results from these tests are given in Figure 9 in terms of maximum drift profiles and storey shear-drift diagrams. The equivalent strength

and deformation capacity developed for the SC specimen showed a moderate improvement with respect to the IN frame, however, the 2nd storey drift demands were much higher for the SC tests. This may be explained by the fact that the infill panels at this storey were not replaced after the previous tests (an inter-storey drift of 0.27% was experienced at this storey, which induced damage in the infill panels).

Two main aspects should be highlighted from these tests, namely: a) the beneficial effects of shotcrete, which avoids premature cracking and crushing of the infill walls; and b) shear-out of the external columns in their upper part, leading to local collapse (*warning - negative dangerous effect*), resulting from a combination of the shear forces developed in the infill panel and of the overturning moment effects (up-lift of the upper beam inhibits transmission of shear forces between the panel and the beam, leading to direct shear-out of the top of the column). This is an aspect that deserves special attention, because it is common practice to apply these strengthening techniques for repair and strengthening of infilled structures after earthquakes. Strengthening of infill walls in frame structures should be made with appropriate doweling to the adjacent beams in order to transfer the shear forces gradually to the surrounding frame. In fact, for infill panels located at the frame extremities (external bays) the overturning moments tend to decrease the vertical contact forces between the beam and the infill panel, so that most of the forces developed in the panels are directly transmitted to the external columns, inducing failure in the joint region. It is presumed that this phenomenon depends on the characteristics and detailing of the column. However, it is known that existing frame structures are poorly detailed and that no transversal reinforcement is usually provided in the joint regions. Therefore, strengthening of infill panels in existing vulnerable frame structures should be avoided unless appropriate dowels are provided to transfer most of the forces developed in the walls directly to the surrounding beam/slab members.

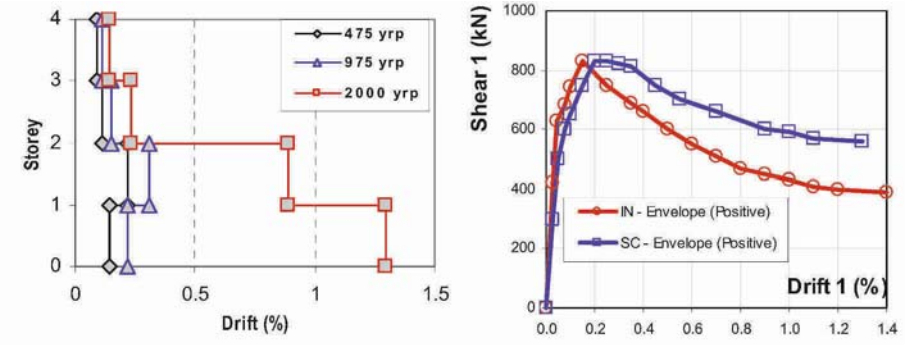

Figure 9. Shotcrete (SC) tests: Maximum drift profiles and 1st storey shear-drift (envelope curves) for the infilled (IN) and shotcrete tests

8. K-bracing with Shear-Link – DSEBS

A ductile steel eccentrically braced system (DSEBS) was used to retrofit one of the storeys of the infilled frame which was subjected to displacement controlled cyclic tests of increasing amplitude. In order to maintain the symmetric layout of the structure, it was decided to retrofit the second storey frame by replacing the infilled wall of the 5.00 *m* wide central bay with the DSEBS assembly as shown in Figure 10.

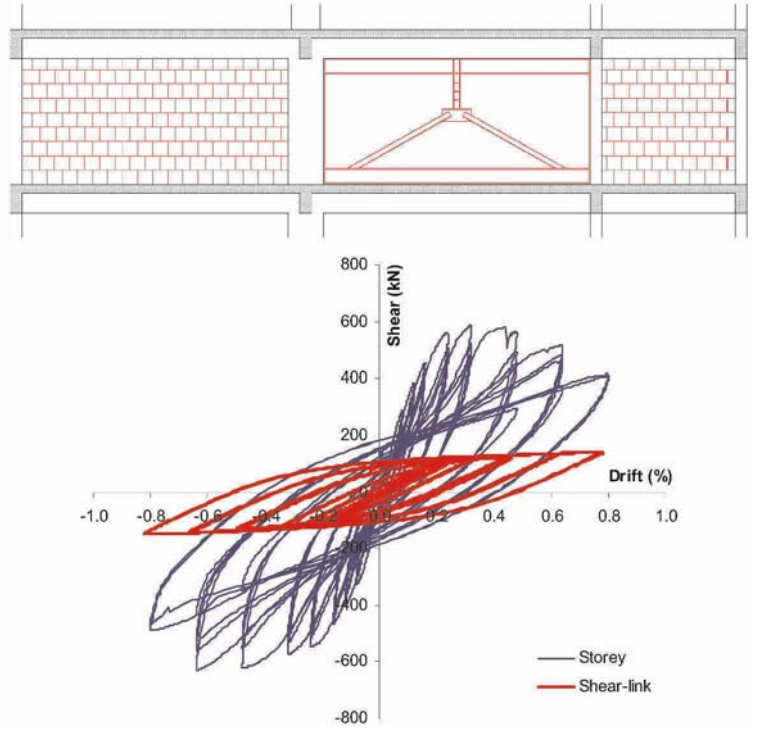

Figure 10. DSEBS: a) Test assembly b) Storey shear – drift and shear-link force-drift results

The DSEBS consists of an assembly of steel beams, diagonal braces and a centrally located ductile vertical shear link replacing the infilled masonry of a single bay in a concrete infilled frame. Conceptually, the design aims at developing a retrofit system, which has a total storey-shear resistance more or less equal to the lateral resistance of the original infilled system (to prevent the introduction of increased loads to the foundation) but with a substantially increased ductile energy absorbing capacity. Other significant characteristics of the DSEBS are drift capacities of up to 9%, and the shear-strain hardening of the web of the shear link that leads under increasing displacements to a cyclic plastic shear resistance equal to about twice the initial lateral resistance at yield.

This increase allows the shear links to compensate for progressive failure and loss of resistance of the non-retrofitted infilled walls.

The results of these tests, in which the retrofitted storey was subjected to cyclic displacement-controlled deflections of increasing magnitude (by holding the lateral displacement of the 2nd floor constant and imposing identical displacements at the 3rd and upper floor levels), showed the soundness of the concept. An excellent agreement between the predicted response and the experimental results was observed. In fact, as shown in Figure 10, the post-peak behaviour of the frame was substantially improved – the drift reached approximately 1% without important loss of strength and the DSEBS dissipated approximately 50% of the total dissipated energy.

9. Summary and Conclusions

A series of pseudo-dynamic tests on two full-scale models of a 4-storey R/C frame representative of existing structures designed without specific seismic resisting characteristics were carried out at ELSA.

The analysis of the test results and the comparison between the behaviour, earthquake vulnerability and performance of the different test models has been presented. The results from the test campaigns permit drawing of the following conclusions: 1) The high vulnerability of the original bare frame (BF) was confirmed. The structure reached imminent collapse at the 3rd storey (2.4% inter-storey drift) for an input intensity slightly higher than the nominal one (1.3 times, in terms of PGA and corresponding to a 975 years return period input motion); 2) The SR frame showed rather improved seismic performance. In fact, it was subjected to the same input motions as the BF with limited structural damage and was able to withstand 1.8 times the intensity of the nominal input motion (corresponding to a return period of 2000 years), maintaining its load carrying capacity with repairable damage. The retrofitting operation addressed and solved the irregularity problem, while the confining steel plates increased the limited deformation capacity of the central stocky column. 3) The infilled frame showed a completely different behaviour as compared to the bare frame. While infills may protect the RC structure, they prompt the development of soft storey mechanisms, and can cause shear-out of external columns in the joint regions; 4) Shotcrete of infill walls in existing structures improves the behaviour of the walls, but can cause premature loss of the vertical load-carrying capacity of the structure shearing-out the external columns. Shotcrete can be beneficial only if appropriate doweling is provided to adjacent beams/girders; 5) Retrofitting solutions based on k-bracing and dissipative devices, such as a shear-link, can substantially improve storey behaviour and increase energy dissipation capacity. More detailed results from the tests and

corresponding analysis can be found elsewhere (Pinto et al. 2002a, 2002b; Bouwkamp et al., 2001, Varum, 2003).

ACKNOWLEDGMENTS

This research developed in the framework of the EC Contracts (FMRX-CT96-0022) and (FMGE-CT95-0027). The co-operation and contribution of the EU researchers is gratefully acknowledged. Sincere gratitude is expressed to E. Carvalho, A. Elnashai, J. Bouwkamp, E. Coelho and R. Pinho for their key contribution to the successful completion of the test campaigns.

References

Bouwkamp, J., Gomez, S., Pinto, A., Varum, H., Molina, J., 2001, Cyclic tests on a R/C frame retrofitted with k-bracing and shear-link, *Report EUR*, Joint Research Centre, Ispra, Italy.

Carvalho, E. C., Coelho, E., Campos-Costa, A., 1999, Preparation of the full-scale tests on reinforced concrete frames - Characteristics of the test specimens, materials and testing conditions, *Report LNEC*, Lisbon.

EC6 - Eurocode N° 6 (EN 1996), Design of masonry structures (Part 1-1: General rules for buildings - Rules for reinforced and unreinforced masonry), CEN, Brussels.

EC8 - Eurocode N° 8 (EN 1998), Design provisions for earthquake resistance of structures (Part 1-4: Buildings in seismic regions - strengthening and repair), CEN, Brussels.

Elnashai, A., Pinho, R., 1999, Icons Topic 2 - Pseudo-dynamic testing of RC frames - proposal for selective repair/strengthening of specimen B, *Report Imperial College of London*, U.K.

Griffith, M. C., Pinto, A. V., 2000, Seismic retrofit of reinforced concrete buildings - a review and case study, in: *Proceedings of the 12th World Conference on Earthquake Engineering*, Auckland, New Zealand, Paper No. 2327.

Pinho, R., 2000, Selective retrofitting of RC structures in seismic areas, PhD Thesis, Imperial College, London, U.K.

Pinto, A. V., 1998, Introduction to the European research projects in support of Eurocode 8, in: *Proceedings of the 11th European Conference on Earthquake Engineering*, A. A. Balkema, Rotterdam.

Pinto, A., Varum, H., Molina, J., 2002°, Assessment and retrofit of full-scale models of existing RC frames, in *Proceedings of the 12th European Conference on Earthquake Engineering*, Elsevier Science Ltd. (Paper Reference 855).

Pinto, A., Verzeletti, G., Molina, J., Varum, H., Coelho, E., Pinho, R., 2002, Pseudo-dynamic tests on non-seismic resisting RC frames (bare and selective retrofit frames), Report EUR, Joint Research Centre, Ispra, Italy.

Pinto, A., Verzeletti, G., Molina, J., Varum, H., Coelho, E., 2002, Pseudo-dynamic tests on non-seismic resisting RC frames (infilled frame and infill strengthened frame tests), *Report EUR*, Joint Research Centre, Ispra, Italy.

Varum, H., 2003, Seismic assessment, strengthening and repair of existing buildings, PhD Thesis, University of Aveiro, Dept. of Civil Engineering, Aveiro, Portugal.

DEVELOPMENT OF INTERNET BASED SEISMIC VULNERABILITY ASSESSMENT TOOLS

AHMET TURER*
Middle East Technical University, Civil Engineering Department, 06531 Ankara Turkey

BARIS YALIM
Department of Civil and Environmental Engineering, Florida International University, Miami, FL, USA

Abstract. Seismic assessment methods are commonly divided into three phases: a) quick assessment b) detailed analysis and c) advanced methods. The dilemma between the large number of buildings to be assessed and low number of technical personnel and funding to assess buildings makes large cities wait on halt. Internet Earthquake Project (InEP) initiated as a Middle East Technical University BAP project in full conjunction with NATO-SfP977231 project, targets internet users to process the buildings in which they reside to carry out the time consuming process of collecting building data. Furthermore, the internet site has a target to disseminate knowledge about basic civil engineering principles and build earthquake vulnerability awareness. Projection of about 5 million internet users in Turkey by the year 2005 builds a good potential for processing the existing building stock. The Internet Earthquake Project's web site is currently fully functional except for ongoing studies of improvement. "Simplistic" and "Complicated" evaluation options are expected to fulfill the beginner and advanced level internet user's level of competency. Concerns about the reliability of entered data and legal (reliability) issues are still under discussion. This study can be viewed as a "first attempt" to carry seismic assessment of existing buildings to the internet, rather than as a final product.

Keywords: Internet; building; assessment; vulnerability; online

* Ahmet Turer, Department of Civil Engineering, Middle East Technical University, 06531 Ankara, Turkey; Tel: +90-312-210 5419, Fax: +90-312-210 1193 E-mail: aturer@metu.edu.tr

S T. Wasti and G. Ozcebe (eds.), Advances in Earthquake Engineering for Urban Risk Reduction, 369–378.

1. Introduction

Earthquake vulnerability assessment of existing reinforced concrete buildings in Turkey is a major need following the updates in the earthquake design code. Istanbul being a large metropolitan area of more than 10 million people is now trying to assess its shabby building stock. After the 17 August 1999 Golcuk-Izmit and 12 November 1999 Duzce Earthquakes, a large magnitude earthquake is expected to hit the city of Istanbul in the future. Limitations of time and resources (such as trained personnel, data collection and post-processing, financial issues) put limitations on the assessment process. Retrofit or demolition-rebuild studies linger on waiting for the assessment as the risk of the earthquake increases.

Istanbul is not the only city at risk, but similar scenarios do exist for other large or small size cities since about 95% of Turkey's population and surface area is under seismic risk. Assessment studies are sreamlined using multiple levels of evaluation: "quick assessment" (walk-down survey), "detailed analysis" (member sizes are used, commonly linear analysis), and "advanced methods" (such as push over analysis, time history). Nevertheless, a fast, efficient, and low-cost alternative would be desirable to assess the seismic vulnerability of existing reinforced concrete buildings.

The number of internet users in Turkey has accelerated from 293 000 users in 1998 to 1 250 000 users in 2000, and 2 660 000 users in 2002[1] in geometric progression and may be expected to exceed 5 million users by 2005. Structural information belonging to about 4 million existing buildings in Turkey can be partially or fully collected through internet as now the number of internet users is rapidly growing in every city. Less developed and small cities may not receive as much attention as the bigger and more industrialized cities (such as Istanbul), but if the data can be collected via internet, the assessment can be automatically done. Since the residents of each house enter the structural parameters, the need for staff to collect data is eliminated.

The two major drawbacks of internet based assessment are 1) reliability and accuracy of the collected data, and 2) liability issues about the assessment results. The details of the internet-based assessment method are given below.

2. Internet-Based Assessment Methodology and Advantages

The internet-based assessment method consists of a main server which is accessed through multiple users through the internet. Building related information is entered and sent to the server. Each assessment request is put in to a queue and processed consecutively. The assessment results based on the input data are generated using the developed software and send back to the user.

Internet based approach combines multiple advantages associated with the internet. The advantages can be listed as follows:

- Large number of users can use the system at the same time.
- Users may access to the assessment server any time at their convenience.
- Residents of houses enter information about their own buildings which eliminates the need for trained personnel and pertinent costs.
- The assessment service is free-of-charge which enables low income residents with internet access to have a general evaluation of their building.
- The internet site and generated information can reach a large number of people very fast which fulfills a very important need.
- Information gathered from a wide spread and comprehensive database would help allocation and optimization of resources for additional assessment planning or retrofit studies.

The objectives of the method are summarized in a bullet list as follows:

- Development of a fast, low-cost, efficient, internet-based earthquake vulnerability assessment tool for existing (or being designed) reinforced concrete buildings.
- Minimization of the problems caused by insufficient technical staff to collect data from an unmanageably large R/C building stock of about 4 million buildings, nationwide.
- Major earthquakes are expected in the future: expedite a well spread assessment process which will enable optimization of related retrofit work by utilizing resources to the districts with worst condition building stock.
- Initiate an approach which may be used internationally for countries that are in similar conditions as Turkey.
- Raise awareness about earthquake risk and vulnerability of buildings.
- Disseminate basic information about civil engineering / construction practice and educate people at a simplified level.
- Calibration of weighting factors of simplistic approach by studying observed building damage after a major earthquake by matching against recorded building information in our database. (The internet site and assessment methods will evolve as earthquakes occur in Turkey. Damage level of buildings that already exist in InEP database will be correlated against predictions and coefficients will be updated after each event.)

The assessment method is defined in two levels of complexity as “simplistic” and “detailed” levels. Each approach is explained in detail below:

2.1. SIMPLISTIC APPROACH

The simplistic approach is composed of an HTML sheet that contains 17 simple questions. The location of each building (address) is asked in order to obtain the seismic zone of the region. Email address of the user is also learned for sending additional information or new assessment results if the evaluation is modified. The following simplistic questions are asked to obtain building related parameters, which are also supported by explanatory graphics.

- number of floors,
- construction date,
- first floor height
- typical floor height,
- building shape and dimensions (width, length),
- irregularity in elevation,
- soil type,
- ground water issues at the basement,
- slope of the ground,
- size of window frames,
- existence of mezzanine,
- soft story and eccentricity,
- apparent concrete quality,
- existence of short column,
- strong beam - weak column,
- overhang in four directions, and
- potential of hammering effect in three directions

Sucuoglu[2] and Yazgan implemented a system of rapid evaluation inspired from ATC-22[3], ATC-21[4] / FEMA 154 by using Duzce database and came up with coefficients (Table 1). An initial starting score is assigned by the number of storeys and peak ground velocity zone (Table 1).

The answers obtained from the internet user are used to assign initial score and deduct points similar to Sucuoglu's[2] work. Since the peak ground velocities are not known for cities in Turkey, the table is modified to use the Earthquake Zoning Map of Turkey (Figure 1). The three zones listed in Table 1 are extrapolated to four zones and the maximum coefficient is modified to be equal to 100 while linearly scaling all of the remaining coefficients (Table 2). Additional questions are asked at the "simplistic" internet site and used to

deduct additional points based on engineering judgment (Table 3). The calibration of coefficients listed in Table 2 and Table 3 can be possible done following a major earthquake (since available building database from previous earthquakes lack that information). Recorded building information in InEP database and observed damage in the future would be matched against each other for preferably a large number of buildings, and the coefficients would be calibrated for an improved assessment confidence level.

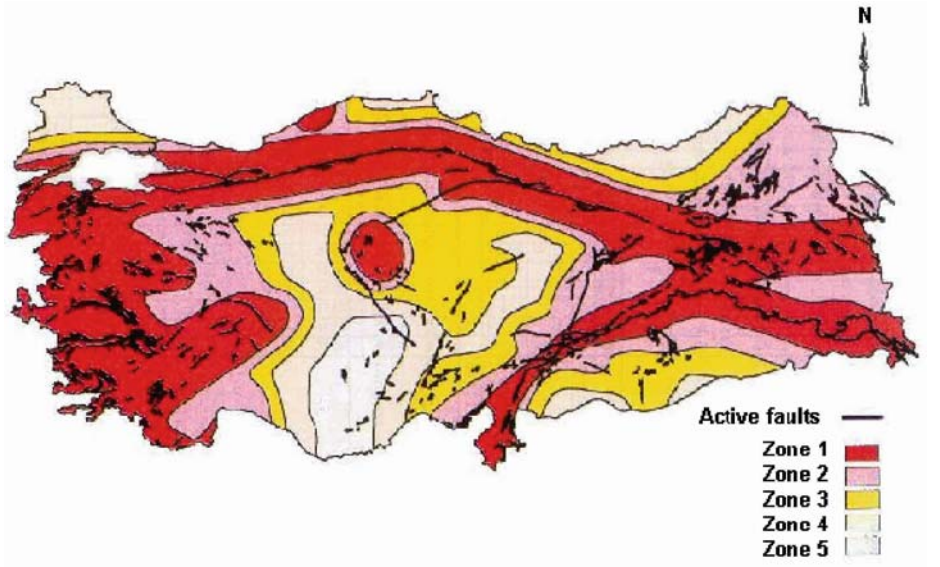

Figure 1. Earthquake zoning map of Turkey

TABLE 1. Sucuoglu[2] and Yazgan's rapid evaluation coefficients

Number of Stories	Zone 1: 60 ≤ PGV ≤ 80	Zone 2: 40 ≤ PGV ≤ 60	Zone 3: 20 ≤ PGV ≤ 40	Soft Story	Heavy Overhangs	Apparent Concrete Quality	Short Column	Hammering Effect	Plan Irregularity
1 or 2	95	130	170	0	-5	-5	-5	0	0
3	90	125	160	-10	-5	-10	-5	-2	-2
4	90	115	145	-15	-10	-10	-5	-3	-2
5	90	105	130	-15	-15	-15	-5	-3	-5
6 or 7	80	90	105	-20	-15	-15	-5	-3	-5

TABLE 2. Modified coefficients by scaling the highest score to 100 (questions 1-8)

Number of Stories	Zone 1	Zone 2	Zone 3	Zone 4	Soft Story	Heavy Overhangs	pparent oncrete Quality	Short Column	Hammering Effect	Plan Irregularity
1 or 2	44.2	60.5	79.1	100.0	0	-2.3	-2.3	-2.3	0	0
3	41.9	58.1	74.4	90.7	-4.7	-2.3	-2.3	-2.3	-0.9	-0.9
4	41.9	53.5	67.4	83.7	-7.0	-4.7	-4.7	-2.3	-1.4	-0.9
5	41.9	48.8	60.5	76.7	-7.0	-7.0	-7.0	-2.3	-1.4	-2.3
6 or 7	37.2	41.9	48.8	58.1	-9.3	-7.0	-7.0	-2.3	-1.4	-2.3

TABLE 3. Additional points assigned for the variables obtained in questions 9-17

PARAMETER	EVALUATION	OPTION 1	OPTION 2	OPTION 3	OPTION 4	OPTION 5
Date of Construction	If doc<1975 → -1 If 1975≤doc≤1998 → -0.5 If doc≥1999 → 0	NA	NA	NA	NA	NA
Vertical Discontinuity (vd)		0	-1	NA	NA	NA
Soil Type (st)		0	-0.5	-0.8	-1	NA
Basement (b)		0	0	-0.3	-0.6	-1
Ground Inclination (gi)		0	-0.3	-0.8	NA	NA
Window Size (ws)		0	-0.2	-0.5	NA	NA
Mezzanine (m)		0	-1	NA	NA	NA
Strong Beam-Weak Column (sb-wc)		0	-1	NA	NA	NA

As the user answers 17 simple questions, the submit button is clicked and the background program calculates a score which is based on the starting score and all the points that are deducted from the starting score. The best and worst case scenarios define the boundaries between 100 points and 1.5 points.

A report is automatically generated including the building score, list of deducted points, earthquake zoning map[5] of the corresponding city, and 7-8 page long report. The report is automatically generated using an expert system which has certain report pieces readily defined. Each report piece is selected based on the answers received for questions and combined together to generate a report. The report discusses general issues about the following:

- amplification of earthquake waves on soft soil
- earthquake zoning map of the selected city
- design code used based on building construction date
- hammering effect
- symmetry in construction, irregularities, architectural issues
- eccentricity (role of windows and infill walls)
- soft storey and effects of mezzanine
- role of overhand
- water table, mechanism and risk of liquefaction
- slope of the land
- importance of concrete quality, segregation, alkali silica reaction etc.
- reinforcement, confinement of concrete, detailing,
- short column and problems associated with it
- strong beam – strong column problem and related information
- disclaimer and histogram showing the buildings entered so far (the user can relatively evaluate his/her building).

The user is also invited to use the "detailed" evaluation program which includes additional questions on the structural system and conducts analysis for evaluation purposes. Further details about the detailed evaluation are provided in the next section.

2.2. DETAILED APPROACH

The detailed approach is based on the finite element analysis of a building. The user is required to download software from the internet site which is developed to function as an advanced user interface (Figure 2). The graphical interface is used to define column and beam properties such as dimensions and reinforcement data. The floor plans (column-beam layout and slab) are defined. Multiple floors can be defined at the same time and changes to selected floor properties (columns, beams, openings in the slab, etc.) can be defined one at a time. The graphical user interface collects data, organizes information, and sends it to the server for processing. Once data reaches the server, a developed structural analysis program conducts a linear analysis and calculates member forces. Member capacities are also calculated based on the member properties defined by the user. The demand-capacity ratios are calculated for each member. A building score (BS) is then found by taking the weighted averages

of all demand-capacity ratios (D/C) with respect to their importance factors (IF) as shown in Eq. (1).

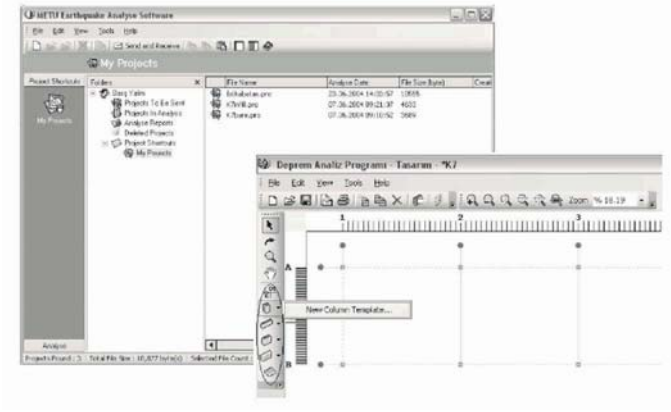

Figure 2. Graphical user interface for the detailed approach

$$BS = \frac{\sum IF_{column\_i} * (D/C)_{column\_i} + \sum IF_{beam\_j} * (D/C)_{beam\_j}}{\sum IF_{column\_i} + \sum IF_{beam\_j}} \quad (1)$$

The program also automatically generates a detailed electronic report that lists all of the member forces, 3D graphical member load graphs (Figure 3), and animated mode shapes (Figure 4). The detailed approach is tested using the Duzce building damage database for randomly selected 36 buildings. Three damage levels "none-light", "medium", and "severe" are defined using the building scores obtained from the analysis program. The selected building population was successfully separated by defining threshold values. The success rates obtained for different performance levels are: severe →100%, medium →66.7%, none/light →94.4%.

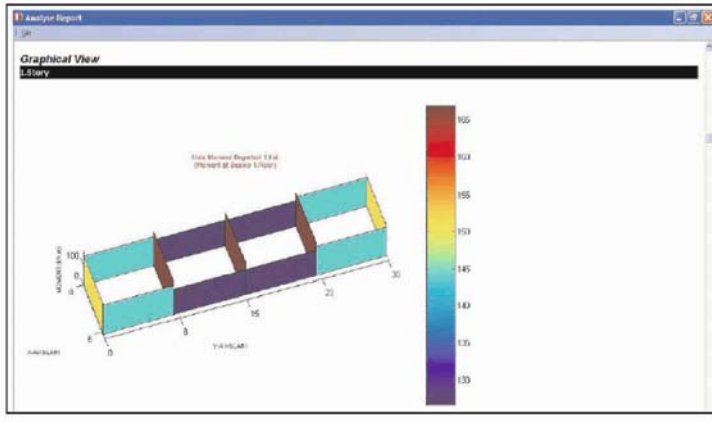

Figure 3. Graphical display of member force distribution

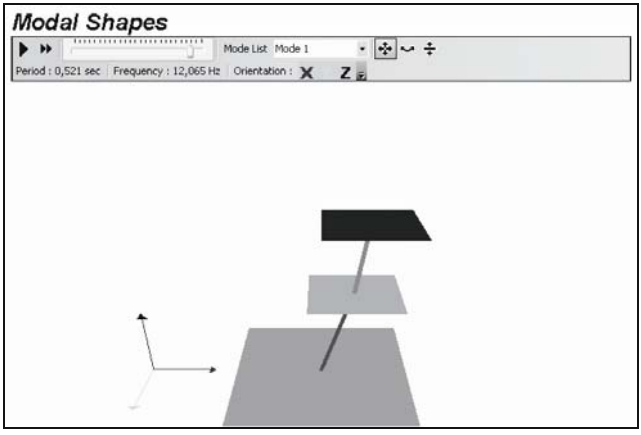

Figure 4. Simplistic mode shape animation

3. Conclusions

The study presented in this paper is a part of ongoing process. The internet earthquake project web site has started demonstration broadcasting at the address http://www.idp.metu.edu.tr and alternatively at http://144.122.101.72/ however there are certain issues left to be solved. Legal issues are carefully being investigated and concerns about the liability exist.

The internet based earthquake vulnerability assessment studies conducted so far is an attempt to carry the evaluation process to the internet which has an ever growing user number that reaches 5 million users in Turkey. The project is very promising for rapidly screening a large number of reinforced concrete buildings that exist in Turkey (about 4 million buildings) at almost no cost to the university or to the user. The extensive database collected from a large number of users would be used for future calibration studies as new earthquakes occur: the building damage levels can be compared against the predictions for the buildings that already exist in the InEP database and improvements to the evaluation engine can be made.

The internet site's role on disseminating practical information about building construction and behavior to residents is noteworthy especially since control on building construction is not perfect and Turkey is located on many major faults that are seismically active. The internet site also carries an ethical dimension as it is equally reachable to all citizens independent of the income level and geographic location.

ACKNOWLEDGEMENTS

This study is supported by BAP-2003-03-03-03 (METU, Science Research Project), PROAD program, and NATO-SfP977231 project. The dissemination of knowledge related activities are also included under TUBITAK ICTAG-577 project.

References

1. "Bilgi toplumunda yeni ekonomi ve e-dönüşüm stratejileri", Prof.Dr.E.Oktay et al. http://iibf.ogu.edu.tr/kongre/bildiriler/04-02.pdf (in Turkish).
2. Sucuoglu, H., Yazgan, U., "Simple Survey Procedures for Seismic Risk Assessment in Urban Building Stocks", Proceedings of the NATO Science for Piece Workshop on Seismic Assessment and Rehabilitation of Existing Buildings, edited by S.Tanvir Wasti and Guney Ozcebe, pp.97-118, Izmir 2003.
3. Applied Technology Council, "A Handbook for Seismic Evaluation of Existing Building" (ATC-22), Federal Management Agency Report FEMA-178, California, 1989.
4. Applied Technology Council, "Rapid Visual Screening of Buildings for Potential Hazards" A Handbook, (ATC-21), Federal Management Agency Report FEMA-154, California, 1988.
5. Ministry of Public Works and Settlement. General Directorate of Disaster Affairs, "Specifications for Structures to be Built in Disaster Areas", Ankara, 1998.

A COMPARATIVE STUDY OF DISPLACEMENT, FORCE AND PUSHOVER APPROACHES FOR DESIGN OF CONTINUOUS SPAN BRIDGES

MICHELE CALVI
University of Pavia, Department of Structural Mechanics, Pavia, Italy

CHIARA CASAROTTI
European School for Advanced Studies in Reduction of Seismic Risk (ROSE School), Pavia, Italy

RUI PINHO
European School for Advanced Studies in Reduction of Seismic Risk (ROSE School), Pavia, Italy

Abstract. Common force-based design approaches require significantly increased design effort, in the form of successive iterations, to be incorporated within a performance-based framework. Recently, displacement-based design methods have been developed with the objective of overcoming such limitation, directly designing a structure able to sustain a pre-defined level of damage under a pre-defined level of earthquake intensity. However, application of those methods in the design of bridges requires a number of assumptions that may, in some cases, lead to not-necessarily cost-effective solutions. A pushover-based design procedure for continuous RC bridges is proposed herein, which can be incorporated into a performance-based design philosophy. The background and development of this alternative design procedure is presented first, followed by a comparative study, carried out in order to compare the proposed design method to simplified force and displacement-based procedures. Pros and cons of each strategy, as well as possible lines of development, are then identified.

Key words: performance; displacement; force; pushover; adaptive; bridge design; DAP

S.T. Wasti and G. Ozcebe (eds.), Advances in Earthquake Engineering for Urban Risk Reduction, 379–394.

1. Introduction

The current state of practice witnesses the widespread use of force-based methods for seismic design of bridges, in which damage and hence performance is very difficult to be quantified for a particular earthquake level. As illustrated by Kawashima (2000) and Calvi (2004), amongst others, such elastic design approaches carry, however, a number of shortcomings that may lead to unsatisfactory bridge seismic performance.

Design for seismic resistance has been undergoing a critical reappraisal in recent years, when attention focused on limit states design, with the emphasis changing from "strength" to "performance". The philosophy of performance-based earthquake engineering consists in designing a structural system which would achieve, rather than be bounded by, a given performance limit state under a given seismic intensity: it is generally agreed that deformations are more critical parameters for defining performance, and it is argued that seismic design methods should largely be based on them. Traditional and current code seismic design methods are force-based in nature and conceptually not based on the perspective of achieving the goal of performance-based engineering.

A promising design philosophy is constituted by direct displacement-based design (DDBD) methods (Priestley, 1993; Kowalsky et al., 1995 and 2002), due to their inherent possibility of explicitly specifying displacements, which are well correlated with deformations, as design targets. However, application of DDBD in the design of bridges requires a number of assumptions that may, in some cases, lead to not-necessarily cost-effective solutions.

Recent studies (Casarotti, 2004) reported the viability of using a design procedure for continuous concrete bridges, which employs a Displacement-based Adaptive Pushover (DAP) to estimate the seismic structural response.

A comparative study is carried out in order to compare to the proposed design method to other simplified procedures: pros and cons of each strategy are compared in terms of reliability, optimization of the required materials, simplicity and velocity of implementation.

2. Current Design Methods for Bridges

Bridges have been designed by reference to acceleration response spectra, for the past 40 years, apparently for historical reasons, related to the common practice of design for static loads. In the 1950's and 1960's, the concept of 'ductility' was adopted, in order to reconcile inconsistencies in the fundamental basis of force-based seismic design; ductility was then related to some kind of "equivalent strength" by a number studies (Newmark and Hall, 1973), by means of the well known concepts of conservation of acceleration, velocity and

displacement as a function of the fundamental period of vibration of the structure. The current state of practice still relies on these concepts: elastic acceleration spectrum is reduced as a function of an assumed structural ductility capacity, and 'capacity design principles' (Park and Paulay, 1975) are applied to ensure the development of the assumed post elastic mechanism.

From a design point of view, a number of performance-based design approaches aimed at reducing local damage or ductility has been proposed advocating only minor changes to existing design approaches: they are basically still force-based procedures, with the addition of a displacement check to ensure that acceptable performance levels are achieved in the design earthquake.

Bertero and Zagajeski (1979) and Fintel and Ghosh (1982) proposed force-based code design for preliminary strength determination, with inelastic time-history analyses to check inelastic deformation, and a subsequent design "optimisation" to reduce inelastic deformation at all locations to acceptable limits. A similar approach was suggested by Stone and Taylor (1994) for bridges, using local damage indices rather than inelastic deformation as acceptance criteria.

It was argued (Kappos, 1997) that the computational effort involved in the successive approximation implied by these methods may be excessive, and that the reliance on a simple SDOF model for initial design may be too simplistic, particularly when modern design codes generally require 3D modal analysis. Kappos (1997) proposed a modified form of these approaches applied to building structures.

Fardis and Panagiotakos (1997) suggested a simplified design procedure in which design forces for ductile elements are calculated for the serviceability level earthquake, based on an interpretation of the consequences of the cross-section stiffness required by EC8 (CEN, 2002). This leads to a force-reduction factor of 5, applied to the full design elastic forces: presented results indicated that simple elastic analysis under a triangular lateral acceleration distribution will provide adequate estimates of drifts.

2.1. ISSUES WITH FORCE-BASED DESIGN PROCEDURES

In force-based design approaches, performance is very difficult to be quantified for a particular earthquake level, since forces are poor indicators of damage potential, and force-reduction factors, which are meant to imply damage levels, are highly variable and often disagreed upon. All the procedures illustrated above are basically force-based, and may be considered as reasonable design approaches that will lead into safe structures, but that does not directly address performance criteria at the initial stage of the design.

Priestley (2000) outlined a number of conceptual and philosophical problems associated with force-based/displacement-check design: (i) the use of characteristic force-reduction or ductility-dependent factors results in non-uniform risk, thus being philosophically incompatible with the use of uniform-risk design spectra; (ii) for many structures, code drift limits are found to govern, and, as a consequence, iterative design increases design complexity; (iii) the emphasis placed in some design code on complex 3D modal analysis seems to bring little benefit if capacity design principle are applied; (iv) assuming the elastic structural characteristics as an indicator of inelastic performance, as implied by force-based design, is clearly of doubtful validity.

Moreover, distributing forces among structural members according to an initial pre-assigned stiffness implies that the structural stiffness is independent of strength, and that yield displacement is directly proportional to strength, whilst experimental evidence shows exactly the opposite.

Kowalsky (2002) showed that spectral analysis assuming elastic properties utilized in force-based design can at times be very accurate and at other times incur significant errors, especially when large stiffness irregularities are introduced, particularly for systems with abutment restraint, thus highlighting the unpredictable performance of the method.

2.2. THE DIRECT DISPLACEMENT-BASED DESIGN PROCEDURE

The alternative design procedure known as ‘direct displacement-based design’ (Priestley, 1993; Kowalsky et al., 1995; Priestley and Calvi, 1997; Kowalsky, 2002) has been developed with the objective of directly designing a structure to reach a predetermined displacement when subjected to an earthquake consistent with the design level event: contrarily to force-based approaches, design forces are obtained from the inelastic response of the system for a desired performance level.

The basic method is defined by a response spectrum-based approach that employs the substitute structure concept (Gulkan and Sozen, 1974) to model an inelastic system with equivalent elastic properties. The structural hysteretic behaviour is represented by an equivalent elastic secant stiffness at the design displacement associated to a consistent equivalent viscous damping, and the structural response is determined from elastic over-damped response spectra. Essentially, the DDBD procedure for MDOF bridge structures can be reduced to the following steps: (i) determination of the inelastic displacement pattern, (ii) characterisation of the equivalent SDOF, (iii) application of the DBD approach to the SDOF, (iv) determination of required strength and design of the columns.

The application of DDBD requires that assumptions are made regarding the inelastic deformed pattern, the base shear distribution and the estimation of the system equivalent viscous damping. In particular:

- The inelastic deformed pattern is represented by means of an approximate sinusoidal shape function: the dependence of the inelastic deformed shape on the relative contributions of deck, piers and abutment restraints renders "the most natural" inelastic pattern possibly more complicated, depending on the regularity of the system. This type of regular deformed pattern might be valid only for symmetric bridge configurations, and even more if the highest piers are centrally located. In the most updated version of the method (Alvarez, 2004), an iterative procedure is applied to the deformed pattern, in which the final displaced shape may differ from the initial assumption.
- The equivalent viscous damping is first estimated per element, and then for the entire system, by means of weighted averages based on the work carried out by each member and on the relative proportion of the total seismic load shared among abutments and piers.
- The total base shear is shared inversely proportional to the pier height, and an assumption of the seismic load carried by the abutments is needed. This passage thus implies that all piers have an elastic-purely plastic response and the same geometry and reinforcement.

Kowalsky (2002) reports case studies where the pier forces, and consequently the supplied longitudinal steel, coming from a DDBD approach are two or three times the forces estimated with a force-based procedure. The latter issue is strictly related to the DDBD approach: the design deformed pattern, corresponding to a limit state maximum response, leads to a large magnitude equivalent displacement. The latter determines the total shear demand on the structure, resulting in a large moment demand if compared with the FBD approaches, which make use of force-reduction factors.

3. A Pushover-Based Performance Design Procedure (PBPD)

Recent studies (Casarotti, 2004) reported the viability of employing Displacement-based Adaptive Pushover (Antoniou and Pinho, 2004) to estimate seismic response of bridges. Contextually, a pushover-based design procedure has been proposed and incorporated into a performance-based design philosophy, in an attempt to overcome some of the difficulties encountered with other simplified design methods, previously introduced. The procedure, applied here to design of continuous concrete bridges with flexible/rigid superstructures

and varying degrees of abutment restraint, caters for estimation of the distribution of the seismic demand on the structure in terms of displacements and base moments, without the need for any assumption that cannot be verified.

The proposed performance-based design approach combines elements from the DDBD and the Capacity Spectrum (Freeman, 1998; Fajfar, 1999) methods, elaborated within an "adaptive" perspective, for which reason it can also be seen as an adaptive capacity spectrum method. The procedure essentially consists in deriving an adaptive SDOF capacity curve and plotting it versus the Acceleration-Displacement Spectrum of the design earthquake, thus obtaining the design intersection. An initial assumption on the pier longitudinal reinforcement is needed, in order to perform the pushover analysis. The method can be reduced to the following basic steps:

1. Determination of the "Equivalent SDOF Adaptive Capacity Curve": a reliable pushover analysis is performed on the structure to derive the "Equivalent SDOF Adaptive Capacity Curve", by calculating the equivalent system displacement $\Delta_{sys,k}$ and acceleration $S_{a\text{-}cap,k}$ based on the current deformed shape at each analysis step k, as described in Eq. (1), where $V_{b,k}$ is the total base shear of the system and $M_{sys,k}$ is the effective system mass (Eq. 2).

$$\Delta_{sys,k} = \frac{\sum_i m_i \Delta_{i,k}^2}{\sum_i m_i \Delta_{i,k}} \text{ and } S_{a\text{-}cap,k} = \frac{V_{b,k}}{M_{sys,k} g} \tag{1}$$

$$M_{sys,k} = \frac{\sum_i m_i \Delta_{i,k}}{\Delta_{sys,k}} \tag{2}$$

2. Application of the demand spectrum to the "Equivalent SDOF Adaptive Capacity Curve": a visual evaluation of the structural performance under the earthquake ground motion is obtained by intersecting the capacity curve and the demand spectrum, and estimating the inelastic acceleration and displacement demands (i.e. design point), as shown in Figure 1(a). A swift iterative procedure is required at this stage in order to use the correctly damped demand spectrum: with the design point obtained with the 10% damped spectrum, the system damping is calculated with a SDOF damping model. As an example, the Takeda degrading-stiffness-hysteretic response based model is shown in Eq. (3), where r and μ_{sys} are the post-yielding ratio and the ductility of the SDOF system, as calculated by bi-linearising the capacity curve at the design point; the procedure is iterated up to the

convergence of the damping value, which usually occurs within a couple of iterations.

$$\xi_{sys,\,eff} = 0.05 + \frac{1-(1-r)/\sqrt{\mu_{sys}} - r\sqrt{\mu_{sys}}}{\pi} \tag{3}$$

3. Determination of the inelastic deformed shape and of the base moment distribution: target displacements and base moments correspond to the design point level in the pushover analysis output, as shown in Figure 1b.

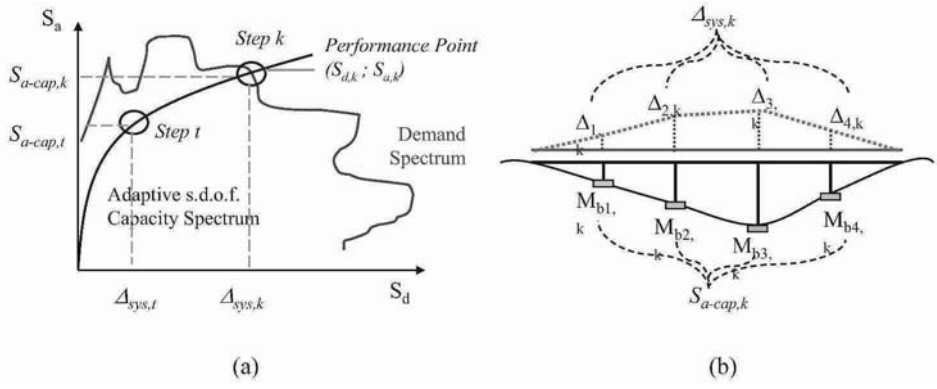

Figure 1. Schematic representation of proposed PBPD procedure

4. Check of acceptability criteria (column required displacement and strength): longitudinal reinforcement supply is checked to assess if it suffices to resist the design moments, whilst transverse reinforcement is designed to warrant the attainment of the design displacements. If the longitudinal steel assumed at the beginning of the procedure results inadequate, a different assumption is made and the whole procedure is re-iterated; simply re-run the pushover with different reinforcement ratios, introducing modifications only when required (i.e. on a limited number of members), thus optimising the design outcome.

The proposed design procedure (PBPD), even though inspired by the Capacity Spectrum Method, features one important conceptual difference: it makes use of an equivalent SDOF curve which does not refer to any given pre-defined mode shape nor to the displacement of a reference node. Indeed, equivalent SDOF quantities are calculated step-by-step based on the current deformed pattern (thus implying that also Msys varies at each step, which is also not the case in traditional Capacity Spectrum methods). In other words, and as stated above, the proposed procedure can be viewed as an adaptive variant of the CSM approach with incorporation of elements of DDBD.

PBPD was applied in the design of a set of asymmetric bridges with different length, pier layout and types of abutments, assuming a minimum initial reinforcement ratio (0.8%) and making use of Displacement-based Adaptive Pushover to run the necessarily reliable nonlinear static analyses. The resulting deformed shapes, corresponding to the design point, have been compared with results obtained from inelastic dynamic analysis: the matching of results appeared to be quite reasonable in the majority of cases, as illustrated in Figure 2, which shows exemplificative results obtained for a highly irregular bridge configuration (B2331312), the characteristics of which can be found in Casarotti (2004).

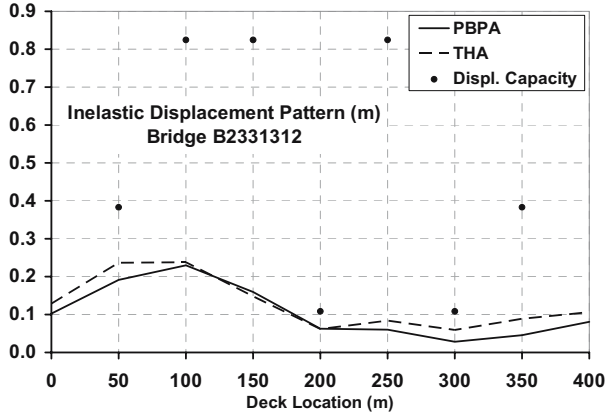

Figure 2. Inelastic displacement pattern obtained with PBPD, for a highly irregular bridge

4. Preliminary Comparative Study

A relatively limited parametric study was carried out in order to preliminarily assess how the proposed design method compared with other simplified procedures: pros and cons of each strategy are evaluated in terms of reliability of response predictions, required design reinforcement and simplicity of application. The following procedures have been applied to design a set of four-span continuous deck bridges: (i) Force-based Design (FBD); (ii) Direct Displacement-based Design (DDBD) in its Priestley and Calvi (2003) version; (iii) Pushover-Based Performance Design (PBPD); (iv) Direct Displacement-based Design based on the inelastic displacement pattern resulting from the pushover (DDBDpo), without iterating on it.

The input parameters for all the procedures are: column diameter and height, inertia masses, material properties, design spectra, and, for PBPD only, assumed steel ratio. The Force-based design procedure applied in this study featured the following steps:

1. Determination of Lateral Forces: the elastic period is determined based on reduced section stiffness, and elastic response acceleration is obtained from the design spectrum. A reduction factor (e.g. 4, consistent with current Caltrans recommendations) is applied to the elastic spectrum-derived forces, which are distributed according to the modal shape.
2. Elastic Analysis: the procedure is repeated for as many modes as needed until 90% of the total mass has been considered: results are then combined using the SSRS rule.
3. Section Design: longitudinal reinforcement for required lateral force is designed (it is assumed that adequate confinement detailing, necessary to warrant the attainment of predicted displacements, would also be introduced).

The applied DDBD procedure, on the other hand, followed the steps described below:

1. Determination of the inelastic displacement pattern: the target lateral drift is identified for each individual column, a starting deformed shape is assumed and scaled on the first damaged element displacement.
2. Characterisation of the equivalent SDOF: system target displacement, hysteretic Damping and effective mass are calculated.
3. Application of the DDBD approach to the equivalent SDOF: the effective period is derived from the damped displacement spectrum and the effective stiffness and base shear are calculated.
4. Determination of the column required strength and design: the lateral seismic force is distributed in proportion to masses and displacements and elastic analysis is performed based on secant stiffness; iterations are made on the deformed pattern up to convergence.

Further details on the application of both design methodologies can be found in the work by Casarotti (2004).

4.1. CASE-STUDIES AND MODELLING

The designed bridge configurations, listed in Table 1, consist of four-span (40 m, 50 m, 50 m, 40 m span length) continuous deck bridges with two types of abutments. The superstructure weight is taken as 200 kN/m, and the moment of inertia (referred to the transverse bending) as 50 m^4, the superstructure depth, i.e. the distance between the pier top and the center of the deck is 2 m; the transverse pier/superstructure connections are assumed to be monolithic, and the columns are fully fixed at the base; the column diameter is 2.2 m, the

concrete compression strength is 40 MPa and 43 mm diameter rebars with strength of 455 MPa are employed. The reference maximum drift is chosen as 4% of the column height.

The employed seismic excitation is defined by a historical record scaled to match the 10% probability of exceedance in 50 years uniform hazard spectrum for Los Angeles (SAC Joint Venture, 1997). The main characteristics of the record (LA03) are a PGA value of 0.39g, a PRA of 1.43g and a significant duration of 8.52s (out of 40s total duration). The design earthquake is 1.6 times such record.

TABLE 1. Designed Bridge configurations

Bridge Label	Abutments	Pier 1	Pier 2	Pier 3
B212el	Linear Elastic	16 m	8 m	16 m
B212fx	Fixed			
B312el	Linear Elastic	24 m	8 m	16 m
B312fx	Fixed			
B321el	Linear Elastic	24 m	16 m	8 m
B321fx	Fixed			
B222el	Linear Elastic	16 m	16 m	16 m
B222fx	Fixed			
B121el	Linear Elastic	8 m	16 m	8 m
B121fx	Fixed			

The Finite Elements Analysis package used in the present work, SeismoStruct (SeismoSoft, 2005), is a fibre-element based program for seismic analysis of framed structures, which can be freely downloaded from the Internet. The program is capable of predicting the large displacement behaviour and the collapse load of framed structural configurations under static or dynamic loading, accounting for geometric nonlinearities and material inelasticity. Its accuracy in predicting the seismic response of bridge structures has been demonstrated through comparisons with experimental results derived from pseudo-dynamic tests carried out on full or large-scale models (e.g. Casarotti, 2004). Further, the package features also the readily availability of the displacement-based adaptive pushover algorithm employed in this study.

4.2. OBTAINED RESULTS

Results are shown in Table 2, per each bridge pier and per each design procedure, in terms of the ratios between the design prediction and the time history results (carried out on the designed specimens) of the deck drifts and of the pier base moments. Design outcomes are then summarised in terms of total number of employed rebars.

TABLE 2. Time history verification (values close to unity indicate good design predictions)

Bridge	Design method	Design prediction/time history verification						Number of rebars
		Δ1	Δ2	Δ3	M1	M2	M3	
B212el	FBD	1.09	0.68	1.09	0.64	0.91	0.64	104
	DDBD	0.95	0.91	0.95	1.05	0.90	1.05	198
	PBPD	1.00	0.90	1.00	1.00	0.91	1.00	120
	DDBDpo	1.06	0.96	1.06	0.96	0.92	0.96	140
B212fx	FBD	0.52	0.43	0.52	0.32	0.83	0.32	94
	DDBD	0.84	0.83	0.85	1.06	0.92	1.06	156
	PBPD	0.73	0.70	0.73	0.95	0.91	0.95	94
	DDBDpo	0.75	0.73	0.75	1.00	0.92	1.00	110
B312el	FBD	1.22	0.48	0.95	0.45	0.90	0.63	90
	DDBD	1.06	0.93	0.87	1.30	0.91	1.05	200
	PBPD	0.91	0.83	0.99	0.85	0.92	1.00	136
	DDBDpo	0.95	0.81	1.08	0.31	0.92	0.04	160
B312fx	FBD	1.03	0.83	0.93	0.28	0.91	0.47	124
	DDBD	0.82	0.81	0.82	1.07	0.90	1.02	140
	PBPD	0.75	0.71	0.73	0.71	0.91	0.91	98
	DDBDpo	0.84	0.84	0.89	1.05	0.91	1.03	122
B321el	FBD	0.71	0.47	0.19	0.45	0.74	0.72	66
	DDBD	0.97	1.00	1.17	1.05	1.00	1.00	154
	PBPD	0.87	0.87	0.92	0.95	0.97	0.95	104
	DDBDpo	1.05	1.13	1.47	1.14	0.97	1.00	214
B321fx	FBD	1.81	1.38	0.89	0.51	0.94	0.92	108
	DDBD	1.18	1.09	1.04	1.08	0.99	0.93	90
	PBPD	1.33	1.22	1.15	0.99	1.00	0.94	84
	DDBDpo	1.34	1.24	1.18	0.83	0.71	0.94	86
B222el	FBD	0.46	0.47	0.46	0.79	0.87	0.78	72
	DDBD	1.20	1.13	1.20	1.01	0.98	1.01	204
	PBPD	1.05	0.99	1.05	1.00	1.00	1.00	196
	DDBDpo	1.01	0.99	1.01	1.00	1.00	1.00	204
B222fx	FBD	0.64	0.65	0.64	0.63	0.87	0.63	68
	DDBD	1.09	1.07	1.09	0.97	0.90	0.96	114
	PBPD	1.14	1.11	1.14	0.99	0.95	0.99	128
	DDBDpo	1.09	1.07	1.09	0.97	0.91	0.97	114
B121el	FBD	0.87	1.07	0.87	0.92	0.81	0.92	118
	DDBD	1.15	1.08	1.15	0.95	0.96	0.95	110
	PBPD	1.05	1.01	1.05	0.93	1.00	0.94	80
	DDBDpo	1.17	1.09	1.17	0.92	0.97	0.92	114
B121fx	FBD	1.00	1.09	1.00	0.94	0.80	0.94	118

Bridge	Design method	Design prediction/time history verification						Number of rebars
		Δ1	Δ2	Δ3	M1	M2	M3	
	DDBD	1.23	1.20	1.24	0.92	0.93	0.92	66
	PBPD	1.11	1.08	1.11	0.93	0.98	0.93	66
	DDBDpo	1.23	1.19	1.23	0.76	0.76	0.76	66

In order to obtain an overview of the effectiveness of the methods, the above results are then averaged along each bridge, and graphically represented in Figure 3, where the total number of employed rebars is normalised with respect to number of rebars requested by the method which required the lowest amount of steel. The following observations can be drawn from this preliminary set of results:

- a fairly good prediction (i.e. values close to unity or to 100%) of the inelastic displacement pattern (Figure 3a) is provided by the three performance-based methods, whilst their force-based counterpart shows great dispersion of results, with a tendency for strong underestimation;
- as for the case of deck drifts, force-based design methods seem to under predict moment demand at the base of the piers (Figure 3b), for the majority of cases, whilst the three performance-based methods present similar level of prediction reliability;
- in terms of requested longitudinal reinforcement, FBD tends to lead to the lowest amount of required steel (Figure 3c), however the conspicuously unsafe inconsistency between the design predictions and the time history verification, renders the method effectively ineligible for comparison in this regard;

DDBD, as implemented in this work, did cater for an effective and full control on both displacement and moment demand. However, it also led to relatively large amounts of longitudinal reinforcement, possibly due to inadequate assumptions of the deformed pattern, which did not seem to be the optimum even when obtained through iteration (when a pushover-obtained displaced shape was employed instead, DDBDpo, improved results were warranted);

In general, the pushover-based design method, PBPD, seemed to provide the best compromise in terms of matching dynamic analyses results and optimising the required design reinforcement. Another advantage of this methodology is that design can be optimised on different piers, either through design iterations or already at the initial assumption stages, if some preliminary conceptual guidance based on bridge configurations is available.

On the other hand, however, it is equally undeniable that, compared to the others methodologies employed, PBPD features a higher level of computation

and implementation complexity even if, contrary to the other simplified performance-based design methods, it did not present any convergence difficulties when applied to highly asymmetric bridge configurations.

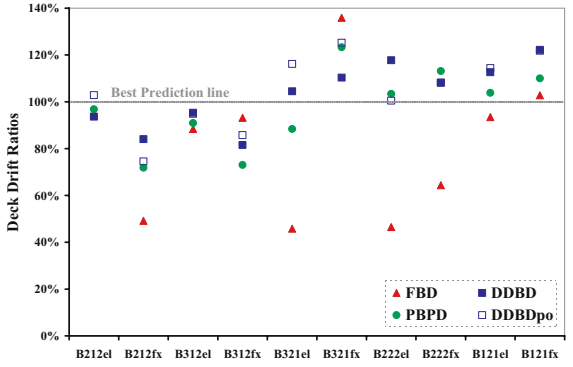

(a)

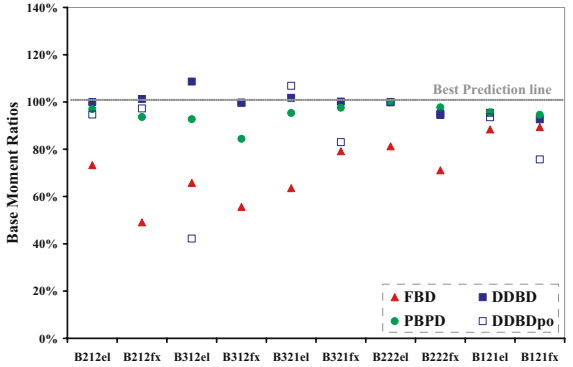

(b)

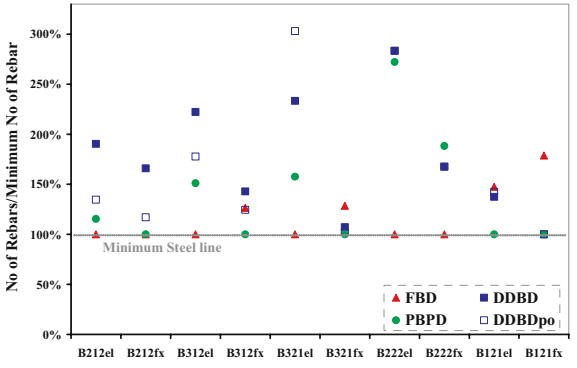

(c)

Figure 3. Ratios of design/verification values: (a) drifts, (b) moments, (c) reinforcement

5. Concluding Remarks

Common force-based design approaches require significantly increased design effort, in the form of successive iterations, to be incorporated within a performance-based framework. This comes as result of the fact that such methods do not provide a direct control over the deformational response of structures; displacements are a design result rather than a design target. Consequently, alternative displacement-based design methods have been recently developed and introduced with the objective of overcoming such limitation, directly designing a structure able to sustain a pre-defined level of damage under a pre-defined level of earthquake intensity.

Direct displacement-based design methods, some versions of which have been briefly described applied in the body of this paper, do prove to be very effective in prescribing a desired non-linear deformation pattern to continuous span bridges, thus leading to a design whereby damage is fully controlled. However, it has been shown that, on occasions, such control requires the employment of a relatively high quantity of pier longitudinal reinforcement, mainly due to the fact that an "unnatural" deformed shape has been assumed and imposed at the early design stages.

A pushover-based design procedure, which can also be considered as an adaptive variant of the capacity spectrum method incorporating elements of direct displacement-based design, has been proposed and employed in the design of continuous span bridges. By virtue of its adaptiveness, the methodology tends to lead to optimum deck deformed shapes, which are therefore not imposed but rather come as a result of adaptive displacement-based pushover analyses.

A number of case studies has been considered and designed according to the different force-, displacement- and pushover-based approaches considered in this preliminary work. It was shown that non-iterative force-based design provides little or no control on the response of the structure, for which reason its employment cannot be recommended by the authors. Displacement-based approaches, on the other hand, present full control on the dynamic response of the bridges, even if at higher cost in terms of pier longitudinal reinforcement. Finally, the pushover-based design method seemed to provide the best compromise in terms of matching dynamic analyses results and optimising the required design reinforcement, this being however achieved with an increased computational effort.

It is thus clear that further studies are called for, with the objective of investigating the possibility of deriving guidance rules, probably based on the geometrical configuration of the bridges that will assist designers in their initial deformed shape assumptions, required as part of simplified direct displacement-

based design procedures. Further, a careful and thorough re-appraisal of the rules employed in these methods to redistribute forces/amongst the different piers and abutments might also lead to the individuation of optimised alternatives.

In other words, despite the apparently superior results obtained with the pushover-based design methodology, the authors still believe that, given the additional complexity of the latter, with respect to simplified direct displacement-based design approaches, it is very much justified that future research effort is placed in the improvement of these latter simplified methods, with the objective of rendering these capable of consistently producing not only performance- but also cost-effective design outcomes. Moreover, such future research developments should also aim at identifying possible boundaries beyond which the employment of simplified approaches is not longer adequate, and thus alternative more complex methods, such as the proposed pushover-based one, are called for.

ACKNOWLEDGEMENTS

Part of the current work has carried out under the financial auspices of the European Commission through the FP6 Integrated Project LESSLOSS (Risk Mitigation for Earthquakes and Landslides). Such support is gratefully acknowledged by the authors.

References

Antoniou S., Pinho R., 2004, Development and verification of a displacement-based adaptive pushover procedure, *Journal of Earthquake Engineering*, **8**(5):643-661.

Bertero V.V, Zagajeski S.W., 1979, Optimal inelastic design of seismic resistance reinforced concrete framed structures, *Proceedings International Symposium on Nonlinear Design of Concrete Structures*, University of Waterloo, Canada, pp. 219-272.

Calvi G.M., 2004, Recent experience and innovative approaches in design and assessment of bridges, Keynote Lecture, *Proceedings of the Thirteenth World Conference on Earthquake Engineering*, Vancouver, Canada.

Casarotti C., 2004, *Adaptive pushover-based methods for seismic assessment and design of bridge structures*, *PhD Thesis*, European School for Advanced Studies in Reduction of Seismic Risk (ROSE School), University of Pavia, Italy.

Comité Européen de Normalization, 2002, *Eurocode 8: Design of Structures for Earthquake Resistance - Part 2: Bridges*, PrEN 1998-2: 2003, 2 April 2002, CEN, Brussels, Belgium

Fajfar P., 1999, Capacity spectrum method based on inelastic demand spectra, *Earthquake Engineering and Structural Dynamics*, **28:**979-993.

Fardis M.N., Panagiotakos T.B., 1997, Displacement-based design of RC Buildings: Proposed approach and applications, in: *Seismic Design Methodologies for the Next Generation of*

Codes, P. Fajfar ,H. Krawinkler (Eds.), Proceedings of International Conference at Bled, Slovenia. A.A. Balkema, Rotterdam/Brookfield, 1997, pp.195-206.

Fintel M. and Ghosh S.K., 1982, Explicit inelastic dynamic design procedure for aseismic structures, *Journal ACI*, **79**(2):110-118.

Freeman S.A., 1998, Development and use of capacity spectrum method, *Proceedings of the Sixth National Conference of Earthquake Engineering*, Seattle, CD-ROM, EERI, Oakland.

Gulkan P., Sozen M., 1974, Inelastic response of reinforced concrete structures to earthquake motions, *ACI Journal*, **71**(6):604-610.

Kappos A.J., 1997, Partial inelastic analysis procedure for optimum capacity design of RC buildings, in: *Seismic Design Methodologies for the Next Generation of Codes,* P. Fajfar ,H. Krawinkler (Eds.), Proceedings of International Conference at Bled, Slovenia. A.A. Balkema, Rotterdam/Brookfield, 1997, pp.229-240.

Kawashima K., 2000, Seismic design and retrofit of bridges, Keynote address, *Proceedings of the Twelfth World Conference in Earthquake Engineering*, Auckland, New Zealand.

Kowalsky M.J., 2002, A displacement-based approach for the seismic design of continuous concrete bridges, *Earthquake Engineering and Structural Dynamics*, **31:**719-747.

Kowalsky M.J., Priestley M.J.N., MacRae G.A., 1995, Displacement-based design of RC bridge columns in seismic regions, *Earthquake Engineering and Structural Dynamics*, **24**(12): 1623-1643.

Newmark N.M., Hall W.J., 1973, Procedures and criteria for earthquake resistant design, building practice for design mitigation, *Building Science Series 45*, National Bureau of Standards, Washington, pp 209-236.

Park R., Paulay T., 1975, *Reinforced Concrete Structures*, John Wiley & Sons.

Priestley M.J.N., Calvi G.M., 2003, Direct displacement-based seismic design of concrete bridges, *Proceedings of the Fifth International Conference on Seismic Bridge Design and Retrofit for Earthquake Resistance*, La Jolla, California.

Priestley M.J.N., 2000, Performance based seismic design, *Proceedings of the Twelfth World Conference on Earthquake Engineering*, Auckland, New Zealand, Paper 2831.

Priestley M.J.N., Calvi G.M., 1997, Concepts and Procedures for Direct Displacement-Based Design and Assessment, in: *Seismic Design Methodologies for the Next Generation of Codes,* P. Fajfar ,H. Krawinkler (Eds.), Proceedings of International Conference at Bled, Slovenia. A.A. Balkema, Rotterdam/Brookfield, 1997, pp. 171-182.

Priestley M.J.N., 1993, Myths and fallacies in earthquake engineering —conflicts between design and reality, *Proceedings of the Tom Paulay Symposium - Recent Developments in Lateral Force Transfer in Buildings*, University of California, San Diego, pp. 229–252.

SAC Joint Venture, 1997, *Develop Suites of Time Histories*, Project Task: 5.4.1, Draft Report, March 21, 1997, Sacramento, CA, USA

Seismosoft, 2004, *Seismostruct - A Computer Program for Static and Dynamic nonlinear analysis of framed structures [online]*, available from URL: http//www.seismosoft.com.

Stone W.C., Taylor A.W., 1994, ISDP:Integrated approach to seismic design of reinforced concrete structures, *ASCE Journal Structural Engineering*, **120**(12):3548-3566.

SEISMIC REHABILITATION USING INFILL WALL SYSTEMS

ROBERT J. FROSCH
Purdue University, 550 Stadium Mall Dr, W Lafayette, IN 47907

Abstract. In seismic regions throughout the world, a large inventory of reinforced concrete structures exist that lack both strength and ductility. The economic impact resulting from a loss of these structures during a seismic event is enormous. Many facilities are vital in terms of their operational benefits. The functional capabilities of many of these facilities cannot be shut down or even suspended. Consequently, there is a great need for efficient, effective, and inexpensive rehabilitation strategies that are minimally invasive and minimize disruption to building operations. While a variety of techniques are available to meet these requirements, the use of an infill wall presents a significant advantage when attempting to minimize both costs and disruption. Furthermore, construction plays a vital role in the success of any rehabilitation scheme. This paper will evaluate infill construction techniques with a focus on a precast infill scheme. The retrofit of a two-story laboratory structure incorporating the precast system will be discussed. Due to the nature of the precast system, the performance of the connections is vital. Consequently, their design and construction will be highlighted. The effectiveness of this rehabilitation scheme will be demonstrated through the overall behavior of the structural system.

Keywords: infill wall; reinforced concrete; seismic rehabilitation; shear wall

1. Introduction

In seismic regions throughout the world, a large inventory of reinforced concrete structures exist that lack both strength and ductility. The economic impact resulting from a loss of these structures during a seismic event is enormous. While it is extremely important to reduce losses related to structural collapse, recent earthquakes have demonstrated that significant economic losses have resulted even though collapse did not occur. As an example, economic losses from the Northridge earthquake have been estimated between 20 and 40

S.T. Wasti and G. Ozcebe (eds.), Advances in Earthquake Engineering for Urban Risk Reduction, 395–409.

billion US dollars while the majority of the resulting losses were not caused by structural failure.

It is important to realize that many facilities are vital in terms of their operational benefits. The functional capabilities of many of these facilities cannot be shut down or even suspended. With many processing facilities and high tech industries, economic losses of an individual facility can amount to millions of dollars per hour of suspended operations. Consequently, there is a need for efficient, effective, and inexpensive rehabilitation strategies that are minimally invasive and minimize disruption to building operations.

2. Rehabilitation

Structures can be rehabilitated by increasing the displacement capacity of the structure to meet the demands imposed by an earthquake Δ_{EQ}. As a simplified example, a building may possess a lateral resistance F_4 and a ductility level of two (μ=2) which provides a displacement capacity of Δ_1 as shown in Figure 1. The building may be strengthened by increasing the lateral force resistance to F_2 (assuming the ductility remains constant), by increasing the ductility to a level of four (μ=4), or by a combination of the two. In other words, the building can be rehabilitated by increasing the strength, ductility, or a combination of the two.

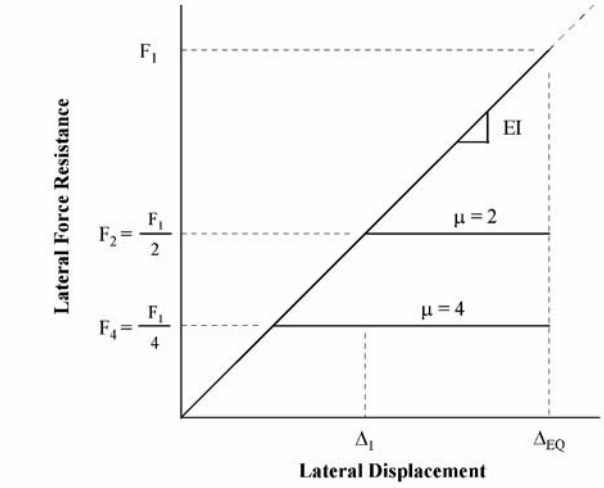

Figure 1. Structural Response

Structures can also be rehabilitated by reducing the demands imposed by an earthquake. The structure's period can be modified by making the structure stiffer or more flexible to change the ground acceleration amplification. Depending on the period of the structure and the period shift, it is possible that

the displacements may decrease or increase which can be determined from the displacement spectrum for the specific case investigated. There are many locations where ground motion characteristics require a change in the dynamic response of the structure to meet the performance requirements established for the structure. Generally, this can be done by changing the stiffness of the lateral load resisting system.

The effect of the rehabilitation scheme on the strength, ductility, and period must be considered together since modification of one can affect the others. The goal of the design or rehabilitation scheme is to provide for displacement capacity of the structure greater than the displacement demands of the earthquake.

A report on the seismic rehabilitation of existing structures is provided in the NEHRP Handbook of Techniques for the Seismic Rehabilitation of Existing Buildings.[1] The following three techniques are listed for rehabilitating reinforced concrete moment frame buildings.

- Increasing the ductility and capacity by jacketing the beam and column joints or increasing the beam or column capacities.
- Reducing the seismic stresses in the existing frames by providing supplemental vertical-resisting elements (i.e., additional moment frames, braces, or shear walls).
- Changing the system to a shear wall system by infilling the reinforced concrete frames with reinforced concrete.

3. Infill Walls

The building frame can be infilled with a concrete wall to change the lateral load system to a shear wall (Figure 2). The addition of infills can dramatically increase both the lateral strength and stiffness of the structure in addition to changing its dynamic response. Due to the high stiffness of the wall, the moment frames do not contribute to the lateral force resistance. Therefore, the weak links and problems exhibited in the existing structure are eliminated provided that the deformations are within the range which will not severely damage the existing columns, beams, or joints. Infill walls can also be used to provide supplemental stiffness for structures where existing shear walls or bracing elements are inadequate.

Infill walls, however, subject the existing structure to various forces for which it was not designed. The performance of the infill wall depends on the existing columns to serve as boundary elements which carry large tension and compression forces. In many structures, the columns have been designed for gravity loads and do not have sufficient tensile capacity to act as a boundary

element for the new structural wall. Typically, tensile capacity is provided by jacketing or adding vertical reinforcement in the infill which is made continuous through the floors near the column. Additionally, the diaphragms must be capable of transferring the forces to the infill wall.

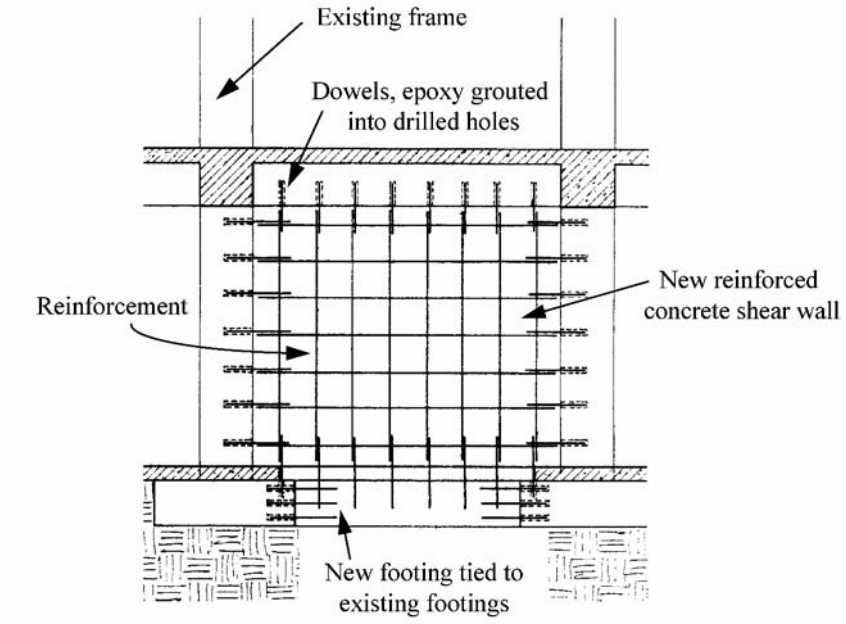

Figure 2. Infill Wall

Infill walls can be costly if the foundation requires upgrading. Additionally, connections to the existing frame with interface dowels may be expensive and time consuming. Finally, the infill wall can obstruct the functional use of the building by impeding access and functional circulation. However, due to the high stiffness of an infill wall, only a limited number of walls are typically required in a structure. Therefore, it is possible to locate walls to minimize disruption both during and after construction.

4. Economic Rehabilitation

The various techniques such as jacketing, bracing, and infill walls have proven to be constructible, to be economically feasible for many structures, and are backed by some experimental data and field experience. However, the cost of such rehabilitation projects remains an obstacle for many owners. The costs may involve not only the actual construction, but the expenses associated with relocation of operations and loss of rental revenue or production during the period of construction.

Therefore, it is desirable that a rehabilitation scheme be designed to not only correct the "weak links" that may exist in the existing structure, but also to simplify the construction process; reduce the time, cost, and inconvenience of construction; and reduce the obstruction to functional use of the structure both during and after construction. The infill wall system meets many of the general objectives desired. However, as mentioned, there are several aspects that make the method inconvenient, costly, and time consuming. The following objectives were identified to make the infill wall system a more economically viable rehabilitation solution.

1. Eliminate interface dowels.
2. Eliminate extensive concrete formwork
3. Eliminate movement and placement of large volumes of fresh concrete.
4. Increase column tensile capacity without column jacketing.

5. Precast Infill System

A precast panel system was developed to enable panels to be assembled into an infill wall taking advantage of the infill wall system while achieving the objectives discussed above.[2,3] A precast system can be constructed rapidly without the need for extensive formwork and the relatively cumbersome and sometime difficult procedures associated with moving and placing large quantities of fresh concrete within an existing building. The precast panels can be brought into an existing structure through the use of elevators and light forklifts. The panels have shear keys along the sides to allow for force transfer and are connected to one another through the use of a reinforced grout strip. Panels are connected to the existing frame through the use of steel pipes (shear lugs) that eliminate the need for interface dowels. The existing structure is cored in selected locations to allow for insertion of pipes and continuity of the wall vertical reinforcement. A schematic of the precast wall system is presented in Figure 3.

Out-of-plane resistance of the wall system is achieved through the combination of continuous vertical reinforcement in the grout strips, shear resistance of the steel pipes, and the constraint provided by the boundary elements that provides for in-plane compression under bending (arching action). The components contributing to out-of-plane resistance are shown in Figure 4.

The tensile capacity of the existing frame columns must be increased to provide overturning capacity to the infill wall. Many existing structures were constructed with only compression lap splices which do not provide for tensile yielding of column reinforcement. A post-tensioning system located adjacent to

the existing frame columns (boundary elements) is used to improve the column tensile capacity without using conventional jacketing. The post-tensioning system is illustrated in Figure 5.

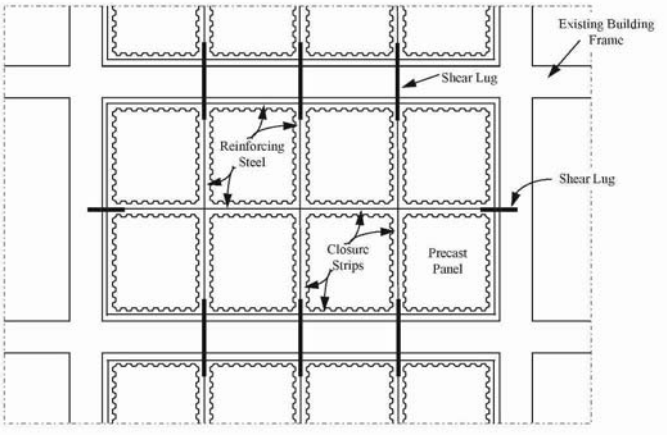

Figure 3. Precast Infill System

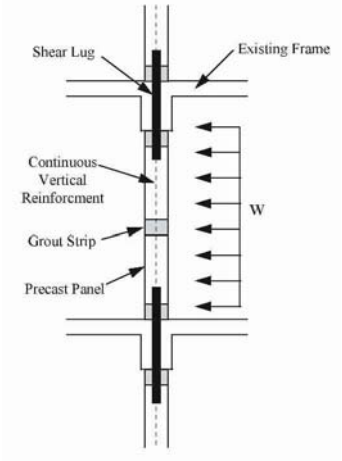

Figure 4. Out-of-Plane

6. Connection System

For successful implementation of the precast infill wall system, the performance of connections is essential. Experimental studies were conducted to specifically evaluate the performance of the panel-to-panel[4] and the panel-to-frame connections[5] as well as to develop minimum design recommendations. Design recommendation for the connections is presented below. Design recommendations for the entire structural system are presented in Reference 3.

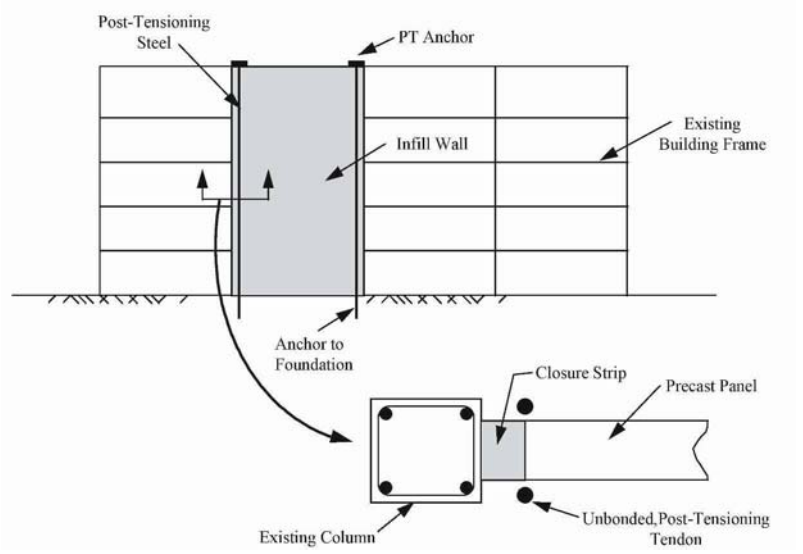

Figure 5. Post-Tensioning System

6.1. PANEL-TO-PANEL CONNECTIONS

The following design recommendations are made concerning design of the grout connection between precast panels.

Grout Strip Reinforcement: Shear must be transferred across the joints through the use of reinforcement placed in the grout strip. The grout strip reinforcement can be designed using the shear friction provisions of ACI-318.[6] These recommendations apply for normal-weight concrete as light-weight was not tested.

$$V_n = A_{vf} f_y \mu$$

where:

V_n = Nominal joint shear strength
A_{vf} = Cross-sectional area of vertical joint reinforcement
f_y = Yield strength of reinforcing steel
μ = 1.0 (Coefficient of friction)

Wall Design Considerations: The shear strength of the wall cannot be more than the capacity of the wall to transfer forces to the joint. The shear capacity of the wall should be checked in addition to the interface shear capacity at the joint.

6.2. PANEL-TO-FRAME CONNECTION

The following design recommendations are made regarding the shear lug connection to an existing building frame.

Pipe Design: Shear must be transferred from the wall to the existing frame through the use of a shear lug. The pipe should be designed based on the shear force required to be transferred at the interface. The design level should be based on the shear yielding capacity of the pipe which can be determined as follows:

$$V_n^{Pipe} = 0.6 A_s F_y$$

where:

V_n^{Pipe} = Nominal pipe shear strength of one pipe
A_s = Cross-sectional area of pipe
F_y = Yield strength of pipe steel

Pipe Embedment: The pipe embedment lengths should be determined by the following method based on bearing of the pipe on the concrete. An overstrength factor of at least 1.25 is recommended to account for material overstrength of the pipe. It is recommended on the wall side to neglect any effects of the supporting surface being wider than the loaded area. Due to the small concrete cover near the pipe, it does not seem reasonable to include this factor. On the frame side, however, it is possible to take advantage of the confinement factor (square root of A_2/A_1) provided by ACI 318.[6]

$$\alpha V_n^{Pipe} = \phi \left(0.85 f_c^{'} \sqrt{\frac{A_2}{A_1}} \right) \varnothing_{OD} d$$

where:

V_n^{Pipe} = Nominal pipe shear strength
$\alpha \geq 1.25$ (Overstrength factor)
$\phi = 0.65$ for concrete bearing
$f_c^{'}$ = Compressive strength of concrete
$\varnothing_{OD}$ = Outside diameter of steel pipe
d = embedment depth

7. Construction

To demonstrate both the construction efficiency and structural effectiveness of precast infill wall system, a two-story laboratory structure was rehabilitated. Construction of the wall progressed in four stages and is illustrated in Figure 6. Again, for proper performance of the system and to minimize construction time,

the details used at the connections were important. Details of the construction stages and sequence are presented below.

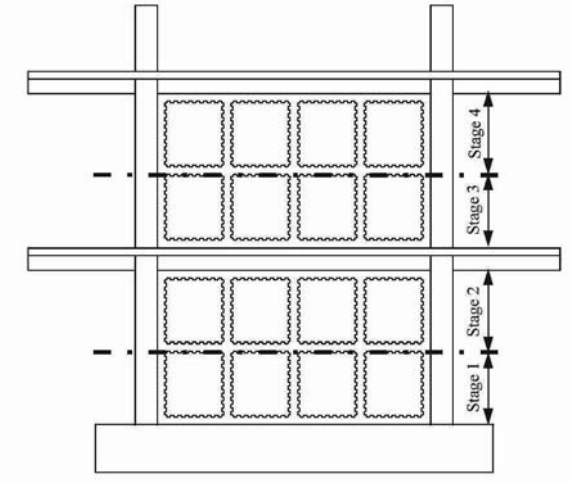

Figure 6. Construction Sequence

Following placement of the bottom row of panels, the base shear lugs were placed along with the grout strip reinforcement as shown in Figure 7. The shear lugs were grouted in the footing to ensure proper location (Figure 8). Following pipe grouting, the strips were formed and grouting proceeded from the top of the closure strips. Consolidation was achieved through the use of a vibrator in the vertical strips and simultaneously through vibration in access holes provided in the horizontal strips. The access holes were spaced roughly at the third points of the panels with two access holes horizontally for each panel. Following grouting of the first row, the horizontal column shear lugs were grouted into position along with the horizontal strip steel as shown in Figure 9.

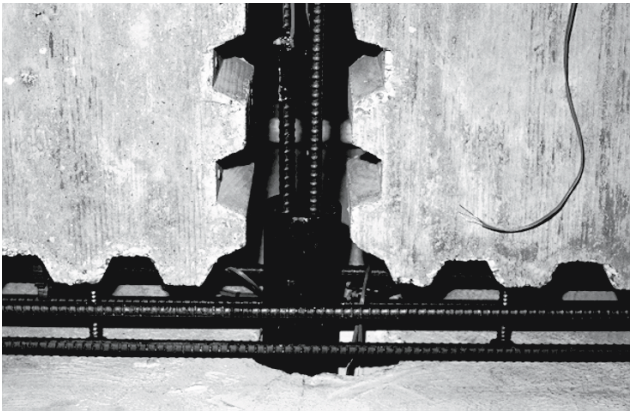

Figure 7. Base Shear Lugs

Figure 8. Grouting Operation

Figure 9. Grouting of Column Shear Lugs

Formwork was stripped the day after grouting, and the next level of panel construction commenced. The top row of panels for the first story was placed along with the reinforcing steel. Subsequently, all closure strips were formed (Figure 10). The grout was placed from the floor above through the beam core holes. The vertical strips were vibrated through the core hole while both the middle and top (below the beam) horizontal strips were vibrated through access holes (Figure 11). Simultaneous horizontal and vertical vibration was essential for good grout flow. The second floor pipe lugs (Figure 12) and the vertical strip reinforcing steel that was spliced inside the pipe at this location (Figure 13) were installed after grouting of the strips in the panels below was completed. A stop should be provided on or under the pipe lugs to ensure proper embedment lengths because vibration will cause the pipe to settle.

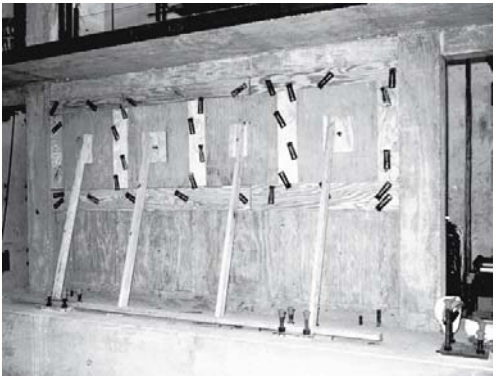

Figure 10. Closure Strips

Figure 11. Grout Vibration

Figure 12. Shear Lug Installation

Figure 13. Strip Reinforcement

Construction proceeded for the second story in the same manner as the first. The strengthened structure after wall construction was completed is shown in Figure 14.

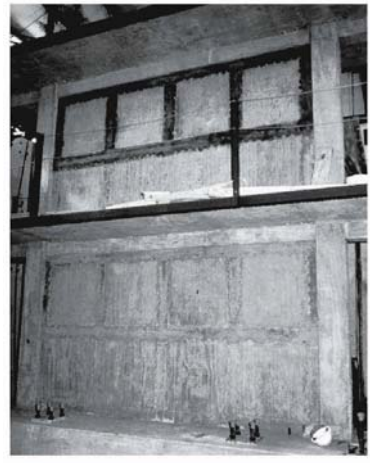

Figure 14. Completed Construction

Inspection of the grouting quality followed each stage of construction. Overall, the grout quality was excellent even in the strip underneath the existing beam where poor grouting is often seen. The only voids noticed along this interface were at one top beam/column corner on the first story as shown in Figure 15 where the corner was not completely filled. The other opposite corner, however, was in excellent condition. During grouting, it could not be determined if the corner was filled since formwork covered the region. To ensure proper grouting of the top beam/column corner for the second story wall, a small hole in the formwork provided at this location was used to check that the joint was filled. The observation hole worked well, and excellent grouting was achieved. With the use of self consolidating concrete (SCC), additional ease in the grouting operation is possible.

Attention to detailing can simplify and ease construction. The vertical steel in the panel to panel connections (grout strips) was spliced inside the pipe lugs between the first and second stories to allow for continuity. Since the splice steel was discontinued at the middepth of the beam for testing purposes, the bars were inaccessible. During pipe installation, there was difficulty slipping the reinforcing bars inside the pipe because the bars could not be held together. After considerable effort, the bars were tied together inside the beam core hole to permit the pipe to be installed. In the field, the bars from the story below should be continued through the beam to allow for easy threading through the pipe.

Figure 15. Beam/Column Joint Void

8. System Behavior

The infill wall system was tested to establish the behavior of the rehabilitation technique.[7] The specimen was tested cyclically using a triangular load distribution applied at the two floor levels to simulate first vibration mode effects for the structure. Flexural and shear strength were investigated to examine the precast panel connections and overall infill wall design procedure. The cracking pattern for the first and second floors is presented in Figures 16 and 17, respectively.

Diagonal cracks were continuous through panels and grout strips. There was no indication of distress along grout strips. The cracking pattern indicated that the wall behaved in a monolithic fashion even though it was constructed of smaller, individual units. A maximum crack width of 0.8 mm was measured during testing. After reaching this width, it was noticed that additional cracks would open so that the initial crack would close slightly.

Overall, the system performed exceptionally well. The system behaved monolithically, and both the panel and frame connections performed according to design. Cracks were evident at the locations of the shear lugs in the footing

and the frame, but failure did not appear to be imminent. At ultimate, the shear strength of the structure was controlled by concrete crushing of the primary compressive strut. The system reached a base shear that was 3.4 times greater than its design level.[7]

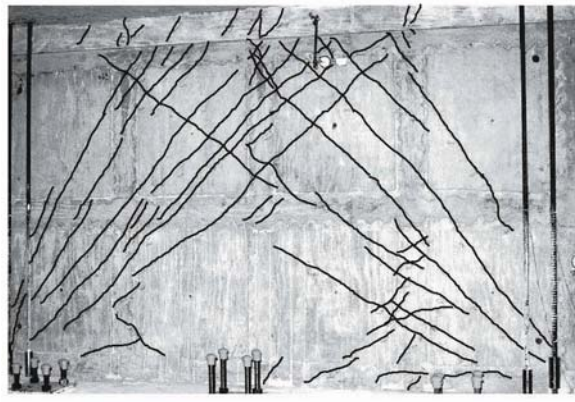

Figure 16. First Floor Cracking Pattern

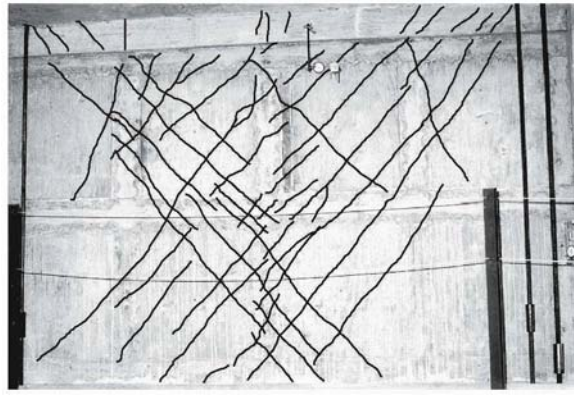

Figure 17. Second Floor Cracking Pattern

9. Summary and Conclusions

For the rehabilitation of many structures, costs are always an issue. While construction cost is typically of primary concern for many owners, costs associated with disruption and loss of operation can be of considerably more importance.

Infill wall systems can be used to help minimize these disruptions as rehabilitation can be concentrated in select building locations. While cast-in-place infills have been traditionally used, precast infill wall systems can eliminate many of the costly and time-consuming procedures present in cast-in-

place construction. Rehabilitation using the precast infill system was demonstrated in a laboratory study using a model structure. For this 2/3 scale structure, infills were able to be constructed at a rate of one floor per two days. One day was required for each row of panels. This construction rate is considered reasonable for actual placement as two rows of panels will typically be required.

The precast system provides engineers with a technique that offers the potential to reduce overall costs of rehabilitating existing structures while allowing the rehabilitation to be tailored to the requirements of the owner.

ACKNOWLEDGEMENTS

This study was conducted at the Phil M. Ferguson Structural Engineering Laboratory and was sponsored by the National Science Foundation (Grant No. BCS-9221531). The author would also like to thank Jim Jirsa and Mike Kreger for their advice throughout the research. Thanks are also extended to Wanzhi Li and Michael Brack for their help during the experimental phase of the research and to Loring Wyllie, Jr. of Degenkolb Engineers and Tom Sabol of Engelkirk and Sabol Consulting Engineers for their contributions and constructive criticism to keep the work relevant to practice.

References

1. Building Seismic Safety Council, *NEHRP Handbook of Techniques for the Seismic Rehabilitation of Existing Buildings*, FEMA-172, Federal Emergency Management Agency, Washington, D.C, (1992).
2. R.J. Frosch, Seismic Rehabilitation Using Precast Infill Walls, *Ph.D. Dissertation*, University of Texas at Austin, pp. 234(1996).
3. R.J. Frosch, W. Li, J.O. Jirsa, and M.E. Kreger, Retrofit of Non-Ductile Moment-Resisting Frames Using Precast Infill Wall Panels, *Earthquake Spectra*, 12(4), pp. 741-760(1996).
4. R.J. Frosch, Panel Connections for Precast Concrete Infill Walls, *ACI Structural Journal*, Vol. 96, No. 4, July-August 1999, pp. 467-472.
5. R.J. Frosch, Shear Transfer Between Concrete Elements Using a Steel Pipe Connection, *ACI Structural Journal*, Vol. 96, No. 6, November-December 1999, pp. 1003-1008.
6. ACI Committee 318, "Building Code Requirements for Reinforced Concrete (ACI 318-02) and Commentary (ACI 318R-02)," American Concrete Institute, Farmington Hills, MI, (2002).
7. R.J. Frosch, J.O. Jirsa, M.E. Kreger, Experimental Response of a Precast Infill Wall System, Seismic Assessment and Rehabilitation of Existing Buildings, S.T. Wasti and G. Ozcebe (eds.), Kluwer Academic Publishers, pp. 383-406(2003).

SHAKE TABLE EXPERIMENT ON ONE-STORY RC STRUCTURE WITH AND WITHOUT MASONRY INFILL

ALIDAD HASHEMI
Department of Civil and Environmental Engineering, University of California, Berkeley

KHALID M. MOSALAM•
Department of Civil and Environmental Engineering, University of California, Berkeley

Abstract. The results of a shake table experiment on a one story reinforced concrete moment resisting frame structure with unreinforced masonry (URM) infill wall are presented. The experiment consists of three stages. In the first stage, the intact structure with URM infill wall is tested to study the effects of the infill on the behavior of the structure. This stage is concluded after the complete collapse of the wall. In the second stage, the behavior of the structure after the collapse of the wall is studied to better understand and isolate the effects of the URM wall on the structural system. In the third stage, the incipient collapse mechanism of the damaged structural system is investigated. Important global response parameters such as maximum drift, maximum base shear and stiffness of the structure as well as some local response parameters such as rotations at column-foundation joint and beam-column joint are discussed.

Keywords: Earthquakes; Hybrid system; Infilled frame; Reinforced concrete; Shake table; URM wall.

1. Introduction

Complex structures with multiple dissimilar components (hybrid systems) are frequently built in seismically active regions. Examples include reinforced

• Associate Professor, E-mail: mosalam@ce.berkeley.edu

S.T. Wasti and G. Ozcebe (eds.), Advances in Earthquake Engineering for Urban Risk Reduction, 411–426.

concrete (RC) building frame with masonry infill walls or steel bridge decks supported on RC piers. In order to develop new modeling techniques and study the behavior of such systems, a two-phase experimental study, consisting of a shake table experiment and a pseudo-dynamic experiment, is developed. The shake table experiment serves as a benchmark test for the development of a unified on-line experimental technique combined with simulations utilizing the pseudo-dynamic concepts[1] with substructuring[2].

The shake table experiment is carried out on a one-story RC moment-resisting frame structure with unreinforced masonry (URM) infill wall on the shake table test facility of the University of California, Berkeley in January 2005. The ¾-scale test structure represents the first story middle frames of a five-story RC prototype structure designed based on the requirements of ACI318-02[3] and NEHRP recommendations[4] in seismic regions. A URM wall is assumed inside one of the interior frames as illustrated in Figure 1.

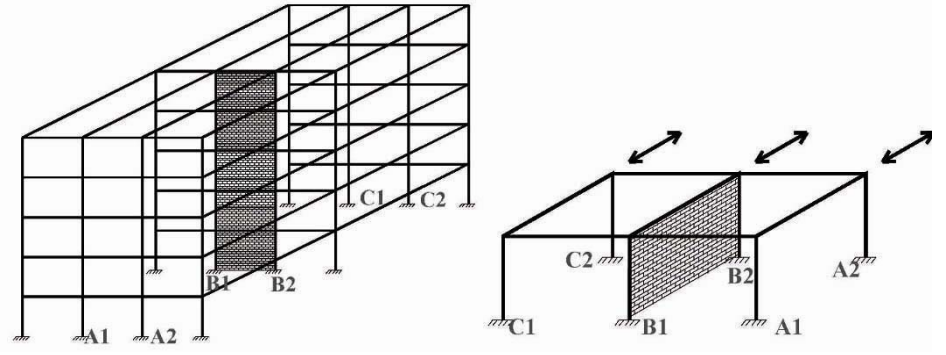

(a) Prototype structure

(b) Model of the test structure

(c) Test structure on the shake table

Figure 1. Development of the shake table test structure

In the pseudo-dynamic experiment, two separate RC frames are tested simultaneously. One frame is bare and the other is infilled with URM. These two frames correspond to frames A1-A2 and B1-B2 respectively, as illustrated in Figure 1. While the two frames constitute the physical specimens in the test, the response of the remaining frame (C1-C2 in Figure 1) is obtained from symmetry of the test structure, and the slab connecting the frames is simulated numerically, making use of the substructuring technique. Figure 2 shows the two RC frames connected to the dynamic actuators used in the pseudo-dynamic experiment.

(a) URM infilled frame

(b) RC bare frame

Figure 2. Pseudo-dynamic experiment with two physical substructures

The experimental study is complemented by an analytical investigation. In that respect, the experiments serve the purpose of calibrating analytical models being developed using Open System for Earthquake Engineering Simulation

(OpenSees)[5]. The objectives of the modeling effort are to enable accurate representation of the in-plane and out-of-plane behavior of URM infill walls, and to refine the modeling techniques of hysteretic strength and stiffness degradation in RC elements and joints. Under extreme loading, the experimental data are to validate numerical algorithms being developed for updating boundary conditions such as in brittle failure, hinge formation, and ultimately automatic element removal for modeling progressive collapse of URM infilled RC framed structures.

This paper focuses on the results of the recently completed shake table experiment. The results of the ongoing pseudo-dynamic experiment and the computational simulations will be discussed in future publications.

2. Configuration of Test Structure

The overall dimensions of the test structure are 16'-0"×14'-6" (4.88 m×4.42 m) in plan and 11'-3" (3.43 m) in height. The center-to-center span of each frame is 13'-6" (4.11 m) and the frames are 6'-0" (1.83 m) apart. The frames are connected using a 3¾" (95 mm) thick RC slab with #3 (10 mm) rebars top and bottom at 12" (305 mm) on center each way. Column sections are 12"×12" (305 mm×305 mm) with 8-#6 (19 mm) longitudinal rebars and an unbonded 1¼" (32 mm) prestressing central rod to represent column axial loads from the upper stories of the prototype building. The transverse rebars of the columns consist of #3@3$^3/_4$" (#10@95 mm) over 24" (610 mm) from the face of the joints and #3@6" (#10@152 mm) elsewhere. Long direction single-span beam sections are 10½"×13½" (267 mm×343 mm) with 3-#6 (19 mm) top and bottom longitudinal rebars. Beam transverse rebars are #3@2$^3/_4$" (#10@70 mm) over the 28" (711 mm) from the face of the beam-column joint and #3@8" (#10@203 mm) elsewhere. Short direction double-span beam sections are 12"×9" (305 mm×229 mm) with 2-#6 (19 mm) longitudinal top and bottom rebars and #3@12" (#10@305 mm) transverse rebars. Foundation sections are 14"×18" (356 mm×457 mm) with 4-#7 (22 mm) longitudinal top and bottom rebars and #3@4" (#10@102 mm) transverse rebars. The concrete cover is ¾" (19 mm) everywhere. The reinforcement is specified as ASTM A615 Grade 60[6]. The specified 28-day compressive strength of the standard concrete cylinder[7] is 4.5 ksi (31 MPa). The masonry wall is made of clay bricks with modular size of 4"×8"×2$^2/_3$" (102 mm×203 mm×68 mm) and ASTM C270 Type N mortar[8]. The measured average 28-day compression strength of the standard masonry prism[9] is 2.46 ksi (17 MPa).

Uniformly-distributed mass is added to the slab in the form of stacked lead ingots bolted to the slab using $^3/_8$" (10 mm) diameter high strength rods. This mass is calculated to account for the tributary live load of the first story, in

addition to the effects of the inertial forces from the dead and live loads of the upper stories. The amount of this additional mass is determined such that the computationally-determined base-shear on the test structure matches that of the three middle frames of the prototype building model when subject to the design ground motion. Static tests confirm that the friction forces between the slab and the lead ingots are large enough to accommodate up to 4.0g lateral acceleration at the slab level.

To measure the base and roof accelerations, 18 accelerometers are installed in different directions over the slab and in various locations on the shake table and the foundation. To measure global and local displacements and rotations, a total of 95 displacement transducers are utilized during the experiment. Moreover, a total of 78 strain gauges out of more than 150 strain gauges installed on the rebars are used during each run of the shake table. As some of the strain gauges are damaged during the runs, alternative gauges are selected and monitored. The prestressing rods are also gauged and monitored during the test to serve as load cells inside the columns.

3. Ground Motions

Three different ground motions as described in Table 1 are used in different stages of the experiment. In this table, PGA, PGV, and PGD refer to peak ground acceleration, velocity, and displacement, respectively. These ground motions are intended to be unidirectional in the direction parallel to the URM infill wall of the test structure. Each ground motion is scaled to generate different levels of intensity as expressed in Table 2. The scaling is based on the equivalent single degree of freedom spectral acceleration (assuming 5% damping) and comparing the average (over a small window of the natural frequency of the test structure) spectral response to that of the NEHRP design spectrum. The scaled spectra of the three selected ground motions and the design spectrum are shown in Figure 3. Level 1 is selected as a small amplitude motion to check the performance of the shake table and data acquisition system. Levels 2, 3, 4 and 6 correspond to 50/50, 30/50, 10/50 (design) and 2/50 (MCE) spectra, respectively. Note that, e.g. 10/50 means 10% probability of being exceeded in 50 years. Levels 7, 8 and 9 are selected to achieve higher demands on the test structure considering the limits of the shake table. The ground motion records are also compressed in time by $\sqrt{3/4}$ factor to account for the reduced length scale of the test structure. A low amplitude white noise with approximately constant amplitude over frequency range of 1-10 Hz is applied before and after each run. The frequency response of the test structure to this signal is studied to assess the change in the natural frequency of the test structure during the experiment as a damage indicator.

TABLE 1. Ground motion specifications

Ground Motion	Station	Direction	PGA [g]	PGV [in/sec (mm/sec)]	PGD [in (mm)]
Northridge, CA, 1994	Tarzana	090	1.570	36.23 (920)	5.13 (130)
Duzce, Turkey, 1999	Lamont	N	0.762	12.97 (329)	0.75 (19)
Loma Prieta, CA, 1989	Bran	000	0.426	17.43 (443)	2.28 (58)

TABLE 2. Scale factors for different levels of input ground motions

Level	1	2	3	4	6	7	8	9
Northridge, CA, 1994 (TAR)	0.05	0.17	0.23	0.39	0.59	-	-	-
Duzce, Turkey, 1999 (DUZ)	-	-	-	-	-	1.50	2.00	2.53
Loma Prieta, CA, 1989 (LomaPr)	-	0.31	0.44	0.67	1.00	1.50	1.95	2.19

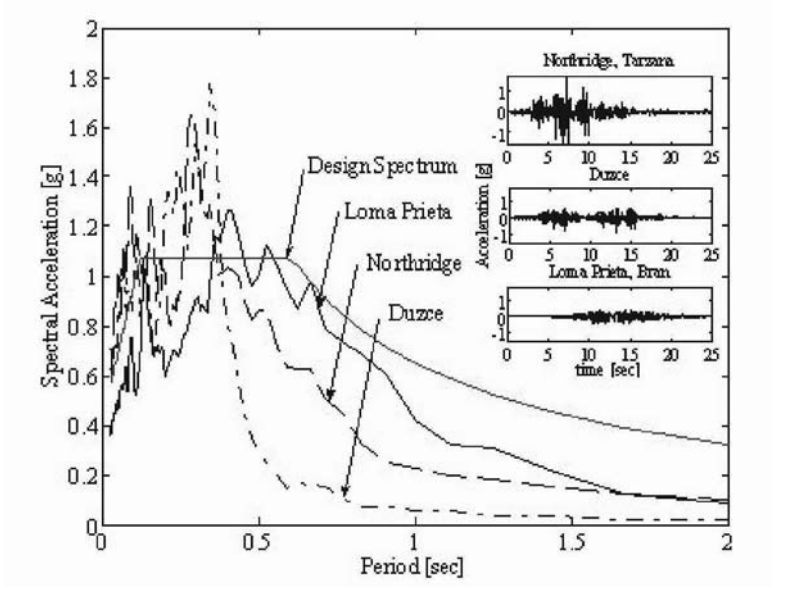

Figure 3. Five percent damping response spectra for the selected ground motions

4. System Properties

Pull (snap-back) tests are performed on the test structure before and after the wall construction to determine the stiffness, natural frequency and damping ratio of the structural system before starting the shake table experiment. These tests are conducted for both in-plane and out-of-plane directions of the test structure, separately. The results of these tests are summarized in Table 3.

TABLE 3. Snap-back test results (refer to Figure 1(c) for orientation of the North (N) direction)

Conditions of the test structure at time of the snap-back (pull) test	In-plane (North-South direction)			Out-of-plane (East-West direction)		
	Natural Period [sec]	Damping Ratio [%]	Stiffness [kips/in (kN/mm)]	Natural Period [sec]	Damping Ratio [%]	Stiffness [kips/in (kN/mm)]
Before building the wall / Nno additional mass	0.135	4.30	113.3 (19.84)	0.134	4.40	134.0 (23.47)
After building the wall / Columns Prestressed. / No additional mass	0.055	5.70	425.5 (74.52)	0.122	4.30	167.1 (29.26)
After building the wall / Columns Prestressed / With additional mass	0.134	6.85	431.0 (75.48)	0.232	4.25	168.0 (29.42)

5. Test Results and Discussion

The shake table experiment is performed in three distinct stages. At the first stage, the intact test structure with the URM wall is subjected to a sequence of ground motions starting from Northridge Tarzana level 1 to 6 (denoted by TAR 1 through TAR 6) and Duzce levels 7, 8 and 7 again (denoted by DUZ 7, DUZ 8 and DUZ 7-2). Due to the stiff URM infill, before the occurrence of any significant damage (up to TAR 6), the lateral behavior is governed by the high strength and stiffness of the URM wall. This is not the case after the displacement demand on the wall exceeds its capacity and the wall is practically disintegrated (DUZ 7-2 and later). A transitional phase can be defined in between, i.e. DUZ 7 and DUZ 8, where the overall behavior is dictated by the level of damage of the URM wall and the interaction between the URM wall and the bounding RC frame.

In order to discuss the progression of damage during the first stage of the experiment, the base-shear versus displacement plots for selected test levels are presented in Figure 4. As shown in Figure 4(a), the stiffness of the test structure during level TAR 3 is about 386 kips/in (67.60 kN/mm). From Table 3, the initial stiffness of the test structure is 431.0 kips/in (75.48 kN/mm), which confirms that up to TAR 3 of stage 1, there is no significant damage in the test

structure (only 10% reduction of the initial stiffness). The response of the test structure in level TAR 4 (design level) as depicted in Figure 4 (b) shows some drop in the stiffness (about 17% reduction), but the overall behavior is more or less linear. Close observation of the wall after the completion of TAR 4 reveals small visible cracks at the wall-column interfaces.

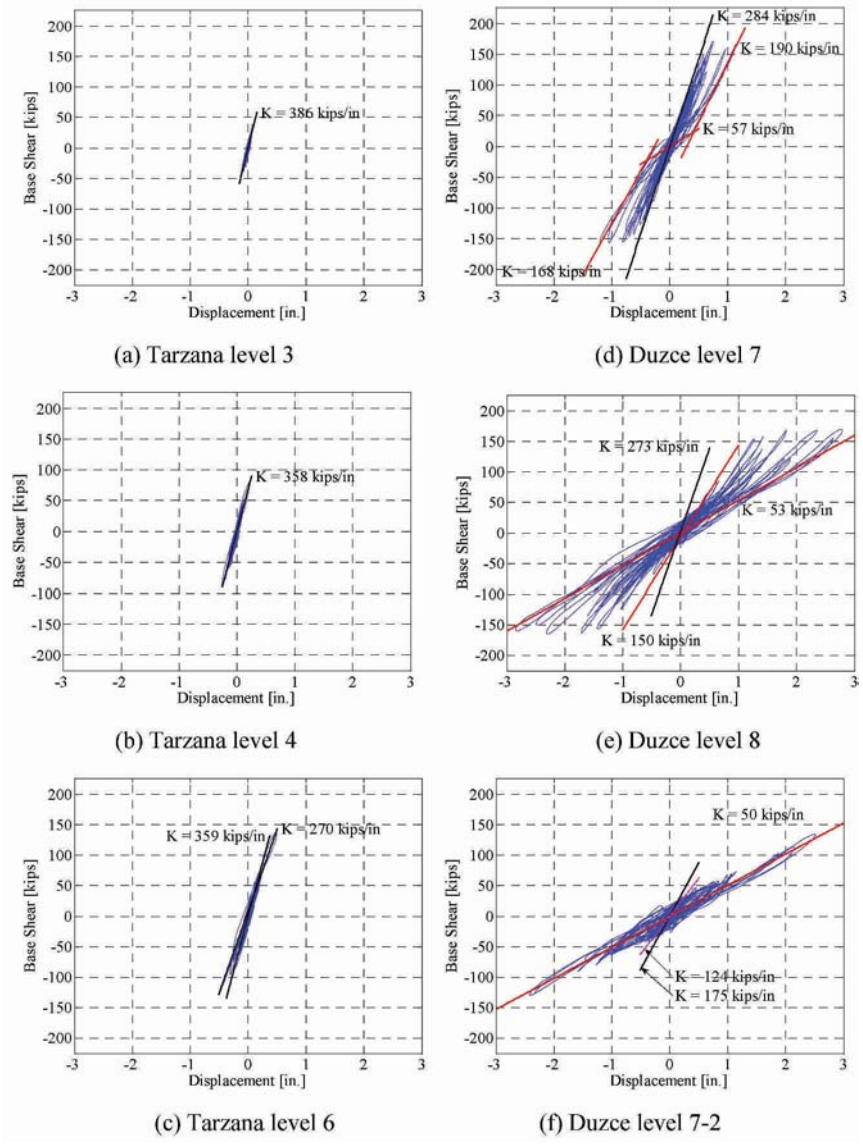

Figure 4. Base shear versus lateral displacement for different test levels [1 kip=4.45kN, 1 in=25.4 mm]

Figure 4 (c), corresponding to level TAR6, shows the first significant signs of damage. The stiffness of 359 kips/in (62.87 kN/mm) in the initial motion shifts to 270 kips/in (47.28 kN/mm) at the peak of the ground motion (25% shift). Observations after the test suggests that some cracks are developing especially along the column-wall interface and some small vertical cracks are observed in the mortar joints at the corners. The maximum total base shear force reached in this stage is 136 kips (605 kN).

The response of the test structure during level DUZ 7, Figure 4 (d), shows the most significant change in the structural behavior. The stiffness at the beginning of this level is 284 kips/in (49.74 kN/mm). Significant wall cracks with clear pattern and load path definition are formed during this test level. The main failure mode of the wall is characterized as *large cracks at 60^o with the horizontal axis starting form top corners of the wall and connecting with a long horizontal crack to a series of 45^o cracks propagating into the opposite bottom corners in each diagonal direction*. At the same time early signs of corner crushing are observed at the top corners. Dark markings in Figure 5 (a) show the observed crack patterns in the wall at this test level. The force-displacement behavior of the assembly at this point can be described as a bi-linear relationship. For small displacements (less than about ¼" (6 mm)), the cracks on the wall open and close without engaging the remaining portions of wall resulting in an observed lateral stiffness of about 57 kips/in (9.98 kN/mm). Once the cracks close, the remaining portions of the wall pick up the load causing further damage in the wall and stiffness increase up to 190 kips/in (33.27 kN/mm). The peak total base shear force observed during all stages of the test, namely 167 kips (743 kN) at roof displacement of 1.15" (29.2 mm) is observed at this stage of the test and right before the main horizontal crack is developed.

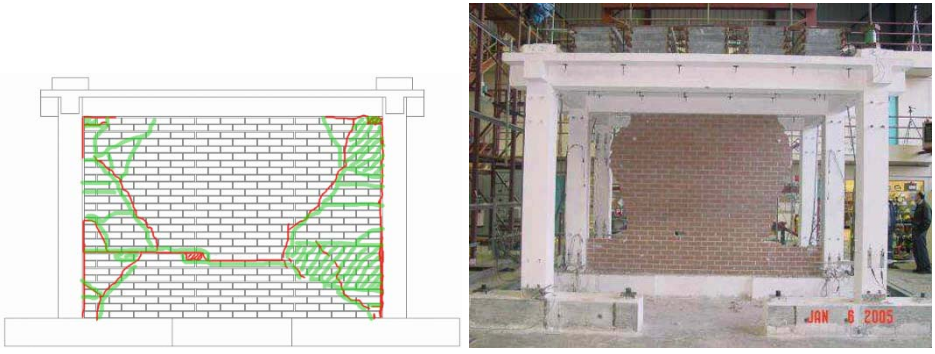

Figure 5. Observed damage of the test structure (a) Crack pattern after Duzce level 8; (b) Test structure after Duzce level 7-2 (end of stage 1)

Figure 4 (e) shows the gradual disintegration of the wall as the test structure is cycled back and forth in level DUZ 8. The measured initial stiffness of the test structure at the beginning of DUZ 8 is 273 kips/in (47.81 kN/mm) for small displacements. Comparison between this stiffness and that of the previous run (284 kips/in (49.74 kN/mm)) with only 4% reduction suggests that at small force demands, the force transferred through the wall is not enough to overcome the static friction between the cracked surfaces. Accordingly, at such small forces, the wall acts as a whole increasing the apparent stiffness of the structural system. Once the force demands at the crack surfaces exceed the static friction (at about 25 kips (111 kN)), the cracked portions start to move with respect to each other and the stiffness reduces to that of RC frames including the intact portions of the URM wall, i.e. 150 kips/in (26.27 kN/mm). Note that the stiffness of the test structure before building the wall (Table 3) is 113.3 kips/in (19.84 kN/mm). As the test structure goes through large displacements, the damage in the URM wall coincides with the damage in the RC frame mostly concentrated at the bases of the columns. Also, partial collapse of the top corners and sides of the wall follows. The final stiffness of the test structure at the end of this level is reduced to 53 kips/in (9.28 kN/mm) and from this point on, the URM wall is structurally insignificant. Thick markings on Figure 5 (a) show the final crack patterns on the wall at the end of level DUZ 8.

Finally, Figure 4 (f) shows the results obtained from the repeat run of level DUZ 7, i.e. DUZ 7-2. Beyond the static friction at the beginning of the motion, the stiffness of the test structure is 50 kips/in (8.76 kN/mm) (only 6% reduction from that at the end of DUZ 8) while the velocity of the motion causes the loose portions of the wall to collapse. Figure 5 (b) shows the state of the test structure at the end of DUZ 7-2 at the conclusion of the first stage of testing. Subsequently, the remaining portions of the URM wall are removed in preparation for the initiation of the second stage of testing.

To further understand the behavior of the test structure in the first stage of the shake table experiment, the change in the “effective” stiffness of the structure in each level of testing is plotted along with the measured initial stiffness of the test structure with and without URM infill wall in Figure 6(a). This effective stiffness denotes the average secant stiffness of the test structure after the demand force exceeds the static friction at about 25 kips (111 kN). It can be observed that the existence of the wall considerably increases the stiffness of the structural system. As the wall undergoes damage, the stiffness of the structure reduces. This reduction occurs most rapidly during levels TAR 6, DUZ 7 and DUZ 8 suggesting the occurrence of significant disintegration of the wall in these levels. Damage in the URM infill also causes significant increase in the natural period of the structure (from 0.134 sec to 0.358 sec with 167% increase) as shown in Figure 7. Note that the stiffness of the test structure

reduces to a level less than the stiffness of the elastic structure without the wall, which confirms the accumulation of damage in the RC frame itself.

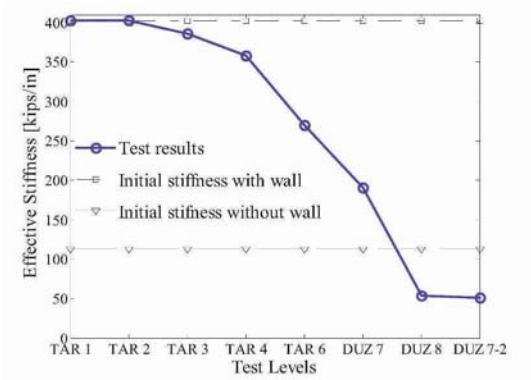

(a) Variation of the effective stiffness

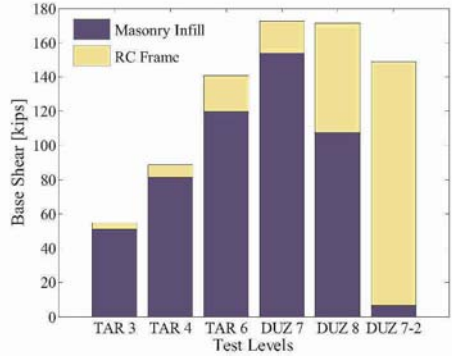

(b) Distribution of base shear between the URM infill wall and the RC frames

Figure 6. Effect of progression of damage in the test structure during the first stage of the experiment [1 kip=4.45kN, 1 in=25.4 mm]

Figure 6 (b) highlights the role of the URM wall on the distribution of forces between the elements of the test structure. The plot shows the portion of the total base shear which is carried by the URM infill versus that portion which is carried by the three RC frames at the peak of the total base shear in selected testing levels. The shear force carried by the RC frames is the sum of the column shears obtained from the static analysis of the columns given the top and bottom moments, which are calculated using the strain gauge data and the section properties. The plot confirms that the behavior of the test structure is governed by the undamaged URM infill before level TAR 6. As the wall experiences damage, the RC frames pick up more of the load. At level DUZ 7-2, the wall is completely disintegrated and can be considered structurally insignificant as the load is carried almost entirely by the three RC frames.

The second stage of the experiment is performed after removal of all the debris and loose parts of the URM wall. The goal of this stage is to better isolate the effects of the URM infill wall on the structural system. Therefore, the same sequence of ground motions as the first stage is applied to the test structure in addition to Duzce level 9 where the physical limit of the shake table is reached. These motions are denoted as AWR-TAR 1 through AWR-TAR 6 and AWR-DUZ 7 through AWR-DUZ 9. Note that AWR stands for "After Wall Removal". Since a large shift in the natural frequency of the test structure is obtained at the end of the loading sequence, a different ground motion with high low-frequency spectral response is needed to match the design spectra for the bare test structure. From Figure 7, Loma Prieta ground motion is suitable for this purpose. The natural frequencies shown in this figure are the frequencies corresponding to the maximum amplitude of the Fourier transform of the acceleration response of the test structure to the low-amplitude white noise input signals applied after each level of testing.

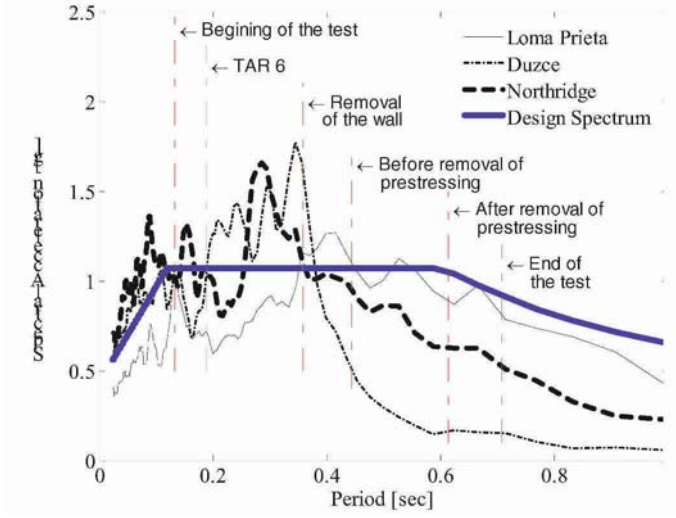

Figure 7. Change in spectral demand due to the change in natural period of the test structure

With the progress of the shake table experiment, more spalling at the bases of the columns and beam-column joints is observed. Significant yielding of the gauged rebars is recorded for shaking beyond Loma Prieta level 7. The most severe damage occurs with the propagation of diagonal cracks in the foundation. These cracks soften the column-foundation connection and in effect produce plastic hinges at the column bases. On the one hand, the development of such hinges reduces the stiffness of the test structure resulting in a significant increase in its natural period. Therefore, the spectral demands on the test structure is reduced as shown in Figure 7 which represents the single degree

freedom elastic spectral response for 5% damping ratio. On the other hand, the hinges developed at the foundation increase the relative demands on the beam-column joints causing further spalling and yielding at the top of the columns. This is quantified by analyzing the results from column strain gauges and displacement transducers and calculating the corresponding moments and rotations at the base and top of each column. It can be observed that, depending on the severity of the previous damage in each column, similar values of the maximum rotations at the bases correspond to different moments at each column-foundation joint. The more the corresponding section of the column at its base is damaged, the less is the maximum moment sustained by that column section. Figure 8 (a) and Figure 8 (b) show the maximum base moment versus maximum measured base rotation for columns A2 and B1 (refer to Figure 1 (b)), respectively. Figure 8 (c) and Figure 8 (d) show the maximum moment versus maximum rotations at the top of columns A2 and B1 (refer to Figure 1 (b)), respectively. These plots suggest significant increase in the bending moment demands on the beam-column joints for both columns compared to the results in the first stage of the experiment. The difference between the results for column A2 and B1 suggests more severe damage at the base of the column A2, which results in higher demands and more damage at the top of that column compared to column B1. Visual inspections after the experiment confirm these results.

The third and final stage of the shake table experiment is performed to investigate the incipient collapse mechanism of the test structure without the URM infill wall. In order to achieve this goal, the prestressing rods in the columns are removed. Removal of these prestressing rods causes considerable increase in the natural period of the test structure (from 0.44 sec to 0.61 sec with 39% increase) as shown in Figure 7. In this final stage, the test structure is only subjected to the Loma Prieta ground motion sequence. The maximum drift ratio reached at this stage is about 6% corresponding to the formation of extremely flexible hinges at the foundation and significant spalling at the top of the columns. Referring to Figure 8 (a) and Figure 8 (b), it can be observed that the maximum moment in the column-foundation joint is further reduced, particularly for column A2, and more base rotations, measured using displacement transducers, are observed at the bases of the columns. Moreover, Figure 8 (c) and Figure 8 (d) show more rotations, taking place at the beam-column joints especially for column A2 as discussed before and at lower moments confirming further damage at the beam-column joints. It is to be noted that for stages 2 and 3 of the shake table experiment, the Loma Prieta ground motion is repeated several times to induce damage to the test structure and this is indicated by the repetition number as shown in Figure 8. For example, LomaPr 9-6 implies the sixth repetition of LomaPr 9.

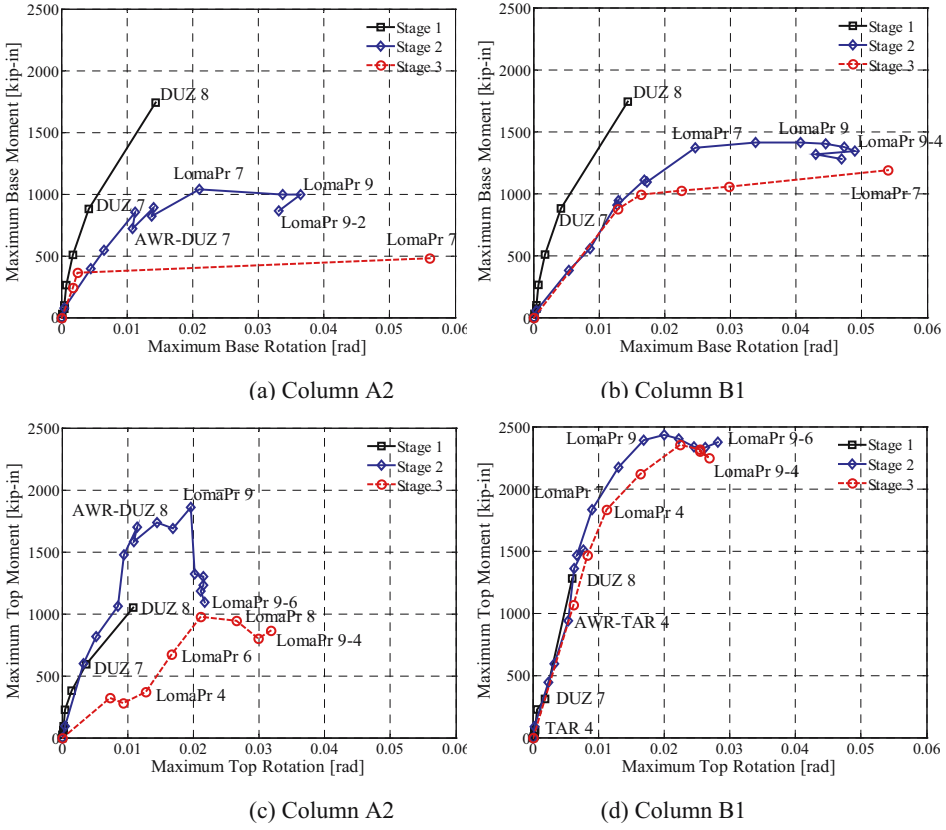

Figure 8. Maximum moment versus maximum rotation at top and bottom of selected columns [1 kip=4.45kN, 1 in=25.4 mm]

In order to compare the global response of the test structure during all three stages of the experiment, the maximum base shear versus maximum drift percentage at each level of testing is shown in Figure 9. The maximum base shear of 172 kips (765 kN) at the first stage corresponds to 1.07% drift in the test structure. However, the maximum drift in this stage is 2.58% corresponding to the base shear of 171 kips (761 kN) suggesting a significant decrease in the stiffness but not in the strength of the test structure. The maximum base shear of 163 kips (725 kN) at the second stage occurs at 4.71% drift ratio during Loma Prieta level 9. Further repetitions of this ground motion level leads to reduction of the maximum base shear and increase in the maximum drift. The maximum drift ratio recorded in the second stage is 5.34% at level Loma Prieta 9-6, i.e. the sixth repetition of LomaPr 9. After the removal of the prestressing rods, the stiffness of the test structure is reduced even further. The maximum base shear of 114 kips (507 KN) in the third stage corresponds to a drift ratio of 5.74% in level Loma Prieta 8. Despite the increase in the intensity of the ground motion

at level Loma Prieta 9 and its repeated runs, smaller values of maximum base shear and maximum drift ratio are reached. This is explained by noting the shape of the ground motion spectra, as shown in Figure 7, where as the test structure softens, the natural period of the test structure increases and the demand forces and displacements on the test structure reduce.

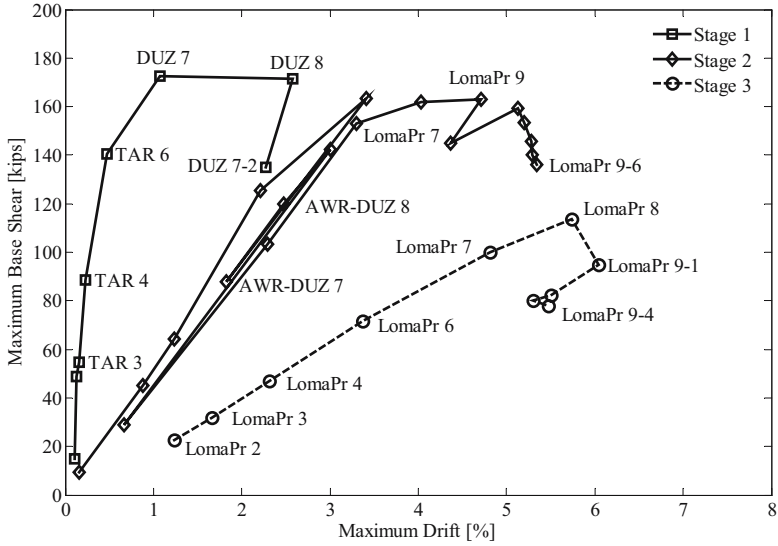

Figure 9. Global results for different stages and levels of shake table experiment [1 kip=4.45kN, 1 in=25.4 mm]

6. Concluding Remarks

The effects of unreinforced masonry infill wall on a reinforced concrete structure are studied using shake table experiments. It is observed that the masonry infill wall significantly changes not only the demands on the structure but also the key global and local response parameters of the structure such as drift ratio, base shear and joint rotations. The sequence of damage and the failure modes of the masonry infill wall are also observed and discussed. The behavior of the structure after the collapse of the masonry infill wall is evaluated and the changes in the force demands and distribution of internal forces on the structure are noted.

The experimental findings are also intended as benchmark dynamic test data to validate a newly developed experimental approach of performing on-line experimentation with multiple physical and computational substructuring. These substructures may have significantly different stiffness characteristics as the case of bare versus masonry infilled frames.

ACKNOWLEDGEMENTS

The authors gratefully acknowledge the financial support provided by the National Science Foundation under the NSF Contract No. CMS0116005. The reinforcing bars for this project were generously donated by Mr. Tom Tietz, Western Regional Manager of the Concrete Reinforcing Steel Institute (CRSI). The continuous help of Mr. Tarek Elkhoraibi during all steps of the experiment from planning to the smallest details is greatly appreciated. Special thanks are due to EERC laboratory personnel especially Mr. Wesley Neighbour for his counsel and assistance during the shake table experiment.

References

1. K. M. Mosalam, R. N. White and G. Ayala, Response of Infilled Frames Using Pseudo-dynamic Experimentation, *Earthquake Engrg and Struct. Dyn.*, 27, 589-608(1998).
2. S. N. Demitzakis and S. A. Mahin, Development of Substructuring Techniques for On-Line Computer Controlled Seismic Performance Testing, *UBC/EERC-85/04,* Earthquake Engrg. Res. Ctr., University of California, Berkeley(1985).
3. Building Code Requirements for Structural Concrete (ACI 318-02) and Commentary (ACI 318R-02), American Concrete Institute, ACI Committee 318
4. NEHRP Recommended Provisions for Seismic Regulations for New Buildings and Other Structures, Part 1:Provisions (FEMA368) and Part 2: Commentary (FEMA369), Building Seismic Safety Council, Washington D.C.,2000
5. Open Systems for Earthquake Engineering Simulation, Pacific Earthquake Engineering Research Center, Website: http://opensees.berkeley.edu/
6. ASTM A 615/A 615M, Standard Specification for Deformed and Plain Carbon-Steel Bars for Concrete Reinforcement, ASTM, West Conshohocken, PA
7. ASTM C 837-99, Standard Test Method for Compressive Strength of Concrete Cylinders Cast-in-Place in Cylindrical Molds, ASTM, West Conshohocken, PA
8. ASTM C 270, Standard Specification for Mortar for Unit Masonry, ASTM, West Conshohocken, PA
9. ASTM C 1314, Standard Test Method for Compressive Strength of Masonry Prisms, ASTM, West Conshohocken, PA

OPPORTUNITIES AND CHALLENGES OF MODERN CONCRETE TECHNOLOGY IN EARTHQUAKE HAZARD MITIGATION

CHRISTIAN MEYER
Columbia University

Abstract. Concrete technology has made significant advances in recent years, which are slowly finding their way into design practice to improve the behavior of structures in seismic regions. Reinforced concrete has long been considered less suitable for earthquake-resistant construction than other materials, until engineers learned how to make it ductile through proper reinforcement. Utilizing latest advances in fiber-reinforced concrete technology it is now possible to engineer the properties of the material such that it not only becomes very ductile, but also exhibits strain hardening, thereby making it ideally suited not only for blast- and impact-resistant structures but also for earthquake-resisting structures. If properly designed, it should be possible to eliminate much or all of shear and confinement reinforcement, thereby considerably improving the constructability, performance, and cost of concrete structures. There remain numerous challenges to achieve such a goal. A lack of consensus in the research community has so far prevented the adoption of standards for mechanical property tests and quality control. In addition, issues of randomness of material properties, with which the industry always had to cope with, need to be addressed in a comprehensive manner to allow designers to offer acceptable reliability at a reasonable cost. This paper briefly summarizes advances in high-performance fiber-reinforced cement composites and in self-consolidating concrete and their implications for earthquake-resistant design of structures. It concludes with comments on the current status of efforts at standardization and codification to facilitate technology transfer to engineering practice.

Keywords: concrete technology; hazard mitigation; strain hardening; ductility

S.T. Wasti and G. Ozcebe (eds.), Advances in Earthquake Engineering for Urban Risk Reduction, 427–439.

1. Introduction

Concrete is one of the oldest and doubtless the most important building material worldwide. The industry uses more than 10 billion tons of it each year, and life, or modern civilization, as we know it is unthinkable without it.

There are several reasons for this widespread popularity. If produced properly, concrete has excellent mechanical properties and can be very durable – some ancient Roman structures are testimony for that. Concrete is adaptable, formable and fire resistant. Its ingredients are available all over the world and very affordable, compared with most other construction materials. One advantage, which is not always properly appreciated, is the fact that concrete is an engineered material. It can be designed to satisfy almost any set of reasonable performance specifications, such as high strength, light weight or improved thermal resistance.

Of course, concrete also has disadvantages, primarily a relatively low tensile strength and associated brittleness, which can lead to early cracking and reduced durability. Also noteworthy is the high statistical scatter of its tensile strength as determined in standard tests, which lowers its reliability. In other words, concrete's tensile strength is literally unreliable. But these disadvantages can be seen as challenges to the research community to be overcome.

A major advance in concrete technology was made in the 1960s and 1970s, when it was determined that proper confinement reinforcement improves the ductility sufficiently to make reinforced concrete a viable structural material for use in seismic regions.

Other advances have been made in the field of concrete technology during the last 20 – 30 years, which are comparable to those made in the preceding 150 years – ever since John Aspdin developed modern Portland cement concrete. In this paper, two of these recent advances shall be discussed because of their potential impact on concrete construction in seismic regions, namely self-consolidating concrete (SCC) and fiber-reinforced concrete (FRC) in general and high-performance fiber-reinforced cement composites (HPFRCC) in particular.

2. Fiber-Reinforced Cement Composites

Concrete's low tensile strength has traditionally been overcome by reinforcing it with steel, leading to a kind of "division of labor": the steel resists the tensile forces, the concrete the compression. However, we know that even in ordinary reinforced concrete, the concrete material is still subjected to tension. In fact, reinforced concrete would not work were it not for the concrete's low and unreliable tensile strength. For example, a member without shear reinforcement

may fail in “diagonal tension”, and the resistance to hoop tension created by deformed reinforcing bars is the basis for bond strength. Even the compressive strength of concrete is indirectly related to its tensile strength, since it is well known that concrete subjected to pure uniaxial compression will fail by splitting.

In principle, steel reinforcement does not alter the mechanical properties of the concrete itself, unless in an indirect way, when confinement reinforcement is arranged such as to produce multiaxial states of stress, under which the strength and especially the ductility of the material is increased possibly by orders of magnitude.

Fiber reinforcement plays basically a similar role as steel reinforcing bars do in regular reinforced concrete. However, since the fibers are relatively small, there are possibly millions per m^3, and these are theoretically oriented randomly and distributed uniformly in space. This makes fiber-reinforced concrete a nearly isotropic material. That means, up until cracking, we may apply composite theory, assuming that within a representative volume element, the material has equal mechanical properties in any arbitrary direction, and these are determined by both the concrete matrix and the fibers. As long as the fibers guarantee a certain minimum tensile strength, it is conceivable that in certain situations no other reinforcement is necessary. For example, facade elements reinforced with glass fibers and nothing else are widely used in the United States [1].

In engineering practice, a multitude of fibers are used – metallic (steel or stainless steel), synthetic (polypropylene, nylon, polyolefin, polyvinyl alcohol, etc), mineral (glass, basalt) or natural fibers (sisal, horsehair, etc). The subsequent discussion shall be limited to steel fibers.

It is known that in ordinary reinforced concrete the reinforcing bars become effective only after cracking of the concrete. The situation is similar in fiber-reinforced concrete, where the fibers are activated only after cracking of the concrete matrix. The compressive strength is hardly affected, as fiber volumes rarely exceed a few percent. Using the law of mixtures, it is easily understood that also the tensile strength is increased only moderately by the fibers. But once the concrete has cracked, the energy necessary to rupture the fibers or pull them out of the matrix can be considerable. By carefully designing the fiber properties it is possible to create multiple cracking before such a failure occurs. If this leads to strain hardening, the resulting ductility and energy absorption capacity of the composite are increased possibly by orders of magnitude. This, then, is the definition of a high-performance fiber-reinforced cement composite (HPFRCC), Figure 1. The condition for this to occur can be derived using basic laws of mechanics.

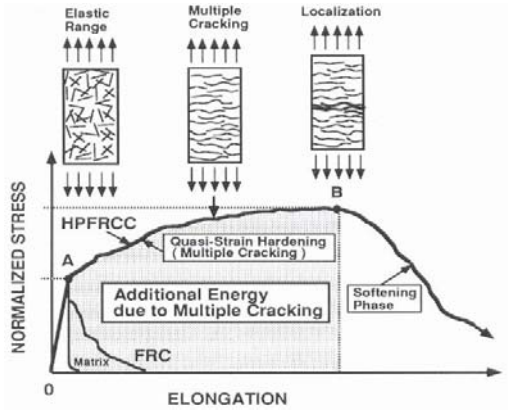

Figure 1. Definition of High-Performance Fiber-Reinforced Cement Composite (Naaman and Reinhardt [2])

3. Mechanics Considerations

Let us consider a single fiber of length L and diameter *d*, embedded within a concrete matrix. We assume that the tensile strength of the fiber, f_y, is considerably higher than that of the matrix, σ_{mu}, so that the matrix fails first, Figure 2.

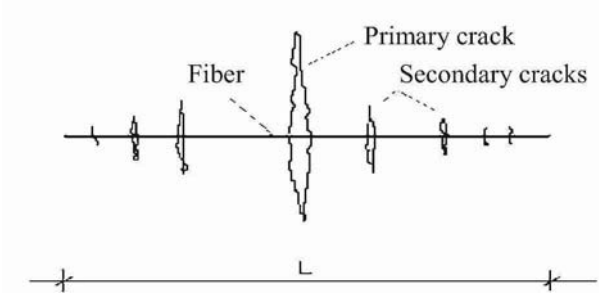

Figure 2. Fiber with Multiple Cracks

The question is whether subsequently the fiber will fail or pull out of the matrix. In either case it is possible that additional cracks develop in the matrix along the fiber before that happens. That means that the externally applied stress can increase, i.e. the stress-strain curve exhibits strain hardening. The critical fiber volume that leads to such strain hardening can be determined using basic equations of mechanics. There are several theories available. For example, we can follow the composite theory of Naaman and Reinhardt [3] who stipulate that by definition of strain hardening, the maximum post-cracking stress, σ_{pc}, cannot be less than the stress at the first cracking, σ_{cc}, i.e.,

$$\sigma_{cc} \le \sigma_{pc} \tag{1}$$

The stress at first cracking can be estimated as,

$$\sigma_{cc} \le \sigma_{mu}(1 - V_f) + \alpha_1 \alpha_2 \tau V_f L/d \tag{2}$$

where σ_{mu} = matrix tensile strength, V_f = fiber volume fraction, τ = bond strength between fiber and matrix, α_1 = coefficient to reflect the mobilized bond strength at first cracking, and α_2 = efficiency factor to recognize the randomness of the fiber orientation. The maximum post-cracking stress can be expressed as,

$$\sigma_{pc} \le \lambda_1 \lambda_2 \lambda_3 \tau V_f L/d \tag{3}$$

where λ_1 = expected pull-out length ratio (= ¼, according to probability considerations), λ_2 = efficiency factor for the fiber orientation, λ_3 = factor representing the number of fibers pulling out per unit area (or density of fiber crossings). By combining Eqs. (1)-(3), it is possible to determine the minimum fiber volume that will cause strain hardening:

$$V_f \ge V_{f,crit} = \frac{1}{1 + \dfrac{\tau}{\sigma_{mu}} \dfrac{L}{d} (\lambda_1 \lambda_2 \lambda_3 - \alpha_1 \alpha_2)} \tag{4}$$

This solution is plotted in Figure 3 [3] and again in Figure 4, where the objective was to obtain strain hardening of the load-deflection curve for a beam in flexure. Similar expressions can be derived using the principles of micromechanics [4] or fracture mechanics [5], although the results are somewhat different.

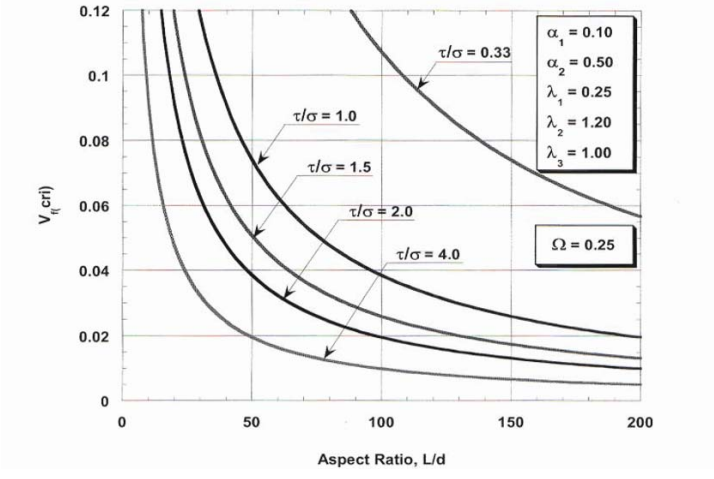

Figure 3. Minimum Fiber Volume for Strain Hardening of Tensile Stress-Strain Curve [3]

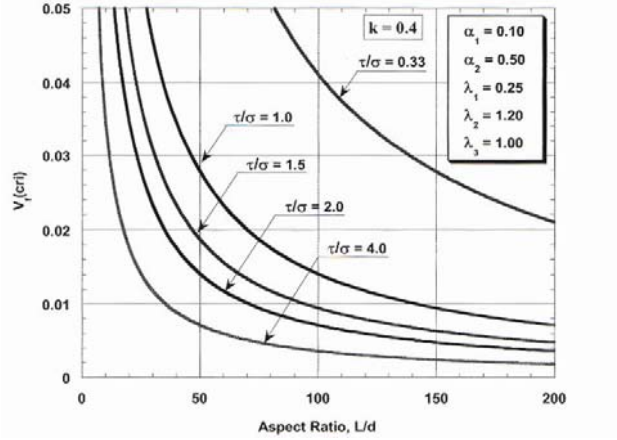

Figure 4. Minimum Fiber Volume for Strain Hardening of Flexural Stress-Strain Curve [3]

Thus, the most important parameters that determine whether the material is a high-performance composite, are the fiber aspect ratio (L/d), the bond strength relative to matrix tensile strength (τ/σ), and the fiber volume, expressed here as the minimum fiber volume ratio $V_{f,crit}$. For example, Figure 3 shows that for L/d = 50 and τ/σ = 2, a fiber volume of at least $V_{f,crit}$ = 4% is required to assure strain hardening of the stress-strain curve for a tensile test specimen. For strain hardening to occur in the load-deflection curve of a beam, a fiber volume of only $V_{f,crit}$ = 1.5% is required, according to Figure 4.

Concerning Figs. 3 and 4, it should be stressed that it is difficult to produce good concrete mixes with fiber volumes exceeding 2%. It is also difficult to work with fibers with L/d > 100. And since the τ/σ - ratio rarely exceeds 1.0, it is practically quite difficult according to Figure 3 to achieve strain hardening in a tensile test specimen. According to Figure 4, however, there exists a small domain within which such behavior is achievable in flexural members [6].

Li and his coworkers [7-9] have developed so-called “Engineered Cement Composites“ (ECC), which can be considered a sub-category of HPFRCC. Their main approach was to physically modify the surface properties of the fibers and to use micromechanics to obtain the desired results.

4. Implications for Engineering Practice

Safety and reliability considerations have always played a major role in engineering practice. It is not uncommon that such considerations dictate the preference of materials, which have mechanical properties with relatively little statistical scatter, as these are by definition more reliable. For example, the use of unreinforced concrete is acceptable only in exceptional cases exactly because

of the poor reliability of its tensile strength. The high statistical scatter of tensile strength data of concrete is the result of a number of factors, most of which can barely be influenced in construction practice. Good quality control can improve the concrete quality to some extent, for example, with careful aggregate grading, mixture proportioning, placing and curing. But the chemical composition of individual cement batches and variations in the mineralogy of natural aggregate, are not readily controlled, not to mention environmental factors such as temperature, humidity, and age. This means that the tensile strength of concrete must be considered a classical random variable with relatively large standard deviations.

The statistical scatter of reinforcing steel properties such as the yield strength is much lower than that of concrete's tensile strength. This is only partially attributable to the better quality control in steel mills compared with that in concrete production facilities. Assigning the tensile forces to reinforcing steel not only benefits the tensile and flexural capacity, but also the reliability of the composite properties. By properly under-reinforcing a flexural member, the mechanical properties of the concrete become less important, and as a result the reliability of a reinforced concrete member is much closer to that of a structural steel member than that of an unreinforced concrete member.

A similar situation is encountered when the concrete is reinforced with short randomly distributed steel fibers, particularly in the case of HPFRCC. Such a composite can properly be referred to as a new structural material, the mechanical properties and reliability of which are closer to those of structural steel than of concrete. Therefore it is conceivable to produce structural members with HPFRCC and no additional steel reinforcement.

At this point it is appropriate to recall some fundamental aspects of structural engineering. In theory it is possible to produce structural elements with unreinforced concrete subjected not only to compression but also flexure. The main problem is the concrete's low and unreliable tensile strength, which is often already impaired due to shrinkage cracks prior to any external load application. Thus, unreinforced concrete members would have to be grossly over designed. The lack of ductility is another reason why standard building codes generally do not permit the use of unreinforced concrete members subjected to flexure. Structural engineers prefer ductile failure modes with ample warning of impending failure. For example, at present, structural glass is gaining increasing attention of architects. Its extreme brittleness can be dealt with only by specifying appropriately high safety margins. Theoretically, unreinforced concrete could be dealt with in a similar manner. However, coupled with the low tensile strength, this would lead to generally unacceptably massive members and waste of natural materials.

When considering HPFRCC, the demands for tensile strength and ductility have to be dealt with separately. In applications with low levels of criticality, such as pavements, additional steel reinforcement could be hard to justify. In structurally critical elements, such as beam-column joints of frames subjected to strong seismic loads, it is known that conventional confinement reinforcement can lead to congestion and difficulties of concrete placement. In such applications the use of HPFRCC could permit sufficiently lower confinement reinforcement (if not altogether avoid it) to ease concrete placement.

An entirely separate issue is that of economics. Since short fibers are generally distributed uniformly and oriented randomly throughout the concrete volume, they are not likely to be as effective as reinforcing bars that are oriented in the direction of principal tension. For example, if we have the option of distributing two volume percent of steel in the form of short randomly distributed fibers or in the form of reinforcing bars in the region of maximum tension, the latter one will be unquestionably more economical [10]. On the other hand, the pure material cost constitutes only a fraction of total cost. Whereas the placement of reinforcing bars is very labor intensive and costly, the addition of steel fibers to a concrete mix has a much smaller effect on the concrete cost. Also, when considering long-term costs, the relative economics of fibers is likely to be more favorable, because the fibers keep cracks small and therefore improve the durability of a structure, reducing cost for maintenance and repair.

In some cases, improved material performance outweighs slight cost increases, as for example in the case of important structures that need to be hardened against blast or impact. Fiber-reinforced concrete in general and HPFRCC in particular have been shown to be so effective in such applications, that there exist few alternatives. Although good corroborating data are sparse, it can be surmised that fiber reinforcement can play a similar role in earthquake resistant design of concrete structures.

5. Applications

Possibly the most significant applications are those where fiber reinforcement can reduce or replace altogether conventional shear reinforcement. In the case of aseismic structures this has been an issue for quite some time [11]. Coupled with modern computational mechanics it is now possible to thoroughly evaluate specific applications. A simple example shall serve as an illustration. In 1962, Bresler and Scordelis have tested beams with and without shear reinforcement [12] and their results have served to calibrate mathematical models since. In a recent exploratory study [13], the program Vector [14] of the University of Toronto was used to simulate the experiments. First, the model was calibrated

to reproduce the test results of beams with and without shear reinforcement. Then, since no test data for comparable beams with fiber reinforcement were available, the theory of Minelli and Vecchio [15] was used to estimate the effect of fiber reinforcement and to compare it with that of conventional shear reinforcement. The results, illustrated in Figure 5, show that even 2 volume percent of steel fibers do not have the same effect as 0.15% shear reinforcement. However, the beneficial effect fibers on stiffness, strength, and ductility are obvious, and because of the preliminary nature of this numerical study, no definite conclusions should be drawn from it.

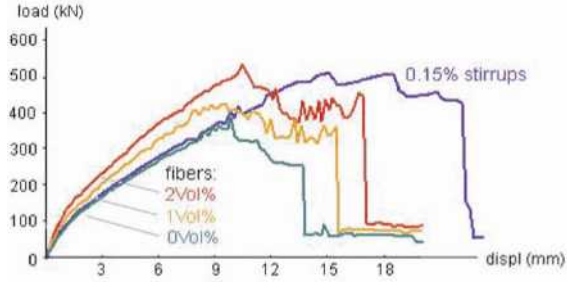

Figure 5. Load-Deflection Curves of Beams With Fiber and Shear Reinforcement [13]

Fischer and Li [16,17] have studied both theoretically and experimentally the effectiveness of Engineered Cement Composites (ECC) in concrete columns subjected to strong cyclic loading. Their results point to a clear and enormous increase of ductility and energy absorption capacity by the fibers, Figure 6. These results are significant because they illustrate that ECC may partially or completely replace conventional confinement reinforcement, thereby improving constructability. They also indicate the enormous potential of ECC to improve the response of structural members to strong seismic ground motions, which is clearly comparable if not greater than that of conventional reinforcement.

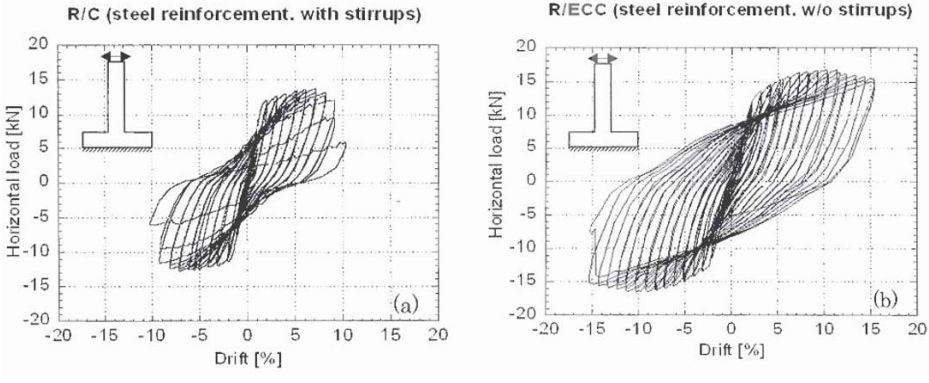

Figure 6. Hysteresis Behavior of Columns with a) stirrups and b) ECC [16]

Since HPFRCC products are amenable to novel production technologies such as extrusion, it is safe to assume that this new type of material will spread in construction practice, although more in precast concrete than cast-in-place applications. Before FRC in general and HPFRCC in particular can expect more widespread acceptance, further research is necessary. Also, standard testing protocols are needed to determine the important material properties, such as tensile strength and fracture toughness, as well as quality control measures to assure that the fibers are in fact uniformly distributed and oriented in space. Once such standard tests are available, it can be expected that this new material will be incorporated into the various building codes and standards – an essential prerequisite for technology transfer into engineering practice.

These obstacles to technology transfer were subject of a recent workshop on advanced fiber-reinforced concrete [18], during which the following steps were identified to overcome those obstacles.

Since many different kinds of fibers are used in construction practice, the pertinent codes and specifications should contain criteria which are generally valid, regardless of the type of fiber, even though the available test data for the various types of fibers are of different quality and quantity.

Based on strain hardening potential, a distinction should be made between regular fiber-reinforced concrete (FRC) and high-performance fiber-reinforced cement composites (HPFRCC). In this regard it is noteworthy that the special properties of HPFRCC are called for only in regions subjected to extreme loading conditions, such as beam-column joints of earthquake-resisting frames, i.e., where plastic deformations are to be expected.

The stress-strain curve for uniaxial tension can be determined from a bending test of a beam with or without notch. Other test setups have been recommended as well. But since the results of direct tension tests are more reliable than those of bending tests, the latter ones would require higher safety factors.

The lack of universally accepted standard tests to determine basic material properties is at present the main obstacle against widespread use of FRC in engineering practice. Discussions are still ongoing as to which test setups should serve as standard tests to determine fracture properties of the various types of concrete. However, the pertinent RILEM committee has made recommendations [19].

Once standard test methods have been accepted, recommendations to the appropriate code-writing authorities can be made. This is the last and most essential step before this new type of material can be expected to be used widely.

6. Self-Consolidating Concrete

Enormous advances in concrete technology have been made in recent decades. A major breakthrough came with the introduction of superplasticizers, also known as water reducing admixtures. These eliminated the age-old dilemma caused by the fact that an increase of the water-cement ratio improves workability but lowers strength. Superplasticizers greatly improve the flowability of fresh concrete, so that the water-cement ratio can be reduced with its beneficial effects on strength and durability, without adversely affecting workability.

A new concrete materials technology generally attributed to Okamura [20,21] is now known as self-consolidating or self-compacting concrete (SCC) and closely related to self-leveling concrete. The original impetus for this development was the need for skilled workers in Japan and elsewhere to achieve high-quality and durable concrete through proper consolidation, especially in applications with dense steel reinforcement. The solution of this problem required a complex optimization problem. A sufficient viscosity of the fresh concrete was required to avoid segregation. Next, the maximum size of coarse aggregate obviously played a major role. Then, the optimum grading of coarse and fine aggregate needed to be determined. Finally, it was found that the addition of water to increase flowability led to an unacceptable decrease in viscosity. This dilemma was solved again by the addition of a superplasticizer, which increases flow, without decreasing viscosity.

Shortly after the breakthrough of achieving self-compacting concrete, standard tests were proposed, such as a U-shaped container, with a gate and obstacles representing steel reinforcing bars in the center. After placing the concrete into one leg of the container, the gate is opened, and the difference in height between the concrete levels in the two legs reached after a specified time interval is taken as a measure of self-compactability.

The significance of this development for the concrete industry cannot be overemphasized. Since the fresh concrete can flow through long distances without segregation and no skilled labor is required to consolidate it, the cost of labor to place concrete is reduced considerably, productivity is increased, and the quality of the end product improved. This new technology will also affect concrete construction in seismic regions, because earthquake-resisting structures typically require significant amounts or reinforcement, which often lead to congestion and difficulties of concrete placement. In addition, high-performance concrete is achievable at relatively little additional material cost and with less skilled labor. Okamura claims that the use of self-consolidating concrete for the construction of the anchorage blocks for the Akashi Straights Bridge shortened the construction time from 2.5 to 2 years [21].

7. Conclusions

During the last 20 – 30 years, greater advances in concrete technology have been made than in the prior 150 years – ever since John Aspdin developed Portland cement. Two of those recent developments were highlighted here: high-performance fiber-reinforced cement composites (HPFRCC) and self-consolidating concrete (SCC). Both of these have already had major impacts on concrete construction in general and are expected to affect the construction of earthquake-resisting concrete structures in particular.

HPFRCC can be considered a new material, with which design professionals still need to familiarize themselves. It has been shown that properly engineered cement composites can achieve ductilities and energy absorption capacities one or two orders magnitude higher than of regular concrete. Such performance is bound to make them attractive for the construction of earthquake-resisting structures. However, the lack of generally accepted standard tests constitutes currently the major hurdle to be overcome before these materials can be incorporated in building codes.

SCC represents a category of novel concrete mix designs with such superior flow properties that high-performance concretes with excellent durability can be placed even in the presence of highly congested reinforcement. Thus, designers of ductile concrete structures have two previously unavailable options: 1) to use conventional reinforcement details in conjunction with SCC, 2) to utilize HPFRCC, which permits a considerable reduction of conventional confinement reinforcement.

References

1. Committee ACI 544, State-of-the-Art Report on Fiber Reinforced Concrete, American Concrete Institute, Farmington Hills, MI, Report ACI 544.1R-96, 2002.
2. A. E. Naaman, and H. W. Reinhardt, Characterization of high performance fiber reinforced cement composites - HPFRCC, High Performance Fiber Reinforced Cement Composites 2, Proc., 2nd Int. Workshop, Ann Arbor, Michigan, 1995, pp 3-23.
3. A. E. Naaman, and H. W. Reinhardt, Strain-hardening and deflection hardening fiber reinforced cement composites, High Performance Fiber Reinforced Cement Composites 4, Proc., 4th Int. Workshop, Ann Arbor, Michigan, 2003, pp 95-113.
4. V. C. Li, and H. C. Wu, Conditions for pseudo-strain hardening in fiber reinforced brittle matrix composites, J. Applied Mechanics Review, V.45, No.8, 1992.
5. P. Tjiptobroto, and W. Hansen, Tensile Strain hardening and Multiple Cracking in High-Performance Cement Based Composites, ACI Materials Journal, V.90, No.1, 1993.

6. A. E. Naaman, and H. W. Reinhardt, Fiber reinforced concrete: current needs for successful implementation, International Workshop on Advanced Fiber Reinforced Concrete: from Theory to Practice, Bergamo, Italy 2004.
7. V. C. Li, On Engineered Cementitious Composites, a Review of the Material and its Applications, Journal of Advanced Concrete Technology, Vol.1, No.3, 2003, pp 215-230.
8. G. Fischer, and V. C. Li, Influence of Matrix Ductility on Tension-Stiffening Behavior of Steel Reinforced Engineered Cementitious Composites (ECC), ACI Structural Journal, V. 99, No. 1, January-February 2002.
9. H. Stang, and V. C. Li, Classification of fiber reinforced cementitious materials for structural applications, Proceedings of BEFIB, Varenna, Lake Como, Italy, Sept. 2004, pp197-218.
10. B. Mu, C. Meyer, R. Felicetti, and S. Shimanovich, Flexural performance of Fiber-Reinforced Cementitious Matrices, Proc., 3rd Int. Conf. on Concrete under Severe Conditions, Vancouver, June 18-20, 2001.
11. C. H. Henager, Steel Fibrous, Ductile Concrete Joint for Seismic-Resistant Structures, Reinforced Concrete Structures in Seismic Zones, American Concrete Institute, Special Publication SP-53, 1977.
12. B. Bresler, and A. C. Scordelis, Shear Strength of Reinforced Concrete Beams, Journal of the American Concrete Institute, Proc., V.60, No.1, pp.51-72, 1963.
13. A. Wildermuth, High Performance Fiber Reinforced Concrete in Engineering Practice, Diplom Thesis, Universität Stuttgart, 2005.
14. P. S. Wong, and F. J. Vecchio, Vector2 and FormWorks User's Manual, University of Toronto, 2002.
15. F. Minelli, and F. J. Vecchio, Compression Field Modeling of Fiber Reinforced Concrete: Preliminary Numerical Study, Fiber-Reinforced Concretes– BEFIB 2004, M. DiPrisco, R. Felicetti, and G.A. Plizzari, eds., RILEM Proceedings PRO 39, 2004.
16. G. Fischer, Deformation Behavior of Reinforced ECC Flexural Members under Reversed Cyclic Loading Conditions, PhD Dissertation, University of Michigan, 2002.
17. Y. Y. Kim, G. Fischer, and V. C. Li, Performance of Bridge Deck Link Slabs Designed with Ductile ECC, ACI Structural Journal, V101, No. 6, Nov-Dec. 2004, pp792-801.
18. C. Meyer, S. Shah, S. Ahmad, M. DiPrisco and G. Plizzari, eds., Proceedings of the International Workshop on Advanced Fiber Reinforced Concrete: from Theory to Practice, Bergamo, Italy, 2004.
19. RILEM TC 162-TDF, L. Vandewalle, Chair, σ-ε-Design Method, pp.560-567, Bending Test, pp.579-582, Test and Design Methods for Steel Fiber Reinforced Concrete, Materials and Structures, Vol.36, Oct. 2003.
20. H. Okamura, M. Kunishima, K. Maekawa, and K. Ozawa, High-Performance Concrete Based on the Durability Design of Concrete Structures, Proceedings, EASEC-2, No. 1, Jan. 1989, pp 445-450.
21. H. Okamura, Self-Compacting High-Performance Concrete, Concrete International, July 1997.

SHAKING TABLE TESTS OF SCALED RC FRAME MODELS FOR INVESTIGATION OF VALIDITY AND APPLICABILITY OF DIFFERENT RETROFITTING TECHNIQUES

MIHAIL GAREVSKI*
Institute of Earthquake Engineering and Engineering Seismology IZIIS, Skopje, Macedonia

VIKTOR HRISTOVSKI
Institute of Earthquake Engineering and Engineering Seismology IZIIS, Skopje, Macedonia

MARTA STOJMANOVSKA
Institute of Earthquake Engineering and Engineering Seismology IZIIS, Skopje, Macedonia

Abstract. Within the NATO Project SfP977231, three 1/3 scale models (2 story R/C frame specimens) of a 4 story R/C frame building prototype have been designed, constructed and tested on the shaking-table at the IZIIS Laboratory, Skopje, Macedonia. The main goal was to verify the validity and applicability of different seismic retrofitting techniques under the project. The first test specimen was a 3D RC frame structure with infill walls. The second specimen had additional CFRP strips applied on both faces of the infill walls using epoxy. The third specimen was retrofitted with pre-cast concrete panels epoxy glued to the wall and frame members. Several input motions with gradually increasing intensity were applied with peak ground acceleration up to 0.52g. Obtained results from the experiments showed that both retrofitting techniques (CFRP strips and pre-cast concrete panels) have significantly reduced the displacements and improve the structural behavior.

Keywords: Shaking-table tests; seismic retrofit; lap splice failure; CFRP strips

* Mihail Garevski, Institute of Earthquake Engineering and Engineering Seismology IZIIS, Salvador Aljenede 73, 1000 Skopje, Macedonia; email: garevski@pluto.iziis.ukim.edu.mk

S.T. Wasti and G. Ozcebe (eds.), Advances in Earthquake Engineering for Urban Risk Reduction, 441–453.

1. Introduction

The research reported herein has been carried out within the NATO Science for Peace Project SfP977231 “Seismic Assessment and Rehabilitation of Existing Buildings”. It represents a common project realized by the Department of Civil Engineering, Middle East Technical University, Ankara, Turkey in cooperation with The Institute of Earthquake Engineering and Engineering Seismology-IZIIS, University “Ss. Cyril and Methodius”, Skopje, Republic of Macedonia, Department of Civil Engineering, University of Texas at Austin, USA, Center of Research and Technology-CERTH, Thessaloniki, Greece, and FORTH/ICE-HT, Patras, Greece.

The initiative for this project arose from the severe damage that resulted from the last major earthquakes in Turkey. The experience has shown that inadequate lateral stiffness and unsuitable design and construction often lead to substantial damage when the structure is subjected to high lateral loads. Hence proper repair and strengthening of such buildings, as well as seismic retrofit is required in order to avoid catastrophic losses and have safer and stronger buildings.

Generally, repair and strengthening of RC frames damaged by earthquakes, as well as seismic retrofit of existing undamaged RC frames can be realized through *system* and *member* behaviour improvement. The system behaviour improvement approach involves a new lateral load resisting system, which will increase the lateral strength and stiffness of the existing system. One of the most widely used techniques based on this principle is construction of RC walls by infilling some bays of the existing frames. Repair and strengthening or seismic retrofit of some reinforced concrete elements can be performed by epoxy injection, by jacketing or fiber reinforced plastics (FRP), carbon fiber (CF) wrapping.

When constructing a new RC wall in an existing building the occupants need to be evacuated, which makes this rehabilitation technique complicated and not very practical. Therefore the research task has been focused on developing simple methodologies and practical and economical rehabilitation techniques for seismically vulnerable buildings without disturbing the occupants. Within this paper, two strengthening/retrofit techniques have been demonstrated. The first proposed technique uses Carbon Fiber Reinforced Polymers (CFRP) for increasing the capacity and ductility of the masonry infill [1], while the second discussed technique involves pre-cast concrete panels epoxy glued to the wall and to the frame members [3].

2. Experimental Work

All three tested specimens represent pure reinforced concrete 3D frame structure with infill walls specified in such a way to take into account some of the common irregularities and deficiencies detected in these types of buildings during past earthquakes in Turkey.

Details regarding the model design, construction and material characteristics are thoroughly presented in [2]. This paper also contains description of the shaking table on which the specimens were tested as well as the instrumentation used.

2.1. TEST SPECIMENS

The first specimen was designed with an idea to simulate the behaviour of the real four-story frame structure with masonry infill walls, collapsed during the 1999 Izmit Earthquake and to serve as a reference for the strengthened specimens (Figure 1).

Figure 1. Display of the test specimens during construction

The second specimen had an additional Carbon Fiber Reinforced Polymer (CFRP) strips on the inner and outer faces of the masonry infill constructed in the middle bay of both stories. The hollow clay used for all three specimens was to a scale of 1/3. Specimen 2 was strengthened according to the results and conclusions drawn from the previous studies carried out in METU Structural Engineering Laboratory [1]. The most important conclusions from these investigations were that: a) In order to increase the lateral strength, CFRP should be extended and anchored to frame members; b) It is not needed to cover the whole brick panel with CFRP, since diagonally placed CFRP strips are as effective as covering the whole bay; c) A firm anchorage should be provided

between CFRP and the panel; d) For the lap splice problems (as in our case for Specimen 1, where brittle failure occurred), that portion of the frame should also be covered by CFRP strips; and e) Anchor dowels should be used to connect CFRP to the infill and to the frame members.

All foregoing mentioned requirements for proper retrofit (or strengthening) of infill wall members have been applied for construction of Specimen 2. The steps of the incorporation and some details of these CFRP strips are presented in Figures 2, 3 and 4.

Figure 2. Phases of construction of Specimen 2; (left)-anchorage holes are drilled; (right)-anchor dowels are placed; (right) completed model with added carbon fibers

Figure 3. Specimen 2: Some details of CFRP incorporation

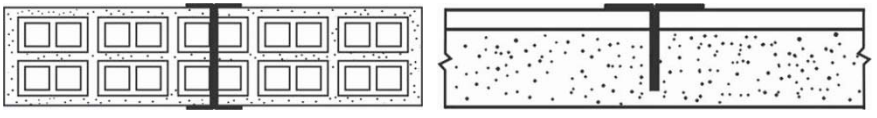

Figure 4. Schematic view of the anchor dowel applications: (left) to infill; (right) to frame members

The used CFRP was composed of an epoxy-based matrix and carbon fibers. The material characteristics of the CFRP strips were the following: a) High strength carbon with packaging rolls: width =0.5 m, length=100 and surface = 50 m^2; b) Superficial density, D_s=0.3 kg/m^2; c) Density of fibre ρ=1820 kg/m^3; d) Effective thickness s=0.165 mm, e) Effective area per unit width, A^{eff}= 0.165 mm^2/mm; f) Tensile strength f_{tk}=3420 MPa; g) Tensile strength per unit width, f_{tkl}=565 N/mm; h) Tensile modulus of elasticity E_{tk}=230 GPa; i) Ultimate deformation, e_u=1.5 %; j) Coefficient of thermal expansion, $\alpha=10^{-7}$ 1/K; k) Thermal conductivity, J=17 1/m.s.K; l) Electrical resistivity, $W=1.6 \times 10^{-5}$.

For the third specimen the existing infill wall was reinforced with a very thin layer of high strength pre-cast concrete elements epoxy glued to the wall and to the frame members. Panels Type 1,2,3,4, and 5 have been placed in four layers in the first floor with height of 1430mm and panels Type 6, 7,8,9,10 have been arranged in the second floor with height of 860mm. Panels were made of concrete with strength of about 40MPa and reinforced with steel plain bars. Figures 5 and 6 show the arrangements, reinforcement details and the dimensions and reinforcement of the panels accordingly.

SIKADUR 31 epoxy repair mortar was used in panel joints and between the panels and the wall plaster. It is a two component mortar with setting time of about 45min at room temperature and the tensile strength of about 20MPa.

SIKA Anchor Fix was used to anchor the dowels into frame members in order to ensure better connection.

The results and conclusions followed from the previous studies carried out in METU [3] were implemented during the strengthening of Specimen 3.

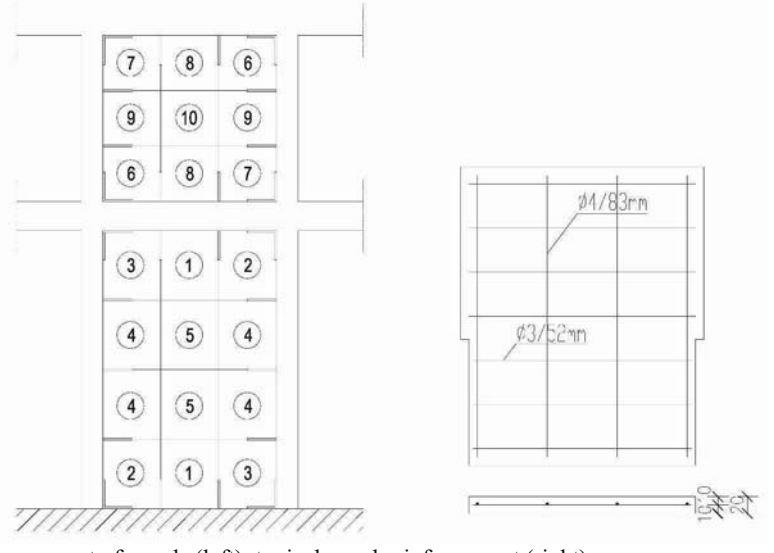

Figure 5. Arrangement of panels (left); typical panel reinforcement (right)

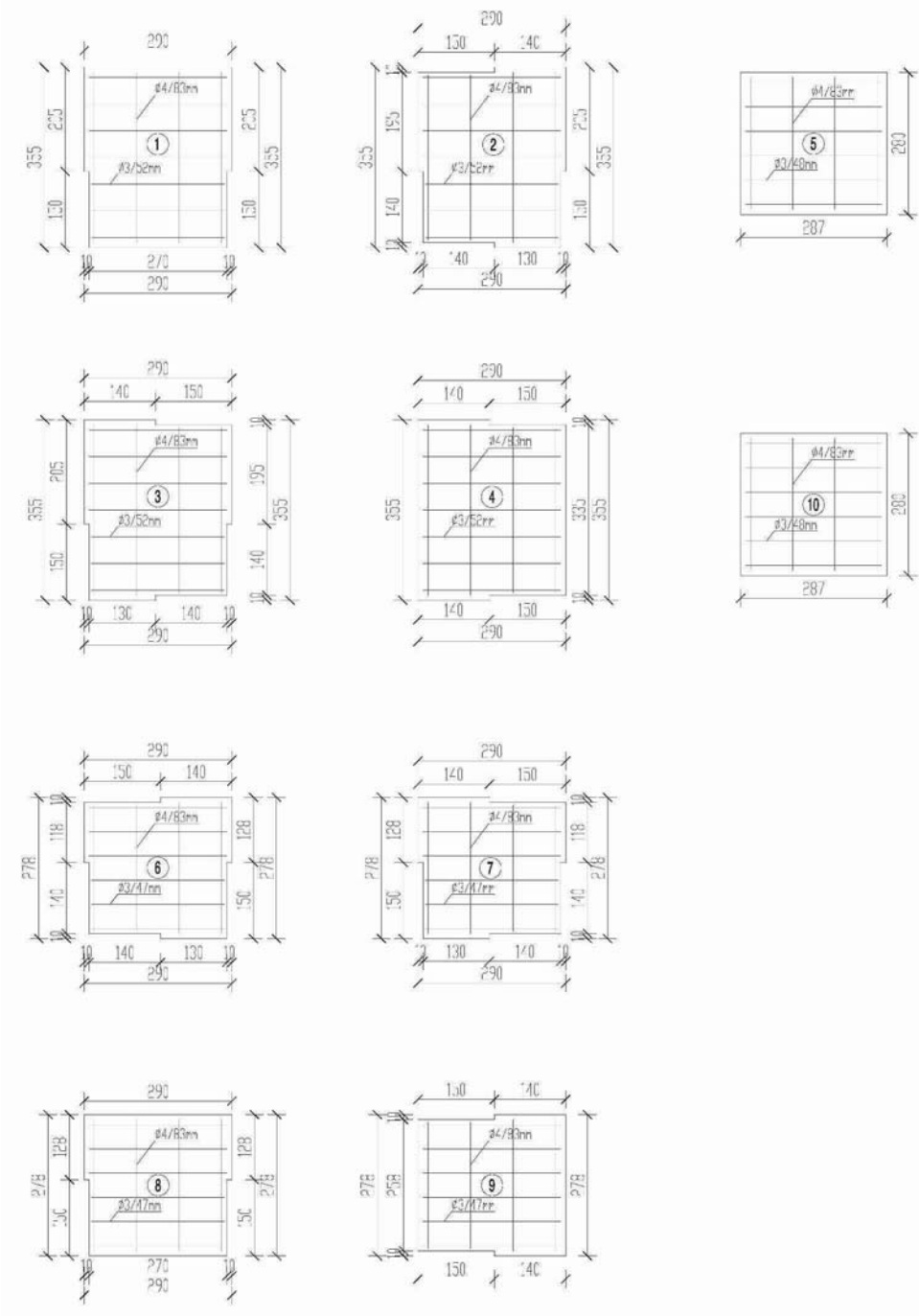

Figure 6. Panel Dimensions

Special attention was paid to panel connections. Though in the first tests shear keys and welded connections (provided by fixing reinforcing steel bars to each other and to dowels epoxy anchored into the frame members) were employed, final results had proved the successful application of epoxy mortar in connecting the panels and inessentiality of the shear keys and welded connections.

Some phases of preparation of the third model are shown in Figures 7-9.

Figure 7. Specimen 3: Placing the anchor dowels (left); general view of the speciment after all anchor dowels are placed (right)

Figure 8. Panels with different geometry (left); glued panels (right)

Figure 9. Completing the model (left); instrumentation installed (right)

3. Test Procedure

Following the curing period of the concrete, Specimen 1 was placed on the shaking table without infill walls. The first step was to load the model with the ballast and excite it with a small shaking table placed on the top slab, in order to measure the mode shapes and frequencies. Checking of the mode shapes has also been performed by using the ambient vibration technique. The same experimental steps were undertaken after construction of the infill walls, to measure the dynamic characteristics of the integral model. The comparison of the natural frequencies has been conducted to establish the influence of the infill walls on the model dynamic characteristics.

The next step was to undertake the shaking table tests in the following order: first a low-level random vibration time history was applied to measure the linear behavior of the model. Following, the scaled Izmit earthquake record (with a_{max}=0.023) was applied to the test model. Afterwards, input motions were applied on the model with peak ground acceleration up to 0.45g. After each earthquake excitation, low-level random vibration tests were undertaken in order to monitor the change of the natural frequencies due to modal material deterioration.

A similar procedure was performed for the other two specimens. For the Specimen 3 minor damage was observed in the infill walls but major crack was detected separating the infill wall from the foundation (Figure 10). Even when the additional mass was added (4 ingots of 1.6t on the first floor slab and 6 ingots of 2.4t on the second floor slab, Figure 11), still no significant damage occurred in the infill wall, demonstrating the effectiveness of the pre-cast panels. Small cracks have been observed in the column-beam joints (Figure 12) and the crack separating the foundation and the infill wall became a bit wider which once again has emphasized the inadequate lap splice length of the longitudinal reinforcement from the foundations.

Figure 10. A major crack infill/foundation

Figure 11. Additional mass added to the model

Figure 12. Small cracks in the column-beam joint

Therefore modified retrofit technique was applied. Additional anchor dowels were placed in the columns, welded to the existing reinforcement, and covered with epoxy mortar (Figure 13).

Figure 13. Modified retrofitted model

4. Obtained Results from the Experimental Tests of the Three Specimens and Discussion

The obtained response from the shaking-table tests of Specimens 1, 2 and 3 subjected to simulated Izmit earthquake, is summarized in Table 1.

TABLE 1. Selected results from shaking-table tests

Span	Max. input acceleration	1st floor		2nd floor	
		abs. accel.	rel. displ.	abs. accel.	rel. displ.
Specimen 1 (not retrofitted)					
035	0.023g	0.028g	0.0060 m	0.045g	0.0059 m
090	0.059g	0.078g	0.0175 m	0.122g	0.0175 m
180	0.112g	0.138g	0.0326 m	0.176g	0.0328 m
360	0.201g	0.265g	0.0690 m	0.325g	0.0710 m
500	0.261g	0.330g	0.1050 m	0.396g	0.1060 m
750	0.450g	0.390g	0.1630 m	0.420g	0.1680 m
Specimen 2 (retrofitted)					
035	0.032g	0.022g	0.0085 m		0.0083 m
070	0.052g	0.039g	0.0168 m		0.0167 m
600	0.410g	0.277g	0.0146 m	0.470g	0.0147 m
601	0.423g	0.740g	0.0113 m	0.420g	0.0870 m
Specimen 3 (retrofitted)					
035	0.032g	0.038g	0.0006 m	0.053g	0.0006 m
600	0.450g	0.500g	0.0076 m	0.659g	0.0079 m
620	0.425g	0.588g	0.0076 m	0.527g	0.0144 m
650	0.486g	0.417g	0.0115 m	0.655g	0.0165 m
700	0.516g	0.380g	0.0143 m	0.552g	0.0226 m
Specimen 3 (retrofitted-extra masses added)					
650	0.396g	0.340g	0.0110 m	0.500g	0.0145m
Specimen 3 (retrofitted-dowels added)					
650	0.459g	0.369g	0.0057 m	0.478g	0.0076 m
700	0.3067g	0.337g	0.0066 m	0.466g	0.0086 m

As mentioned previously, simulation of the behavior of the 4-story frame structures during the Izmit earthquake taking into account all phenomena and deficiencies of the design and construction, is generally very difficult. During the experimental test of Specimen 1, it was possible first to observe the shear-slip failure of the infill wall due to deterioration of the bond between the columns/beams and the masonry, since these contact zones were simulated as they really were in the real structure (poor mortar connection without anchors, Figure 14).

Figure 14. Specimen 1 at the end of test: Shear-slip failure between the concrete elements and masonry infill wall due to poor connection (left);brittle failure between the columns and foundation due to inadequate stirrup lap-splice-length (middle); and crushing and spalling of concrete near beam-column joints(right)

Then, the non-ductile failure of the column basis (lap-splice failure and pull-out of the longitudinal reinforcement) has been observed (Figure 14). This brittle failure practically prevented damage of the upper part of the structures, although concrete crushing (Figure 14) has been observed at some beam-column connections.

It is important to note that the formation of the separated surfaces at the bottom of the columns led to shifting of the basic natural period of vibration of the structure (as could be seen from the random vibration tests with low magnitude preformed after each loading), so that the structure practically behaved as base-isolated. Although considerable deformations have been measured (maximum displacement of 16.3 cm), the structure did not collapse and any serious damage to the structural elements has not been observed. However, even though the experiment did not simulate the spectacular pancake-type failure (as it really happened in the actual structure during the Izmit earthquake), the fact is that several important deficiencies have been simulated (the lack of lap splice length of the longitudinal reinforcement from foundations, as well as the poor quality of the concrete, etc.) which resulted in the overall poor behavior of the structure. Anyway, having in mind the difficulties arising during the design and construction of the non-linear shaking-table models (lack of possibilities for scaling and modeling of constitutive relations for materials, size-effect in concrete especially related to fracturing and bond-deteriorating processes), the basic objectives for simulation of a real 4-story building with 2-story 1/3 model have been achieved.

Obtained results for the Specimen 2 and 3 (Table 1) have shown that both of the proposed retrofit techniques, by using Carbon Fiber Reinforced Polymers (CFRP) and pre-cast concrete panels, can improve the behavior of this kind of structures, increasing their capacity and ductility.

5. Conclusions

From the performed experimental investigations the following conclusions may be drawn:

1. Three specimens of two-story spatial frame system with 1/3 scale have been constructed: the first one to simulate the behavior of the real four-story frame structures with masonry infill walls which collapsed during the 1999 Izmit earthquake, and the other two specimens, strengthened with CFRP strips and pre-cast concrete panels accordingly, to show how these retrofitting techniques can significantly improve the seismic response of this kind of structural system.
2. Shaking-table tests have been performed in order to investigate the influence of the dynamic conditions and real time-history input accelerations (1999 Izmit earthquake) on structural behavior. Although the model design process for this kind of problems can be very uncertain and difficult, having in mind the complexity of the conditions (nonlinear materials, dynamic conditions, complex structural system, etc.), using basic similitude requirements with artificial mass simulation method, rational and logical models have been designed and constructed, which have successfully served for the research purposes and objectives.
3. The experiments have shown that using the proposed techniques for retrofit of these kind of structural systems, the overall behavior under seismic excitation can significantly be improved, as can be seen from the results of these investigations, presented in Table 1, i.e., the maximum displacements dropped from 16.8 cm for the non-retrofitted specimen to 8.7 cm and 2.26 cm for the retrofitted specimens for the strongest applied earthquake record (0.45g and 0.423g input maximum peak acceleration).
4. From the test of Specimen 1, brittle failure at the contact between columns and foundations has been observed due to inadequate lap splice length of the longitudinal reinforcement in columns, which was one of the phenomena observed on real 4-story frame buildings with brick infill walls during the 1999 Izmit earthquake. This deficiency (together with the poor connection between the infill and RC members) has been overcome by applying the proposed retrofitting method, demonstrated on Specimen 2, using CFRP strips and anchor dowels, as shown in Figures 2, 3, and 4. Generally, significant improvement has been achieved regarding the member's behavior, as well as the overall structural behavior in terms of increased structural and member's capacity and ductility, as well as lateral strength.
5. Similar conclusions can be drawn from the third test. Specimen 3 strengthened with epoxy glued pre-cast panels exhibited significant increase

in the load carrying capacity and stiffness as well as considerable ductility improvement and increased energy dissipation. As a critical issue, the lap splice problem in the columns which can lead to premature failures still remains. However additional epoxy anchored dowels in the sections where frame and masonry infill are connected to the foundations have overcome this problem.

6. As compared to other retrofit and strengthening methods (for example incorporation of a new RC infill), both of the strengthening techniques CFRP and pre-cast concrete panels have proved to be applicable more easily and more rapidly, and also do not require evacuation of the occupants. Of course, to choose the most appropriate and most optimal retrofitting or strengthening technique, the cost of application must be considered for each separate case and structural system.

References

1. I. Erdem, U. Akyuz, U. Ersoy, and G. Ozcebe, A Comparative Study on the Strengthening of RC Frames, *NATO SfP977231 Project: "Seismic Assessment and Rehabilitation of Existing Buildings"*, NATO Science Series, IV. Earth and Environmental Sciences-Vol.29, May, 2003, pp.407-432.
2. M. Garevski, A. Paskalov, K. Talaganov and V. Hristovski, Experimental and Analytical Investigation of 1/3-Model R/C Frame-Wall Building Structures – PART I(Model Design and Analytical Evaluation of Dynamic Characteristics of the Model), *NATO SfP977231 Project: "Seismic Assessment and Rehabilitation of Existing Buildings"*, NATO Science Series, IV. Earth and Environmental Sciences-Vol.29, May, 2003, pp.487-498.
3. M. Baran, M. Duvarci, T. Tankut, U. Ersoy, and G. Ozcebe, Occupant Friendly Seismic Retrofit of RC Framed Buildings, *NATO SfP977231 Project: "Seismic Assessment and Rehabilitation of Existing Buildings"*, NATO Science Series, IV. Earth and Environmental Sciences-Vol.29, May, 2003.

ANALYSIS OF INFILLED REINFORCED CONCRETE FRAMES STRENGTHENED WITH FRPS

BARIS BINICI•
Middle East Technical University, Department of Civil Engineering, 06531, Ankara

GUNEY OZCEBE
Middle East Technical University, Department of Civil Engineering, 06531, Ankara

Abstract. In the past various researchers conducted numerous experimental studies, in which different rehabilitation techniques were developed. Among them, use of fiber reinforced polymers (FRPs) was found to be an effective alternative with rapid retrofit time and providing substantial increases in strength with limited ductility. In order to design and detail FRPs based on the results of experiments, analysis and design procedures need to be established. The objective of this study is to fill this gap and propose analysis guidelines for FRP strengthened infill walls for use in seismic evaluation methods. For this purpose, a diagonal compression-strut and tension-tie model is presented to model the strengthened infill wall that is integrated to the boundary frame members. The comparisons of test results with estimated load-deformation curves show that model is capable of estimating stiffness, strength and deformation capacity of FRP strengthened reinforced concrete frames with sufficient accuracy. The outcome of this research is believed to enable the structural engineers to perform retrofit design of deficient infilled reinforced concrete frames with FRPs.

Keywords: Fiber reinforced polymer; analysis; infill wall

• Assistant Professor, Middle East Technical University, Department of Civil Engineering, 06531, Ankara, Email: binici@metu.edu.tr, Tel:+90-312-210-2457

S.T. Wasti and G. Ozcebe (eds.), Advances in Earthquake Engineering for Urban Risk Reduction, 455–470.

1. Introduction

Recent earthquakes in Turkey (Kocaeli 1999, Duzce 1999, Bingol, 2003) demonstrated the vulnerability of existing structures to large seismic demands that were not accounted in their design. Efficient and reliable upgrade methods are needed in order to mitigate the expected seismic loss. Most of these deficient structures in the building stock are reinforced concrete frames with infill walls. The post earthquake reconnaissance surveys[1,2] showed that lack of lateral strength together with insufficient ductility to withstand seismic deformations is responsible for collapses in most cases. To begin rebuilding and retrofitting the infrastructure, practical methods and relevant design procedures are needed for building rehabilitation. Among the available retrofit schemes, adding shear walls is the most commonly chosen alternative for current applications. However, the construction work involved is tremendously demanding. Furthermore, it results in lengthened retrofit time and necessitates the need to relocate the occupants. In order to overcome these shortcomings, alternative retrofit schemes are needed to enhance in-plane load carrying capacity of reinforced concrete frames with infill walls.

Fiber reinforced polymers have been used in strengthening infill and masonry walls in a number of studies[3-5]. Both in plane and out-plane behavior of strengthened walls have been investigated in these studies. Recently, a novel technique that makes use of fiber reinforced polymers (FRPs) in the upgrade of reinforced concrete frames with infill walls was developed as a part of a NATO sponsored extensive research project[6]. The method is based on the premise of limiting inter-story deformations using FRPs bonded on infill walls that are integrated to the boundary frame members. Quasi-static cyclic tests were performed on multi-bay multi story structures in order to experimentally validate the effectiveness of the FRP strengthening system[6-9]. The proposed method was found to be attractive due to its speed and ease of application with little or no disturbance of the occupants. It is believed that this method can efficiently be used in the upgrade of existing reinforced concrete frames with infill walls, especially when the number of buildings that needs rapid rehabilitation measures is immense. This study aims at developing analysis guidelines for the FRP retrofitting of existing reinforced concrete frames with infill walls. In this way, it will be possible for the structural engineers to assess the feasibility of the retrofit procedure, design and detail FRPs for building retrofit.

2. Behavior and Failure Modes

When a reinforced concrete frame with infill walls is subjected to lateral deformations, the infill wall acts as a diagonal strut and the separation of the infill occurs on the opposite side. The idea of the FRP retrofit scheme is to reduce inter-story deformation demands by using FRPs to act as tension ties. In order to achieve this, diagonal FRPs bonded on the infill wall are tied to the framing members using FRP anchors as shown in Figure 1. In this way, a tension tie contributes to the load carrying capacity in addition to the strength provided by the compression strut formed along the infill diagonal. Special embedded fan type FRP anchors formed by rolling FRP sheets are connected in the corner region in order to achieve efficient use of FRP materials (Figure 1). To eliminate premature debonding of FRP from plaster surface anchor dowels are used along the thickness of the infill wall (Figure 1).

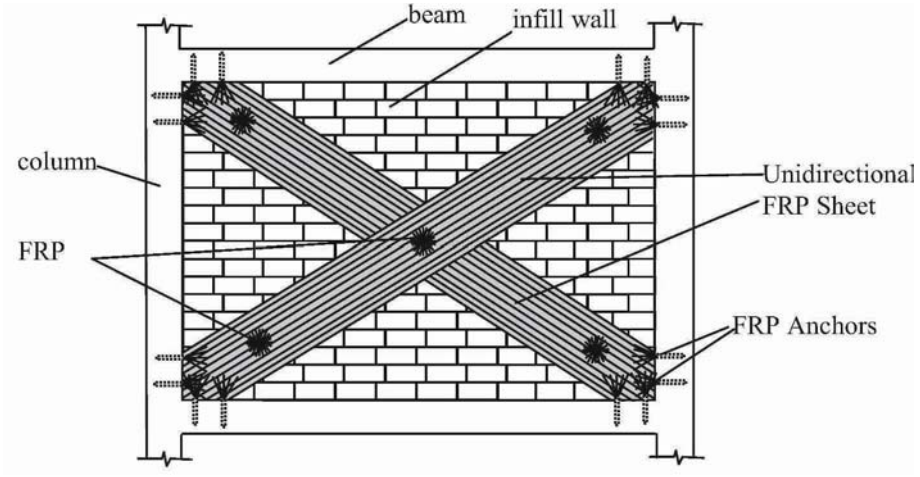

Figure 1. FRP strengthening method for reinforced concrete frames with infill walls

To demonstrate the structural deformations and flow of stresses, a two story frame is analyzed using plane stress elements available in ANSYS[10]. The objective of this analysis is not to reproduce the complete inelastic behavior of a retrofitted specimen. Instead, a qualitative picture of the deformations and flow of stresses is obtained to gain insight for a structural model. Concrete beams and columns are assigned isotropic elastic material properties whereas the infill wall is modeled with orthotropic elastic material properties to reflect the direction dependent behavior of masonry. Frictional contact surface is used between the frame members and the infill wall to capture the separation of the infill from the boundary frame. Second story infill wall represents the conventional infill behavior whereas the first story infill wall mimics the

behavior of an FRP strengthened infill wall. The connection of the infill wall elements are provided only at the nodes where FRP anchors are used for the first story. The deformed shape of the analyzed frame is presented in Figure 2a. It can be observed that separation of the infill occurs in the second story, whereas the first story infill wall acts an integral part of the frame due to the presence of FRP anchors. Principal stresses are shown in Figure 2b for the analyzed frame. The use of FRPs together with proper anchors in the first story results in a tension tie limiting the inter-story displacements in addition to the resistance provided by the compression strut that forms due to bearing of boundary frame on the infill wall. The analysis results show that when an FRP is bonded to the infill wall and tied to the boundary frame, it acts as a tension tie whose width is similar to the width of the provided FRP sheet in the effectively anchored region.

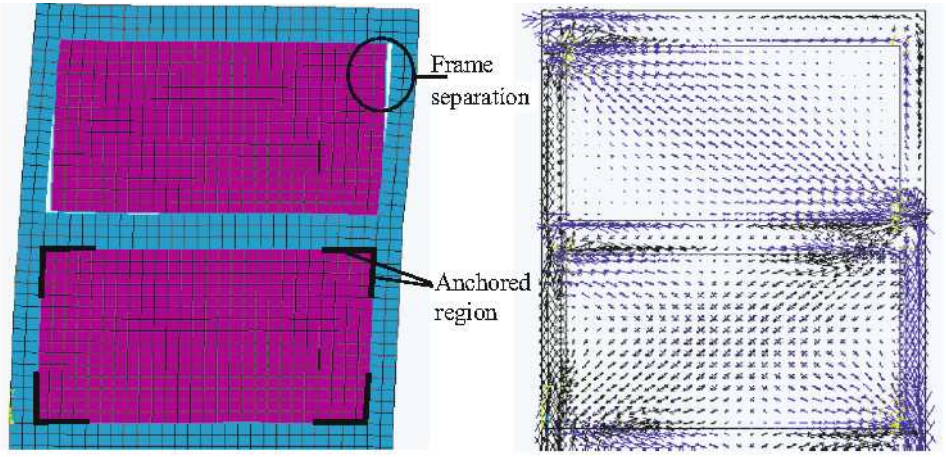

a) Deformed Shape b) Principal Stresses

Figure 2. Finite element analysis results of a two story frame with anchors provided for the first story infill wall

Experiments conducted on FRP strengthened reinforced concrete frames[7-9] with infill walls revealed that there are two dominant failure modes (Figure 3). The first mode initiates with the failure of the FRP anchors in the form of a combined pull-out and slip failure. As soon as the anchors fail, the load carried by the FRP is transferred to the diagonal compression strut and failure of the infill wall occurs due to corner crushing. When three CFRP anchors with a depth of about five times the hole diameter are used per corner on each side of the infill, it has been observed that anchor failure occurs at an effective diagonal FRP strain of about 0.002[9]. Second failure mode occurs because of FRP debonding from the infill wall surface. After FRP debonding, previously formed horizontal cracks start to open and when the tie action of FRP is lost,

sliding shear failure of the infill wall occurs. The first failure mode is mainly due to insufficient anchor depth and can be avoided by increasing the depth and number of anchor dowels[9]. However, the second failure mode marks the limiting strength of the strengthened infill. Tests have shown that beyond a strain level of about 0.006, FRP debonding takes place resulting in a sliding shear failure of the infill followed by a sudden drop of strength[9]. These observations obtained from the finite element analysis and experiments are used to develop structural models for the FRP strengthened RC frames with infill walls.

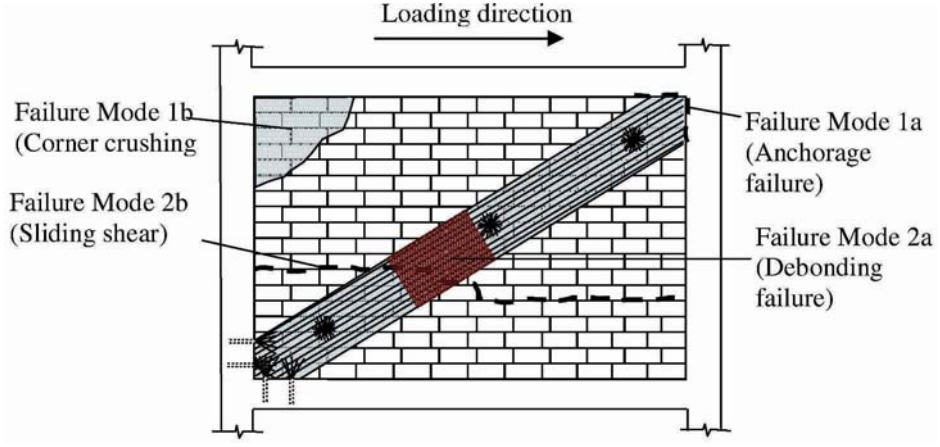

Figure 3. Failure modes of FRP strengthened infill wall in a reinforced concrete frame

3. Analytical Model

3.1. FRAME ELEMENTS

Models using structural elements (frames, trusses, plates etc.) are computationally much more efficient compared to continuum models. Continuum models can provide more accurate information on local stresses and strains at the expense of additional computation time. However, structural models allow the analyses of a number of cases to conduct parametric and reliability studies. The analytical model of a strengthened frame proposed in this study is a structural one and is shown in Figure 4. Frame elements (beams and columns) are modeled using elastic elements with predefined plastic hinge regions at their ends. The cross sections of the plastic hinge regions are discretized into a number of fibers with appropriate uniaxial stress-strain behavior for different materials. Unconfined concrete fibers are modeled using Hognestad stress-strain curve[11] with a linear descending branch up to a strain of

0.004 at zero stress. Modified Kent and Park model[11] is implemented for core concrete fibers confined with transverse reinforcement. Steel reinforcement is modeled with an elastic perfectly plastic material model. The advantage of fiber models is the consideration of axial load moment interaction during analysis and avoiding the need of performing sectional analysis separately. Plastic hinge length, which is the length of the region where inelastic action is expected, is taken equal to the depth of the member. Effective cracked stiffness equal to the 75% of the gross section properties and modulus of elasticity of concrete are used between the plastic hinge regions to model the elastic portion of the frame elements.

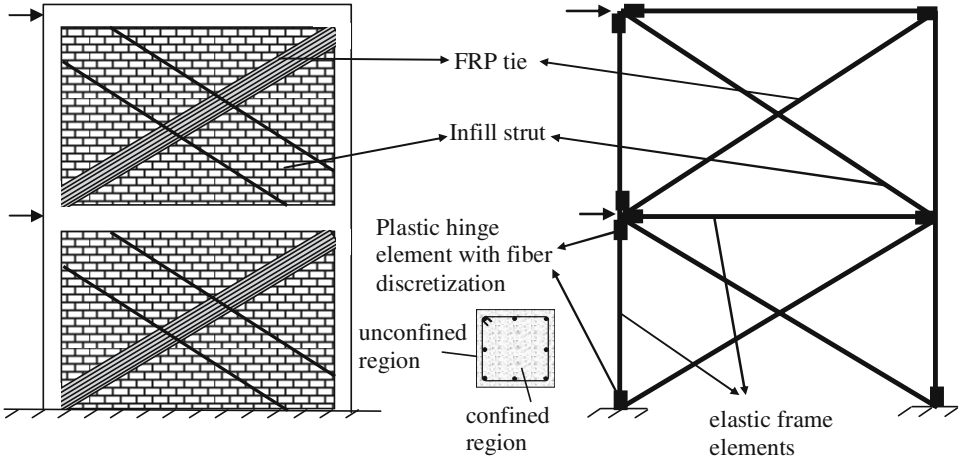

a) Strengthened frame b) Structural model

Figure 4. Structural model of a two-story frame strengthened with FRPs

3.2. FRP TIES

Infill wall strengthened using FRPs is modeled using a compression strut and a tension tie (Figure 4), which adequately represents the load transfer mechanism observed from the experiments and finite element analysis. A trilinear stress-strain response is proposed for the truss members to simulate the behavior of the strengthened infill wall (Figure 5). Experiments conducted on reinforced concrete frames with infill walls with and without plaster showed that presence of plaster on infill wall surface needs to taken into account for accurate estimation of stiffness and strength[12]. Therefore it assumed here that FRP, infill material and plaster on the infill wall surface contributes to the stiffness of the tension tie. The area of the composite tension tie is:

$$A_{tie} = w_f t_{tie} \tag{1}$$

where w_f is the width of the FRP provided and t_{tie} is given by:

$$t_{tie} = t_f + t_p + t_{in} \tag{2}$$

in which t_f, t_p, t_{in} are the thicknesses of FRP, infill and plaster, respectively. It is not unrealistic to assume that mortar used between the infill blocks is similar to the plaster used for exterior coating. Therefore the cracking stress of the tie, f_{crt} can be found from:

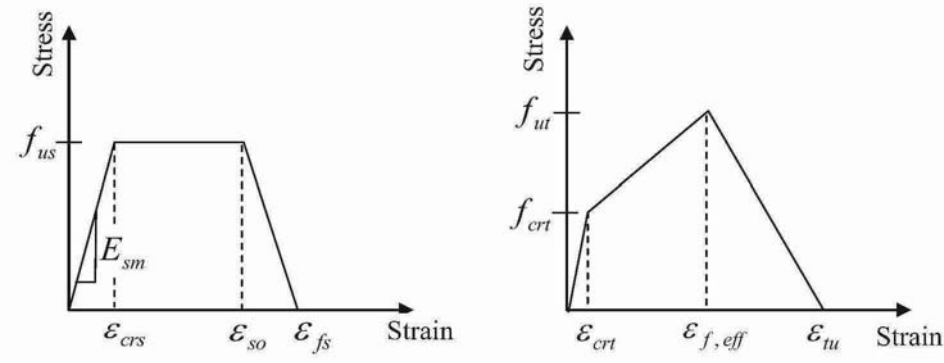

Figure 5. Stress-strain behavior of the infill strut and FRP tie

$$f_{crt} = \frac{V_{crt}}{A_{tie}} \tag{3}$$

$$V_{crt} = f_{pt} w_f \left(\left(t_{in} + t_p \right) + \frac{E_f}{E_m} t_f \right) \tag{4}$$

where f_{pt} is the tensile strength of the plaster, E_f and E_m are the moduli of elasticity of FRP and mortar, respectively. Eq. (4) assumes that cracking of plaster and mortar occurs simultaneously up to which level the three-phase material behaves as a unit. The corresponding cracking strain, ε_{crt} is the cracking strain of the plaster which can be determined from uniaxial tension tests. Beyond cracking, contribution of mortar and plaster to load carrying capacity gradually decreases (Figure 5). The tensile capacity V_{ut}, and tensile strength, f_{ut}, can be computed from Eqs. (5) and (6) respectively, based on the capacity of the FRP at the effective strain obtained from experimental results, $\varepsilon_{f,eff}$, at which anchor failure or debonding initiates.

$$V_{ut} = \varepsilon_{f,eff} w_f t_f E_f \tag{5}$$

$$f_{ut} = \frac{V_{ut}}{A_{tie}} \tag{6}$$

The last definition required for the tension tie is the strain at which complete failure of FRP occurs (ε_{tu}). This strain limit controls descending portion of the global response. The preliminary analyses results showed that three times the effective strain ($\varepsilon_{f,eff}$) can be used to model the strength degradation beyond ultimate strength.

3.3. INFILL STRUTS

The strut stress-strain model is also a trilinear model with a perfectly plastic plateau and limited deformation capacity. The area of the composite strut, A_{str}, is computed by:

$$A_{st} = w_s t_{st} \tag{7}$$

where

$$t_{st} = t_p + t_{in} \tag{8}$$

$$w_s = \frac{(1-\alpha)\alpha h}{\cos\theta} \tag{9}$$

Equation (9) is proposed by El-Dakhakhi et al[13] based on the work by Saneinejad and Hobbs[14] to estimate the effective width of the strut. In Eq. (9), h is the height of the infill wall, θ is the strut inclination angle and α is a dimensionless parameter to account for the frame infill contact length computed by:

$$\alpha = \sqrt{\frac{2(M_{pj} + 0.2M_{pc})}{h^2 t_{st} f_{mc}}} \tag{10}$$

in which M_{pj} is the minimum of the moment capacities of the column or the beam, M_{pc} is the moment capacity of the column and f_{mc} is the compressive strength of the infill plaster composite.

The ultimate strength of the diagonal compressive strut V_{us}, is computed based on the minimum of the two capacities, namely sliding shear, V_{ss}, and corner crushing, V_{cc}.

$$V_{us} = \min\left(V_{ss}, V_{cc}\right) \tag{11}$$

$$V_{ss} = f_{mv} L t_{st} \tag{12}$$

$$V_{cc} = 250 t_{st} f_{mc} \tag{13}$$

and the ultimate strength, f_{us}, can be computed by:

$$f_{us} = \frac{V_{us}}{A_{st}} \tag{14}$$

In Eq. (12), f_{mv} is the shear strength of the mortar (or plaster) bed joint and L is the width of the infill wall. Eq. (13) is an empirical equation calibrated with test results and proposed by Flanagan and Bennett[15] to predict corner crushing strength of infill walls. f_{mc} that appears in Eqs. (10) and (13) and the slope of the stress strain curve in Figure 4 (E_{sm}), can be obtained from uniaxial compression tests of plastered infill walls. In the absence these tests Eqs. (15) and (16) can be used to predict the strength and stiffness of the diagonal strut.

$$f_{mc} = \frac{f_{in}t_{in} + f_m t_p}{t_{st}} \tag{15}$$

$$E_{sm} = \frac{E_{in}t_{in} + E_m t_p}{t_{st}} \tag{16}$$

In Eq. (16), E_{in} is the elasticity modulus of the infill material, which generally varies between 500 to 1500 times the compressive strength of the infill material. The strain value at which strength loss initiates occurs after the failure of the FRP tie. Therefore, ε_{so} should be larger than $\varepsilon_{f,eff}$ in the presence of FRPs and should be equal to the cracking strain of mortar (ε_{crs}) in the absence of any strengthening. The following relationship proved to yield satisfactory estimations for the deformation capacity of the strut:

$$\varepsilon_{so} = \begin{cases} \varepsilon_{crs} \text{ without FRP} \\ 2\varepsilon_{f,eff} \text{ with FRP} \end{cases} \tag{17}$$

Equation (17) implies that no ductility should be expected for the compression strut in the absence of FRP strengthening whereas some ductility is available for the strut when FRPs are used delaying the complete failure. Failure strain of the compression strut, ε_{fs}, was assumed to occur at a strain of 0.01 by El-Dakhakhni et al[13]. A similar assumption is made here for the infill walls without any strengthening or failing due to anchorage failure. This strain limit can be taken as 0.02 when failure of the FRP tie occurs beyond a strain level of 0.005.

4. Experimental Verification

The models described above have been validated by comparing the estimated response curves with the results obtained from the experiments conducted by

different researchers at different institutions. Material properties of the infill walls used in the analyses are presented in Table 1. Specimen details are presented in Table 2. All the analyses were conducted in a displacement controlled mode with the reference loads applied at given proportions at different stories. Opensees[16] analysis platform was used to conduct the analyses. The envelope curves of the quasi-static tests are compared herein with the pushover analyses using the models described above.

TABLE 1. Material properties for analyzed specimens

Researcher	Material	Compressive Strength (MPa)	Tensile Strength (MPa)	Modulus of Elasticity (MPa)
Erduran[7]	FRP	-	3450	230000
	Concrete	15	-	18400
	Plaster	4.3	0.4	9800
	Infill	10 (2)[a]	-	7000 (2000)
Erdem[8]	FRP	-	3450	230000
	Concrete	9.5	-	14600
	Plaster	5	0.5	9800
	Infill	11.2 (2)	-	7000 (2000)
Akguzel[9]	FRP	-	3450	230000
	Concrete	15	-	18400
	Plaster	5	0.5	10600
	Infill	11 (2)	-	7000 (2000)

a) Numbers in parenthesis denote values in the weak direction of infill material.

TABLE 2. Member details for analyzed frames

Researcher	Columns				Beams			Anchors	
	Dimensions (mm × mm)	ρ_l[a] (%)	s[b] (mm)	l_d[c] (mm)	Dimensions (mm × mm)	ρ_l (%)	s (mm)	n[d]	d[e] (mm)
Erduran[7]	100 × 150	1.3	90	300	150 × 150	0.9	90	3	60
Erdem[8]	110 × 110	1.6	100	320	110 × 150	1.4	100	3	70
Akguzel[9]	100 × 150	1.3	95	160	150 × 150	1.3	130	3 (5)[f]	50 (80)

a) Longitudinal reinforcement ratio

b) Spacing of transverse reinforcement

c): Lap splice length in the plastic hinge region

d) Number of anchors provided on one face at a corner

e) Depth of anchors

f) Values for the second specimen failing with FRP debonding

Akguzel[9] tested four two-story one bay frames, two of them unstrengthened and two with FRP upgrades. All the columns in the frame members were deficient for confining steel and had lap splices in the plastic hinge regions. Lateral load was applied incrementally and lateral load ratio of the second story to the first story was two throughout the tests. One of the unstrengthened specimens had no infill walls whereas the other one had infill walls in both stories. Strengthening was achieved through bonding of 200 mm wide FRP sheets on both sides of the frame. Total base shear plotted against roof displacement values are compared for the analytical and experimental results in Figure 6. FRP strain limit was taken as 0.006 for the case when FRP debonding was the failure mode and 0.002 was used when anchor strength was critical. It can be observed that FRP strengthening resulted in an increase of about 100% in base shear capacity when proper anchors were used. Estimations of stiffness and strength of all the test specimens reasonably agree with the measured response.

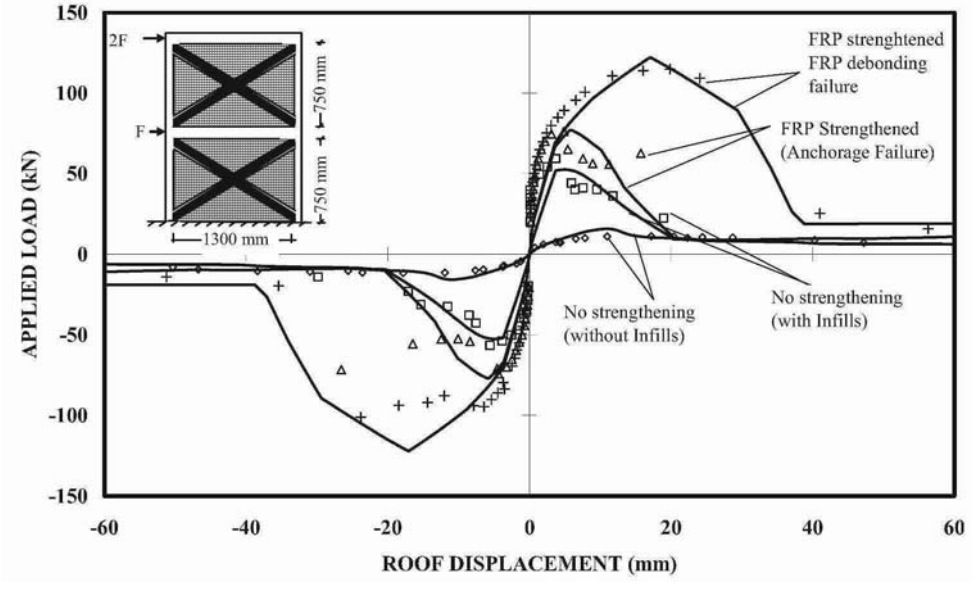

Figure 6. Comparisons of experiments conducted by Akguzel[9] with analysis results (Points are the experimental points, lines are analytical estimations)

Erdem[8] tested two three-bay two-story frames, one bare frame and one infilled frame strengthened with FRPs. Load was applied to the second story floor level only. Strengthened specimen had infills only in the center bay of the frame. Confining steel deficiencies and lap splices in the plastic hinge region existed in these specimens. Strengthening was performed by bonding 400 and 200 mm wide FRPs on the infills of the first and second story infill walls,

respectively. Analyses results are shown together with experimental results for total base shear versus roof displacement in Figure 7. A strain limit of 0.002 was used to curves obtained from these tests are compared herein with the pushover tests using the models described above. It can be observed that capacity of the strengthened frame is approximately twice that of the one prior to upgrading. Furthermore, behavior of the strengthened frame approaches the behavior of the bare frame at large lateral deformations. Analytical estimations of ultimate strength and corresponding deformations agree well with the measured values.

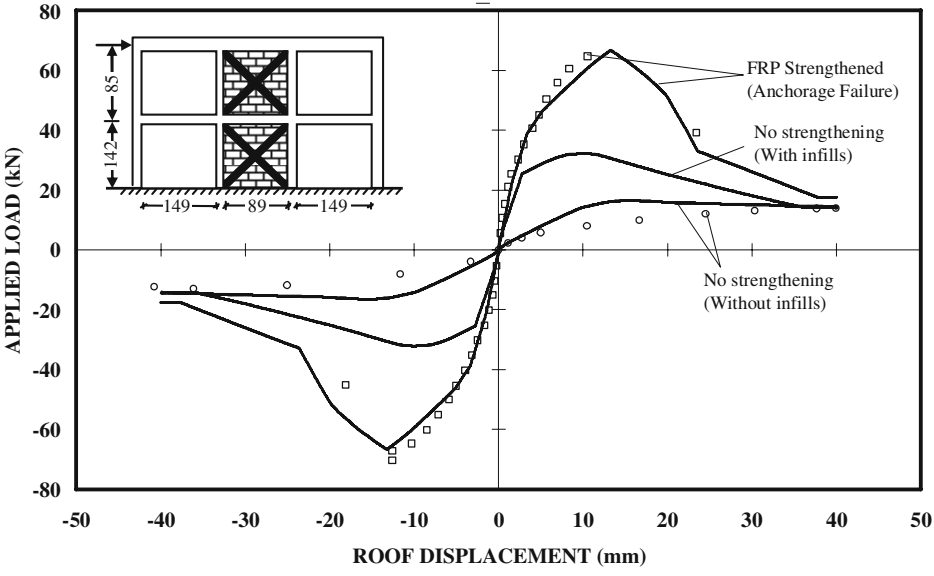

Figure 7. Comparisons of Experiments conducted by Erdem[8] with analysis results (Points are the experimental points, lines are analytical estimations)

Tests of Erduran[7] with FRP strengthening and without any strengthening are compared to the analysis results in Figure 8. Both frames were two-story one bay frames. 200 mm wide FRPs were used in both stories of the one bay two story frames tested by Erduran[7]. An effective strain limit of 0.003 was chosen for FRP ties to simulate anchorage failure of CFRP anchors.

Strength increase obtained compared to the reference specimen with no strengthening was about 85% with significant increase in deformation capacity. Load deformation trends obtained from analyses agree well with the results from experiments. It can be concluded that comparisons presented above on the global load deformation response of the specimens provide confidence on the accuracy of the models proposed in this study.

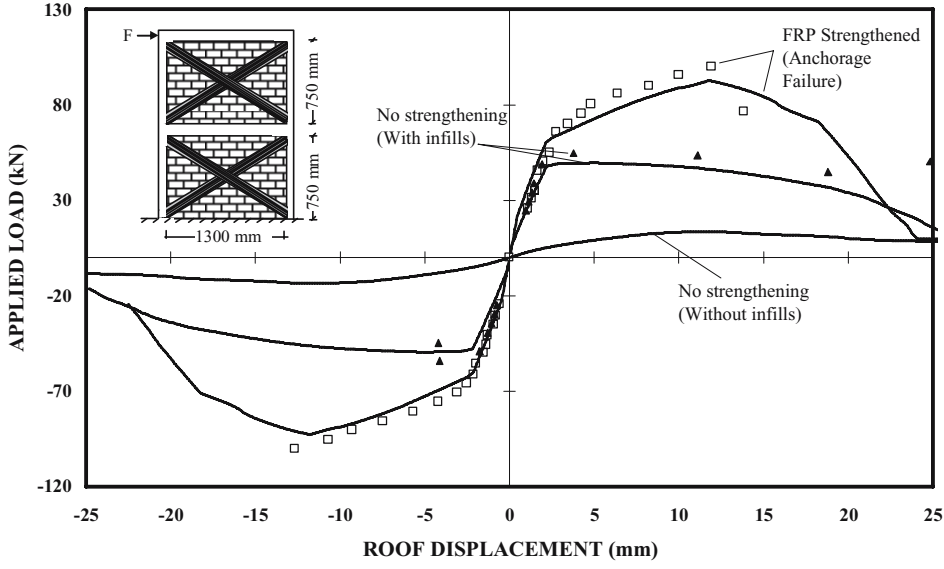

Figure 8. Comparisons of experiments conducted by Erduran[7] with analysis results (Points are the experimental points, lines are analytical estimations)

4.1. CASE STUDY

A typical interior frame of a regular plan building requiring upgrade was analyzed to demonstrate the capacity increases that can be obtained through the use of FRPs. The elevation view of the four-bay, five-story building frame including the locations of the infill walls is shown in Figure 9. All the columns were 400 mm × 400 mm with a longitudinal reinforcement ratio of 1 % whereas the beams had dimensions of 300 mm × 600 mm with 0.5% longitudinal reinforcement ratio. Stirrup spacing of the columns were approximately equal to the effective depth of the section resulting in insufficient confinement for ductile behavior. Concrete strength was 10 MPa simulating typical construction quality in Turkey whereas the reinforcement had a yield strength of 420 MPa. The infill walls were composed of hollow-clay brick with a thickness of 100 mm and a compressive strength of 2 MPa. Additional plaster on the infill walls was 40 mm thick with a compressive strength of about 2 MPa.

Three cases were analyzed by subjecting the frames to an inverted triangular displacement profile along the building height (Figure 9). First analysis was conducted by neglecting the presence of the infill walls. Second analysis was performed by considering the infill walls with the model previously described in this study. A third analysis was conducted by performing an upgrade of the building with carbon fiber reinforced polymers with material properties given in Table 1. Retrofit design was conducted by considering a CFRP width similar to

the width of the estimated compression strut (750 mm). In this way, the compression struts can remain intact and sustain large deformations prior to failure of FRP ties. Sufficient CFRP anchors were provided to eliminate anchorage failures. All the infill walls were retrofitted with CFRPs bonded on two sides of the walls. The normalized base shear ratio was plotted against the normalized roof displacement in Figure 9 to compare the response of different scenarios.

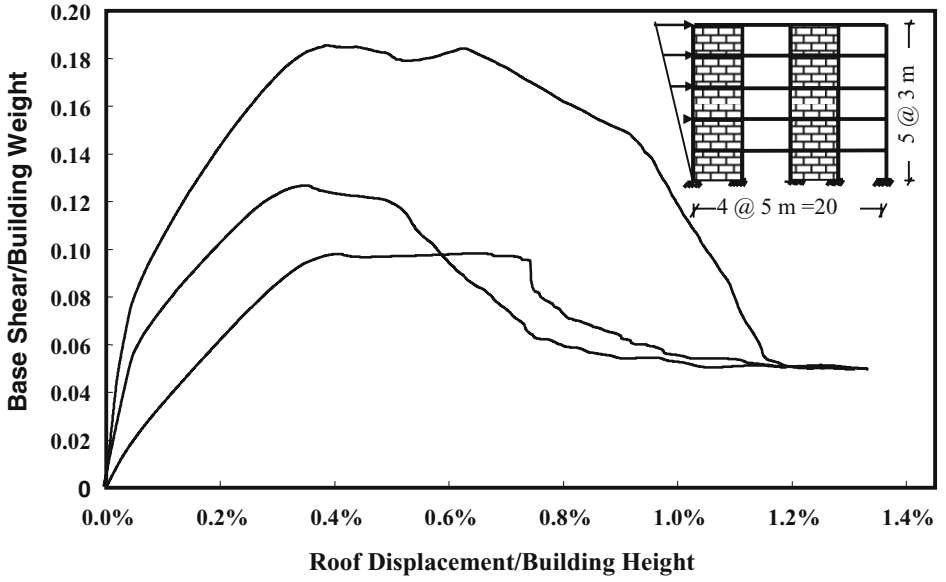

Figure 9. Analysis results for the building frame analysis

It can be observed that presence of the infill walls increases the lateral load carrying capacity by about 30%, whereas the displacement capacity of the building decreases due to rapid degradation of the infill walls and neighboring frame elements once the base shear capacity is reached. Analysis results show that CFRP retrofit resulted in strength increases of about 90% compared to the bare frame whereas the capacity increase was about 50% prior to strengthening with infill walls. For the strengthened frame, some ductility was observed due to progressive failure of the strengthened infill walls. It also can be observed that at large displacements the capacity approaches that of the bare frame. As a result it is possible to say that application of the CFRP retrofit can enhance both the load carrying capacity and deformation capacity of reinforced concrete frames with infill walls.

5. Summary and Conclusions

A structural model is presented in this study to estimate the behavior of FRP strengthened reinforced concrete frames with infill walls. The strengthened infill model is composed of a compression strut and a tension tie with trilinear stress strain response. Frame members are modeled with an elastic beam with hinges that are defined by fibers with appropriate stress-strain relations. Static inelastic analyses were conducted to verify the proposed models and comparisons with test results were presented. A good agreement between measured and estimated stiffness, strength and deformation capacity was observed. A case study of typical reinforced concrete frame with infill walls was analyzed with and without upgrades. Substantial strength and deformation capacity increases were observed as a result of the applied retrofit design.

The proposed model for inelastic static analysis of FRP strengthened reinforced concrete frames can be used in seismic evaluation where pushover analysis is required to obtain a capacity curve. It is believed that the outcome of this research will help structural engineers in making a decision on the retrofit scheme as the models developed have proven to provide reasonable estimates of strength and deformation capacities.

References

1. M. Aschheim, P. Gulkan, H. Sezen, M. Bruneau, A. Elnashai, M. Halling, J. Love, and M. Rahnama, Performance of Buildings, *Earthquake Spectra* 16, 237 (2000)
2. G. Ozcebe, J. A. Ramirez, S. T. Wasti, and A. Yakut, 1 May 2003 Bingol earthquake engineering report, TUBITAK Structural Engineering Research Unit, Publication No: 2004-01, 2004, p. 125.
3. M. R. Valluzzi, D. Tinazzi, and C. Modena, Shear behavior of masonry panels strengthened by FRP laminates, *Construction and Building Materials*, 16(7), 409-416 (2002)
4. T. C. Triantafillou, Strengthening of masonry structures using epoxy-bonded FRP laminates, *ASCE, Journal of Composites for Construction*, 2(2), 96-104 (1998).
5. S. A. Hamoush, M. W. McGinley, P. Mlakar, D. Scott, and K. Murray, Out-of-plane strengthening of masonry walls with reinforced composites, *ASCE Journal of Composites for Construction*, 5(3), 139-145, (2001).
6. G. Ozcebe, U. Ersoy, T. Tankut, E. Erduran, R. S. Keskin, and H. C. Mertol, Strengthening of brick-infilled RC frames with CFRP, TUBITAK Structural Engineering Research Unit Report, No. 2003-01, 2003, p. 67.
7. E. Erduran, Behavior of brick infilled reinforced concrete frames strengthened by CFRP reinforcement: Phase 2, MS thesis submitted to Middle East Technical University, Department of Civil Engineering, 2002, p. 77.
8. I. Erdem, Strengthening of existing reinforced concrete frames, MS thesis submitted to Middle East Technical University, Department of Civil Engineering, 2003, p. 123.

9. U. Akguzel, Seismic retrofit of brick infilled R/C frames with lap splice problem in columns, MS thesis submitted to Bogazici University, Department of Civil Engineering, 2003, p. 125
10. ANSYS 6.1 Documentation, http://www.oulu.fi/atkk/tkpalv/unix/ansys-6.1/content/
11. B. D. Scott, R. Park, and M. J. N. Priestley, Stress-strain behavior of concrete confined by overlapping hoops at low and high strain rates, *ACI Journal*, 79(1), 13-27 (1982).
12. F. Marjani, Behavior of brick infilled reinforced concrete frames under reversed cyclic loading, Ph.D thesis submitted to Middle East Technical University, Department of Civil Engineering, 1997, p. 185.
13. W. W. El-Dakhakhni, M. Elgaaly, and A. A. Hamid, Three-strut model for concrete masonry infilled steel frames, *ASCE, Journal of Structural Engineering*, 129(2), 177-185, (2003).
14. A. Saneinejad, and B. Hobbs, Inelastic design of infilled frames, *ASCE, Journal of Structural Engineering*, 121(4), 634-650 (1995).
15. R. D. Flanagan, and R. M. Bennett, In-plane behavior of structural clay tile infilled frames, *ASCE, Journal of Structural Engineering*, 125(6) 590-599 (1999).
16. OpenSees, Open system for earthquake engineering simulation user manual, PEER Center, http://opensees.berkeley.edu/OpenSees/manuals/usermanual/OpenSeesManual.pdf

TENSILE CAPACITIES OF CFRP ANCHORS

GOKHAN OZDEMIR
Department of Civil Engineering, Earthquake Engineering Research Center, Middle East Technical University, 06531 Ankara, Turkey

UGURHAN AKYUZ•
Department of Civil Engineering, Earthquake Engineering Research Center, Middle East Technical University, 06531 Ankara, Turkey

Abstract. In reinforced concrete buildings inserting adequate amount of reinforced concrete infills is an effective strengthening technique. Another promising technique is to strengthen the existing hollow clay tile infill with diagonally placed CFRP sheets. In this technique, CFRP sheets are extended to the frame members. The connection between CFRP sheets and frame members is provided by CFRP anchors. If an adequate amount of CFRP anchoring is used, CFRP applied hollow clay tile infill becomes a unique part of the reinforced concrete frame. Thus in this strengthening technique, the effectiveness is dictated by the CFRP anchors. In this study, by means of the prepared test setup, the pull-out strength capacities of CFRP anchors are measured. The effects of concrete compressive strength, anchorage depth, anchorage diameter, and number of fibers on the tensile strength capacity of CFRP anchor are studied.

Keywords: Adhesive anchor; carbon fiber reinforced polymer (CFRP); CFRP anchor; strengthening; bond model

• Ugurhan AKYUZ, Department of Civil Engineering, Earthquake Engineering Research Center, Middle East Technical University, 06531 Ankara, Turkey; e-mail: han@metu.edu.tr

S.T. Wasti and G. Ozcebe (eds.), Advances in Earthquake Engineering for Urban Risk Reduction, 471–487.

1. Introduction

In comparison with steel, FRP possess many advantages such as high corrosion resistance, high strength to weight ratio, electromagnetic neutrality and ease of handling. FRPs are generally constructed of high performance fibers such as carbon (CFRP), aramid (AFRP) or glass (GFRP). By selecting among the many available fibers, geometries and polymers, the mechanical and durability properties can be adapted accordingly. Such a synthetic quality makes FRP a good choice for civil engineering applications. The first applications of FRP in strengthening were seen in the retrofitting of damaged columns and beams, which provide member improvements only. In the recent studies, knowing that strengthening with FRP is successful for member repair, it was used in rehabilitation of undamaged structures with a new technique in which the goal was the system improvement rather than member rehabilitation. This technique is called as seismic retrofit by carbon fiber sheet (SR-CF system).

The most important point in SR-CF application is the performance of the special connection. Because, this technique is based on load transfer from the hollow clay tile infill wall covered with CFRP to the frame members. This can only be possible with proper connection details. For this purpose, special devices namely, carbon fiber reinforced polymer (CFRP) anchors, were developed. The effectiveness of SR-CF system highly depends on the capacity of CFRP anchors.

This study discusses the direct tensile load capacities of single CFRP anchors embedded into concrete. The experimental study was conducted under the effects of concrete strength, anchor embedment depth, anchor hole diameter, and CFRP sheet width. Any multiple anchor effect is not addressed here.

1.1. STRENGTHENING WITH CFRP

An experimental study was performed by Erdem et al.[1] to investigate the behavior of an RC frame with hollow clay tile infill wall strengthened with CFRP sheets, in the Structural Mechanics Laboratory of Middle East Technical University (METU). The test specimen was a two story three bay 1/3 scale reinforced concrete frame. This frame had common deficiencies of the buildings in Turkey, such as low strength concrete (10 MPa) and a soft story (h_1/h_2=1.5). To strengthen this frame, first, the middle bay of the frame was infilled with hollow clay tiles. Then, CFRP sheets were glued on both surfaces of the infill diagonally. The load transfer from strengthened hollow clay tile infill wall to the frame members was provided by the CFRP anchors. The specimen was subjected to quasi-static reversed cyclic lateral load at the second story level with an axial load applied to the columns during the test.

The most remarkable conclusion drawn from this experimental study was the importance of the connections, namely CFRP anchors, in the effectiveness of the strengthening application with CFRP. In the light of the experimental study conduced by Erdem et al.[1], it is well understood that the CFRP anchors should be designed properly. For design purposes, tensile capacities of the CFRP anchors were investigated under the effects of the previously mentioned parameters.

All tests were carried out in unconfined and uncracked concrete specimens. To determine the behavior of CFRP anchors under uniaxial tensile tests, two series of tests were conducted. These series differ from each other in the manner of the preparation of the CFRP anchors.

2. Background

In this study, the anchors considered are adhesively bonded CFRP anchors. An adhesive anchor is an anchor installed into a drilled hole with an adhesive to provide bond between the anchor and concrete. Adhesives used in this kind of application can be either pre-packaged or comprise two component mixtures which are proportioned by the user.

2.1. DESIGN CONCEPTS OF ADHESIVE ANCHORS

In the literature, there are several methods to predict the tensile capacities of anchors embedded into concrete. These methods can be subdivided into two groups: concrete cone models and bond models. These two groups can also be sub grouped such as bond models neglecting the shallow concrete cone or combined cone-bond models. In concrete cone models, the tensile capacity of the anchor depends on the embedment depth and the compressive strength of the concrete where anchors are installed. The effect of anchor diameter is ignored in concrete cone models.

Similar to cone models, bond models also depend on the embedment depth in addition with the effects of bond strength between concrete and adhesive, and anchor diameter. Besides these, some researchers revealed that the compressive strength of the concrete is another parameter influencing the capacity[2,3] while some others did not[4]. Bond models, neglecting the effect of shallow concrete cone, differ from the other models by the embedment length definition. The length of the anchor is reduced to account for the shallow concrete cone.

2.1.1. *Bond models*

Cook et al.[5] proposed an elastic bond model in which the tensile capacity of the anchor changes with the embedment depth:

$$P_u = \tau_{ave} \pi d_o \left[\frac{\tanh(\lambda h_{ef})}{\lambda} \right] \tag{1}$$

In the above equation, τ_{ave} is the bond stress, d_o is the hole diameter, λ is the stiffness characteristic of the adhesive anchor system, and h_{ef} is the embedment depth of the anchor. The term inside the bracket in Equation (1) is equal to h_{ef} for shallow embedment depths and the above equation behaves like uniform bond stress model (Equation (2)) for shallow depths. However, the bracketed term becomes less than h_{ef} for deeper embedment depths. When these two limit cases compared, it is clear that the tensile strength of the bonded anchors is not directly related to the embedment depth. Different from Equation (1), d is the outer diameter of the anchor in Equation (2).

$$P_u = \tau_{ave} \pi d h_{ef} \tag{2}$$

In the case of bond models ignoring the shallow concrete cone, the embedment depth of the anchors is reduced by a certain amount. For this purpose, Cook et al.[5] assumed an effective embedment depth which is equal to actual embedment depth of the anchor minus 50 mm. The equation used to predict the tensile capacity by this model is given below.

$$P_u = \tau_{ave} \pi d (h_{ef} - 50) \tag{3}$$

Finally, for the combined cone-bond model, it is assumed that the tensile capacity of the anchor is the combination of both cone model and bond model. In their model, Cook et al.[5] determine a cone depth which is calculated by Equation (4). The ultimate tensile capacity of the anchors with suggested cone depth was calculated as in Equation (5).

$$h_c = \frac{\tau_{ave} \pi d}{1.84 \sqrt{f_c}} \tag{4}$$

$$P_u = 0.92 h_c^2 \sqrt{f_c} + \tau_{ave} \pi d (h_{ef} - h_c) \tag{5}$$

3. Experimental Program

3.1. TEST SPECIMENS

To determine the direct tensile capacities of CFRP anchors, five concrete blocks were cast with three different compressive strengths. 28-day and test-day compressive strengths of these blocks are given in Table 1.

TABLE 1. Desired and actual 28-day compressive strengths of these blocks

Specimen	Compressive Strength of Concrete (MPa)	
	28 day	Test day
1st beam	10.7	10.7-11.3
2nd beam	15.8	15.8-16.4
3rd beam	19.4	19.4-20.1
4th beam	10.2	10.2-10.5
5th beam	16.3	16.3-16.5

3.2. CFRP ANCHORS

CFRP anchors were prepared by MBrace produce C1-30 unidirectional fiber sheets. CFRP anchors were two component systems composed of an epoxy based matrix and C1-30 carbon fibers. The epoxy based matrix was also a two component mixture, consisting of an epoxy resin cross-linked with a curing agent. The epoxy resin is designated as compound A and the curing agent as compound B by the manufacturer. A room temperature cure epoxy resin adhesive, namely saturant, is used as the component of the CFRP. The properties of C1-30 fiber sheets and epoxy resin are given in Tables 2 and 3, respectively.

3.3. TEST SERIES

3.3.1. *Type 1*

This first set of anchors was prepared by rolling the CFRP sheet around itself such that it has a cylindrical form (Figure 1.a). In this type, three different sheet widths (w) were studied: 80 mm, 120 mm, and 160 mm. The rolled CFRP sheets were embedded into epoxy resin so that a 1 cm portion from the bottom was covered with epoxy. By the time end of the anchor hardened, some portion of the CFRP sheet, which is equal to embedment depth, was coated with epoxy and inserted into drilled holes. With the help of the 1 cm stiff portion from the bottom of the CFRP anchor, one can push the epoxy coated cylindrical sheet

into the hole full of with epoxy by means of a very thin steel wire. The diameters (d) of the anchor holes were 12 mm, 14 mm, and 16 mm in this series. The bond free part of the CFRP anchor was also perfectly bonded to a steel rod to apply a tensile force (Figure 1.b). In Type-1, three different embedment depths (h); 70 mm, 100 mm, and 150 mm, three different concrete compressive strength (f_c); 10 MPa, 16 MPa, and 20 MPa were chosen as the study parameters together with the mentioned hole diameters and CFRP sheet widths.

TABLE 2. Properties of C1-30 fiber sheets

Property	Amount	Unit
Unit Weight	0.300	kg/mm^2
Effective Thickness	0.165	mm
Characteristic Tensile Strength	3,430	MPa
Characteristic Elasticity Modulus	230,000	MPa
Ultimate Strain	0.015	mm/mm

TABLE 3. Mechanical properties of epoxy resin (provided by MBrace)

Property	Amount
Compressive Strength	>80 MPa
Direct Tensile Strength	>50 MPa
Flexural Tensile Strength	>120 MPa
Elasticity Modulus	>3000 MPa
Ultimate Strain	>0.025

3.3.2. *Type 2*

Different from Type-1 anchors, these CFRP anchors were prepared completely out of the hole and then installed into the concrete. In this type, first the desired width of CFRP sheet is cut and coated with epoxy resin. Then, the epoxy coated CFRP sheet is rolled over a silicon rod 10 mm longer than the embedment depth and the steel rod through which the force is applied (Figure 2). The diameters of the silicon rod and the steel rod are the same. This technique is developed to have straight anchors in which the fibers of the CFRP sheets are oriented in the same alignment. The part of the anchor that is rolled around the silicon rod is embedded into the drilled hole and bonded there. The extra part of the silicon rod stands above the concrete level to prevent a discontinuity at the critical section. The parameters studied in this type are four different embedment depths; 50 mm, 70 mm, 100 mm, and 150 mm, and two different concrete compressive strengths; 10 MPa, and 16 MPa. The CFRP sheet width is chosen as 120 mm, and the anchor hole diameter is chosen as 20 mm.

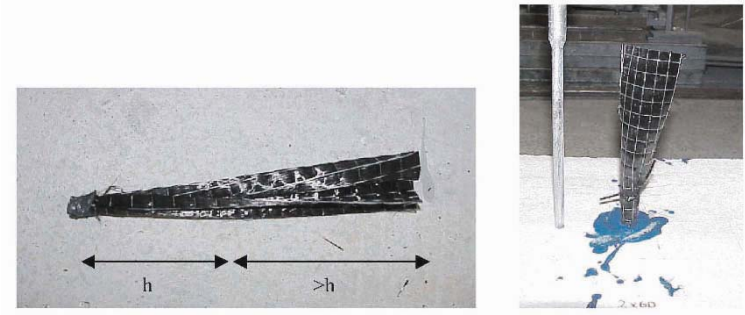

Figure 1. a)Rolled CFRP sheet (left) and b)CFRP anchor embedded into concrete (right)

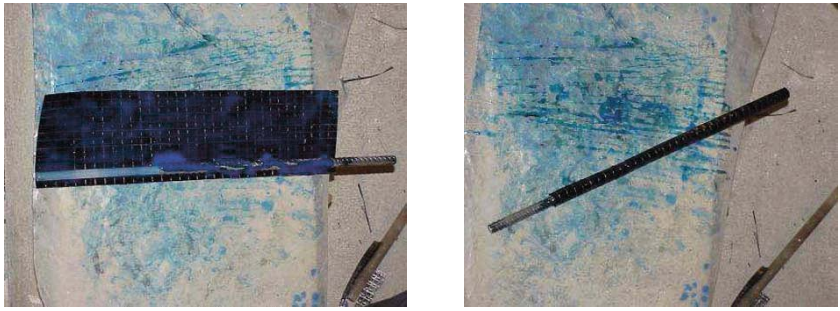

Figure 2. Epoxy coated CFRP sheet rolled around silicon and steel rod

3.3.3. *Testing apparatus and procedure*

The steel frame, which is used to apply the tensile force to the embedded anchor, is shown in Figure 3. The load was applied by means of a center hole hydraulic jack and the load was measured by a load cell. Applied load was transferred to the CFRP anchors through the steel rod extending along the loading equipment.

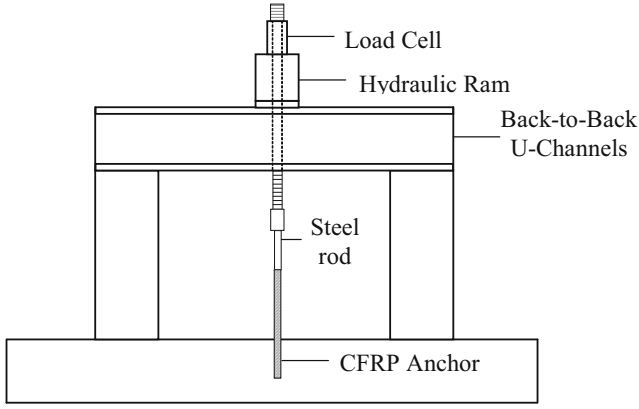

Figure 3. Schematic view of test set-up

4. Test Results

The test results are presented in two parts. In Type-1, 121 tests were conducted while in Type-2 there are 23 tests results. It should be mentioned that all of the tensile capacities observed during the tests were normalized with the tensile capacity of the CFRP sheet provided by the manufacturer. The capacity of the CFRP sheet with a desired width was calculated by

$$P_{FRP} = w \times t \times f_u \text{ (N)} \tag{6}$$

In Equation (6), w is the CFRP sheet width in mm, t is the thickness of the CFRP sheet in mm, and f_u is the characteristic tensile strength of the carbon fibers in terms of MPa. t and f_u are declared by the manufacturer as 0.165 mm and 3,430 MPa, respectively.

4.1. TYPE-1 TEST RESULTS

In Type-1, all of the CFRP anchors failed due to CFRP rupture. Discussion of the parameters will be done under the name of each parameter in the following paragraphs.

4.1.1. *Effect of anchor hole diameter (d):*

To have an effective bonding, manufacturers usually suggest 2-3 mm free space between concrete and anchor for adhesive. The purpose of choosing the diameter of the anchor hole as a parameter is to investigate the effect of additional free space for bonding on the tensile capacity of the CFRP anchor. To do this, the anchor hole diameter was changed from 12 mm to 14 mm and 16 mm while other parameters remained constant.

Figure 4 shows the change in normalized tensile capacities of CFRP anchors as a function of anchor hole diameter for w=120 mm, f_c=16 MPa, and h=150 mm. As is seen, the normalized tensile capacities of the CFRP anchors are almost equal to 30~32% of the CFRP sheets. There is no significant increase or decrease in normalized capacities due to change in hole diameter d.

4.1.2. *Effect of concrete compressive strength (f_c):*

Figure 5 shows the test data of CFRP anchors with 160 mm sheet width, 100 mm embedment depth, and 14 mm hole diameter. As it is seen, the variation is so small that it can be neglected. The normalized tensile capacities change in between 0.31 and 0.33.

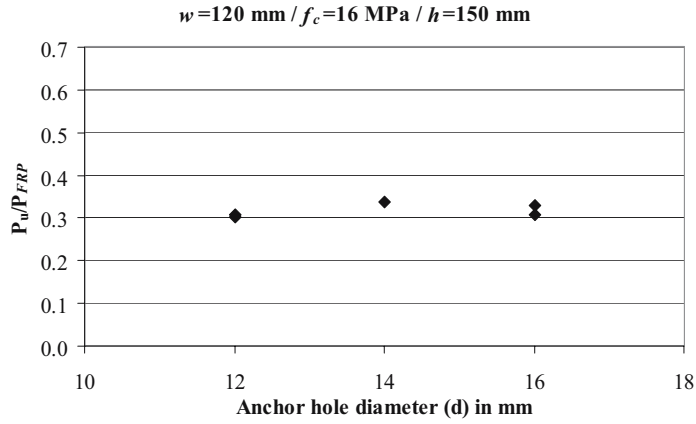

Figure 4. Effect of anchor hole diameter (w=120 mm, h=150 mm, and f_c=16 MPa)

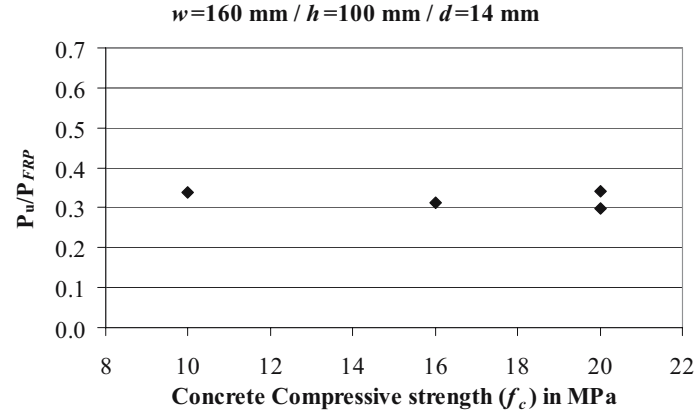

Figure 5. Effect of concrete compressive strength (w=160 mm, h=100 mm, and d=14 mm)

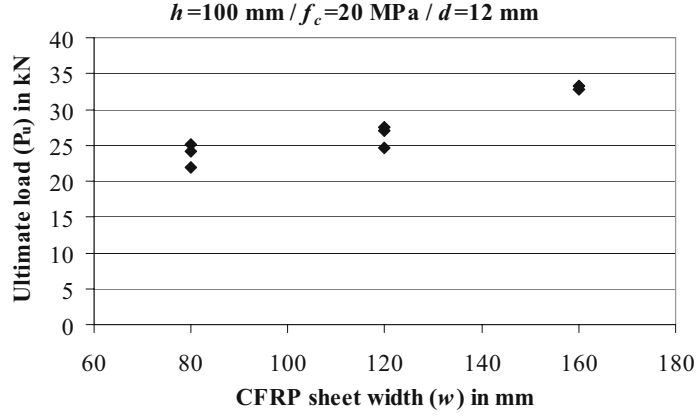

Figure 6. Ultimate tensile load versus CFRP sheet width (h=100 mm, d=12 mm, and f_c=20 MPa)

4.1.3. *Effect of CFRP sheet width (w):*

To investigate the effect of the sheet width on the tensile capacity of CFRP anchors, in Figure 6 the ultimate tensile capacity versus CFRP sheet width is plotted. In addition, Figure 7 shows the normalized tensile capacity of the same data set. As expected, test results show that load capacity increases with an increase in CFRP sheet width (Figure 6). However, the behavior is not linearly proportional to the sheet width. The tensile capacities of the anchors do not increase in the same amount with the sheet widths (Figure 7).

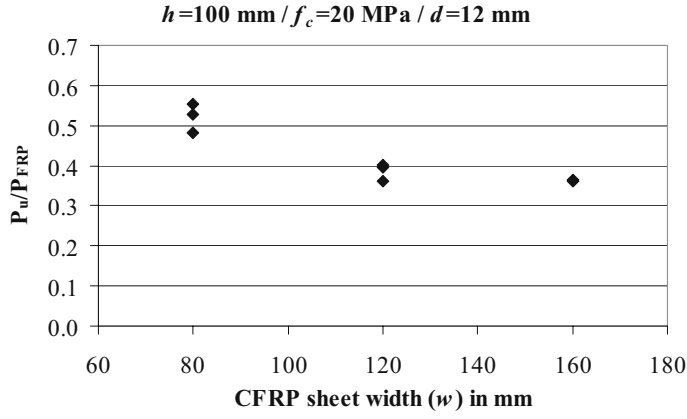

Figure 7. Effect of CFRP sheet width (h=100 mm, d=12 mm, and f_c=20 MPa)

4.1.4. *Effect of embedment depth (h):*

Most of the previous studies that investigate the behavior of the anchors are mostly interested in the effect of the embedment depth of the anchors[4-6]. To investigate the change in tensile capacity of CFRP anchors, the embedment depth increased from 70 mm to 100 mm and 150 mm while the other parameters kept constant. As is seen in Figures 8 and 9, the normalized tensile capacity of a CFRP anchor increases as embedment depth increases from 70 mm to 100 mm. However, there is a decrease in the CFRP anchor capacity when the embedment depth increases from 100 mm to 150 mm.

4.2. TYPE-2 TEST RESULTS

All of the anchors tested in this part have 120 mm sheet width and installed into a hole with 20 mm diameter. The main difference observed during Type-2 tests is in the failure types. A concrete cone observed for anchors with 50 mm embedment, while a combined cone-bond failure observed for 70 mm and 100 mm embedment depths. The failure of the CFRP anchors with 150 mm embedment was due to rupture of CFRP sheet.

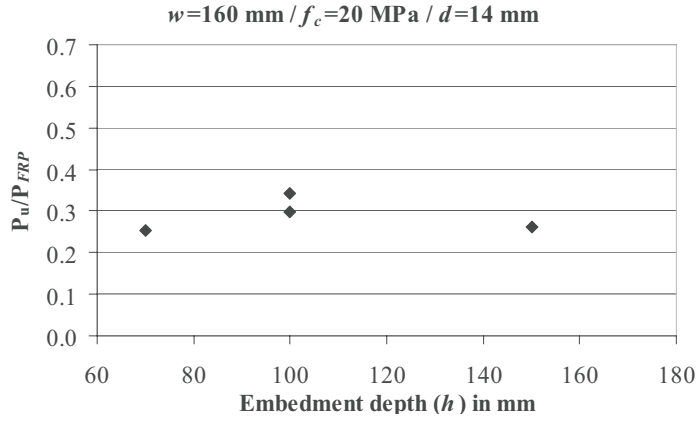

Figure 8. Effect of embedment depth (w=160 mm, d=14 mm, and f_c=20 MPa)

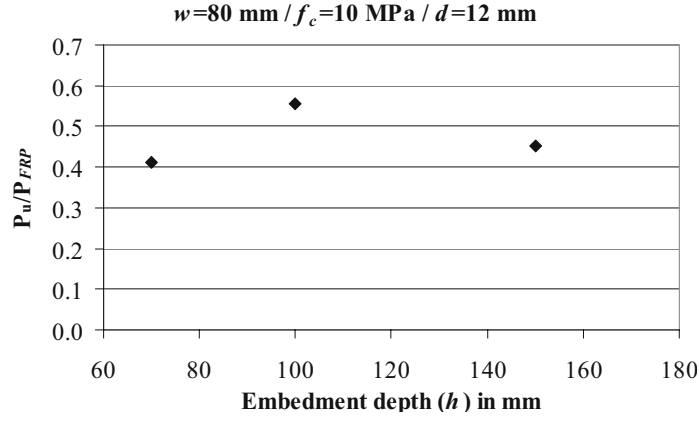

Figure 9. Effect of embedment depth (w=80 mm, d=12 mm, and f_c=10 MPa)

4.2.1. *Effect of concrete compressive strength (f_c):*

Normalized tensile capacities for all embedment depths, namely 50 mm, 70 mm, 100 mm, and 150 mm, are given in Figure 10. It is seen that the highest normalized tensile capacity of a CFRP anchor is reached for an embedment depth of 100 mm. As is also seen, normalized data for 50 mm embedment depth are close to each other, the difference in tensile capacities of anchors installed into the 10 MPa concrete beam and 16 MPa concrete beam is negligible. However, as the embedment depth increases, the significance of the concrete compressive strength increases. For the highest normalized tensile capacity, i.e. for h=100 mm, the effect of concrete compressive strength is most significant.

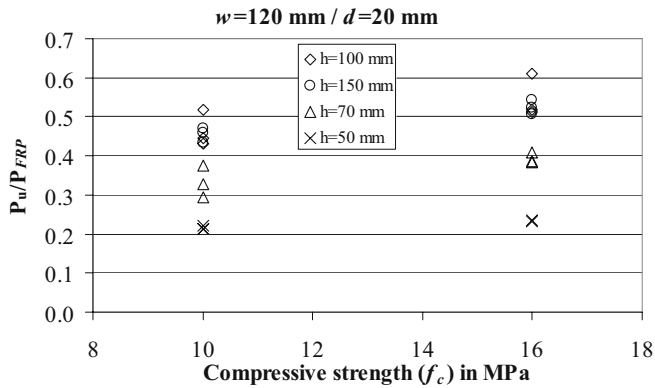

Figure 10. Concrete compressive strength versus normalized tensile capacities for w=120 mm, d=20 mm

4.2.2. *Effect of embedment depth (h)*

Figure 11 gives the normalized test results of anchors installed into a concrete beam of 10 MPa. As expected, the normalized tensile capacity of a CFRP anchor increases as the embedment depth increases. However, there is an effective depth beyond which the capacity becomes almost constant. For the parameters studied, effective embedment depth seems to be 100 mm. The capacities of CFRP anchors that are embedded to 150 mm are almost equal to those of 100 mm embedment depth. Figure 12 shows the change in normalized tensile capacities of anchors installed into a concrete beam of 16 MPa compressive strength. Similar behavior is observed for this concrete compressive strength also. Tensile capacities of CFRP anchors increase up to 100 mm embedment depth. Beyond this depth, the capacity becomes constant and equal to that of 100 mm.

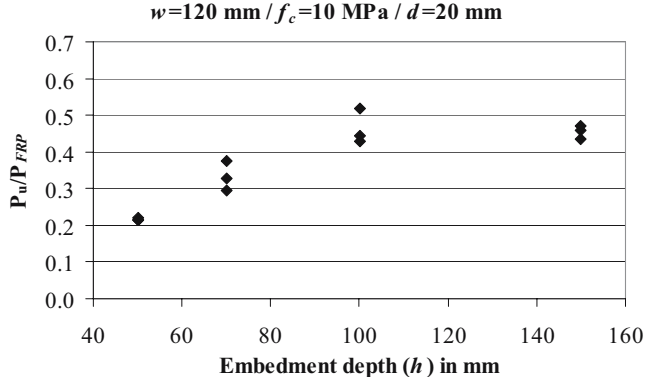

Figure 11. Embedment depth versus normalized tensile capacities for w=120 mm, f_c=10 MPa, d=20 mm

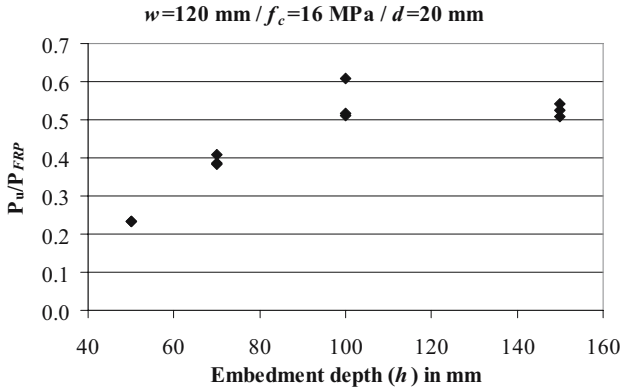

Figure 12. Embedment depth versus normalized tensile capacities for w=120 mm, f_c=16 MPa, d=20 mm

5. Prediction of Tensile Capacity of CFRP Anchors

There are several methods that can be used to predict the strength of adhesive steel anchors in the literature. However, there is as yet no successful way of predicting the tensile capacities of CFRP anchors. Equation (6) is used to give an idea about the tensile capacity of the CFRP sheet used to prepare the anchor. Similar to this approach, one may want to compute the tensile capacity of the carbon fibers after the application of epoxy resin to the carbon fibers. For this purpose, tensile coupon tests of CFRP sheet with epoxy resin (composite material) were done. The thickness of composite specimen was 1.2 mm. Stress-strain relationship of this specimen is given in Figure 13. As is seen, the maximum tensile stress is obtained as 650 MPa. Then, the tensile capacity of this composite can be calculated as

$$P_{CMPST} = w \times 1.2 \times 650 \quad \text{(N)} \qquad (7)$$

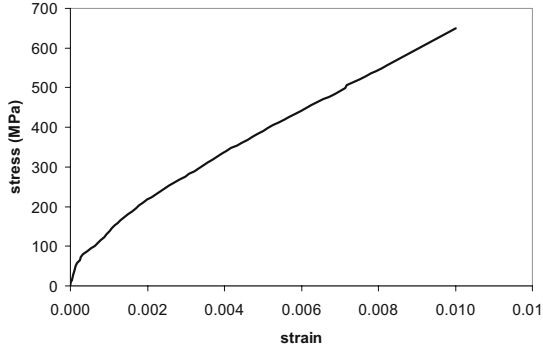

Figure 13. Coupon test result of CFRP sheet

Equations (6) and (7) are based on the capacity of the carbon fibers in a chosen sheet width. On the other hand, the effect of the concrete strength can be considered by calculating the tensile capacity of the concrete cone given in Figure 14 as:

$$h < 50 \text{ mm} \qquad P_{CONE} = 0.33\sqrt{f_c} \times h \times (d + h)\pi \tag{8.a}$$

$$h > 50 \text{ mm} \quad P_{CONE} = 0.33\sqrt{f_c} \times 50 \times (d + 50)\pi + \tau_{ave} \times \pi \times d(h - 50) \tag{8.b}$$

In Eqs. (8a) and (8b), f_c is concrete compressive strength, h is embedment depth of anchor, d is hole diameter, and τ_{ave} is the average bond stress of the concrete through the embedment depth. CFRP anchors with embedment deeper than 50 mm have a shallow cone followed by a slip through the remaining part in failure. The concrete cone depth is almost equal to 50 mm for all embedment depths. Therefore, for embedment depths greater than 50 mm, to represent the bond failure Eq. (8.b) is proposed. Equations (9a) and (9b) are based on the assumption that the concrete cone occurs with a crack angle of 45 degrees. The concrete cone depth is taken as 50 mm for all embedment depths based on experimental observations.

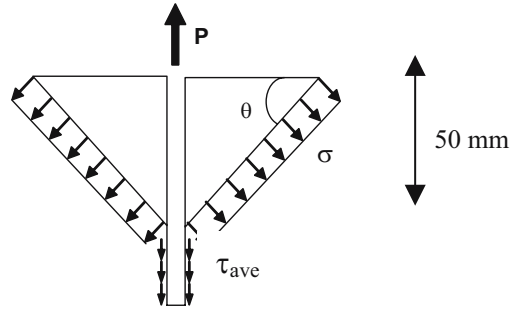

Figure 14. Stress distribution along the embedment depth of the anchor

In Equation (8.b), τ_{ave} is obtained from Equation (4) by equating h_c to 50 mm. Equations (8a) and (8b) are obtained for a concrete cone with crack angle of 45 degrees. One may want to change these equations into a form in which the angle of crack pattern is also a variable. In that case, these two equations are modified as

$$h < 50 \text{ mm} \qquad P_{CONE} = 0.33\sqrt{f_c}\left(d + \frac{h}{\tan\theta}\right)\frac{\pi h}{\sin\theta} \tag{9.a}$$

$$h > 50 \text{ mm} \quad P_{CONE} = 0.33\sqrt{f_c}\left(d + \frac{50}{\tan\theta}\right)\frac{\pi \times 50}{\sin\theta} + \tau_{ave} \times \pi d \times (h - 50) \tag{9.b}$$

To determine the bond stress (τ_{ave}) along the embedment depth of the CFRP anchor, a series of partially bonded direct tensile tests were also carried out. To do this test, a plastic pipe was placed into the drilled anchor hole to prevent the bonding between CFRP anchor and concrete along the pipe. The length of the pipe was chosen so that the bond will not be affected by the loading at the upper bound of the concrete. Thus, a complex state of stress around the surface was eliminated, (Figure 15).

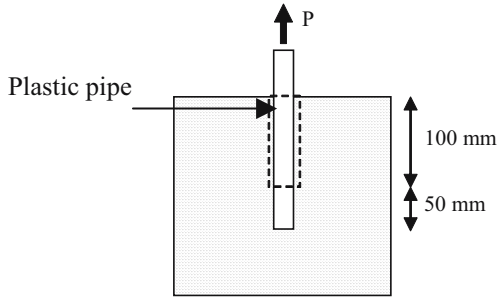

Figure 15. Pullout test without confinement

The ultimate loads obtained from these tests were divided by the circumferential area of the bonded part of the CFRP anchor. This is based on the assumption that the bond stress distribution along the bonded part is uniform. So, the average bond stress τ_{ave} can be found by Equation (2) in which h_{ef} is equal to 50 mm, which is the bonded length of the CFRP anchor. Table 4 gives the ultimate loads observed during the partially bonded tests together with the corresponding average bond stress. These bond stresses are then inserted into the Equation (4) by which the concrete cone depth can be calculated. The calculated cone depths are used to predict the ultimate tensile capacity of CFRP anchors using Equation (5).

TABLE 4. Shear stresses with corresponding concrete compressive strength end bonded length

Embedment depth (mm)	Bonded length (mm)	f_c (MPa)	P_u (kN)	τ (MPa)
150	50	10	27.44	8.73
150	50	10	28.65	9.12
150	50	16	34.30	10.91
150	50	16	36.44	11.60

In Figures 16 and 17, the comparisons of the discussed methods are given for the data obtained from Type-2 tests. In these figures, tensile capacities are computed by Eqs. (8) and (9). The average bond stresses were taken as 9 MPa, and 11 MPa for concrete blocks of 10 MPa and 16 MPa compressive strengths, respectively.

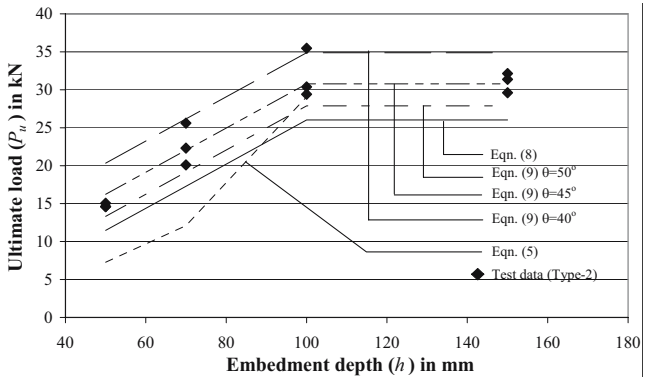

Figure 16. Comparison of prediction methods with Type-2 tests (10 MPa compressive strength)

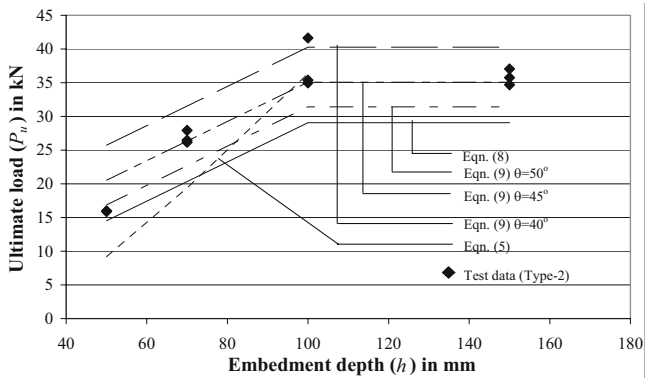

Figure 17. Comparison of prediction methods with second series of tests (16 MPa compressive strength)

6. Conclusions

In strengthening of the hollow clay tile infill with CFRP sheets, CFRP anchors are used both in masonry and in reinforced concrete members to provide a sufficient load transfer mechanism between the CFRP sheet and the masonry and the reinforced concrete member. Better connections lead to higher energy dissipation and higher ductility. Thus, the capacity increase in the existing structure mostly depends on the load transferred through the CFRP anchors, or simply the increase in capacity of the structure depends on CFRP anchor capacity. In this experimental study, direct tensile capacities of CFRP anchors were investigated for different parameters. The effect of CFRP sheet width, embedment depth of adhesive anchor, hole diameter of anchor and compressive strength of concrete on the uniaxial tensile capacity of the CFRP anchors were determined. With the help of the test results, the conclusions below are reached:

For the studied parameters, the maximum tensile load capacities are obtained for CFRP anchors which have 100 mm embedment depth. This indicates that there is an effective bond length beyond which load capacity does not increase. The increase in tensile load capacities can be assumed linear up to 100 mm embedment depth.

For shallow embedment depths, i.e. 50 mm, the effect of concrete compressive strength, in the range of 10 MPa to 16 MPa, on the tensile capacity of CFRP anchor is not significant. However, as the embedment depth increases, the effect of concrete compressive strength becomes more significant.

The comparison of prediction methods to the test results show that the better prediction can be done using Eq. (9) with 45^{o} crack angle. The capacity calculated with Equation (5) gives very close results for 100 mm embedment depth which is stated as effective depth in this study. However, this model is far from being representative for other embedment depths.

ACKNOWLEDGMENT

This study has been partially supported by NATO (grant no: SfP-977231) and The Scientific and Technical Research Council of Turkey (grant no: ICTAG I575).

References

1. I. Erdem, 2003, *Strengthening of Existing Reinforced Concrete Frames*, Master's thesis, Middle East Technical University, 123 pp.
2. E. Makitani, I. Irisawa, N. Nishiura, 1995, Investigation of Bond in Concrete Member with Fiber Reinforced Plastic Bars, *Proceedings of International Symposium on Fiber Reinforced Plastic Reinforcement for Concrete Structures*, *ACI SP-138*, pp. 315-331.
3. A. Hattori, S. Inoue, T. Miyagawa, M. Fujii, 1995, A Study on Bond Creep Behavior of FRP Rebars Embedded in Concrete, *Proceedings of 2nd International RILEM Symposium on Non-Metallic FRP Reinforcement for Concrete Structures*, pp. 172-179.
4. R. A. Cook, J. Kunz, W. Fuchs, and R. C. Konz, 1998, Behavior and Design of Single Adhesive Anchors under Tensile Load in Uncracked Concrete, *ACI Structural Journal*, Vol. 95, No. 1, Jan.-Feb., pp. 9-26.
5. R. A. Cook, 1993, Behavior of Chemically Bonded Anchors, *Journal of Structural Engineering*, Vol. 119, No. 9, September, pp. 2744-2762.
6. R. A. Cook, G. T. Doerr, R. E. Klingner, 1993, "Bond Stress Model for Design of Adhesive Anchors", *ACI Structural Journal*, Vol. 90, No. 5, Sep.-Oct., pp. 514-524.

USING A DISPLACEMENT-BASED APPROACH FOR EARTHQUAKE LOSS ESTIMATION

JULIAN J. BOMMER*
Department of Civil and Environmental Engineering, Imperial College London, UK.

RUI PINHO
European School for Advanced Studies in Reduction of Seismic Risk (ROSE), Pavia, Italy.

HELEN CROWLEY
European School for Advanced Studies in Reduction of Seismic Risk (ROSE), Pavia, Italy.

Abstract. A displacement-based earthquake loss assessment procedure currently under development is presented. Predictions of the degree of damage to buildings under both ground shaking and liquefaction-induced ground failure can be carried out with this method. Earthquake actions and structural reactions are represented by displacements following the observed correlation between building damage and lateral displacements. The main concept is to compare the mechanics-derived displacement capacity of the building stock and the imposed displacement demand from the earthquake. A probabilistic framework has been incorporated to account for the epistemic (knowledge-based) uncertainty in the capacity parameters. Options for treating the aleatory variability in the ground motion are presented for estimates of losses from single and multiple earthquake scenarios. A discussion of the influence of the epistemic uncertainty on the results of a loss model is also presented. The method can be calibrated for different locations and building practices and this advantage forms the base for a proposed new approach for calibrating seismic design codes.

Keywords: displacement-based; loss assessment; vulnerability; epistemic uncertainty; aleatory variability

* Julian Bommer; email: j.bommer@imperial.ac.uk

S.T. Wasti and G. Ozcebe (eds.), Advances in Earthquake Engineering for Urban Risk Reduction, 489–504.

1. Introduction

Earthquake loss modeling is of fundamental importance for emergency planners and the insurance and reinsurance industries, as well as seismic code drafting committees. An earthquake loss model requires the convolution of four basic components: seismic hazard, building exposure, building vulnerability and specific cost.

The seismic hazard should be modeled using a ground-motion parameter which shows a good correlation with damage and that accounts for the frequency content of the ground motion and the fundamental period of vibration of the buildings. The exposed buildings should be divided into building classes with similar construction types, height and response mechanisms. The vulnerability of the buildings should be modeled using a procedure that can be applied to hundreds or even thousands of buildings and can be easily modified for different regions of interest. An analytical procedure for the assessment of structural and non-structural vulnerability of different classes of reinforced concrete buildings that convolves the displacement demand with the displacement capacity is presented in Section 2 of this paper.

A large amount of input data needs to be collected to model the earthquake activity, the ground conditions, the building stock and infrastructure exposure and the vulnerability characteristics of the exposed buildings in a loss model. Regardless of the methodology employed, one of the most important aspects of constructing a loss model is to identify, quantify and incorporate into the estimates the uncertainties with each of the input parameters. The uncertainties can generally be classified as aleatory (random variability) and epistemic (resulting from incomplete knowledge): the important distinction between the two is that the former cannot be reduced whilst the latter (at least in theory) can be decreased provided sufficient investment in data collection is made. The influence of epistemic uncertainty and aleatory variability on an earthquake loss model is also discussed herein. The use of the method to calibrate seismic design codes is also briefly presented.

2. Vulnerability Assessment

2.1. TRADITIONAL VULNERABILITY ASSESSMENT

The seismic vulnerability of a building might be thought of as its likelihood to be damaged by an earthquake. The aim of a vulnerability assessment is to obtain the probability of a given level of damage to a given building type due to an earthquake of a given intensity. The various methods for vulnerability assessment that have been proposed in the past for use in loss estimation can

generally be divided into three categories: empirical, analytical or hybrid. Empirical methods are based on the observed damage of buildings from earthquakes or expert judgment and might take the form of Damage Probability Matrices (e.g. Whitman et al., 1973; ATC, 1985) or vulnerability functions (e.g. Spence et al., 1992). These types of vulnerability assessments are generally based on macroseismic intensity or peak ground acceleration (PGA). Many shortcomings can be highlighted with the use of these two parameters. The determination of the intensity of shaking is subjective, being based on the observations rather than measurements, and thus cannot be judged as an exact procedure, whilst PGA shows almost no correlation with the damage potential of the ground motion. In addition, neither parameter accounts for the relationship between the frequency content of the ground motion and the dominant period of the buildings. In order to compensate for the aforementioned shortcomings, assessment methods which are based on response spectra are preferred. Analytical methods have recently been proposed which use structural mechanics theory and relate the capacity of the structure to the demand using response spectra (e.g. FEMA, 1999; Calvi, 1999; Ordaz et al., 2000).

2.2. DISPLACEMENT-BASED VULNERABILITY ASSESSMENT

2.2.1. *Proposed methodology*

The underlying principles of the Direct Displacement-Based Design methodology (e.g. Priestley, 2003) were used by Calvi (1999) in the derivation of a displacement-based method for deriving the capacity of column-sway (soft-story) reinforced concrete frames, starting from basic principles of structural mechanics and seismic response to arrive at an estimation of seismic vulnerability of classes of buildings. As a follow up to this proposal, which featured displacements as the fundamental indicator for damage and a spectral representation of the earthquake demand, Pinho et al. (2002) introduced a displacement-based vulnerability assessment methodology for reinforced concrete (RC) buildings that was then developed by Glaister and Pinho (2003), and subsequently by Crowley et al. (2004). This probabilistic displacement-based loss assessment procedure (DBELA) uses mechanics-derived formulae to describe the displacement capacity of classes of buildings at three different structural and non-structural limit states.

Damage to the structural (load-bearing) system of the building class is estimated using three limit states of the displacement capacity. The building class may thus fall within one of four discrete bands of structural damage: none to slight, moderate, extensive or complete. A qualitative description of each

damage band for reinforced concrete frames is given in the work by Crowley et al. (2004) along with quantitative suggestions for the definition of the mechanical material properties for each limit state, taken from the work of Priestley (1997) and Calvi (1999). Damage to non-structural components within a building can be considered to be either drift- or acceleration-sensitive (Freeman et al., 1985; Kircher et al., 1997). Drift-sensitive non-structural components such as partition walls can become hazardous through tiles and plaster spalling off the walls, doors becoming jammed and windows breaking. Acceleration-sensitive non-structural components include suspended ceilings and building contents. At present, only drift-sensitive non-structural damage is considered within this methodology, using three limit states of drift capacity. Inter-story drift can be used to predict drift-sensitive non-structural damage and the suggestions given by Calvi (1999) for three non-structural limit states have been followed (see Crowley et al., 2004). The non-structural components will again fall within one of four bands of damage: none, moderate, extensive or complete.

The seismic response of reinforced concrete buildings is currently modeled using a single bare frame with either a beam-sway or column-sway response mechanism and the modeling of infill panels, structural walls, stairwell cores and other irregularities in plan, which all have an important influence on the behavior of buildings, is not currently considered in the methodology. Current research work is being carried out to include these factors in the DBELA methodology. The following section describes how the displacement capacity equations used in DBELA can be derived from structural mechanics principles and how they are convolved with the demand to attain the vulnerability of a building class.

2.2.2. *Convolution of displacement demand and capacity*

DBELA can be used to predict the damage to building classes under both liquefaction-induced ground deformations and strong ground shaking. The former procedure requires a direct comparison between the displacement demand (due to differential movement of foundations) on the structural members of the building and the displacement capacity of these members. The latter procedure requires the building to be modeled as a substitute structure with equivalent displacement capacity and effective period of vibration, and the demand is obtained from a displacement demand spectrum. The same structural mechanics principles are required to define the displacement capacity for both procedures, as described below.

A typical cross section of a column is shown in Figure 1a and the strain profile at that section is shown in Figure 1b. At any cross section, the curvature can be computed by the sum of steel and concrete strains (ε_s and ε_c,

respectively) at the two extremes of the section, divided by the effective depth, *d'*.

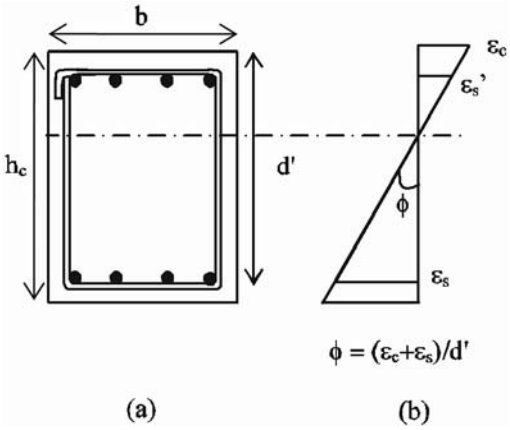

Figure 1. (a) Typical poorly-confined reinforced concrete column section, (b) strain profile and definition of curvature

A cantilever column member, with a height, h_s, with the section as described above is presented in Figure 2a. When the section at the base of the column reaches the yield curvature, ϕ_y, the first limit state is reached and the curvature distribution with height can be conservatively approximated as triangular (Figure 2b). Priestley (1998) has shown that the yield curvature is independent of the strength and can be evaluated from the yield strain and the geometrical properties of the section. By integrating the curvature distribution along the length of the deformed member, the tangent yield rotation, θ_y, in Figure 2d, is obtained and the yield displacement capacity at the top of the column can be computed by the moment-area method (e.g. Gere and Timoshenko, 1997). The curvature distribution of the column at the post-yield limit states is presented in Figure 2c: the plastic curvature, ϕ_p, can be found from the difference between the limit state curvature and the yield curvature at the base of the section. The dotted lines in Figure 2c show the approximate plastic curvature distribution which can be assumed in order to simplify the integration of the actual curvature profiles. By multiplying the plastic hinge length, l_p, by the plastic curvature, the plastic rotation is attained, which can then be multiplied by the height of the column to obtain the plastic displacement capacity. The total limit state displacement capacity can then be found by adding the yield displacement to the plastic displacement capacity.

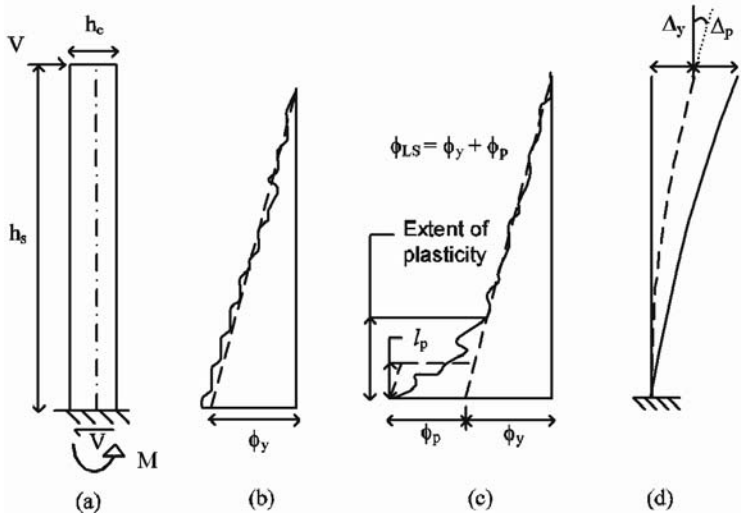

Figure 2. (a) reinforced concrete cantilever, (b) curvature distribution with height when the base section reaches yield curvature (limit state 1), (c) curvature distribution with height at post-yield limit states, (d) total lateral tip deflection (adapted from Paulay and Priestley, 1992)

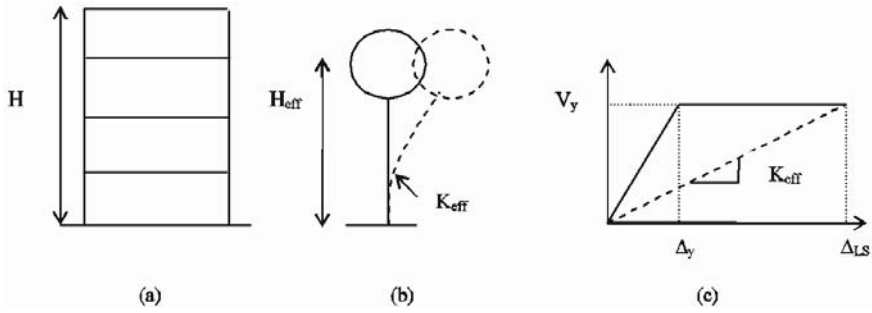

Figure 3. (a) MDOF building, (b) SDOF substitute structure, (c) force vs. displacement relationship for substitute structure (dotted line)

Formulae can thus be derived to give the limit state displacement capacity of the members of a reinforced concrete building as a function of the geometrical and material properties. The displacement capacity of the ground floor columns of a building can be directly compared with the displacement demand imposed by the various liquefaction-induced modes of differential deformation of the flexible foundations beneath a building (see Bird et al., 2004).

When the vulnerability of a structure to strong ground shaking is to be considered, the structure needs to be modeled as a single-degree-of-freedom (SDOF) substitute structure, as illustrated in Figure 3. The displacement capacity of the SDOF substitute structure can be derived using the same

principles described previously, and is thus dependent on the geometrical and material properties of the reinforced concrete members, as observed in Eq. (1), which defines the post-yield displacement capacity of a RC beam-sway frame:

$$\Delta_{SLSi} = 0.5 ef_h H_T \varepsilon_y \frac{l_b}{h_b} + 0.5(\varepsilon_{C(Lsi)} + \varepsilon_{S(Lsi)} - 1.7\varepsilon_y) ef_h H_T \quad (1)$$

where Δ_{SLSi} is the structural limit state i (2 or 3) displacement capacity; ef_h is the effective height coefficient; H_T is the total height of the original structure; ε_y is the yield strain of the reinforcement; l_b is the length of beam; h_b is the depth of beam section; $\varepsilon_{C(Lsi)}$ is the maximum allowable concrete strain for limit state i; and $\varepsilon_{S(Lsi)}$ is the maximum allowable steel strain for limit state i.

Non-structural damage to the components of a building that are drift-sensitive (e.g. dry partition walls) can be predicted by computing the displacement capacity of the SDOF substitute structure once the limit state inter-story drift capacity (ϑ_i) of the non-structural members is reached. The potential for concentrated damage at the ground floor of a column-sway frame and distributed damage in a beam-sway frame is considered. Equation (2) displays the post-yield non-structural displacement capacity of a RC building with a soft-story at the ground floor:

$$\Delta_{NSLSi} = \vartheta_i h_s + 0.43(ef_h H_T - h_s)\varepsilon_y \frac{h_s}{h_c} \quad (2)$$

where h_s is the height of the story, h_c is the depth of the ground floor column section and the other variables are as described previously.

By substitution of the height of the buildings in Eq. (1) and Eq. (2) through a formula relating height to the limit state period (Crowley and Pinho, 2004), displacement capacity functions in terms of period are attained. This offers the advantage that a direct comparison can now be made at any period between the displacement capacity of a building class and the displacement demand predicted from a response spectrum. The concept is illustrated in Figure 4, whereby the range of structural periods with displacement capacity below the displacement demand is obtained and transformed into a range of heights using the aforementioned relationship between limit state period and height. From a purely deterministic and conceptual viewpoint, this range of heights could then be superimposed onto the cumulative distribution function of building stock to find the proportion of buildings failing the given limit state.

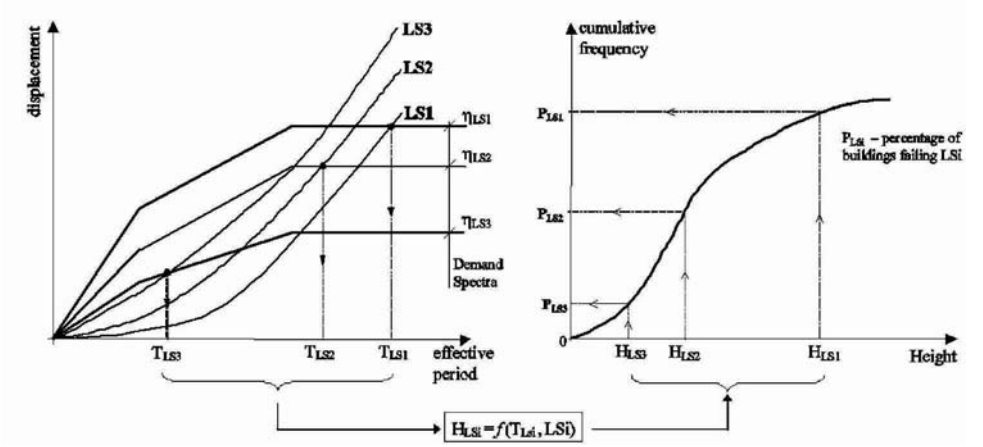

Figure 4. A deformation-based seismic vulnerability procedure (Pinho et al., 2002). (LS stands for limit state.)

2.2.3. *Probabilistic framework*

The translation of the above procedure to a probabilistic framework was carried out by Crowley et al. (2004), building upon the work of Restrepo-Velez and Magenes (2004) who adapted the classical time-invariant reliability formulation described in Pinto et al. (2004). In this way, the method can duly cater for the uncertainty in the displacement demand spectrum and the uncertainty in the displacement capacity that arises when a group of buildings, which may have different geometrical and material properties, is considered together.

For a single scenario earthquake, the aleatory variability in the demand is modeled using the widely accepted assumption of a log-normal distribution of residuals and the cumulative distribution function (CDF) of the displacement demand can be found using the median displacement demand values and their associated logarithmic standard deviation at each period; the inclusion of the aleatory variability when multiple earthquakes are considered is discussed in Section 2.2.4. The CDF gives the probability that the displacement demand exceeds a certain value, x, given a response period, T_{Lsi}, for a given magnitude-distance scenario. In Figure 5a, an illustrative example of a displacement demand CDF is shown, cut-off at 3 seconds to allow the indication of the 50-percentile (median), 16-percentile and 84-percentile values of the displacement response.

The random variation in material properties (with respect to manufacturers' specifications) and in member dimensions (with respect to design drawings) are both considered to be small in comparison with the variations caused by the simplifying assumption of grouping many different buildings into a single class for the purpose of modeling losses. For this reason, only the more significant

latter variations, arising from differences in design and construction, are considered in DBELA. The variation of the material properties and member dimensions within a building classification is an epistemic uncertainty since by detailed inspection of all buildings the exact distribution could actually be determined. For modeling purposes, however, the simplifying assumption is made that this variation can be represented as a random (i.e. aleatory) variability. This assumption makes it considerably simpler to handle the variation of these properties in the loss calculations, as discussed below.

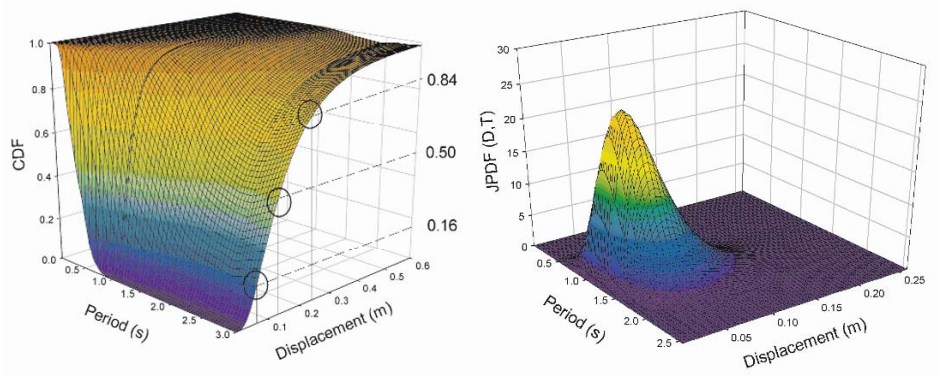

(a) (b)

Figure 5. (a) CDFs of the demand displacement at each period, with median, 16-percentile and 84-percentile values of displacement response indicated at 3 seconds, b) Example JPDF of capacity for a 4 story column-sway RC building class (Crowley et al., 2004)

The probability density functions (PDF) of the limit state displacement capacity and period are found using the first-order reliability method (FORM). Essentially, FORM can be used to compute the approximate cumulative distribution function of a non-linear relationship of correlated parameters, such as the limit state displacement capacity equation (Δ_{Lsi}) and limit state period equation (T_{Lsi}). The uncertainty in Δ_{Lsi} and in T_{Lsi} is accounted for by constructing a matrix composed of the mean values and standard deviations of each parameter in the equations. By assigning probability distributions to each parameter, FORM can be used to find both the PDF of the limit state displacement capacity, conditioned to a period, and the PDF of the limit state period. For a given number of stories, the probability density of the periods may be multiplied by the PDF of the corresponding displacement capacity so that the joint probability density function (JPDF) of period and displacement can be obtained, as exemplified in Figure 5b, for a four-story column-sway building class. The JPDF can then be used in conjunction with the demand CDF in the classical time-invariant reliability formulation to find the probability of exceeding the limit state for each number of stories for a scenario earthquake.

In the DBELA methodology, once the probability of failure of each structural or non-structural limit state has been found, the proportion of buildings, *P*, within distinct damage bands (none/slight, moderate, extensive and complete) can be calculated as follows:

$$P_{none/slight} = 1 - P_{f1} \tag{3}$$

$$P_{moderate} = P_{f1} - P_{f2} \tag{4}$$

$$P_{extensive} = P_{f2} - P_{f3} \tag{5}$$

$$P_{complete} = P_{f3} \tag{6}$$

A composite measure of the damage (mean damage ratio, MDR) that relates the estimated cost of loss to the rebuilding cost can be calculated by applying damage ratios to the proportion of buildings in each damage band, and the results are then integrated. The choice of damage ratios should ideally be based on detailed local data on insurance claims rates for different damage states of distinct building types.

2.2.4. *Deriving loss curves*

The above framework, which is to be applied for a single earthquake scenario, can be very useful for communicating seismic risk to the public and to decision makers. However, for many applications, including decision-making processes within the insurance and reinsurance industries and in seismic code drafting committees, it is necessary to estimate the effects of many, or even all, possible future earthquake scenarios that could impact upon the urban areas under consideration. In such cases, the purpose of the loss calculations is to estimate the annual frequency of exceedance (or the return period) of different levels of loss due to earthquakes (i.e. loss curves).

An important consideration in the derivation of loss curves is the consideration of the inter- and intra-event components of the aleatory variability. For each earthquake scenario, the inter-event variability (σ_{inter}) will cause the ground motions at all locations to be lower or higher than the median estimates from the predictive equation, whilst the intra-event variability (σ_{intra}) will lead to large fluctuations of the ground motion between locations having the same site classification and being at the same distance from the earthquake source.

One option for representing the demand in a loss model for multiple earthquakes is to first perform a probabilistic seismic hazard analysis (PSHA) and then convolute the hazard curves at different locations with the exposure and vulnerability of the building stock; it should be noted that with the use of

PSHA-derived hazard curves, the aleatory variability should be removed from the vulnerability calculation described in Section 2.2.3 to avoid double-counting this variability (i.e. Figure 5a becomes a step curve at each period ordinate). The use of PSHA to generate loss curves is appealing because of the great computational efficiency that it offers; however, performing independent PSHA calculations simultaneously at several locations, effectively treats the hazard at all sites as being mutually exclusive and perfectly correlated and the intra-event component of the aleatory variability, which represents spatial variability, is thus treated as inter-event variability.

Another option to model the seismic demand is through the triggering of large numbers of earthquake scenarios that are compatible with the seismicity model; different loss curves will be obtained depending on where the aleatory variability (sigma) is included in the calculations. The various possibilities for the treatment of sigma in the derivation of loss curves are discussed in Bommer and Crowley (2005) and can be summarized as follows:

- Generate random scenarios of magnitude and location and include the total sigma in the vulnerability calculation at each site (i.e. use the scenario-based methodology described in Section 2.2.3).
- Generate random scenarios of magnitude, location and ε_{inter} (where ε signifies the number of logarithmic standard deviations) and include σ_{intra} in the vulnerability calculation at each site.
- Generate random scenarios of magnitude, location, ε_{inter} and a random ε_{intra} at each site (and thus remove sigma from the vulnerability calculation).

The most rigorous approach for the production of loss exceedance curves using multiple earthquake scenarios is to generate large numbers of magnitude-location-ε_{intra}-ε_{inter} scenarios using Monte Carlo simulation (Bommer and Crowley, 2005; Crowley, 2005). This procedure inevitably leads to appreciably larger computational effort than when PSHA is employed, but both the temporal (inter-event) and spatial (intra-event) variability of the ground motions can be robustly modeled in this way and the results are conceptually sounder.

3. The Impact of Epistemic Uncertainty on an Earthquake Loss Model

The reliability of the results from an earthquake loss model will be controlled by the most uncertain elements, hence there is little to be obtained from refinement of one component if another, with similar or even greater impact on the results, remains poorly defined. Therefore, establishing the relative impact of the epistemic uncertainty in the vulnerability and site classification parameters, both of which can be reduced by expenditure of time and effort,

compared to the epistemic uncertainty in the ground-motion predictions (which probably cannot be significantly reduced in the foreseeable future) is essential for guiding decision making regarding the cost-benefit of additional data retrieval through structural inspection and geotechnical investigation.

The region to the north of the Sea of Marmara in Turkey was chosen by Crowley et al. (2005) as the test case for a sensitivity study of a single-event loss model using DBELA because of the high levels of hazard and exposure in this area, and also to take advantage of the data and experience of previous earthquake loss modeling work in Turkey (e.g. Bommer et al., 2002). The DBELA methodology is well suited to sensitivity studies because the vulnerability of all the building classes in the study can be accurately computed within minutes, for every parametric change in the model variables. If the capacity of the building stock is estimated through pushover curves, then detailed non-linear finite element analyses for each building class would be required each time a change in capacity parameters needs to be introduced and a sensitivity study could become unfeasible.

For this study, the scenario was assumed to be a magnitude M_w 7.2 earthquake on a fault segment below the Sea of Marmara at a distance of approximately 15 km from the coastline of Istanbul City. Systematic variations of the parameters defining the demand (ground motion) and the parameters in the structural capacity equations (see Eq. 1) were carried out to identify the relative impacts on the resulting losses. The main conclusions that were drawn from the results for this loss model are as follows:

- The epistemic uncertainty inherent in the choice of ground-motion prediction equation had the largest influence of all the demand parameters on the loss.
- The period at which the constant displacement plateau is reached was found to have a minor influence on the loss results due to the low levels of ductility inherent in the Turkish building stock.
- It was found that the building classes could be grouped into a range of story numbers (e.g. 1-9) provided that the median, as opposed to the central value, story number was used to represent the range; a large reduction in computational effort can thus be attained.
- It was found that once distinctions between ‘good’ and ‘poor’ buildings within the building stock had been made, a further division of the ‘poor’ buildings into beam-sway or column-sway mechanisms could be made by engineering judgment alone.
- A variation of the mean value assigned to each capacity parameter was seen to have a large effect on the capacity equations. The most influential

parameters were found to be the geometrical properties of the structural elements, which can be reliably determined by field investigation.

- The simultaneous variations of the capacity parameters gave rise to a significant variation in the loss model results: the influence was almost four times that obtained considering the uncertainty in the choice of ground-motion prediction equation.
- The formula used in the study for calculating the MDR was seen to exaggerate the influence of the changes made to the demand and capacity parameters when the results were compared with an alternative formula.

The overall conclusion for this particular loss model was that the capacity parameters, and particularly the geometrical properties, had a very significant impact on the calculated losses, even in comparison with uncertainty in the demand. This suggests that there is significant benefit to be obtained from investing time and effort in defining the vulnerability characteristics of the exposed building stock. It is important, however, to bear in mind that some important sources of variation were not considered in the current methodology, such as the influence of infill panels and irregularities in plan, which when accounted for might change the results attained. Additionally, these conclusions cannot necessarily be extended to loss models in general as they concern the estimated losses from a single earthquake scenario and a specific region.

4. Using DBELA for the Calibration of Seismic Design Codes

Codes for the earthquake-resistant design of structures are an essential tool in the mitigation of seismic risk, enabling the achievement of minimum levels of safety to be ensured in all structures that could be exposed to earthquake shaking, even by engineers without specialist training in earthquake engineering. The basic performance objective in most seismic design codes has always been related to ensuring the life safety of the building occupants, which is usually interpreted as collapse prevention. The ground motions for which life safety is to be ensured by the design, at least until recently, have been based on the same criterion in almost every seismic design code throughout the world: the 5%-damped spectral acceleration with a return period of 475 years.

A new paradigm for the calibration of codes for performance-based design has been suggested (Bommer et al., 2005) wherein the matching of seismic loading and performance levels is based on a quantitative comparison of the incremental costs of adding seismic resistance and of the associated losses that can be thus avoided. The DBELA methodology is ideal for this cost-benefit approach to code calibration as the structural parameters, such as those presented in Eq. (1) and Eq. (2), can easily be adapted to model increasing

levels of seismic resistance, and thus enhanced design criteria. The main steps of the proposed framework are as follows:

1. Model the building stock within a given area in terms of building classes.
2. Define the basic hazard levels within a given region in terms of zonation or microzonation maps.
3. Identify different levels of earthquake resistance (DL_j) through increments of stiffness, strength and ductility over and above those resulting from non-seismic design according to the relevant building regulations (DL_0).
4. The enhanced design levels are assigned to the building stock exposed within each zone or micro-zone, and each of these combinations can be assigned a label reflecting the collective seismic capacity, SC_k, for which the incremental cost of adding the seismic resistance above SC_0 (all buildings in all zones designed to DL_0) can be estimated. SC_1, for example, may involve applying DL_1 to zone 1 buildings and maintaining DL_0 for buildings in other zones; SC_2 might apply DL_1 to zones 1 and 2, and so on.
5. Each level of building stock resistance is then subjected to the model of the seismic hazard in order to derive MDR exceedance curves for various levels of seismic resistance for a given construction type.
6. An uncomfortable but necessary decision must be taken by politicians, planners and code drafters regarding the tolerable levels of death, injury and persons rendered homeless as a result of an earthquake ground motion with a specified annual frequency of exceedance.
7. These threshold levels can be correlated to structural damage and so the seismic resistance levels which have higher exceedance frequencies than allowed at the threshold damage level are eliminated from further consideration and thus the minimum seismic resistance is defined.
8. Cost-benefit considerations are applied to the remaining seismic resistance levels to ascertain the optimum seismic resistance.
9. The final outcome of these analyses will be an optimal SC_k, which represents a particular combination of design levels, DL_j, in the different seismic hazard zones.

The procedure outlined above represents a rather radical departure from the current format of seismic design codes. The philosophy behind the procedure proposed is that the experts in engineering seismology and structural earthquake engineering charged with drafting the code should do more of the work outside the code, making the best use of their hazards models and their analytical tools, and only pass on to the engineer in the design office the outcome of these calculations.

5. Conclusions

The DBELA methodology for the loss assessment of urban areas based on displacement-based mechanics principles has been presented herein and the use of this methodology in a sensitivity study of a loss model and for the calibration of seismic design codes has been discussed. The prediction of the structural and non-structural damage to reinforced concrete frames due to ground shaking and liquefaction-induced ground deformations can currently be carried out with this method, whilst additional developments are being incorporated to include further building classes, the influence of infill panels and irregularities in plan. Furthermore, components of the substitute structure concept such as the use of equivalent linearization, and thus secant stiffness to define the inelastic response of buildings, as well as the characterization of equivalent viscous damping of inelastic systems, are part of ongoing research to improve the methodology.

ACKNOWLEDGEMENTS

The authors are especially grateful to Selamet Yazici of the General Directorate of Insurance, the Prime Ministry, Turkey, for authorizing the use of the building stock data, without which the sensitivity study of the Marmara region could not have been realized.

References

ATC, 1985, Earthquake damage evaluation data for California, *Report ATC-13*, Applied Technology Council, Redwood City, California.

Bird, J.F., Crowley, H., Pinho, R. and Bommer, J.J., 2004, Assessment of building damage due to liquefaction, *Submitted to Géotechnique*.

Bommer, J.J., and Crowley, H., 2005, The effect of ground-motion variability in earthquake loss modelling, *Submitted to Bulletin of Earthquake Engineering*.

Bommer, J.J., Spence, R.J.S., Erdik, M., Tabuchi, S., Aydinoglu, N., Booth, E., Del Re, D., and Peterken, O., 2002, Development of an earthquake loss model for Turkish catastrophe insurance, *Journal of Seismology* **6**(3): 431-446.

Bommer, J.J., Pinho, R., and Crowley, H., 2005, Using displacement-based earthquake loss assessment in the selection of seismic code design levels, *Proceedings of 9th International Conference on Structural Safety and Reliability (ICOSSAR'05)*, Rome, Italy.

Calvi, G.M., 1999, A displacement-based approach for vulnerability evaluation of classes of buildings, *Journal of Earthquake Engineering* **3**(3): 411-438.

Crowley, H., 2005, An investigative study on the modelling of earthquake hazard for loss assessment, *Individual Study*, ROSE School, Pavia, Italy.

Crowley, H., and Pinho, R., 2004, Period-height relationship for existing European reinforced concrete buildings, *Journal of Earthquake Engineering* **8**(Special Issue 1): 93-119.

Crowley, H., Pinho, R., and Bommer, J.J., 2004, A probabilistic displacement-based vulnerability assessment procedure for earthquake loss estimation, *Bulletin of Earthquake Engineering*. **2**(2): 173-219.

Crowley, H., Bommer, J.J., Pinho, R., and Bird, J.F., 2005, The impact of epistemic uncertainty on an earthquake loss model, Accepted for publication in *Earthquake Engineering and Structural Dynamics*.

FEMA, 1999, *HAZUS99 – Earthquake Loss Estimation Methodology*: *User's Manual*, Federal Emergency Management Agency, Washington, DC.

Freeman, S.A., Messinger, D.L., Casper, W.L., Mattis, L.W., Preece, F.R., and Tobin, R.E., 1985, Structural Moments No. 4. Drift Limits: Are they realistic? *Earthquake Spectra* **1**(2): 203-390.

Gere, P., and Timoshenko, S., 1997, *Mechanics of Materials*, 4th Edition, PWS Pub. Co., Boston.

Glaister, S., and Pinho, R., 2003, Development of a simplified deformation-based method for seismic vulnerability assessment, *Journal of Earthquake Engineering* **7**(Special Issue 1): 107-140.

Kircher, C.A., Nassar, A.A., Kustu, O., and Holmes, W.T., 1997, Development of building damage functions for earthquake loss estimation, *Earthquake Spectra* **13**(4): 663-682.

Ordaz, M., Miranda, E., Reinoso, E., and Pérez-Rocha, L.E., 2000, Seismic loss estimation model for Mexico City, *Proceedings of 12th World Conference on Earthquake Engineering,* Auckland, New Zealand, Paper no. 1902.

Paulay, T., and Priestley, M.J.N., 1992, *Seismic Design of Reinforced Concrete and Masonry Buildings*, John Wiley and Sons, INC, New York.

Pinho, R., Bommer, J.J., and Glaister, S., 2002, A simplified approach to displacement-based earthquake loss estimation analysis, *Proceedings of 12th European Conference on Earthquake Engineering,* London, England, Paper no. 738.

Pinto, P.E., Giannini, R., and Franchin, P., 2004, *Methods for Seismic Reliability Analysis of Structures*, IUSS Press, Pavia, Italy.

Priestley, M.J.N., 1997, Displacement-based seismic assessment of reinforced concrete buildings, *Journal of Earthquake Engineering* **1**(1): 157-192.

Priestley, M.J.N., 1998, Brief comments on elastic flexibility of reinforced concrete frames and significance to seismic design, *Bulletin of the New Zealand National Society for Earthquake Engineering* **31**(4): 246-259.

Priestley, M.J.N., 2003, *Myths and Fallacies in Earthquake Engineering, Revisited*, The Mallet Milne Lecture, IUSS Press, Pavia, Italy.

Restrepo-Vélez, L., and Magenes, G., 2004, Simplified procedure for the seismic risk assessment of unreinforced masonry buildings, *Proceedings of 13th World Conference on Earthquake Engineering*, Vancouver, Canada, Paper no. 2561.

Spence, R.J.S., Coburn, A.W., and Pomonis, A., 1992, Correlation of ground motion with building damage: the definition of new damage-based seismic intensity scale, *Proceedings of 10th World Conference on Earthquake Engineering*, Rotterdam: AA Balkema, pp. 551-556.

Whitman, R.V., Reed, J.W., and Hong, S.T., 1973, Earthquake Damage Probability Matrices, *Proceedings of 5th World Conference on Earthquake Engineering,* Rome, Italy.

NONLINEAR DRIFT DEMANDS ON MOMENT-RESISTING STIFF FRAMES

ASLI METIN
Department of Civil Engineering Middle East Technical University 06531 Ankara, Turkey

SINAN AKKAR*
Department of Civil Engineering Middle East Technical University 06531 Ankara, Turkey

Abstract. Drift demands for stiff moment-resisting frames are investigated. A total of 8 regular frame models with 3- to 9-stories are subjected to 40 soil site records. The moment magnitude and source-to-site distance of the ground motion data set varies between $5.7 \leq M \leq 7.6$ and $2.5 \text{ km} \leq d \leq 23 \text{ km}$, respectively. The ground motion data set is divided into 2 equal bins to represent different seismic hazard levels. The frames conform to the seismic code provisions for the median design spectra of the ground motion bins and they are classified as stiff frames according to their fundamental periods. Nonlinear response history analyses are conducted to present the height-wise variation of maximum lateral displacement profiles and story drift demands for the frame models considered. The accuracy in estimating the maximum roof and interstory drifts is investigated through simplified procedures that use the first-mode approach. The statistics presented show that the maximum interstory drift is strongly correlated with the building configuration and ground-motion features. Use of first-mode approach associated with building elastic dynamic properties generally yields conservative maximum roof drift estimations. A novel approach is also evaluated that can reveal preliminary information about the nonlinear maximum interstory drift if the concern is not the exact location of this deformation demand.

Keywords: Nonlinear MDOF analyses; drift demands; statistical analyses; simplified procedures; moment resisting frames

S.T. Wasti and G. Ozcebe (eds.), Advances in Earthquake Engineering for Urban Risk Reduction, 505–519.

1. Introduction

A realistic seismic performance evaluation of structures requires the estimation of deformation demands imposed by the earthquake ground motions. The choice of deformation demand measures for performance assessment depends on the performance target (a selected performance level at a given seismic hazard) and they should be related to the lateral strength capacity of the structural system as far as the nonlinear behavior is concerned. The maximum roof and interstory drifts along the building height, variation of maximum story drifts and story ductility can be considered as useful deformation demand measures if the performance targets of interest are directly related to downtime and monetary losses.

Much of work has been done to estimate the above demand measures as a function of lateral strength capacity for different seismic hazard levels[1-6]. The underlying basic concept in these and similar procedures is to reduce the multi-degree-of-freedom (MDOF) building system into an equivalent single-degree-of-freedom (SDOF) system using nonlinear static procedures (pushover analysis) that generally introduce an invariant lateral force distribution along the building height to represent the likely global capacity of the structure under seismic excitation. The nonlinear maximum response of the equivalent SDOF system is then determined using either the response history analysis or approximate methods[7-9] that employ the response spectrum concept. The MDOF deformation demands are extrapolated from this information via empirical relationships that relate MDOF-SDOF behavior. The present state of practice that is addressed in most of the guidelines[10-12] under the framework of performance-based earthquake engineering (PBEE) consists of these fundamental steps within the context of suggested approximate procedures. The premise in these approximate procedures is such that the accuracy of the predicted deformation demands should perform well in terms of central tendency for general structural behavior under a given seismic hazard level. This rational presupposition has been challenged as presented in various studies[13-15] by evaluating such methods either in a statistical manner or for particular cases. The epistemic and aleatory uncertainties in earthquakes (generally referred to as record-to-record variability in the engineering literature), sophisticated dynamic behavior of structures and peculiar variations for distinct deformation demands due to the intricate interaction between the ground motion and structural behavior perpetuate such studies. Recent research effort has been devoted to establish advanced probabilistic approaches to estimate the MDOF deformation demands produced by earthquakes considering proper seismic intensity measures that yield the minimum dispersion around the central tendency of the deformation demand investigated[16, 17]. These efforts are

aimed at quantifyig the losses due to earthquake hazard via fragility functions which is one of the ultimate goals in PBEE.

The preliminary results for some of the above seismic deformation demands on regular stiff moment-resisting frames (MRFs) are presented in this paper. Model frames of 3-, 5-, 7- and 9-story are designed conforming the recent seismic design provisions[18, 19]. The maximum roof and interstory drifts and the height-wise variation of story drifts of these models are presented in a statistical manner using a total of 40 strong ground-motion records. The computer program IDARC 2D[20] is used for nonlinear response history analysis to compute the "exact" response of the frame models. No degradation is associated in the nonlinear response history analyses as all the models comply with the provisions required by the seismic codes. The influence of second order effects (P-delta) is insignificant as none of the models experienced the near-collapse failure mode. The ground motions represent soil site records with source-to-site distances varying between 2.5 km $\leq$ d $\leq$ 23 km and moment magnitudes of 5.7 $\leq$ M $\leq$ 7.6. Records with pulse signals are excluded from the ground-motion data set that may introduce significant differences in terms of structural behavior due to their particular seismological features[21]. The statistical results presented in this study should not be generalized for near-fault ground motions with pulse but they may affirm the seismic deformation demands for moderate to severe near-fault events that do not exhibit dominant pulse effects. The paper also presents some relevant statistics to observe the adequacy of first mode approach in describing the expected drift demands on stiff MRFs. This is achieved by using an approach similar to the performance-based guidelines[11, 12] and a recently proposed procedure[22]. The elementary results covered in this paper are believed to be useful for some of the essential issues that have been the subject of research in PBEE related studies as briefed in the preceding paragraph.

2. Ground Motions, Building Models and Global Capacities

Two ground-motion bins of 20 soil site records in each group are used to scrutinize the statistical variation of nonlinear drift demands on stiff MRFs. Figure 1 presents a general view for the pseudo-acceleration spectra (PSA) of the records in each ground-motion bin together with the median (50th percentile) spectra. The median spectra are computed by assuming lognormal distribution. The plots also show the 84th percentile PSA variation in order to display the inherent dispersion in the ground motions used. The curves in Figure 1 suggest that seismic hazard level of Group I ground motions are higher with respect to these in Group II when central tendencies are considered. The moment magnitude and source-to-site distances of the ground-motion bins

range between 5.7 ≤ M ≤ 7.6 and 2.5 km ≤ d ≤ 23 km, respectively. A special effort was put forward to exclude the records with pulse signals that have distinct effects on the linear/nonlinear behavior of frame structures as described by various researchers[21]. The reader is referred to Akkar and Ozen[23] for a detailed description of the important seismological features of the ground motions used here.

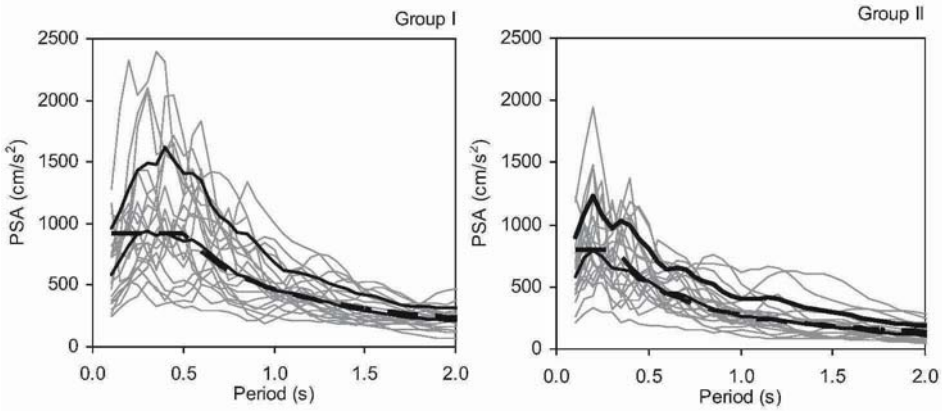

Figure 1. Pseudo-acceleration spectra of the records in each ground-motion bin together with the median and 84th percentile values. The dashed thick lines represent the smoothed median spectra used for design

The median spectrum for each ground-motion bin is smoothed by the procedure described in the FEMA-356[11] document to design 2D regular special MRFs of 3-, 5-, 7- and 9-story that comply the recent seismic code provisions in the U.S[18, 19]. Conventional, force-based elastic response spectrum analysis is used for design and the contribution of all vibration modes are included using the well-known CQC modal combination rule. All the model buildings are 3 bay special MRFs with beam and column lengths of 5 m and 3 m, respectively. A dead load of 30 kN/m and a live load of 6.6 kN/m are assumed to be uniformly distributed along the beam spans. These are reduced by 25 percent at the roof level. The height-wise distribution of lateral stiffness is computed to achieve equal story drifts in all stories under the seismic load combinations defined by the provisions used. No lateral stiffness reduction is applied along the building height for Group I model frames whereas the member section areas are reduced by 10 percent at every 2 story after the first 3 stories in Group II model frames. The fundamental vibration modes ($T_{1,ex}$) of the frames that are presented in Table 1 suggest that these generic MRFs can be classified as stiff and they approximately follow T = 0.1n relationship where n is the number of stories. The major difference between these two groups is the lateral stiffness

distribution along the building height that is invariant for Group I whereas it is uniformly decreased for increasing height in Group II.

TABLE 1. Fundamental mode periods and idealized dynamic properties of the frames obtained from the global capacity curves

	Group I				Group II			
	3 story	5 story	7 story	9 story	3 story	5 story	7 story	9 story
$T_{1,ex}$ (s)	0.27	0.45	0.63	0.82	0.47	0.55	0.68	0.92
$T_{1,ideal}$ (s)	0.27	0.45	0.64	0.82	0.45	0.55	0.66	0.88
PSA_y (g)	0.41	0.30	0.25	0.19	0.28	0.30	0.19	0.14
$S_{d,y}$ (cm)	0.74	1.54	2.55	3.27	1.42	2.23	2.12	2.68
α[1]	0.02	0.03	0.03	0.04	0.03	0.04	0.03	0.04

[1] Post yield to elastic stiffness ratio.

The global capacity envelope (roof displacement vs. base shear coefficient) of each frame model is determined using the pushover analysis. The computer program IDARC 2D[20] is used for this purpose. This information is used for evaluating the nonlinear deformation demands that are presented in the following sections. The height invariant inverse triangular force distribution is used for nonlinear static analysis considering the structure is subjected to a linear distribution of acceleration throughout the building height. This is one of the suggested distributions in building codes for structures deforming primarily in the first mode. Bilinear idealization is then performed on the global capacity curves by matching the areas under the global capacity curve and its bilinear representation. The initial branch of the bilinear curves is obtained by drawing a straight line from the origin that is tangent to the initial slope of the global capacity curve. This line reveals information about the idealized period (T_{ideal}) of the equivalent SDOF system. The second line that represents the post yielding in the idealized bilinear curve intersects the first line by drawing it from the ultimate point of the capacity curve back to the first line. The slope of the second line (post yield stiffness) is varied until the areas below the global capacity and bilinear idealization are equal[10]. The bilinear curves are transformed to S_d – PSA (spectral displacement vs. pseudo-acceleration) curves using the first mode elastic dynamic properties of the model frames. The intersection of the initial branch and the post yielding branch of the idealized bilinear curves are accepted as the global yielding points (i.e., $S_{d,y}$ and PSA_y) for the frame models. A representative illustration of global capacity envelopes and their bilinear idealization both in terms of roof displacement vs. base shear coefficient and S_d vs. PSA for Group I frames is shown in Figure 2. The elementary dynamic properties obtained from the idealized bilinear curves are listed in Table 1.

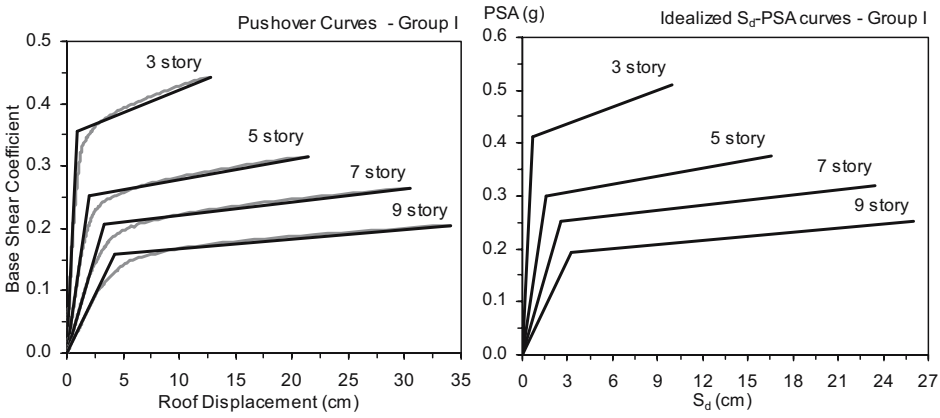

Figure 2. Representative global capacity curves and their idealizations for Group I frames

3. Nonlinear Drift Demands from Response History Analysis

Figure 3 shows the global relationship between the maximum roof (MRDR) and maximum interstory (MIDR) drift ratios for the Group I and Group II frames considered in this study. Some researchers[5, 24] employed similar relationships to estimate the MIDR in frame systems using the maximum roof drift information. This relationship is independent of the lateral strength capacity that obliges one to define some specific limits on this capacity parameter for its practical use. It is also independent of the ground motion intensity if the data set is not assembled for a specific intensity measure by considering its uncertainties associated with the above demand measures.

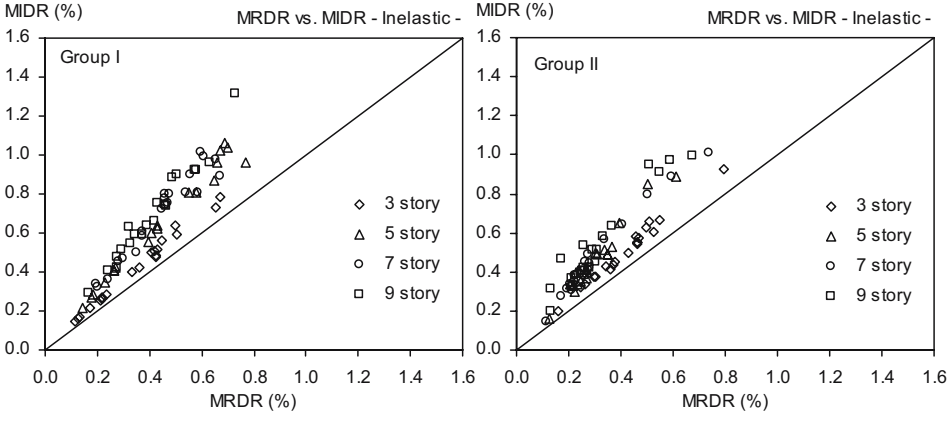

Figure 3. Global relationship between maximum roof and interstory drift for the frame models

Using the limited amount of data presented in this study, a similar deterministic relationship is derived to predict the MIDR for a given MRDR.

$$MIDR = 4.61(1 - e^{0.35 MRDR}) \quad (1)$$

This equation can be used for stiff MRFs conforming seismic code provisions with fundamental periods less than 1.0 s and normalized strength ratios (R, elastic to yield strength ratio) less than 7 that can be computed from the idealized bilinear global capacity curve and the earthquake specific PSA. The reader is referred to the references[5, 9] for detailed information on this issue.

Figure 4 shows the inelastic-to-elastic ratios of MRDR in terms of R for the subject frame models. The scatter plots for roof drift indicate that the inelastic roof drift tends to be less than the elastic roof drift with increasing story number. The inelastic roof drift demands on 3-story models are, in general, higher than their elastic counterparts for both groups. This can be attributed to the sensitivity of short-period nonlinear deformation demands to the changes in strength particularly when the lateral strength of the short period system is less than the elastic strength that would maintain the system to respond linearly. This observation is more noticeable for the 3-story model in Group I that is subjected to a relatively higher seismic hazard level.

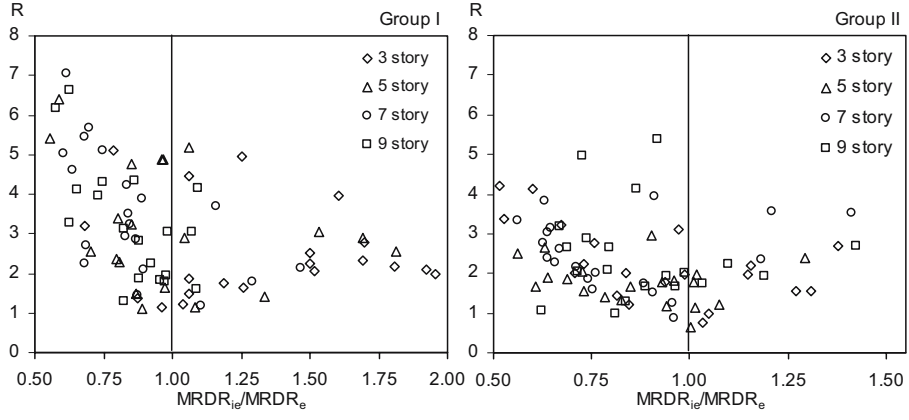

Figure 4. Variation of maximum roof drift as a function of normalized strength for the frame models. (Scale is not the same for abscissa)

Figure 5 presents similar scatter plots for MIDR. The scatter plots of Group I suggest a similar trend for inelastic-to-elastic MIDR ratio as in the case of MRDR but this time the variations are more dispersive suggesting that the behavior of MIDR is more complex with respect to MRDR. This observation is particularly valid for Group II model frames that are designed considering a uniform decrease in the lateral stiffness. The intricate behavior of MIDR is illustrated by plotting the story-wise logarithmic standard deviations of nonlinear maximum story drifts and story displacements for Group II. The lognormal standard deviations that are presented in Figure 6 describe a fairly

uniform story-wise dispersion for lateral displacements that is not observed for story drifts. The story drift standard deviations vary with respect to height and attain their maximum in the lower stories where the interstory drifts are expected to become maxima for the model frames investigated in this study.

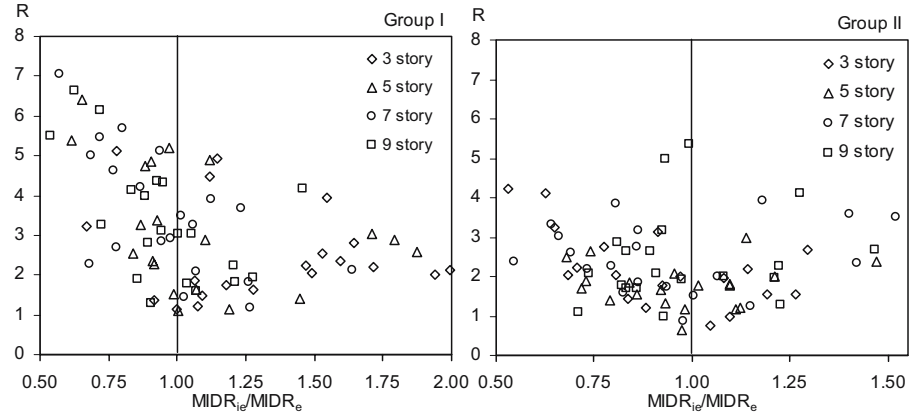

Figure 5. Variation of maximum interstory drift as a function of normalized strength for the frame models. (Scale is not the same for abscissa)

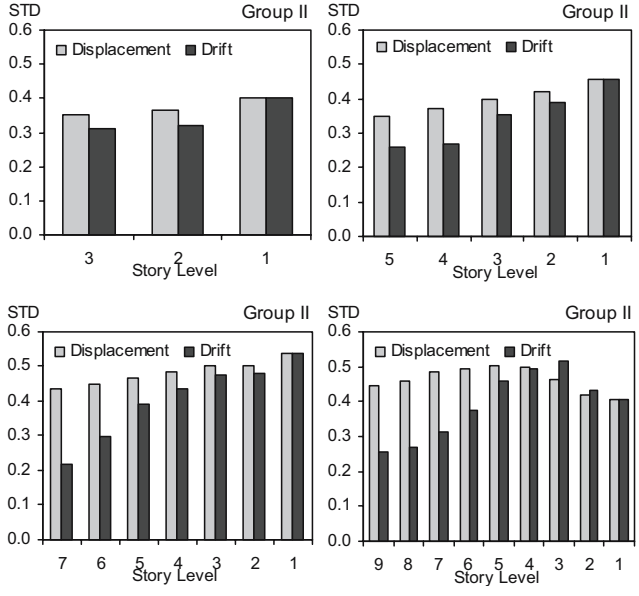

Figure 6. Story-wise dispersions for maximum lateral displacements and story drifts for Group II frames

The plots in Figure 7 that show the variations of maximum story drifts support the observations presented in the previous paragraph. The overall behavior resembles first mode dominancy where the maximum interstory drifts

are expected to occur in the lower stories. However, the height-wise story drift variation shows a considerable dispersion that is particularly more apparent for 2nd group frame models. Considering the close fundamental period patterns for Groups I and II and the common seismic features attributed to the ground motions, the uniform decrease in the lateral stiffness of Group II frames are believed to be the reason for the increased dispersion in Group II story drifts.

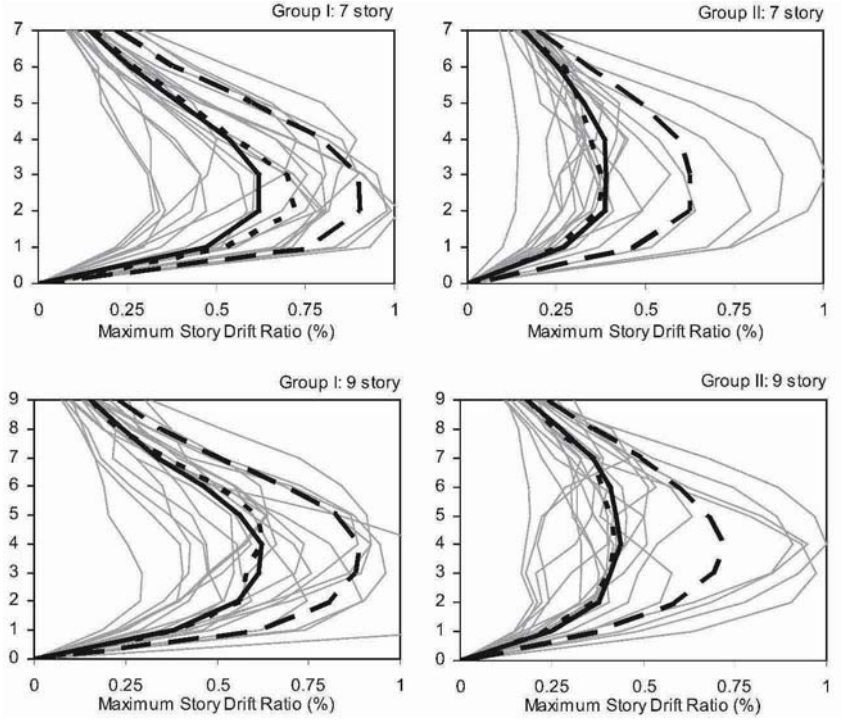

Figure 7. Variation of maximum story drift ratios for 7- and 9-story frame models in Groups I and II. Black solid lines designate the mean variation for each frame model. Solid short and long dashed lines designate the median and 84th percentile variations, respectively

4. Nonlinear Drift Demand Estimations by First Mode Approximations

First mode approach is still the state of practice for estimating the deformation demands in approximate procedures suggested by various performance-based seismic guidelines[10, 11, 12]. Recently, more elaborate methods that consider the higher mode effects have been proposed[6, 25] but this study considers them as conjectural. They have to be evaluated thoroughly for their applicability in the wide array of engineering practice. Table 2 summarizes some of the relevant statistics for the variables that can be used to relate SDOF deformation demands to MDOF deformation demands. More precisely, similar relations are used in

the aforementioned guidelines to estimate the roof displacements from the maximum deformation demands of equivalent SDOF systems obtained from the idealized global capacity curves that are described in the previous sections.

TABLE 2. Statistics to relate SDOF to MDOF deformations using first mode approach

		Group I			Group II		
	Fractiles	$\Gamma_{1,e} \times \phi_{1,e}$	$\Delta_{top,e}/S_{d,e}$	$\Delta_{top,i}/S_{d,i}$	$\Gamma_{1,e} \times \phi_{1,e}$	$\Delta_{top,e}/S_{d,e}$	$\Delta_{top,i}/S_{d,i}$
3-story	50%	1.29	1.29	1.21	1.30	1.40	1.26
	84%		1.30	1.68		1.60	1.64
5-story	50%	1.30	1.32	1.19	1.32	1.34	1.20
	84%		1.35	1.32		1.43	1.43
7-story	50%	1.30	1.31	1.29	1.35	1.41	1.11
	84%		1.34	1.50		1.59	1.34
9-story	50%	1.31	1.32	1.31	1.36	1.51	1.22
	84%		1.39	1.42		1.78	1.39

In Table 2 the variable $\Gamma_{1,e} \times \phi_{1,e}$ is the product of elastic first mode participation factor and the modal roof displacement that is expected to define an accurate relationship between the elastic spectral displacement ($S_{d,e}$) at the first mode and the elastic roof displacement demand as long as the structure primarily deforms in the first mode. The variables $\Delta_{top,e}/S_{d,e}$ and $\Delta_{top,i}/S_{d,i}$ are the elastic ($\Delta_{top,e}$) and inelastic ($\Delta_{top,i}$) roof displacements normalized by the elastic ($S_{d,e}$) and inelastic ($S_{d,i}$) spectral displacements, respectively that are computed from the response history analyses. The spectral quantities are computed by using the equivalent SDOF systems associated with the dynamic properties obtained from the idealized bilinear capacity curves. The fractiles presented in Table 2 are computed by assuming a lognormal distribution. The comparisons between $\Gamma_{1,e} \times \Gamma\phi_{,e}$ and $\Delta_{top,e}/S_{d,e}$ indicate that these two parameters are in good agreement in terms of median statistics and the associated dispersions are small for Group I model frames. This observation changes for Group II buildings where $\Delta_{top,e}/S_{d,e}$ generally yields higher values with respect to $\Gamma_{1,e} \times \phi_{,e}$ and the associated dispersions are significantly higher than the ones presented for Group I. This difference can be attributed to the higher mode effects that seem to be relatively dominant for Group II models when they respond in the elastic range. The comparisons between $\Gamma_{1,e} \times \phi_{,e}$ and $\Delta_{top,i}/S_{d,i}$ parameters reveal that the median values of the latter parameter are less than $\Gamma_{1,e} \times \phi_{,e}$ for all cases. The smaller median values of $\Delta_{top,i}/S_{d,i}$ with respect to $\Gamma_{1,e} \times \phi_{,e}$ can be attributed to the concentration of plastic hinge formations at the lower stories. This causes a diversion in nonlinear deformation patterns from the lateral deformation patterns that are guided by the elastic behavior. This fact is illustrated in Figure 8 using the linear vs. nonlinear lateral deformation profiles of the 9-story model from Group I. The plots show that, on average, the structural behavior is

dominated by the first mode and the nonlinear deformations are less than the corresponding elastic deformations due to the yielding in the lower stories. This observation suggests that, on average, the use of $\Gamma_{1,e}\times \phi_{1,e}$ parameter would yield conservative nonlinear roof drift estimates as will be described in the below paragraphs. The higher dispersion in $\Delta_{top,i}/S_{d,i}$ is believed to be caused by the complex relationship between the nonlinear structural behavior and the ground motions.

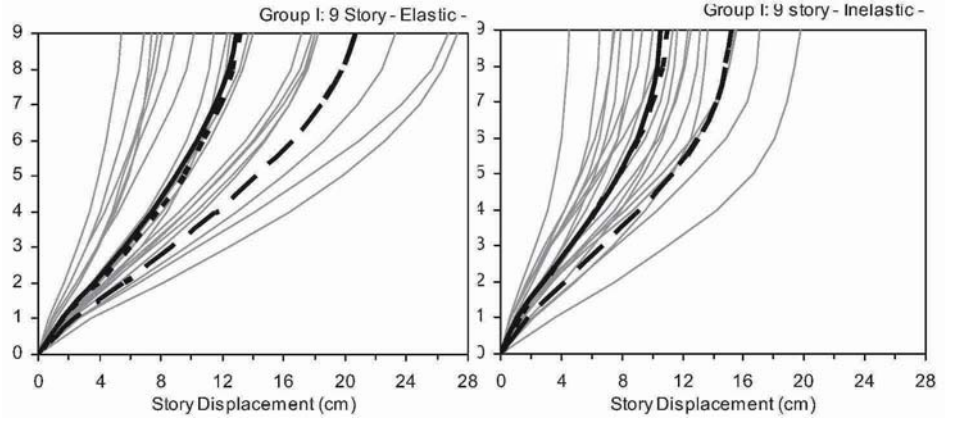

Figure 8. Elastic and inelastic maximum lateral deformation profiles of 9-story, Group I frame model subjected to 20 ground motions. Black solid lines designate the mean variation. Solid short and long dashed lines designate the median and 84th percentile variations, respectively

Tables 3 and 4 present the error statistics for roof and interstory drift demands, respectively when the first-mode approach is used. The error is computed as the ratio of approximate demand estimated by the first-mode approach to the exact demand computed from the nonlinear response history analysis. Assuming a lognormal distribution 16th, 50th and 84th percentile error values are listed for each frame model. The lower and upper percentiles define an error interval whereas the 50th percentile describes the central tendency of the error. The approximate roof drift demands are computed using Eq. (2).

$$MRDR = \frac{1}{H}\left[\Gamma_{1,e} \times \phi_{1,e} \times S_{d,i}(T_{1,ideal}, \xi = 5\%, R) \right] \quad (2)$$

The variable $\Gamma_{1,e}\times \phi_{1,e}$ is the product of elastic first mode participation factor and the modal roof displacement and H designates the building height. The inelastic spectral displacement ($S_{d,i}(T_{ideal},\xi=5\%,R)$) is computed using the equivalent SDOF system obtained from the idealized global capacity curves. The normalized strength ratio is calculated using the record specific elastic pseudo-acceleration and the PSA_y value of the idealized bilinear curve. This inelastic spectral displacement is the $S_{d,i}$ parameter discussed in Table 2. The damping

ratio ξ is taken as 5 percent for the SDOF nonlinear response history analysis that is consistent with the first mode damping of the frame models. The 50th percentile errors presented in Table 3 indicate that the nonlinear roof drift, on average, is estimated on the conservative side. The estimations shift to a more conservative range as the discrepancy between $\Delta_{top,i}/S_{d,i}$ and $\Gamma_{1,e}\times \phi_{r,e}$ increases in the favor of the latter parameter (i.e. $\Delta_{top,i}/S_{d,i} < \Gamma_{1,e}\times \phi_{r,e}$). This observation is consistent with the discussion presented in the above paragraph.

TABLE 3. Error statistics for roof drift demands using the first-mode approach

	Error Statistics in Fractiles (Error = Approximate / Exact)					
	Group I			Group II		
	16%	50%	84%	16%	50%	84%
3-story	0.82	1.06	1.32	0.84	1.03	1.19
5-story	0.99	1.09	1.35	0.95	1.10	1.35
7-story	0.90	1.01	1.08	1.04	1.22	1.46
9-story	0.94	1.00	1.14	1.01	1.11	1.28

The maximum interstory drift estimations using the first mode approach is computed by Eq. (3).

$$MIDR = \frac{1}{h}\left[\Gamma_{1,e} \times \left|\phi_{1,e}^{n} - \phi_{1,e}^{n-1}\right|_{\max} \times S_{d,i}(T_{1,ideal}, \xi = 5\%, R)\right] \quad (3)$$

This equation is similar to Eq. (2) except that the absolute maximum modal displacement difference between two consecutive stories that is normalized by the story height h is used to estimate the MIDR. The approach in Eq. (3) can not describe the precise location of MIDR as it only uses the elastic properties of the building without considering the complex ground motion influence on the nonlinear structural behavior. The error statistics presented in Table 4 indicate that, on average, this approximate procedure yields conservative estimations for low-rise buildings. The increase in story numbers (7- and 9-story frames for this study) shifts the errors to the unconservative side indicating that the first-mode approach fails to resemble the actual variation in nonlinear structural behavior.

TABLE 4. Error statistics for MIDR using the first-mode approach

	Error Statistics in Fractiles (Error = Approximate / Exact)					
	Group I			Group II		
	16%	50%	84%	16%	50%	84%
3-story	1.09	1.38	1.75	0.86	1.03	1.21
5-story	0.90	0.99	1.26	0.87	1.02	1.24
7-story	0.75	0.86	0.99	0.80	0.92	1.11
9-story	0.76	0.84	0.95	0.67	0.85	1.01

A novel approach[22] that has been tested thoroughly for elastic MDOF behavior is also evaluated in the context of this study to see its efficiency in predicting the nonlinear MIDR. This approach modifies a previously proposed[26] ground-story drift ratio ($GSDR_{sh}$) for shear beam behavior by considering the theoretical first mode moment resisting frame behavior. The basic relationship for MIDR is given in Eq. (4).

$$MIDR(T,\xi,\rho)=\gamma_1(T,\rho)\gamma_2(T,\rho)GSDR_{sh};\quad \gamma_1=c_1+\frac{c_2}{T};\quad \gamma_2=e^{(c_3+c_4/T)} \tag{4}$$

The modifying factors γ_1 and γ_2 are regression expressions derived considering the first mode behavior of MRFs for different ρ values that controls the relative joint rotation in building systems and it is the ratio of beam-to-column stiffness ratio at the story level closest to the building mid-height[27]. The other variables in Eq. (4) are

$$GSDR_{sh}=1.27\sin\left(\frac{\pi h}{2H}\right)\frac{S_d(T,\xi)}{H}$$
$$c_1=\frac{1}{1+0.35/\rho^{0.65}};\ c_2=\frac{1}{8+25\rho^{0.4}};\ c_3=\frac{1}{2\rho+1};\ c_4=\frac{0.07}{\rho^{0.25}} \tag{5}$$

The terms h, and H correspond to the story and building height, respectively. Replacing $S_{d,i}(T_{ideal},\xi=5\%,R)$ by $S_d(T,\xi)$ in Eq. (5), the MIDR values for each model frame are estimated using Eq. (4). This simple replacement accounts for the nonlinear response of the equivalent SDOF system. The statistical results that are listed in Table 5 reveal that this new method is superior with respect to the direct first-mode approach. The median error statistics in Table 5 display that the MIDR predictions of this new procedure are most of the time on the conservative side. Considering the complex relationship between the nonlinear structural behavior and ground-motion records that has been addressed throughout the text, the results obtained from this basic procedure is promising for the preliminary seismic performance assessment of stiff MRFs.

TABLE 5. Error statistics for MIDR using the method proposed by Akkar et al.[22]

	Error Statistics in Fractiles (Error = Approximate / Exact)					
	Group I			Group II		
	16%	50%	84%	16%	50%	84%
3-story	0.91	1.15	1.45	1.01	1.22	1.42
5-story	0.95	1.04	1.33	1.00	1.17	1.43
7-story	0.84	0.94	1.11	1.00	1.15	1.38
9-story	0.86	0.95	1.08	0.82	1.03	1.23

5. Conclusions

Nonlinear drift demands for stiff MRFs are described in a statistical manner using regular 3- to 9-story frames that comply with seismic design provisions. Nonlinear response history analyses are conducted for 40 soil site ground motions to produce the relevant statistics. The statistical results indicate that the variation of story drifts is sensitive to the structural configuration. The first-mode approach, on average, tends to overestimate the roof drift for stiff MRFs. The MIDR estimations are not successful by this approach. A new procedure to estimate the MIDR is also evaluated. The preliminary results indicate that this new method is promising for the preliminary seismic performance evaluation of existing stiff MRFs.

ACKNOWLEDGMENTS

Dr. Ahmet Yakut is greatly acknowledged for his contribution during the design stage of the model frames. This research has been funded by the Scientific Research and Technical Council of Turkey and the Middle East Technical University Scientific Research Projects program.

References

1. G.D.P.K Seneviratna and H. Krawinkler, Evaluation of Inelastic MDOF Effects for seismic Design, Stanford University, John A. Blume Earthquake Engineering Center Report No. 120, 1997.
2. E. Miranda, Approximate seismic lateral deformation demands in multistory buildings, *Journal of Structural Engineering* 125(4), 417-425 (1999).
3. P. Fajfar, A nonlinear analysis method for performance-based seismic design, *Earthquake Spectra* 16(3), 573-592 (2000).
4. Gupta and H. Krawinkler, Estimation of seismic drift demands for frame structures, *Earthquake Engineering and Structural Dynamics* 29, 1287-1305 (2000).
5. R. A. Medina, Seismic Demands for Nondeteriorating Frame Structures and Their Dependence on Ground Motions, Department of Civil and Environmental Engineering, Stanford University PhD Thesis, 2002.
6. K. Chopra, R. K. Goel and C. Chintanapakdee, Statistics of single-degree-of-freedom estimate of displacement for pushover analysis of buildings, *Journal of Structural Engineering* 129(4), 459-469 (2003).
7. J. B. Berrill, M. J. N. Priestley and H. E. Chapman, Design earthquake loading and ductility demand, *Bulletin of the NZ National Society for Earthquake Engineering* 13(3), 232-241 (1980).
8. A. Nassar and H. Krawinkler, Seismic Demands for SDOF and MDOF Systems, Stanford University, John A. Blume Earthquake Engineering Center Report No. 95, 1991.

9. J. Ruiz-García and E. Miranda, Inelastic displacement ratios for evaluation of existing structures, *Earthquake Engineering and Structural Dynamics* 32, 1237-1258 (2003).
10. Applied Technology Council (ATC), Seismic valuation and Retrofit of Concrete Buildings, Report No. ATC-40 (1996).
11. Federal Emergency Management Agency (FEMA), Prestandard and Commentary for the Seismic Rehabilitation of Buildings, Report No. FEMA-356 (2000).
12. Applied Technology Council (ATC), Improvement of Nonlinear Static Seismic Analysis Procedures, Report No. FEMA-440 (2005).
13. M. A. Aschheim, J. Maffei and E.F. Black, Nonlinear static procedures and displacement demands, Proc. 6th U.S. Conference on Earthquake Engineering, Seattle Washington, CD-ROM Paper No. 167 (1998).
14. E. Miranda and J. Ruiz-García, Evaluation of approximate methods to estimate maximum inelastic displacement demands, *Earthquake Engineering and Structural Dynamics* 31, 539-560 (2002).
15. S. D. Akkar and E. Miranda, Statistical evaluation of approximate methods for estimating maximum deformation demands on existing structures, *Journal of Structural Engineering* 131(1), 160-172 (2005).
16. P. Giovenale, C. A. Cornell and L. Esteva, Comparing the adequacy of alternative ground motion intensity measures for the estimation of structural responses, *Earthquake Engineering and Structural Dynamics* 33, 951-979 (2004).
17. Y.C. Kurama and K. T. Farrow, Ground motion scaling methods for different site conditions and structure characteristics, *Earthquake Engineering and Structural Dynamics* 32, 2425-2450 (2003).
18. American Concrete Institute (ACI), 318-99/318R-99: Building Code Requirements for Reinforced Concrete and Commentary, ACI 318-02 (2002).
19. Building Seismic Safety Council (BSSC), NEHRP Recommended Provisions for Seismic Regulations for New Buildings and Other Structures, Report No. FEMA-450 (2003).
20. R.E. Valles, A.M. Reinhorn, S.K. Kunnath, C. Li and A. Madan, IDARC 2D version 4.0: A Program for the Inelastic Damage Analysis of Buildings, State University of New York at Buffalo, National Center for Earthquake Engineering Research Report No. NCEER-96-0010, 1996.
21. B. Alavi and H. Krawinkler, Behavior of moment-resisting frame structures subjected to near-fault ground motions, *Earthquake Eng. and Struct. Dyn.,* 33, 687-706 (2004).
22. S. Akkar, U. Yazgan and P. Gulkan, Drift estimates in frame buildings subjected to near-fault ground motions, *Journal of Structural Engineering*, 133(7) (2005).
23. S. Akkar and O. Ozen, Effect of peak ground velocity on deformation demands for sdof systems, *Earthquake Engineering and Structural Dynamics*, 34 (2005).
24. A. Ghobarah, On drift limits associated with different damage levels, Performance-Based Seismic Design Concepts and Implementation Proceedings of the International Workshop Bled, Slovenia, June 28–July 1, 2004 Report No. PEER 2004-05, 2005.
25. N. M. Aydinoglu, An incremental response spectrum analysis procedure based on inelastic spectral displacements for multi-mode seismic performance evaluation, *Bulletin of Earthquake Engineering* 1(1), 3-36 (2003).
26. P. Gulkan and S. Akkar, A simple replacement for drift spectrum, *Engineering Structures* 24(11), 1477-1484 (2002).
27. J. A. Blume, Dynamic characteristics of multistory buildings, *Proceedings of the ASCE Journal of Structural Divisions* 94(ST 2), 377-402 (1968).

THE SEISMIC WELL-BEING OF BUILDINGS: DIAGNOSTICS AND REMEDIES

SYED TANVIR WASTI
Department of Civil Engineering Middle East Technical University 06531 Ankara, Turkey

UGUR ERSOY
Department of Civil Engineering Middle East Technical University 06531 Ankara, Turkey

Abstract. An overview of old as well as emerging problems and solutions in earthquake engineering with particular emphasis on the assessment and rehabilitation of seismically vulnerable buildings is presented. Earthquakes continue to result in vast loss of life and damage to property especially in populated urban areas. As a result, with an increase in both awareness and experience, traditional repair and strengthening techniques are giving way to more efficient methods applicable on a larger scale and with greater speed, in order to ensure that as many existing buildings as possible are retrofitted in advance of future earthquakes.

Keywords: retrofitting; traditional methods; occupant-friendly methods; system improvement; infill walls; FRP; externally bonded panels; NATO SfP977231

I have mixed with a crowd and heard free talk
    In a foreign land where an earthquake chanced;
And a house stood gaping, naught to balk
    Man's eye wherever he gazed or glanced.
The whole of the frontage shaven sheer,
    The inside gaped: exposed to day,
Right and wrong and common and queer,
    Bare, as the palm of your hand, it lay.

From Robert Browning, *House*.

S.T. Wasti and G. Ozcebe (eds.), Advances in Earthquake Engineering for Urban Risk Reduction, 521–534.

1. Prefatory Remarks

The huge earthquake off the coast of the island of Sumatra towards the end of 2004 caused huge tsunamis that took a vast toll of life and property in many countries, some of which were thousands of miles away from the epicenter. The very scale of this gigantic event and the ubiquitous availability of portable photographic equipment resulted in the catastrophe being well recorded. Never before in human history has earthquake damage been so forcefully brought to the forefront of the world's attention. The natural disaster which resulted in more than a quarter of a million dead also highlighted – once again – the responsibility of engineers and builders to ensure, as much as is possible, that the structures they design and construct will provide a high level of safety and security.

The present work is a sequel to an earlier paper* wherein a global overview of the pre- and post- earthquake assessment and rehabilitation of buildings was discussed in the light of NATO SfP Project 977231 which, in early 2003, was in its initial stages of implementation. It is intended herein to examine the same subject with the hindsight afforded by the completion of the various stages of the project. In view of the predominance of reinforced concrete (RC) in Turkey, especially in urban building construction, it is intended to focus the presentation primarily on reinforced concrete buildings.

Although RC is known to be a versatile, sturdy, and economical construction material, especially where the availability of structural steel sections is limited, its very popularity often results in poor concrete quality, sloppy workmanship, inattention to proper detailing of joint regions, deficiency in the provision of suitable confinement steel which, combined with the lack of effective supervision, result in serious damage to RC buildings in the event of an earthquake. It must furthermore be pointed out that much greater experience has been gained – especially in view of frequent large earthquakes in Turkey since 1992 – in the investigation as well as strengthening of buildings that have already suffered damage as opposed to those that might be considered suitable candidates for retrofitting in advance of future earthquakes.

In most countries, extensive programs of structural appraisal with the intention of structural repair/strengthening are only conducted following some large scale natural disaster. Before the rehabilitation process can begin, a post-

* Syed Tanvir Wasti and Ugur Ersoy, "Bringing to Buildings the Healing Touch – A Challenging Task for Engineers", in S. T. Wasti and G. Ozcebe (eds.), Seismic Assessment and Rehabilitation of Existing Buildings, Kluwer Academic Publishers, Dordrecht / Boston / London, 2003, pp. 1 – 10.

disaster field investigation needs to be carried out to assess [within a very limited period] which buildings in a given area need to be demolished, which ones require only minor repair and which ones can be considered for strengthening. After this initial assessment, based on a prototype form involving an expert system that provides numerical values and penalty points to structural characteristics and defects, an overall cumulative damage score is calculated. Decisions on the future of moderately damaged structures have to be made by investigators using systematic approaches involving cataloguing of damage. Families occupying houses or individuals running their business in the damaged buildings have been entitled, in the past, to receive damage compensation from the government in accordance with the rated damage due to the Disaster Law so as to restore their living after the disaster. However, particularly with seismically vulnerable megalopolitan areas such as Istanbul, the incentive to conduct pre-emptive programs of structural assessment and retrofitting to ward off future loss of life and property has now taken root.

A fundamental aspect of the present work is the appraisal and comparison of what might be considered "traditional" methods of post-earthquake structural amelioration, which tend to favor in-situ installation of RC shear walls and concrete jacketing of columns, with more "occupant friendly" methods involving new materials and techniques. The main idea behind these new seismic rehabilitation techniques is to strengthen the existing infill walls [which are usually constructed of hollow clay tiles] using Fiber Reinforced Polymers (FRP) or precast panels which will upgrade them to structural walls. Moreover, it is essential that such interventions should not necessitate the evacuation of buildings.

2. Structural Evaluation of an Existing and/or Damaged Building

Near-and near-and nearer still,
As the Earthquake saps the hill,
First with trembling, hollow motion,
Like a scarce awakened ocean,
Then with stronger shock and louder,
Till the rocks are crushed to powder...

From Lord Byron, *The deformed transformed.*

The general outline of the process for the assessment of the safety of an existing building is given in the steps below:

- Review of documentation related to the building

  Before proceeding to the site for an inspection of the structure to be rehabilitated, the architectural project drawings, the structural drawings, design calculations, soil test data including site boring information and all pertinent information must be assembled and studied thoroughly. Copies of such documents are expected to be deposited with the local municipal authorities, but it is usually not possible to retrieve these documents, especially after a disaster. For each building to be rehabilitated, the as-built plans therefore need to be re-drawn with architectural and engineering features marked on them.

- Observations on site and evaluation of all available field data

  Dimensions and details of columns, beams and slabs should be examined. Concrete strength, in-situ checking of quality and quantity of reinforcement, corrosion, etc. should be assessed. The possibility that the actual amount of steel reinforcement is less than that required by the structural calculations should definitely be investigated. Contractors often tend to cut down on ties, stirrups and sometimes even main reinforcement. All other evidence of structural distress or damage such as excessive deflections, cracking, should be catalogued on accepted standard damage assessment forms, as such data are essential for the design of the repair/strengthening system. Soil and foundation conditions need to be appraised. This may require expert assistance and also the preparation of a boring map for the site.

- Analytical studies, including earthquake criteria, choice of mathematical model, and choice of local site earthquake intensity

  The selection of an analytical method for the evaluation of an existing structure is based on available geological, structural design information, computer facilities and also engineering judgment. A simple seismic coefficient to evaluate the lateral load as given in most earthquake codes may be used initially. Since the natural vibration periods of many buildings fall into the short or intermediate period range, a constant seismic coefficient of 0.2 is often employed. Similarly, it is usually accepted that the modulus of elasticity of columns and beams is between 30% and 60% lower than the original values assumed in design, respectively. A modal response spectrum or a complete time history analysis may be needed for other cases. Computer programs for push over analyses and the inclusion of inelastic effects such as stiffness degradation are also available. For existing buildings, structural response analysis is more reliable than in the case of design, because after construction the building exists and its structural properties can be assessed with greater accuracy.

3. Structural Repair/Strengthening of an Existing and/or Damaged Building

We learn geology the morning after the earthquake.
From Ralph Waldo Emerson, *The Conduct of Life.*

Each building or structure in need of repair and strengthening is unique in many ways. Based on the constraints on the site, a responsible decision has to be made about the rehabilitation procedure for each structure. The basic criterion in seismic retrofit of a damaged building is to upgrade its resistance to the level required by the current seismic code. The current Turkish Earthquake Code[1] describes the seismic hazard with a 10% probability of exceedance in 50 years. This generally yields a high level of peak ground acceleration in a severe earthquake zone of (say) 0.40 g. The elastic design acceleration spectrum is then reduced by a factor which takes into account that a certain amount of acceptable damage may be suffered by the building in the event of a moderate to severe earthquake without endangering life safety or resulting in the collapse of the building. This reduction factor, called the response modification factor in most earthquake Codes, is 4 for frame/wall concrete systems if the system is considered ordinary (non-ductile) and 7 if it is ductile. Since the strengthened system is composed of a non-ductile existing frame and ductile added walls, a reduction factor of 5 is generally considered acceptable in design. A life safety performance is expected from such buildings under the described seismic hazard.

Techniques for the rehabilitation of damaged or undamaged RC structures are numerous, and the choice of a suitable strategy is a matter of engineering judgment based on experience, damage level, economic considerations and site conditions. Rehabilitation or retrofitting is not connected only with pre- or post-disaster structural strengthening measures; it may also be necessitated by increased structural performance requirements required as a result of the updating of building codes. The Turkish Earthquake Specifications are currently (2005) being modified to include a new section on requirements for structural rehabilitation.

3.1. TRADITIONAL REPAIR/STRENGTHENING TECHNIQUES

The traditional process of RC building rehabilitation involves the following procedures:

- Strengthening of individual members or components, by jacketing with reinforced concrete or with steel angles and built-up sections or by externally bonded steel plates.

- System improvement, in which the existing deficient lateral load resisting system is replaced by a new lateral load resisting system which usually consists of braced frames or structural walls.

Repair/strengthening is a complex operation and must be left to professionals if the desired structural behavior is afterwards to be attained. Repair and/or strengthening of damaged or deficient members without considering the overall behavior of the structure may weaken the structure instead of strengthening it. Injudicious strengthening may also lead to an increase in demand which can exceed the strength increase provided. Repair and strengthening strategy thus requires not only the assessment of damage or weakness and their possible causes, but also a re-examination by rigorous analysis of the eventual performance [including strength, safety and ductility] of the structure after the repair/strengthening is complete.

3.1.1. *Component strengthening*

In general, columns are regarded as the most critical and important structural members, followed by beam-column joints and beams. Slabs are generally less critical and relatively easy to replace or strengthen. Depending on the level of weakness or damage, as well as the envisaged level of post-intervention structural strength, all structural elements may be subjected to injection of epoxy or grout, or replacement of damaged parts by fresh parts, or jacketing with RC or with steel angles and sections or by externally bonding steel plates. However, such strengthening cannot be given the label of rehabilitation, although a large volume of literature is available on the subject.

In natural disasters such as earthquakes, it is usually observed that columns suffer the greatest damage. Although proper design procedures are meant to encourage the formation of plastic hinges due to high loads or deflections in the beams rather than in the columns of a reinforced concrete structure, very often the reverse is found to be the case, with slender columns and heavy beams. Furthermore, if the space between successive columns is not filled up [with a shear or infill wall] to the level of the upper beam, thus causing a band-like gap, severe damage occurs due to the ‘captive column’ or ‘short column’ effect. Ordinary repair of columns involves supporting the beam-slab region surrounding the column so as to substantially reduce the column load. The joint region between columns and beams should be examined and in order to ensure suitable transfer of shear and moment, reinforcing bars from both beams and column should be made continuous through the joint region. Column repair/strengthening techniques may involve concrete jacketing, concrete wing walls, steel angles or plates, which will result in an increase in the column dimensions. In all cases, the concrete ends of columns have to be well confined.

Beams are the most important structural members after columns. The tensile strength of beams can be increased by the provision of extra reinforcement and subsequent shotcreting[2]. The compressive region in beams can also be strengthened by the provision of a new reinforced concrete layer. Attention has to be paid to the bond and shear connection between the new and old layers. Thin steel plates [usually up to 3 mm in thickness] can be bolted or fixed by epoxy adhesive at different locations of a beam[3] to increase tensile and shear resistance. External or internal stirrups should be employed to counteract the increased demand due to increased flexural strength. The use of prestressed tie-rods to strengthen beams is common but is not suitable for cyclic or reversed loading.

Floor slabs do not usually create serious structural problems. However, in some cases, the diaphragm action of the slab is found to be inadequate or the serviceability conditions not satisfied. Furthermore, in flat plate structures, the punching strength of the slab may be less than required by the code. In such cases, a new reinforced concrete top layer may be added to strengthen the existing slab.

3.1.2. *System improvement*

System improvement becomes more feasible than component strengthening when there are too many individual members to be conveniently rehabilitated and/or when the lateral stiffness is insufficient. In Turkey, system improvement is carried out by infilling the selected bays of the frame by RC walls in both principal directions. These cast-in-place walls are connected to the existing frame by embedded dowels anchored to the frame members with epoxy bonding. In order to counteract torsional effects more efficiently, these RC structural walls are usually located along the peripheral axes of the structure if possible. Depending on the degree of connection provided between the infill and the main frame skeleton, the infill wall will act as a shear wall, thus forming a new lateral load resisting system. The so-called ‘Infilled Frame Technique’ not only improves the seismic behavior and strength, but also the lateral stiffness significantly. In Turkey, this system was first applied in 1968 by Middle East Technical University (METU) staff[4] and since then several research projects were carried out to understand the behavior of such systems and to develop design criteria as well as construction details.

Experience during the rehabilitation and structural upgrading work in 1992 on public buildings in Erzincan, which is a highly seismic area, led to the choice of cast in place composite steel and RC shear walls in both directions at suitable locations over the height of each strengthened building so as to impart the required resistance to lateral forces. Cast-in-place RC shear walls as infills in structural frames have also been found to give very satisfactory results when

the system is tested under reversed cyclic loading. This technique was adapted for the repair and strengthening of moderately damaged RC structures after the 1995 Dinar and 1998 Ceyhan earthquakes and the on-site application was found to be satisfactory.

Rehabilitation work conducted by the METU research group indicates that when the infilled frame technique is used in damaged buildings it is not necessary to repair the damaged frame members as the lateral load is resisted by the newly formed structural system consisting of structural walls (infilled frames). This conclusion was reached on the basis of three experimental research projects in which frames were tested in the laboratory under reversed cyclic loading until considerable damage occurred (e.g. yielding of column reinforcement, cracking in beams and beam-column joints). The damaged frames were strengthened with RC infill but members and joints were not repaired. When tested under reversed cyclic loading, such frames performed adequately well[5] and demonstrated that the use of infill walls for system improvement eliminates the need for repair of damaged frame members as long as the RC is of adequate quality. In practice, of course, some of the damaged columns may require repairs for cosmetic purposes. Furthermore, if the concrete strength in the boundary columns is very low, the anchorage of the dowel bars becomes a problem and, in such cases, the boundary columns of the infilled frames are jacketed to provide stronger anchorage for the dowels.

The following design requirements have been established as a result of the extensive research conducted at METU in this area:

- Sufficient 'RC infilled frame area' (shear wall area) must be provided in both principal directions to ensure that the total base shear is resisted by this system.
- The cross-sectional area of the 'RC infilled frames' in each orthogonal direction should not be less than 0.25% of the total floor area nor less than 1% of the floor area at the base of the building.
- The shear stress in the walls (RC infilled frames) should not exceed $0.35\sqrt{f_{ck}}$ in SI units.
- The total tensile strength of the dowels (horizontal anchors) anchored to the columns should not be less than the total tensile strength of the horizontal infill reinforcement.

Another technique for the provision of system improvement is to strengthen the structure by means of precast infill panels to carry both vertical and horizontal loads. Much work has been done in this area in recent decades. Details of a sophisticated system, incorporating precast panels that can be assembled or combined to form a stout infill wall are given in Frosch, Jirsa and

Kreger[6]. The panels are equipped with shear keys on all edges and are connected to each other by means of reinforced grout strips. A separate connection, involving shear lugs formed from steel pipes, is used to join the panels to the external RC frame. In order to provide the resulting infill wall with overturning capacity, the tensile capacity of the existing frame columns on either side of the infill walls needs to be augmented, and this is achieved by a post-tensioning system. All in all, the system is very effective, but somewhat complicated.

3.2. CONTEMPORARY REPAIR/STRENGTHENING TECHNIQUES

Traditional repair and strengthening techniques as described above have several drawbacks. Although practical implementation and laboratory experimentation have proved that they are very effective in upgrading the lateral resistance of the structure, they are intrusive and can often be messy. If and when applied to buildings which have suffered moderate damage in an earthquake, it is likely that the building to be rehabilitated is either vacant to begin with, or shall need to be vacated for weeks or even months. Traditional methods become unpractical if a building lacks seismic safety and needs to be retrofitted while it is occupied and in full use, e.g. before damage is caused by an earthquake. Attention has therefore been focused in recent investigations on methods that will enable the swift and efficient strengthening of buildings without interrupting their functioning, i.e. the development of 'occupant-friendly' strengthening techniques.

The vast majority of RC buildings have a moment resisting framework of beams and columns which may be further strengthened by the presence of shear walls in both principal directions. Spaces between the beams on successive floors and consecutive columns are usually filled in with lightweight masonry walls that are assumed not to participate in bearing horizontal or vertical loads. Such infill walls are present primarily to enclose the space and provide openings for doors and windows.

Practical contemporary solutions for 'occupant-friendly' retrofitting include the following:

- component strengthening by wrapping RC columns and/or beams with carbon fiber reinforced polymers [CFRP]

  CFRP wraps not only enhance the strength of RC columns, but studies indicate that the deformability of CFRP wrapped RC columns also increases significantly[7]. An important factor in favor of using CFRP wraps is that they do not materially alter the dimensions of the columns or beams that are rehabilitated.

- system improvement by strengthening existing masonry infills

  One of the main objectives of recent research conducted under the general direction and guidance of the METU research group was to develop "occupant-friendly" rehabilitation techniques for strengthening seismically deficient buildings while creating minimum disturbance for the occupants. The main idea behind the research projects, which were sponsored by NATO and TUBITAK, was to strengthen existing masonry infills so as to convert them into structural walls.

Two different techniques were employed: a) strengthening of masonry infills by externally bonding CFRP sheets or strips and b) strengthening of masonry infills by externally bonding precast panels.

a) strengthening of masonry infills by externally bonding CFRP sheets or strips

In the experimental program, the masonry infills of seismically deficient RC frames were strengthened by bonding CFRP sheets or strips on the infills. Two story – one bay and two story – three bay frames in which only the interior bay was infilled were tested at METU under reversed cyclic loading[8,9]. Different CFRP configurations were tried and special anchors were developed. The two story – three bay specimen in which the infill is strengthened with CFRP strips is shown in Figure 1. Tests on specimens with lapped splices in column longitudinal bars were tested by Ozden[10] as a part of the NATO and TUBITAK projects.

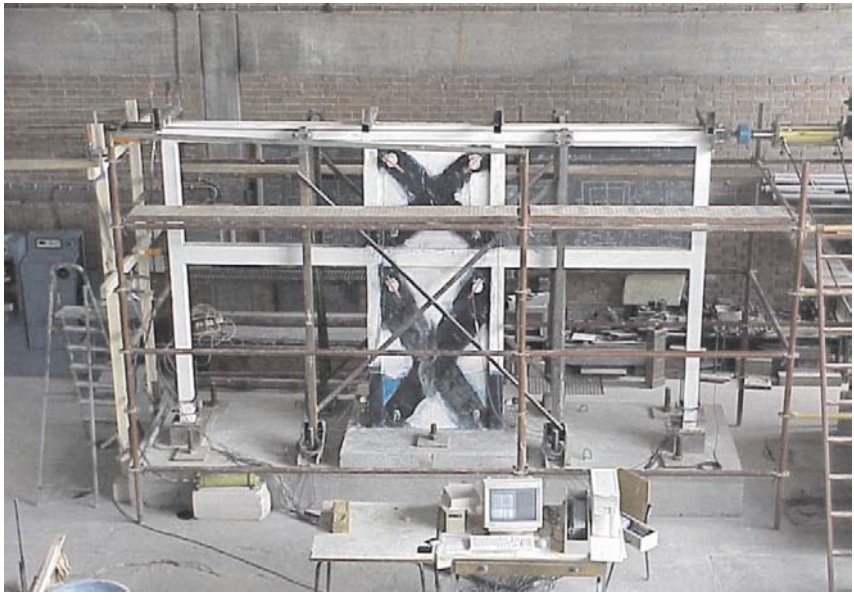

Figure 1. Two story – three bay frame ready for testing after CFRP strengthening

b) strengthening of masonry infills by externally bonded precast panels

In the experimental program conducted at METU, the seismically deficient two story – one bay RC frames with hollow clay tile infills were strengthened by bonding precast panels of manageable sizes on such infills[11]. Basically, two different shapes were used for the precast panels and different connection details were tried. All specimens were tested under reversed cyclic loading.

Experimental results indicated that even unstrengthened masonry infills increased both the strength and the stiffness of the frames significantly. However, once the infill failed, the performance under reversed cyclic loading became very unsatisfactory. The performance was significantly improved when the masonry infill was strengthened using CFRP strips or precast panels bonded to the infill and connected to the frame members. Typical base moment – lateral displacement curves of seismically deficient RC frames strengthened using different techniques are shown in Figure 2 together with that of the bare frame.

It may be observed that the strength of the specimen in which the infill was strengthened using CFRP strips came close to the strength of the specimen having an RC infill. However, once the ultimate strength was reached, a sudden drop in the load carrying capacity occurred due to the failure of the anchors securing the strips. Specimens in which the masonry infills were strengthened with precast panels had strengths comparable to those with RC infills but the ductility was reduced.

From Figure 2 it is evident that both strength and stiffness increase significantly when the infill is introduced.

4. Summing Up

The earthquake came, and rocked the quivering wall,
And men and nature reeled as if with wine.

Lord Byron, *Love and Death.*

Structural rehabilitation, amelioration and retrofitting which, like earthquake engineering, were unknown at the time Byron wrote the lines of his last poem, have come a long way in the ensuing span of nearly two hundred years. Concomitantly, however, the increase in world population and the lack of suitably engineered buildings in most countries have ensured that the problems of structural inadequacy and failure persist, causing loss of life and property with every major earthquake. Significant improvements in the seismic design and construction of new and large structures are, indeed, taking place. By contrast, the dissemination and implementation of available techniques, as well as the development of efficient retrofit methods are required to ensure that the

large stock of seismically deficient buildings still in use for residential and business purposes can be equipped to withstand earthquakes during the remainder of their lifetime and to provide at least life safety.

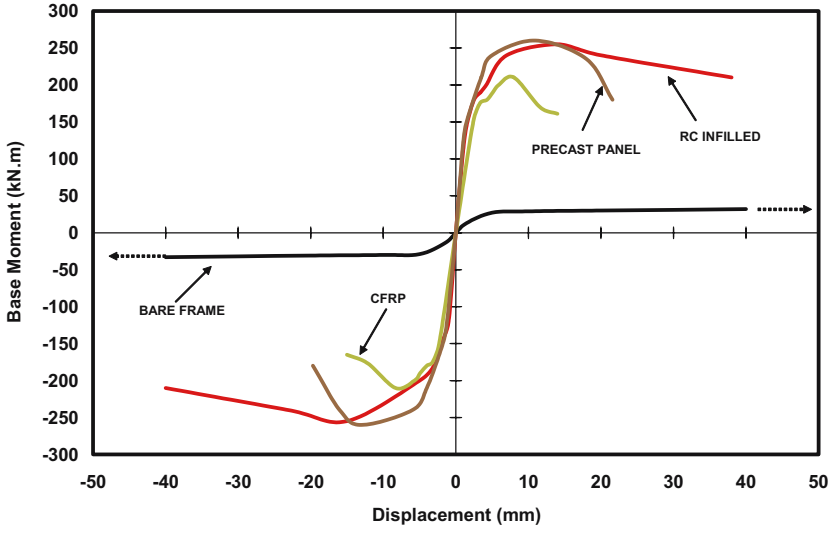

Figure 2. Relative load – drift behavior for unstrengthened and rehabilitated frames

Research conducted under NATO Project SfP977231 and associated Turkish projects sponsored by TUBITAK under the general direction and guidance of METU faculty members has, in the past few years, concentrated to a significant extent on the analytical and experimentation validation of both traditional as well as contemporary methods of retrofitting RC structures. Traditional methods have usually incorporated the removal of existing non-structural infills and replacing them with in-situ RC structural walls, whereas more contemporary methods have tended to provide structural upgrading by converting masonry infill walls into structural walls either by the application of CFRP strips or layers or by externally bonding precast panels of manageable dimensions. The lessons learnt from the project substantially indicate that in the interests of time, economy and convenience, it is expedient to prefer more contemporary techniques for the seismic retrofitting of RC buildings that are occupied and in use. An important result from these projects has been the development of design criteria for the analysis and detailing of buildings in which simple masonry infills have been strengthened by various methods. However, the last word on the matter probably lies further down the road and more experimental information needs to become available to be able to improve the recommendations already made.

An associated problem, especially in seismically vulnerable countries like Turkey, is the retrofitting of the vast stock of rural or semi-urban building stock

that comprises masonry structures. Hitherto, large scale post-earthquake rehabilitation of such buildings has either been avoided by recommending demolition. Medium scale rehabilitation of masonry structures has usually employed traditional methods of strengthening in the form of component strengthening including incorporation of in-situ RC columns and strengthening of masonry load-bearing walls with external jackets of shotcrete reinforced with wire-mesh[12].

Each building or structure in need of repair and strengthening is unique in many ways and decisions can only be made with this in mind. A greater choice in current versus traditional methods will result in enhanced flexibility for the engineer faced with recommending retrofitting techniques especially for large numbers of seismically vulnerable buildings.

References

1. Ministry of Public Works and Settlement, Specifications for Structures to be built in Disaster Areas, [in Turkish], Ankara, 1997.
2. ACI, Recommended Practice for Shotcreting, American Concrete Institute Standard No. 506-66, Detroit, 1966.
3. M. D. MacDonald, The flexural performance of 3.5 m concrete beams with various bonded external reinforcements, TRRL Suppl. Report No. 728, Transport and Road Research Laboratory, Crowthorne, Berkshire, 1982.
4. U. Ersoy, and S. Z. Uzsoy, The behavior of infilled frames [in Turkish], TUBITAK Report MAG-205, Ankara, 1971.
5. E. Canbay, U. Ersoy, G. Ozcebe, Contribution of RC Infills to the Seismic Behavior of Structural Systems, ACI Structural Journal, V.100, Iss.5, pp.637-643, Sept. 2003.
6. R. J. Frosch, J. O. Jirsa, and M. E. Kreger, Experimental response of a precast infill wall system, in S. T. Wasti and G. Ozcebe (eds.), Seismic Assessment and Rehabilitation of Existing Buildings, Kluwer Academic Publishers, Dordrecht / Boston / London, 2003, pp. 383 – 406.
7. S. N. Bousias, and M. N. Fardis, Experimental Research on Vulnerability and Retrofitting of Old-Type RC Columns under Cyclic Loading, in S. T. Wasti and G. Ozcebe (eds.), Seismic Assessment and Rehabilitation of Existing Buildings, Kluwer Academic Publishers, Dordrecht / Boston / London, 2003, pp. 245 – 268.
8. U. Ersoy, G. Ozcebe, T. Tankut, U. Akyuz, E. Erduran and I. Erdem, Strengthening of Infilled Walls with CFRP Sheets, in S. T. Wasti and G. Ozcebe (eds.), Seismic Assessment and Rehabilitation of Existing Buildings, Kluwer Academic Publishers, Dordrecht / Boston / London, 2003, pp. 305 – 334.
9. I. Erdem, U. Akyuz, U. Ersoy and G. Ozcebe, A Comparative Study on the Strengthening of RC Frames, in S. T. Wasti and G. Ozcebe (eds.), Seismic Assessment and Rehabilitation of Existing Buildings, Kluwer Academic Publishers, Dordrecht / Boston / London, 2003, pp. 407 – 432.

10. S. Ozden, U. Akguzel and T. Ozturan, Seismic Retrofit of R/C Frames with CFRP Overlays, in S. T. Wasti and G. Ozcebe (eds.), Seismic Assessment and Rehabilitation of Existing Buildings, Kluwer Academic Publishers, Dordrecht / Boston / London, 2003, pp. 357 – 382.
11. M. Baran, M. Duvarci, T. Tankut, E. Ersoy and G. Ozcebe, Occupant Friendly Seismic Retrofit (OFR) of RC Framed Buildings, in S. T. Wasti and G. Ozcebe (eds.), Seismic Assessment and Rehabilitation of Existing Buildings, Kluwer Academic Publishers, Dordrecht / Boston / London, 2003, pp. 433 – 456.
12. S. T. Wasti, M.A. Erberik, H. Sucuoglu and C. Kaur, Studies on the strengthening of rural structures damaged in the 1995 Dinar earthquake, Proc. Eleventh European Conf. on Earthquake Eng., CD-ROM, Paris, France (1998).

ENVOI

Over the four years of its tenure, NATO SfP Project 977231 entitled Seismic Assessment and Rehabilitation of Existing Buildings has proved to be a successful vehicle for the friendly interchange of scientific ideas via brainstorming sessions, informal discussions and e-mail. Under the gentle umbrella of the Public Diplomacy Division of NATO, the project has also formally coordinated and brought together the efforts of academics and research engineers working in the areas of earthquake engineering and structures. The three successful workshops [Antalya, 2001; Izmir, 2003 and Istanbul, 2005] conducted under the Project provide tangible proof of achievements in analytical methods, experimental investigations, design and construction techniques whose ripple effects are already being felt within the engineering disciplines of seismic assessment, structural rehabilitation and hazard mitigation, especially in Turkey and the Balkan countries.

The proceedings of the Izmir Workshop have already been published in book form in the NATO Science Series as S. T. Wasti and G. Ozcebe (eds.), *Seismic Assessment and Rehabilitation of Existing Buildings*, Kluwer Academic Publishers, Dordrecht / Boston / London, 2003, 546 pp.

The present volume, also in the NATO Science Series, comprises the proceedings of the Istanbul Closing Workshop. Both volumes contain valuable contributions from many persons in the very forefront of the earthquake engineering profession in several countries of the world. Urban risk reduction is a subject that concerns the whole world.

Apart from the presentation of "cutting edge" research developments, the guiding theme behind the workshops related to NATO Project SfP977231 has been the dissemination of information related to aspects of earthquake engineering at all levels. In the programme of the Closing Workshop, the last item of formal activity was a Panel that brought together all participants in an informal 'brainstorming' session. There was, indeed, a general consensus among the participants about the severity of the seismic risk especially in urban areas with deficient construction, typified by Istanbul. Many measures for the pre-emption as well as mitigation of the urban seismic problem on the macro and micro scales were put forward. However, it was felt that more was required than just preaching to the converted. One of the suggestions included the formulation of ideas and decisions within the general purview of earthquake engineering that might usefully be conveyed to municipal as well as governmental authorities – especially those in the corridors of power willing to listen. While engineers may provide the main analytical thrust behind such

ideas, the practical implementation on the ground is usually the responsibility of civil servants who cannot be expected to be experts in seismic planning, assessment and rehabilitation.

The following items represent a selection of the topics encapsulating the thoughts and hopes expressed by many of the workshop participants:

Ugur Ersoy:

The 1999 Marmara Earthquake has dramatically demonstrated what might happen in a major earthquake in highly populated areas in Turkey. A similar earthquake with an epicenter closer to Istanbul is expected in the near future. Such an earthquake will not only cause thousands of casualties but also will smash the Turkish economy.

Upgrading all vulnerable buildings and structures in seismic regions will not be a feasible solution because such a project will take decades and cannot be financed. Sidewalk observations made on buildings under construction in Istanbul and other cities indicate that even after the 1999 event the supervision is inadequate. Many of these new buildings do not conform to the code and give the impression that they have little chance of resisting a major earthquake.

Time is running out and actions which had to be taken yesterday should be taken today without losing time. The recommended actions should be realistic and practical. I believe the three actions listed below should be taken simultaneously as soon as possible.

- *Effective supervision should be provided for the new buildings to be constructed in regions of high seismic risk.*
- *Public buildings and structures such as hospitals, schools, power stations and bridges should be rehabilitated without losing time. Loans with low interest rates should be provided to the owners of private buildings for rehabilitation.*
- *City by-laws should be revised to encourage demolishing very vulnerable buildings and to build seismically resistant buildings on the same lot. Certain incentives should be provided to encourage rebuilding.*

To enable the above mentioned actions, the related laws need to be revised. The codes and/or guidelines for seismic rehabilitation should be as simple as possible so that the practicing engineers can understand and apply them without any difficulties.

To accomplish these tasks, a central committee should be established and required legal, financial and technical authority should be given to this committee. Such a committee is a must.

Robert Frosch:

A large variety of techniques have been developed for the seismic assessment and rehabilitation of existing structures both through the NATO project as well as from other research projects conducted around the world. While the NATO workshop has clearly demonstrated that rehabilitation technologies are available to substantially increase the safety of the built environment, it is obvious that public safety will not be increased without implementation. Implementation is imperative and cannot be achieved in a vacuum. A directed, coordinated, and systematic effort is required that must be supported at the highest levels of government. The risk of a major earthquake in Istanbul as well as many other major cities around the world is real and cannot be ignored as the economic, social, cultural, and political consequences are enormous.

Polat Gulkan:

No city was created in a single day. This is a continual process that evolves over centuries, takes up- or down-turns according to the twists of fate of its inhabitants, and is inherited by successive generations. Yet, the destruction of an urban settlement, or a significant portion of it, can last less than a minute when it is visited by a strong enough earthquake. The urban building stock, and the wealth and historic heritage it represents must be protected against such an eventuality if it becomes evident that these would be in serious jeopardy when the ground motion hits them.

Recent surge of interest in structural retrofit and assessment methods is the worldwide response of the structural engineering community to the challenge posed by awareness that many of the world's major cities display a deficiency of seismic capacity in the face of the earthquake hazard they face. This situation is acutely true for cities in the less developed countries where the risk is growing unchecked every day. We must devise effective ways of understanding the degree that a given building is vulnerable, how this may be addressed, and work out quick and effective methods for bringing it to the required capacity so that its occupants will not risk their lives. This is not a task that is suited to easy generalizations or quick and untested fixes. The workshop has reviewed only a tiny cross section of building retrofit technologies, but it is hoped that with further empirical confirmation most of these will become the standard tools of improvement of building safety.

It has been said of scientific articles that they should be as short as possible (an advice that the growing pile of literature on my desk confirms is not well heeded), but not shorter. The same is true for buildings: they

should be as strong as needed, but not stronger. This is a tall order to realize, but the community of concerned engineers and scientists in the earthquake field should keep on exchanging ideas and experience to help make it come true one day.

Guney Ozcebe:

NATO SfP Project 977231 entitled Seismic Assessment and Rehabilitation of Existing Buildings has provided an international forum for the meeting of minds and brought together the efforts of academics and research engineers working in all areas of earthquake engineering.

The project was one of a number of earthquake studies aimed at increasing earthquake-preparedness and people's safety, which were recommended by a working group set up by the NATO Science Committee, in the wake of the two destructive earthquakes that Turkey suffered in 1999.

Successful completion of the project studies yielded seismic vulnerability assessment procedures on a regional scale. Moreover, innovative rehabilitation techniques were also developed. These rehab technologies are of special value especially when the rehabilitation of large building stocks is under consideration. Through the course of the project, necessary verification studies and pilot applications were conducted to validate the reliability of the methodologies proposed.

Over the four years of its tenure, the project has brought together researchers from four countries, namely Macedonia, Greece, Turkey and the United States. In the joint research activities, research teams from 7 different research institutes and universities collaborated for the common goal of earthquake risk mitigation in big cities. The achievements reached have, one more time, shown clearly that the scientific community is single-minded in solving the problem. Regrettably, the implementation of the solution is not only in the hands of the scientists. Creating seismically proof cities demands a concomitant and equal determination in the political arena. In the light of the knowledge provided by science, a strong political will and equally strong community participation would essentially lead to the solution.

As a national risk mitigation program would require long-term planning [normally spanning between 20 to 30 years] at least 5-6 different successive governments may be expected to take part in this marathon run. Past experiences have shown that the orchestration of these activities should be made by an autonomous authority independent of any political influence. Furthermore this authority should be unaffected by changes in political trends. The establishment of such an autonomous authority should also be supported by realistic budgetary arrangements. All these

arrangements require patience, steadfastness and fortitude devoid of political considerations. For this reason, the present government should urgently recognize the problem as a high priority national problem and short-, medium- and long-term action plans should immediately be developed and put into action with no further delay.

Mete A. Sozen[*] *and the members of the Doganbey Workshop, July 2005* [†]

We the undersigned concerned experts in earthquake engineering from Japan, Turkey, and the United States have studied the relevant engineering and scientific reports about the consequences of such a damaging earthquake in the metropolitan area. We believe that such an earthquake will have extremely negative social and economic effects on the city and the nation. There will be many thousands of casualties. Industries and institutions will be unable to operate for a considerable amount of time, thus reducing the living standards of the entire country. We believe that immediate action is a national responsibility involving Turkish resources and people at all levels, government and private. We further believe that a priority list for immediate action can be constructed and initiated at once.

Given the extreme importance of this earthquake threat in Turkey, and based on a record of success in California and Japan, we recommend that a new authority should be established, called for example the Istanbul Earthquake Authority. This Authority would be charged with establishing and guiding an integrated earthquake hazard reduction program. In the interest of effectiveness the Authority should not exceed seven members. The composition of the Authority should be drawn from wide elements of Turkish public and private institutions, including two members of the parliament and a member from the Istanbul Metropolitan Municipality. The Authority should report regularly to the Prime Minister of Turkey and the Governor and Mayor of Istanbul.

---

[*] *Mete A. Sozen, Purdue University, Indiana, U.S.A.*

[†] *Bruce A. Bolt (deceased), University of California, Berkeley;*
Polat Gülkan, Middle East Technical University, Ankara; Turkey.
Tsuneo Okada, Tokyo University, Japan;
Nobuo Shuto, Nihon University, Japan;
Shunsuke Otani, Chiba University, Japan;
Takao Kagawa, Geo-Research Institute, Kyoto, Japan;
Ayhan Irfanoglu, Wiss Janney Eltsner, Emeryville, California; U.S.A.
Jake Griffiths, Purdue University, Indiana; U.S.A.
Santiago Pujol, Wiss Janney Eltsner, Emeryville, California; U.S.A.
Ahmet Yakut, Middle East Technical University, Ankara, Turkey.

Among the first actions of the Authority should be the enabling of the retrofit of public buildings, including all schools, and general public education about the threat. Retrofitting of the schools, hospitals,utilities,and transportation arteries must be completed on a priority basis by the end of the current decade.Turkey possesses the necessary material and manpower resources to accomplish such a task. It should now demonstrate its determination to take effective action for control of its own future because the challenge facing us requires nothing less.

Haluk Sucuoglu:

Earthquake risks will perhaps be much easily manageable in the next century due to the wealth of accumulated knowledge, much more effective implementation of earthquake resistant standards and a stronger global economy for supporting risk reduction efforts in settled regions. The existing risks will significantly be reduced at least by attrition through which the majority of infrastructure with high seismic risk is replaced by earthquake safe structures in accordance with the natural course of development. The situation in this century is not so promising, however. There is a huge building stock inherited from the last century that is built with insufficient, or no consideration of seismic safety. Moreover, the bulk of this vulnerable building stock is distributed over the mega metropolises of developing countries. The main task for earthquake researchers and risk planners in this century therefore is to find realistic solutions to reduce these risks to acceptable, manageable levels. The NATO Project on "Seismic Assessment and Rehabilitation of Existing Structures" and its closing Istanbul workshop provide a meaningful example of what has to be done by the earthquake research society in the 21st Century. It remains now to convey the developed ideas and methodologies to the society leaders who have the power of implementing them, presuming that they have the willingness to do so. We are confident that the societies under earthquake risk will benefit enormously from the results of the NATO project on seismic risk reduction in urban environments.

S. Tanvir Wasti:

In his famous Rede lecture in 1959, C. P. Snow, who was well-known both as a professional research scientist and as a very successful novelist, first introduced the phrase of "the two cultures". Snow forcefully suggested that there was a widening gap between the "two cultures" – the sciences and the humanities – as a result of which the world's problems were being compounded. He even went further and argued that there were far more people in the scientific community who could read and understand a play by

Shakespeare than those in the humanities who had even heard of the Second Law of Thermodynamics, let alone know what it was about. When it comes to earthquakes and their effects on the built environment, there is increasingly a 'dialogue of the deaf' in many countries between engineers on the one hand and politicians and bureaucrats who control the purse strings on the other. Charismatic politicians do not like having to take cues from back-room boffins who talk about base forces and lateral drifts. Entrepreneurial contractors prefer not to be bogged down by what appear to be expensive and constricting technical requirements for extra seismic safety. Of course, administrations and governments do act swiftly and take brave relief measures after a disaster strikes, but no amount of eloquent scientific persuasion seems to convince them that prevention is better than cure or that a stitch in time will save nine. Engineers will need to become more suave and eloquent in order to beat the politicians at their own games. Sophisticated codes, competent engineers and all forms of know-how and technology are available, but all applications need to be strictly monitored and supervised. Earthquakes must be downgraded from being a calamity to being a structural nuisance. A time will come when no excuse will suffice for the loss of even a single life as a result of an earthquake.

M. Semih Yucemen:

In Turkey, the State used to have a legal obligation to fund the costs of reconstructing buildings after an earthquake. This responsibility of the State naturally brought an unplanned burden on the national economy and on the already limited central budget in the case of catastrophic seismic events. After the two major earthquakes in 1999, the Government of Turkey has decided to enforce earthquake insurance on the nationwide basis with the sole purpose of privatizing the potential risk by offering insurance via the Turkish Catastrophic Insurance Pool (TCIP) and then exporting the major part of this risk to the international reinsurance and capital markets. Although the main aim was to reduce government's fiscal exposure, it was also intended to encourage risk mitigation and safer construction practices. To achieve these purposes all registered residential dwellings are required to be within the compulsory earthquake insurance coverage. Initially funded by the World Bank, the TCIP program became effective as of March 2001.

Turkish Catastrophic Insurance Pool has a potential to become one of the largest earthquake insurance companies in the world provided that the penetration rate be increased significantly. However, since the Law on Natural Disaster Insurance has not become effective yet, no legal enforcement is possible. Besides, governmental officials, instead of encouraging the earthquake insurance, have provided State constructed

housing in recent earthquakes. It is very important that the Law on Natural Disaster Insurance be made effective as soon as possible. The State should encourage and support participation at all levels in the compulsory earthquake insurance scheme. The earthquake problem in Turkey is too urgent and too severe for any political considerations to override it.

Natural disasters are usually violent – and mostly unpredictable. It is a sobering thought that as these lines are being written the colossal loss of life and huge damage caused by Hurricane Katrina in the south-eastern states of the United States of America continue to dominate headlines in the media. The path of Katrina towards the mainland was approximately mapped out days in advance but, in spite of this, its effects were devastating. Earthquakes, by contrast, arrive suddenly and without warning; the minute-long reign of terror of an earthquake leaves in its wake destroyed lives and property turned to debris. Earthquakes also tax engineering ingenuity – and buildings, in the form of houses and homes, are indisputably among the earliest of engineering structures. However, as indicated above, the technical facilities for changing the grim post-earthquake picture are now available. It is up to the world to get its act together and to remember that 'in delay there lies no plenty'.

S. Tanvir Wasti
Guney Ozcebe

Ankara, September 2005

ACKNOWLEDGMENTS

NATO SfP Project 977231 has differed from many other research projects in its width of scope and in being extended across so many countries and institutions. The full-length papers of the Closing Workshop have been published in book form as part of the NATO Science Series courtesy of the NATO Public Diplomacy Division. Here it should be reiterated that if the project has produced outstanding results, then a large part of the credit goes to the NATO Public Diplomacy Division and the other sponsors – TUBITAK and Middle East Technical University, who have provided both funding and understanding, and have pared down red-tape to a minimum. The project has provided an excellent example of cooperation towards specific goals and, as such, thanks are due to many organizations and individuals for the success of the Closing Workshop and in connection with the publication of the present volume.

- Throughout the duration of the Project, the NATO Public Diplomacy Division, Brussels, maintained close and efficient liaison with the researchers. Dr Chris de Wispelaere and Dr Susanne Michaelis need to be thanked for their assistance, sponsorship and kindness
- The Scientific and Technical Research Council of Turkey [TUBITAK] provided financial support and encouragement
- The well-known publishing firm of Springer-Bertelsmann has set an extraordinarily high standard in the production of this book and their representative Wil Bruins has been both helpful and cheerful
- Prof. Dr. Ural Akbulut, President, Middle East Technical University, Ankara, took a personal interest in the progress of the project
- Research Assistant Koray Kadas provided much infrastructural support during the preparation of manuscripts for the press
- BAKHUS Travel and Tours, Ankara provided professional management of local hospitality at the highest level

Syed Tanvir Wasti
Guney Ozcebe

INDEX

A

B

C

D

E

F

G

H

I

J

L

M

N

O

P

Q

R

S

T

U

V

W

Z